

AD  
601500

203

486p

\$6.00

*Proceedings of the*

## FLUID AMPLIFICATION SYMPOSIUM

*May 1964*

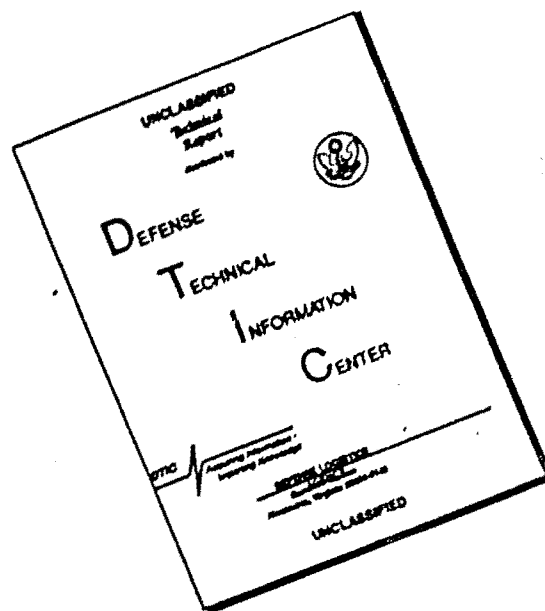
Volume II



**HARRY DIAMOND LABORATORIES**  
FORMERLY: DIAMOND ORDNANCE FUZE LABORATORIES  
**ARMY MATERIEL COMMAND**

WASHINGTON 25, D. C.

# DISCLAIMER NOTICE



THIS DOCUMENT IS BEST QUALITY AVAILABLE. THE COPY FURNISHED TO DTIC CONTAINED A SIGNIFICANT NUMBER OF PAGES WHICH DO NOT REPRODUCE LEGIBLY.

**UNITED STATES ARMY MATERIEL COMMAND  
HARRY DIAMOND LABORATORIES  
WASHINGTON 25, D.C.**

**Proceedings of the  
FLUID AMPLIFICATION SYMPOSIUM**

**Volume II**

**Sponsored by the Harry  
Diamond Laboratories,  
26, 27, and 28 May 1964**



## HARRY DIAMOND LABORATORIES

Milton S. Hochmuth  
Lt. Col, Ord Corps  
Commanding

B. M. Horton  
Technical Director

### MISSION

The mission of the Harry Diamond Laboratories is:

(1) To perform research and engineering on systems for detecting, locating, and evaluating targets; for accomplishing safing, arming, and munition control functions; and for providing initiation signals: these systems include, but are not limited to, radio and non-radio proximity fuzes, predictor-computer fuzes, electronic timers, electrically-initiated fuzes, and related items.

(2) To perform research and engineering in fluid amplification and fluid-actuated control systems.

(3) To perform research and engineering in instrumentation and measurement in support of the above.

(4) To perform research and engineering in order to achieve maximum immunity of systems to adverse influences, including counter-measures, nuclear radiation, battlefield conditions, and high-altitude and space environments.

(5) To perform research and engineering on materials, components, and subsystems in support of above.

(6) To conduct basic research in the physical sciences in support of the above.

(7) To provide consultative services to other Government agencies when requested.

(8) To carry out special projects lying within installation competence upon approval by the Director of Research and Development, Army Materiel Command.

(9) To maintain a high degree of competence in the application of the physical sciences to the solution of military problems.

The findings in this report are not to be construed as an official Department of the Army position.



## CONTENTS

THE IMPACT MODULATOR, B. G. Bjornsen, Research and Development Division, Johnson Service Company.....	5
SOME PROPERTIES AND APPLICATIONS OF DIRECT AND TRANSVERSE IMPACT MODULATORS, T. J. Lechner and P. H. Sorenson, Research and Development Division, Johnson Service Company.....	33
CONTROL CHARACTERISTICS OF VORTEX VALVES, E. A. Mayer and P. Maker, Bendix Corporation, Research Laboratories Division.....	61
EXPERIMENTAL STUDY OF A PROPORTIONAL VORTEX FLUID AMPLIFIER, B. A. Otsap, The Marquardt Corporation.....	85
CHARACTERISTICS OF A VORTEX FLUID THROTTLE, D. P. Miller, Research Laboratories, United Aircraft Corporation.....	125
CHARACTERISTICS OF COUNTER-VORTEX OSCILLATORS, T. Sarpkaya, University of Nebraska.....	147
APPLICATION TECHNIQUES FOR PROPORTIONAL PURE FLUID AMPLIFIERS, C. A. Belsterling and K. C. Tsui, The Franklin Institute.....	163
STATIC DESIGN OF PNEUMATIC LOGIC CIRCUITS, H. T. Saghafi, IBM General Products Division, Development Laboratory.....	191
APPLICATION OF PURE FLUID LOGIC TO ON-OFF CONTROL SYSTEMS, D. J. Nelson and H. Iwata, The Marquardt Corporation.....	221
THEORETICAL ANALYSIS OF FLUID AMPLIFIER DESIGN, R. E. Denker, Whittaker Controls and Guidance Division of Telecomputing Corporation.....	243
THE TURBULENCE AMPLIFIER IN CONTROL SYSTEMS, R. N. Auger, Fluid Logic Control Systems.....	261
MULTIPLE-BALL PNEUMATIC AMPLIFIERS, J. J. Eige, Control Systems Laboratory, Stanford Research Institute.....	273
THE STAGING OF PRESSURE PROPORTIONAL AMPLIFIERS TO PROVIDE STABLE, MEDIUM GAIN, DUAL CONTROL, SINGLE OUTPUT PURE FLUID SYSTEMS, W. L. Cochran and R. W. Van Tilburg, Corning Glass Works.....	289
DEVELOPMENT OF A PROPORTIONAL FLUID AMPLIFIER FOR MULTI-STAGE OPERATION, R. W. Van Tilburg and W. L. Cochran, Corning Glass Works.....	313
EXPERIMENTS IN ANALOG COMPUTATION WITH FLUIDS, S. Katz, J. M. Goto, and R. J. Dockery, Harry Diamond Laboratories.....	335

## CONTENTS

A FLUID ENCODING SYSTEM, C. K. Taft, Case Institute of Technology.....	375
FEASIBILITY STUDY OF A FLUID AMPLIFIER STEAM TURBINE SPEED CONTROL, W. A. Boothe, Advanced Technology Laboratories, General Electric Company.....	377
APPLICATIONS OF PURE FLUID TECHNIQUES TO A SPEED CONTROL, J. R. Colston and E. M. Dexter, Bowles Engineering Corporation.....	405
A PURE FLUID HYDROFOIL CONTROL SYSTEM, R. E. Bowles and E. U. Sowers, III, Bowles Engineering Corporation.....	431
A STATUS REPORT ON THE EXPERIMENTAL DEVELOPMENT OF A HOT GAS VALVE, J. C. Dunaway and V. H. Ayre, Control Systems Branch, Army Inertial Guidance and Control Laboratory, Directorate of Research and Development, Army Missile Command, Redstone Arsenal, Alabama.....	459
DEVELOPMENT OF TWO PURE FLUID TIMERS, G. V. Lemmon -- Sandia Corporation; E. R. Phillips -- UNIVAC, Div. of Sperry Rand Corp.....	481
DISTRIBUTION LIST.....	497

# THE IMPACT MODULATOR

Bjorn G. Bjornsen<sup>1</sup>

Research and Development Division

Johnson Service Company

Milwaukee, Wisconsin

## Abstract

The paper explains how the familiar mechanical motion-balance concept has been applied to the design of a new basic pure fluid component called the Impact Modulator\*. Two design versions called the Transverse Impact Modulator and the Direct Impact Modulator are discussed in regard to pressure and flow gains.

The output signals can be above and/or below standard atmosphere, i.e. positive and/or negative output flows and pressures are possible.

The DIM incorporates a unique input signal method\* which not only can accept positive and/or negative signals in the above sense, but also has a very high input impedance, approaching infinity, which increases its sensitivity and reduces several loading problems as exemplified by the cascading of two DIM yielding a pressure gain of approximately 8000:1 and a starting input pressure of 0.00125 psig.

---

\*Patent applied for by Johnson Service Company

<sup>1</sup>Senior Research Engineer, Johnson Service Company, Milwaukee, Wisconsin

# THE IMPACT MODULATOR

Bjorn G. Bjornsen<sup>1</sup>

Research and Development Division  
Johnson Service Company  
Milwaukee, Wisconsin

Pure fluid devices and circuits can duplicate many of the achievements of electronic devices and circuits. Fluid flow, however, and the effect of fluid phenomena, are mechanical in nature and the mechanical principles which must be adapted and employed in the design of pure fluid instruments have limited their analog.

Besides the inherent slower response of pure fluid devices, insufficient pressure and flow gains, low signal to noise ratio, and low input impedance, are common limitations, the latter being in the author's opinion the most serious. Low input impedance lowers the sensitivity and prevents the attainment of high gains by the cascading of units.

The following is a discussion of how the adaption of a common mechanical instrument design principle, yields a pure fluid device which combines high pressure and flow gain, i.e. power gain, with a high input impedance approaching infinity.

The basic principles of mechanical instrument design are force balance and motion balance. Both are essentially the same, except the force balance system measures relative force changes, while the motion balance system measures a required change in force balance position following a relative force change.

---

<sup>1</sup>Senior Research Engineer, Johnson Service Company, Milwaukee, Wisconsin

When a fluid jet issues into ambient fluid, the common assumption is made that the jet's total momentum flux remains constant in the downstream direction. [1]\* Then, because of fluid entrainment and the decrease in jet velocity downstream, it follows that the momentum flux density decreases with increasing distance from the emitting nozzle.

If we measure, therefore, the jet strength by integrating its momentum flux over a finite area, [2] the force becomes a function of the downstream position of the integrating area.

Such an "integration" is illustrated in Figure 1 where the compression of the spring is a measure of the force on the finite area.

The system in Figure 1 is also a motion balance system. For any change in jet strength, the area will move in the axial direction until a new position is reached where the jet force on the finite area and the spring force again are in equilibrium, i.e., a stable system.

Figure 2 illustrates a pure fluid motion-balance system established by the direct impact of two fluid jets. The motion is the axial movement of the resulting radial jet, and the gain is the total movement per unit relative change in momentum flux density.

It may well be, as is the case when two jet "cores" impact that the movement required to find a balance position is in excess of nozzle separation. Even for two identical jets impacting in this manner, the equilibrium position is indeterminate [2] in contrast to a mechanical force balance system where it is established by the fixed space coordinates of the forces.

---

\*References are shown at the end of this paper.

The movement of the radial jet can be measured by a pitot tube located transverse to the common axis of the impacting jets. Then by varying one of the jet supply pressures, the radial jet moves past the pitot tube, and the resulting velocity profile can be recorded.\*

Figure 3 shows such recordings for four different distances between the nozzles. One pressure is maintained at 15 psig with the probe equidistant from the nozzle openings. The greatest distance used is roughly 15 jet nozzle diameters. The broadest profile corresponds, according to the discussion above, to the smallest gain.

The movement of the balance position, i.e., the radial jet, is illustrated by the recordings in Figure 4. Here the distance between the jet nozzles is kept fixed while the pitot tube moves in the axial direction locating the position of the radial jet for various supply pressure combinations. How the radial jet has occupied various positions between the two nozzles can be seen in Figure 4.

The transverse pitot tube method of sensing the radial jet motion does not suffice when flow in addition to pressure output is required. A "radial" pitot tube consisting of a mechanical cavity with two axially aligned orifices may be used. Such a sensing scheme allows a  $360^\circ$  collection whereby greater flows can be obtained.

A "radial" pitot tube method for collection of the radial jet is illustrated in Figure 5 where one of the axially aligned orifices serves as the emitting nozzle for one of the impacting jets.

---

\*All accompanying recordings have been obtained using air at room temperature.

The arrangement shown in Figure 5 yields various input-output characteristics depending upon which jet supply pressure is designated the input, thus determining whether the impact jet moves into or out of the output cavity for increasing input values.

Figure 6 shows direct, i.e., positively sloped input-output pressure characteristics. The direct characteristics are obtained by keeping the upstream pressure of the jet emerging into the output cavity constant, while that of the other, being the input, increases and forces the radial jet from the outside into the output, increasing this pressure accordingly.

A reverse acting characteristic, shown in Figure 7, is obtained by letting the jet supply pressure associated with the output cavity be the input. The other supply pressure is maintained at a value which, relative to the starting pressure of the input, yields an impact position within the output cavity. Then as the input increases, the radial jet moves out with corresponding decrease in output pressure.

Depending upon physical design and supply pressure values, aspiration may occur. Hence minimum output pressures range in values from less than atmosphere to more than atmosphere. The particular examples in Figures 6 and 7 are seen to have minimum output pressures below atmosphere.

In the discussion above it has been shown how the concept of mechanical motion balance has been applied to pure fluid instrumentation. A particular application, shown in Figures 6 and 7, yields relatively high gains which alone may serve as a pure fluid amplifying unit whenever the low sensitivity is not prohibitive. The low sensitivity, i.e., the high level around which the input has to vary, is introduced by using one of the power supplies as an input signal.

The system illustrated in Figure 5 constitutes a "power amplification unit" to which one or several "input systems" can be added to facilitate local and/or total momentum flux changes.

In one simple Impact Modulator\* design shown in Figure 8, the input signal consists of a third jet which intercepts and deflects one of the impacting power jets which now are maintained at constant supply pressures. Relative to the direction of the undeflected jet from the output side, its total strength and flux density is reduced, with the result that the output signal decreases from its initial value. Thus for an increase in input signal, a corresponding reduction in output signal results, yielding a negative gain device.

In Figures 9a and 9b two typical characteristics illustrate the flexibility of the design. Since the initial output pressure is determined by the relative magnitude of the power jets, it is possible, as in Figure 9b, to select zero psig as the initial output. This then results in a negative gain, negative output characteristic. (Negative input values are obviously not practical in this design.)

The sensitivity is high, but the input impedance has a fixed value which depends upon the physical dimension of the input nozzle, and the input power required for stream deflections limits the sensitivity.

How the finite input impedance affects its application is amply discussed in reference [3].

---

\*Patent applied for by Johnson Service Company



In the more advanced Impact Modulator\* design, shown in Figure 10, a second orifice has been added. The input signal is introduced into the new cavity, creating several advantages such as higher input impedance and greater sensitivity, together with the possibility of employing negative and/or positive input signals.

Due to the "symmetric" design of the modulator, the following nomenclature has been introduced. The power signals are designated by capital letters, and the input and output signals by lower case. Subscripts 1 and 2 refer to input and output sides respectively. The orifices located concentrically to the impacting jets are called input and output control orifices, and the corresponding cavities for input and output control spaces. The region outside the control spaces is called the reference and is normally kept at atmospheric pressure.

The former design shown in Figure 8, has been called the Transverse Impact Modulator (TIM), where "transverse" refers to the method of momentum flux modulation. The advanced design shown in Figure 10, has for a similar reason regarding the method of momentum flux modulation, been called the Direct Impact Modulator (DIM).

A complete analysis of the input control-space and orifice functions cannot be given at this time, but an appreciation of the problem and its complexity can be obtained from the following discussion. [4].

If the input pressure is equal to or less than 0.528 of the power jet supply pressure  $P_1$ , the supply flow is choked at the exit of the (power jet) nozzle wherefrom the jet begins to expand.

---

\*Patent applied for by Johnson Service Company

If the input pressure is greater than  $0.528 P_1$  the exit supply nozzle pressure equals the input. If there is a negative pressure gradient through the input control orifice to a reference pressure equal to or less than  $0.528 P_1$ , the power jet continues to converge downstream from the power jet nozzle to a position in the input control where the static pressure equals  $0.528 P_1$  from where the jet starts to expand.

Depending upon jet nozzle and control orifice dimensions, together with the relative values of supply, input and reference pressures, the power jet may occupy the control orifice completely such that the input flow is zero for absolute values of input pressures above or below the reference. The input impedance is then infinite.

In addition to the direct influence of input pressure on supply flow condition and, thereby, on jet momentum flux; the input flow and pressure controls the boundary displacement and momentum thickness in the control orifice. Changes in said "thicknesses" alter the control orifice coefficients with resulting changes in jet momentum flow.

When the power jet only partially occupies the control orifice, the throat for the input flow is formed by the annular area between the orifice wall boundary layer and the jet. The pressure in the control orifice, which is the static pressure of the input and supply flow, may at some point along the control orifice have a value equal to  $0.528$  of the input pressure value. The input flow is then choked

with its throat at that position. As the input pressure changes and, thereby, the control orifice pressure gradient the throat can move to different positions in the control orifice. A plot of input flow versus input pressure for such a condition has a portion with essentially zero slope as shown in Figure 11. Such a situation may be associated with "zero" conductance because

$$\frac{dw_1}{dp_1} = 0$$

w = mass flow  
p = pressure

although the absolute conductance is not zero. By proper selection of physical dimensions and supply pressure, the zero slope portion will coincide with zero flow in which case the impedance is infinite as already discussed.

When this "direct" method of flux modulation is used in the Impact Modulator, a device with high pressure and flow gain results without the use of stream deflection. Its high input impedance not only increases the sensitivity, but also reduces many of the loading problems of pure fluid circuitry.

The individual performance of the Direct Impact Modulator is well illustrated by the input-output pressure characteristics shown in Figure 12. These were obtained by first selecting the supply pressure on the input side  $P_1$ . Keeping the input pressure equal to the reference, in this case standard atmospheric,  $P_2$  is increased until the output reaches the same. With  $P_2$  fixed at this value the output pressure will increase with increasing input pressure. Figure 13 illustrates the flow gain of the same modulator.

Cascading two Direct Impact Modulators resulted in a gain of approximately 8000:1 as shown in Figure 14 which also illustrates the high sensitivity, by a starting point of approximately 0.00125 psig.

In our work, we have for the most part, employed circular orifices and nozzles, such units being much easier to manufacture. With a view towards circuit application we have also tried to miniaturize these devices. Figure 15 shows a photograph of two plastic molded Direct Impact Modulators.

The main objective has been to demonstrate how the familiar mechanical motion balance principle has been applied to the design of new pure fluid components, and how this principle, together with a unique input signal method, makes output modulation possible without having to employ stream deflection. An added feature of this method of direct flux modulation, in addition to pressure and flow gain, is the high input impedance, with increased sensitivity and reduced loading problems.

The concepts employed do not require any mathematical formulation. That does not imply the non-existence of analytical problems, however. Severe difficulties are associated with the detailed analysis and optimum design of the input section of the Direct Impact Modulator, the output section being equally complex. Experimental verification of analytical results is also a formidable problem when dealing with small critical dimensions and when a single physical parameter cannot always be varied without affecting others.

The results of our effort, recently supported by our contract with the Harry Diamond Laboratories,<sup>1</sup> have increased our conviction of the great potentialities of the Impact Modulators.

---

<sup>1</sup>Contract No. DA-49-186-AMC-28(X).

## References

1. H. Schlichting, "Boundary Layer Theory", McGraw-Hill Book Company, Inc., New York, New York, 1955. (Translated from the German "Grenzschicht-Theorie", G. Braun, Karlsruhe, Germany, 1951.)
2. L. M. Milne - Thompson "Theoretical Hydrodynamics", The Macmillan Company, New York, New York, 1960
3. "Some Properties and Applications of Direct and Transverse Impact Modulators", T. J. Lechner and P. H. Sorenson, paper presented at this symposium. (HDL Symposium on Pure Fluid Amplification, May, 1964.)
4. "Ejector-Nozzle Flow and Thrust" H. E. Weber. Paper presented at the Hydraulic Conference, Ann Arbor, Michigan, April 13-15, 1959, of The American Society of Mechanical Engineers.

"MECHANICAL "INTEGRATION" OF  
JET MOMENTUM FLUX."

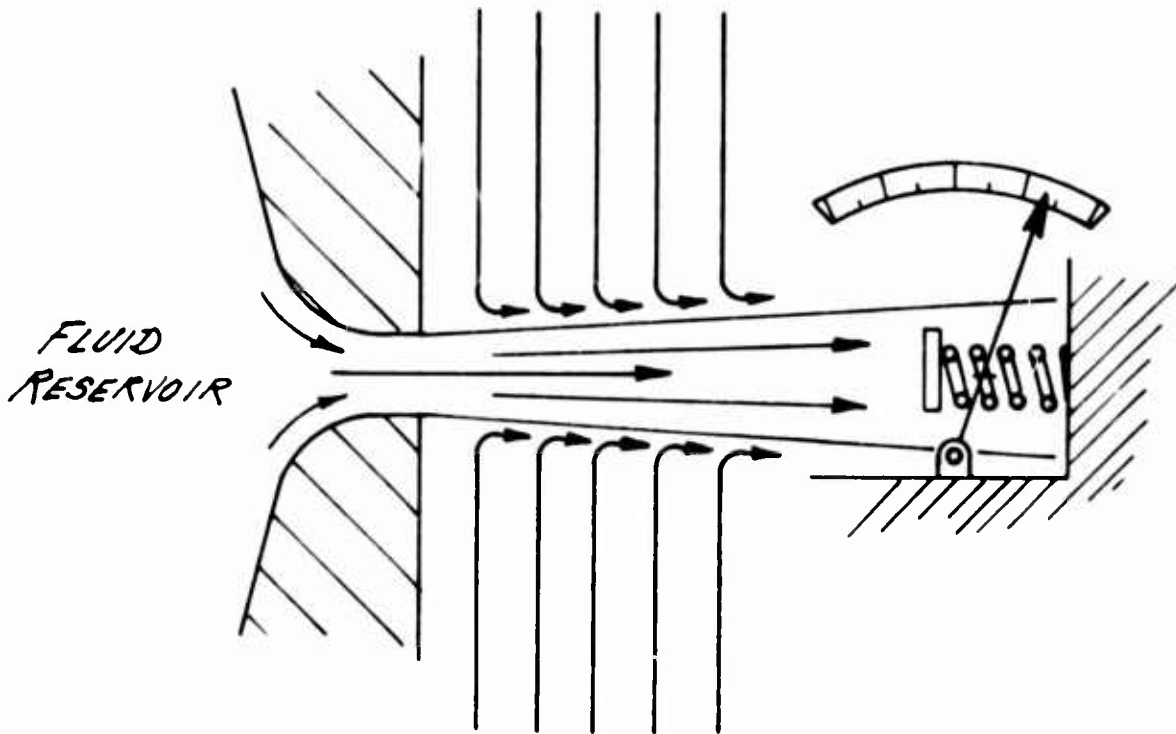


FIG. 1

"THE DIRECT IMPACT OF TWO JETS CONSTITUTE A  
PURE FLUID MOTION-BALANCE SYSTEM"

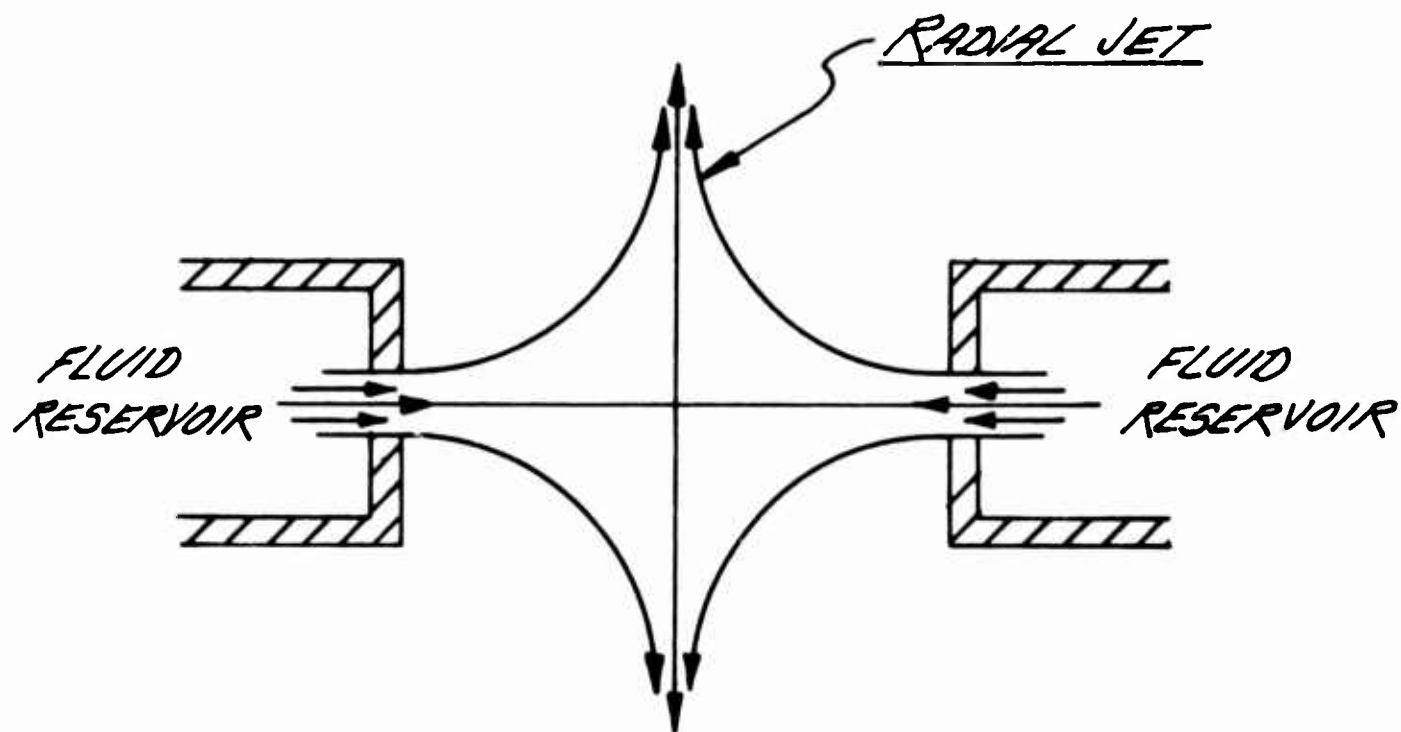


FIG. 2

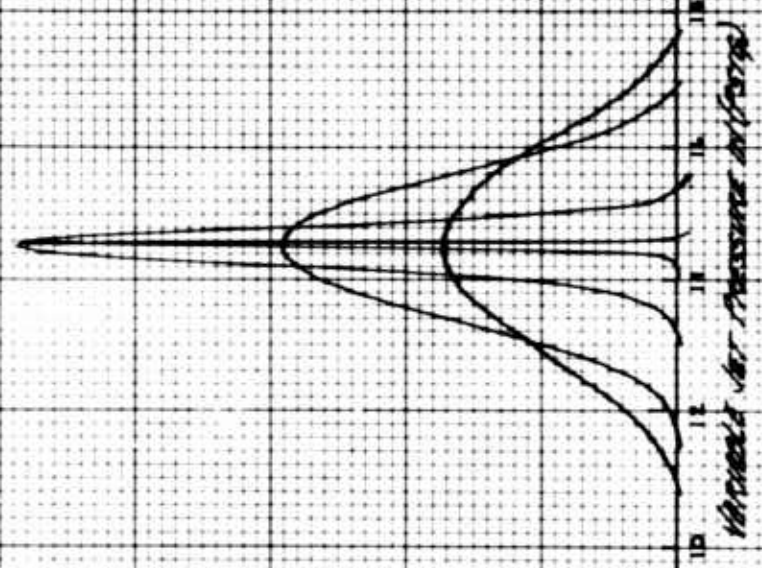


*Pressure Jet Profiles for Different Nozzle Separations*

THE PROFILES ARE OBTAINED BY KEEPING ONE JET SUPPLY PRES-  
SURE CONSTANT WHILE THE OTHER  
VARIES OVER THE RANGE  
INDICATED.

THE TOTAL HEAD OF THE RADIAL  
JET IS SENSED BY A PITOT TUBE  
EQUIDISTANT FROM THE TWO  
OPPOSING NOZZLES AND ORIENTED  
NORMAL TO THEIR COMMON AXIS.

THE NARROWER PROFILE CORRES-  
PONDS TO THE SMALLER NOZZLE  
SEPARATION.



*Pressure Jet Profiles for Different Nozzle Separations*

*Fig. 3*

# DIFFERENT POSITIONS IN A PURE FLUID MOTION BALANCE SYSTEM

NOZZLE SEPARATION IS FIXED  
AT 0.200" AND ONE JET SUPPLY  
PRESSURE (LEFT IN FIGURE) IS  
KEPT AT 15 PSIG. FOR THE  
VARIOUS PRESSURE COMBINATIONS,  
SHOWN ABOVE THE PROFILES, THE  
LOCATION OF THE RADIAL JET IS  
INDICATED BY THE PITOT TUBE  
TRAVEL.

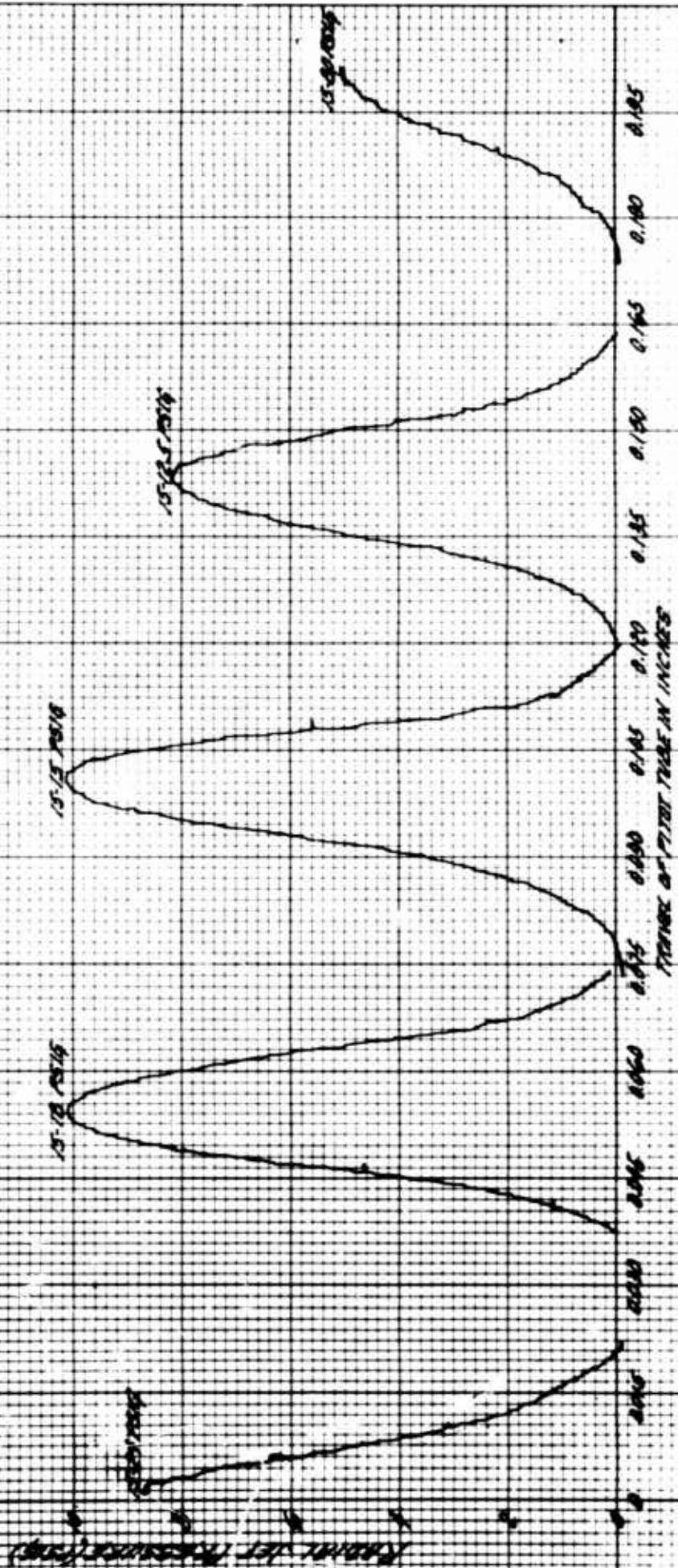


Fig. 4

"IDENTIFICATION OF RADIAL JET POSITION  
- RELATIVE TO A SINGLE ORIFICE"

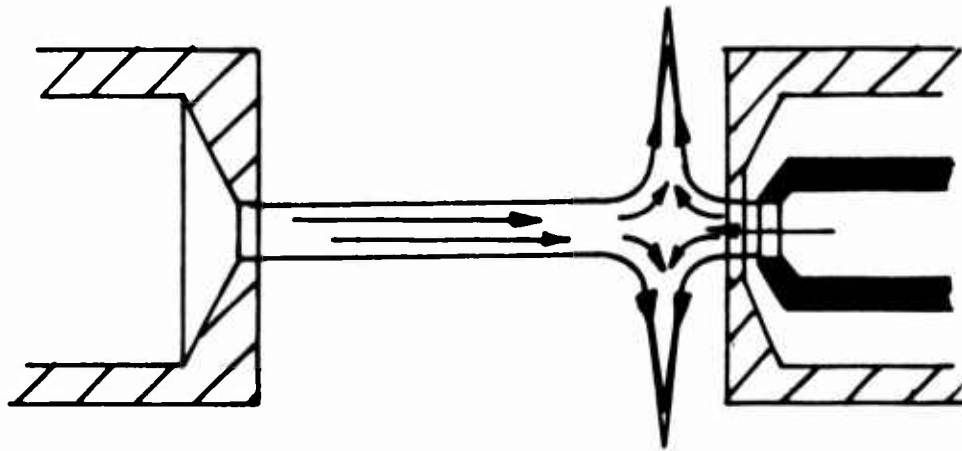


Fig. 5

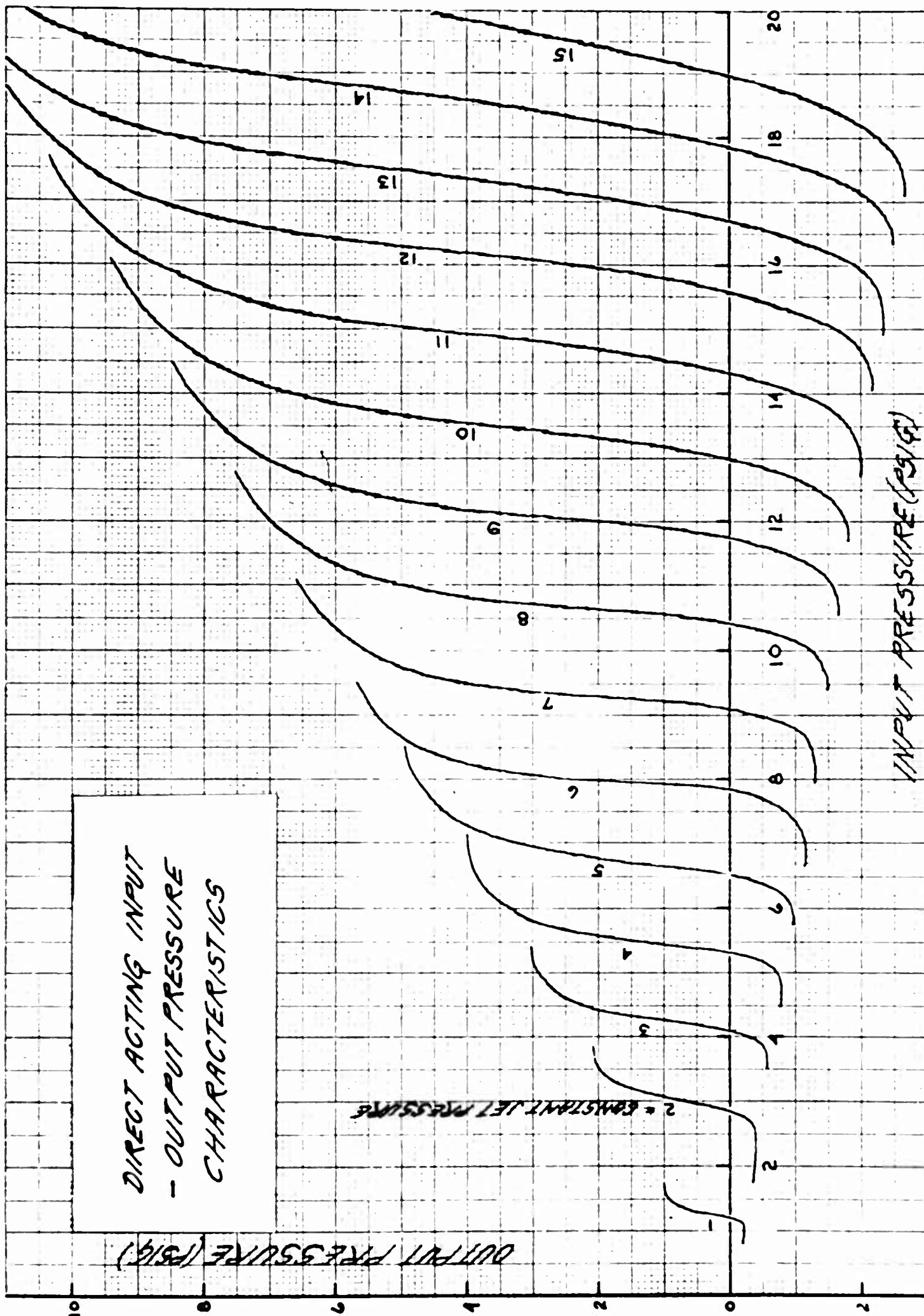


FIG. 6



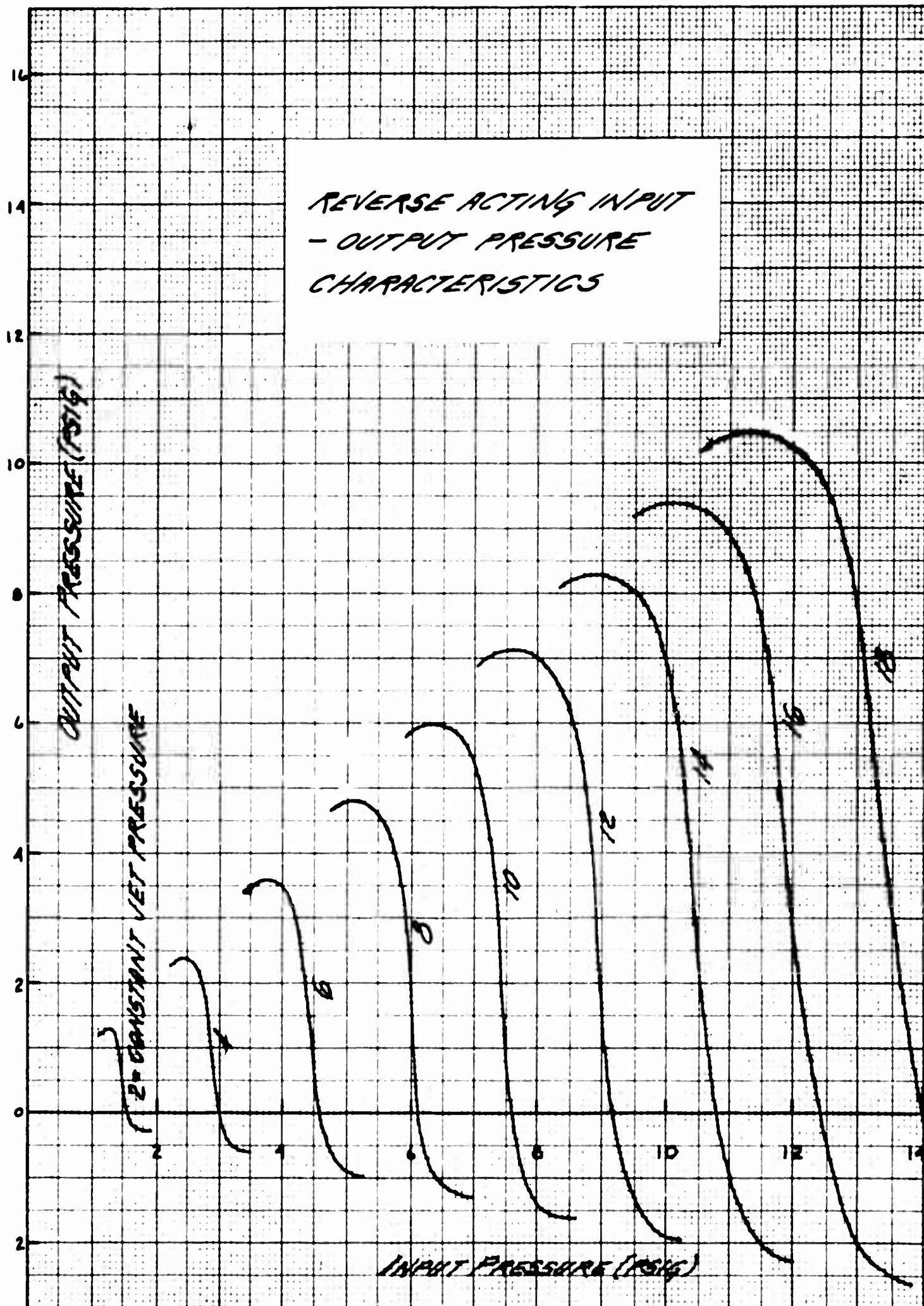


FIG. 7

## "IMPACT MODULATOR"

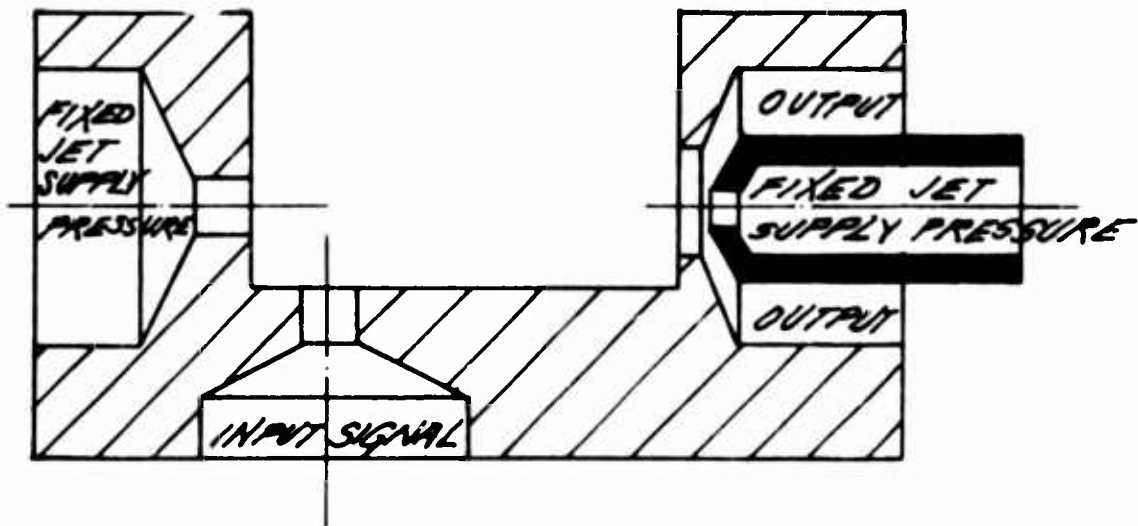


FIG. 8

"INPUT-OUTPUT  
CHARACTERISTICS"

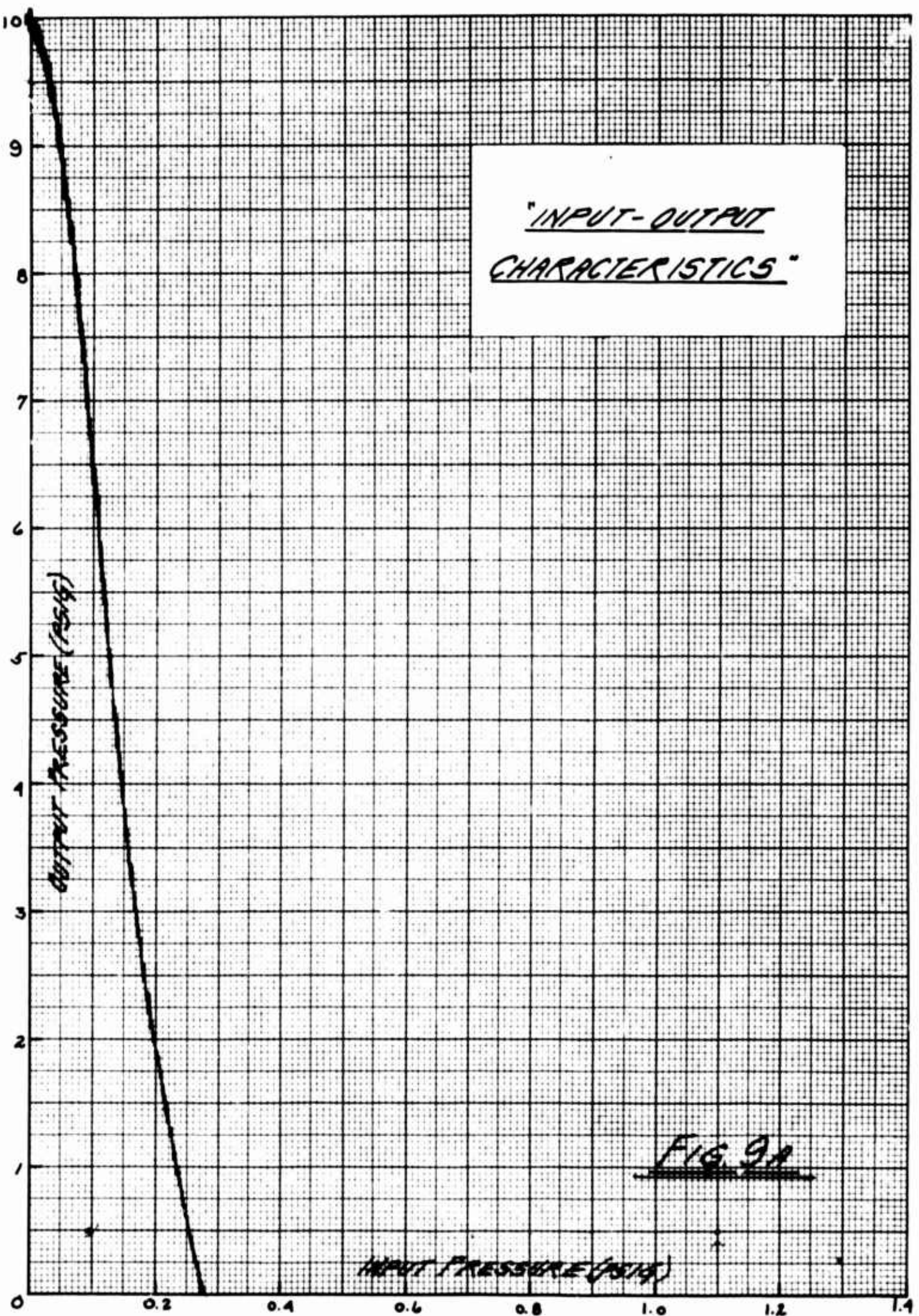


FIG. 9A

"THREE STAGE NEGATIVE GAIN, NEGATIVE OUTPUT -  
IMPACT MODULATOR"

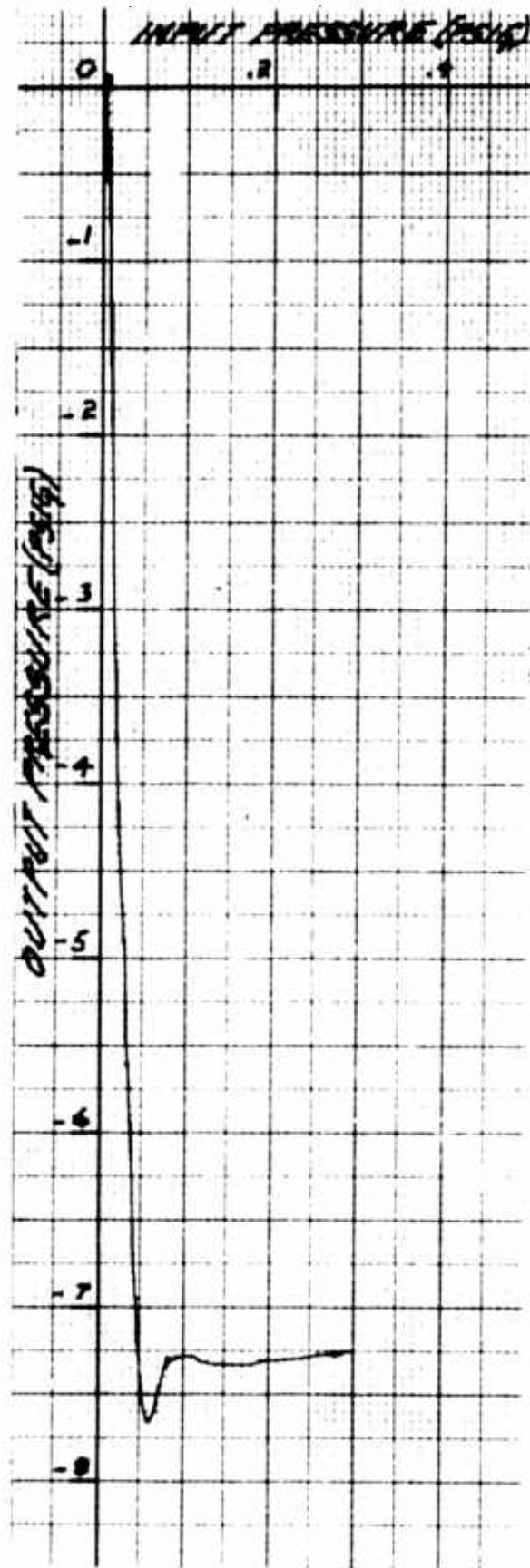
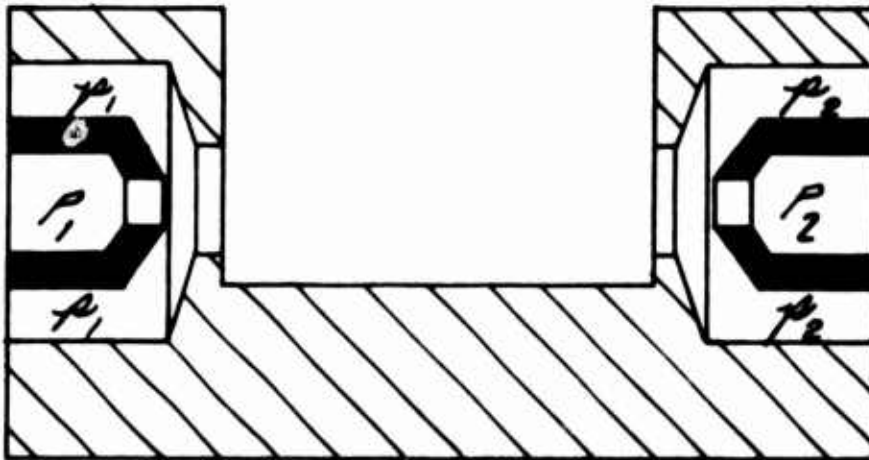


FIG. 9B



## "DIRECT IMPACT MODULATOR"



$P_1$  &  $P_2$  ARE SUPPLY  
PRESSURES  
 $p_1$  IS INPUT SIGNAL  
 $p_2$  IS OUTPUT SIGNAL

FIG. 10

INPUT CONDUCTANCE : INPUT FLOW  
VERSUS INPUT PRESSURE

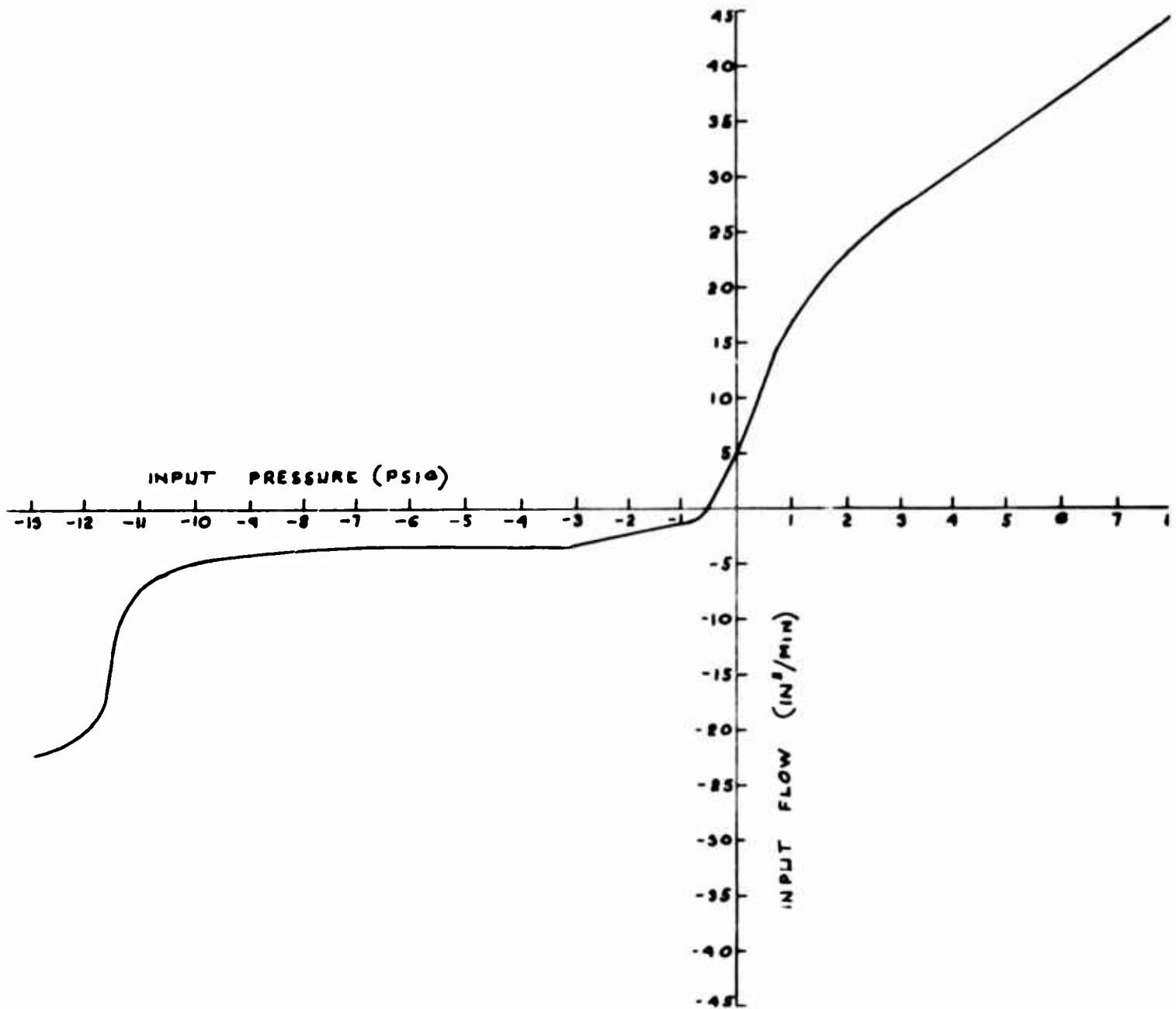


FIG. 11

"INPUT-OUTPUT PRESSURE CHARACTERISTICS OF A  
DIRECT IMPACT MODULATOR"

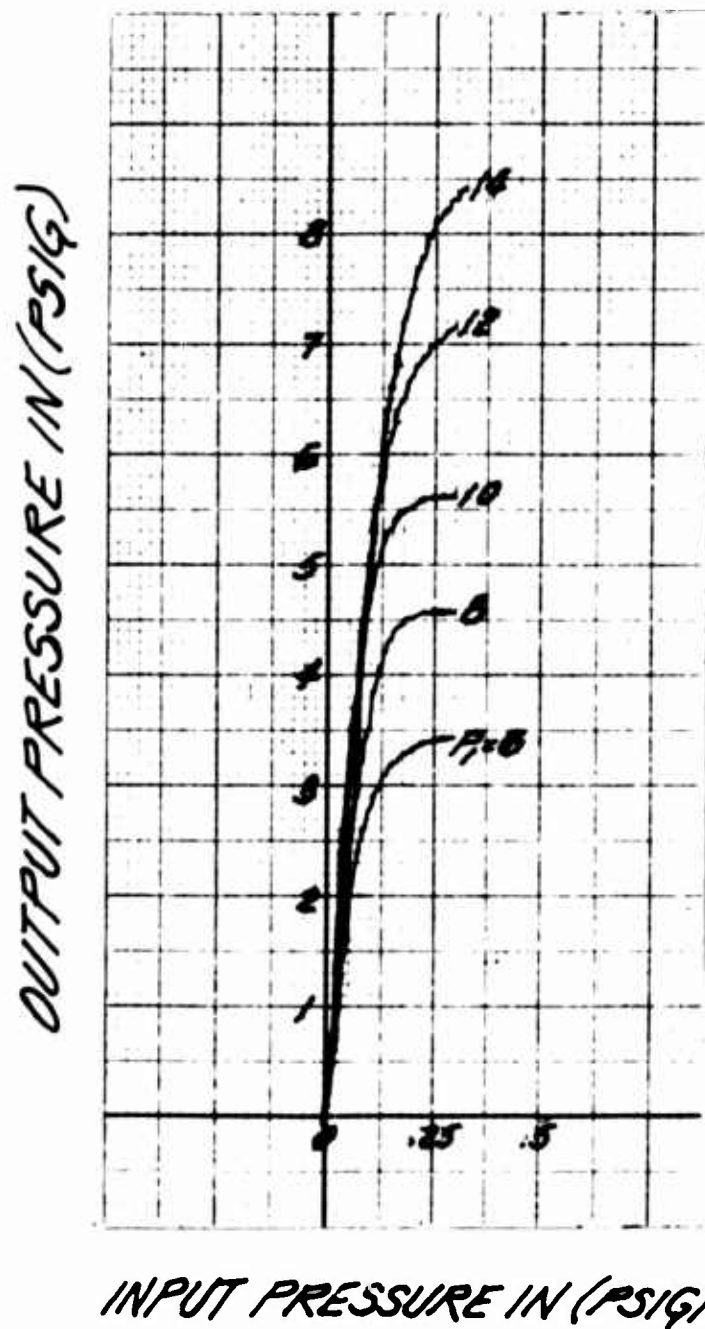
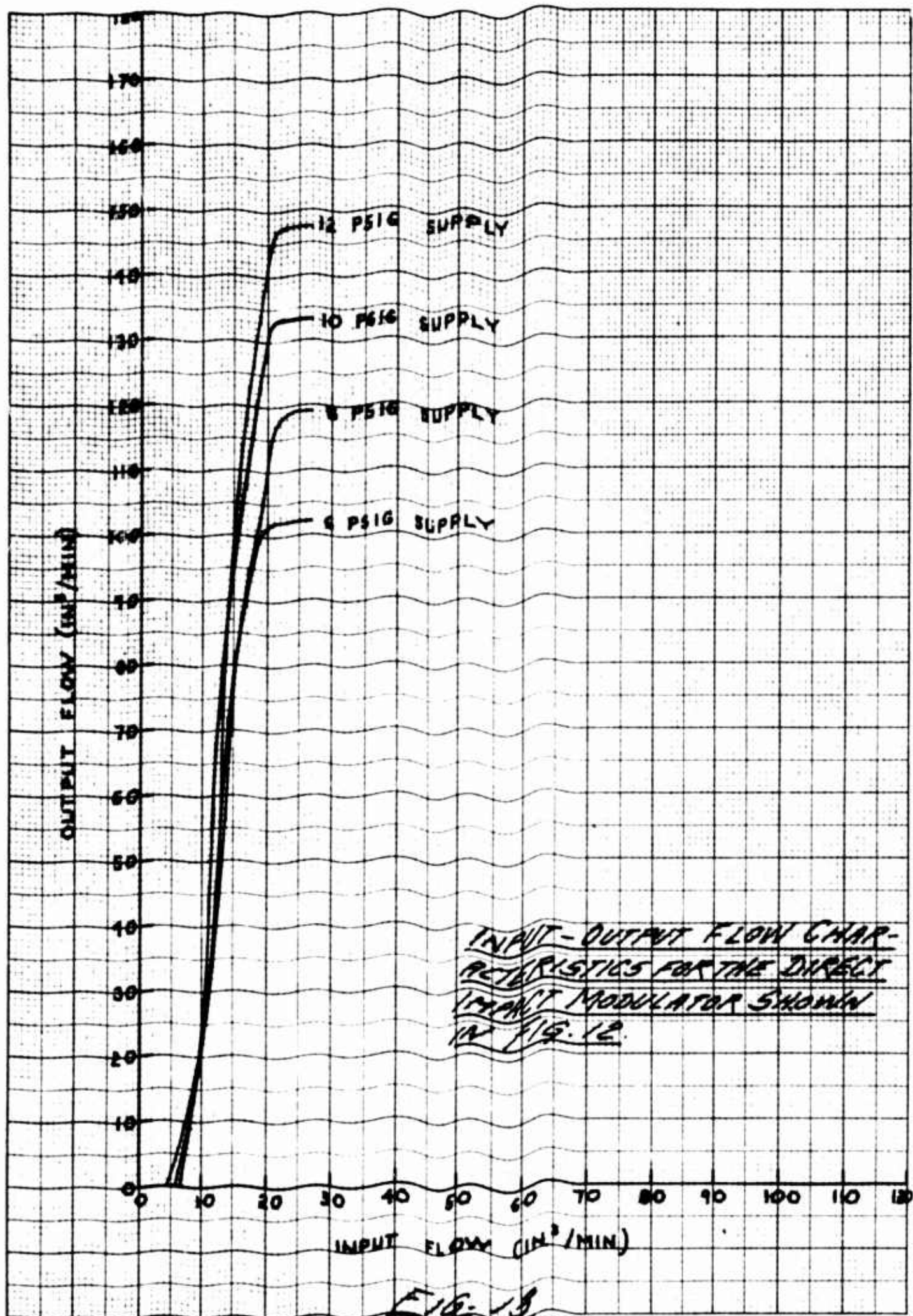


FIG. 12



"INPUT-OUTPUT PRESSURE CHARACTERISTIC OF A -  
TWO-STAGE DIRECT IMPACT MODULATOR"

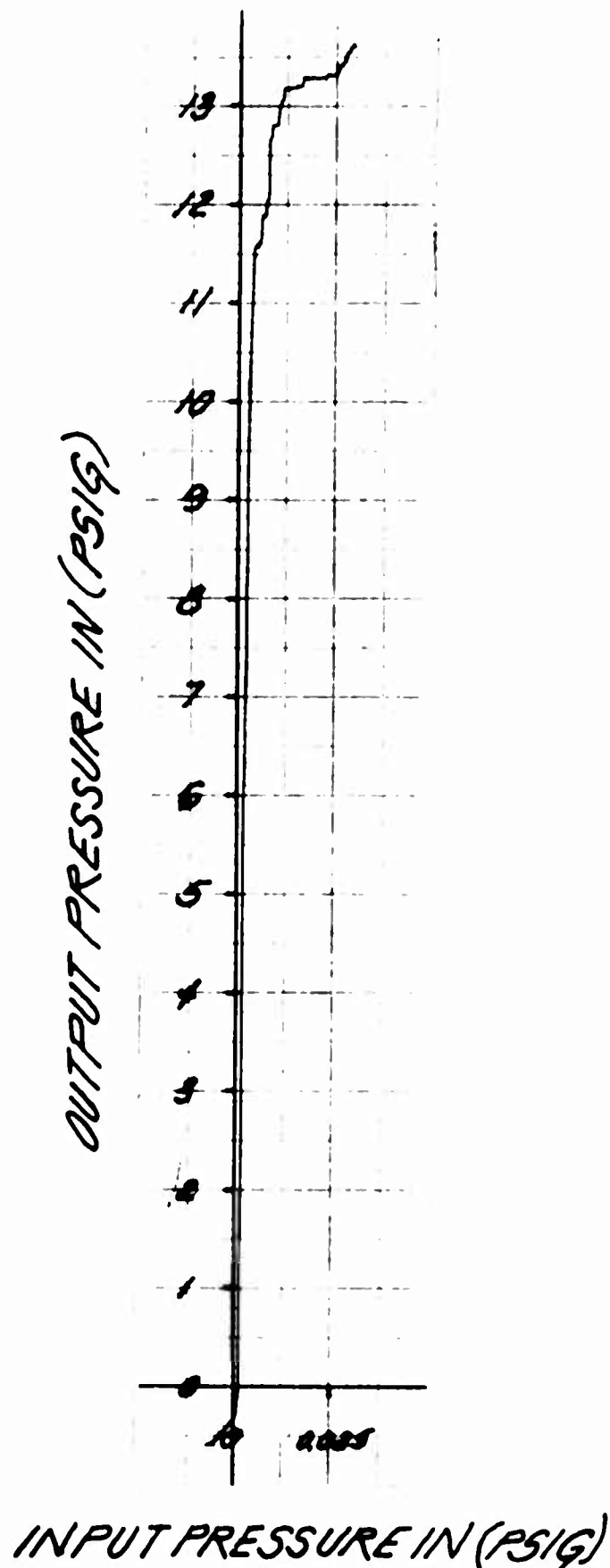


FIG. 14

"PLASTIC MOLDED DIRECT IMPACT -  
MODULATORS."

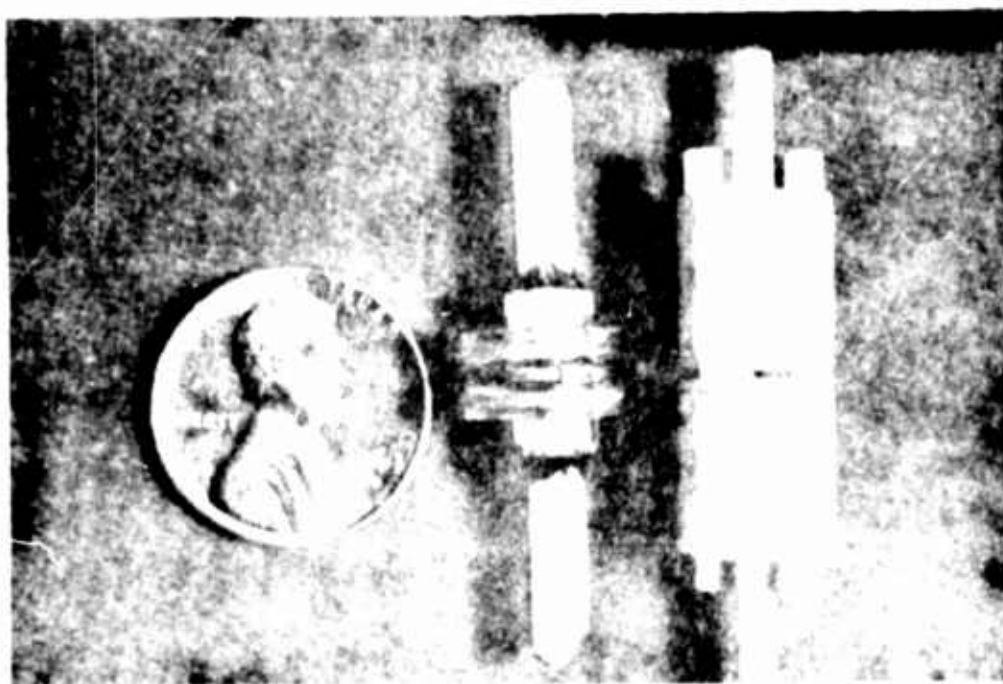


Fig. 15

SOME PROPERTIES AND APPLICATIONS OF  
DIRECT AND TRANSVERSE IMPACT MODULATORS

T. J. Lechner<sup>1</sup> and P. H. Sorenson<sup>2</sup>

Research and Development Division  
Johnson Service Company  
Milwaukee, Wisconsin

This paper describes some of the properties and applications of a unique pure fluid amplifying element called the Impact Modulator.<sup>3</sup> A brief discussion of the operating principles of the two types of modulators (Direct and Transverse) is given, but a more complete description is given in another paper, "The Impact Modulator", of this symposium.<sup>4</sup>

The compatibility characteristics of these devices such as output impedance, transfer curves, etc., are presented. These characteristic curves are used to construct a four stage amplifier with a 12,000:1 pressure gain. This amplifier is used to form the forward loop of a pure fluid operational amplifier. The performance characteristics such as gain, linearity, offset etc., of this amplifier are then discussed, and suggestions for improvement are included.

---

<sup>1</sup>Senior Research Engineer, Johnson Service Company, Milwaukee, Wisconsin

<sup>2</sup>Associate Research Engineer, Johnson Service Company, Milwaukee, Wisconsin

<sup>3</sup>Patent applied for by Johnson Service Company

<sup>4</sup>"The Impact Modulator", B. G. Bjornsen, paper presented at the Fluid Amplification symposium, Washington, D.C., May, 1964.

SOME PROPERTIES AND APPLICATIONS OF  
DIRECT AND TRANSVERSE IMPACT MODULATORS\*

T. J. Lechner<sup>1</sup> and P. H. Sorenson<sup>2</sup>

Research and Development Division

Johnson Service Company

## I Introduction

The Johnson Service Company Research and Development Division, under the sponsorship of the Harry Diamond Laboratories, has for the past year been involved in applied research in order to develop certain components for a pure fluid operational amplifier. The active element considered for this amplifier design is the impact modulator, a unique amplifying element conceived at Johnson Service Company prior to this development work. This paper is an extension of another paper on this program [1], and is intended to show the desirable performance characteristics for incorporation of the impact modulator into pure fluid systems.

The successful coupling of pure fluid components requires a knowledge of both the input and output characteristics of each component. The necessary characteristics (such as input impedance, output impedance, gain, etc.) associated with the impact modulator performance will be discussed with respect to both the direct and transverse methods of signaling. An evaluation of the two signaling

---

\*This work has recently been supported by the Harry Diamond Laboratories, Washington 25, D. C. under Contract No. DA-49-186-AMC-28(X).

<sup>1</sup>Senior Research Engineer, Johnson Service Company, Milwaukee, Wisconsin

<sup>2</sup>Associate Research Engineer, Johnson Service Company, Milwaukee, Wisconsin



techniques will be made whenever possible to point out their basic differences in operation. The characteristics presented here, differ in concept from other pure fluid devices, in that the impact modulators have a dual supply, which implies a combination of supply conditions for any operating point. It will also be shown that because of the two supplies, an optimum gain exists at any operating condition. From a description of the impact modulator characteristics the methods necessary to design an effective operational amplifier circuit will be presented.

## II General Description of Impact Modulators

The impact modulator is pure fluid amplifier based on the field balance of two axially opposed fluid jets. The resultant flow from this balance point is a radial flow core which is collected as the output of the amplifier. If either power jet is affected so as to change its strength, the balance point will move and, therefore, change the collected pressure. This principle has manifested itself in two types of fluid amplifiers, the transverse impact modulator and the direct impact modulator. [1]

The transverse impact modulator (TIM) is a negative gain amplifier, Figure 1. It is, in the basic design, signaled by a round jet stream whose momentum transversely impinges on a power stream of higher strength, causing the latter to be deflected. This deflection is reflected as a decrease in strength of that power jet at the balance point, causing a decrease in output. The no load pressure gain of these units is generally of the order -20 to -100, while the full load flow gains are of the order -5 to -30. The input to output impedance ratios of the transverse impact modulator are usually in the neighborhood of 1:1 to 3:1.

The direct impact modulator (DIM) is a positive gain amplifier, Figure 2. It is a device in which the impact balance point is caused to move by the application of a pressure signal applied around one power stream. The signal, applied at the exit of one power nozzle causes a change in the downstream momentum or momentum distribution of that power stream thereby changing the location of the balance point. This method of signaling causes no deflection of either power stream. Pressure gains of this device have been as high as 200:1, and there is no reason to believe this to be a limit. As this type of signaling requires only a pressure signal and very little power, the flow gain is high.

### III Performance Characteristics

The performance characteristics describing the impact modulators are all of a dimension higher than those of other fluid devices because of the extra supply pressure. For example, the output characteristics which are normally presented as a curve of output flow versus output pressure for different constant input pressures with a fixed power jet pressure, are a five dimensional space. The output characteristics for an impact modulator are a six dimensional space because of the second supply pressure. This practically eliminates the possibility of achieving enough necessary design information on a two dimensional graph. For this reason a simplified version of describing these operating characteristics is presented here.

## A. Output Pressure-Supply Curves

The (nulled) output pressure supply curves, Figure 3, are simply the output pressure plotted versus supply pressure with the second supply fixed, and with no input signal. These curves are somewhat analogous to pressure recovery curves in that they depict the maximum output pressure range that can be achieved with any particular supply pressures.

If one wants to draw an analogy, however, the supply  $P_2$  could be functionally compared to the grid bias voltage of a vacuum tube, in that it biases the output flow to positive, zero, or negative values with no input signal. This is, therefore, the method whereby the modulator is biased into the proper output range in a manner that most favorably suits the particular load.

The characteristics shown in Figure 3, are essentially the same for both the direct and transverse impact modulator except that they usually have different operating points (DIM has positive gain while the TIM has negative gain).

The difference between the DIM and the TIM that should be mentioned is that the control orifice in the DIM can be so arranged to provide nonlinear spacing of the output pressure-supply curves so that in these regions of uneven spacing the gain can be much higher than in the symmetric units. It might also be pointed out that when the DIM's are operated as bistable elements, the output pressure-supply curves are hysteresis loops.

## B. Input Impedance

The input impedance of the TIM is that of the signal orifice since there is no interference from the supply or power jet. The input impedance of the DIM is a function of the supply ( $P_1$ ) and is usually decades higher than that of the TIM. In fact there are input pressure ranges where the input impedance can be infinite or negative depending on the configuration of the primary supply and control orifices. Further information on this subject can be found in the paper referenced as [1]. Typical input impedance curves for both types of modulators are shown in Figure 4.

## C. Output Impedance

The usual output impedance characteristic curve is a plot of output flow and output pressure, taken as the load resistance is varied through the range from 0 to  $\infty$ . This plot is made for different constant input values giving one page of curves for each supply pressure. These characteristics for the impact modulators, however, have to be projected into the third dimension to include the range of secondary supply pressures ( $P_2$ ) that are possible. This extra variable does increase the complexity of design, but in return it allows a selection of supply pressures that produce the same output range, making it a more versatile component. In a sense it is the same as a unit with variable geometry that can be adapted to the particular load that it must drive. Figure 5 shows that for a particular (constant signal) operating point ( $q_2, p_2$ ) there is a range of supply pressures that satisfy that point. The implication of this curve is that the output conductance ( $\partial q_2 / \partial p_2$ ), can be regulated by choosing different supply pressure combinations. It could further be shown that this is also true of transconductance and amplification factor.

#### D. Transfer Curves

Once the supply pressures have been selected and the output impedance characteristic curve has been obtained, another graph can be formed that relates the input pressure to the output pressure through the load line. This graph is a plot of the output flow versus signal pressure for constant output pressures and is called the static transfer curve. Both the output and static transfer curves are shown in Figure 6. From this curve the transconductance ( $\partial q_2 / \partial p_1$ ) can be measured.

#### E. Cascading Techniques

In order to describe the methods of cascading these devices, examples involving the TIM will be used. They are more difficult to match because of the fact that the range of one must exactly coincide with the input range of the one it drives in order to assure a nulled output.

When two modulators are to be cascaded it must first be determined what supply settings will give optimum performance. Then the conventional dynamic transfer curves can be found to determine the gain, distortion, etc. Figure 7 shows the (nulled) output pressure-supply curves of a typical TIM (modulator A) plotted against  $P_2$  where the lines of constant  $p_{1c}$  indicate the amount of signal necessary to drive the output to cutoff from any zero signal setting. If the device is operated from the maximums of the  $p_{1c}$  curves it can be seen that the gain of the unit is about -36:1. Figure 8 shows the same characteristics of a different TIM (modulator B) loaded with the input of modulator A. If the modulator A were to be driven through the range 0-7.5 psi by modulator B then the supply settings

of the two, and the overall signal range can easily be found from Figures 7 and 8. From Figure 7 knowing that the maximum output of 7.5 psi is desired, it can be seen that one set of near optimal values would be.

$$\begin{array}{ll} \text{Unit A} & P_1 = 18.0 \text{ psig} \\ & P_2 = 13.0 \text{ psig} \\ & P_{1c} = 0.24 \text{ psig} \end{array}$$

Realizing that the maximum signal of A must correspond to the maximum output of B we can, through Figure 8, find:

$$\begin{array}{ll} \text{Unit B} & P_1 = 0.75 \text{ psig} \\ & P_2 = 0.55 \text{ psig} \\ & P_{1c} = 0.025 \text{ psig} \end{array}$$

The overall pressure gain ( $G_p$ ) of these two units is then approximated by:

$$G_p = \frac{(\text{output B})_{\max}}{(\text{input A})_{\max}} = \frac{7.5}{0.025} = 300$$

Figure 9 shows the pressure gain of this combination. It can also be shown that these are the optimal values of supply pressures as far as overall gain is concerned. The next step in the process would be to plot the dynamic transfer curves for the combination to determine the distortion, exact pressure gain, etc.

#### IV Operational Amplifier

A generalized schematic of an operational amplifier control circuit is given in Figure 10. The active amplifying element "K" is in this case a series of cascaded stages of impact modulators. The output pressure ( $P_{\text{out}}$ ) is fed back through the passive element (H) to be compared with the input signal ( $P_{1n}$ ) in the summing point.

The output is then corrected according to the error signal ( $P_e$ ). The steady state transfer function or amplifier gain can then be written as  $\frac{P_{out}}{P_{in}} = \frac{K}{1+HK}$ , where K and H are the gains of the forward loop and feedback respectively. Since the loop gain (KH) is much greater than one, the gain of the circuit can be determined by the value of feedback gain. Although several variations of this control circuit are under investigation, only one is presented here.

#### A. The Active Amplifying Element

From the transfer function shown above, it is evident that if a passive element is used in the feedback, i.e.,  $0 \leq H \leq 1$  the gain may be varied from K to  $\frac{K}{1+K}$ . If several stages of the impact modulator are used to obtain the high gain K, (here in excess of  $10^4$ ) the gain can vary from K to approximately 1. In the previous section, it was shown how two transverse impact modulators could be cascaded to obtain a gain of 300:1 psi/psi. By adding two more stages to this combination, the gain was increased to 12,000:1 psi/psi, see Figure 12. This four stage amplifier was then assumed sufficient for use as the active amplifying element.

#### B. The Summing Point

The usual operating conditions for the summing point is that  $P_e = P_{in} - P_f$ . However, it would be sufficient if  $P_e = aP_{in} - bP_f$  where (a) and (b) are constants of proportionality. The first approach used to obtain this action was to use a stream deflection principle in the following manner. The input signal ( $P_{in}$ ) is applied at an orifice  $d_1$ , Figure 11. It is then collected on the opposite side in a collector orifice  $d_3$ . If then the feedback

signal is applied to an orifice,  $d_2$ , normal to the input-collector axis, the input stream will be deflected away from the collector reducing the collected pressure proportionally to the magnitude of the feedback signal. This device might be considered a simple three dimensional stream deflection or momentum amplifier with a single control and collector orifice. This device, called a three terminal modulator (3TM) operates according to the relation

$P_{in} + P_c = A(P_{in}^b)P_f^{1-b}$  where  $A$  and  $b$  are constants dependent upon the geometry of the unit. By imposing the conditions of a control circuit and further algebraic manipulation of this equation, the 3TM can be shown to follow the relation  $P_c = \alpha P_{in} - \frac{m}{1-b} P_f$  where  $m$  and  $\alpha$  are determined by the circuit relationships. Then the 3TM follows the necessary characteristics of a summing point. By including this relation in the total circuit equation, the following transfer function is obtained,  $\frac{P_{out}}{P_{in}} = \frac{K}{1+M'HK}$  where  $M' = \frac{m}{1-b}$ .

The value of  $\alpha$  in the transfer function can be of significance in the performance of the circuit.  $\alpha$  is dependent upon the geometry of the 3TM and the impedance which the error signal sees in the first stage of amplification. When the input impedance of the first stage is known, the 3TM can be designed for a maximum  $\alpha$ . [2] This impedance match will also assure maximum impedance in the feedback and at the same time minimize the gain loss in the forward loop.



### C. Feedback

Of all the circuit components, the feedback element must meet the most rigid specifications. The feedback gain must be variable from zero to one and linear over the full pressure drop of the output range. Although almost any passive flow resistance element can meet the gain range requirements, none of these are linear enough for feedback elements. Capillaries, if long enough, can present a relatively linear resistance but usually have to be paralleled in order to pass sufficient flow. Porous materials, in some instances, present extremely linear resistance, but are sensitive to manufacturing techniques and have tendencies to become clogged. One method of attaining an approximately linear resistance is with a pair of axially opposed orifices with variable spacing between them. The gain is determined by the space between the orifices and the amplifier output sees the same impedance even as the feedback gain is varied. This scheme will be used in the following amplifier design.

### D. Evaluation

To evaluate the effectiveness of the circuit design, it is necessary to examine the actual characteristics of the operational amplifier. The input characteristics can simply be described as flow through an orifice. The gain characteristics can be determined from the value of the feedback. The output characteristics, however, must be determined through an experimental plot of output flow and pressure with changing load. With these characteristics then, the entire operation of the amplifier can be described.

The gain curves show the range of gains available. Figure 12 shows the forward gain of the circuit under actual circuit loading condition. This gain is in the order of magnitude of  $10^4$  psi/psi. Figure 13 shows the total range of gains available, from approximately  $10^4$  with no feedback, to approximately .5 psi/psi with full feedback. Although only two intermediate gains are shown, there is infinite resolution of gain between the maximum and the minimum.

The output characteristics must be examined to determine the linear range of operation of this device when coupled with similar computing devices. Figure 14 shows the output characteristics of this circuit. The dashed lines indicate the ideal output characteristics of an operation amplifier. The loss of pressure with increased load before sharp cutoff is due to the lack of sufficient gain in the forward loop. The cutoff slope is due to load of the feedback orifice. It can be shown that the cutoff curve is identical to the feedback load line. When this circuit is to be coupled with another computing device, the input characteristic of that device can be plotted directly over this output curve. The intersection of this load line and cutoff curve will show the maximum output pressure to which linear amplification will occur. According to this output curve the greater the output load, the more limited the operating range. When the impedance of the feedback load is increased the operating range of the amplifier will also increase. This output characteristic thus has certain undesirable features, but it does show that pure fluid operational amplifiers can be designed that exhibit the same type of performance as their electronic counterparts.

## V Discussion

### A. Passive Differential Amplifier

Although the impact modulator has been presented as an active amplifying element, its principle of operation offers an additional feature of acting as a passive amplifying element, i.e., a device which amplifies the difference of two signals. Consider the two supply pressures  $P_1$  and  $P_2$  as signals, and the output pressure,  $p_2$  and input pressure  $p_1$  as two outputs, one positive and one negative, Figure 2. Under these conditions it can be shown that the output pressures  $p_1$  and  $p_2$  are proportional to the difference in the signal pressures  $P_1$  and  $P_2$ . Consider first the condition that  $P_1 > P_2$ . The negative pressure  $p_1$  will always remain less than or equal to zero. The positive output  $p_2$  will read some amplified portion of the difference. It should be noted that the pressure drop across the orifice  $D_2$  is greatly reduced and, therefore, the flow is greatly reduced. If then,  $P_1 > P_2$  the impedance of signal  $P_1$  remains that of an orifice, while the impedance of signal  $P_2$  is greatly increased. Because of the symmetry of the direct impact modulator, the exact reverse of this situation is also true. When the two signals  $P_1$  and  $P_2$  are equal, the output of either side, is zero. This device when used as a passive element has the properties of a difference amplifier or summing point.

By replacing the 3TM with the impact type summing point, the loading effect of the feedback on the output is greatly reduced. This, however, presents certain inherent limitations. The opposing orifice type feedback element can no longer be used as it destroys any improvement in feedback impedance. In order to retain the high impedance a "closed" type restrictor must be used.

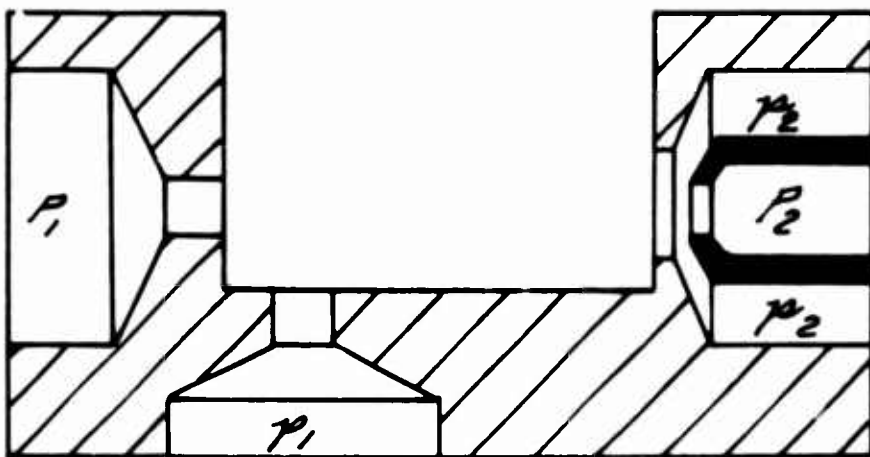
## VI Concluding Remarks

In defining the techniques involved in designing an operational amplifier using the impact modulator, many details in the physical construction have been bypassed. This omission has been intentional so that the principles of operation would not be overshadowed by the many details of physical design. It should also be pointed out that the model amplifier presented in this paper was not meant to be an optimum design but rather an example to present the techniques used for describing impact modulators and their applications.

## BIBLIOGRAPHY

1. Bjornsen, B. G. "The Impact Modulator" Fluid Amplification Symposium, Harry Diamond Laboratories, May, 1964.
2. Lechner, Thomas J. and Wambsganss, Martin W., "Proportional Power Stages for Impedance Matching Pure Fluid Devices, " Fluid Amplification Symposium, Diamond Ordnance Fuze Laboratories, October, 1962.

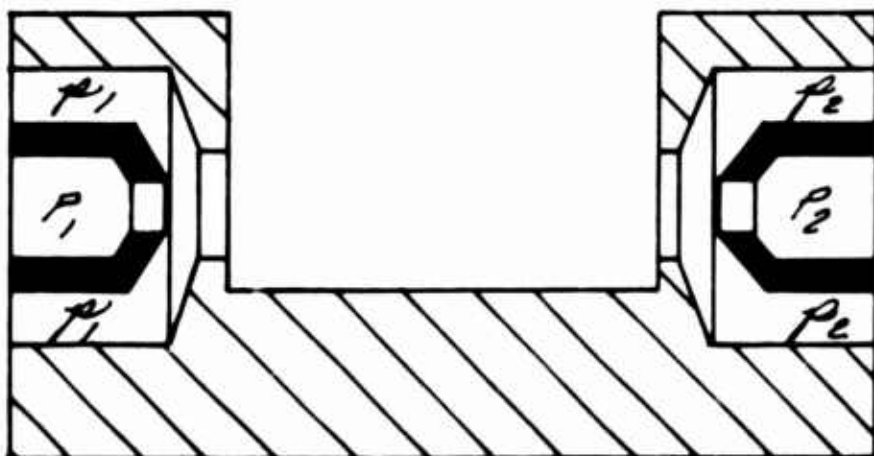
# TRANSVERSE IMPACT MODULATOR (TIM)



$P_1, P_2$  ARE SUPPLY  
PRESSURES.  
 $P_1$  IS INPUT SIGNAL  
 $P_2$  IS OUTPUT SIGNAL

FIG. 1

# DIRECT IMPACT MODULATOR (DIM)



$P_1, P_2$  ARE SUPPLY  
PRESSURES.  
 $P_1$  IS INPUT  
 $P_2$  IS OUTPUT

FIG. 2

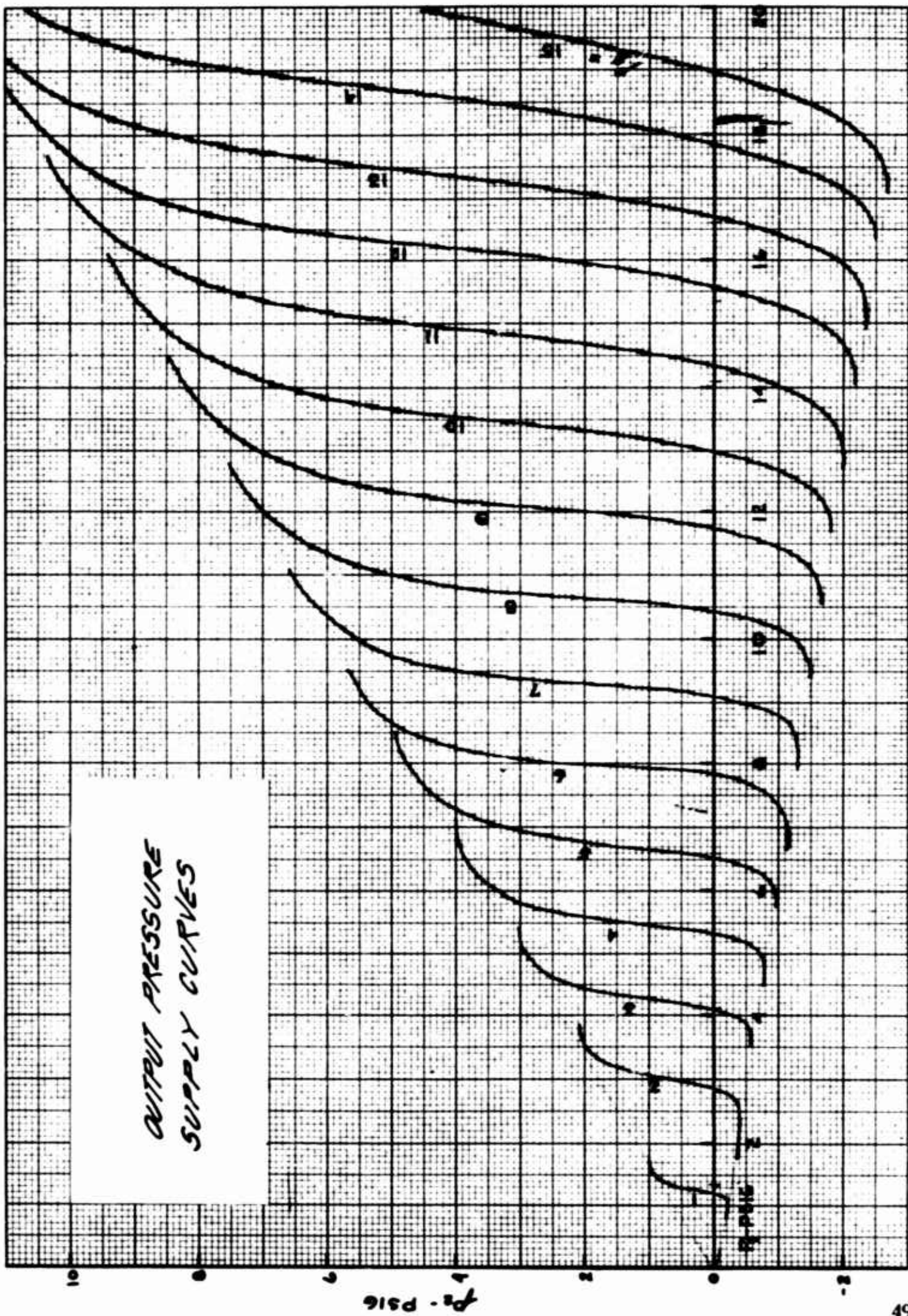


FIG. 3



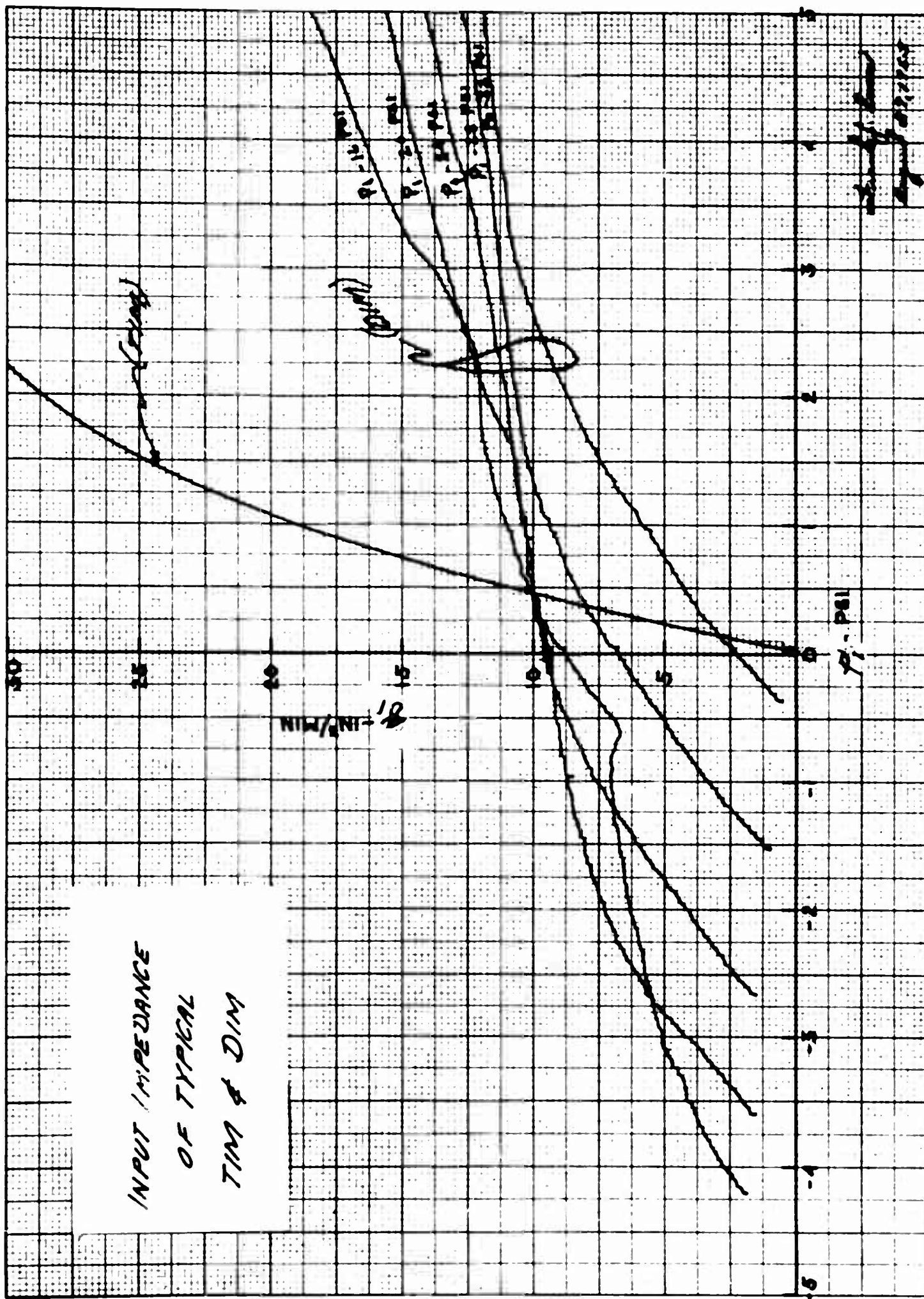


FIG. 4

INPUT IMPEDANCE  
OF TYPICAL  
TIM & DIM



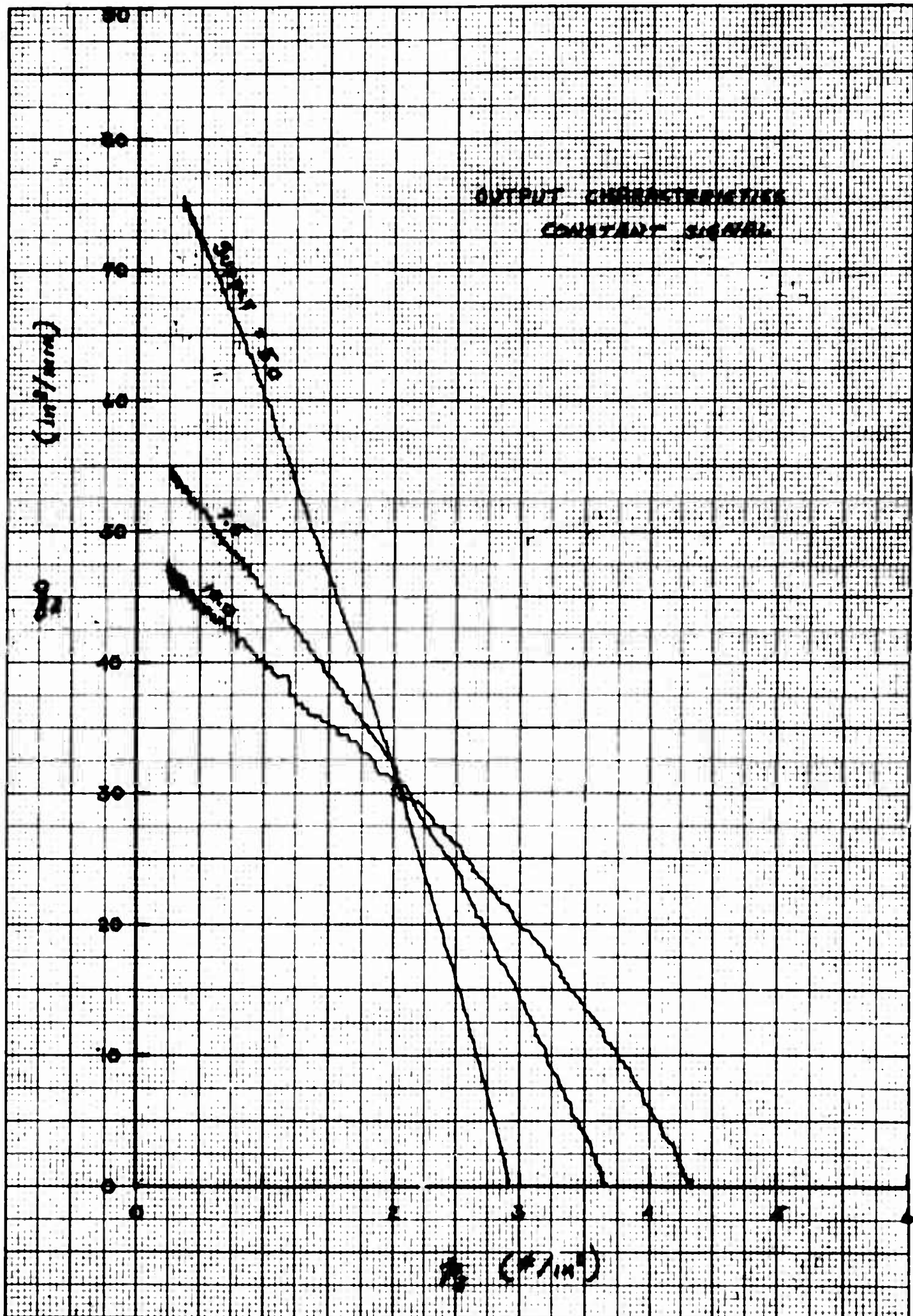


FIG. 5

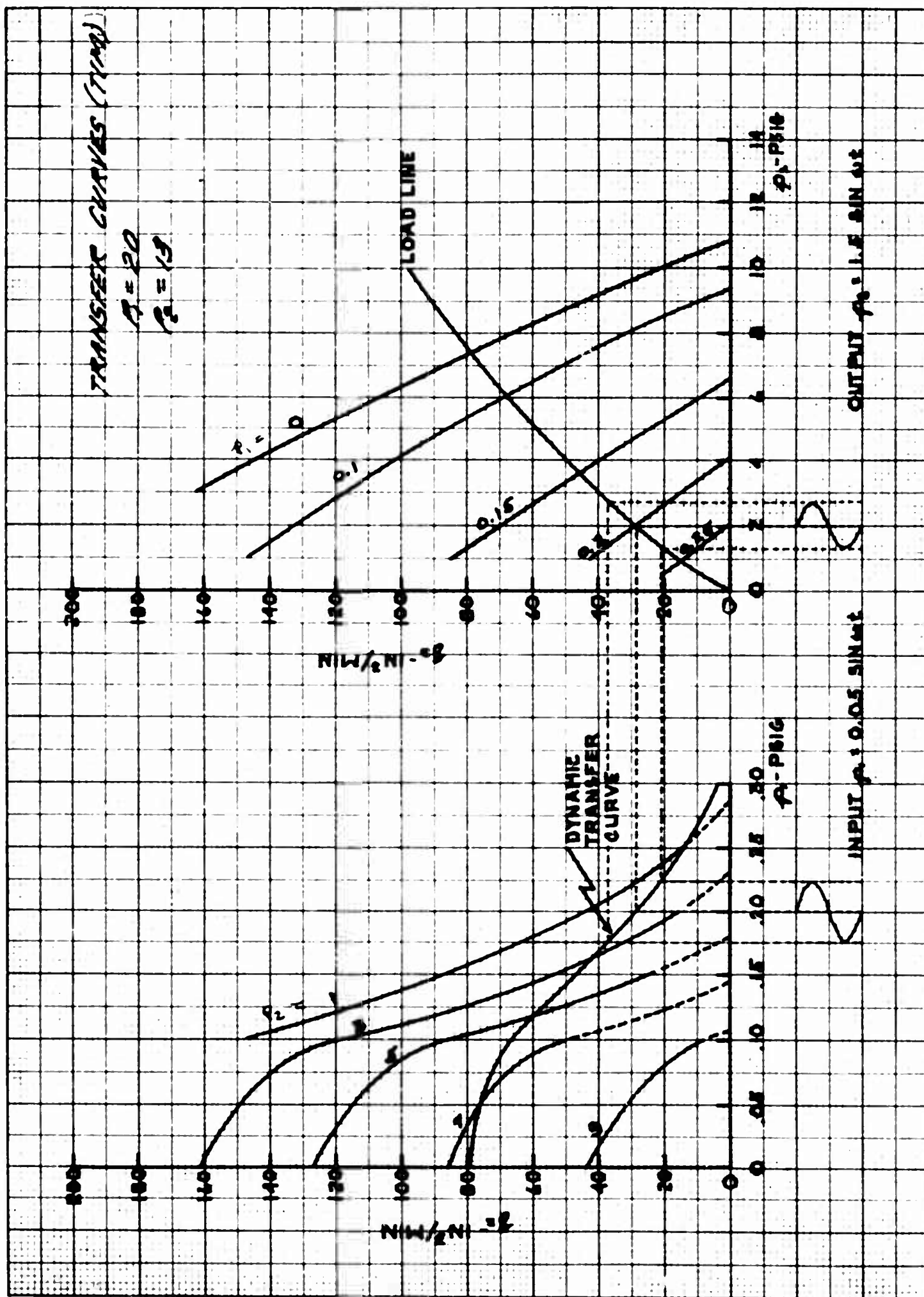


FIG. 6

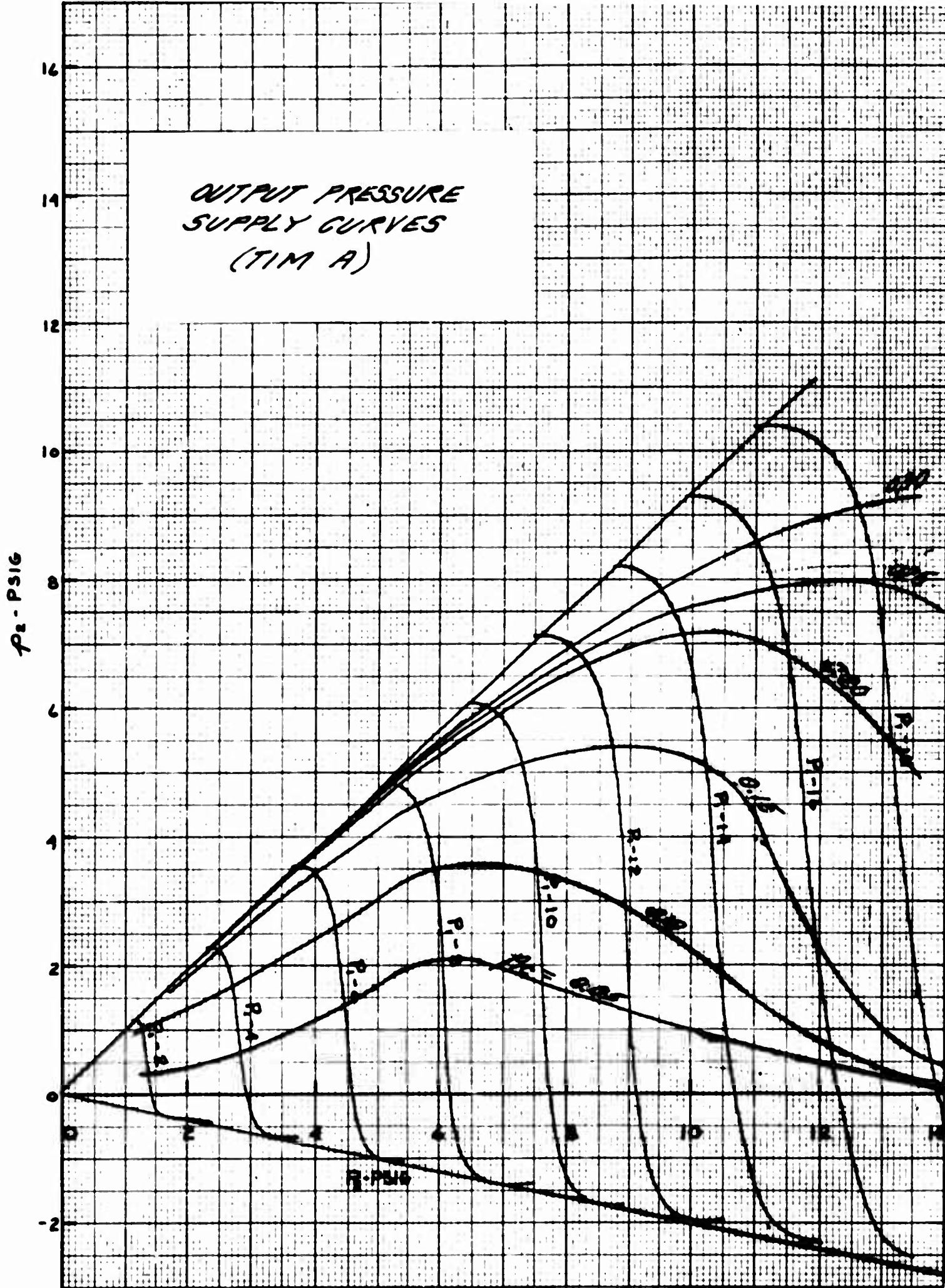


FIG. 7





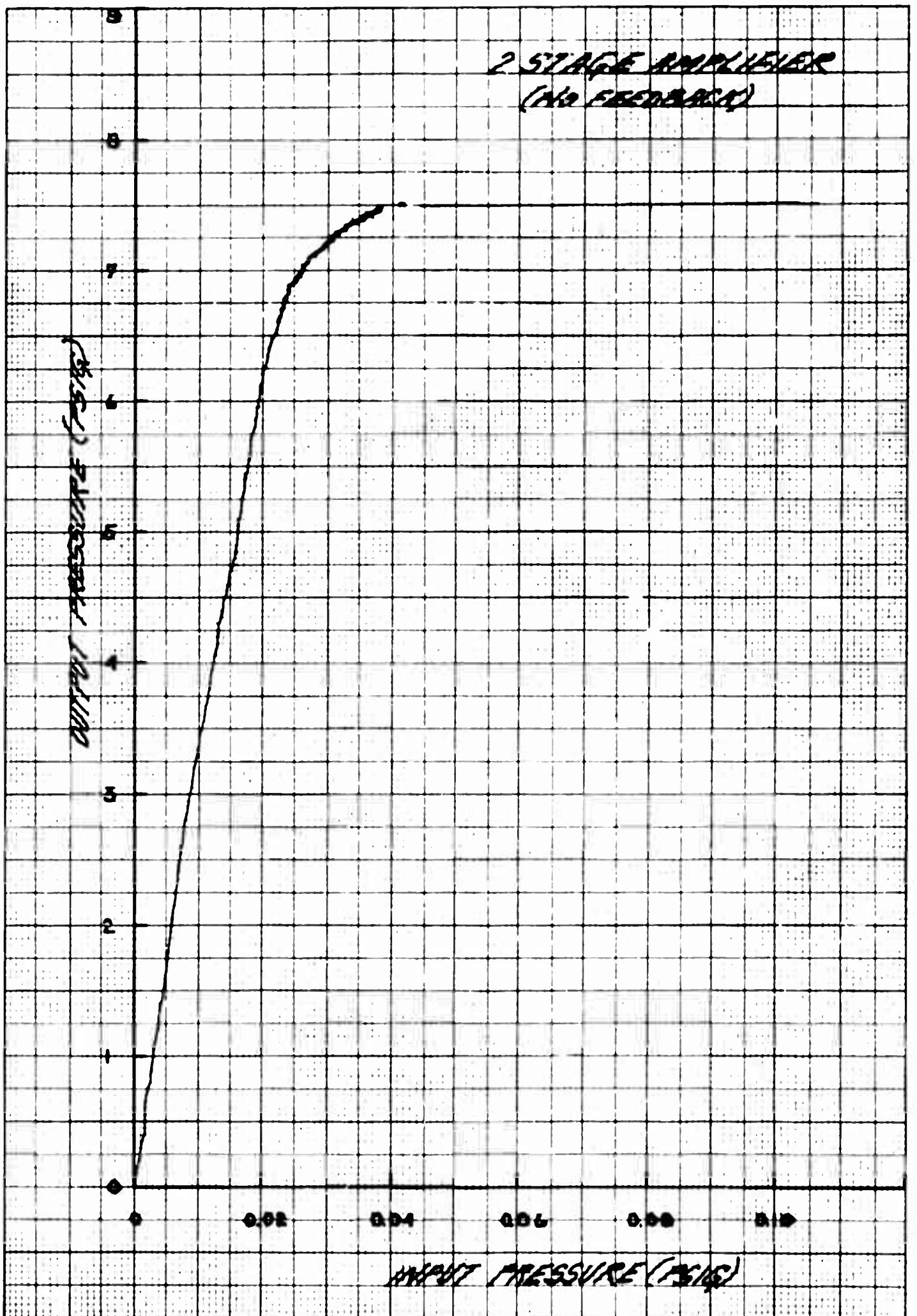


FIG. 9

## OPERATIONAL AMPLIFIER SCHEMATIC

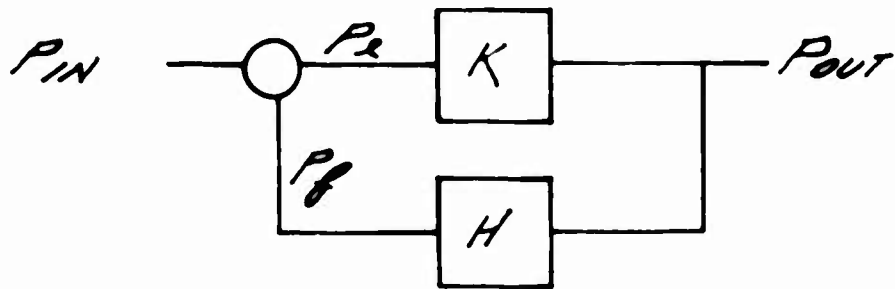


FIG. 10

## THREE TERMINAL MODULATOR (3TM)

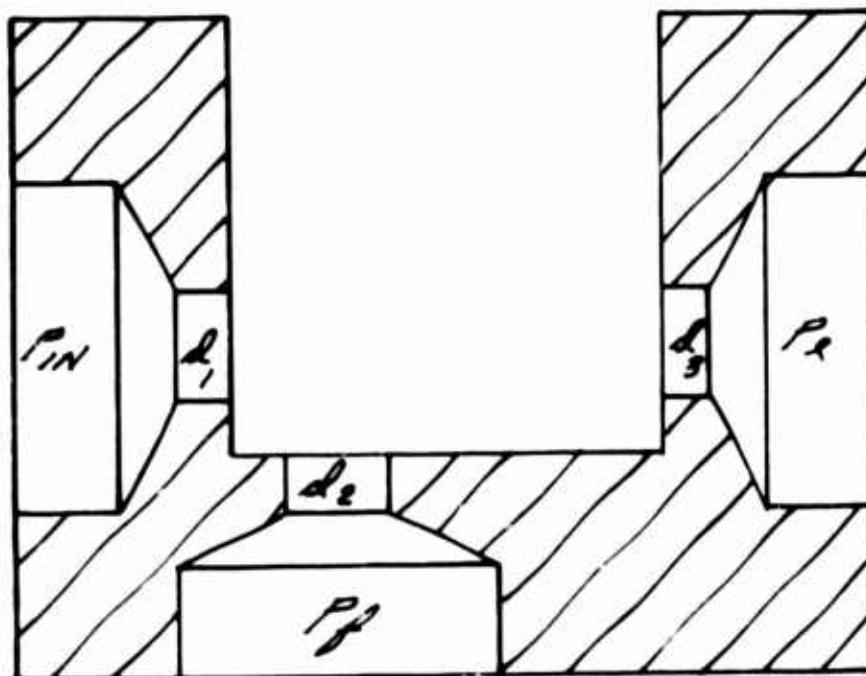


FIG. 11

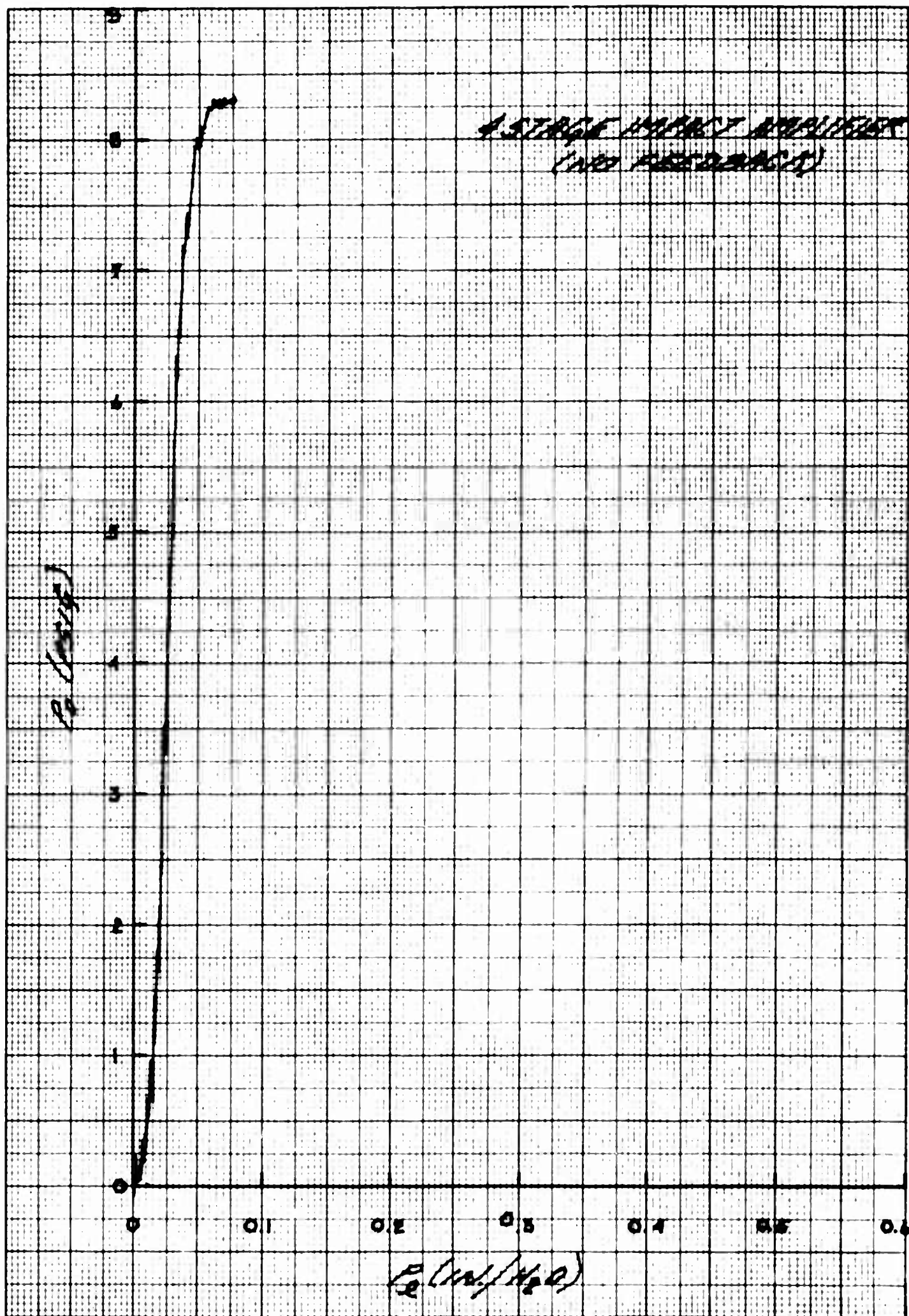


FIG. 12

# 1 STAGE OPERATIONAL AMPLIFIER W/ FEEDBACK





# OPERATIONAL AMPLIFIER OUTPUT CHARACTERISTICS

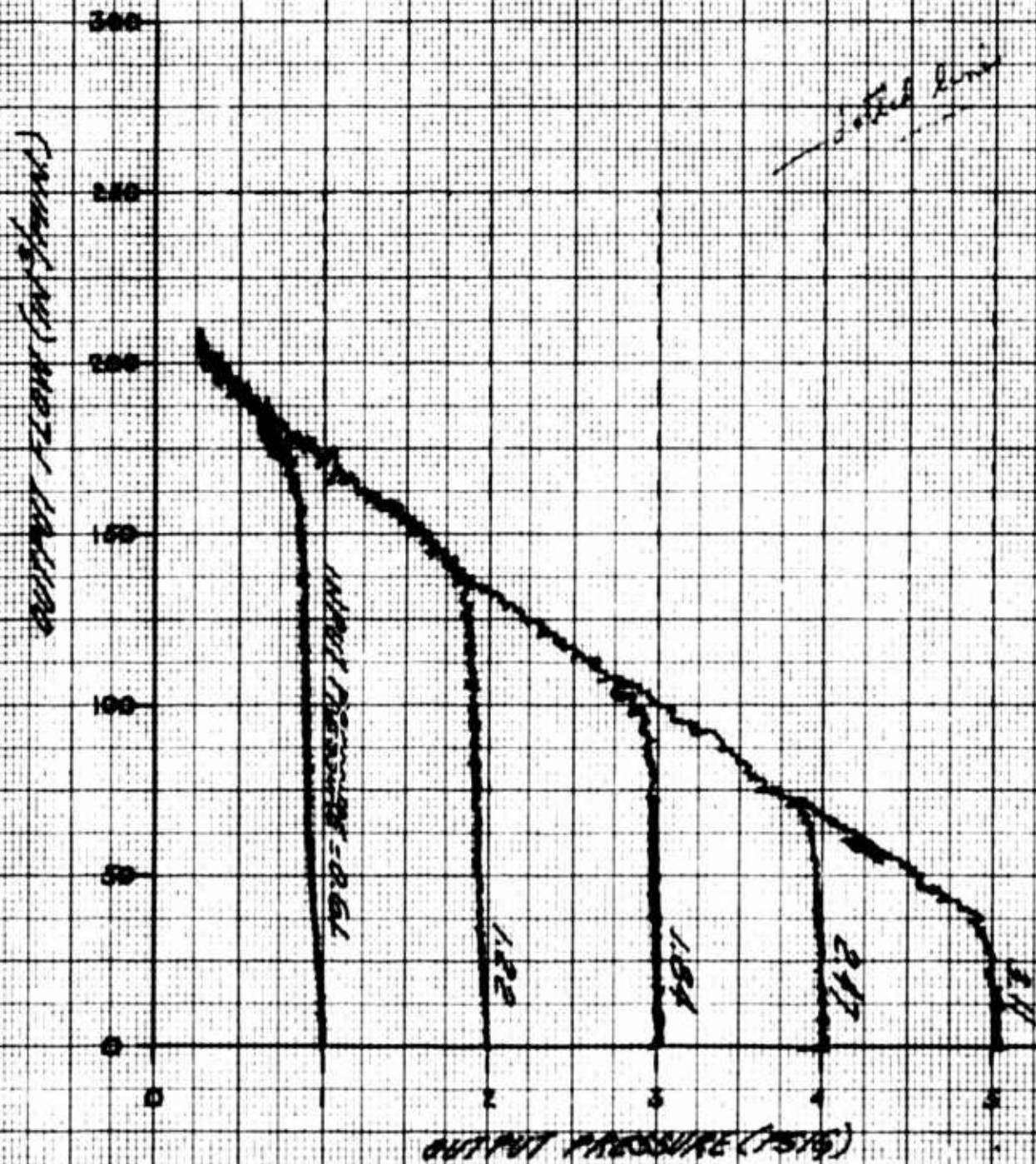


FIG. 14

# CONTROL CHARACTERISTICS OF VORTEX VALVES

Endre A. Mayer \*

Paul Maker \*

## INTRODUCTION

*A plane vortex has two velocity components, a radial component and a tangential component. The interaction between these components may be used to accomplish a valving function, using no moving mechanical elements other than the fluid flows. This feature makes the vortex valve a desirable control element in the output stages of fluid power systems.*

The basic operating mechanism of the vortex, the three-dimensional flow field, defies rigorous analysis. Since the work on energy separation by Ranque in 1931, a number of analytical approaches have been proposed.

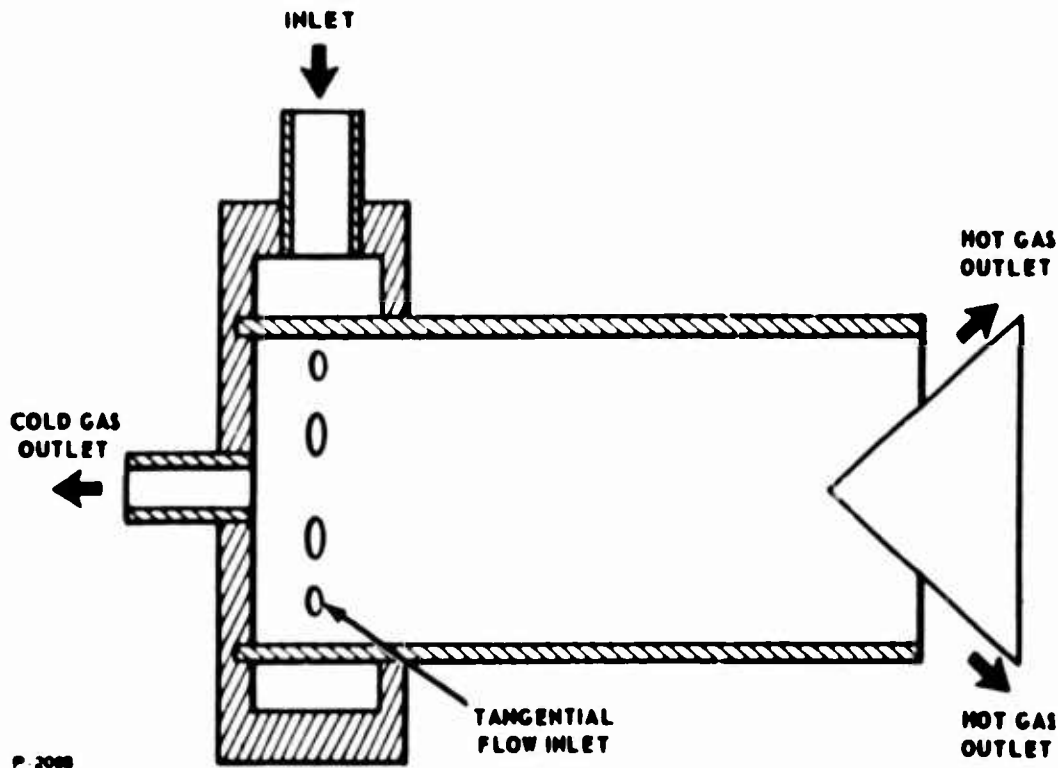


FIGURE 1 - RANQUE-HILSCH TUBE-SCHEMATIC REPRESENTATION

\*Staff Engineer, Energy Conversion and Dynamic Controls Laboratory,  
Bendix Research Laboratories, Southfield, Michigan

The scope of vortex investigations, both analytical and experimental has become very broad since the rediscovery and extension of Ranque's work by Hilsch in 1946, leading to the development of the Ranque-Hilsch tube.

The Ranque-Hilsch tube has remained a challenging analytical problem to the fluid dynamicist over the years. This device is described here only briefly, because a large number of publications on analytical and experimental investigations serve as a foundation for the present, simplified approach to vortex valve design. Figure 1 is a schematic of a counterflow Ranque-Hilsch tube. Air, or any compressible gas, enters the tube through tangential inlet nozzles at near Mach 1 velocity. The swirling flow travels down the tube at a considerably lower axial velocity and discharges through an annular orifice in one end of the tube. In the vicinity of the axis of the tube a counterflow takes place and discharges through a centrally located orifice near the inlet end. The gas passing through the center nozzle is at a lower total temperature than the inlet gas, while the gas discharging through the annulus at the far end of the tube is at a higher total temperature than the inlet gas.

A comprehensive bibliography by Westley (1) summarizes the Ranque-Hilsch tube research. At first the device seemed to be an extremely simple and attractive means of refrigeration, however the relative inefficiency of the device, when compared to a mechanical refrigerator has limited practical applications of the Ranque-Hilsch tube. In spite of the limited application, the Ranque-Hilsch tube has served to spark a large area of interest in vortex investigations, both analytical and experimental. The present paper describes a simple analytical approach to a vortex valve operating with a compressible gas.

### Vortex Valve Analysis

The vortex valve is an "all-fluid" control element having no mechanical moving parts. The flow control is produced by interaction between two fluid flows. The schematic of a typical vortex valve is shown in Figure 2. The main supply flow enters the plenum behind the mixing region at negligible velocity. The flow passes through a mixing zone in an annular sheet into the main vortex chamber. In the absence of control flow, the main flow proceeds radially inward toward the central outlet of the vortex chamber. In this condition the maximum flow passes through the valve.

The tangential control flow imparts a rotational component to the main supply flow, and the combined flows pass into the vortex chamber

with both tangential and radial components. The angular momentum may be written as:

$$\vec{M} = m r U$$

or:

$$\vec{M} = m r^2 \omega$$

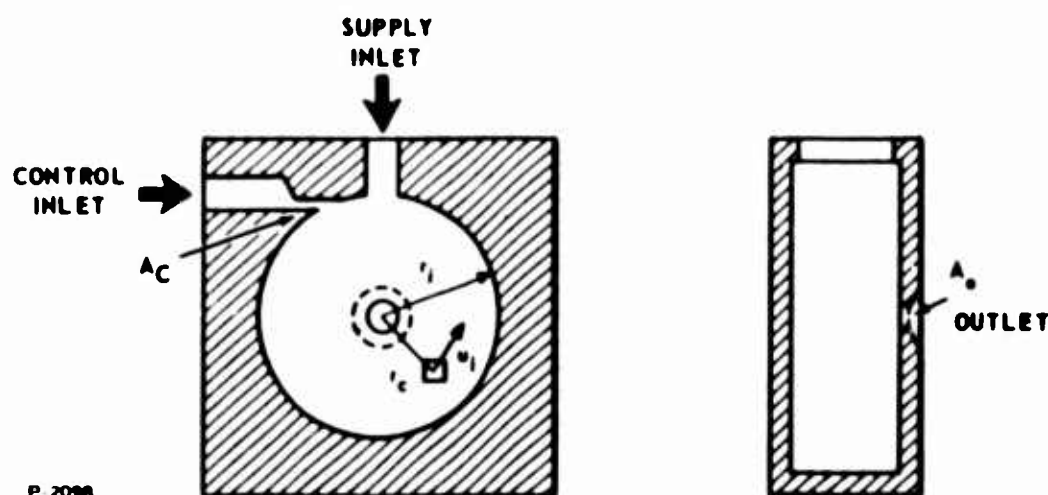


FIGURE 2 - VORTEX VALVE-SCHEMATIC REPRESENTATION

and conservation of momentum requires that the tangential velocity  $U$ , and the angular velocity  $\omega$ , both increase as the flow moves inward, with decreasing  $r$ . The velocity changes cause shear stresses in the rotating fluid mass, tending to accelerate the outer layers and slow the inner layers. This coupling amounts to a feedback, with the net effect of further increasing the average angular velocity. The energy increment involved is supplied by the pressure drop in the fluid as it moves inward against the centrifugal field.

Near the outlet port the two-dimensional vortex field begins to change to a three-dimensional vortex due to the "sink" flow from the exit opening. The maximum velocities, both tangential and angular, occur near the center of the vortex chamber slightly inside the radius of the exit hole. At smaller radii in the exit jet, shear forces bring the fluid jet practically to a "wheel" rotation, of constant angular velocity.

A comprehensive, general analytical approach to the solution of the three-dimensional vortex flow of a viscous, compressible flow is considered impractical. The assumptions by the authors of previous papers on vortex phenomena made the results specific to the particular

applications concerned, and there has been no generally valid mathematical basis developed for the descriptions of these phenomena. These assumptions have, in general, defined the velocity field within the vortex by indirect means. The large changes in tangential velocity occurring in a vortex chamber, operating from zero to maximum rotational velocity in a vortex valve, may require continuous adjustments of the assumed coefficients.

In flow control applications of a vortex valve, knowledge of the relationship between control pressure and total weight flow is desired. The following analysis is directed toward a simple approach for predicting valve performance with viscous compressible fluids over a large range of physical variables, such as vortex chamber diameter, length, chamber diameter to outlet orifice ratio, ambient pressure, and supply and control gas pressures and temperatures.

The basic assumption of the analysis is that of the tangential velocity distribution itself. With an assumed velocity distribution, pressure losses in the chamber may be calculated with relative ease. In addition, the pressure distribution across the outlet port may be calculated, thus the total flow through the vortex valve may be computed.

The following three basic rotational velocity fields may be encountered in a vortex valve:

The solid body rotation or forced vortex flow may occur under high viscous coupling. At extreme velocities the apparent viscosity becomes very large: values of the order of a thousand times the normal viscosity have been estimated in experimental reports on the Ranque-Hilsch tube. At such high viscous coupling the velocity field resembles solid body rotation. In solid body rotation the angular velocity remains constant at any point, and the tangential velocity is a direct function of the radius.

$$\omega_i = \omega_1 \quad (1)$$

$$U_i = U_1 \frac{r_i}{r_1} \quad (2)$$

Free vortex rotation is defined by constant angular momentum. This mode is approached in bodies of gases rotating at comparatively low velocities when the effective viscosity becomes negligible.

$$\omega_i = \omega_1 \left( \frac{r_1}{r_i} \right)^2 \quad (3)$$

$$U_i = U_1 \frac{r_1}{r_i} \quad (4)$$

Constant tangential velocity is a unique intermediate velocity distribution between the free vortex and forced vortex rotation. The tangential velocity is constant at any point in the vortex chamber and the rotational velocity is an inverse function of the radius.

$$\omega_i = \omega_1 \frac{r_1}{r_i} \quad (5)$$

$$U_i = U_1 \quad (6)$$

Equations (1) to (6) indicate that the velocity profiles may be described for all conditions by exponential equations:

$$\omega_i = \omega_1 \left( \frac{r_1}{r_i} \right)^n \quad (7)$$

$$U_i = U_1 \left( \frac{r_1}{r_i} \right)^{n-1} \quad (8)$$

The particular velocity distributions given may now be defined by particular values of the exponent (n) where:

n = 0 for a free vortex velocity distribution

n = 1 for constant tangential velocity

n = 2 for a forced vortex velocity distribution

Only a relatively small amount of experimental data has been published on vortex field velocities. Several investigators have questioned the value of velocity measurements entirely, because even the smallest available velocity probe may upset the local vortex pattern due to eddy formations, thus producing erratic or misleading results.

Figure 3 compares the three velocity distribution patterns with a typical experimental curve given by Lay (22) in a report on a Ranque-Hilsch tube investigation. The distribution of the velocity data lies between constant tangential and the theoretical forced vortex velocity; perhaps closer to the constant tangential velocity distribution. At lower tangential velocities ( $M_t \sim 0.05$ ) Yeh (21) found that the velocity distribution very closely approached that of a free vortex velocity distribution. Using the typical observed data, the tangential velocity distribution was defined arbitrarily for the present analysis.

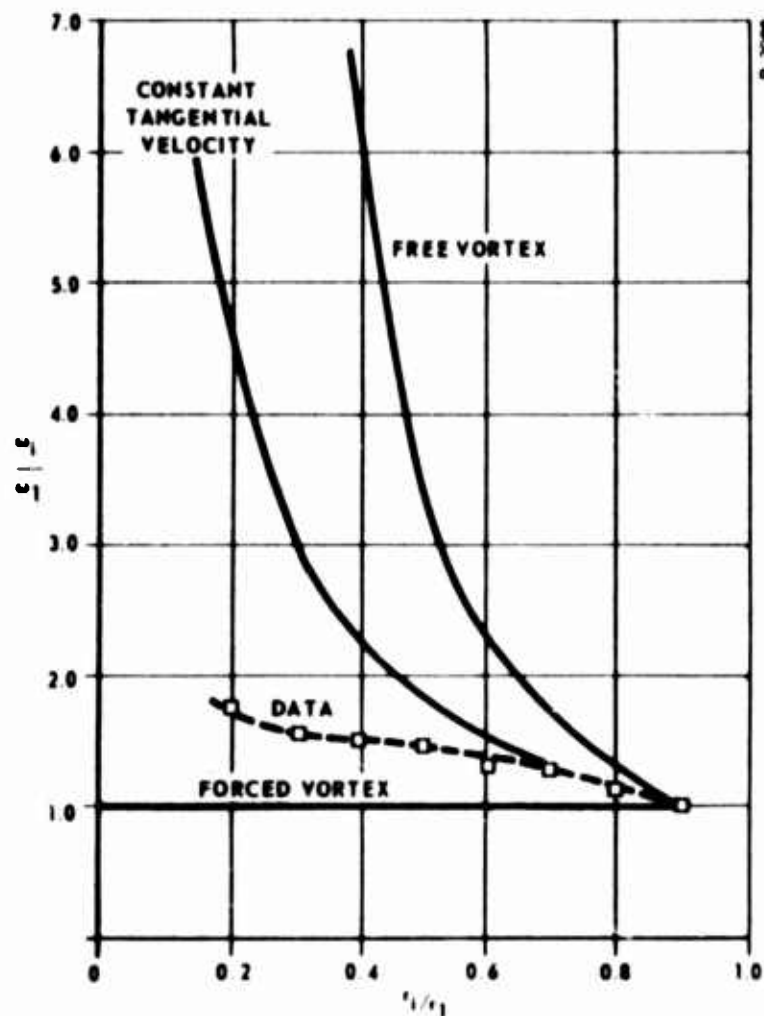


FIGURE 3 – THEORETICAL AND EXPERIMENTAL VORTEX VELOCITY DISTRIBUTIONS

The exponent ( $n$ ) in Equations (7) and (8) is a function of both local tangential velocity and location in the vortex chamber. For the present analysis the exponent was defined by a curve composed of five linear segments starting with  $n = 2$  at very low tangential velocities



and finishing at  $n = 1$  for sonic velocity. In order to correlate various tangential velocity curves, the definition is in Mach Number as given in Table I.

Table I

Mach No, $M_t$	1.0	0.5	0.1	0.01	0.001
Exponent, $n$	1.0	1.31	1.5	1.8	2.0

The effect of losses due to boundary layers within the chamber may be included in the computation by modifying the velocity distribution curve. Preliminary estimates indicated that the effects of boundary layer may be reduced by allowing sufficient chamber length. No published experimental data was found on the effects of boundary layer on the vortex chamber velocity distribution. For these reasons the analysis did not include variations in the exponent ( $n$ ) as functions of location or radial position within the vortex chamber.

The starting point for the vortex valve design may be conveniently taken as the operation at zero control flow. The restricting flow area is that at the center hole in this vortex chamber design. The minimum area may be either that of the outlet hole area:

$$A_o = \pi r_o^2 \quad (9)$$

or that of the annulus at the periphery of the hole:

$$A_a = 2 \pi r_o l \quad (10)$$

However, if the chamber length is equal to or greater than the hole diameter, the annular area is at least four times that of the hole, and the resistance of the annulus may be neglected. This is the case with the valve design discussed here.

The flow from the vortex chamber may be calculated by the adiabatic flow formulas. For high supply pressures the flow is sonic:

$$W_{s \max} = C_{d1} A_o P_s \sqrt{\frac{2g}{R_o \tau_s}} \sqrt{\frac{k}{k+1} \left( \frac{2}{k+1} \right)^{\frac{2}{k-1}}} \quad (11)$$



when:

$$\frac{P_e}{P_s} \leq \left( \frac{2}{k+1} \right)^{\frac{k}{k-1}} \quad (= 0.526 \text{ for } k = 1.4) \quad (12)$$

Above this critical pressure ratio the flow becomes subsonic:

$$W_{s \max} = C_{d1} A_o P_s \sqrt{\frac{2g}{R_o T_s}} \sqrt{\frac{k}{k-1} \left( \frac{P_e}{P_s} \right)^{\frac{2}{k}} \left[ 1 - \left( \frac{P_e}{P_s} \right)^{\frac{k-1}{k}} \right]} \quad (13)$$

As long as the flow areas in the vortex chamber and the mixing zone are maintained at least 4 to 8 times the size of the outlet area, the pressure at the outlet orifice annulus will remain at a value very close to that of the supply pressure due to the low pressure losses in the vortex chamber.

The control flow to the valve may be calculated in a similar manner, using the control pressure as the upstream pressure and the supply pressure the downstream pressure at the control port. Below the critical pressure ratio:

$$\frac{P_s}{P_c} \leq \left( \frac{2}{k+1} \right)^{\frac{k}{k-1}} \quad (14)$$

and

$$W_c = C_{d2} A_c P_c \sqrt{\frac{2g}{R_o T_c}} \sqrt{\frac{k}{k+1} \left( \frac{2}{k+1} \right)^{\frac{2}{k-1}}} \quad (15)$$

and above the critical pressure ratio, in the subsonic flow range:

$$W_c = C_{d2} A_c P_c \sqrt{\frac{2g}{R_o T_c}} \sqrt{\frac{k}{k-1} \left( \frac{P_s}{P_c} \right)^{\frac{2}{k}} \left[ 1 - \frac{P_s}{P_c}^{\frac{k-1}{k}} \right]} \quad (16)$$

Assuming complete mixing of supply flow and control flow in the

mixing zone the tangential velocity of the gas entering the vortex chamber may be calculated.

$$U_i = V_c \frac{W_c}{W_o} \quad (17)$$

where:

$$W_o = W_s + W_c \quad (18)$$

The control velocity may be computed using the known upstream conditions in terms of either velocity or Mach number. The only limiting factor is the sonic velocity of the control flow at the critical pressure ratio; thus at the critical pressure ratio and lower pressure ratios, the sonic velocity was used for  $V_c$ . For the subsonic control the adiabatic formula was used for flow velocity.

$$V_c = c M_c = \sqrt{g R_o T_c k} \sqrt{\frac{2}{k-1} \left[ 1 - \left( \frac{P_s}{P_c} \right)^{\frac{k-1}{k}} \right]} \quad (19)$$

For the assumed tangential velocity profile and with known entrance flow conditions, the pressure gradient due to the swirl is given by:

$$dP = \frac{\rho_i U_i^2}{g} \frac{1}{r_i} dr \quad (20)$$

In this equation, both density and velocity are functions of the radial position. A numerical solution of this equation may be readily obtained to any desired degree of accuracy on a digital computer. In the initial hand calculations the equation was solved over the assumed velocity profile using graphic means. The assumed velocity profile (Table I) is shown in Figure 4 as a function of radial location, for tangential velocities between Mach numbers 0.001 and 1.00 at the outer edge of the vortex chamber and radius ratios from 1.00 to 0.001. Figure 4 may be used to find the tangential velocity at any point within the vortex chamber for a given entry condition.

The pressure drop may be solved by simple hand calculation under

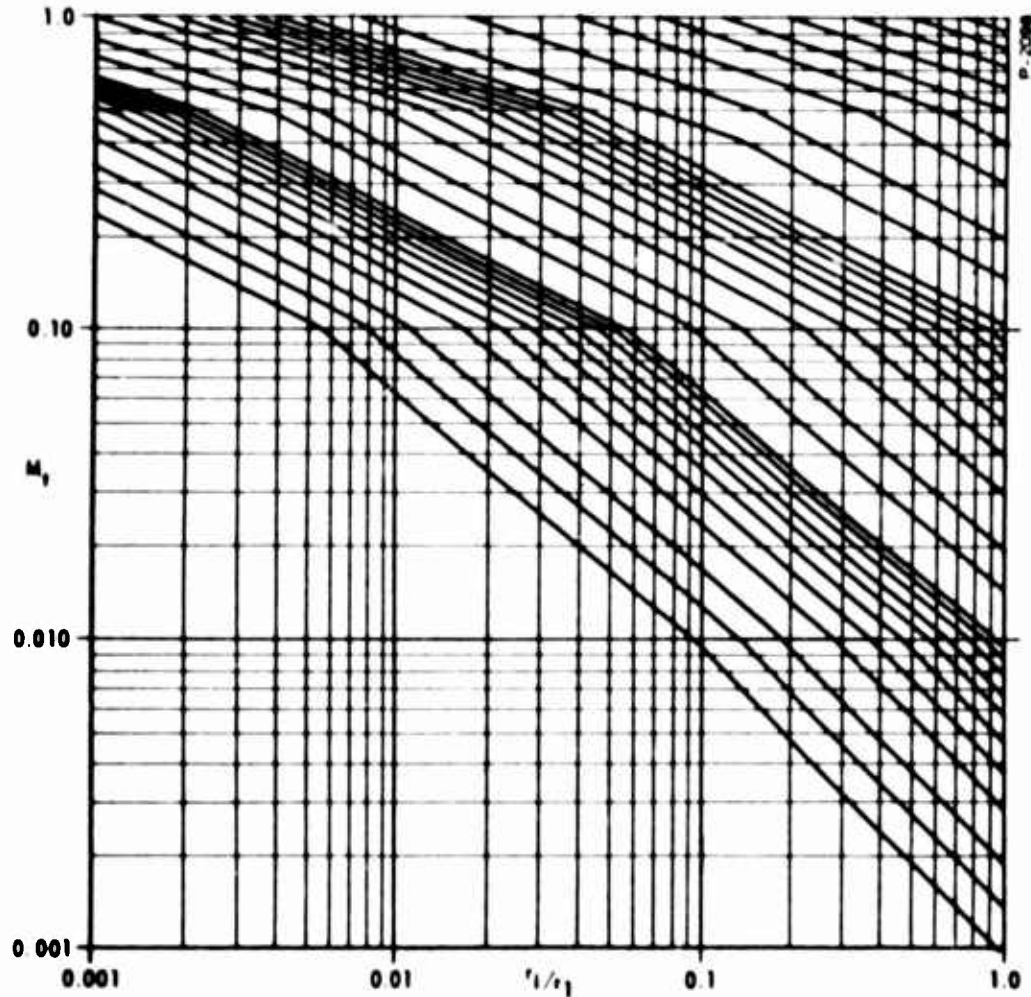


FIGURE 4 – ASSUMED TANGENTIAL VELOCITY DISTRIBUTION

the condition that the absolute pressure is high compared to the pressure loss across the vortex valve, by assuming  $\rho_i$  to be constant:

$$\rho_i \approx \frac{P_s}{R_o T_o} \quad (21)$$

At lower operating pressures, or if the pressure drop in the vortex field is sufficient to affect the density, Equation (20) may be solved by stepwise numerical integration. Using twelve segments the pressure equation was solved in a modified form.

$$dP = \frac{\rho C^2}{g} F(M_{t_1} r) \quad (22)$$

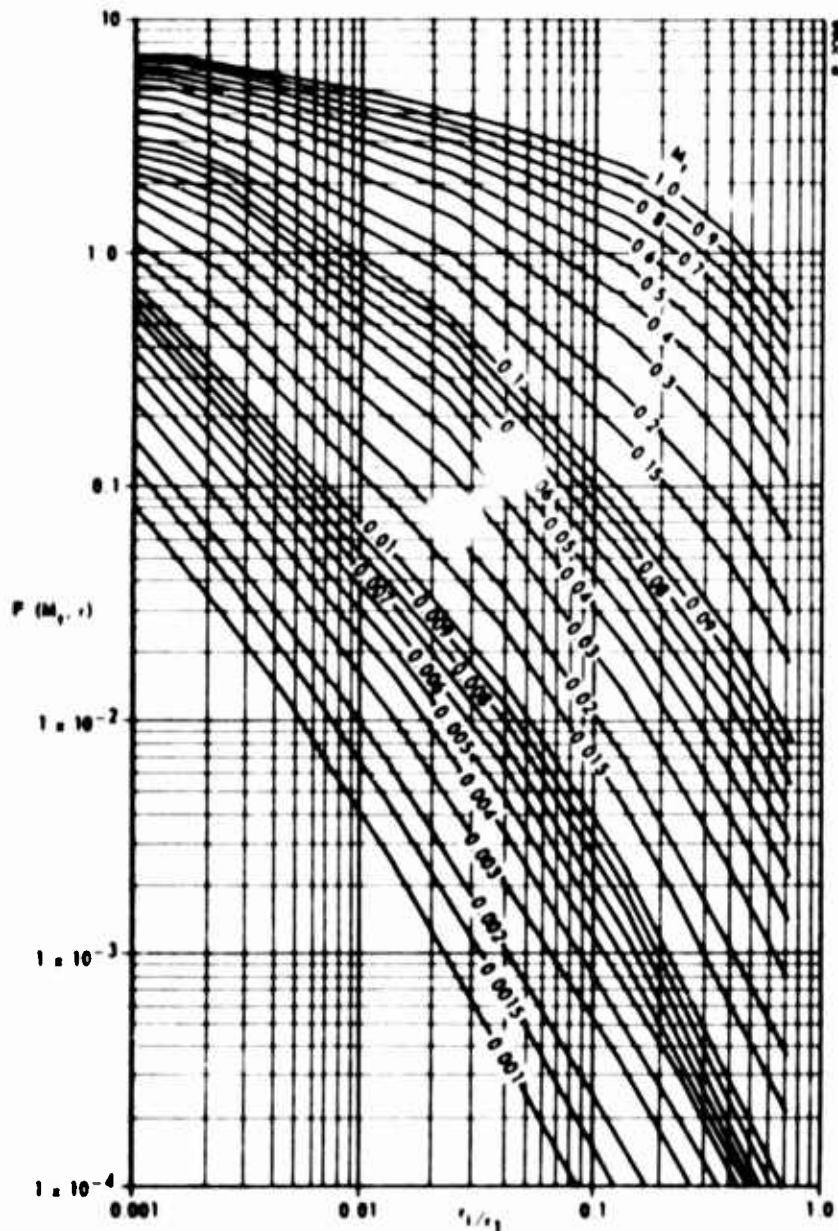


FIGURE 5 — PRESSURE LOSS FUNCTION IN A VORTEX FIELD

The value of  $F(M_{t1}, r)$  was calculated for initial Mach numbers of 0.001, 0.01, 0.1 and 1.0 using 12 linear segments in each case. Figure 5 shows  $F(M_{t1}, r)$  for the range calculated. Using Figure 5, the pressure distribution in the valve may be calculated.

#### Experimental Verification of Vortex Analysis

An experimental program was conducted to verify the analytical performance prediction. The test schematic is shown in Figure 6. Variable area Rotameters were used for flow measurements. The

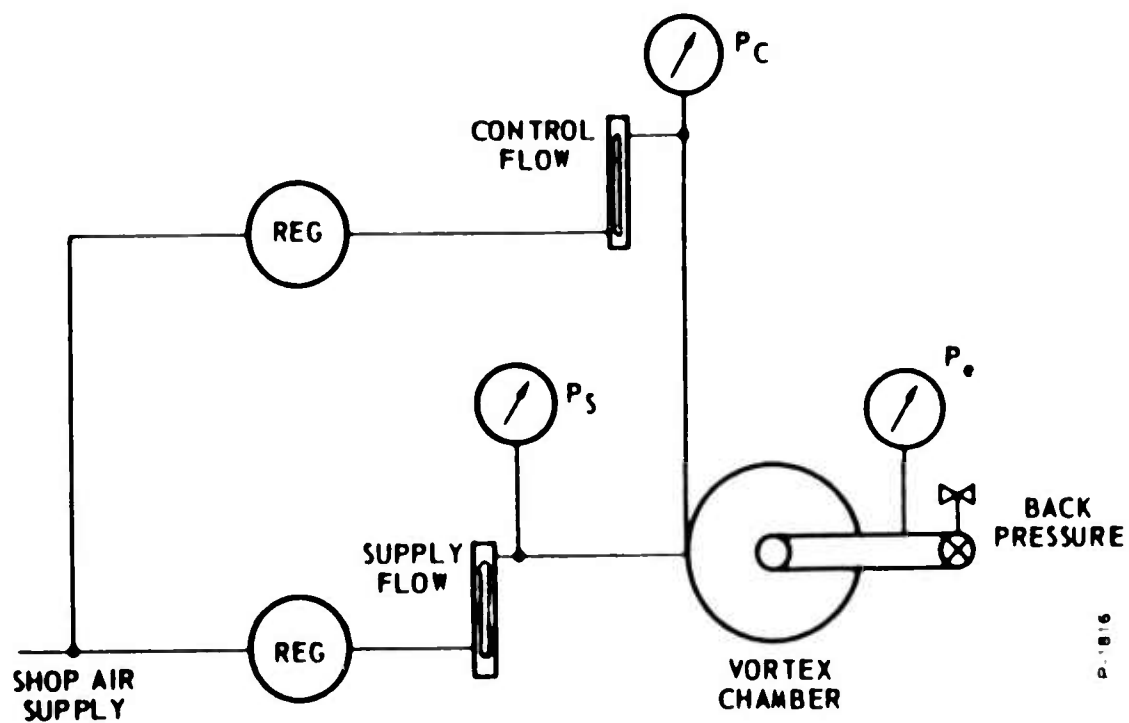


FIGURE 6 – TEST SCHEMATIC

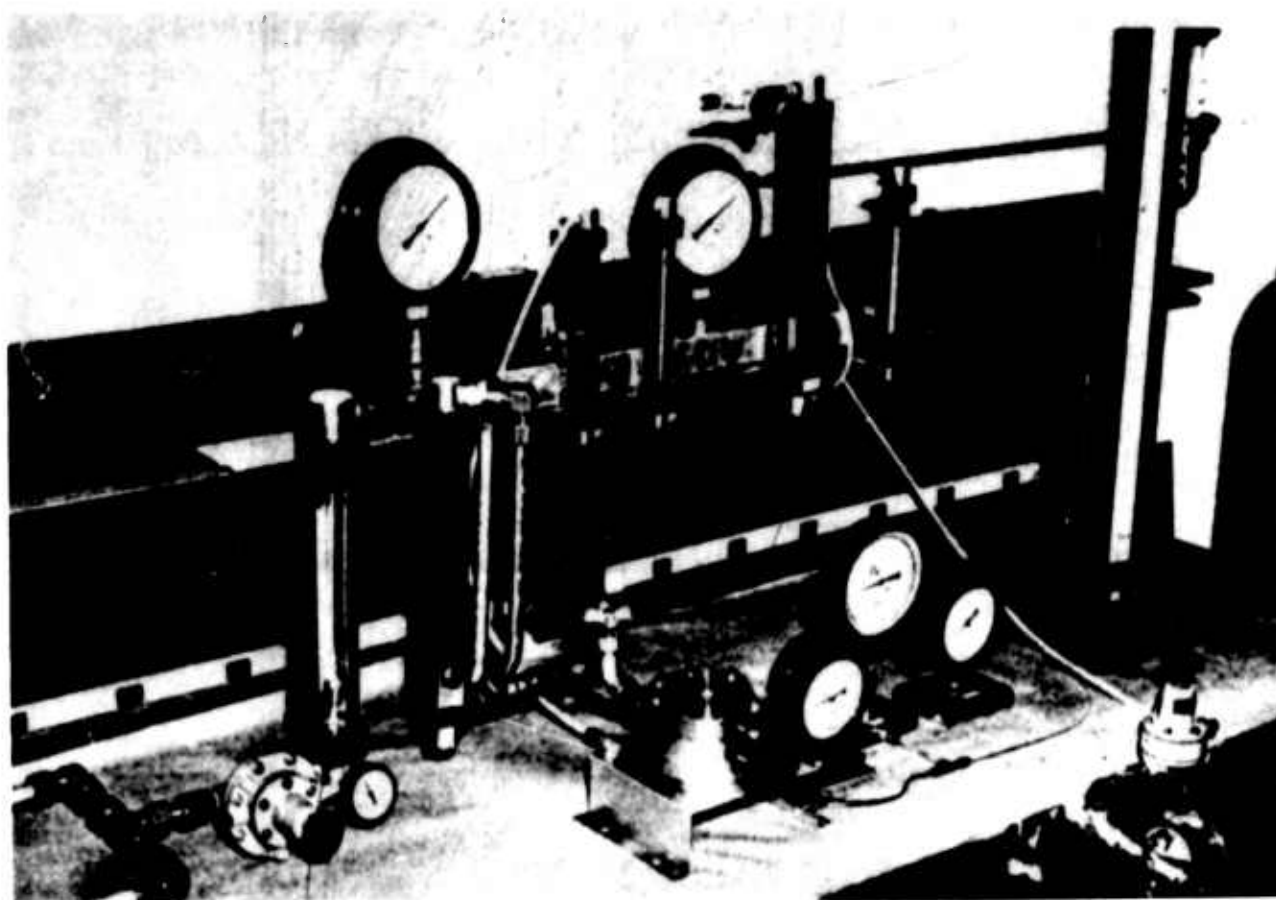


FIGURE 7 – TEST SETUP

verification tests were carried out using shop air at ambient temperature as the fluid.

Figure 7 is the general view of a typical test setup. The vortex valve shown in the center foreground is a model with a 4.00-inch diameter vortex chamber.

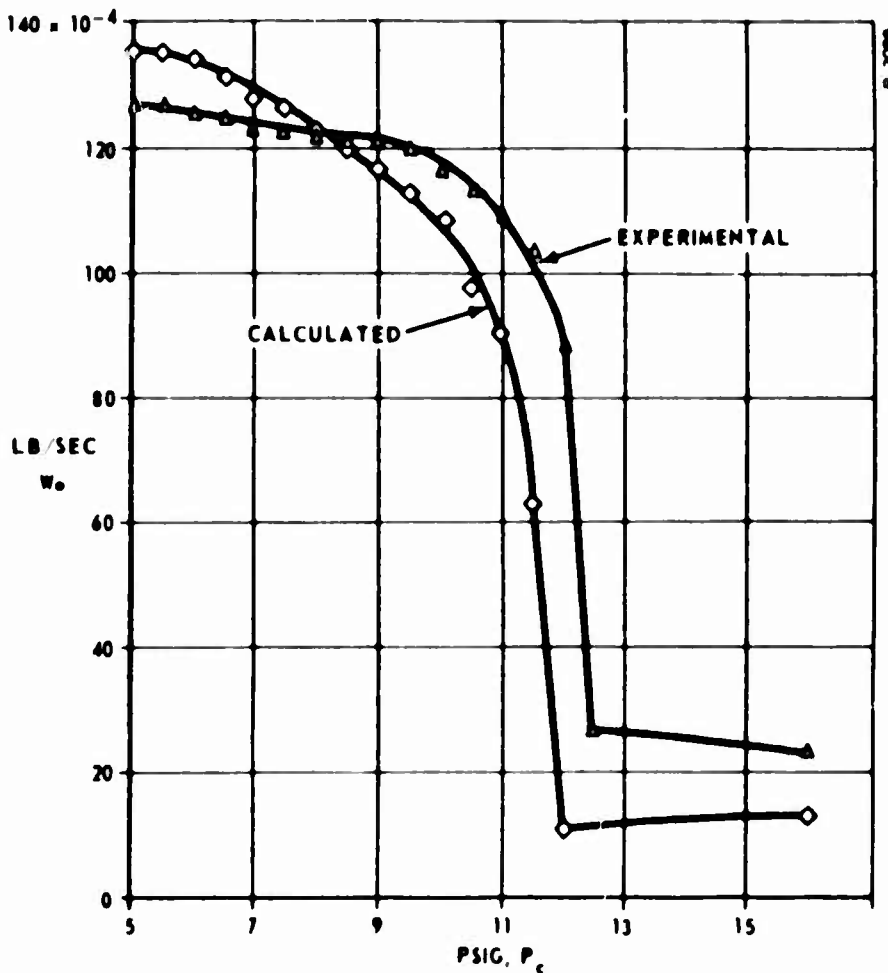


FIGURE 8 – THEORETICAL AND EXPERIMENTAL FLOW CORRELATION

Figure 8 indicates the correlation between calculated and experimental vortex valve performance. The agreement is good both for gain and the location of the cutoff control pressure. The major difference between the calculated values and the experimental data is in the weight flow ratio  $W_o/W_{s \text{ max}}$ . The calculated minimum is 8 percent, but the experimental minimum is 17 percent. The deviation could not be traced to any single source. On the basis of the otherwise good correlation found, no attempt was made to adjust the assumed velocity profiles. The experimental data suggested that the tangential velocity may be

decreasing as the center of the valve is approached and the velocity field approaches solid body rotation, with the resultant reduction of exponent ( $n$ ) to 0 instead of the values shown in Figure 4, the assumed tangential velocity distribution.

Further experimental evaluation of additional vortex valves models indicates that turndown ratios of 6.5:1 between maximum outlet flow and minimum outlet flow are obtainable from vortex valves operating on compressible gases from room temperature to 1400°F supply gas temperatures. Figure 9 shows a vortex valve designed for 2000°F ambient operation and with outlet flow turndown capability of 6.5:1.

The operating characteristic of the high temperature vortex valve is shown in Figure 10. The lower curve indicates operation at 70°F ambient and using nitrogen at the ambient temperature. The upper curve was obtained at 1300°F ambient temperature with the valve operating with 1400°F nitrogen as the control source and 1200°F nitrogen for supply gas. The tests were conducted in a radiant heat furnace. The difference in the performance between the heat exchangers used for heating the control and supply gas accounted for the 200°F temperature difference. The shift in the curve is in the same sense as expected from the analytical calculation due to the temperature difference between the control and the supply gas.

The vortex valve, as any pneumatic control element, is sensitive to loading. Typical load characteristics of a vortex valve and different sizes of downstream orifices is shown in Figure 11. As the outlet area downstream of the valve is decreased using one of four different sizes of throttling orifices, the maximum flow decreases correspondingly. The nearly vertical load lines indicate the natural tendency for a vortex valve to act as a pressure control valve. The load characteristics of vortex valves may be modified to a considerable extent by adjusting chamber length and the geometry in the mixing zone.

The basic vortex valve is primarily a flow control device. Typical incremental flow gain is 200. The flow gain may be varied by changing the size of the control port of the valve. Incremental power gain is approximately 275. The values given for both flow gain and power gain were measured at room temperature using the valve shown in Figure 9.

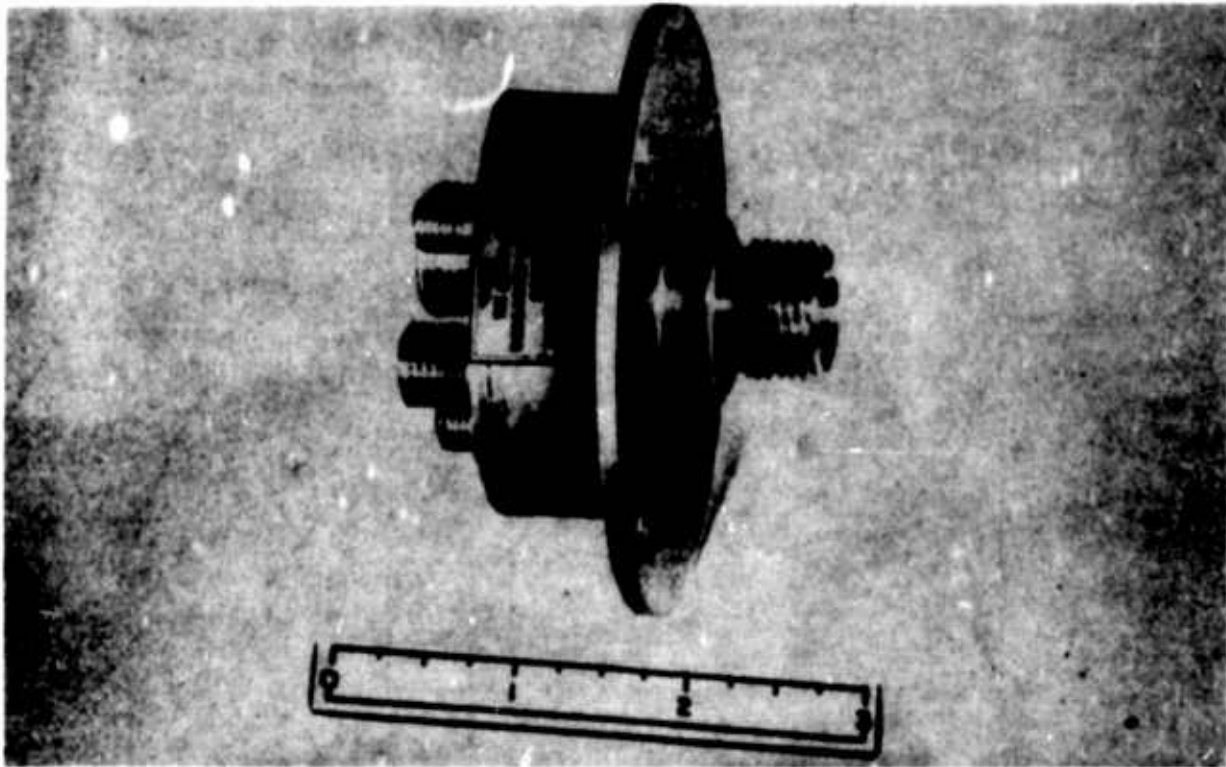


FIGURE 9 – HIGH TEMPERATURE VORTEX VALVE

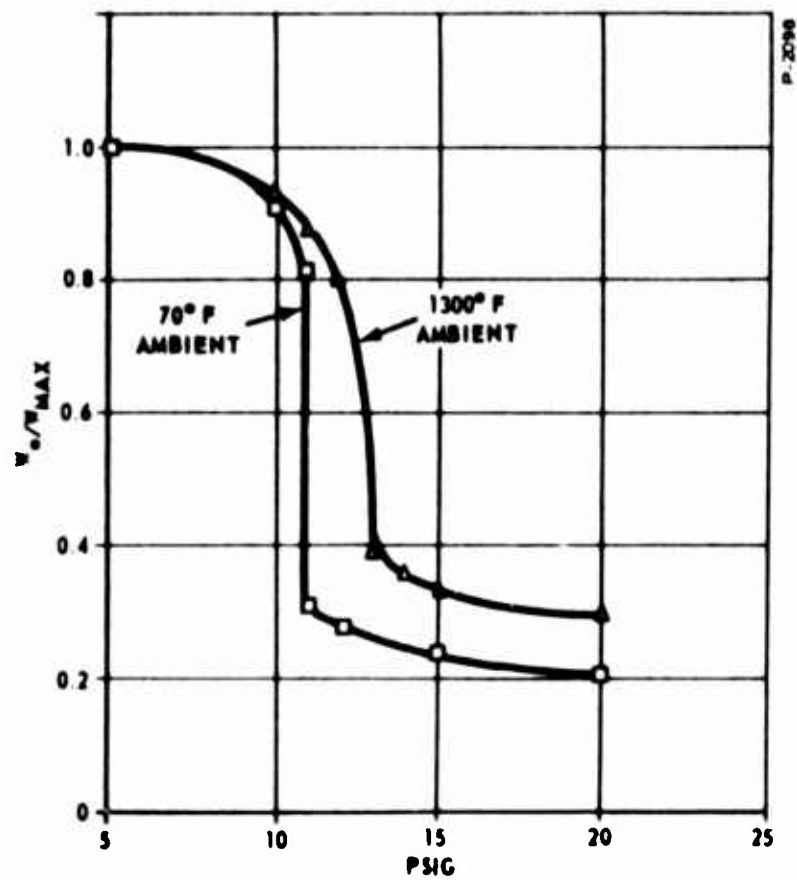


FIGURE 10 – HIGH TEMPERATURE VORTEX VALVE CHARACTERISTICS



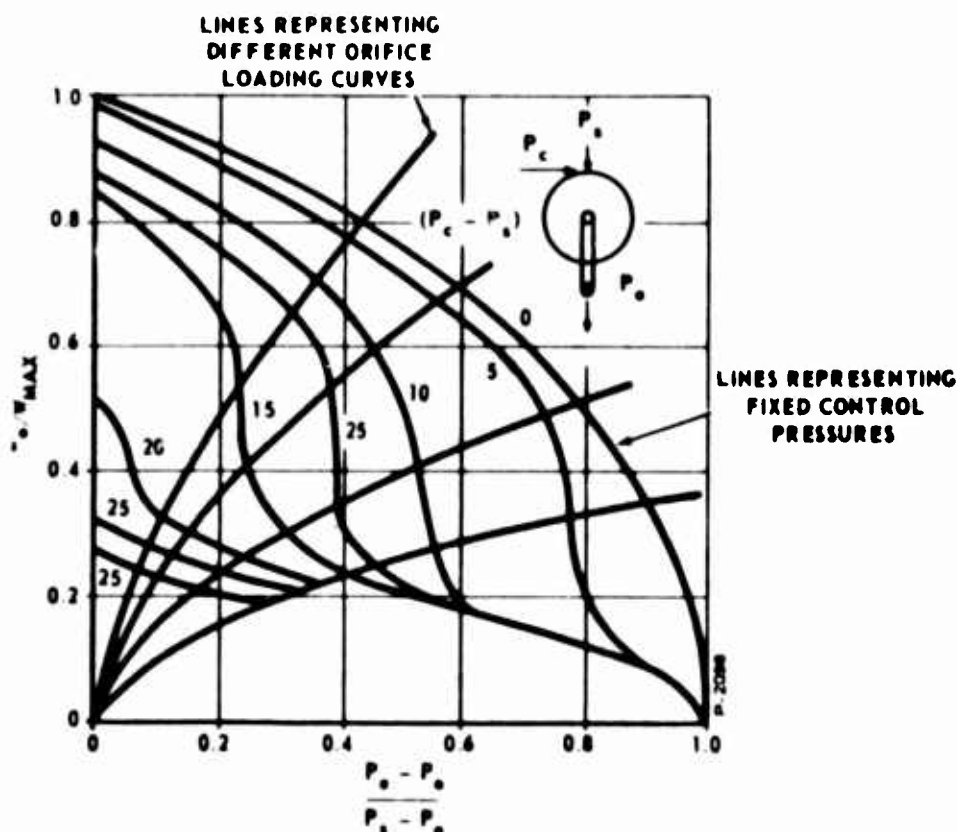


FIGURE 11 – VORTEX VALVE FLOW CHARACTERISTICS

## CONCLUSIONS

An attempt was made to define and develop analytical techniques leading to an engineering capability in the design of vortex valves. These techniques were examined experimentally and were verified to an adequate degree of accuracy. The assumed velocity profile technique lends itself to a direct and relatively simple experimental verification. Hot wire anemometer probes or pitot tube velocity measurements could directly confirm these assumptions. However, the agreement between predicted performance and experimental data for the present work and the relative complexity of both vortex models and instrument probes has discouraged direct velocity profile measurements.

## ACKNOWLEDGEMENTS

This investigation was conducted at the Research Laboratories Division, The Bendix Corporation, under joint sponsorship of the Eclipse-Pioneer Division and the Research Laboratories Division. The investigation was initiated as a follow-on to previous vortex investigations con-

ducted at the Products Division, The Bendix Corporation. The construction of the vortex test models was conducted under the supervision of L. Marion. Mr. R. H. Pospeshil made all primary measurements. Mr. L. B. Taplin, Mr. W. F. Datwyler, and Mr. J. P. Madurski contributed with their helpful suggestions both to the analytical and to the experimental program.

## NOMENCLATURE

<u>Symbol</u>	<u>Description</u>	<u>Unit</u>
$A_a$	Annular flow area at the outlet orifice	in. <sup>2</sup>
$A_c$	Control orifice areas	in. <sup>2</sup>
$A_o$	Outlet orifice areas	in. <sup>2</sup>
$C$	Velocity of sound	in./sec
$C_{d1}$	Outlet orifice contraction coefficient	
$C_{d2}$	Control orifice contraction coefficient	
$g$	Gravitational constant	in./sec <sup>2</sup>
$k$	Ratio of specific heats of gas	
$l$	Vortex chamber length	in.
$\vec{M}$	Local angular momentum	in.lb sec
$M_c$	Control flow Mach number	
$M_t$	Total flow tangential Mach number	
$n$	Velocity distribution exponent	
$P_c$	Control pressure	lb/in. <sup>2</sup>
$P_e$	Exit pressure	lb/in. <sup>2</sup>
$P_s$	Supply pressure	lb/in. <sup>2</sup>
$r_l$	Vortex chamber radius	in.
$r_i$	Radius at location (i)	in.
$r_o$	Radius of outlet orifice	in.

$R_o$	Gas constant	in/°R
$T_c$	Control gas temperature	°R
$T_s$	Supply gas temperature	°R
$U_l$	Tangential velocity at $r_l$	in./sec
$U_i$	Tangential velocity at location (i)	in./sec
$V_c$	Control flow velocity	in./sec
$W_c$	Control gas weight flow	lb/sec
$W_o$	Outlet gas weight flow	lb/sec
$W_s$	Supply gas weight flow	lb/sec
$\rho$	Gas density	lb/in. <sup>3</sup>
$\rho_i$	Gas density at location (i)	lb/in. <sup>3</sup>
$\omega_l$	Rotational velocity at $r_l$	rad/sec
$\omega_i$	Rotational velocity at $r_i$	

## BIBLIOGRAPHY OF VORTEX PUBLICATIONS

The following is a chronological list of vortex related publications.

UP to 1945

1. WESTLEY, R.

A Bibliography and Survey of the Vortex Tube. College of Aeronautics, Cranfield, Note 9, March 1954.

Lists 116 vortex tube publications, giving a brief summary of the contents and also a survey of vortex development between 1931 and 1953. The publications listed by Westley are not included in the following bibliography with exception References 3 and 4.

2. HEIM, R.

An investigation of the Thoma Counterflow Brake. Trans. Hydr. Inst. Munich Tech. U., Bulletin 3, 1929.

3. RANQUE, G. J.  
French Patent applied for 12 December 1931, issued 1932.
4. HILSCH, R.  
The use of the expansion of gases in a centrifugal field as cooling process. The Review of Scientific Inst. Vol. 18, No. 2. February 1947 pp 108-113.
5. BINNIE, A. M. and HOOKER, S. G.  
The Radial and Spiral Flow of a Compressible Fluid. Philosophical Magazine; Vol. 23; pp 597-606.
6. RINGLEB, F.  
Exacte Losungen Der Differential Gleichungen Einer Adiabatischen Gasstromungen  
Abstract in Journal of the Royal Aeronautical Soc.; Vol. 46, 1942; pp 403-404 Translation Ministry of Aircraft Production; Great Britain; R.T.P. Translation; 1609, 1942.
7. GARRICK, I. E. and KAPLAN, C.  
On the Flow of a Compressible Fluid by Hodograph Method. NACA (Tech.) Reference 790, 1944.

1945 to 1955

8. PORITSKY, H.  
Compressible Flows Obtainable from Two Dimensional Flows through the Addition of a Constant Normal Velocity. Journal of Applied Mechanics Vol. 13, Trans. ASME; Vol. 68, 1946; pp A-61-65.
9. EINSTEIN, H. A. and LI, H.  
Steady Vortex in a Real Fluid  
Heat Transfer and Fluid Mechanical Inst., 1951, pp 33-43.
10. SCHULTZ, F. - GRUNOV  
How the Ranque-Hilsch Vortex Tube Operates  
Refrigerating Engineering, Vol. 59, 1951, pp 52-53.
11. BICKLEY, W. G.  
Some Exact Solutions of the Equations of Steady Homentropic Flow of an Inviscid Gas  
Modern Developments in Fluid Dynamics; Vol. 1, Edited by L. Howarth, Clarendon Press, Oxford, England, 1953.

12. SYMPOSIUM

The Vortex Tube as a True Free Air Thermometer

Armour Research Foundation, Chicago, Illinois, May 24, 1955.

13. KREITH, F.

The Influence of Curvature on Heat Transfer to Incompressible Fluids Trans. ASME, Vol. 77, 1955, p 1247-1256.

14. PACKER, L. S. and BOX, N. C.

Vortex Tube Free Air Thermometry  
ASME Paper No. 55-A-22; 1955.

1956 to 1959

15. HARNETT, J. P and ECKERT, E. R. G.

Experimental Study of the Velocity and Temperature Distribution in a High-Velocity Vortex-Type Flow  
Transaction ASME, May 1957.

16. deNEUVILLE, A.

The Dying Vortex  
Proc. 5th Midwestern Conf. Fluid Mechanics  
U. of Mich., 1957.

17. PENGELLEY, C. D.

Flow in a Viscous Vortex  
J. A. P. Vol. 28, No. 1, January 1957.

18. STEVENS, J. C. and KOLF, R. C.

Vortex Flow through Horizontal Orifices  
SAE Paper 1461, December 1957 SA 6; Am. Soc. of Civ. Eng.,  
San Engr. Div.  
Journal 83, 1957, 1461 1 to 22

19. DEISSLER, R. G. and PERLMUTTER, M.

An Analysis of the Energy Separation in Laminar and Turbulent Compressible Vortex Flows  
Heat Transfer and Fluid Mechanics Inst.; 1958, p 40.

20. DREITH, F. and MARGOLIS, D.

Heat Transfer and Friction in Swirling Turbulent Flow  
Heat Transfer and Fluid Mechanics Inst., Stanford U.  
Press 1958.

21. YEH, HSUAN  
Boundary Layer Along Annular Walls in a Swirling Flow  
Transaction, ASME, May 1958.
22. LAY, J. E.  
An Experimental and Analytical Study of Vortex-Flow  
Temperature Separation by Superposition of Spiral and  
Axial Flows  
Part 1, Transaction ASME, August 1959.
23. LAY, J. E.  
An Experimental and Analytical Study of Vortex-Flow  
Temperature Separation by Superposition of Spiral and  
Axial Flow  
Part 2, Transaction ASME, August 1959.
24. SULLIVAN, R. D.  
A Two Cell Vortex Solution of the Navier-Stokes Equation.  
Journal of Aerospace Sciences; Vol. 26, No. 11, November 1959.

1960 to PRESENT

25. DEISLER, R. G. and PERLMUTTER, M.  
Analysis of the Flow and Energy Separation in a Turbulent  
Vortex. International Journal of Heat and Mass Transfer  
1960, Vol. 1, pp 173-91
26. DERGARABEDIAN, P.  
The Behavior of Vortex Motion in an Emptying Container  
Proc. of 1960 Heat Transfer and Fluid Mech. Inst.; pp 47-62;  
Stanford U.
27. DONALDSON, C. D. and Sullivan, R. D.  
Behavior of Solutions of the Navier-Stokes Equation for a  
Complete Class of Three Dimensional Viscous Vortices;  
Proc. of 1960 Heat Transfer and Fluid Mech. Inst.,  
Stanford U., pp 16-31
28. KEYES, J. J.  
An Experimental Study of Gas Dynamics in High Velocity  
Vortex Flow  
Proc. of 1960 Heat Transfer and Fluid Mech. Inst.,  
Stanford U., pp 31-47.

29. MACK, L. M.  
The Compressible Viscous Heat-Conducting Vortex  
Journal of Fluid Mechanics, Vol. 8, Part 2, 1960.
30. DEXTER, E. M.  
Vortex Valve Development  
April 17, 1961 (ASME presentation)
31. HOLMAN, J. P. and MOORE, G. D.  
An Experimental Study of Vortex Chamber Flow.  
Transaction, ASME, December 1961.
32. KERREBROCK, J. L. and MEGHREBLIAN, R. V.  
Vortex Containment for the Gaseous-Fission Rocket.  
Journal of the Aerospace Sciences; Vol. 28, 1961, p 710-724.
33. NISSAN, A. H. and BRESAN, V. P.  
Swirling Flow in Cylinders  
AICHE Journal Vol. 7, No. 4, 1961.
34. PRENTICE, J. J.  
Velocity Distribution in Vortex Flow Between Concentric  
Cylinders.  
Thesis-MS-Air U., Wright Patterson; 1961.
35. ROSENZWEIG, M. L.  
Velocity Recovery and Shear Reduction in Jet Driven Vortex  
Tubes  
AFBMD, Report TDR-594(1203-01)TN-1 1961.
36. SAVINO, J. M. and RAGSDALE, R. G.  
Some Temperature and Pressure Measurements in Confined  
Vortex Fields  
Journal of Heat Transfer, ASME Vol. 83 Series C No. 1, p 33-38.
37. DONALDSON, C. D. and Snedeker, R.S.  
Experimental Investigation of the Structure of Vortices in  
Simple Cylindrical Vortex Chambers.  
AD-296-874, December 1962.
38. GREENBERG, R. A.  
Nonequilibrium Vortex Flow in a Dissociating Gas  
Journal of Aerospace Sciences, Vol. 29, p 1483, 1962.
39. STAHLER, A. F.  
The Free-Surface Water Table Analog of Compressible



Source-Vortex Flow

Journal of Aerospace Sciences; Vol. 29, p 998, 1962.

40. WANG, K. C.

Vortex Flow in a Dissociating Gas

Journal of Aerospace Sciences, Vol. 29, p 623, 1962.

41. CHANAUD, R. C.

Experiments Concerning the Vortex Whistle

Journal of the Acoustical Society

July, 1963 p 253.

42. BLATT, T. A. and TRUSCH, R. B.

An Experimental Investigation of an Improved Vortex Cooling  
Device

ASME paper No. 62-WA-200, 1963.

# EXPERIMENTAL STUDY OF A PROPORTIONAL VORTEX FLUID AMPLIFIER

by

Ben A. Otsap

of

The Marquardt Corporation

## Abstract

An experimental investigation was conducted on a vortex-controlled proportional fluid amplifier exhibiting unique characteristics of high pressure gain of 200, high pressure recovery, fast response and high signal-to-noise ratio. The performance characteristics were investigated, analyzed and are presented in terms of nondimensional quantities and nondimensional design parameters. The adaptation of the high pressure gain of a fluid amplifier to network application is presented. An approach to staging and circuit application is presented with suggested notation and schematization. Performance comparison to "pressure controlled" and "momentum controlled" fluid amplifiers are presented utilizing nondimensional parameters.

## Introduction

The present state-of-the-art of fluid amplification without moving parts reached a status where system application could be considered and conceived utilizing existing elements developed by Harry Diamond Laboratory, Massachusetts Institute of Technology, and others. Here at Marquardt, emphasis is placed on the adaptation of fluid amplification concepts to actual systems application utilizing "non-moving parts" fluid amplifiers.

Mechanization of these systems and optimization of their performances resulted in the need for special purpose units with particular performance characteristics suitable to the system requirements. It was therefore necessary to modify existing units to meet circuit requirements or conceive new types of elements with the required characteristics.

Investigating the adaptation of "pure fluid" concept to ramjet control systems created the need for a single ended\* "non-moving part" proportional fluid amplifier exhibiting high pressure gain characteristics (over 100), high pressure recovery at high output impedance (blocked load) and capabilities of operation with pressure ratios (supply to ambient) up to 6.0. Typical application is the inlet control system of ramjet with high impedance actuator as the output load. The vortex fluid amplifier presented in this paper was conceived and designed to meet these specific requirements.

Formulating a mathematical model describing the operation of the vortex amplifier requires the solution of the "Navier-Stokes" equation for three-dimensional flow. In light of the complex nature of the flow, the design does not lend itself to analysis, and emphasis has been placed on experimental evaluation of performance of this unit, allowing for utilization of data obtained in deriving mathematical expressions. This paper is limited to the experimental investigation described below.

The paper presents an evaluation of the TMC vortex amplifier supported by experimental data with emphasis placed on its performance under actual system condition, compressible fluid (air) and blocked load. Performance criteria investigated were pressure gain, pressure recovery, response and signal-to-noise ratio. Design parameters controlling the performance characteristics of the vortex amplifier were investigated and evaluated. The objective was to optimize performance and present the data in terms of design parameters to serve as a guide in selecting a vortex amplifier suitable to a specific application.

## Performance

The performance characteristics of the vortex amplifier shown in Figure 1 are presented in terms of pressure gain, pressure recovery, response and signal-to-noise ratio. These four parameters are considered to be the primary factors in evaluating the performance capabilities of the vortex amplifier and in its adaptation to control system applications. Other parameters such as flow gain, hysteresis, threshold, deadband, etc., are not considered in this paper, but are under investigation, and the results will be presented at a later date.

### Pressure Recovery

Pressure recovery, at blocked output, is the ratio of output total pressure ( $P_o$ ) to supply total pressure with no input signal. Percent total pressure recovery (R) represents the fluid utilization factor for pressure

---

\*Single ended pure fluid amplifier is defined as a unit with a single input, output, and signal ports. Analogous to a transistor or triode tube.

gain fluid amplifiers. Pressure recovery provides the means for evaluating the pressure losses in a pure fluid control system, the connection and arrangement of elements in a network, and configuration necessary in maximizing output pressure levels.

$$R = \frac{P_o}{P_s} \times 100 \quad (1)$$

where  $P_s$  = Supply total pressure

$P_o$  = Output total pressure

Consequently, an investigation was conducted to evaluate the relationship between the design parameters throat area ratio ( $C_1$ ), supply area ratio ( $C_2$ ), depth area ratio ( $C_3$ ) and the total pressure recovery. This investigation was correlated with the pressure gain study to determine their relationship so that pressure recovery could be maximized without a reduction in the pressure gain capabilities. The results are summarized in Figures 2 and 3. Percent pressure recovery varies from 100 percent to 80 percent for pressure ratios ( $P_s/P_a$ ) of 1 to 4 as shown. The design parameter that influences the recovery is  $C_1$  as shown in Figure 2. Figure 3 shows that the pressure recovery is not dependent on the supply area ratio  $C_2$ . Reducing  $C_1$  increases the pressure recovery at low pressure ratios but decreases the recovery at high pressure ratio (above 4).

To evaluate the total pressure recovery at laminar and turbulent flow conditions and provide a common denominator for comparison of the performance to other fluid amplifiers, the pressure recovery was analyzed and is presented as a function of Reynolds number ( $N_R$ ), see Figure 4. It was assumed that  $N_R < 4000$  represents laminar flow and  $N_R > 4000$  turbulent flow. It could be summarized that the percent recovery for laminar flow is between 99 percent and 98 percent and for turbulent flow between 98 percent to 70 percent (for  $N_R$  up to 60,000). This variation in performance indicates that the final configuration will be adopted to match a particular application.

### Pressure Gain

The pressure gain characteristics of the fluid vortex amplifier are presented and evaluated in terms of a specific application (blocked output). These types of elements were specifically designed for operation at blocked load condition such as high impedance actuators in ramjet application. Other load conditions would require modification of design parameters, and are not considered in this paper. The vortex amplifier is a single ended element, and its pressure gain,  $G_p$  is defined as the

ratio of change in output pressure ( $P_o$ ) to change in signal pressure with the supply pressure remaining constant ( $P_s$ ).

$$G_p = \frac{\Delta P_o}{\Delta P_i} \quad (2)$$

The pressure gain characteristics are a function of the design parameters and the method of applying signal pressure. Injecting the signal pressure tangent and in opposition to vortex motion, the pressure gain characteristic approaches a sharp "S" shape curve with pressure gains up to 200 (see Figure 5). Injecting the signal in the center of the vortex reduces the pressure gain to 100 and tends to flatten the pressure gain curve (see Figure 6). Injecting the signal with the vortex motion reduces the pressure gain to 60 and further flattens gain curve approaching a linear relationship.

A study was conducted to evaluate the pressure gain characteristics as a function of the major nondimensional design parameters throat area ratio ( $C_1$ ), supply area ratio ( $C_2$ ), and depth area ratio ( $C_3$ ). The results of this investigation are summarized in Figures 7, 8, and 9.

The investigation showed that a change in  $C_1$  from 7.5 to 4.5 increased the pressure gain from 45 to 150 without affecting the linearity through the operating range. These characteristics are shown in Figure 9. However, if  $C_1$  is  $< 4.0$ , the vortex amplifier operated as a digital amplifier with two pressure modes (high and low) and pressure gains of over 250. When  $C_1 < 2.0$  the unit is unstable. The other controlling parameter is the supply area ratio ( $C_2$ ). Reducing  $C_2$  from 28.5 to 10 increased pressure gain and improved linearity. However, when  $C_2 < 10.0$  the unit operated as a digital amplifier; and when  $C_2 < 5.0$  the unit is unstable. It is, therefore, obvious that the performance of the vortex amplifier could be adapted to numerous specific applications by carefully selecting the proper design parameters. Figure 7 shows the performances of an optimized configuration selected for ramjet application.

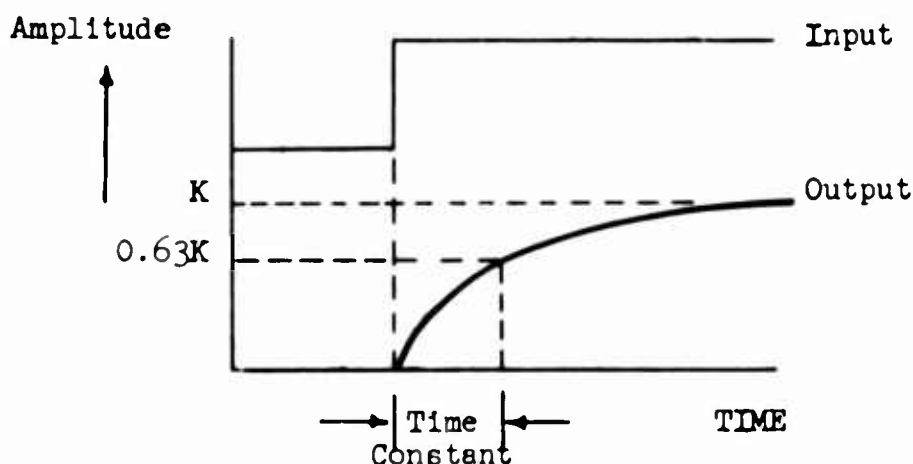
### Response

Two experimental methods were utilized to investigate the dynamic characteristics of the vortex fluid amplifier: steady state frequency response and transient response. The open loop frequency response tests were based on the application of a steady state sinusoidal pneumatic signal to the input, and the measurements of the magnitude of input and output pressure levels and their phase relationship. The test setup is shown in Figure 10. The transient response characteristics were obtained by applying a step input (square wave) and recording the output response. This was accomplished after the establishment of the transfer function for the vortex amplifier. The transfer function is a first order lag,  $G = K/(1 + TS)$  as indicated below.

A summary of the frequency response test data is presented in Figures 11 through 15. The tests were conducted on a representative element (Model A) with frequencies up to 125 cps. A plot of the amplitude ratio

(db) and phase shift (degrees) as a function of frequency is presented in Figure 15. The results indicate that the open loop characteristics approximate a first order lag transfer function ( $G = K/[1 + TS]$ ), with a break frequency of 27 cps.

Transient response tests were conducted on four similar units with different internal plenums. The time constant was established by determining the point where the output reached 63 percent of steady state level as indicated below.



The time constant was investigated as a function of chamber plenum of the unit, e.g. time constant was related to chamber plenum ratio ( $V_R$ ), which is the ratio between Model "A" and the other models (B,C,D). The results of this investigation are summarized in Figures 16 and 17. It appears that the time constant is closely related to the chamber plenum. A change in  $V_R$  from 1.0 to .5 reduces the time constant from .010 sec. to .0065 sec. It could be concluded that the transfer function of the vortex amplifier is a first order lag and it appears to be independent of scaling; however, the time constant or break frequency is a function of the internal volume of the unit.

#### Signal-to-Noise Ratio

In general it may be assumed that a primary factor limiting the amplification of any fluid amplifier is its signal-to-noise ratio. Any noise introduced or generated will be amplified along with the desired signal, so that if the noise level is an appreciable portion of the desired signal, further amplification will introduce significant distortion. The total noise present in a fluid amplifier can be divided into two main categories: Noise that is introduced from an outside source and noise that is generated by the fluid amplifier itself.

This section presents the results of an investigation conducted to determine the magnitude of the internal noises generated by the unit itself in comparison to output signal, i.e. signal-to-noise ratio. The

signal-to-noise ratio was investigated with respect to two parameters: supply to ambient pressure ratio ( $P_s/P_a$ ) and frequency. The pressure ratio range under investigation was 1.0 to 7.0 with frequency range of 0.5 to 100 cps. Summary of the test data is presented in Figures 18 through 23.

The investigation showed that pressure ratios (up to 7.0) have a secondary effect on the magnitude of the noise (signal-to-noise ratio of approximately 30 db or noise is approximately 3 percent of signal). However it is believed that higher pressure ratios will significantly influence the level of internally generated noises. Frequency of 0 to 25 cps have no effect on noise level as shown in Figure 23. At frequencies above 25 cps the noise level increases with the increase in frequency and at 100 cps the signal-to-noise ratio is approximately 14 db or noise is 20 percent of signal. This behavior could be related to the frequency response characteristics in attenuating the output signal level without effecting the internal noise level generated by the element itself. The signal level is reduced but the noise level remains constant and as a result the signal-to-noise ratio is reduced; in other words, the noise is a larger portion of the signal.

#### Staging and Circuit Application

The staging of vortex fluid amplifiers can be accomplished with three basic techniques: series connection, parallel connection, and series inverted connection, and any combination thereof, as shown in Figures 24 through 27.

Employing the series connection method, the amplifiers are cascaded and the output of the first stage is the signal to the second stage and so on....as shown in Figure 25. The number of stages will depend on the signal-to-noise ratio, the impedance matching, and the required amplification. Ideally, the total amplification  $K_T$  is:

$$K_T = K_1 \cdot K_2 \cdot K_3 \cdot \cdot \cdot K_n = \prod_{n=1}^n (K_n) \quad (3)$$

However, due to the impedance matching problem and other losses, the total amplification factor is reduced by a factor  $\phi_s$ .

$$\phi_s = f\left(N, \frac{P_s}{P_a}, K_1, Z\right) \quad (4)$$



where

$N$  = number of stages

$\frac{P_s}{P_a}$  = pressure ratio

$K_1$  = gain of the individual elements

$Z$  = system impedance

Therefore

$$K_T = \phi_s \prod_{n=1}^n (K_n) \quad (5)$$

In parallel connection approach, the output of the first stage serves as the power supply to the next stage and the pressure signal is applied simultaneously to both stages as shown in Figure 26. The number of stages is determined by the pressure recovery characteristics. The required output pressure level, at zero signal, is primarily a function of the recovery of each stage. Therefore

$$\left(\frac{P_{on}}{P_a}\right) = \left(\frac{P_s}{P_a}\right) \prod_{n=1}^n (R_n) \quad (6)$$

where

$\frac{P_{on}}{P_a}$  = output pressure ratio of  $n^{th}$  stage

$\frac{P_s}{P_a}$  = supply pressure ratio

$R_n$  = recovery of the  $n^{th}$  stage

$N$  = number of stages

Assume the recovery of all the stages are the same  $R_1 = R_2 = R_3 = \dots R_n$ . We can rewrite equation (7) where

$$\frac{P_{on}}{P_a} = \left(\frac{P_s}{P_a}\right) (R)^N \quad (7)$$

or

$$N = \frac{\log \left(\frac{P_{on}}{P_s}\right)}{\log R} \quad (8)$$

The total amplification  $K_T$  for "parallel connection" is

$$K_T = \phi_P (K)^N \quad (9)$$

Where  $\phi_P$  is the reduction factor and it is a function of

$$\phi_P = \left( N, \frac{P_S}{P_A}, Z \right) \quad (10)$$

The series inverted connection technique utilizes the "vent" flow which is inverted in polarity with respect to the output signal as the input to the next stage as shown in Figure 27. Employing this technique it is possible to increase the network gain without a sign change (plus or minus).

#### Performance Comparison

To relate the characteristics of the vortex fluid amplifier to conventional fluid amplifiers, the performance characteristics of two basic types of fluid amplifiers, "pressure controlled" and "momentum controlled", were experimentally investigated under identical load condition, blocked load, and their performance compared to the data obtained for the vortex amplifier utilizing nondimensional parameters as the common denominator. The results of this investigation are summarized in Figures 28, 29 and 30\*.

The pressure gain capabilities are presented by considering only the linear portion of the data for each element or its approximation, and the absolute magnitude of the signal pressure and output pressure. The performance of the "momentum controlled" unit is inverted to permit a uniform presentation of the data. The pressure gains of the "pressure controlled", "momentum controlled" and "vortex controlled" were 9, 10, and 60 respectively at a supply pressure of 50 psia. At supply pressures of 70 psia, the pressure gains were 11, 16, and 150 respectively.

The pressure recovery characteristics are presented as a function of two nondimensional quantities: pressure ratio and Reynolds number. The percent recovery as a function of pressure ratio varies from 100 percent to 54 percent for the "pressure controlled" unit, 100 percent to 54 percent for the "momentum controlled" unit and 100 percent to 80 percent for the "vortex controlled" unit. For comparison of pressure recovery at

---

\*It should be pointed out that the units used for comparison were fabricated by The Marquardt Corporation in accordance with available data. Variation in fabrication may account for differences in measured performance characteristics.

laminar and turbulent flow conditions, percent pressure recovery is presented as a function of Reynolds number ( $N_R$ ) Figure 30. It was assumed that  $N_R < 4000$  represents laminar flow and  $N_R > 4000$  turbulent flow.

The response characteristics of the three fluid amplifiers ("momentum controlled", "pressure controlled", and "vortex controlled") were similar. The frequency response can be represented by a first order lag transfer function ( $G = K/[1 + TS]$ ) with a time constant,  $T$ , as a function of the internal volume of the element and the supply pressure and pressure drop. The predominant factor controlling the time constant was the internal volume. With similar plenum, the time constants were .18 second, .008 and .012 seconds, respectively for the three units.

### Conclusion

The performance characteristics of the vortex fluid amplifier, as indicated by this preliminary investigation, confirms its application to systems and networks with high load impedance and demonstrates the application of vorticity phenomena to pure fluid amplification. Additional work should be followed to increase its scope of application and formulate the mathematical model for the entire range of operation.

### Acknowledgments

This work was supported by the U.S. Air Force under contracts AF 33(657)-12146 and AF 33(616)-40809.

## References

1. "Flow Visualization - Compressible Fluids" by J.R.Keto, Diamond Ordnance Fuze Laboratories.
2. "The Kinematics of Vorticity" by C.Truesdell, Indiana University Press.
3. "Pneumatic Pulse Transmission with Bistable Jet Relay Reception and Amplification" Sc.D Thesis by F.T.Brown, Massachusetts Institute of Technology.
4. "A Theoretical Study of the Design Parameters of Subsonic Pressure Controlled Fluid Jet Amplifiers" Ph.D. thesis by A.K.Simson, Massachusetts Institute of Technology.
5. "Generalized Performance Characteristics of Proportional and Bistable Fluid Amplifiers" by Silas Katz and R.J.Dockery, Harry Diamond Laboratories.

## VORTEX AMPLIFIER

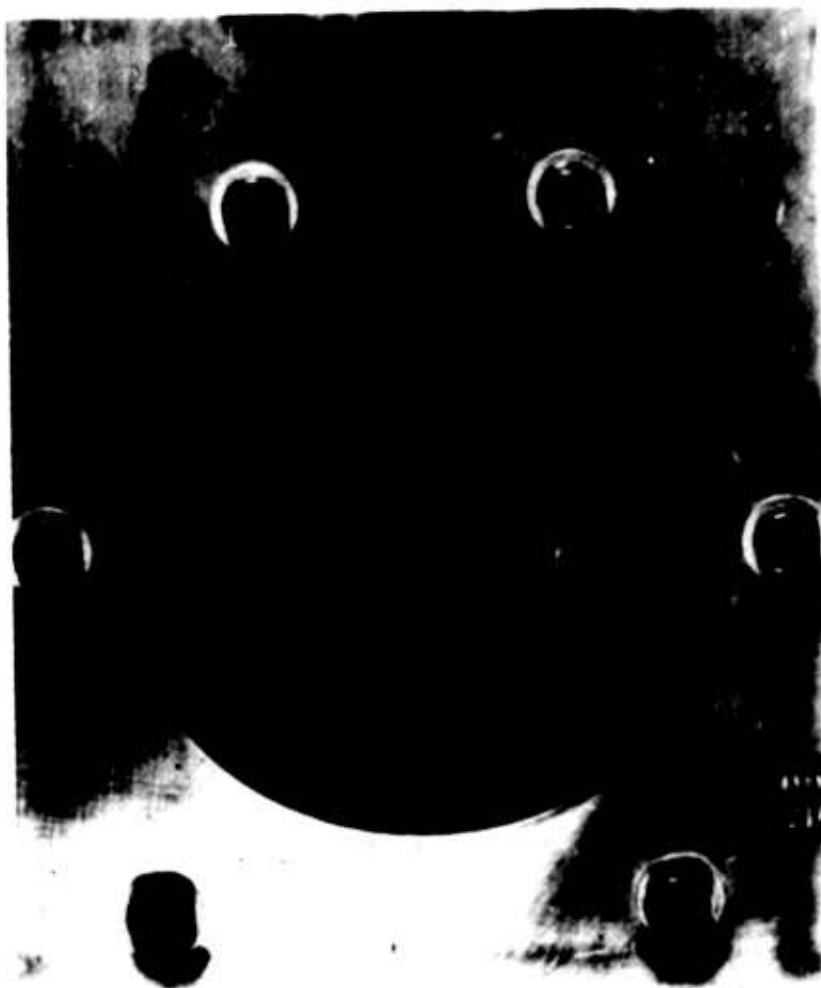


FIGURE 1

# PERCENT PRESSURE RECOVERY TMC VORTEX AMPLIFIER

## BLOCKED OUTPUT

$C_1$  = THROAT AREA RATIO  
FLUID = AIR

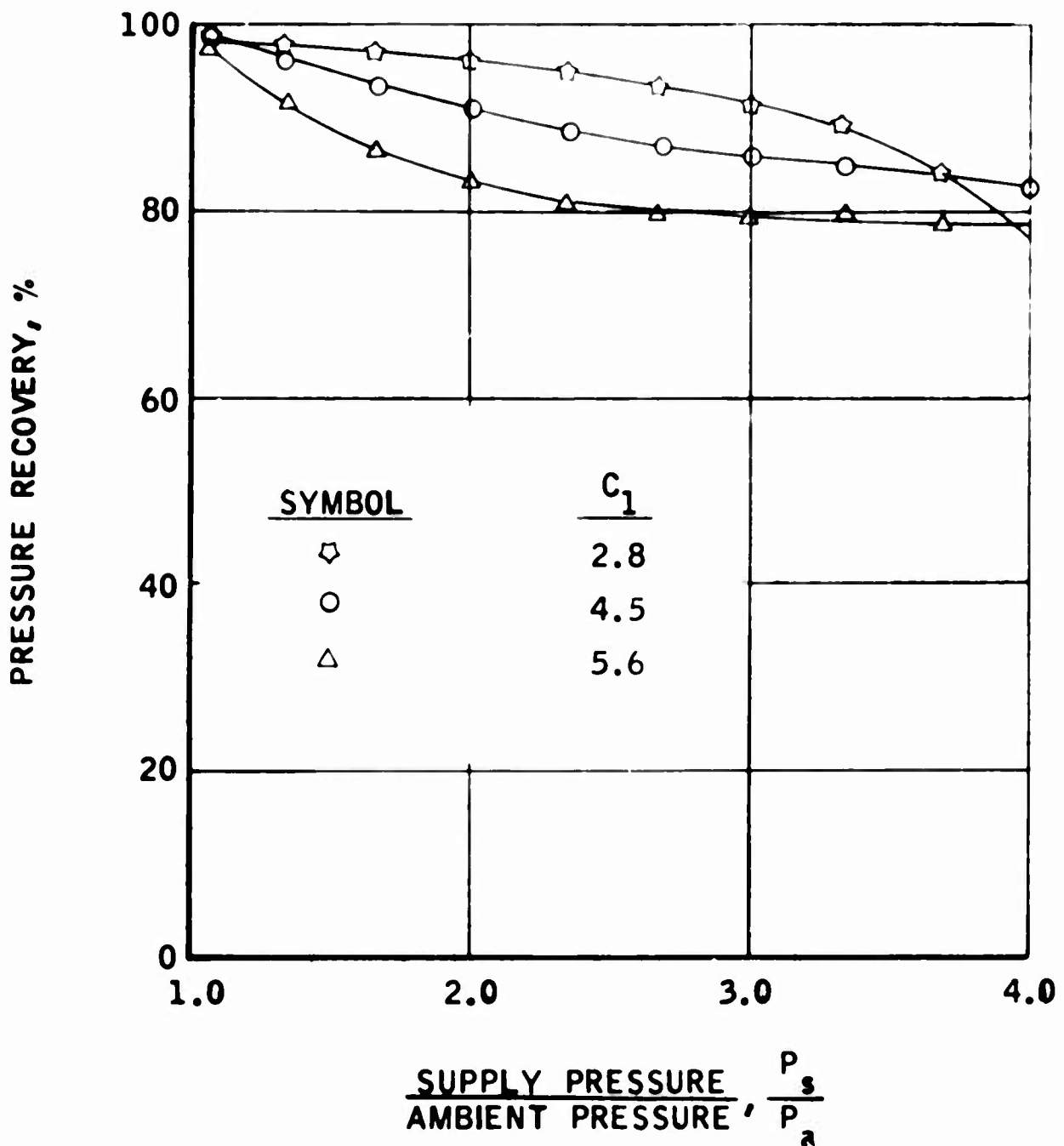


FIGURE 2

# PERCENT PRESSURE RECOVERY TMC VORTEX AMPLIFIER

BLOCKED OUTPUT

$C_2$  = SUPPLY AREA RATIO

FLUID = AIR

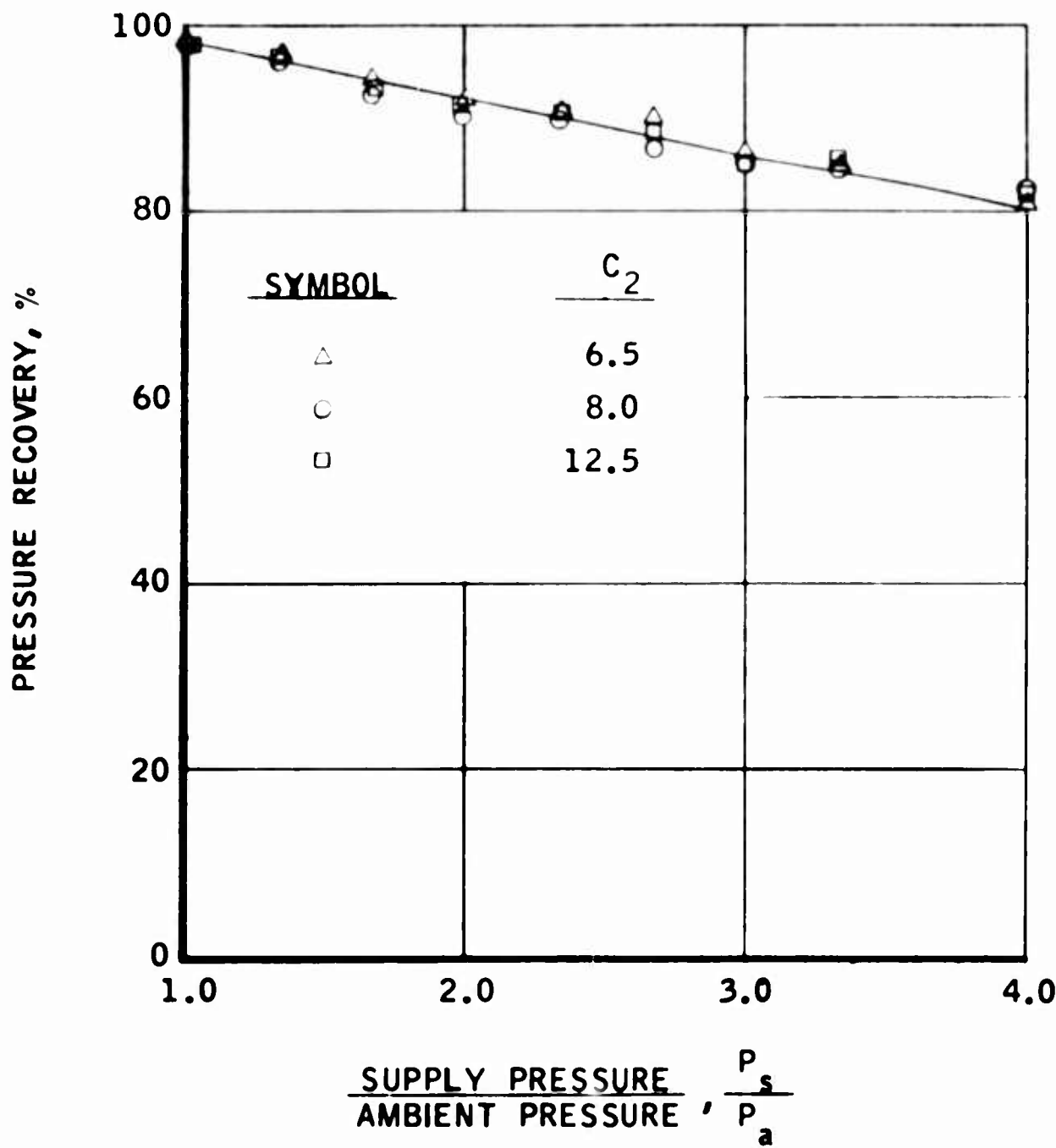


FIGURE 3



# TMC VORTEX AMPLIFIER

SYMBOL	$C_1$
◆	6.00
▼	8.80
●	4.75
▲	18.50
■	10.50
◇	14.50
▽	7.75
◐	12.50
○	22.50
△	28.50
□	10.00
◻	22.00

$C_1$  = THROAT AREA RATIO  
 $C_2$  = SUPPLY AREA RATIO

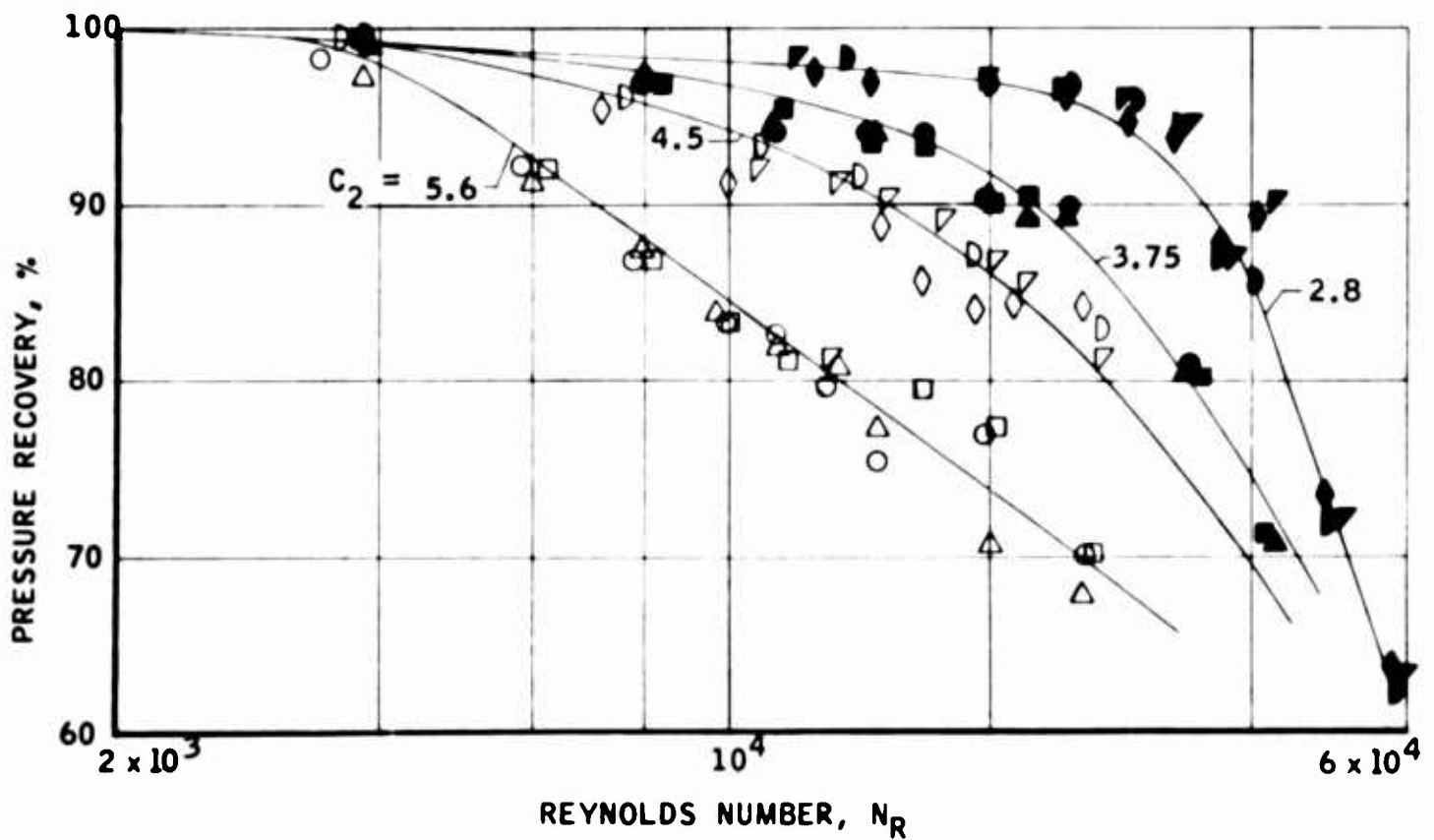


FIGURE 4

## PERFORMANCE OF TMC VORTEX AMPLIFIER

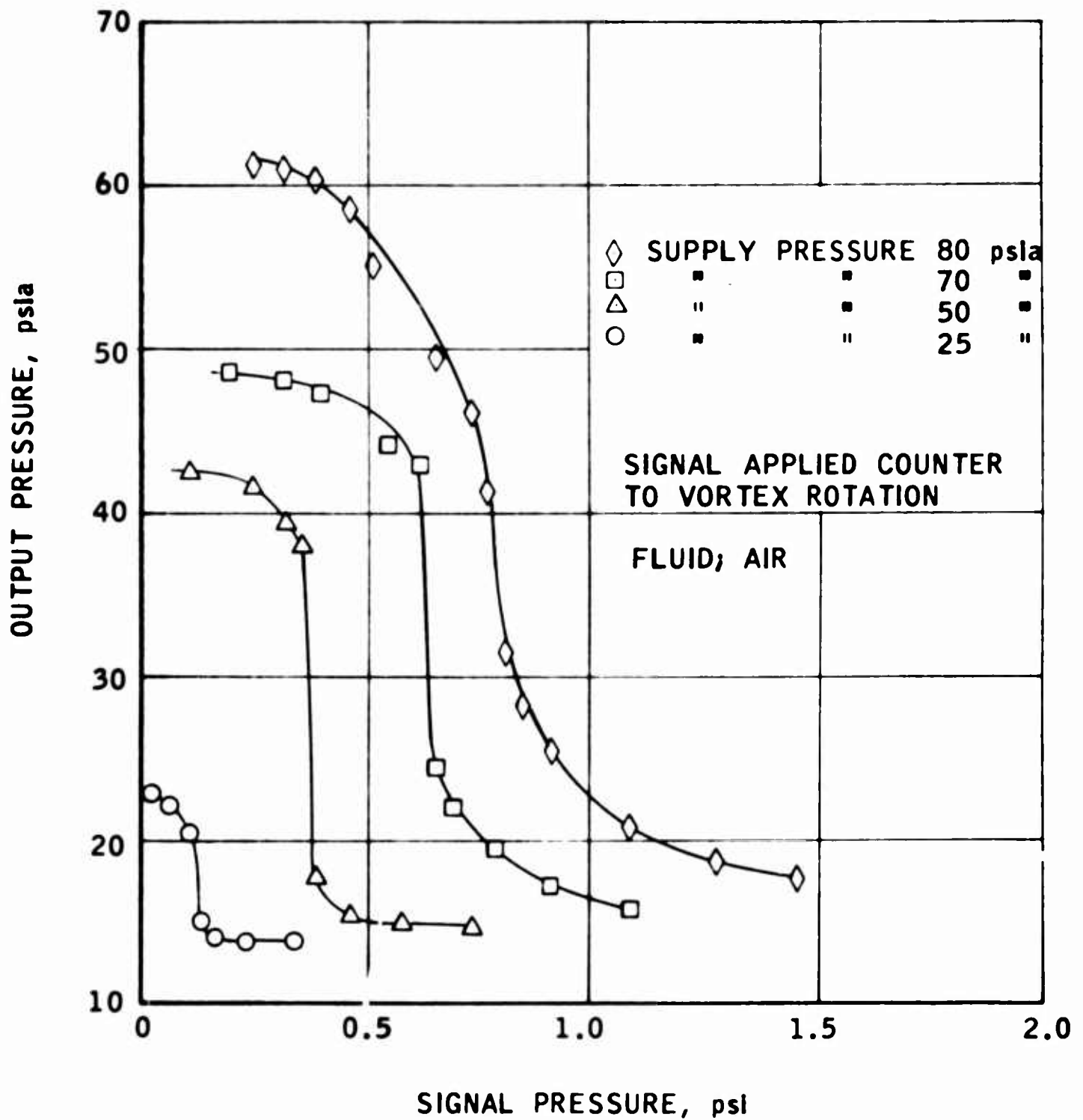


FIGURE 5

PERFORMANCE OF TMC VORTEX AMPLIFIER

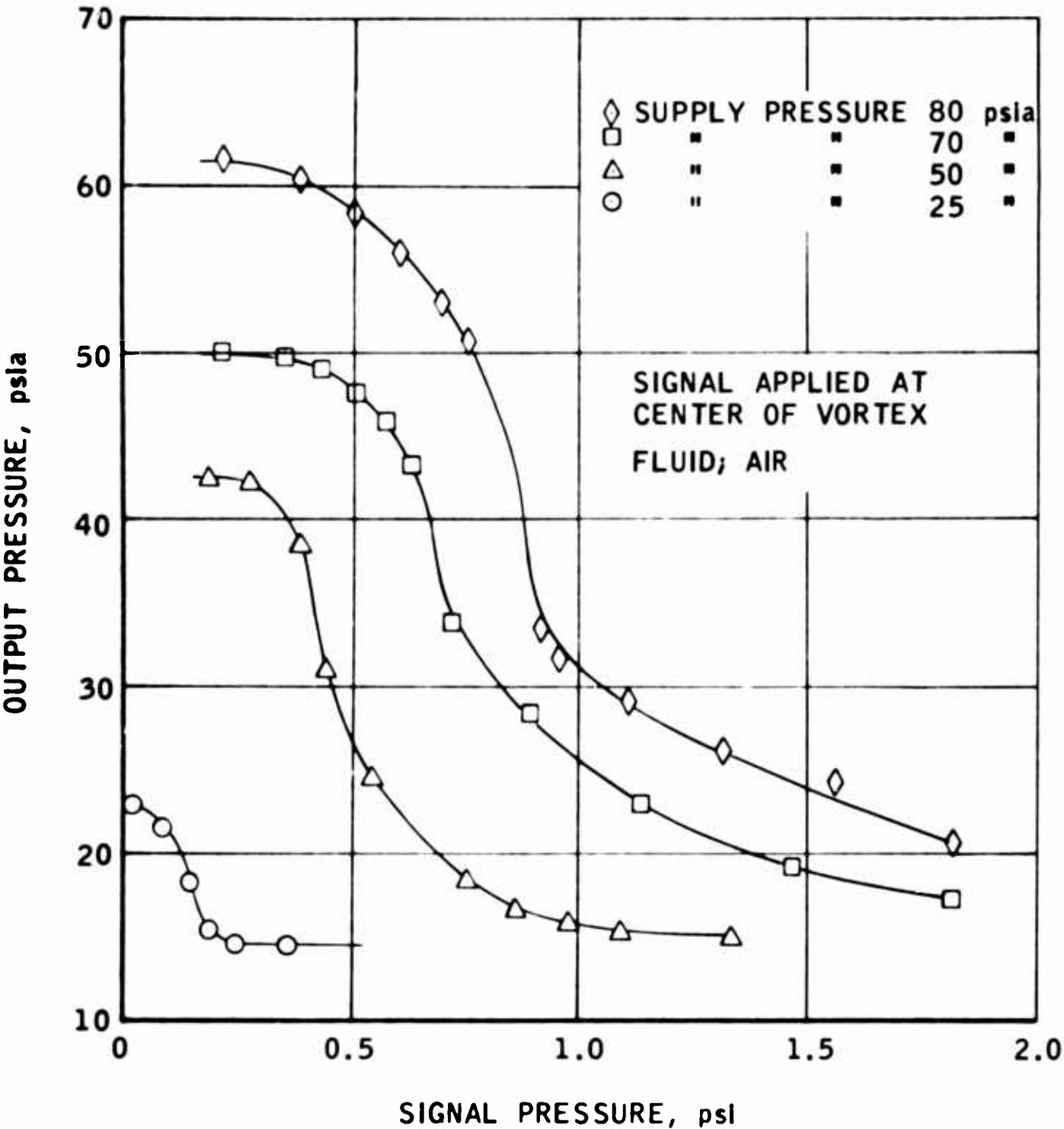


FIGURE 6

# PRESSURE GAIN CHARACTERISTICS TMC VORTEX AMPLIFIER

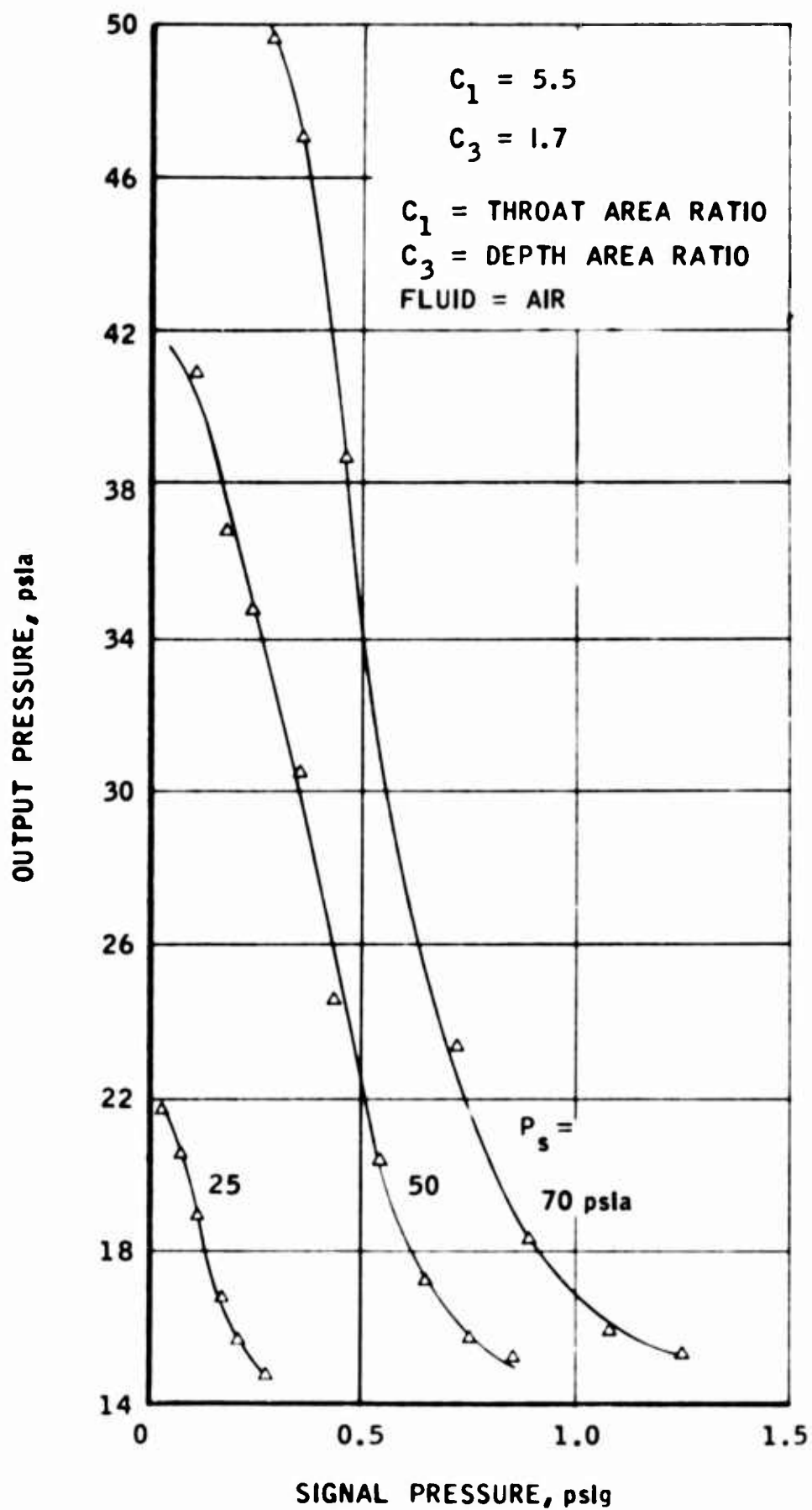


FIGURE 7

## PRESSURE GAIN CHARACTERISTICS

SUPPLY PRESSURE = 50 psia

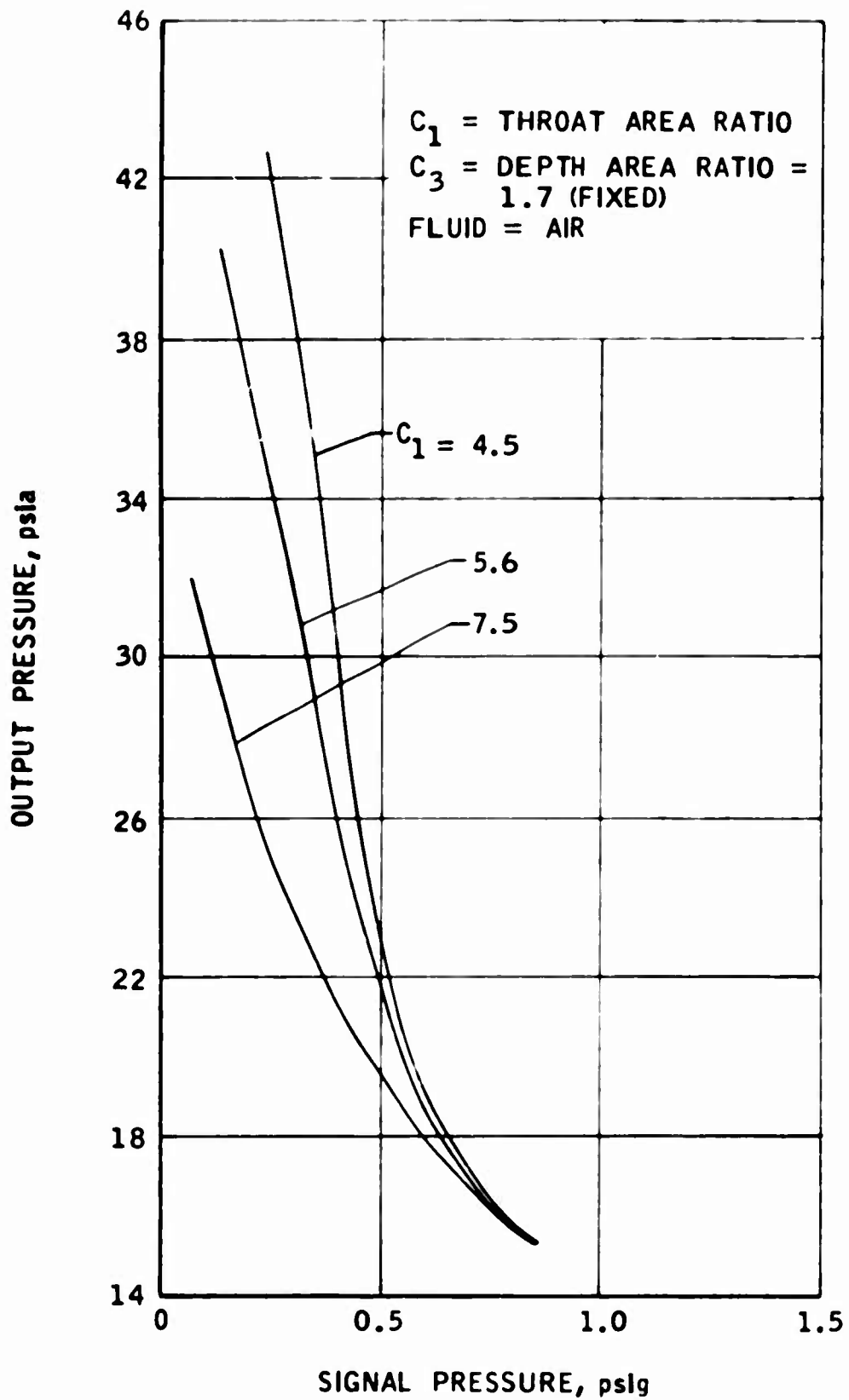


FIGURE 8

## PRESSURE GAIN CHARACTERISTICS

SUPPLY PRESSURE = 50 psia  
FLUID = AIR

$C_2$  = SUPPLY AREA RATIO

$C_3$  = DEPTH AREA RATIO = 5.6 (FIXED)

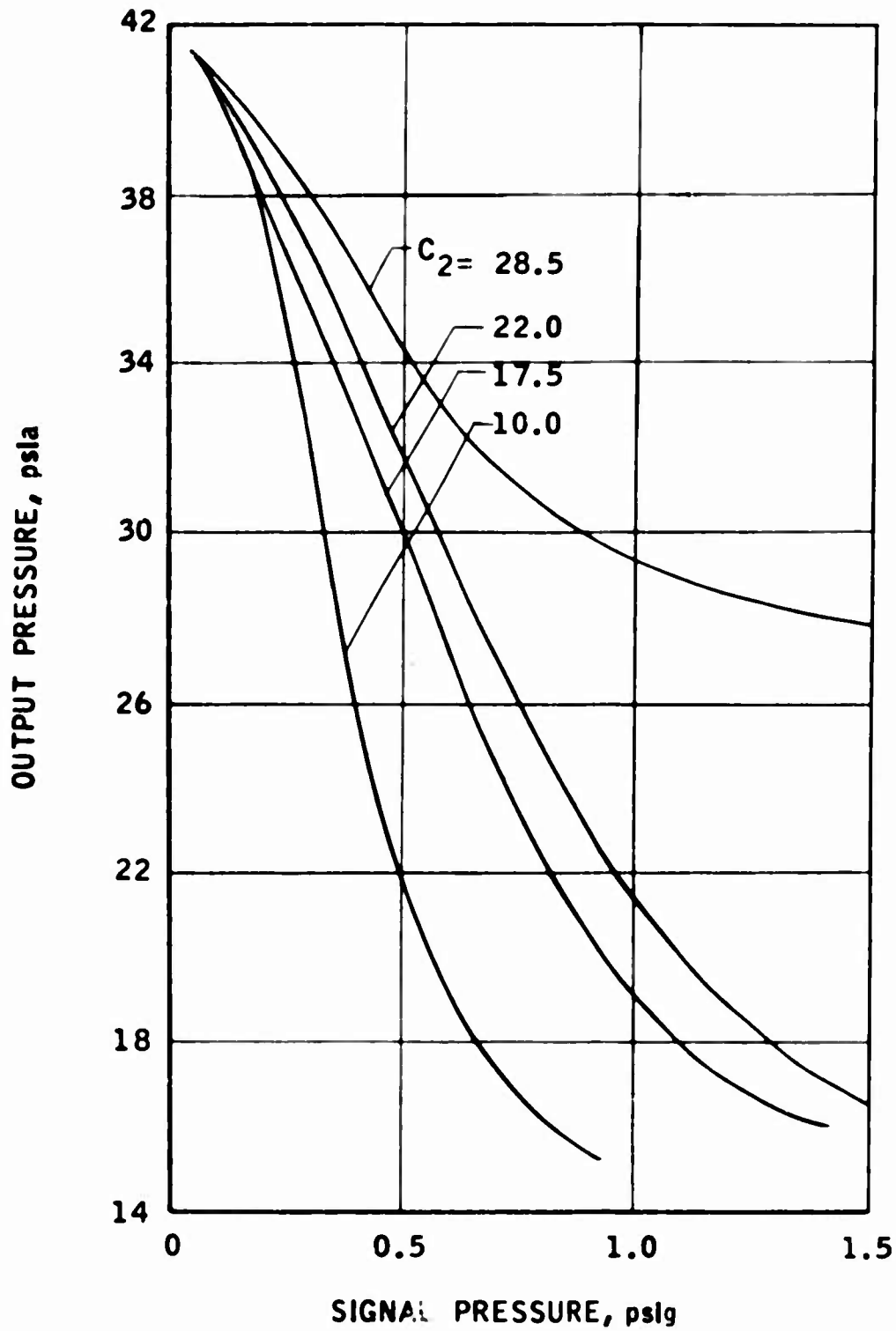


FIGURE 9

# FREQUENCY RESPONSE TEST SETUP VORTEX AMPLIFIER

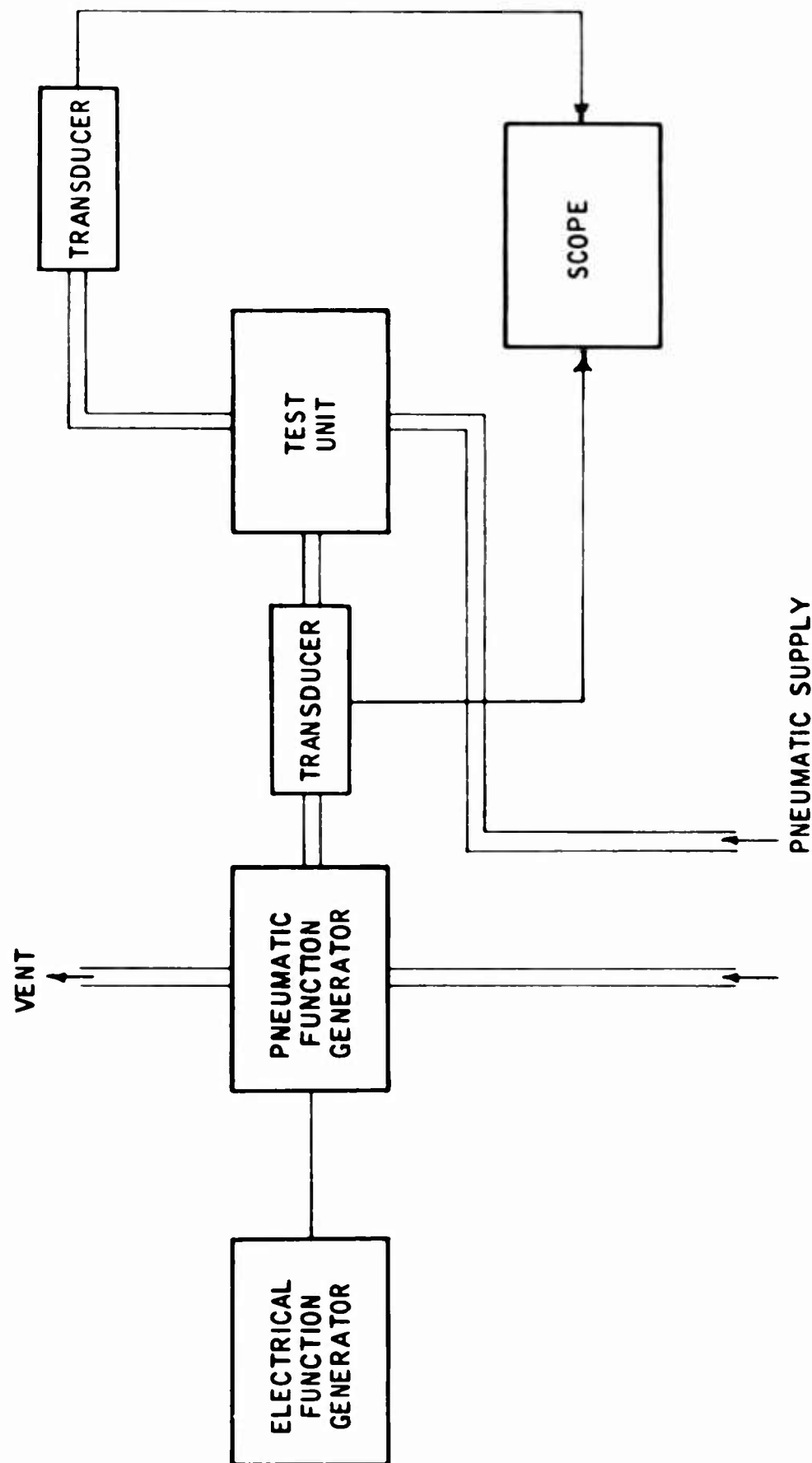
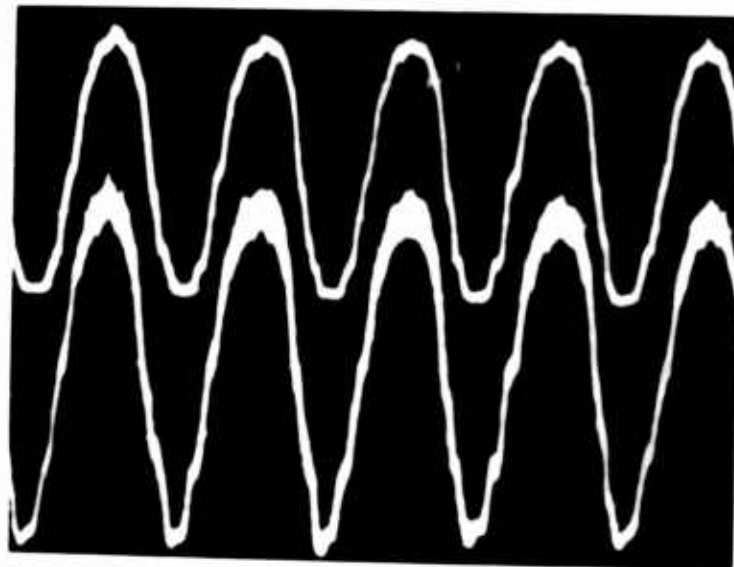


FIGURE 10

## FREQUENCY RESPONSE - VORTEX AMPLIFIER

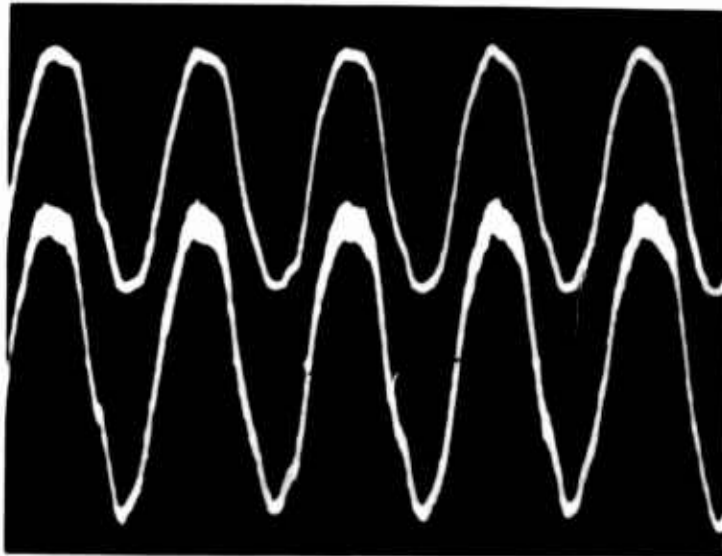


OUTPUT SIGNAL

FREQUENCY = 0.5 cps  
SWEEP = 1 cm/sec  
AMPLITUDE RATIO = 0 db  
PHASE SHIFT = 0°

INPUT SIGNAL

TRAVEL →



OUTPUT SIGNAL

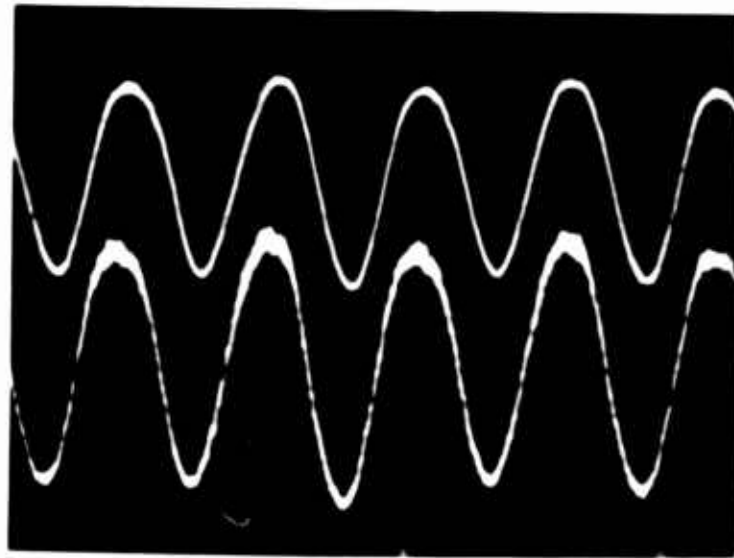
FREQUENCY = 1.0 cps  
SWEEP = 0.5 cm/sec  
AMPLITUDE RATIO = 0.13 db  
PHASE SHIFT = 0°

INPUT SIGNAL

FIGURE 11



## FREQUENCY RESPONSE - VORTEX AMPLIFIER

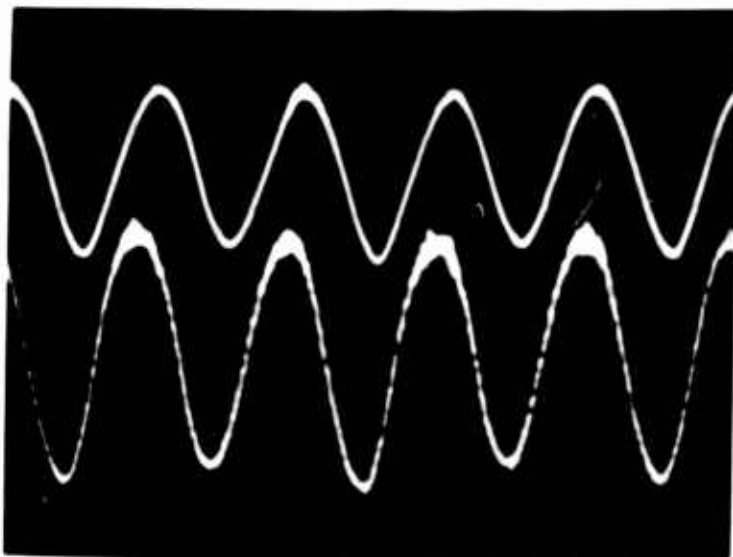


OUTPUT SIGNAL

FREQUENCY = 5.0 cps  
SWEEP = 0.1 cm/sec  
AMPLITUDE RATIO = 0.1 db  
PHASE SHIFT =  $16^\circ$

INPUT SIGNAL

TRAVEL  $\longrightarrow$



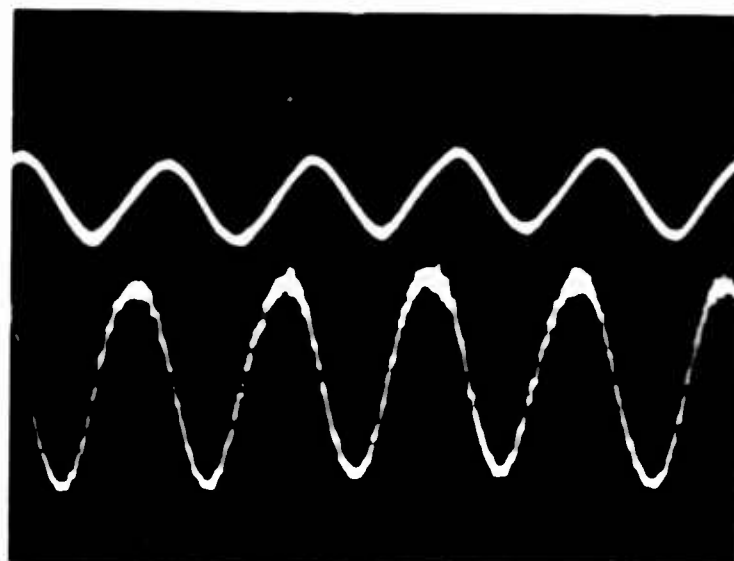
OUTPUT SIGNAL

FREQUENCY = 10 cps  
SWEEP = 0.05 sec/cm  
AMPLITUDE RATIO = 0 db  
PHASE SHIFT =  $25^\circ$

INPUT SIGNAL

FIGURE 12

# FREQUENCY RESPONSE - VORTEX AMPLIFIER

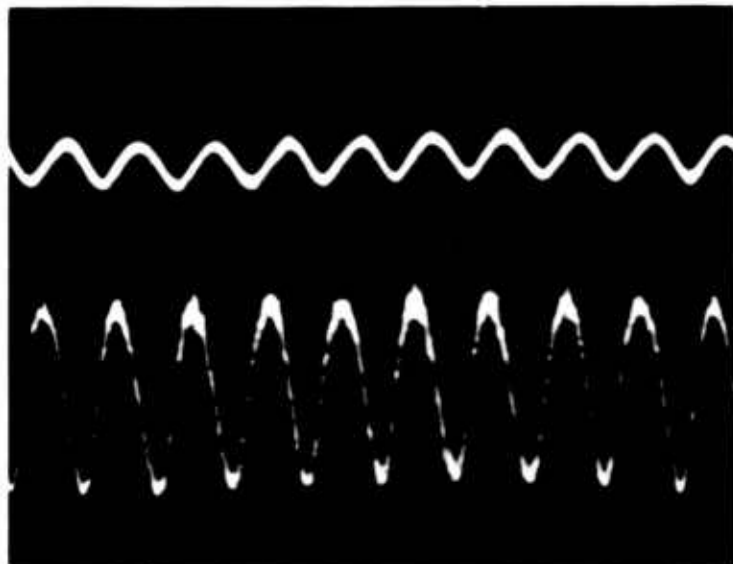


OUTPUT SIGNAL

FREQUENCY = 25 cps  
SWEEP = 0.02 sec/cm  
AMPLITUDE RATIO = -2 db  
PHASE SHIFT =  $41^\circ$

INPUT SIGNAL

TRAVEL  $\longrightarrow$



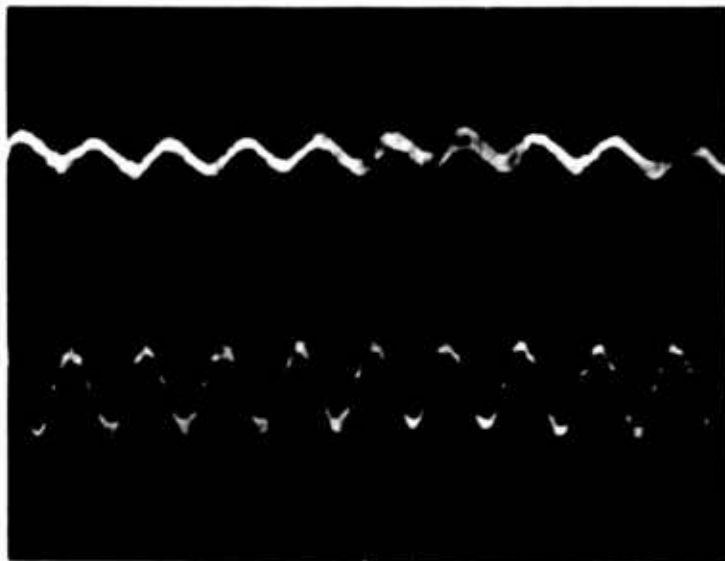
OUTPUT SIGNAL

FREQUENCY = 50 cps  
SWEEP = 0.020 sec/cm  
AMPLITUDE RATIO = -5 db  
PHASE SHIFT =  $56^\circ$

INPUT SIGNAL

FIGURE 13

## FREQUENCY RESPONSE - VORTEX AMPLIFIER

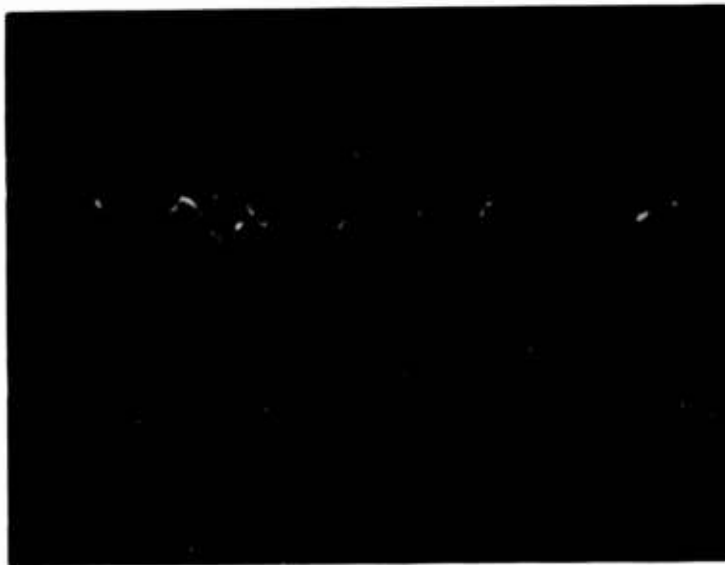


OUTPUT SIGNAL\*

FREQUENCY = 100 cps  
SWEEP = 0.01 sec/cm  
AMPLITUDE RATIO = -10.5 db  
PHASE SHIFT = 83°

INPUT SIGNAL

TRAVEL →



OUTPUT SIGNAL\*\*

FREQUENCY = 125 cps  
SWEEP = 0.01 sec/cm  
AMPLITUDE RATIO = -13.6 db  
PHASE SHIFT = 93°

INPUT SIGNAL

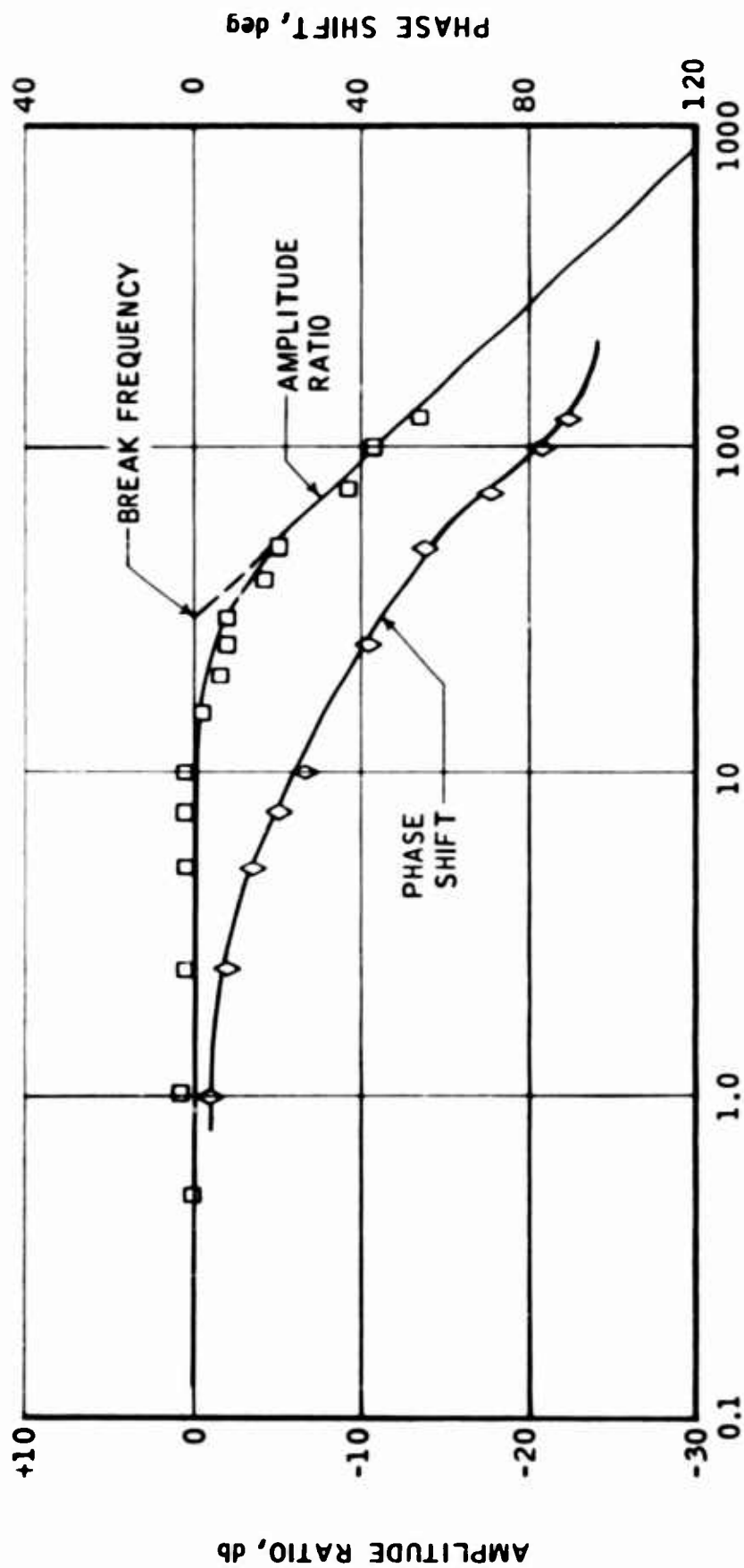
\* AMPLIFIED 2.5 TIMES

\*\* AMPLIFIED 5.0 TIMES

FIGURE 14

# OPEN LOOP FREQUENCY RESPONSE CHARACTERISTICS VORTEX AMPLIFIER

MODEL A

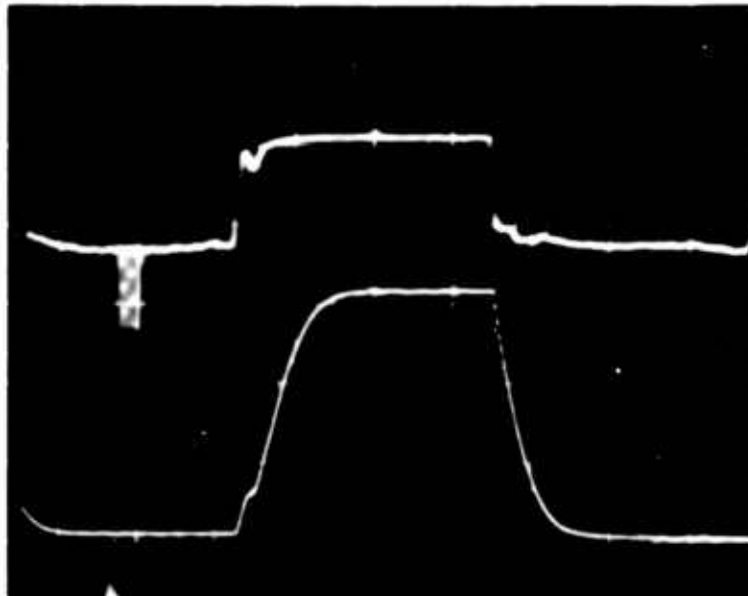


FREQUENCY, cps

FIGURE 15

# RESPONSE TO STEP INPUT SIGNAL VORTEX AMPLIFIER

## MODEL A



INPUT SIGNAL

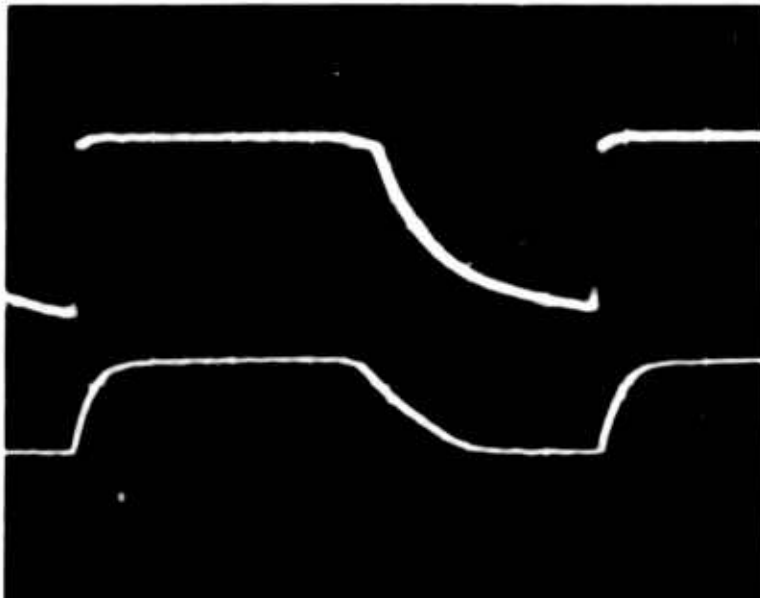
VORTEX CHAMBER  
VOLUME RATIO,  $V_R = 1.0$

SWEEP = 0.02 cm/sec  
TIME CONSTANT = 0.010 sec

OUTPUT SIGNAL

TRAVEL →

## MODEL B



INPUT SIGNAL

VORTEX CHAMBER  
VOLUME RATIO,  $V_R = 0.75$

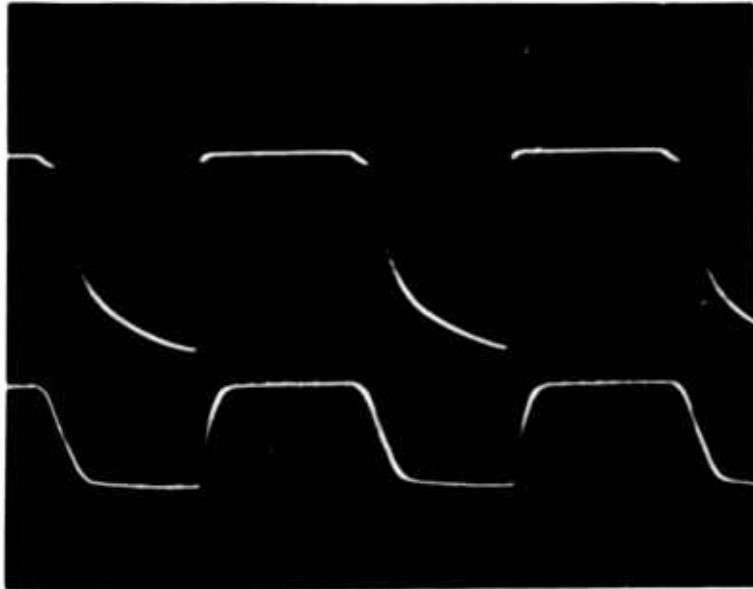
SWEEP = 0.02 cm/sec  
TIME CONSTANT = 0.0075 sec

OUTPUT SIGNAL

FIGURE 16

# RESPONSE TO STEP INPUT SIGNAL VORTEX AMPLIFIER

## MODEL C



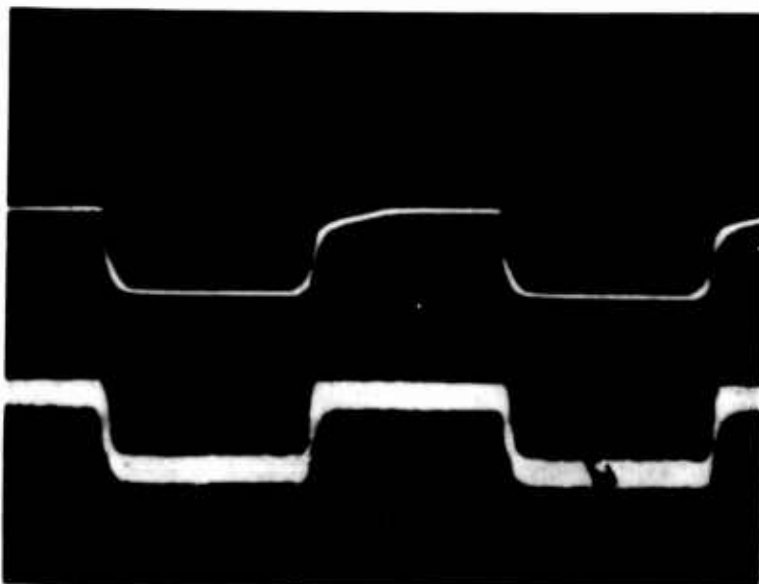
INPUT SIGNAL

VORTEX CHAMBER  
VOLUME RATIO,  $V_R = 0.5$   
SWEEP = 0.05 cm/sec  
TIME CONSTANT = 0.0065 sec

OUTPUT SIGNAL

TRAVEL →

## MODEL D



INPUT SIGNAL

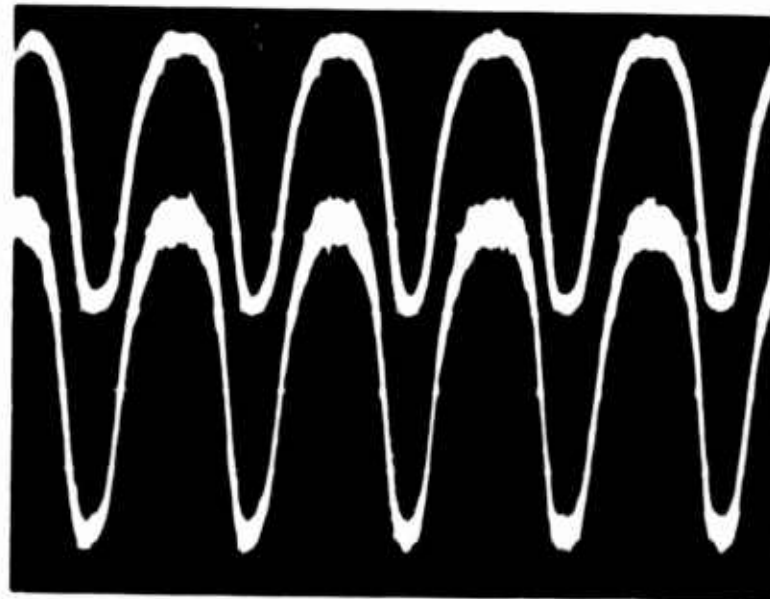
VORTEX CHAMBER  
VOLUME RATIO,  $V_R = 0.35$   
SWEEP = 0.05 cm/sec  
TIME CONSTANT = 0.0045 sec

OUTPUT SIGNAL

FIGURE 17

# SIGNAL TO NOISE RATIO - VORTEX AMPLIFIER

1 cps



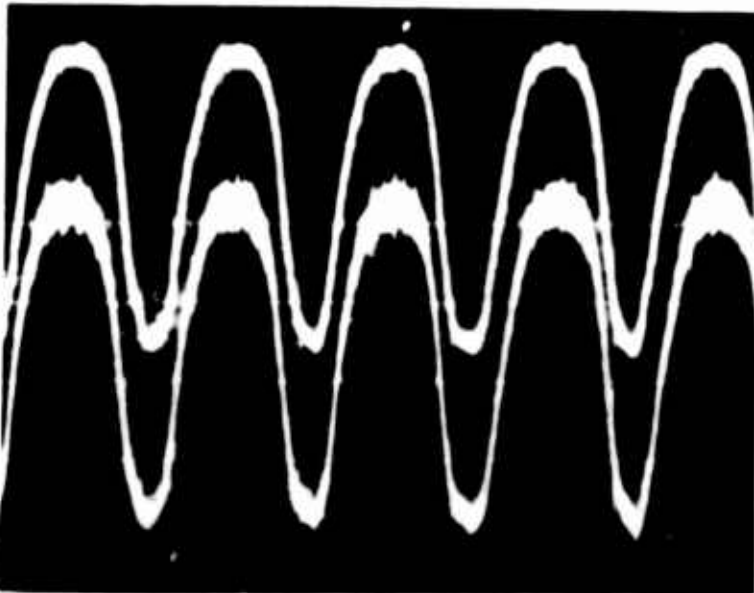
OUTPUT SIGNAL

$$\frac{\text{SUPPLY PRESSURE}}{\text{AMBIENT PRESSURE}}, \frac{P_s}{P_a} = 3.5$$

$$\frac{\text{SIGNAL}}{\text{NOISE}}, Q = 28 \text{ db}$$

INPUT SIGNAL

TRAVEL →



OUTPUT SIGNAL

$$\frac{\text{SUPPLY PRESSURE}}{\text{AMBIENT PRESSURE}}, \frac{P_s}{P_a} = 7.0$$

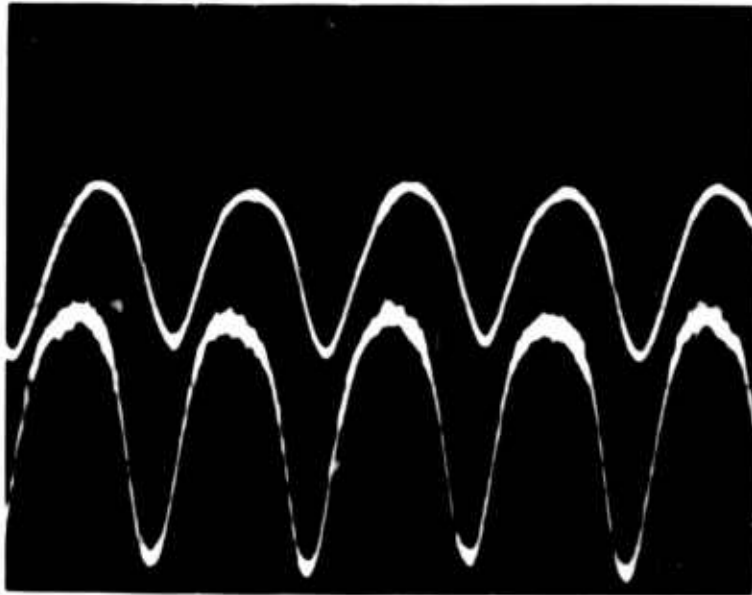
$$\frac{\text{SIGNAL}}{\text{NOISE}}, Q = 29 \text{ db}$$

INPUT SIGNAL

FIGURE 18

# SIGNAL TO NOISE RATIO - VORTEX AMPLIFIER

10 cps



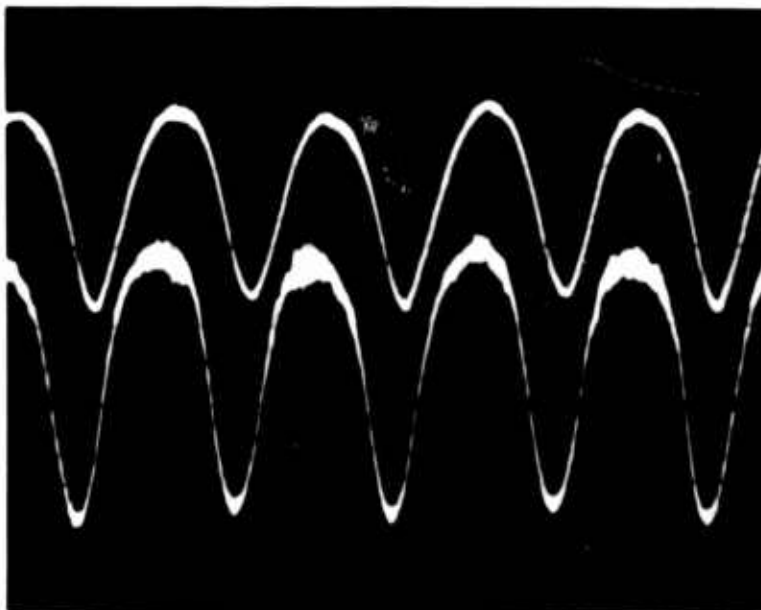
OUTPUT SIGNAL

$$\frac{\text{SUPPLY PRESSURE}}{\text{AMBIENT PRESSURE}}, \frac{P_s}{P_a} = 3.5$$

$$\frac{\text{SIGNAL}}{\text{NOISE}}, Q = 30 \text{ db}$$

INPUT SIGNAL

TRAVEL →



OUTPUT SIGNAL

$$\frac{\text{SUPPLY PRESSURE}}{\text{AMBIENT PRESSURE}}, \frac{P_s}{P_a} = 7.0$$

$$\frac{\text{SIGNAL}}{\text{NOISE}}, Q = 31 \text{ db}$$

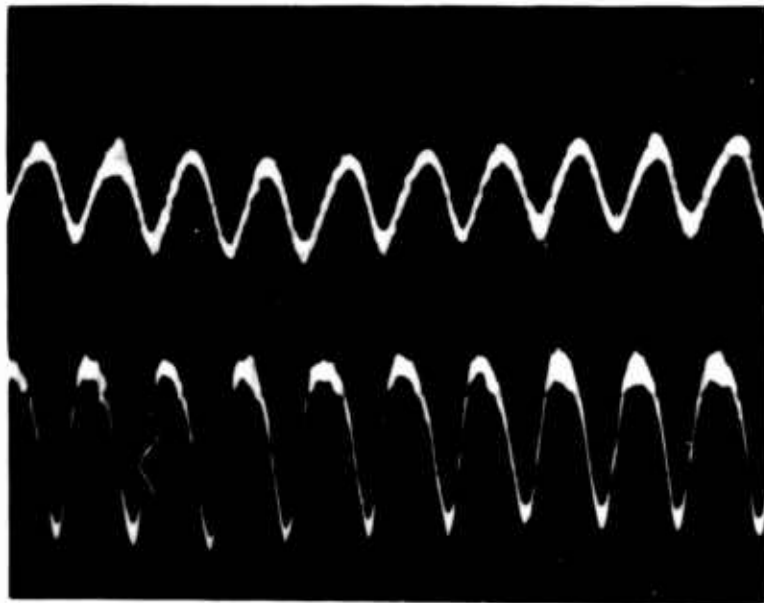
INPUT SIGNAL

FIGURE 19



# SIGNAL TO NOISE RATIO - VORTEX AMPLIFIER

50 cps



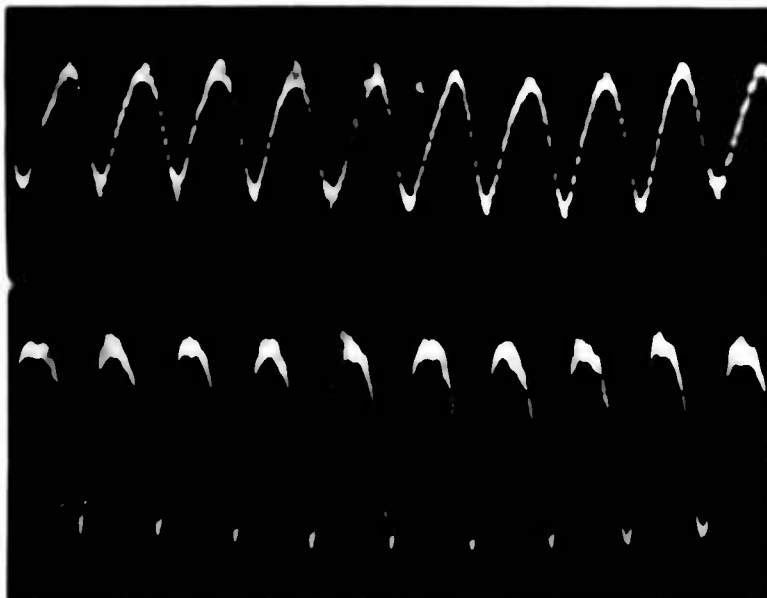
OUTPUT SIGNAL

$$\frac{\text{SUPPLY PRESSURE}}{\text{AMBIENT PRESSURE}}, \frac{P_s}{P_a} = 3.5$$

$$\frac{\text{SIGNAL}}{\text{NOISE}}, Q = 20 \text{ db}$$

INPUT SIGNAL

TRAVEL →



OUTPUT SIGNAL

$$\frac{\text{SUPPLY PRESSURE}}{\text{AMBIENT PRESSURE}}, \frac{P_s}{P_a} = 7.0$$

$$\frac{\text{SIGNAL}}{\text{NOISE}}, Q = 21 \text{ db}$$

INPUT SIGNAL

FIGURE 20

# SIGNAL TO NOISE RATIO - VORTEX AMPLIFIER

75 cps

OUTPUT SIGNAL

$$\frac{\text{SUPPLY PRESSURE}}{\text{AMBIENT PRESSURE}}, \frac{P_s}{P_a} = 3.5$$

$$\frac{\text{SIGNAL}}{\text{NOISE}}, Q = 15 \text{ db}$$

INPUT SIGNAL

TRAVEL  $\longrightarrow$

OUTPUT SIGNAL

$$\frac{\text{SUPPLY PRESSURE}}{\text{AMBIENT PRESSURE}}, \frac{P_s}{P_a} = 7.0$$

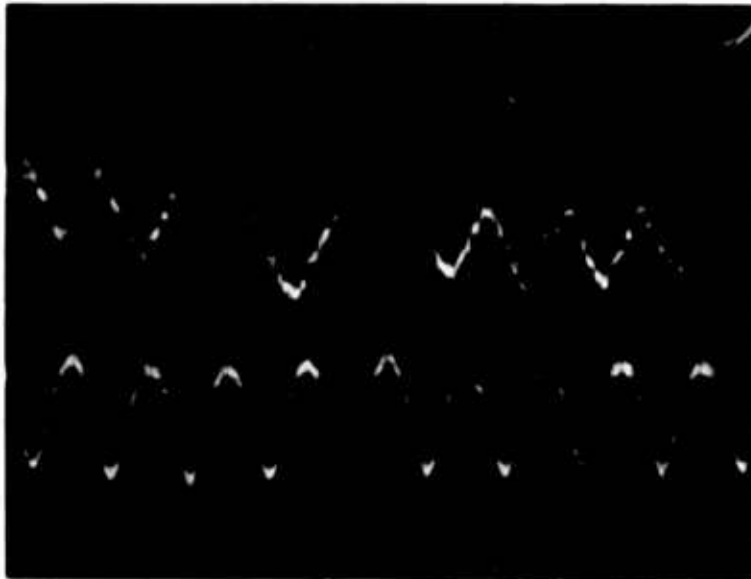
$$\frac{\text{SIGNAL}}{\text{NOISE}}, Q = 16 \text{ db}$$

INPUT SIGNAL

FIGURE 21

# SIGNAL TO NOISE RATIO - VORTEX AMPLIFIER

100 cps



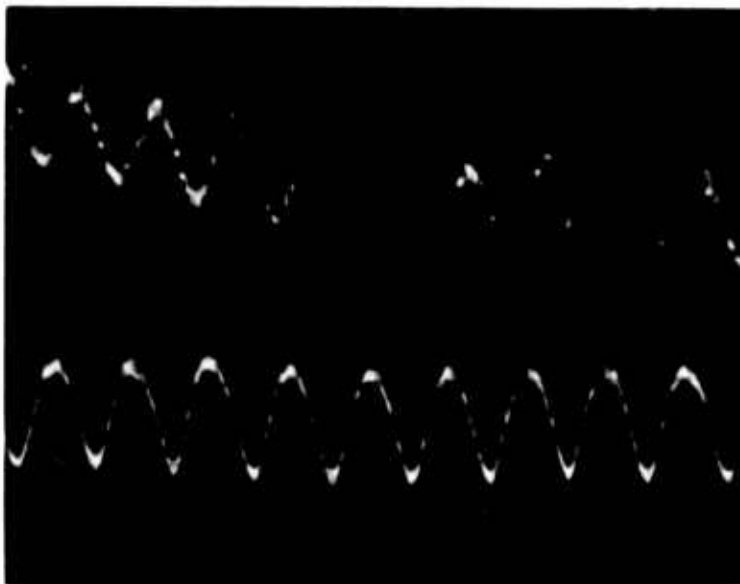
OUTPUT SIGNAL

$$\frac{\text{SUPPLY PRESSURE}}{\text{AMBIENT PRESSURE}}, \frac{P_s}{P_a} = 3.5$$

$$\frac{\text{SIGNAL}}{\text{NOISE}}, Q = 13 \text{ db}$$

INPUT SIGNAL

TRAVEL →



OUTPUT SIGNAL

$$\frac{\text{SUPPLY PRESSURE}}{\text{AMBIENT PRESSURE}}, \frac{P_s}{P_a} = 7.0$$

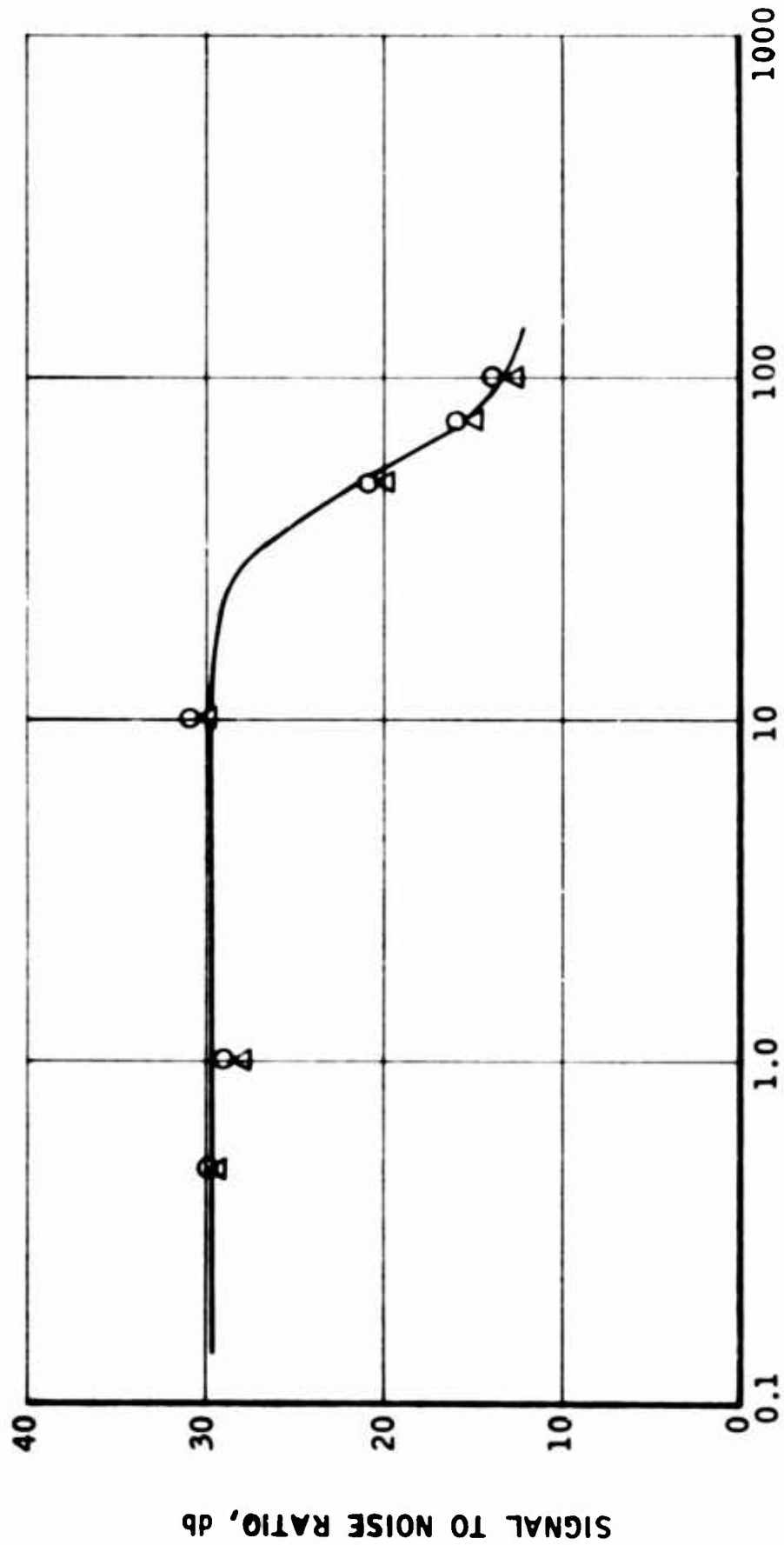
$$\frac{\text{SIGNAL}}{\text{NOISE}}, Q = 14 \text{ db}$$

INPUT SIGNAL

FIGURE 22

# SIGNAL TO NOISE CHARACTERISTICS VORTEX AMPLIFIER

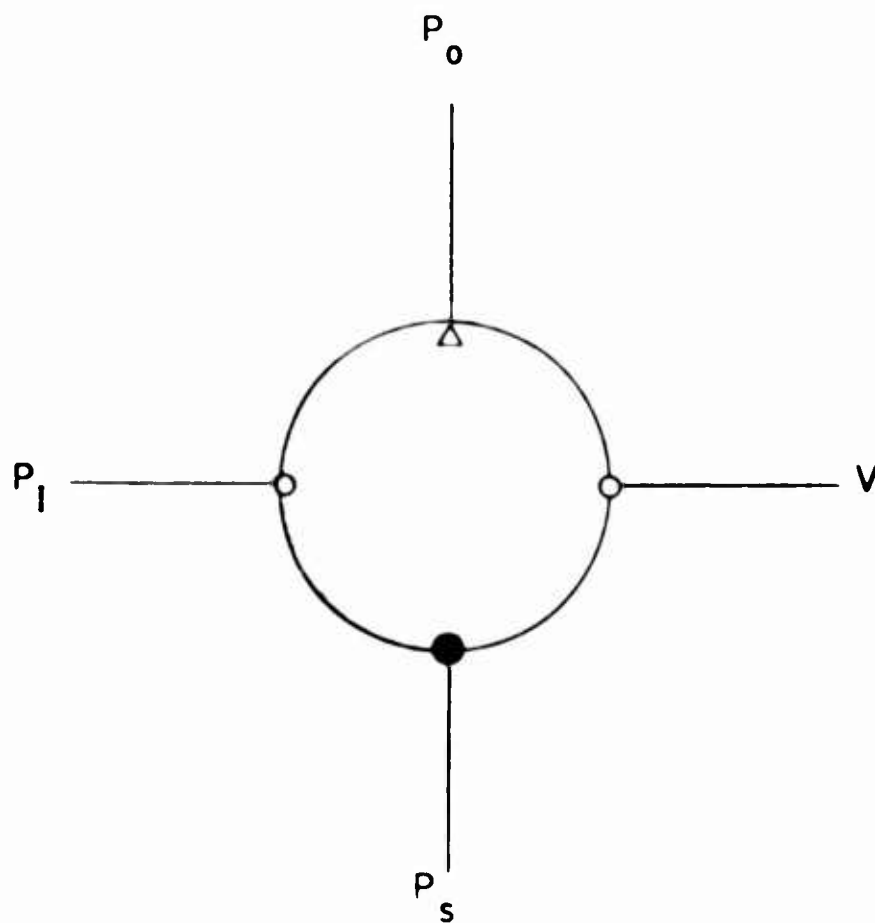
SYMBOL	SUPPLY PRESSURE	
	AMBIENT PRESSURE	
○	7.0	
△	3.5	



FREQUENCY, cps

FIGURE 23

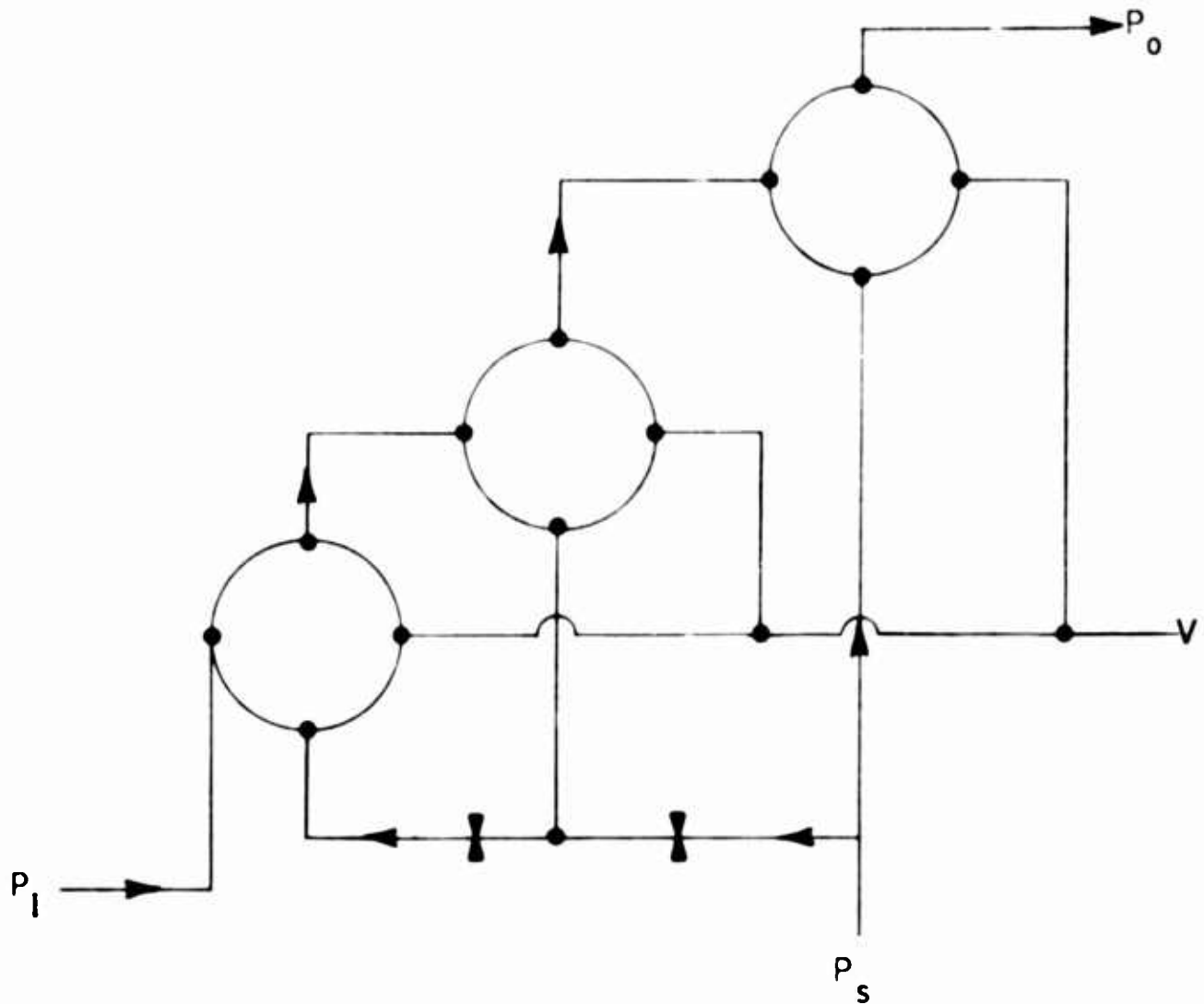
## SCHEMATIC DIAGRAM OF VORTEX AMPLIFIER



$P_i$  = SIGNAL PRESSURE  
 $P_s$  = POWER SUPPLY  
 $P_o$  = OUTPUT PRESSURE  
 $V$  = VENT

FIGURE 24

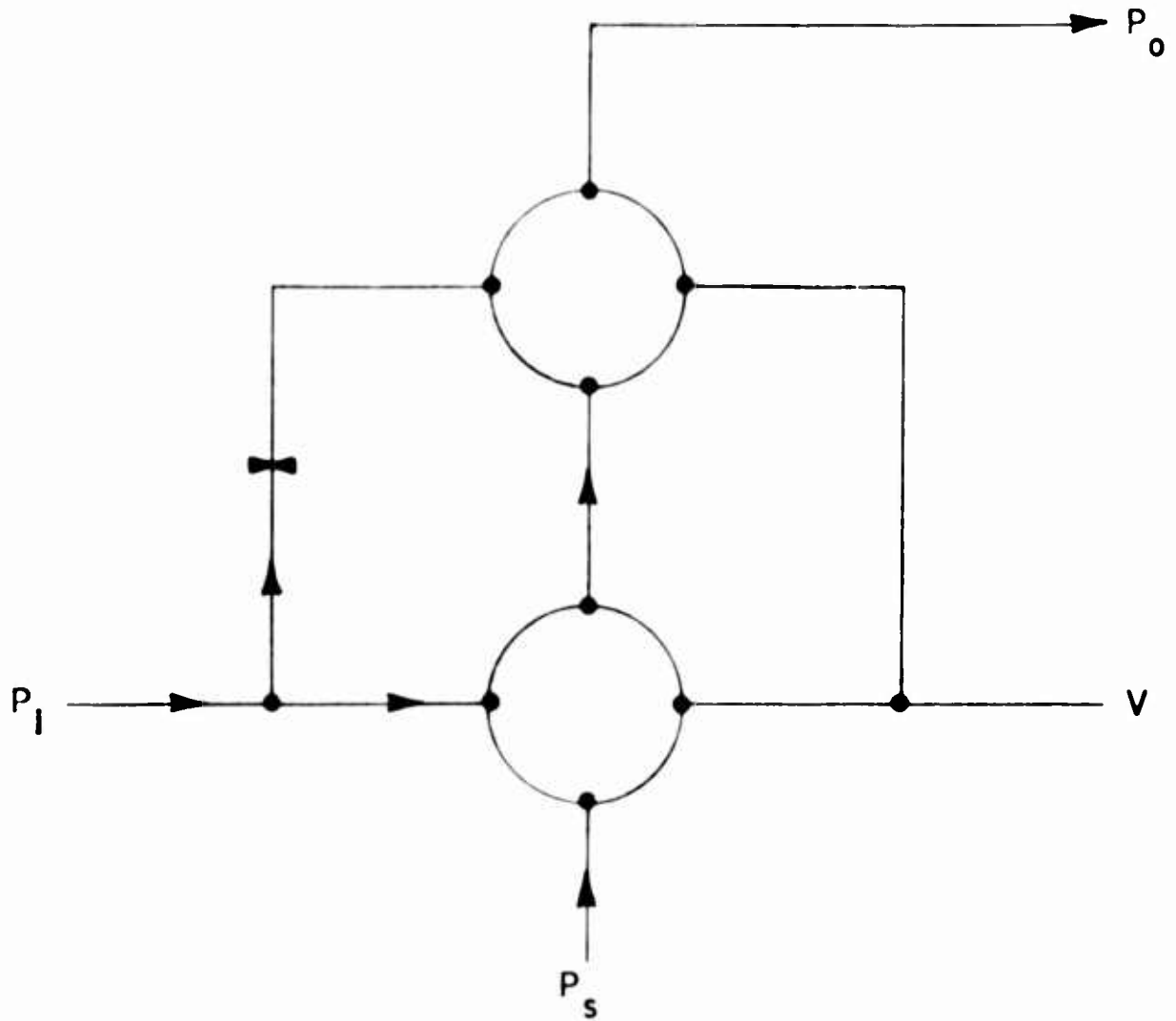
## THREE STAGE "SERIES" CONNECTION CIRCUIT



$P_I$  = SIGNAL PRESSURE  
 $P_S$  = POWER SUPPLY  
 $P_O$  = OUTPUT PRESSURE  
 $V$  = VENT

FIGURE 25

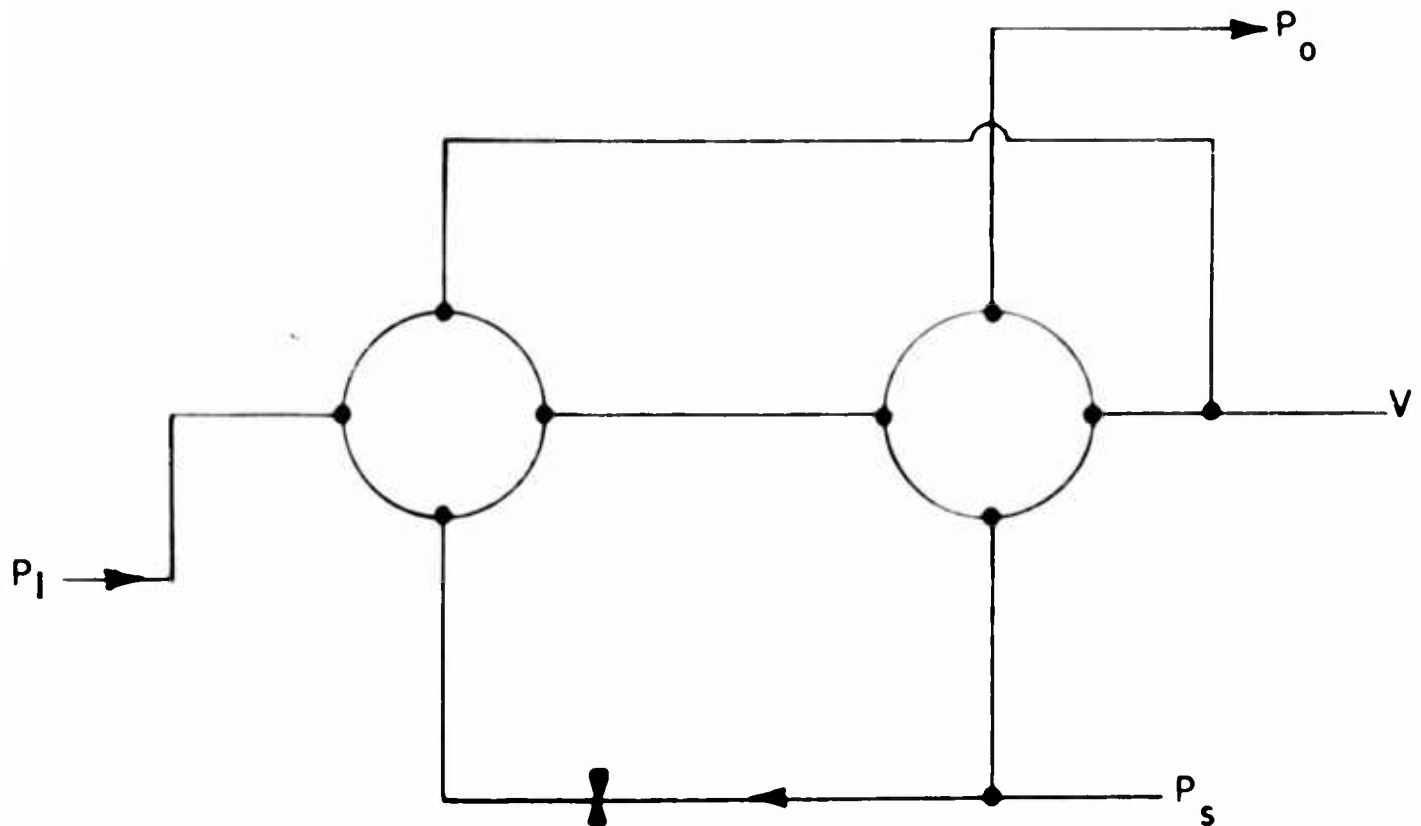
## TWO STAGE "PARALLEL" CONNECTION CIRCUIT



$P_I$  = SIGNAL PRESSURE  
 $P_S$  = POWER SUPPLY  
 $P_O$  = OUTPUT PRESSURE  
 $V$  = VENT

FIGURE 26

## TWO STAGE "SERIES-INVERTED" CONNECTION CIRCUIT



$P_I$  = SIGNAL PRESSURE  
 $P_s$  = POWER SUPPLY  
 $P_o$  = OUTPUT PRESSURE  
 $V$  = VENT

FIGURE 27



# PRESSURE GAIN CHARACTERISTICS - LINEAR REGION

SUPPLY PRESSURE 70 psia

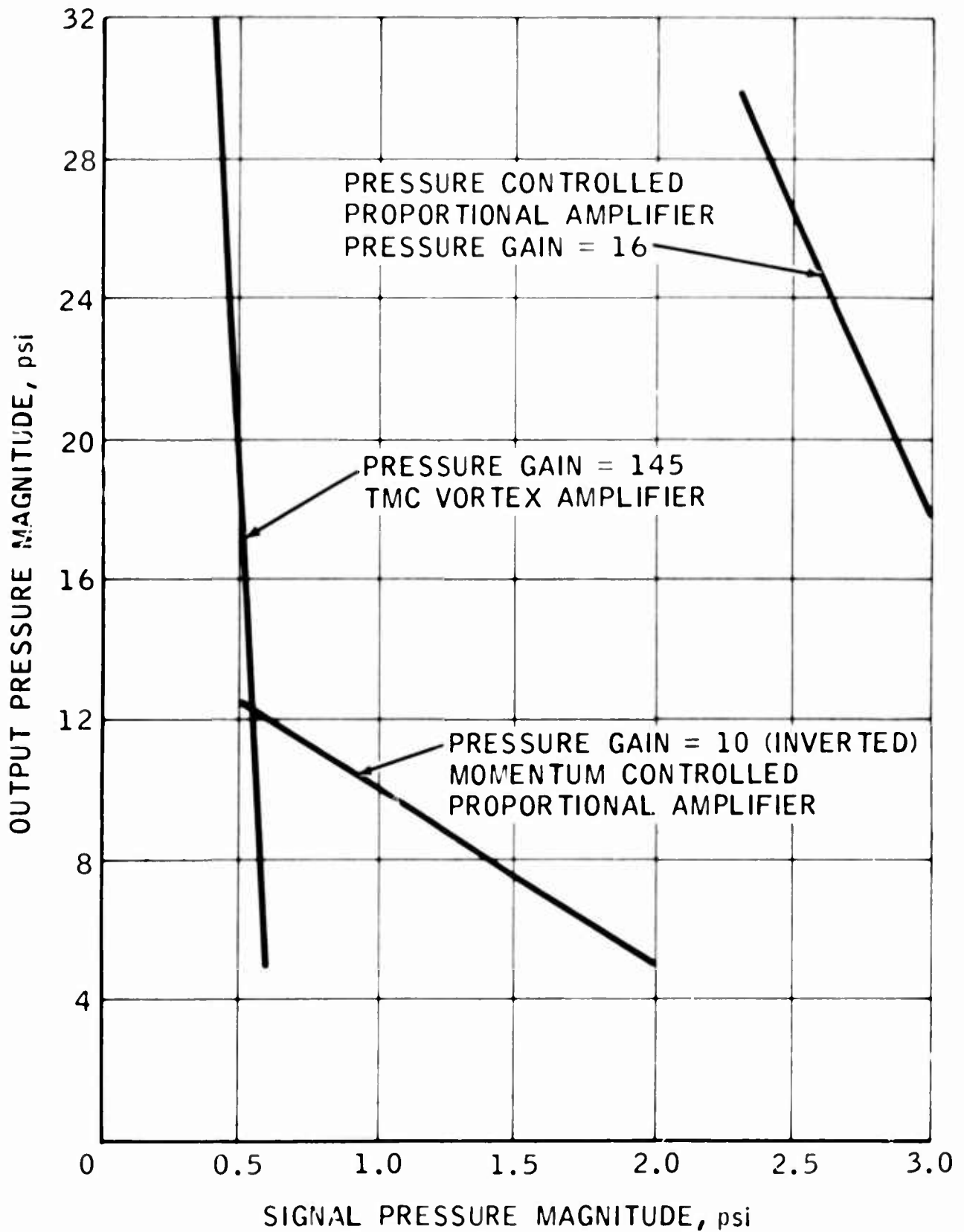


FIGURE 28

# COMPARISON OF PRESSURE RECOVERY FOR THREE FLUID AMPLIFIERS

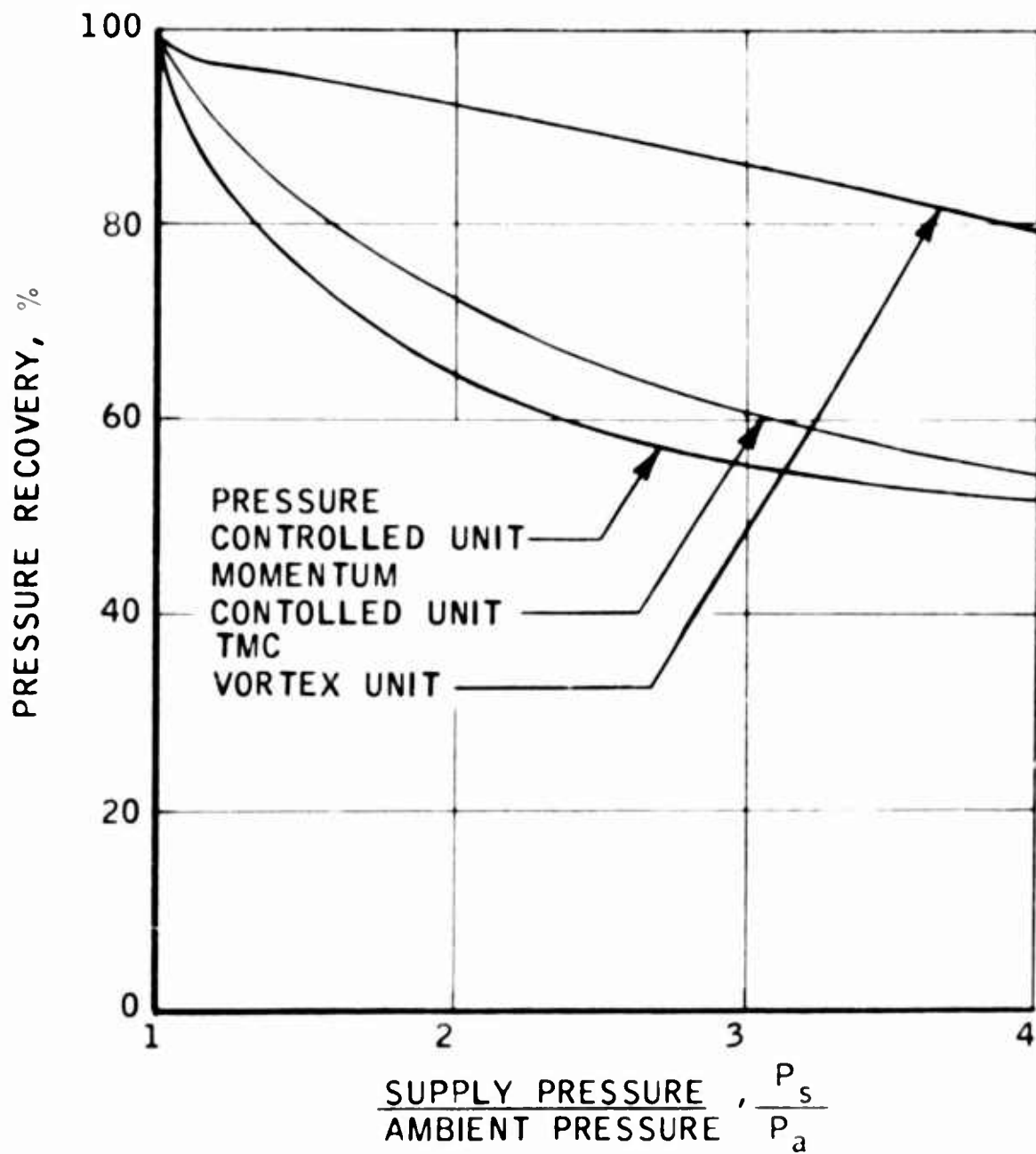


FIGURE 29

COMPARISON OF PRESSURE RECOVERY  
FOR THREE FLUID AMPLIFIERS

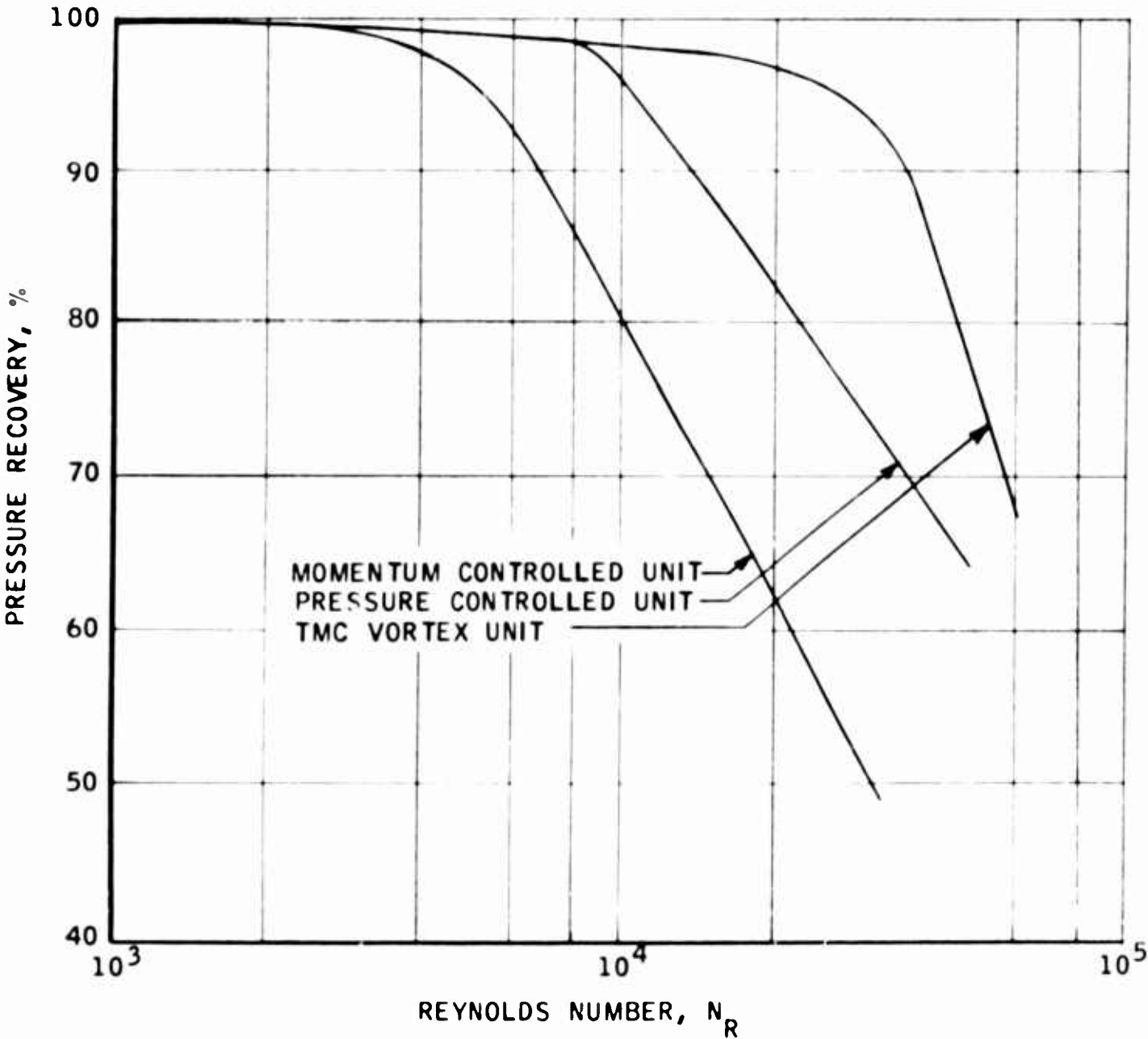


FIGURE 30

# CHARACTERISTICS OF A VORTEX FLUID THROTTLE

by

David P. Miller

of

Research Laboratories  
United Aircraft Corporation

## ABSTRACT

Experimental studies were conducted to determine performance characteristics of a fluid throttle in which secondary air is injected upstream of the nozzle throat tangentially to the wall so as to produce a vortex in the converging section. Conservation of angular momentum requires that the swirl which is produced by the injection must increase through the convergent section of the nozzle. As a result, the axial flow rate is reduced by the flow being forced to follow a helical path of continuously decreasing pitch and by the loss in total pressure resulting from the viscous turbulent mixing of the secondary and primary flows. Data are presented showing static pressure at the wall and pitot pressure along the centerline of the cylindrical chamber ahead of the nozzle as a function of injectant total pressure. The effect of the number and area of the injection ports and of the injection Mach number on the throttling effectiveness of the vortex throttle is also presented. The data are compared with an approximate inviscid theory for swirling flow through a nozzle and its applicability to predicting vortex throttle performance is discussed. Finally, the data for the vortex throttle are compared with the data for a fluid throttle in which air was injected into the throat of a similar nozzle from a circular annulus radially and upstream at angles of 60 and 45 deg relative to the direction of flow.

## INTRODUCTION

Methods for controlling mass flow by pneumatic means are frequently an integral part of systems using fluid amplification elements. Two types of these no-moving-part fluid throttles have been proposed. Throttling action is achieved in one type by reducing the effective flow area of the throat of a nozzle by injecting secondary fluid in an approximately radial direction from an annulus surrounding the throat. This throat injection throttling scheme

has been studied and reported (Ref. 1) as applied to the rocket thrust magnitude control problem. Throttling or flow modulation is achieved in a second type from the effects resulting from establishing a free vortex in the converging section of a nozzle. With no control flow present, the primary flow enters the vortex chamber ahead of the nozzle and passes through the nozzle with little resistance. When a control flow is injected tangentially to the wall of the chamber, a vortex is established. The effective resistance to the primary flow is increased through the rise in back pressure created by the intensification of the swirl through the converging section of the nozzle. Because of the high pressure drop from the outer circumference of the vortex chamber to the centerline, the throttling characteristics of this device are dependent upon the location of the primary flow inlet in the vortex chamber. In most applications conceived to date (Ref. 2), the primary flow is introduced radially into the vortex chamber, that is, perpendicular to the axis of the nozzle. In the throttle considered in this study, the primary flow is introduced on the axis of the vortex chamber. One possible advantage of the use of radial primary inflow is that higher back pressures can be produced at the periphery of the vortex for control of the primary stream, while a disadvantage is that the resistance to the primary flow at zero control flow is higher than for the one considered in this study.

Theoretical analysis of the vortex throttle is complicated by the strong viscous interactions and turbulent mixing between the secondary and primary streams. An approximate solution for the potential swirling flow through a nozzle has been published (Ref. 3) and is useful in that it may represent an upper bound of what can be achieved under ideal conditions even though it does not consider the actual physical mechanism by which the swirl is imparted to the flow ahead of the nozzle. Since theory is not developed to the stage of being useful in predicting the performance characteristics of the vortex throttle, it is generally necessary to determine experimentally the optimum throttle design for a particular application.

The object of this UAC Research Laboratories' Corporate-sponsored study was to study experimentally the general performance and pressure characteristics of a vortex fluid throttle in which the primary air stream is introduced into the vortex chamber at the axis of the nozzle.

## EXPERIMENTAL PROGRAM

A schematic diagram and photograph of the vortex throttle model tested in the experimental program are presented in Figs. 1 and 2, respectively. Primary air was introduced into the cylindrical chamber ahead of the nozzle through a bellmouth located on the axis of the cylindrical chamber. A bucket-shaped baffle plate was located approximately 3 in. from the bellmouth exit in order

to break up a free-jet that was created by the primary flow. The cylindrical chamber preceding the nozzle, termed the vortex chamber, had a length to diameter ratio of 2.7 and was joined through a smooth contour to the convergent exhaust nozzle. The diameter of the throat of the nozzle and of the vortex chamber were 2 in. and 6 in., respectively. The secondary control air or injectant flow from the bellmouth was supplied through 4 hoses to the plenum chamber surrounding the vortex chamber (see Fig. 2). The secondary air was injected through rectangular ports located around the periphery of interchangeable injection inserts. A photograph of a typical insert is shown in Fig. 2 and the geometrical characteristics of the inserts tested are summarized in the following table:

<u>Insert</u>	<u>No. of Ports, N</u>	<u>Width of Ports, b</u>	<u>Total Injection Area, <math>A_i</math></u>
1	3	0.8 in.	0.428 in. <sup>2</sup>
2	4	"	0.426
3	4	"	0.545
4	4	"	0.747

As shown in Fig. 1, wall static taps and centerline pitot probes were located approximately 3.0, 6.0, and 8.5 in. upstream of the injection ports. An additional pitot probe was located 9.5 in. upstream of the injection ports and directed tangentially in order to sense the tangential component of velocity at that station. Static pressures were also measured at the wall of the nozzle throat and in the vacuum chamber downstream of the nozzle. The primary and injectant flow rates were measured using bellmouths having 0.5 and 0.75 in. diameters, respectively.

Air having a stagnation temperature of approximately 80 F and a dew point of less than -20 F was introduced into the primary and secondary flow bellmouths from a 400 psia compressor capable of continuously delivering 5 lb/sec. For these tests the air was throttled so that maximum total pressures for the primary and secondary flow were approximately 130 and 110 psia, respectively. The flow from the nozzle was exhausted into a 4 in. diameter cylindrical chamber that was evacuated by laboratory vacuum pumps.

Tests were conducted by increasing the injectant flow rate in small increments while maintaining a constant primary flow rate. The flow through the primary bellmouth was generally choked and nominal values of 0.10, 0.15, and 0.30 lb/sec were tested. Initial increments in injectant flow rate were about 0.08 lb/sec and were increased with increasing injectant flow rate to increments of about 0.15 lb/sec at the maximum flow rates of about 0.90 lb/sec. Tests were conducted for both a constant exhaust pressure  $P_E$  of approximately

1.0 psia and a variable exhaust pressure in which the ratio of the exhaust pressure  $P_E$  to the wall static pressure  $P_W$  was held constant at values of 0.6, 0.7, and 0.8.

## DISCUSSION OF RESULTS

### Pressure Characteristics

Pressure characteristics of the vortex throttle are presented in Figs. 3 through 7. Figure 3 shows the centerline pitot pressure and the wall static pressure as a function of the injectant total pressure  $P_{T_i}$  for axial stations  $X_u$  located 3.0, 6.0, and 8.5 in. upstream of the injection station. The tests were conducted at a constant primary flow rate  $W_p$  of 0.15 lb/sec and with an insert having a total injection area of 0.545 in.<sup>2</sup>. It is noted that the wall static pressures were nearly independent of axial position and tended to increase linearly with the total pressure of the injectant. In contrast, the centerline pressures exhibited a nonlinear variation with injectant pressure and increased slightly with upstream position. The centerline pressures were essentially the static pressures induced by the vortex since the high contraction ratio of the nozzle resulted in a nominal axial Mach number ahead of the nozzle of only 0.065 so that the ratio of the static to total pressure of the axial component of velocity was 0.997. Comparison of the wall and centerline pressures shows that a relatively strong vortex was induced upstream of the injection position and that its strength was diminished only slightly over the length of the vortex chamber through viscous dissipation. Further evidence of the high strength of the induced vortex is the fact that for this test condition a tangential Mach number of 0.43 existed at a position  $X_u = 9.5$  in. and 0.5 in. from the wall at an injectant total pressure of 84.5 psia.

The effect of the area of the injection ports on the pressure at the centerline and at the wall for axial station  $X_u = 3.0$  in. is presented in Fig. 4. For this case the primary flow has a constant value of  $W_p = 0.15$  lb/sec. Both the centerline and wall pressure increased significantly with injection area at a given value of injectant pressure. Although not shown, both the centerline and wall pressure, and hence the strength of the vortex, have been found to correlate very well with injectant weight flow at a constant value of primary flow. For the three cases shown in Fig. 4 the injectant flow was choked for  $P_{T_i} > 10$  psia so that for this range of injectant pressure the injectant flow rate was proportional to the injectant total pressure  $P_{T_i}$  and a flow coefficient. The flow coefficient is the ratio of the actual mass flow rate through the port to the mass flow rate at the same pressure conditions for the ideal case in which there would be no boundary layer or flow separation on the walls of the port. The flow coefficient of the injection ports was found to be about 0.780 for all cases in which the flow

was choked. Typical values for the flow coefficient of a contoured nozzle or bellmouth would be between 0.97 and 0.99. The relatively low value for the small rectangular injection ports results from the fact that the inlets to the ports had sharp edges rather than a smooth contoured surface.

The centerline pitot pressure and the wall static pressure at the  $X_U = 3.0$  in. station are presented in Fig. 5 for several values of primary flow rate. Data are shown for constant primary flow rates of 0, 0.15, and 0.30 lb/sec in which the area of the injection port was 0.545 in.<sup>2</sup>. Again, as also noted for the case presented in Fig. 3, the static pressure at the wall increased nearly linearly with injectant pressure at each of the primary flow rates in the range which the injection flow was choked ( $P_W/P_T \leq 0.528$ ) and increased uniformly with primary flow rate at a given injectant pressure. From Fig. 5 it is apparent that the centerline pressure exhibits a greater sensitivity to the primary flow rate than does the wall static pressure and that the nonlinear variation of centerline pressure with injectant pressure is produced by the primary flow. These effects on the centerline pressure are due mainly to the primary flow being forced into the low pressure core of the vortex by the large radial pressure gradient.

For the data presented in Figs. 3 through 5 the exhaust pressure  $P_E$  had a constant value of about 1.0 psia so that the axial flow through the nozzle remained choked at all times. Figure 6 presents the variation of the centerline pitot pressure and wall static pressure with injectant pressure and shows the effect of holding the ratio of exhaust pressure to wall static pressure  $P_E/P_W$  constant at several values for which the nozzle was unchoked. The data show that the centerline pressure  $P_{CL}$  ahead of the nozzle was lower than the exhaust pressure  $P_E$  (seen by comparing  $P_{CL}$  with the corresponding value of  $P_W$  multiplied by the value of  $P_E/P_W$ ). For these tests in which the nozzle was unchoked it is apparent that the flow was reversed along the axis of the nozzle since the exhaust pressure  $P_E$  was greater than the centerline pressure  $P_{CL}$  at  $X_U = 3.0$  in. It is important to recognize that reverse flow may be created in a nozzle which is initially unchoked, and a nozzle which is initially choked may become unchoked in the core region through the action of the vortex. The static pressure outside the nozzle then can propagate through the nozzle to affect the flow in the vortex chamber.

The variation of the wall and centerline pressure at  $X_U = 3.0$  in. and of the static pressure  $P_p$  in the inlet duct of the primary flow with injectant flow rate at zero primary flow rate is presented in Fig. 7. It is noted that these pressures correlate very well with the injectant flow rate. The throttling effectiveness of the vortex throttle probably depends on the manner in which the primary flow is introduced into the vortex chamber. Consider a case in which the primary flow would be introduced into the vortex chamber through a port having an area larger than that of the nozzle and with the back pressure in the primary flow inlet equal to the static pressure at the wall of the vortex chamber. As the injectant flow rate is increased,



the primary flow rate would be reduced. The primary flow would be shut off when the static pressure at the wall equals the total pressure in the primary flow source. For the geometry of the test model and the slope of the wall static pressure curve in Fig. 7, the primary flow would be shut off when the ratio of the injectant flow rate to the initial primary flow rate (for a choked nozzle) before injection is 0.40. On the other hand, the throttle effectiveness can be interpreted from the standpoint that the primary flow enters through a small inlet on the axis of the chamber as on the test model. From the slope of the  $P_p$  curve, the ratio of the injectant flow to initial primary flow when the primary flow is shut off would be 9.72. While this ratio appears to be relatively large, it is directly dependent upon the area of the primary flow port (in this case  $A_p = 0.196 \text{ in.}^2$ ). If the measured value of the inlet pressure  $P_p$  is independent of the area of the inlet port, then the ratio of  $W_i/W_p$  when the primary flow is shut off would be  $0.607 A_N/A_p$  for  $A_p \leq A_N$ . Actually, the slope of the  $P_p$  curve is affected somewhat by the diameter of the primary flow inlet port since this pressure adjusts to some average value over the port. This can be seen in Fig. 7 where the pressure  $P_p$  is noted to be between the pressure at the wall and the pressure on the centerline at  $x_u = 8.5 \text{ in.}$  If the vortex throttle is to be used as a flow rate control, rather than a pressure control for a constant primary flow rate, the vortex throttle may operate more effectively if the primary flow is introduced at the periphery of the vortex chamber.

### Weight Flow Characteristics

The primary and injectant weight flow characteristics of the vortex throttle are presented in Figs. 8 through 11. For the data presented in these figures the flow through the nozzle was choked and for a given set of data the primary flow rate was constant. As noted in the previous discussion the injectant flow was generally unchoked for injectant pressures less than 10 psia; the exact injectant pressure at which the flow became choked was dependent upon the area of the injection ports and the primary flow rate. Before examining these results in detail, it is necessary to discuss the significance of the parameters that are employed in the figures. In Figs. 8 and 9 both the primary and injectant flow rates are normalized with respect to a weight flow parameter  $W^*$ . This parameter is equivalent to the flow rate through the nozzle of the throttle for a choked flow condition at a reference pressure. For the general case in which the throttle is operated from a primary flow source having a constant total pressure, the primary flow ratio  $W_p/W^*$  is employed to represent the ratio of the instantaneous primary flow rate to the primary flow rate when the injectant flow is zero. When the throttle is supplied by a primary flow source having a constant flow rate, as was the case for the throttle tested in this study, then the flow parameter must be based on some reference pressure. For the data presented in Figs. 8 through 11 the parameter  $W^*$  is based on the wall static pressure, that is, the throttle is considered as a pressure control. Consequently,

the primary flow ratio  $W_p/W^*$  is a parameter which is inversely proportional to the static pressure on the wall of the vortex chamber. Although not shown, the primary flow ratio  $W_p/W^*$  was found to correlate with the injectant flow ratio  $W_i/W_p$  for a given injection configuration, that is, independent of the primary flow rate  $W_p$ . Therefore, even though a given set of data were measured at a constant primary flow rate  $W_p$ , the primary flow ratio  $W_p/W^*$  of the data presented in Figs. 8 through 11 may also be interpreted as the reduction in primary flow rate ( $W^*$  constant) for a vortex throttle in which the flow rate and pressure of the primary flow are related in such a way that the static pressure at the wall of the vortex chamber remains constant. As will be shown, employing the parameter  $W^*$  is also useful for showing the effects of the injection port area and the injection Mach number on the throttling effectiveness.

The variation of the ratio of the primary flow ratio  $W_p/W^*$  with the injectant flow ratio  $W_i/W^*$  is presented in Fig. 8 and shows the combined effect of varying injection area and injection Mach number. Improved throttling performance is indicated for decreasing area of the injection ports. This increased throttle effectiveness probably can be attributed to the fact that the effective injection Mach number  $M_i^*$  increases with decreasing injection area as indicated in Fig. 8. Actually, since the injection ports were not contoured to a convergent-divergent shape, the injected flow probably remained at the supersonic Mach number  $M_i^*$  at most for a distance equivalent to ten times the height of the injection port and then shocked down to the local static pressure. This suggests however that improved throttle performance may be achieved by using convergent-divergent ports so as to expand the injection flow isentropically to supersonic Mach numbers. Use of this supersonic injection technique would also improve operating efficiency by reducing the total pressure loss of the injectant.

The two graphs in Fig. 9 show the influence of the primary weight flow and of the number of injection ports on the weight flow parameters. Doubling of the primary weight flow is seen to have no significant influence on the effectiveness of the throttle. The second graph shows that only a very slight improvement in the throttling performance was realized when the number of injection ports was increased from three to four while the total area of the injection ports was held constant.

### Analytical Considerations

An approximate solution for swirling potential flow through a nozzle is presented in Ref. 3. Since potential flow is assumed, the tangential velocity is inversely proportional to the radius. Therefore the tangential velocity increases with decreasing radius until the pressure, and therefore the density, become zero. The value of this minimum radius below which the flow ceases to exist, and hence the effectiveness of the throttle, is related to the magnitude

of the swirl imparted to the flow. The chief assumption in this solution is that the radial component of velocity is zero, so the boundary condition that the flow must be tangent to the nozzle wall is not exactly satisfied. In addition, the important viscous effects and the physical mechanism by which the swirl is imparted to fluid are not considered. Despite this departure of the assumed flow model from the actual flow process, the theory is useful in that it may represent an upper bound of the throttling effectiveness that can be achieved under the most ideal conditions.

A comparison between the measured and predicted effectiveness of the vortex throttle is presented in Fig. 10. Again, the experimental results must be interpreted either as a pressure control for a constant primary flow rate or as a flow control for a throttle in which the pressure and flow rate of the primary flow are related in such a way that the static pressure at the wall remains constant. In comparing the data with the theory the total mass flow through the nozzle must be considered, that is, the sum of the primary and secondary flows. Plotting the data on this basis shows in Fig. 10 that the total flow parameter  $(W_i + W_p)/W^*$  approaches asymptotically a value of about 0.43 with increasing injectant flow rate. On the other hand, the theory predicts that the total flow parameter is directly related to the tangential Mach number at the wall of the nozzle throat. It is noted in Fig. 10 that the data apparently approach a value of throttle effectiveness equivalent to that predicted for a throat tangential Mach number slightly less than 0.7. Hence the comparison of the data with the theory may also indicate that improved throttle effectiveness may be possible with supersonic injection. This increase in the tangential Mach number of the flow could be attained through the use of contoured injection ports.

#### Comparison of Performance Characteristics of Fluid Throttles

The performance characteristics of fluid throttles generally are strongly dependent upon the relationship between the inlet pressure and flow rate of the primary and secondary flows. Consequently, the inlet flow conditions must be clearly defined when comparing the performance characteristics of two types of fluid throttles. In certain applications the total pressure of the primary flow may be constant so that the flow rate is variable or the flow rate may be constant so that the total pressure is variable. Also, a combination of these two conditions may exist as in the case of applying a fluid throttle to control the thrust magnitude of a solid propellant rocket engine. Since the burning rate of the propellant is proportional to the chamber pressure raised to a constant power (termed the fuel's pressure exponent), increasing the injectant flow rate not only increases the pressure of the primary flow source but also increases the primary mass flow rate through increased burning of the propellant. In the case of the vortex throttle the presentation of general performance curves is further complicated by the large variations in pressure and velocity throughout the vortex chamber which result in the throttle performance being

dependent upon the way in which the primary flow is introduced into the vortex chamber. In fact, basic studies of free vortex flow in cylindrical cavities have shown that due to end wall effects the characteristics of the vortex itself are strongly dependent upon the geometry of the chamber. Hence the presentation and comparison of fluid throttle data represents a difficult problem and one that requires further investigation.

#### Comparison with the Throat Injection Fluid Throttle

Test data for a fluid throttle in which air was injected into the throat of a nozzle from a circular annulus radially and upstream at angles of 60 and 45 deg relative to the direction of flow are presented in Fig. 11. These data, which were measured in conjunction with a previous test program at the Research Laboratories, are for a model having nozzle and tank dimensions identical to those of the model used for the vortex throttle studies. It was found that injecting the control fluid into the throat of the nozzle increased the pressure uniformly throughout the chamber ahead of the nozzle. The throttling performance was independent of radial location at which the primary flow was introduced into the chamber ahead of the nozzle. Therefore, the data for the throat injection throttle may be interpreted either as a device that controls the primary flow from a constant pressure primary flow source or for one that controls the pressure in the chamber when the primary flow rate is constant. Of the three injection angles considered, it is seen in Fig. 11 that the best throttling performance was obtained when the control air was injected at the intermediate angle of 60 deg.

A comparison between the throat injection throttle and the vortex throttle also is shown in Fig. 11. Because the data of the vortex throttle model cannot be related to the total pressure of the primary flow for a general configuration, the throttle effectiveness of the two devices can only be directly compared in the case of a pressure control for a constant primary flow rate or as a flow regulator for the case in which the pressure and flow rate of the primary flow are related so that the static pressure at the wall of the vortex chamber remains constant. The data in Fig. 11 show that for small values of the injection flow ratio  $W_i/W$  the throat injection throttle is considerably more effective than the vortex throttle. The greater effectiveness of the throat injection throttle at low values of injection flow ratio is due to the fact that the injectant operates directly on the primary flow to reduce the effective throat area of the nozzle whereas the injectant of the vortex throttle operates indirectly on the primary flow by imparting swirl to it. As a result, the vortex throttle does not become more effective than the throat injection throttle until the injectant flow ratio is large enough to establish a strong vortex in the converging section of the nozzle. The dependence of the vortex throttle effectiveness upon the strength of a well-established vortex also accounts for the high degree of nonlinearity exhibited by the data.

# LIST OF SYMBOLS

$A_i$	Total area of injection ports, in. <sup>2</sup>
$A_N$	Cross-sectional area of nozzle throat, 3.14 in. <sup>2</sup>
$A_P$	Cross-sectional area of primary flow bellmouth, 0.196 in. <sup>2</sup>
$b$	Width of injection ports, 0.8 in.
$M_i^*$	Effective Mach number of injection flow
$M_T$	Mach number of tangential velocity at wall of nozzle throat
$N$	Number of injection ports
$P_{CL}$	Pitot pressure on centerline of chamber ahead of nozzle, psia
$P_E$	Exhaust pressure in chamber downstream of nozzle, psia
$P_P$	Static pressure upstream of primary flow bellmouth, psia
$P_W$	Static pressure at wall of chamber ahead of nozzle, psia
$T_T$	Total temperature, deg R
$W^*$	Flow rate parameter, $0.532 \frac{P_W A_N}{\sqrt{T_T}}$ , lb/sec
$W_i$	Injectant flow rate, lb/sec
$W_P$	Primary flow rate, lb/sec
$X_u$	Distance upstream from center of injection ports, in.
$\theta_i$	Angle between injectant flow and axis of nozzle for throat injection throttle (see Fig. 11), deg

## REFERENCES

1. Zumwalt, G. W., and W. N. Jacksonis: Aerodynamic Throat Nozzle for Thrust Magnitude Control of Solid Fuel Rockets. ARS Journal, Vol. 32, No. 12, 1962.
2. Anon.: Fluid Amplifier State of the Art. General Electric Company, Vol. I, December 1963.
3. Mager, Artur: Approximate Solution of Isentropic Swirling Flow Through a Nozzle. ARS Journal, Vol. 31, No. 8, 1961.

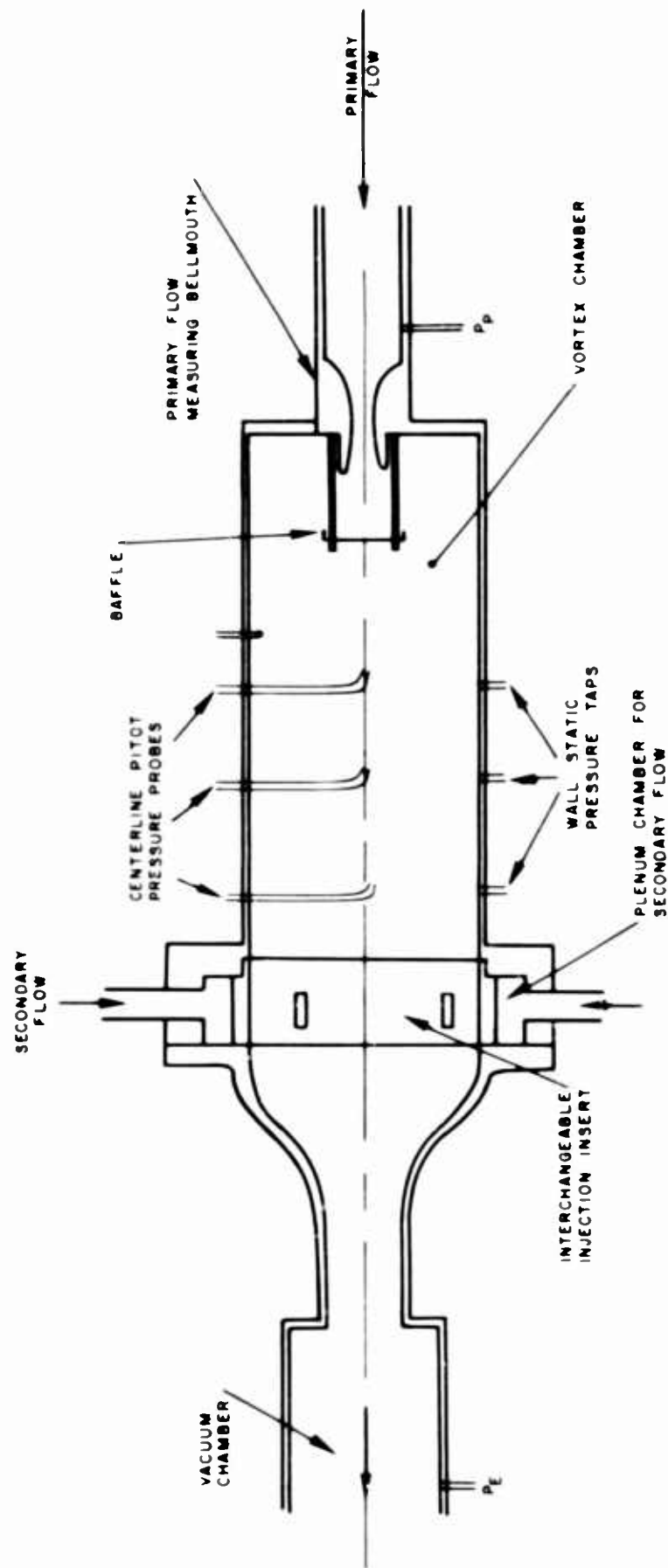
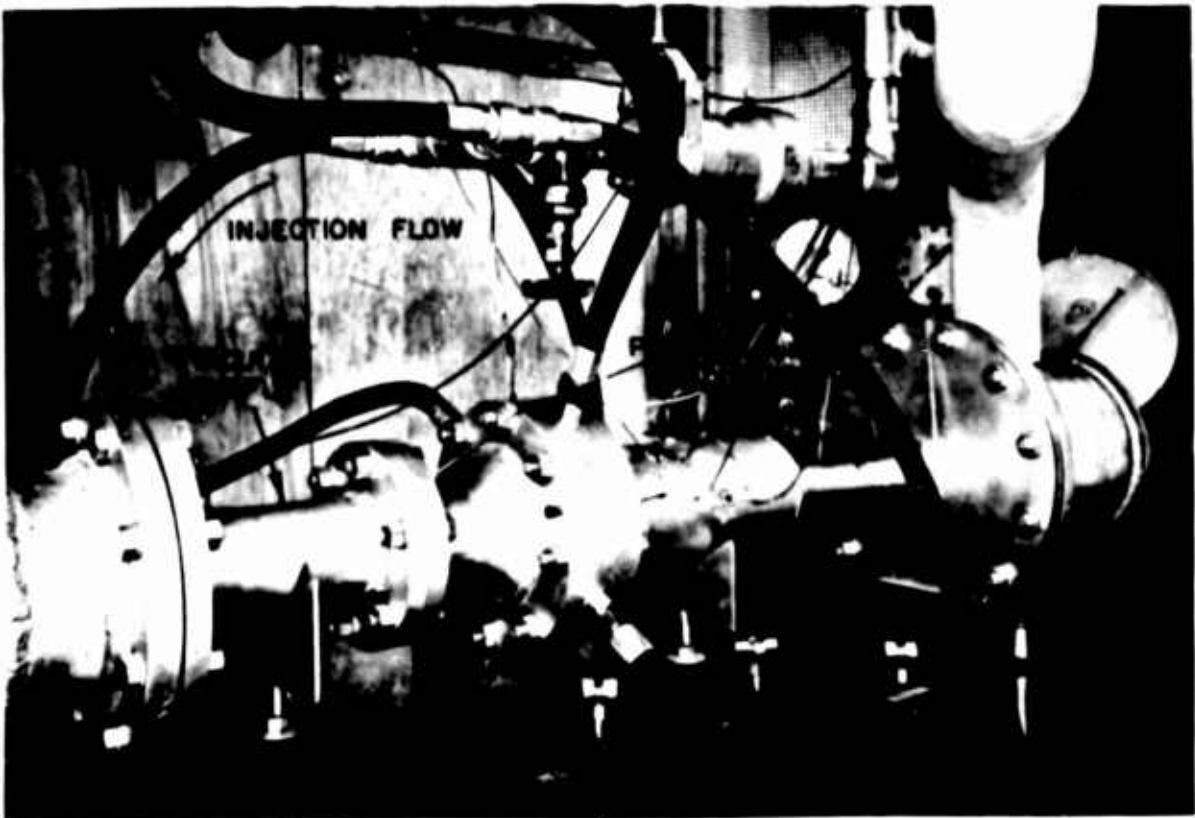


FIGURE 1 SCHEMATIC DIAGRAM OF VORTEX THROTTLE TEST RIG



TYPICAL INSERT SHOWING INJECTION PORTS

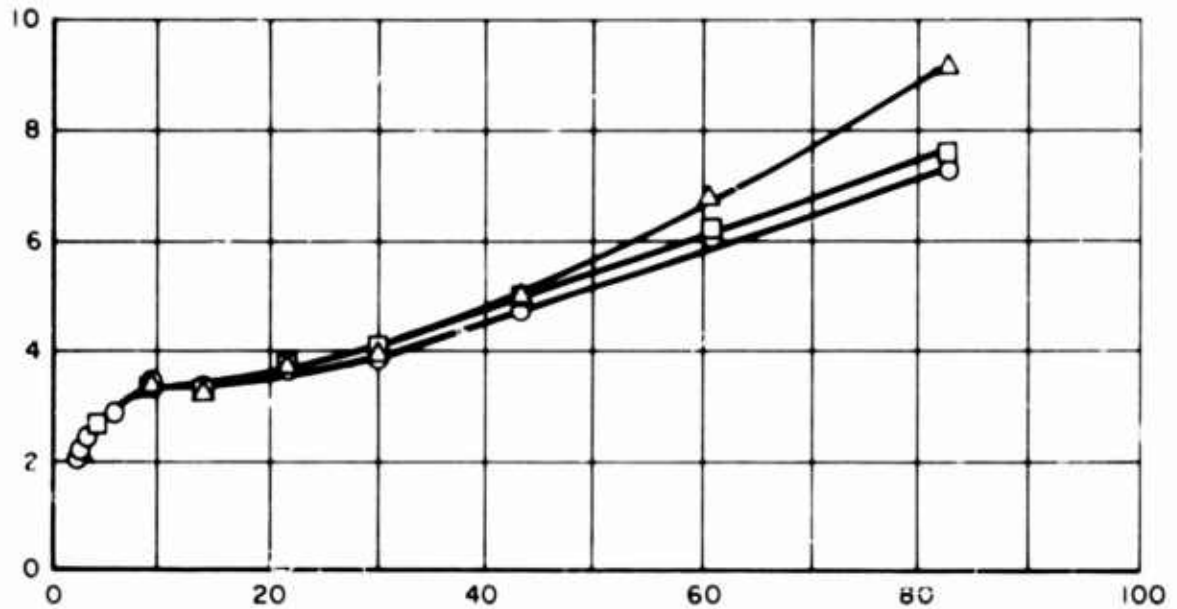
FIGURE 2 PHOTOGRAPHS OF VORTEX THROTTLE TEST RIG



AREA OF INJECTION PORTS  $A_i = 0.545 \text{ IN}^2$   
 PRIMARY FLOW RATE  $W_p = 0.15 \text{ LB/SEC}$

SYMBOL	○	□	△
AXIAL STATION, $x_u$	3.0	6.0	8.5

CENTERLINE PITOT PRESSURE,  $P_{CL}$ , PSIA



WALL STATIC PRESSURE,  $P_w$ , PSIA

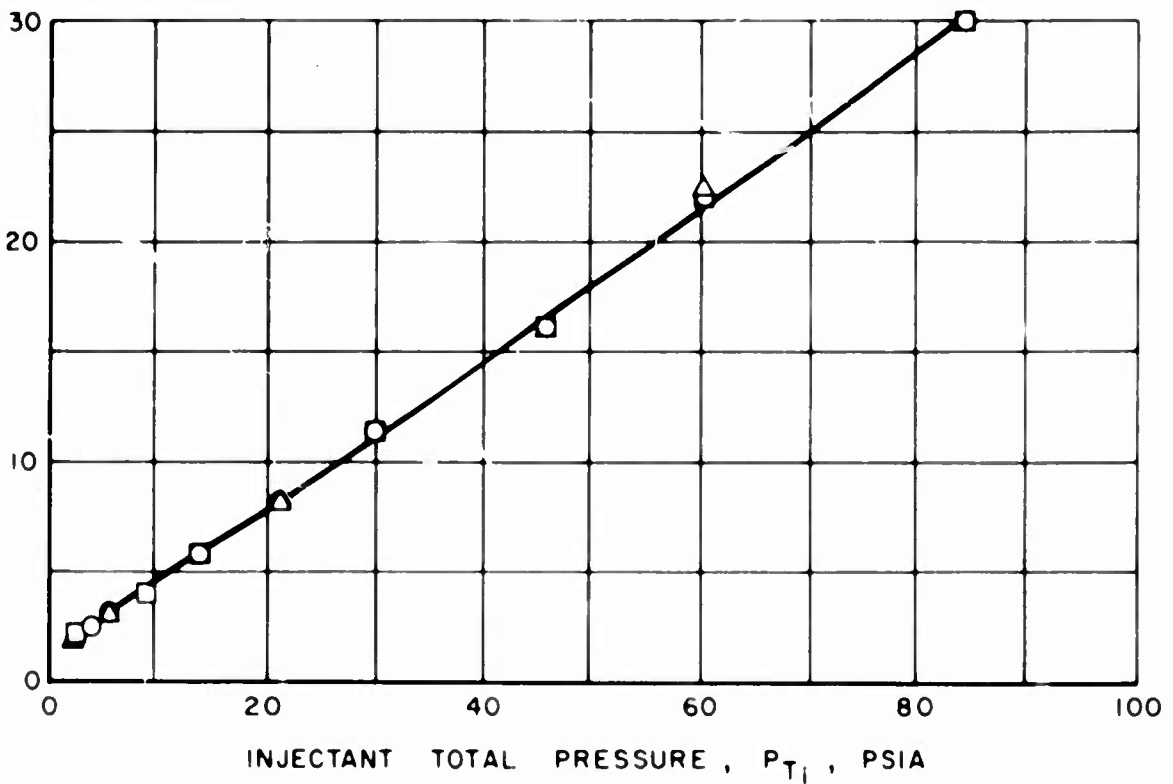
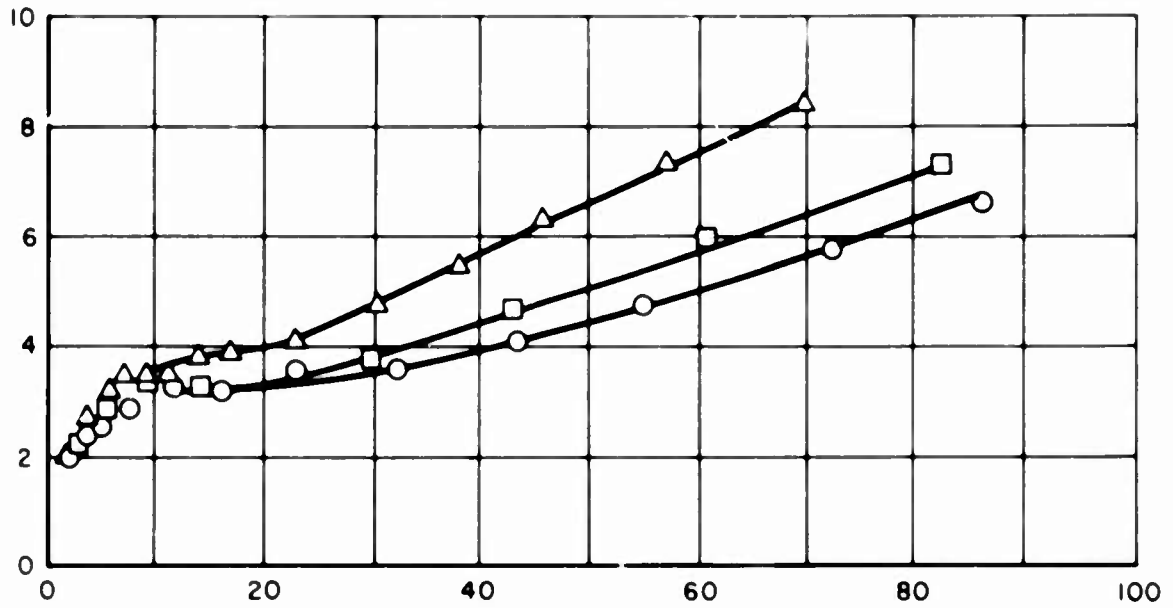


FIGURE 3 PRESSURE CHARACTERISTICS IN VORTEX CHAMBER

PRIMARY FLOW RATE  $W_p = 0.15$  LB/SEC  
 AXIAL STATION  $x_u = 30$  IN

SYMBOL	○	□	△
INJECTION AREA, $A_i$	0.426	0.545	0.747

CENTERLINE PITOT PRESSURE,  $P_{CL}$ , PSIA



WALL STATIC PRESSURE,  $P_w$ , PSIA

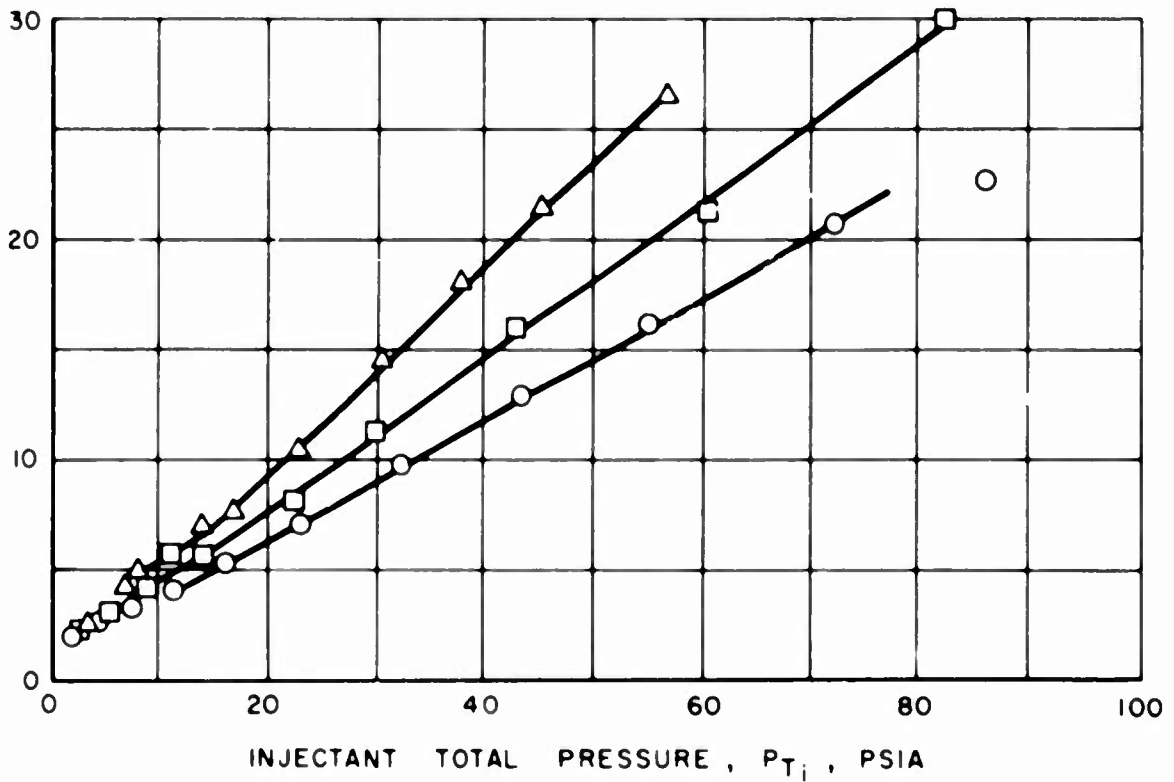
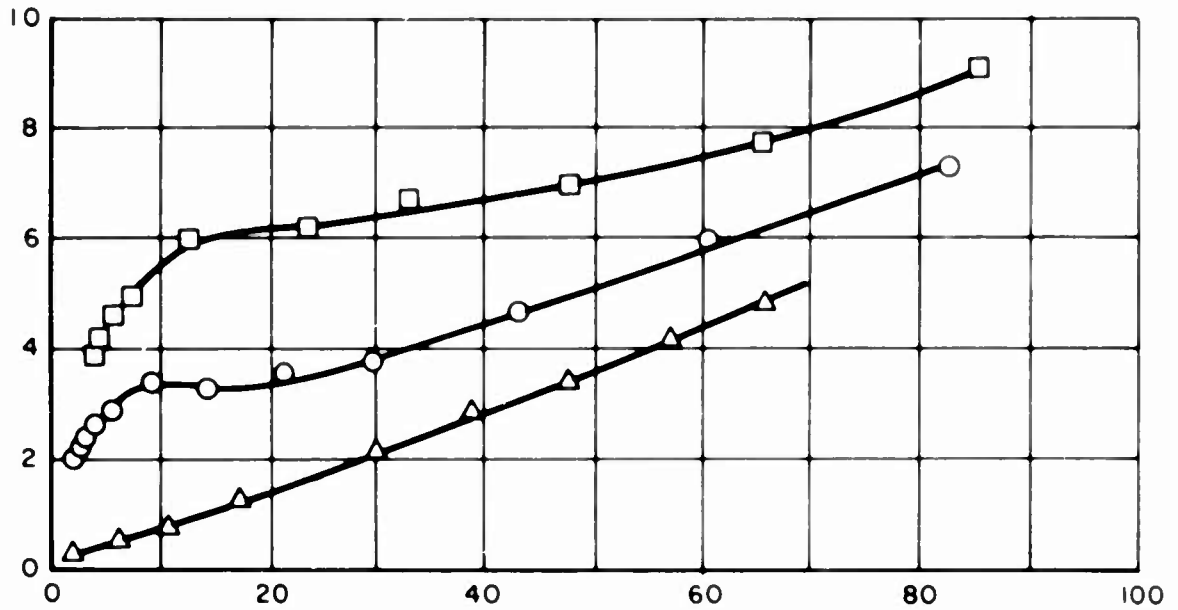


FIGURE 4 EFFECT OF AREA OF INJECTION PORTS ON CENTERLINE PITOT PRESSURE AND WALL STATIC PRESSURE

AREA OF INJECTION PORTS  $A_i = 0.545 \text{ IN}^2$   
 AXIAL STATION  $x_u = 3.0 \text{ IN.}$

SYMBOL	$\Delta$	$\circ$	$\square$
PRIMARY FLOW, $w_p$	0	0.15	0.30

CENTERLINE PITOT PRESSURE,  $P_{CL}$ , PSIA



WALL STATIC PRESSURE,  $P_W$ , PSIA

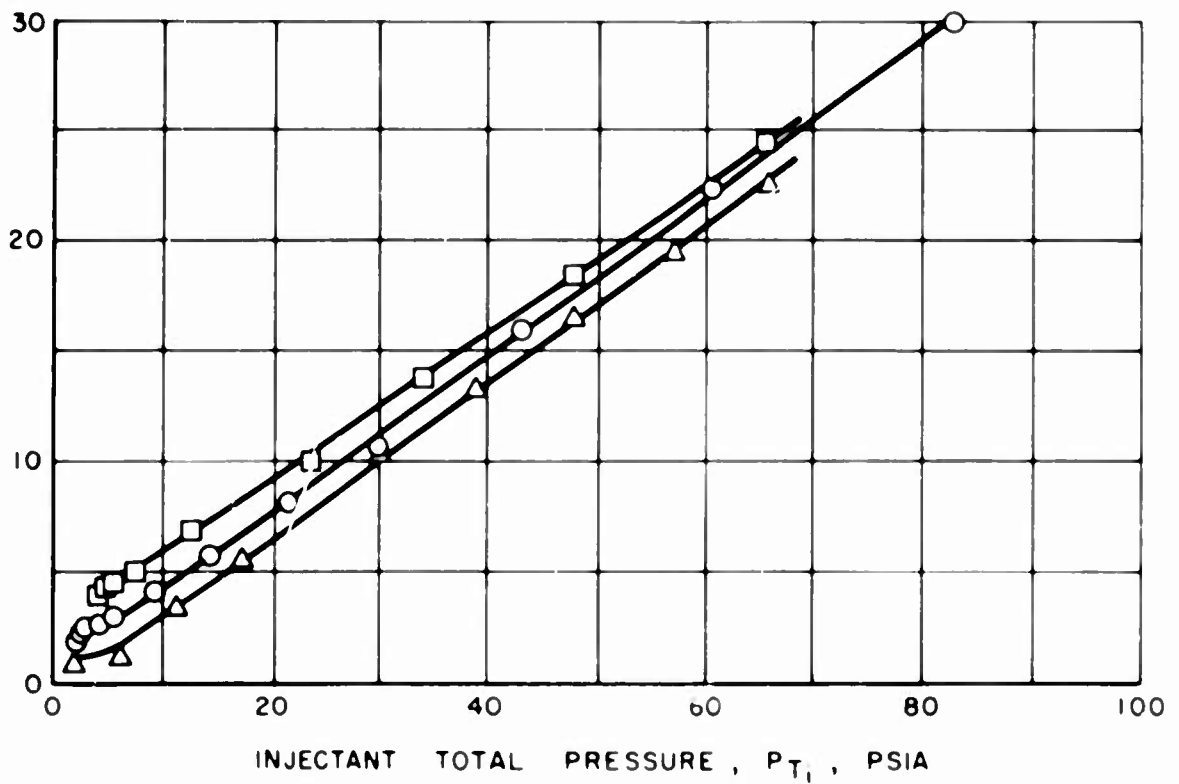


FIGURE 5 EFFECT OF PRIMARY FLOW RATE ON CENTERLINE PITOT PRESSURE AND WALL STATIC PRESSURE

PRIMARY FLOW RATE  $W_p = 0.10$  LB/SEC  
 AREA OF INJECTION PORTS  $A_i = 0.545$  IN.<sup>2</sup>  
 AXIAL STATION  $x_u = 30$  IN.

SYMBOL	○	□	◇
EXHAUST PRESSURE RATIO, $P_E / P_W$	0.6	0.7	0.8

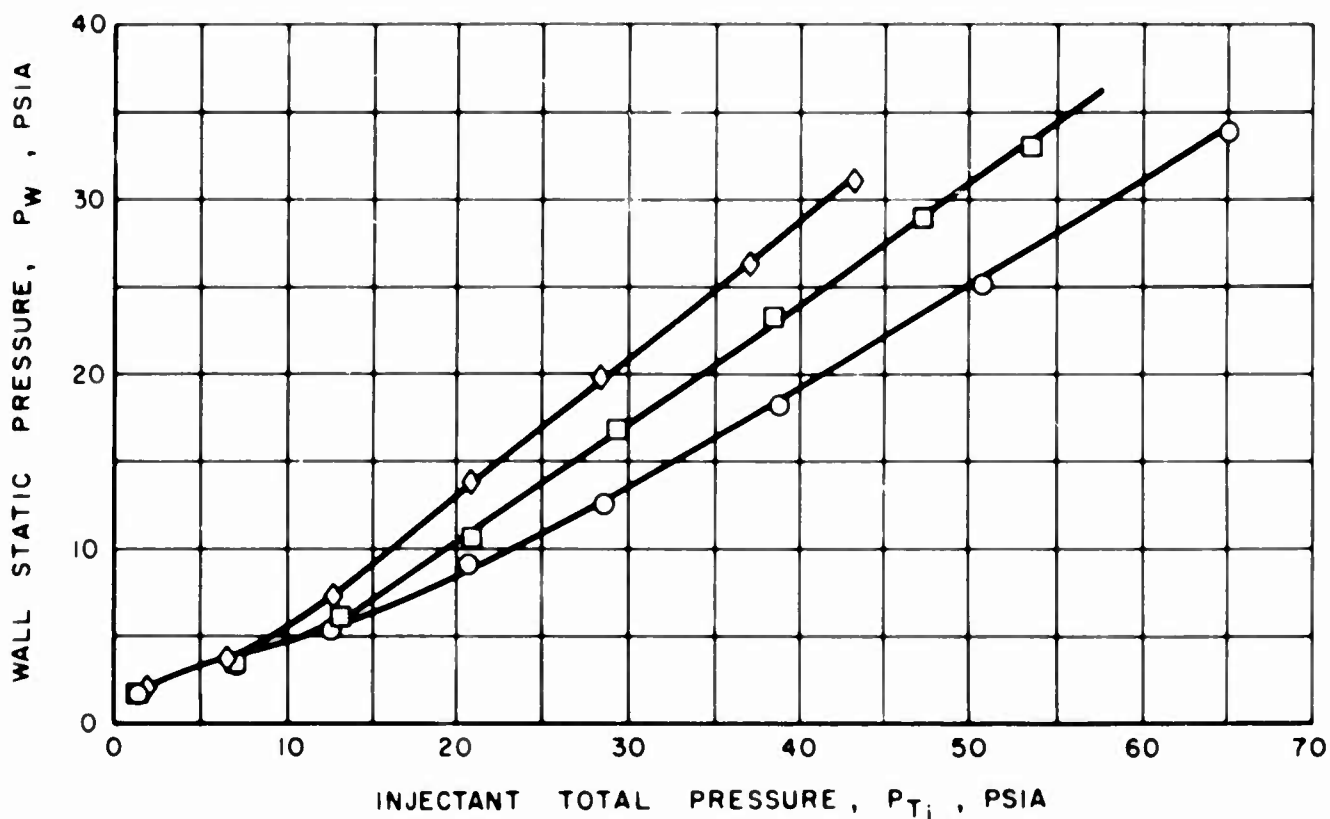
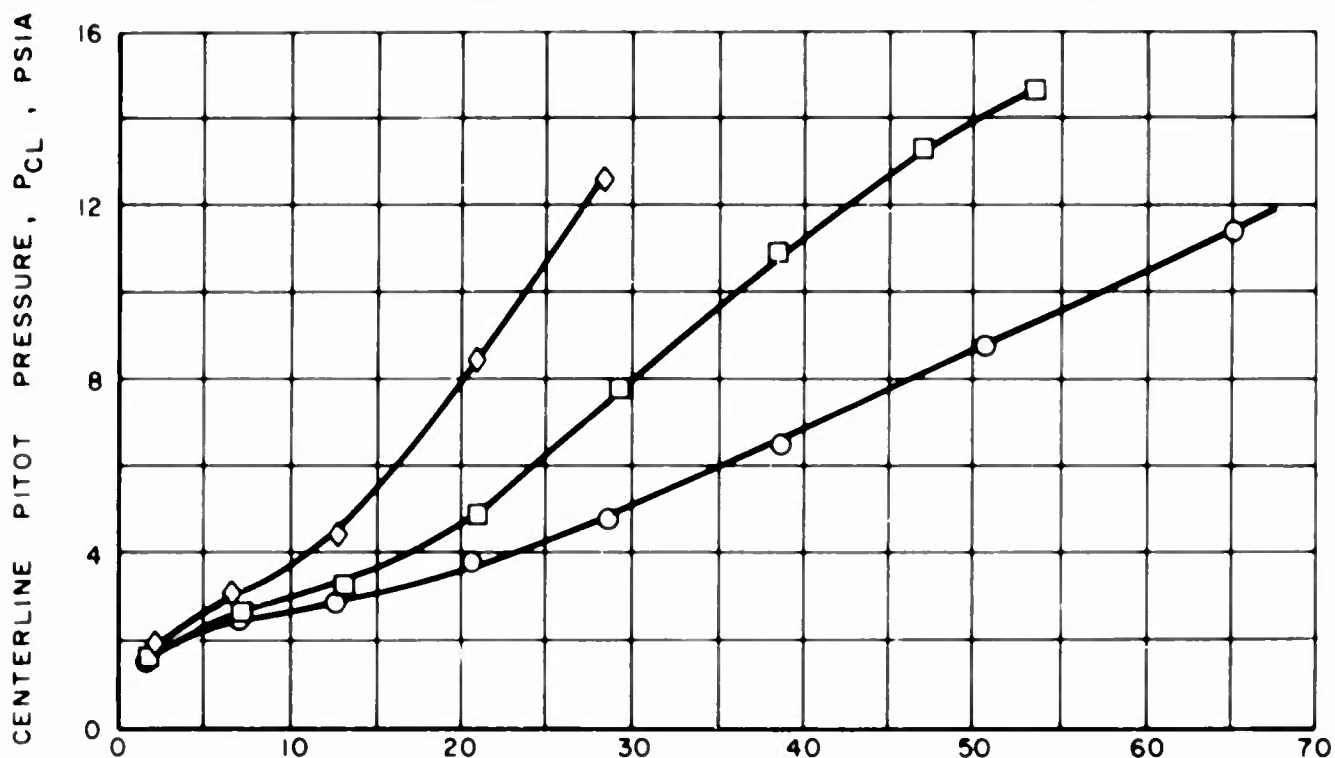


FIGURE 6 EFFECT OF EXHAUST PRESSURE RATIO ON CENTERLINE PITOT PRESSURE AND WALL STATIC PRESSURE

PRIMARY WEIGHT FLOW  $W_p = 0$

SYMBOL	$\Delta$	$\square$	$\circ$
INJECTION AREA, $A_i$	0.426	0.545	0.747

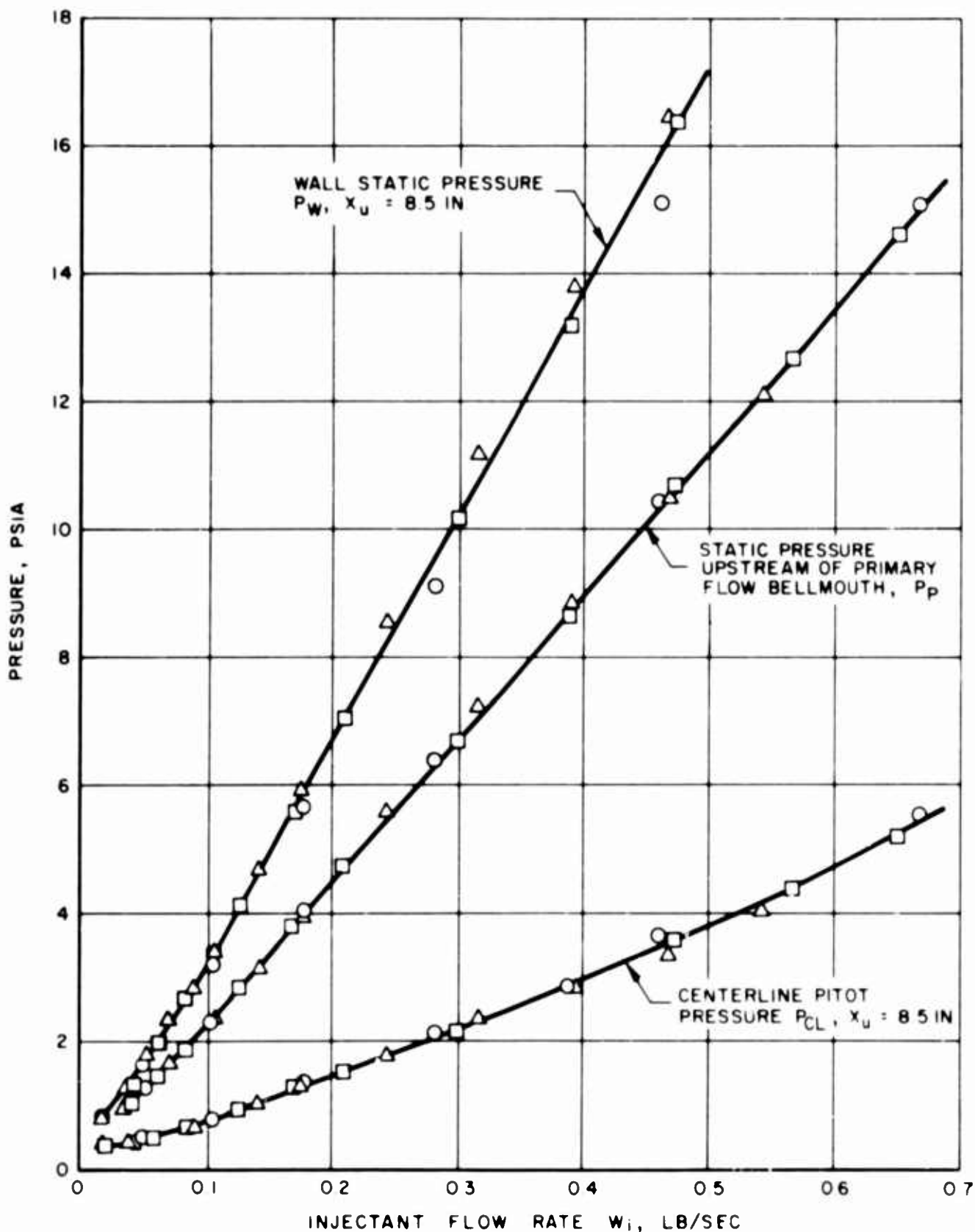


FIGURE 7 PRESSURE CHARACTERISTICS AT PRIMARY FLOW SHUTOFF

PRIMARY WEIGHT FLOW  $w_p = 0.15$  LB/SEC

SYMBOL	○	□	△
INJECTION AREA, $A_i$	0.426	0.545	0.747

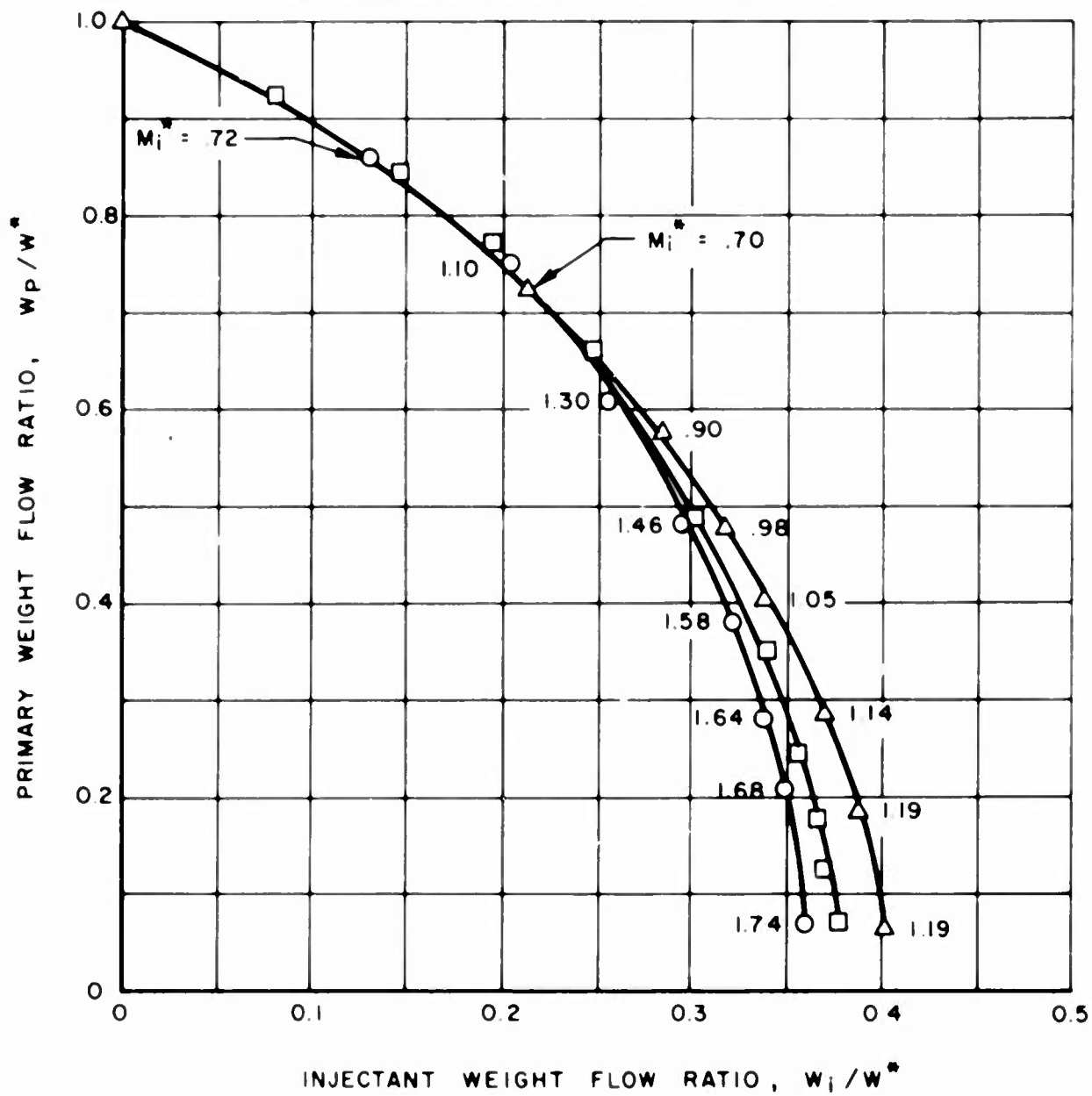


FIGURE 8 EFFECT OF AREA OF INJECTION PORTS ON WEIGHT FLOW CHARACTERISTICS

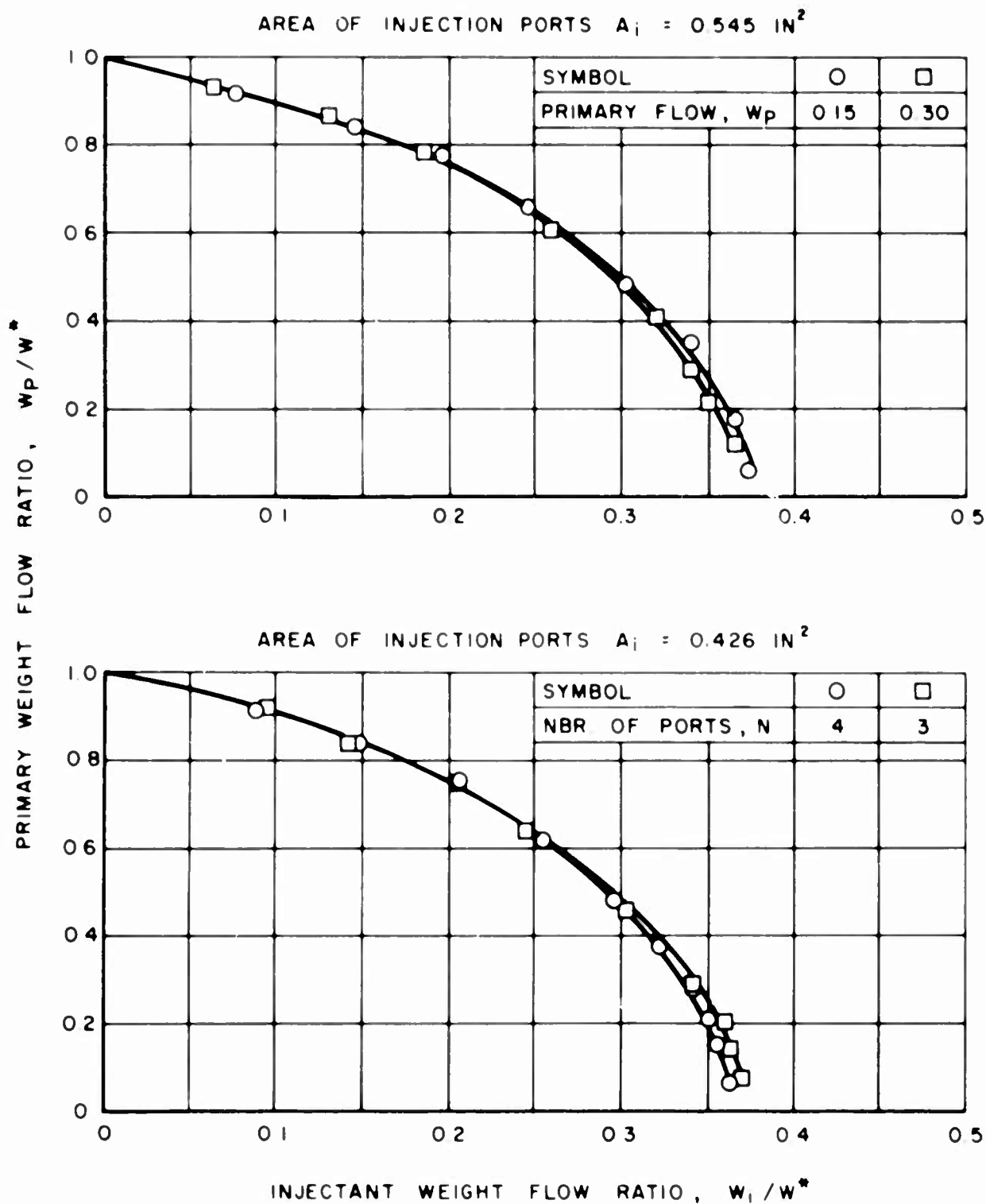


FIGURE 9 EFFECT OF PRIMARY FLOW RATE AND NUMBER OF INJECTION PORTS ON WEIGHT FLOW CHARACTERISTICS

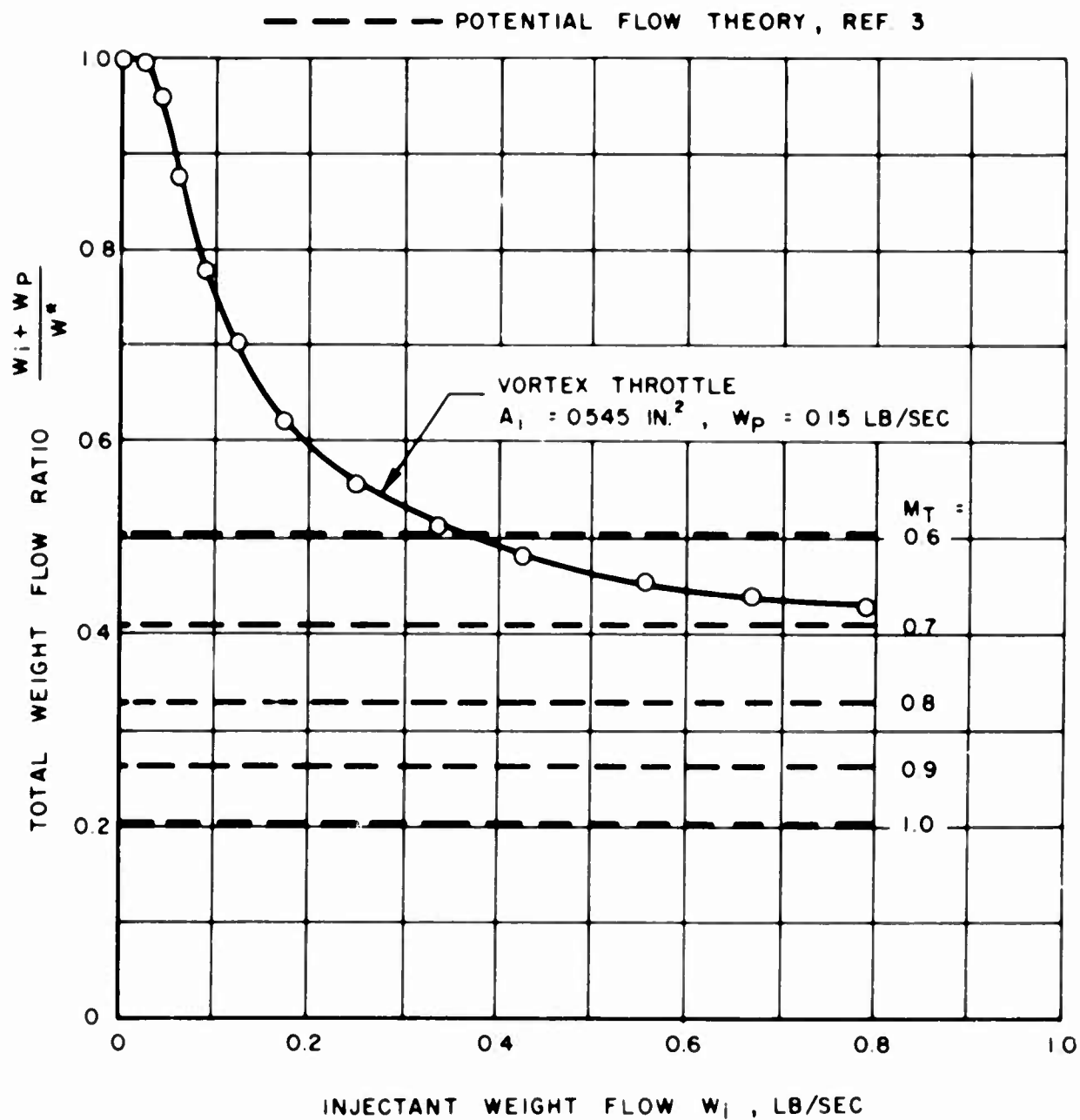


FIGURE 10 COMPARISON OF VORTEX THROTTLE DATA WITH AN APPROXIMATE POTENTIAL FLOW THEORY



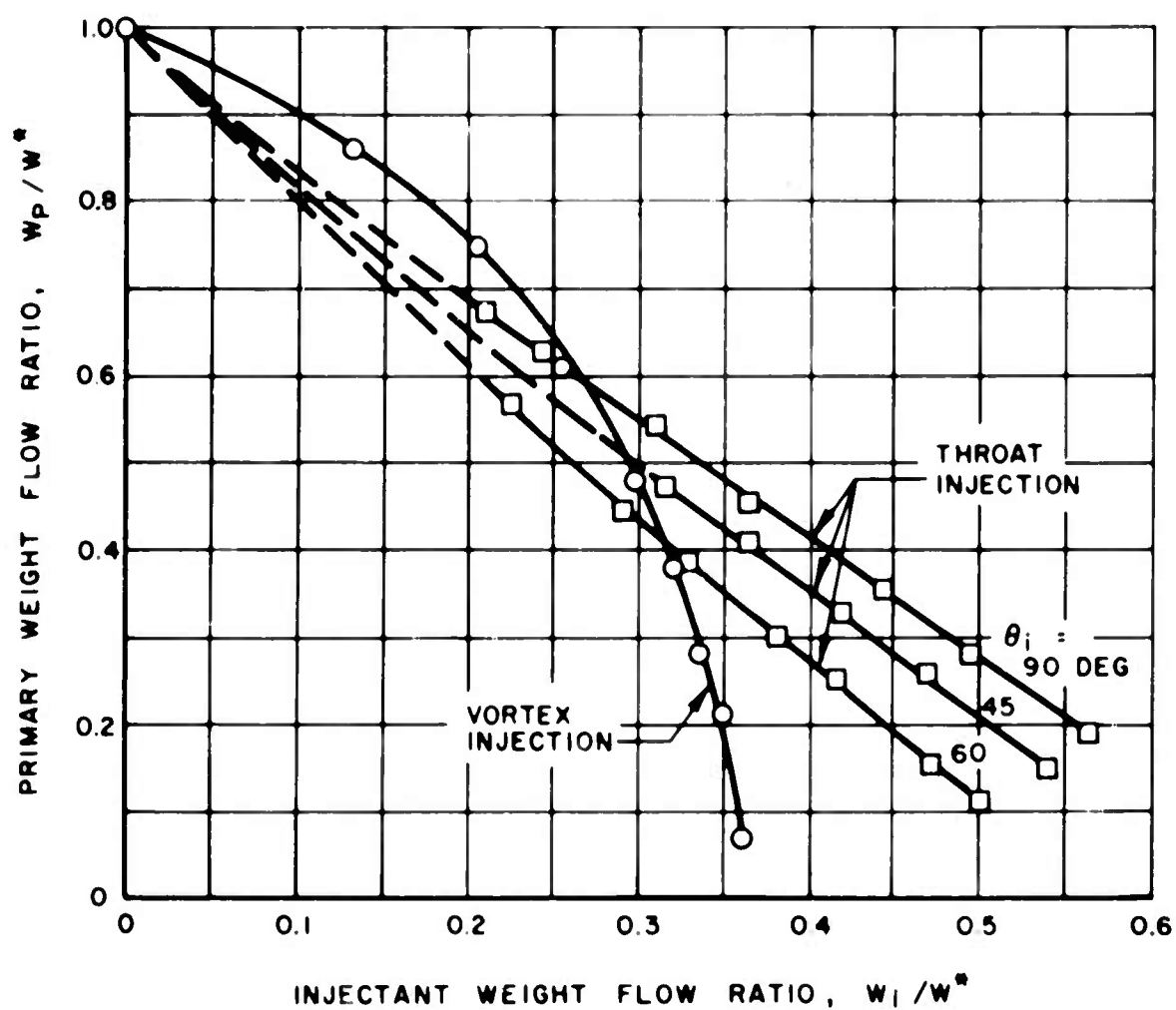
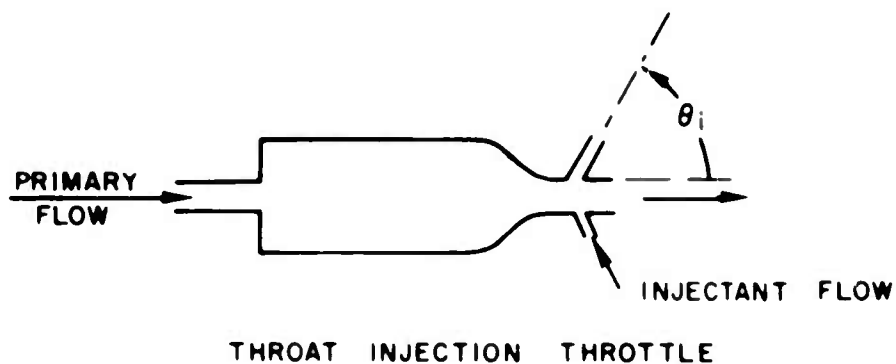


FIGURE 11 COMPARISON OF VORTEX THROTTLE WITH THROAT INJECTION THROTTLE

# CHARACTERISTICS OF COUNTER-VORTEX OSCILLATORS

by

Turgut Sarpkaya

University of Nebraska, Lincoln, Nebraska

## ABSTRACT

The characteristics of the vortex motion created by two vortices rotating in opposite directions in an axially symmetrical vortex tube are investigated. Various geometrically similar units were constructed and tested with air as the working fluid. The median pressures, the amplitude and the frequency of the pressure oscillations at the two vortex chambers were determined. It is found that only the unique combinations of pressure at the two vortex chambers produce oscillations of constant amplitude and frequency. There appears to be a linear relationship between the two pressures.

The initial vortex motion, while irrotational immediately after entry into the vortex tube, does not stay irrotational, but transforms itself partly to rotational flow as it proceeds along the connecting tube. The change from one flow to the other is due to viscosity. The rotational flow has the lesser amount of useful kinetic energy. The amplitude of the pressure oscillations increases with decreasing lengths of the connecting tube while the inverse is true for the frequency. The characteristics of the counter-vortex motion are strongly dependent on the ratio of the tangential velocity to the axial velocity at the jet origin. When this ratio is sufficiently large the axial velocity reverses its direction near the jet axis.

## INTRODUCTION

The possible use of a counter-vortex oscillator, referred to hereafter as a CVO unit, as a diode in fluid-jet amplifiers requires an evaluation of the instability of the counter-vortex motion and of the frequencies and pressure oscillations associated with it. The tangential air jet introduced at the upstream chamber creates a vortex the strength of which remains nearly constant as the vortex enters into the connecting tube of a smaller cross-section. Due to increased tangential velocity, however, the pressure drops very rapidly. Within the connecting tube the energy loss is basically due to viscous and turbulent

energy dissipation, and the rate of fall of pressure is nearly uniform. In the downstream chamber the vortex rotates in a direction opposite to that of the upstream vortex. The velocity distribution in the radial direction is such that the velocity decreases with increasing radial distance. At a radial distance approximately equal to the radius of the connecting tube the velocity of the upstream vortex may be smaller or larger than that produced by the downstream vortex at the same radius. When the two velocities are nearly identical the rotation at the core of the downstream vortex tends to become unstable and changes its direction of rotation with fairly regular frequencies similar to the manner in which a rocker wheel operates in a watch.

Despite the fact that the vortex tube is a very simple device which has no moving parts but consists merely of two chambers and a length of straight tubing, there is to date no theoretical analysis of the instability associated with the motion thus produced. One obvious reason for this is the extreme complexity of the axially symmetrical unsteady motion within and outside of the CVO unit.

Vortex tubes of various kinds have attracted the attention of researchers in the past, particularly for their use in producing hot and cold air simultaneously. Such a vortex tube, called a Ranque-Hilsch tube, has been investigated very exhaustively. Although there is a large amount of experimental data available, none of the various hypotheses advanced are fully able to explain the characteristics of this particular tube. In the present study it was decided to approach the problem as systematically as possible by carrying out the experiments on geometrically similar units. Experiments were performed with air and water although only the experiments conducted with air are reported herein. The results presented in this paper represent the initial portion of these investigations which were undertaken as part of a general investigation of the performance of counter-vortex oscillators being conducted for the Harry Diamond Laboratories under Contract DA-49-186-AMC-51(X).

## ANALYTICAL CONSIDERATIONS

Anything approaching an exact analytical treatment of the counter-vortex oscillator gives every indication of being quite complicated. The complexity of the flow problem in the vortex is undoubtedly further increased in the case of gases by the fact that rather high temperature gradients can exist in the radial direction as the velocities approach supersonic values.

A theoretical flow model for the spiral vortex motion is presented in Fig. 1. The upper portion of the figure shows the unit divided into

three zones; the connecting tube, the upstream and downstream chambers.

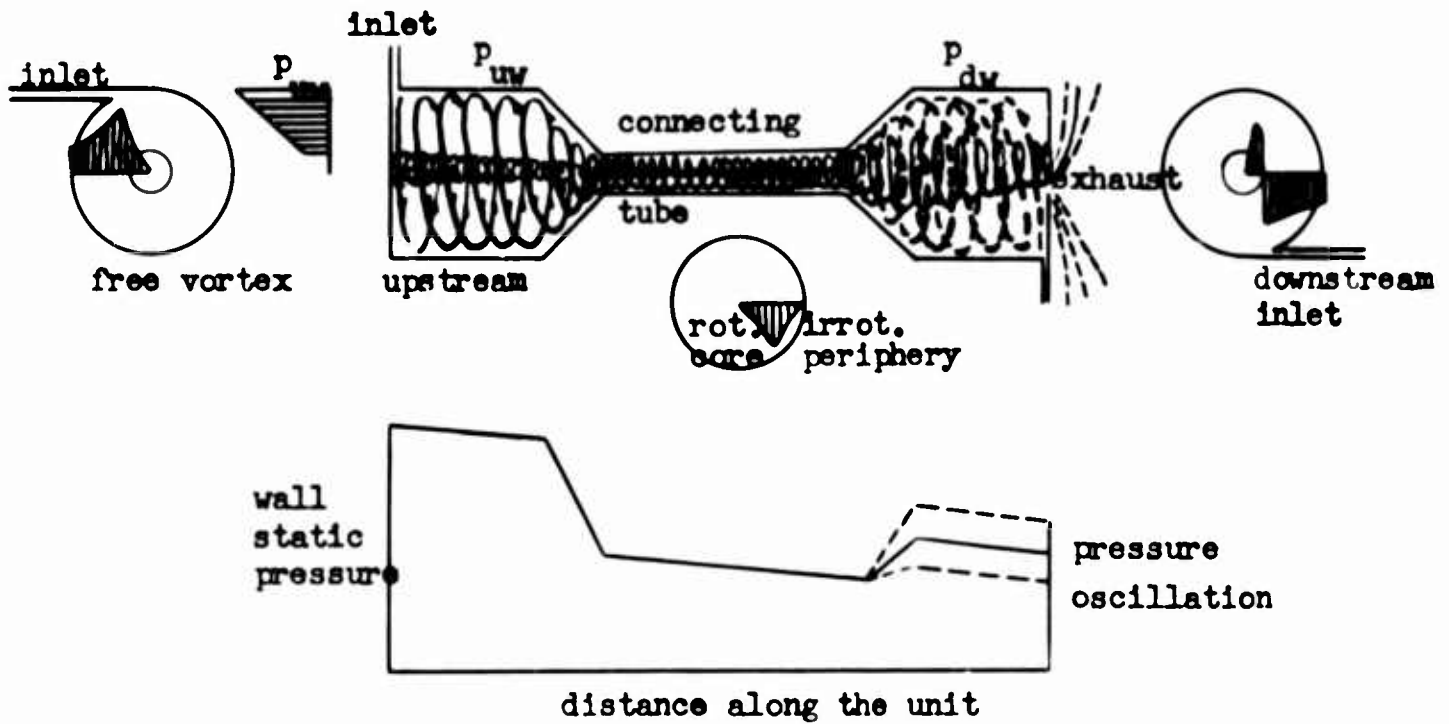


Fig. 1 Flow model and the pressure distribution for a CVO-unit

Also shown in this portion of the figure are typical velocity profiles at various axial stations along the unit. At the upstream chamber the vortex motion is unaffected, at least not to any significant amount, by the viscous resistance, and a relationship between the wall static pressure and the characteristics of the vortex may be derived. The axial component of the velocity,  $V_{ua}$ , is independent of  $r$  in the irrotational portion of the vortex motion.

The differential pressure according to equations of motion is given by

$$dp = \rho \frac{V_{ut}^2}{r} dr \quad (1)$$

With the assumption of isentropic flow and constant total temperature, the energy equation becomes,

$$\frac{dp}{\rho} = -V dV \quad (2)$$

Substituting Eq. (2) into Eq. (1) results in

$$\frac{v_{ut}^2}{r} = -v \frac{dv}{dr} \quad (3)$$

The relationship between  $v_{ut}$  and  $v_{ua}$  can be written as

$$v^2 = v_{ut}^2 + v_{ua}^2$$

or

$$v \frac{dv}{dr} = \frac{1}{2} \left( \frac{dv_{ut}^2}{dr} + \frac{dv_{ua}^2}{dr} \right) \quad (4)$$

Substituting into Eq. (3) yields

$$\frac{2}{r} v^2 = - \left( \frac{dv_{ut}^2}{dr} + \frac{dv_{ua}^2}{dr} \right) \quad (5)$$

Noting the fact that  $2\pi v_{ut} r = \Gamma_u = \text{constant}$ , one has

$$2 \frac{v_{ut}^2}{r} = \frac{2 v_{ut}^2}{r} - \frac{dv_{ua}^2}{dr} \quad (6)$$

or  $v_{ua} = \text{constant}$ .

Having shown that the axial component of the velocity is constant, we can determine the wall static pressure as follows: For isentropic flow and constant total temperature, density and temperature are related by

$$\frac{\rho}{\rho_0} = \left( \frac{T}{T_0} \right)^{\frac{1}{\gamma-1}} \quad (7)$$

Since the total energy in a stream tube must be equal to that in any other stream tube, we have

$$\frac{T}{T_0} = 1 - \frac{v^2}{2 C_p} \quad (8)$$

Combining Eqs.(1), (7), and (8), results in

$$dp = \rho \frac{\Gamma_u^2}{4 \pi^2 r^3} \left[ 1 - \frac{v_{ua}^2 + \frac{\Gamma_u^2}{4 \pi^2 r^2}}{2 C_p T_o} \right] \frac{1}{\gamma - 1} \quad (9)$$

Integrating between the limits  $r_{uc}$  and  $r_{uw}$ , and  $p_{uc}$  and  $p_{uw}$ , one has

$$\frac{p_{uw} - p_{uc}}{p_o} = \left[ 1 - \frac{v_{ua}^2 + \frac{\Gamma_u^2}{4 \pi^2 r_{uw}^2}}{2 C_p T_o} \right]^{\frac{\gamma}{\gamma-1}} - \left[ 1 - \frac{v_{ua}^2 + \frac{\Gamma_u^2}{4 \pi^2 r_{uc}^2}}{2 C_p T_o} \right]^{\frac{\gamma}{\gamma-1}} \quad (10)$$

In order to verify experimentally the validity of Eq. (10), one needs to know the core radius  $r_{uc}$  and the core pressure  $p_{uc}$ . The other variables can either be measured directly or determined from the mass influx and the tangential entrance velocity. The minimum radius at which a free vortex flow can exist is given by the following expression<sup>(1)</sup>

$$r_{uc} = \frac{\Gamma_u}{2 \pi C} \sqrt{\frac{\gamma-1}{\gamma+1}} \quad (11)$$

Physically, this radius represents the point at which the static pressure  $p_{uc}$  has a value of zero psia and corresponds to the core radius. In reality, however, the core forms at a larger radius since zero pressure can never be realized. Furthermore, the upstream vortex is partly choked depending on the conditions prevailing at the exhaust at the downstream chamber. Experiments have shown that the value of  $p_{uc}$  varied between 0.5 psia and 0.7 psia. The observed and the calculated values of  $p_{uw}$  agree fairly well only if the calculated values of  $r_{uc}$  through actually observed  $p_{uc}$  values are used.

For velocities well within the subsonic range a simpler incompressible flow analysis yields,

$$\frac{p_{uw} - p_{uc}}{p_{uw}} = \frac{\rho \Gamma_u^2}{8 \pi^2 p_{uw} r_{uw}^2} \left( \frac{r_{uw}^2}{r_{uc}^2} - 1 \right) \quad (12)$$

Although Eqs. (10) and (12) may also be applicable to the time-averaged values of the downstream chamber for the two flow ranges cited, an experimental verification to this effect is not possible because of the difficulty, if not impossibility, of the determination of the core radius and the lack of understanding of the interaction region of the two opposing vortices.

The expressions developed above are for that region of the tube, relatively near the entrance, where viscosity effects are negligible. As the flow proceeds down the connecting tube, viscosity effects begin to take over, and the free vortex changes into a forced vortex. Using Kassner's<sup>(2)</sup> concept of shear stress in circular turbulent flow, we have

$$\tau_{mt} = (\mu + \rho \epsilon) \left( \frac{dV_{mt}}{dr} - \frac{V_{mt}}{r} \right) \quad (13)$$

Since the velocity distribution at the entrance into the connecting tube is given by:  $\Gamma_m = 2\pi r V_{mt}$ , Eq. (13) reduces to:

$$\tau_{mt} = -2 (\mu + \rho \epsilon) \frac{V_{mt}}{r} \quad (14)$$

The moment of the shearing force acting on an annular element of fluid a distance  $r$  from the axis is found to be,

$$M = -2 (\mu + \rho \epsilon) \Gamma_m \quad (15)$$

which is independent of  $r$  and constant as long as  $\Gamma_m$  remains constant. This renders the sum of internal elemental moments different than zero. Since there is no external torque applied to the flow upon entrance to the connecting tube, the sum of internal moments must be zero. In other words, the flow, while irrotational immediately after entry into the vortex tube, does not stay irrotational, but changes into something else so as to satisfy the above requirement. That this something else is rotational flow can be seen by applying the equations of rotational flow: Since the characteristic equation for the rotational flow is:  $V_{mt} = \omega r$ , it follows that  $dV_{mt}/dr = \omega = V_{mt}/r$ , and

$$\int_0^R 2\pi r^2 (\mu + \rho \epsilon) \left( \frac{dV_{mt}}{dr} - \frac{V_{mt}}{r} \right) dr = \int_0^R M dr = 0$$

Thus, rotational flow is the stabler form of flow to which the initial

flow transforms itself, even though both flows satisfy the conservation of energy principle. The rotational flow, however, has the lesser amount of useful kinetic energy. The inner layers, having too much kinetic energy, transfer part of their energy to the outer layers by being slowed down. The process of conversion ends with rotational flow being attained near the tube exit. The gradual conversion from irrotational to rotational flow causes a gradual rearrangement in velocity and energy distribution. Consequently, the wall static pressure and the strength of the vortex decrease along the connecting tube. In view of the fact that the distribution of velocity, shear stress, inlet and outlet pressures and the variation of  $\Gamma$  and  $p$  are difficult to estimate, neither the equation of momentum in the axial direction:

$$\int_{um} p \, dA + \int_{um} \rho \, v_a^2 \, dA - \int_{dm} \rho \, v_a^2 \, dA - \int_{dm} p \, dA = \int_{mw} \tau_{amw} 2\pi r_m \, dx = C_{a0} \rho_0 \bar{v}_{am}^2 \pi r_m^2$$

nor the equation of angular momentum for the tangential direction:

$$\int_m \rho \, v_a \, v_t \, r^2 \, dr = \int_m \tau_{tmw} r_m^2 \, dx = C_t \rho_0 \bar{v}_{tm}^2 \pi r_m^2$$

help to evaluate the appropriate resistance coefficients. These equations do, however, point out the need and the importance of the measurement of various internal characteristics of the flow within the connecting tube as well as in the upstream and downstream chambers.

## EXPERIMENTAL EQUIPMENT AND PROCEDURE

The experiments were conducted at the Hydrodynamics Laboratory of the Department of Engineering Mechanics of the University of Nebraska.

The compressed air was filtered prior to its introduction into a CVO unit. Since there were no noticeable pressure oscillations in the upstream chamber, the upstream wall pressure  $p_{uw}$  was measured with a calibrated test gage. The downstream wall pressure  $p_{dw}$ , the total fluctuating pressure  $p_{dw}$ , and the frequency  $f$  were determined through the use of a specially designed pressure transducer and a recorder. A sample recording is shown in Fig. 2. From these recordings it was possible to determine the dependent variables cited above with a high degree of accuracy.



The experimental procedure adopted was as follows: The pressure  $p_{uw}$  was set at a certain value, then the pressure  $p_{dw}$  was increased gradually until an oscillation began. The pressure  $p_{dw}$  was then increased to see if the oscillations would stop. When the oscillations stopped,  $p_{dw}$  was reduced slowly to the point where the oscillation started again. Having found a combination of pressures  $p_{uw}$  and  $p_{dw}$ ,  $p_{uw}$  was reread and recorded;  $p_{dw}$  and  $\Delta p_{dw}$  were obtained from the recorder traces. In order to determine the frequency  $f$  accurately, the recorder was run at a chart speed of 100 mm per second for about five seconds and the cycles per second were determined by counting the oscillations within various time intervals.

The units used in the tests were constructed of various materials, including brass, aluminum and plexiglass. The inner surfaces were polished and any burrs that may have been created during the drilling of jet holes and pressure taps were carefully removed. The two entrance jets were made tangent to the inner wall of the vortex chambers. The pressure taps at the upstream and downstream chambers were drilled in the radial direction and connected to pressure measuring devices with short tubes. Pressure taps were drilled along the connecting tube to determine the pressure distribution and the energy loss along the tube. Figure 3 is a picture of some of the units and of the connecting tubes used in the tests. The characteristic length ratios of various CVO units are presented in Table I.

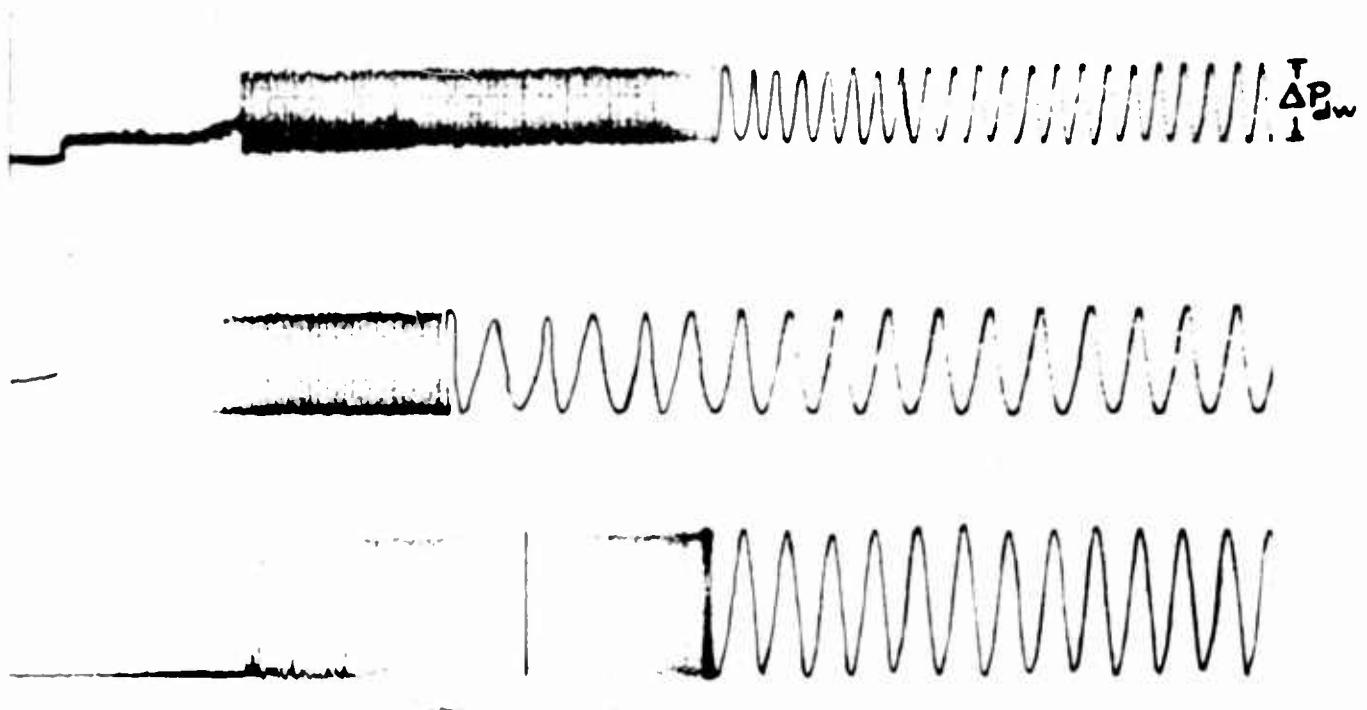


Fig. 2 Sample recordings of pressure oscillations at the downstream vortex chamber.

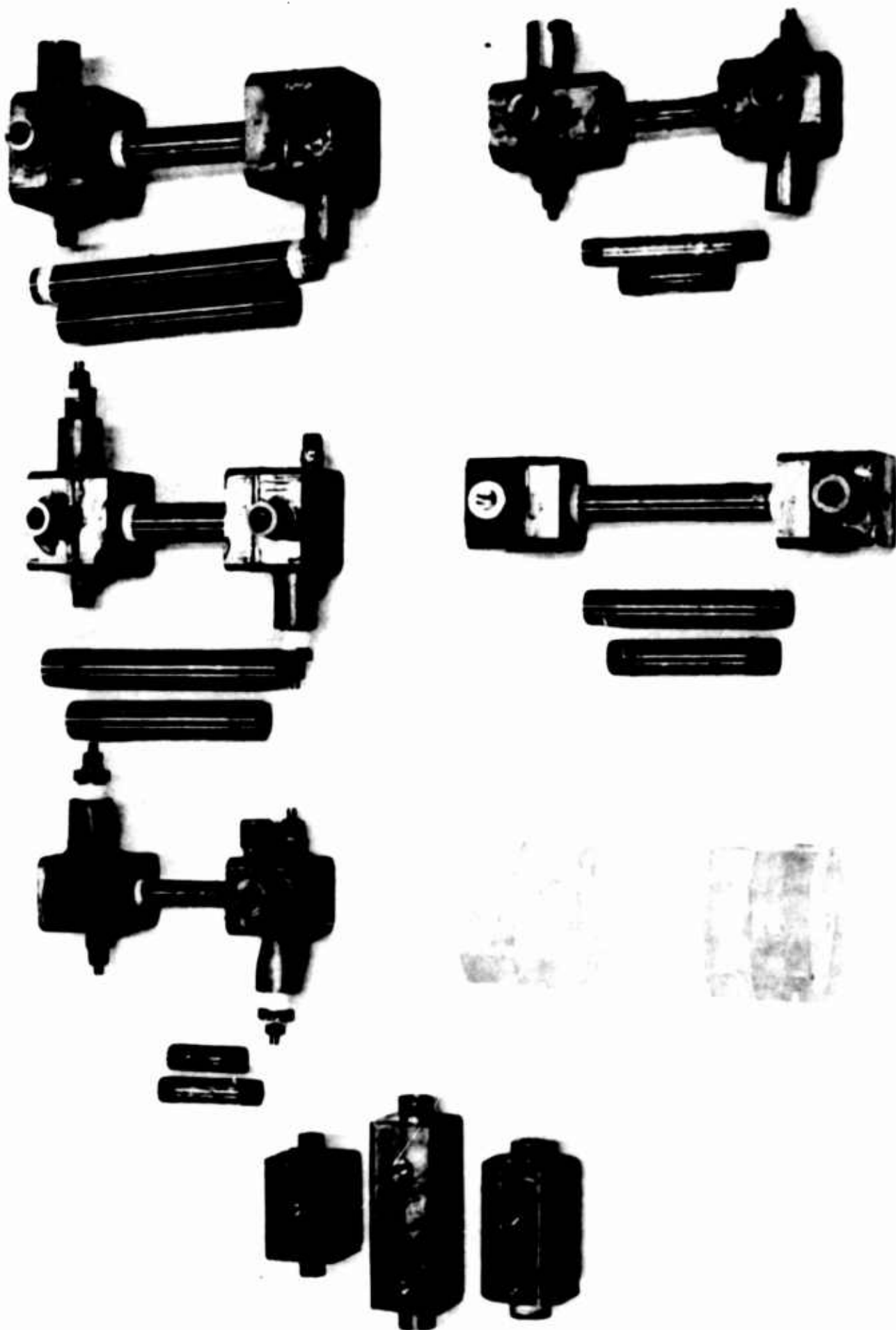
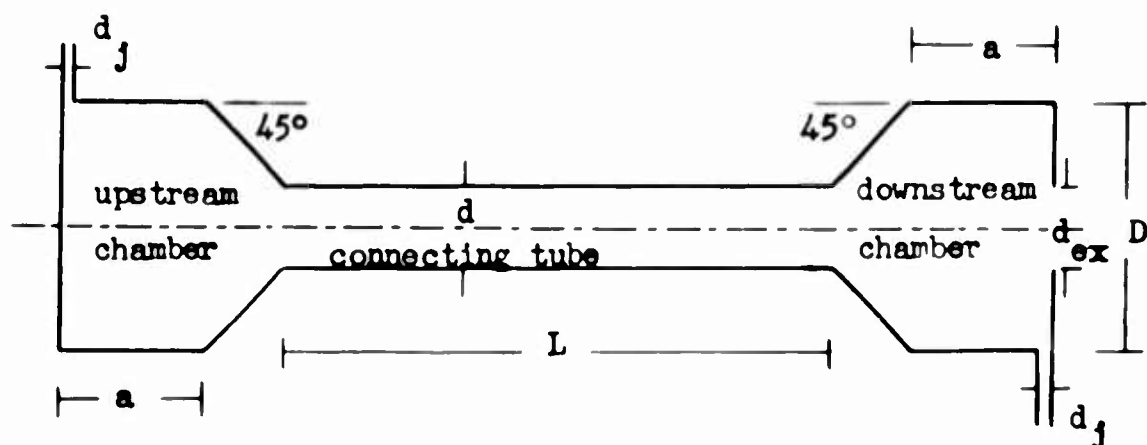


Fig. 3 Picture of various CVO-units used in the tests



Units	$D/d$	$L/d$	$L/D$	$D/d_j$	$d/d_{ex}$
1AA	2.67	10.95	4.10	8	1
2A	2.67	10.95	4.10	8	1 (25% larger than 1AA)
2AA	2.67	10.95	4.10	10	1 (25% larger than 1AA)
1BB	2.67	13.50	5.05	8	1
2B	2.67	13.50	5.05	8	1 (25% larger than 1BB)
2BB	2.67	13.50	5.05	10	1 (25% larger than 1BB)
1CC	2.67	16.40	6.16	8	1
2C	2.67	16.40	6.16	8	1 (25% larger than 1CC)
2CC	2.67	16.40	6.16	10	1 (25% larger than 1CC)
1S	2.67	6.42	2.41	8	1
1SS	2.67	1.42	0.53	8	1

(  $a = 5/16$  inch and kept constant)

Table-I Characteristic length ratios of various CVO-units used in the tests

## DISCUSSION OF RESULTS

The experimental results obtained through the procedure described above were plotted in various dimensional and dimensionless forms. Included herein are only the representative plots. No attempt was made to present all the data obtained for the sake of brevity.

In Figs. 4 and 5 vortex chamber pressures  $p_{vw}$  and  $p_{vw}$  are plotted with respect to each other for the units 1AA, 2AA, 1S, and 1SS. The scatter of the data is within the limits of experimental accuracy. The relationship

between the two pressures is very close to being linear. There is, however, a slight curvature in an imaginary line connecting the test points. For practical purposes it may be concluded that as  $L/d$  increases, the ratio of  $p_{uw}/p_{dw}$  increases. This is, as discussed previously, due to the effect of viscous energy dissipation within the connecting tube. As the length of the connecting tube increases the final strength of the vortex arriving at the end of the connecting tube decreases. This in turn means that the strength of the vortex which must be created at the downstream chamber and hence the pressure  $p_{dw}$  must be smaller. Consequently,  $p_{uw}/p_{dw}$  becomes larger with increasing lengths of the connecting tube.

Furthermore, it is found that as the ratio  $L/d$  increases, the effect of the variation of  $D/d_j$  becomes more noticeable. For small  $L/d$  ratios, however, the variation of the jet diameter relative to the chamber diameter does not appear to have a large influence on the relationship between  $p_{uw}$  and  $p_{dw}$ .

The total fluctuation  $\Delta p_{dw}$  of the median pressure  $p_{dw}$  is plotted with respect to pressure  $p_{dw}$  in Fig. 6 and 7. The scatter of the test data is somewhat larger than otherwise anticipated. This is partly due to the difficulty in the precise determination of small pressure fluctuations. It is observed that for a given  $p_{uw}$ ,  $\Delta p_{dw}$  increases rapidly at first and slowly toward the end as  $L/d$  decreases toward its limiting value of zero.

The frequency of the oscillations determined through the procedure described previously is plotted as a function of  $p_{dw}$  in Fig. 8. The scatter of the experimental data is larger than that which would be desirable. This is partly due to the superposition of secondary harmonics on the major frequency of the pulsations.

In concluding the discussion of the experimental data it suffices to say that for a given unit a definite relationship exists between the parameters  $p_{uw}$ ,  $p_{dw}$ ,  $\Delta p_{dw}$  and the frequency  $f$ . A further understanding of the various relationships existing between these parameters and the establishment of design criteria require the detailed experimental analysis of the energy dissipation in vortex flow along the theoretical lines discussed in this article.

## NOMENCLATURE

C a coefficient  
 $C^*$  speed of sound at Mach 1  
 $C_p$  specific heat coefficient  
 $d_j$  diameter of inlet jets  
 $D$  diameter of vortex chambers  
 $f$  frequency of oscillations  
 $L$  length of connecting tube  
 $M$  moment

## Subscripts

a denotes axial direction  
d downstream direction  
j jet  
m middle section, connecting tube  
t tangential direction  
u upstream chamber  
w denotes on the wall

p pressure  
p pressure fluctuation  
r radial distance  
T temperature  
V velocity

$\epsilon$  eddy diffusivity  
 $\rho$  density of fluid  
 $\gamma$  ratio of specific heats  
circulation  
 $\mu$  viscosity  
 $\omega$  angular velocity  
 $\tau$  shear stress

## REFERENCES

1. A. H. Shapiro, "The Dynamics and Thermodynamics of Compressible Fluid Flow," The Ronald Press Company, New York, 1953, Vol. 1, page 108.
2. R. Kassner and E. Knoerschild, "Friction Laws and Energy Transfer in Circular Flow," Tech. Report No. F-TR-2198-ND, GS-USAF, WPAFB, No. 78, March, 1948.

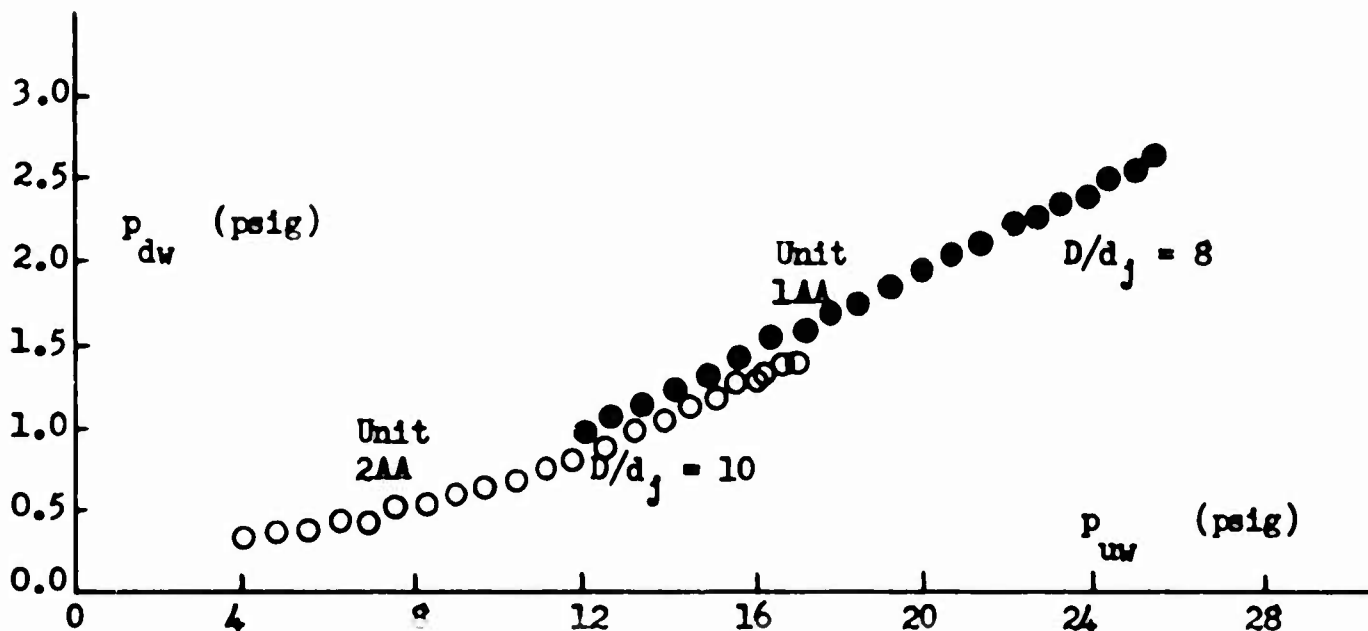


Fig. 4  $p_{dw}$  versus  $p_{uw}$  for the CVO-units 1AA and 2AA.

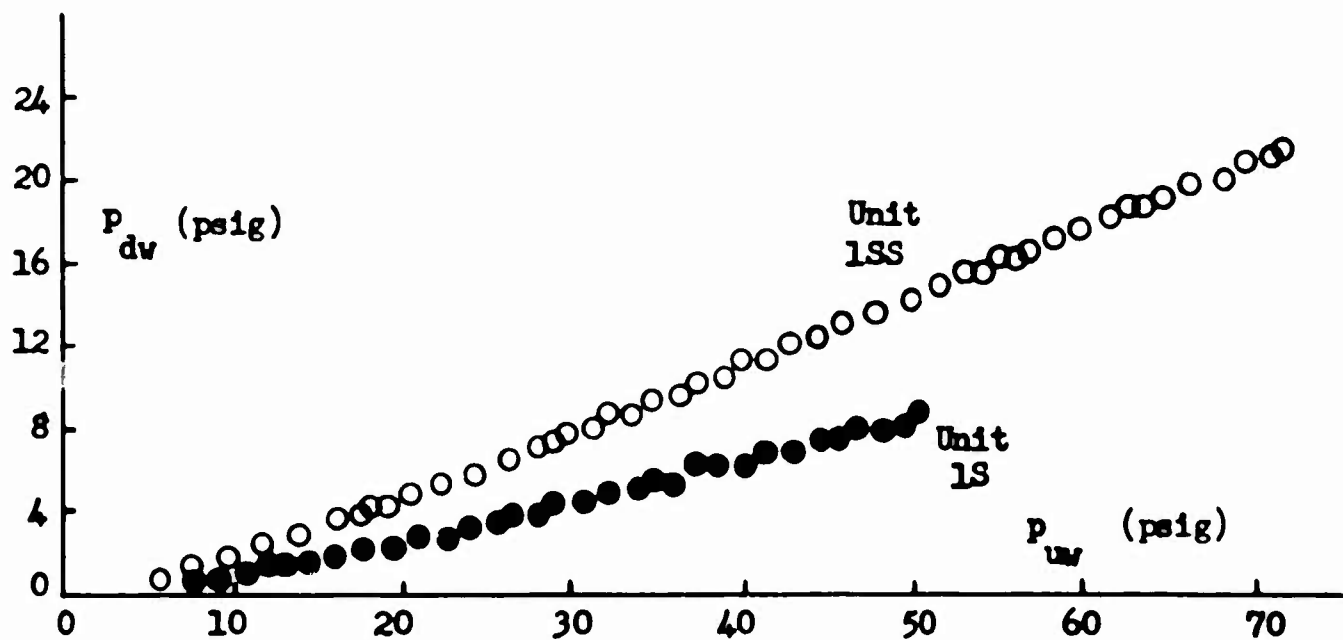


Fig. 5  $p_{dw}$  versus  $p_{uw}$  for the CVO-units IS and ISS.

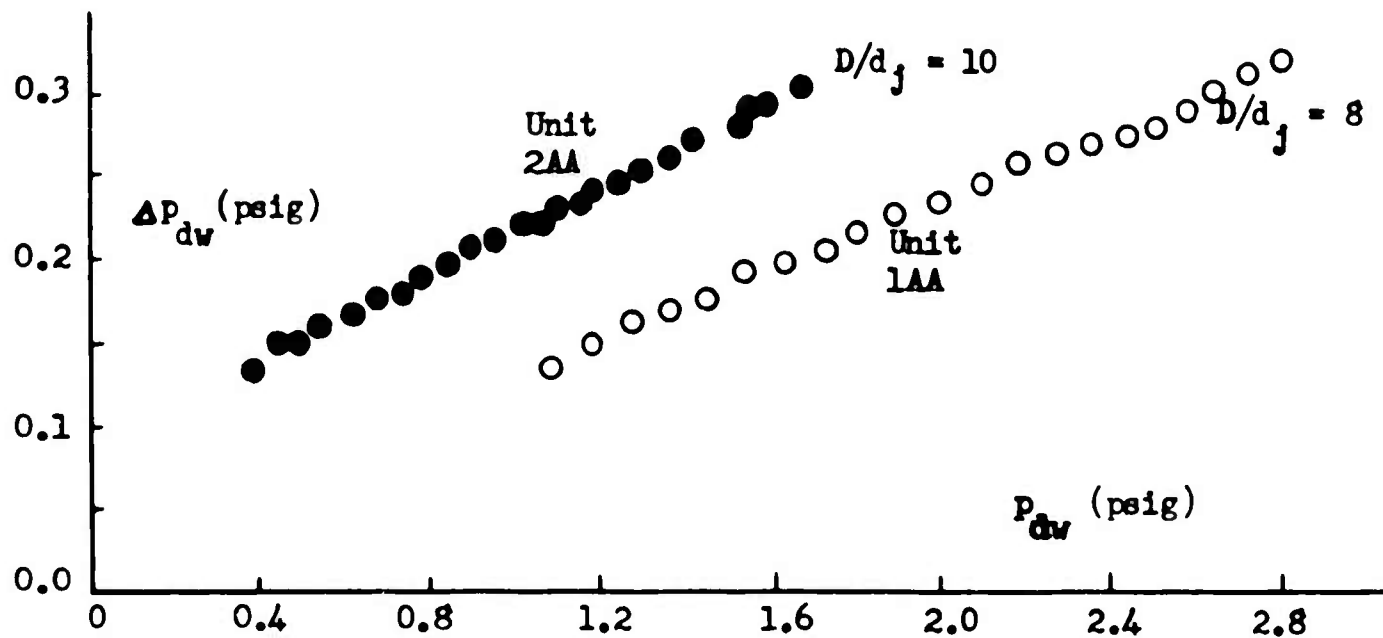


Fig. 6 Total pressure fluctuation versus median pressure in downstream vortex chamber.

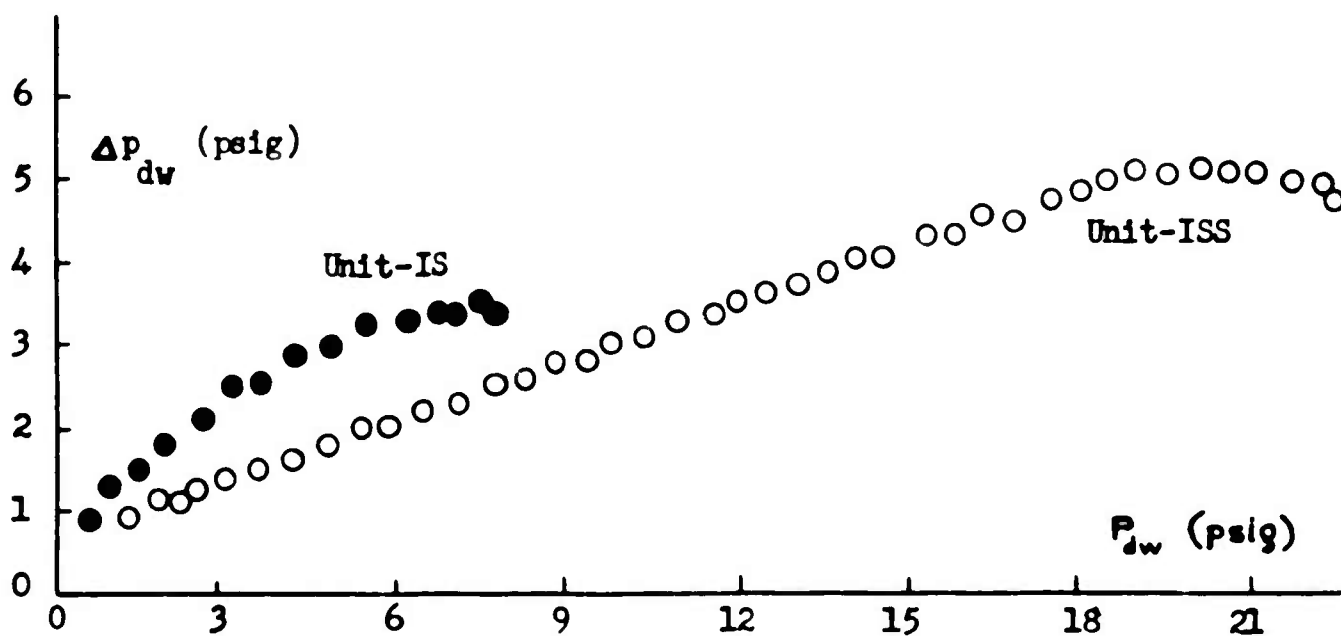


Fig. 7 Total pressure fluctuation versus median pressure in downstream vortex chamber.

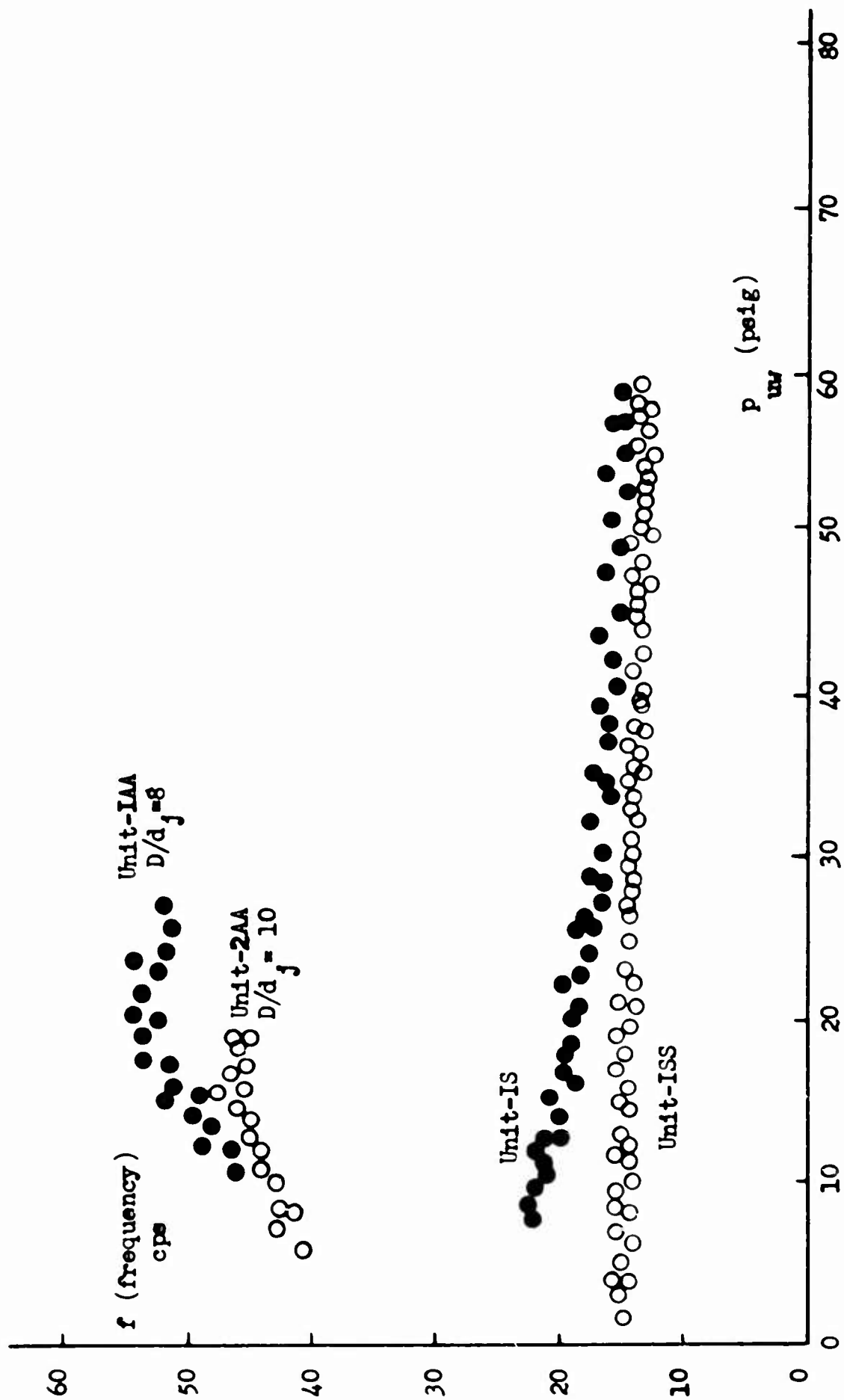


Fig. 8 Frequency of pressure oscillations versus the pressure in the upstream vortex chamber.



APPLICATION TECHNIQUES  
FOR PROPORTIONAL PURE FLUID AMPLIFIERS

by

C. A. Belsterling and K. C. Tsui  
The Franklin Institute, Phila., Pa.

ABSTRACT

This paper describes a program of experimental and analytical research on pure fluid amplifiers currently being conducted at The Franklin Institute.

The ultimate objective of this research program is to promote the application of pure fluid devices in systems, by describing those devices in terms familiar to the control systems engineer. It is intended to define static and dynamic analogies of network parameters, equivalent electrical circuits, and transfer functions; and develop analytical and graphical techniques for more direct system analysis.

To date, load line techniques and equivalent circuits for both static and dynamic cases have been developed. Experimental tests have verified some aspects of the approach. The program is making good progress toward the stated objective but many problems have yet to be resolved.

I. INTRODUCTION

This paper describes a program of experimental and analytical research on pure fluid amplifiers currently being conducted at The Franklin Institute.\*

The concept of pure fluid amplification covered in this work was invented at the Diamond Ordnance Fuze Laboratories (now Harry Diamond Laboratories) in 1959 and since has been the subject of the research and development efforts of a large number of other agencies. However, in spite of the lapse of years, there has been only limited success in applying these devices in practical systems. We believe that this situation can be attributed to the fact that most of the effort has been applied to analyzing the fluid mechanics of the devices, and to the optimization of internal

---

\*Supported in part by Harry Diamond Laboratories.

dimensions. Limited effort has been devoted to describing performance from an external (black box) point of view as required in systems application and this in terms unfamiliar to the systems design engineer.

The ultimate objective of this research program is to promote the application of pure fluid devices in systems, by describing those devices in terms familiar to the control systems engineer. Most control engineers have a working knowledge of vacuum tube and transistor circuits and network theory. Therefore, this work is intended to define static and dynamic analogies of network parameters, equivalent electrical circuits and transfer functions; and develop analytical and graphical techniques for more direct system analysis.

This report covers preliminary studies of both the static and dynamic cases, limited to two different amplifier designs. We develop hypothetical techniques through a relatively unsophisticated treatment of the theory and perform experimental tests to correlate with predicted performance. Later phases of the work will be devoted to a rigorous mathematical treatment and the consideration of second order effects. The immediate goal is to demonstrate the approach and its value as an application aid.

## II. THEORY

### A. General Approach

In this phase of the work we have taken a relatively unsophisticated approach to developing useful application techniques. We have assumed complete duality with vacuum tubes and transistors, and developed graphical characteristics and mathematical techniques along the lines of a well-known undergraduate text<sup>1</sup>. The relatively rigorous methods of network analysis have thereby been avoided but it is obvious that once the basic analogies have been established, those methods will also be applicable to pure fluid amplifier circuits.

### B. Description of the Pure Fluid Amplifier

Comprehensive descriptions of the DOFL type fluid amplifiers are given by others<sup>2</sup> and will not be repeated here. A simplified description, adequate for the present work, is included for completeness.

The basic configuration of the DOFL-type pure fluid amplifier is shown in Figure 1. Pressurized fluid enters the supply port at the bottom and is ejected as a high velocity jet into the interaction chamber. If no

- 
1. ELECTRONIC ENGINEERING PRINCIPLES, John D. Ryder, Prentice Hall, 1947.
  2. "Fluid Amplification: 1. Basic Principles," R. W. Warren and S. J. Peperone, DOFL Report TR-1039, 15 August 1962.

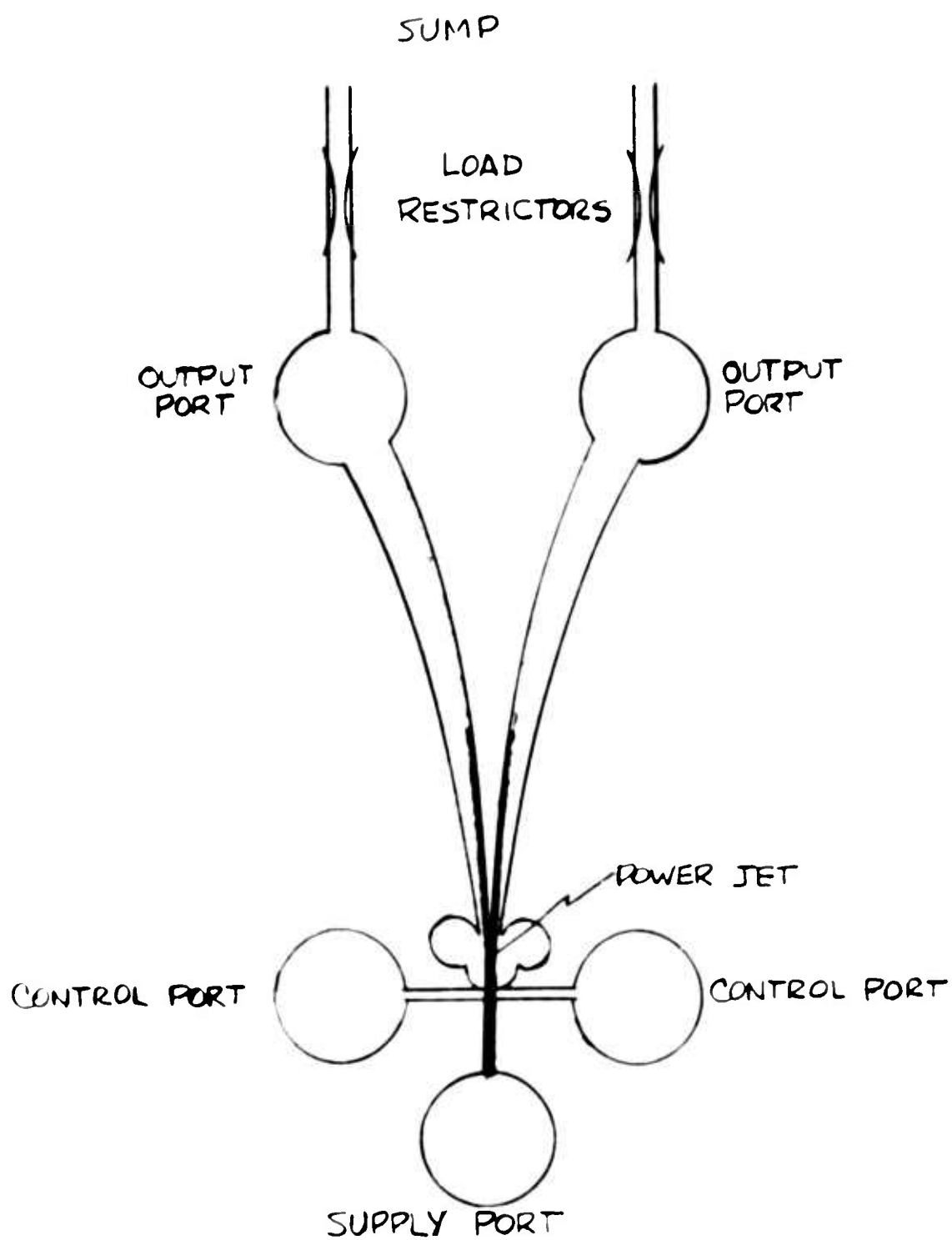


FIG 1 - SKETCH OF PURE FLUID AMPLIFIER

pressure difference exists between opposite sides of the power jet, its centerline will strike the divider and equal amounts of flow will enter the two upper channels and exit through the appropriate output ports. With equal restrictors between the output ports and the sump, the pressure developed at the output ports will also be equal.

If a pressure difference does exist between opposite sides of the power jet in the interaction chamber, a force is present which deflects the power jet so more fluid exits through one output port and less fluid exits through the other. With equal output restrictors, a pressure difference is generated between output ports. Thus a control fluid ejected at low energy into the interaction region can control the relatively high energy fluid in the power jet.

Under certain conditions in the interaction region, the power jet itself will generate pressures on either side which are in unstable equilibrium. In this case the jet is attracted to one side or the other without external control and the amplifier is bistable. Under other conditions the effect of differential pressures generated by the power jet itself are minimized, and the power jet is mainly sensitive to external control. In this case the action is proportional and the force deflecting the control stream can arise from two sources, (1) pressure generated by the control source or (2) momentum of the control jet. It is the proportional case which is of primary interest in the present study.

### C. Graphical Characteristics of the Pure Fluid Amplifier

Since, like the vacuum tube and the transistor, the pure fluid amplifier is a nonlinear device, the most convenient way to express its characteristics is in the form of graphs. This avoids the need for having to deal with the internal fluid mechanics and at the same time embraces all of the nonlinear behavior. The pure fluid amplifier is more complex than the vacuum tube and transistor because (1) it is made up of two active elements connected in a differential circuit, (2) the control is a function of differential pressure and/or flow and (3) the control is also a function of absolute level of control pressure and/or flow.

In the fluid amplifier there are four variables of interest, namely (1) input (control) pressure, (2) input (control) flow, (3) amplifier pressure drop, and (4) amplifier load flow. Thus we must generate the characteristics defining the relationship between (a) control flow and control pressure, (b) load flow and amplifier pressure, and (c) control flow or control pressure and load flow or amplifier pressure. These relationships will then be sufficient to describe amplifier performance.

Referring again to Figure 1, the load circuits of the pure fluid amplifier can be described in terms of pressure drop across each half and flow out of each output port. The characteristics will theoretically be independent of load and can be shown as a family of curves of the

pressure drop versus the flow for each half with control pressure or flow as the parameter. Note that these curves can be taken experimentally with flow measuring devices with greater than zero impedance if the abscissa is amplifier pressure drop. Also note that if the unit is symmetrical and balanced, the characteristics of one side are sufficient to describe the total performance.

The first question which arises is the choice of control variable, control pressure or control flow. Since we intend also to determine the relationship between control flow and control pressure, the choice is a question of convenience. Control pressure has tentatively been selected because experimental plots of proportional amplifiers are typically more regular with respect to this variable and it is more convenient to measure.

In selecting the most useful method of presenting the amplifier load circuit characteristics, the duality with vacuum tube and transistor circuits is taken into account and the result is illustrated in Figure 2. Here the load circuit characteristic curves of the left half and the right half of the fluid amplifier are plotted independently as a function of control differential pressure. We prefer to retain a display of both halves to accommodate the conditions encountered with an unbalanced amplifier.

These characteristics describe the relationship between (1) load flow and amplifier pressure and (2) amplifier pressure and control differential pressure. As mentioned previously, the performance is also a secondary function of the absolute (or bias) level of control pressure. Therefore to be complete, the load circuit characteristics should be three-dimensional (surfaces), with bias level as the second parameter. In the experimental work connected with this study, we avoided the need for a third dimension by plotting separate characteristic curves for the various bias levels used.

In addition to the load circuit characteristics showing the relationships between load flow, amplifier pressure and control pressure, a set is necessary to describe the input circuit. Since we must be concerned with absolute conditions on each side as well as the differential conditions of control, it is necessary to plot control pressure and control flow for both right and left halves as shown in Figure 3. It is then a relatively simple matter to calculate the curve for differential pressure versus differential flow, if it is of interest. Note that for these input characteristics to be valid in defining input impedance according to rigorous network theory, the output should be open circuited or held constant.

#### D. Derivation of the Performance Parameters of the Pure Fluid Amplifier

Because fluid amplifiers are to be used in circuits where the signals are to be varying about a given operating point, their behavior

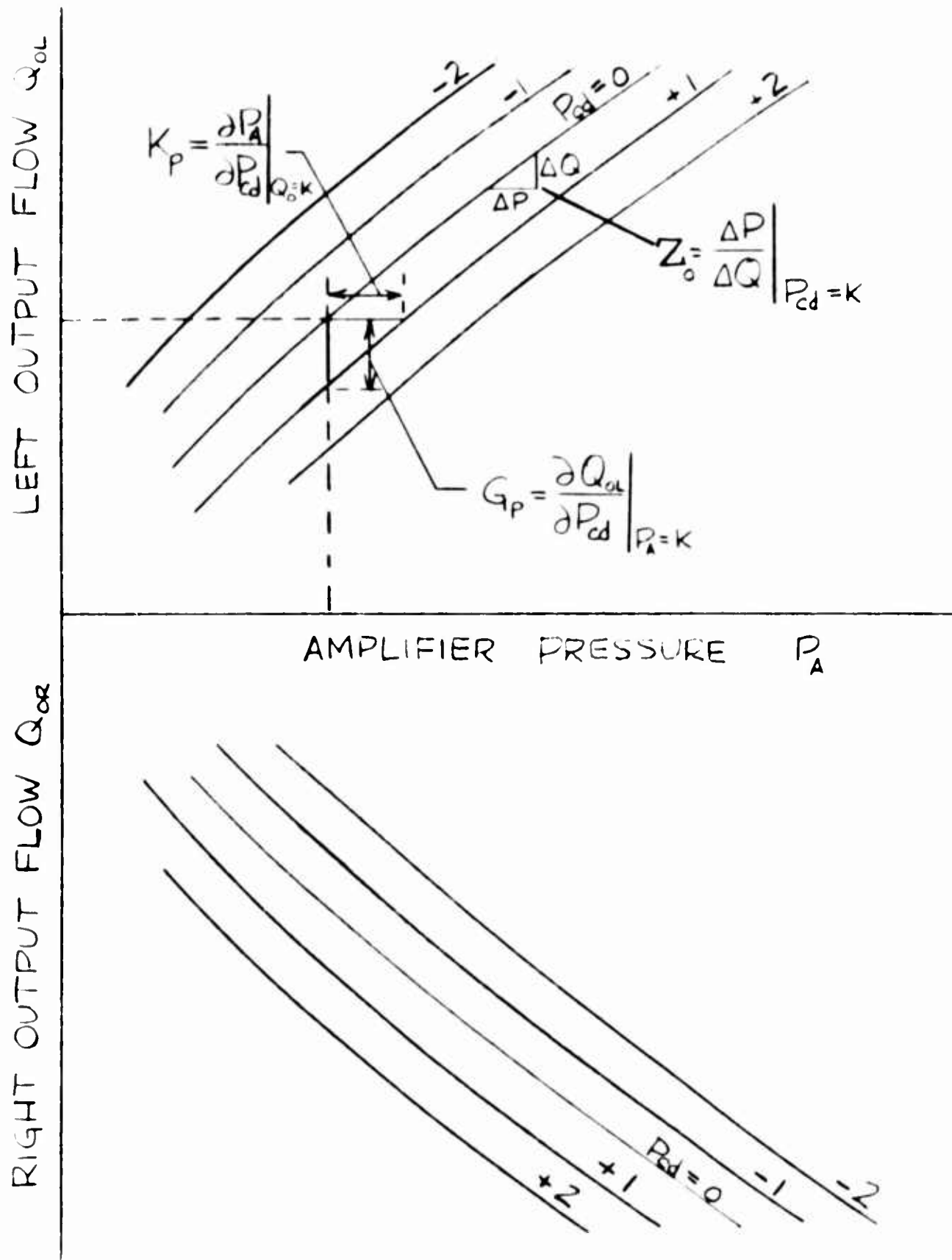


FIG 2 - TYPICAL LOAD CIRCUIT CHARACTERISTICS

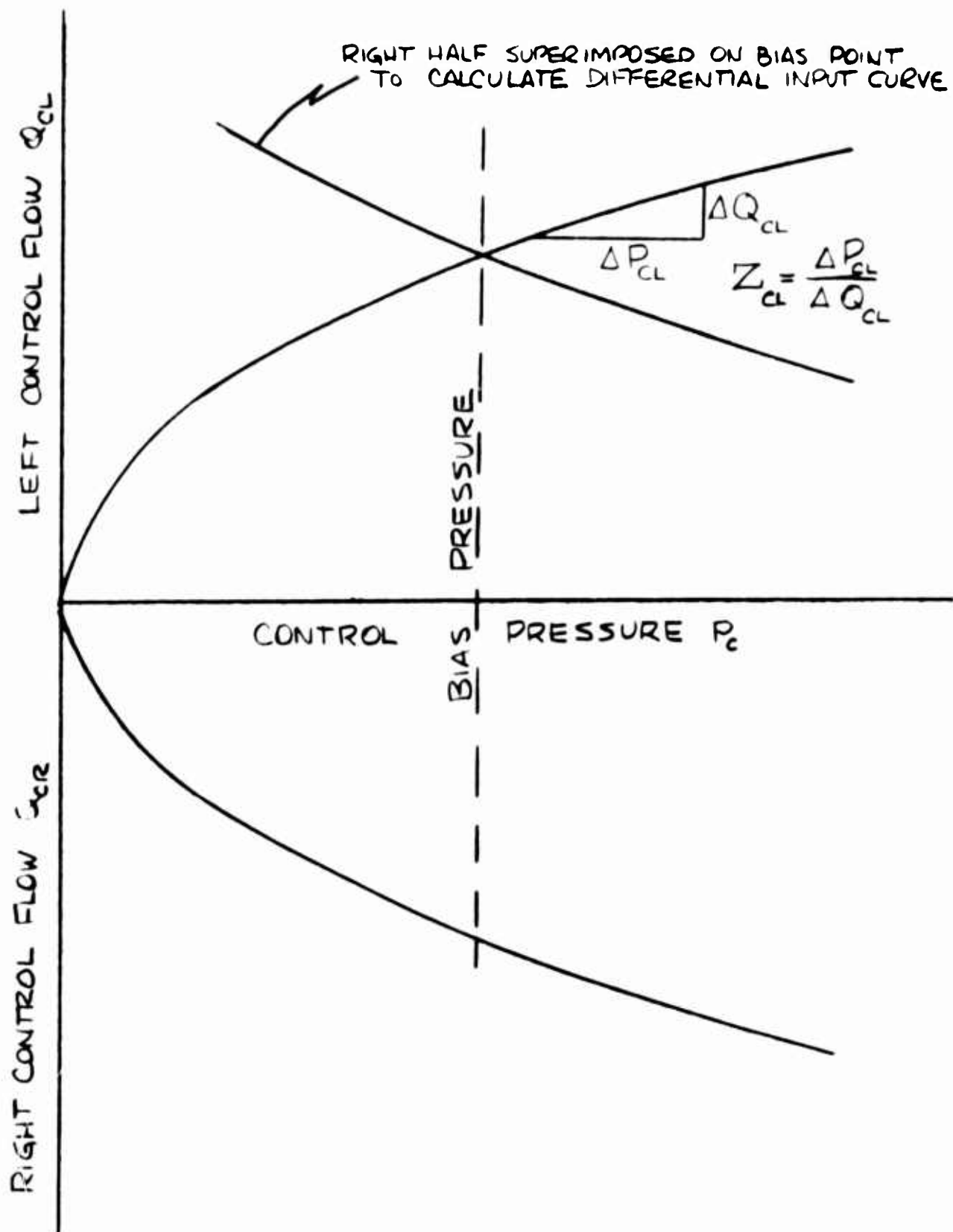


FIG 3 - TYPICAL CONTROL CIRCUIT CHARACTERISTICS

can be described in terms of incremental coefficients. For example referring again to the load circuit characteristics in Figure 2, we can see that for a given control differential pressure, an incremental change in load flow  $Q_{OL}$  will cause an incremental change in amplifier pressure drop  $P_A$  and the slope of the characteristic is

$$Z_O = \left. \frac{\delta P_A}{\delta Q_{OL}} \right]_{P_{cd} \text{ constant}} \quad (\text{output impedance})$$

which has the units of impedance and is directly analogous to the plate resistance  $r_p$  of the vacuum tube.

At a constant level of load flow the effectiveness of the control differential pressure  $P_{cd}$  in changing the amplifier pressure drop  $P_A$  is

$$K_P = \left. \frac{\delta P_A}{\delta P_{cd}} \right]_{Q_{OL} \text{ constant}} \quad (\text{pressure amplification factor})$$

This ratio is dimensionless and is directly analogous to the amplification factor  $\mu$  of the vacuum tube.

At a constant level of amplifier pressure drop the effectiveness of the control differential pressure  $P_{cd}$  in changing the load flow  $Q_{OL}$  is

$$G_P = \left. \frac{\delta Q_{OL}}{\delta P_{cd}} \right]_{P_A \text{ constant}} \quad (\text{pressure transconductance})$$

This factor has the units of conductance relating the flow in the load circuit to the pressure in the control circuit. It is directly analogous to the mutual conductance  $g_m$  in the vacuum tube.

A glance at the graphical construction of these coefficients on the characteristics of Figure 2 shows that  $K_P = G_P Z_O$  which is equivalent to  $\mu = g_m r_p$  in the vacuum tube.

Referring now to Figure 3, the input circuit characteristics, a change in input flow  $Q_{CL}$  is related to a change in input pressure  $P_{CL}$  by

$$Z_{CL} = \left. \frac{\delta P_{CL}}{\delta Q_{CL}} \right]_{Q_{OL} \text{ constant}} \quad (\text{input impedance})$$



which has the dimensions of impedance and is analogous to the input impedance of a vacuum tube amplifier circuit.

#### E. Graphical Performance Analysis

Taken as a whole, the characteristics of the pure fluid amplifier are nonlinear. When operated at the extremes or when driven by a large signal, the parameters are not constant and the output becomes seriously distorted. The graphical method of performance analysis permits one to account for the effects of these nonlinearities without complex mathematics.

Consider the circuit of Figure 4. In the external load circuit

$$P_S = P_{AL} + Q_{OL}Z_{LL} \quad (1)$$

Which is to say simply that at every value of load flow  $Q_{OL}$  the sum of the amplifier pressure  $P_{AL}$  and the pressure drop across the load  $Q_{OL}Z_{LL}$  must equal the supply pressure  $P_S$ . Thus on the characteristic curves the load line for  $Z_{LL}$  can be plotted with one intercept ( $P_{AL} = 0$ ) at  $Q_{OL} = P_S/Z_{LL}$  and the other ( $Q_{OL} = 0$ ) at  $P_{AL} = P_S$ . At all intermediate points the load line follows the equation

$$P_{AL} = P_S - Q_{OL}Z_{LL} \quad (2)$$

Note that

$$Q_{OL} = \frac{P_S}{Z_{LL}} - \frac{P_{AL}}{Z_{LL}} \quad (3)$$

is of the form  $y = b + mx$ , the equation of a straight line of slope  $-1/Z_{LL}$  and intercepts  $P_S$  and  $P_S/Z_{LL}$ . However in the case of the fluid amplifier  $Z_{LL}$  is not usually a constant and the coordinates of the load line must be plotted point-by-point.

In Figure 5 we show a typical load line superimposed on the amplifier characteristics. It is now a relatively simple matter to determine the performance of the amplifier as follows.

With no differential control signal the intersection of the load line and the  $P_{cd} = 0$  characteristic defines the quiescent or stand-by level of the left and right output ports. If either the amplifier or the load restrictors are unbalanced, a difference in pressure across the load restrictors will exist, equal to the difference between the pressure coordinates of the quiescent point of each half of the amplifier. If a unit of control differential pressure is applied in the positive sense ( $P_{CL} > P_{CR}$ ), the operating point of the left half will move along the load line in the direction of decreasing flow to the  $P_{cd} = 1$  curve.

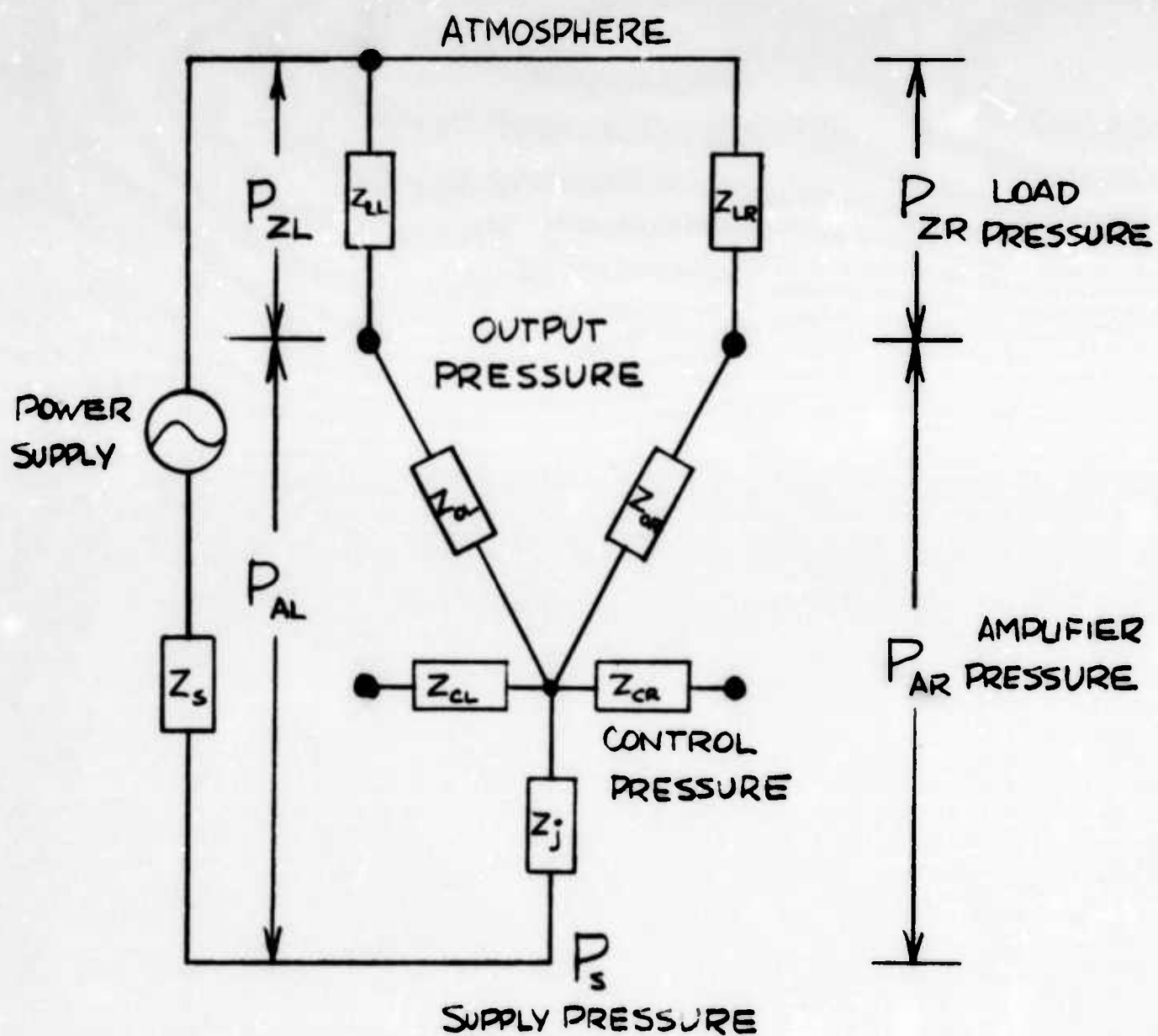


FIG 4 - SCHEMATIC OF THE FLUID AMPLIFIER

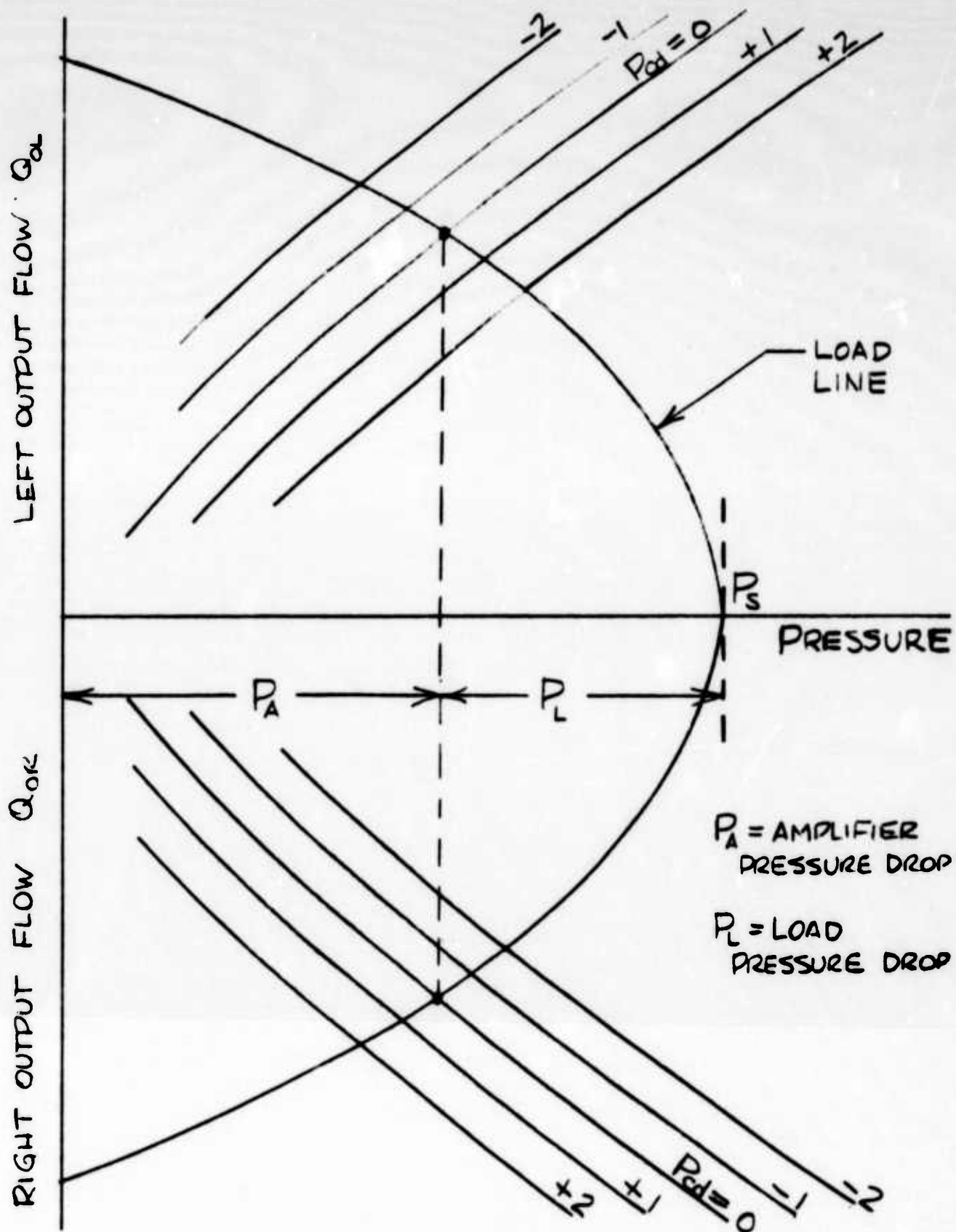


FIG 5- LOAD LINE SUPERIMPOSED ON LOAD CIRCUIT CHARACTERISTICS

The operating point of the right half will move along the load line in the direction of increasing flow to the  $P_{cd} = 1$  curve. The pressures at the output ports of each half are defined by their pressure coordinates and the differential output pressure will be the difference between them. The action is similar but opposite when a negative differential control pressure is applied.

By solving graphically for a number of increments in  $P_{cd}$  it is possible to plot the transfer curve of Figure 6 which relates differential output pressure to differential control pressure of this particular amplifier, this particular load, at this particular bias level and supply pressure. Note that it can reflect the effects of the nonlinear characteristics. We also illustrate the technique for utilizing the transfer curve for determining response of this amplifier circuit to a continually varying input signal.

Since the amplifier characteristics are in terms of differential control pressure, input characteristics were not necessary to the solution of this simple illustrative problem. However, conditions in the input circuit can be analyzed from the input characteristics of Figure 3 in a manner similar to that described above.

In summary, the amplifier load circuit characteristics, the load line and the amplifier input characteristics are sufficient to describe the static and dynamic performance of the pure fluid amplifier in a practical circuit.

#### F. Equivalent Circuit Performance Analysis

Although the graphical methods of analysis are truly general and are equally applicable to small signal amplification, the method involves interpolation and reading of curves and the accuracy becomes generally unsatisfactory. A second convenient method of analysis involves the assumption of linearity for operation with signals of small amplitude, and the development of equivalent electrical circuits of generators and impedances which can be analyzed with conventional mathematical techniques.

##### 1. The Complete Equivalent Circuit

Prior to developing the equivalent circuit for small signal operation it is first necessary to make an intermediate step. That is, to describe the functioning of the fluid amplifier in complete detail in terms of equivalent electrical elements (at least schematically). The characteristics of the elements of this circuit are the complete characteristics and the elements are therefore nonlinear. Thus, if one wants to handle the large-signal performance analysis as a nonlinear mathematical problem, this equivalent circuit would be valid and adequate. It will, of course, include the quiescent (or bias) conditions and is of extreme value in establishing insight into the behavior of the amplifier

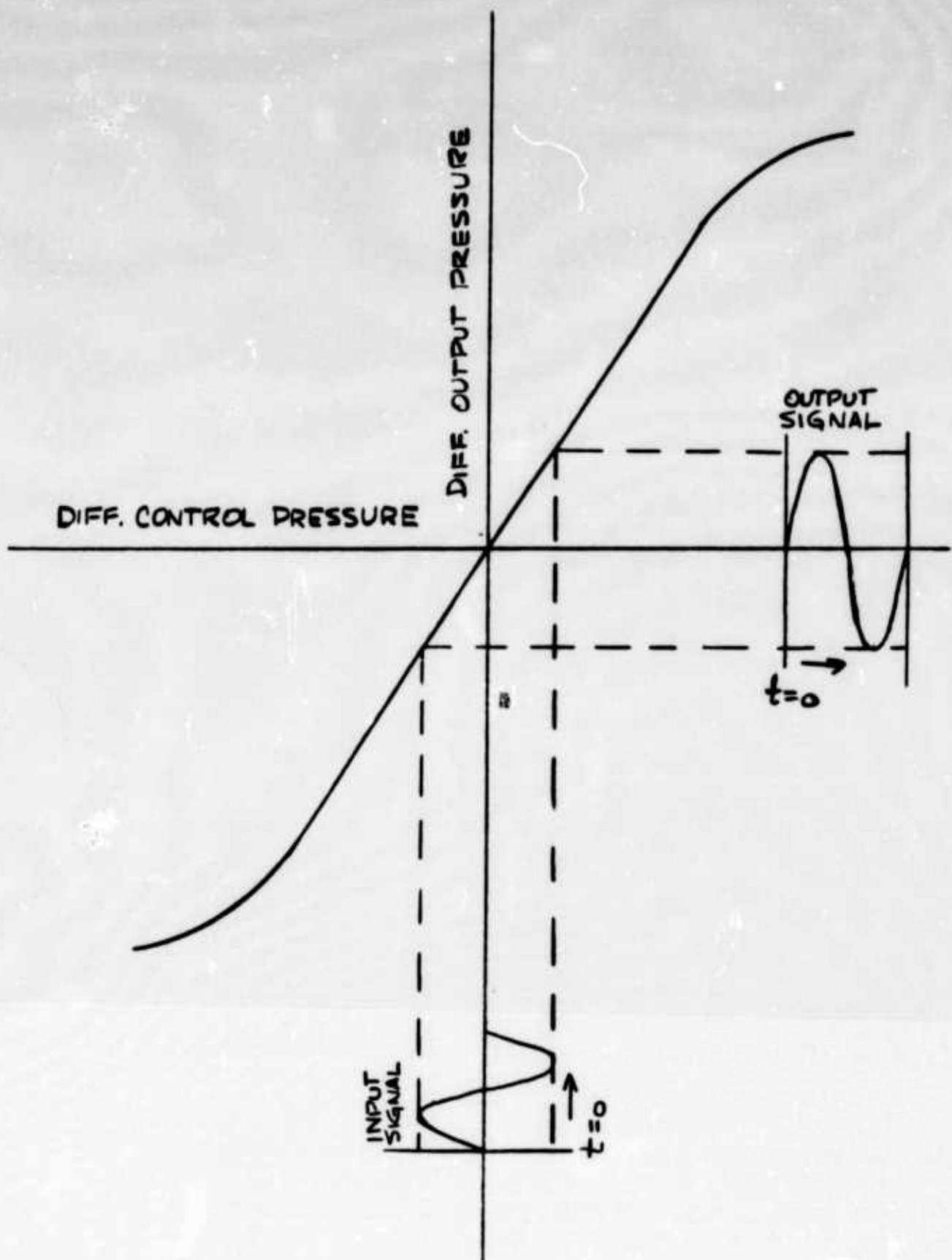


FIG 6 - TYPICAL TRANSFER CURVE

and the problems of cascading stages.

The complete equivalent circuit for the pure fluid amplifier has been developed on a logical basis by studying the theoretical and experimental behavior, then providing circuit elements and interconnections which will behave in an appropriate manner. The results are illustrated in Figure 7. The general layout is directly analogous to the actual device, and each element represents a fluid phenomenon. The power supply is a pressure source developing pressure  $P$  and having an internal impedance  $Z_S$ . The pressure  $P_S$  appears at the supply port of the amplifier, causing a power jet flow  $Q_j$  through the power jet impedance  $Z_j$  and the branch and load impedances  $Z_{OL}$ ,  $Z_{OR}$ ,  $Z_{LL}$  and  $Z_{LR}$ .

In each branch there is a generator with a gain  $K_p$  the calculated amplification factor.  $Z_{OL}$  and  $Z_{OR}$  are the reciprocals of the slopes of the load circuit characteristics at the operating point.  $Z_{LL}$  and  $Z_{LR}$  are the reciprocals of the slopes of the load restrictor characteristics at the operating point.  $Z_B$  is the effective impedance of the bleed ports (if used). The generators are connected differentially and driven by a function of the differential control pressure,  $P_{cd}$ . Differential output pressure  $P_{od}$  is developed at the amplifier output ports.

In the control circuit we have the internal control circuit impedance for each side, shown in two sections, one linear and one nonlinear, to account for the loss in gain at the higher bias levels. There are also zero impedance voltage generators to simulate the suction pressure in the interaction region, generated by the power jet flow  $Q_j$ , having a gain of  $K_g$ . Finally, the absolute levels of control pressure  $P_{CL}$  and  $P_{CR}$  are applied at the control terminals after the signal has passed through the line impedance  $Z_1$ . The effects of internal feedback are neglected.

## 2. The Incremental Equivalent Circuit

The next step is to generate the linearized equivalent circuit for small signals. Referring to the complete circuit of Figure 7, we have in the upper branch of the load circuit

$$P = Q_j(Z_S + Z_j) - K_p P_{cd} + (Q_{OL} - \Delta Q_{OL})(Z_{OL} + Z_{LL}) \quad (4)$$

and in the lower branch

$$P = Q_j(Z_S + Z_j) + K_p P_{cd} + (Q_{OR} + \Delta Q_{OR})(Z_{OR} + Z_{LR}) \quad (5)$$

Subtracting equation (4) from (5) to eliminate the steady conditions and assuming

$$Z_{OL} = Z_{OR} = Z_O \text{ and } Z_{LL} = Z_{LR} = Z_L \text{ and } \Delta Q_{OL} = \Delta Q_{OR} = \Delta Q_O$$



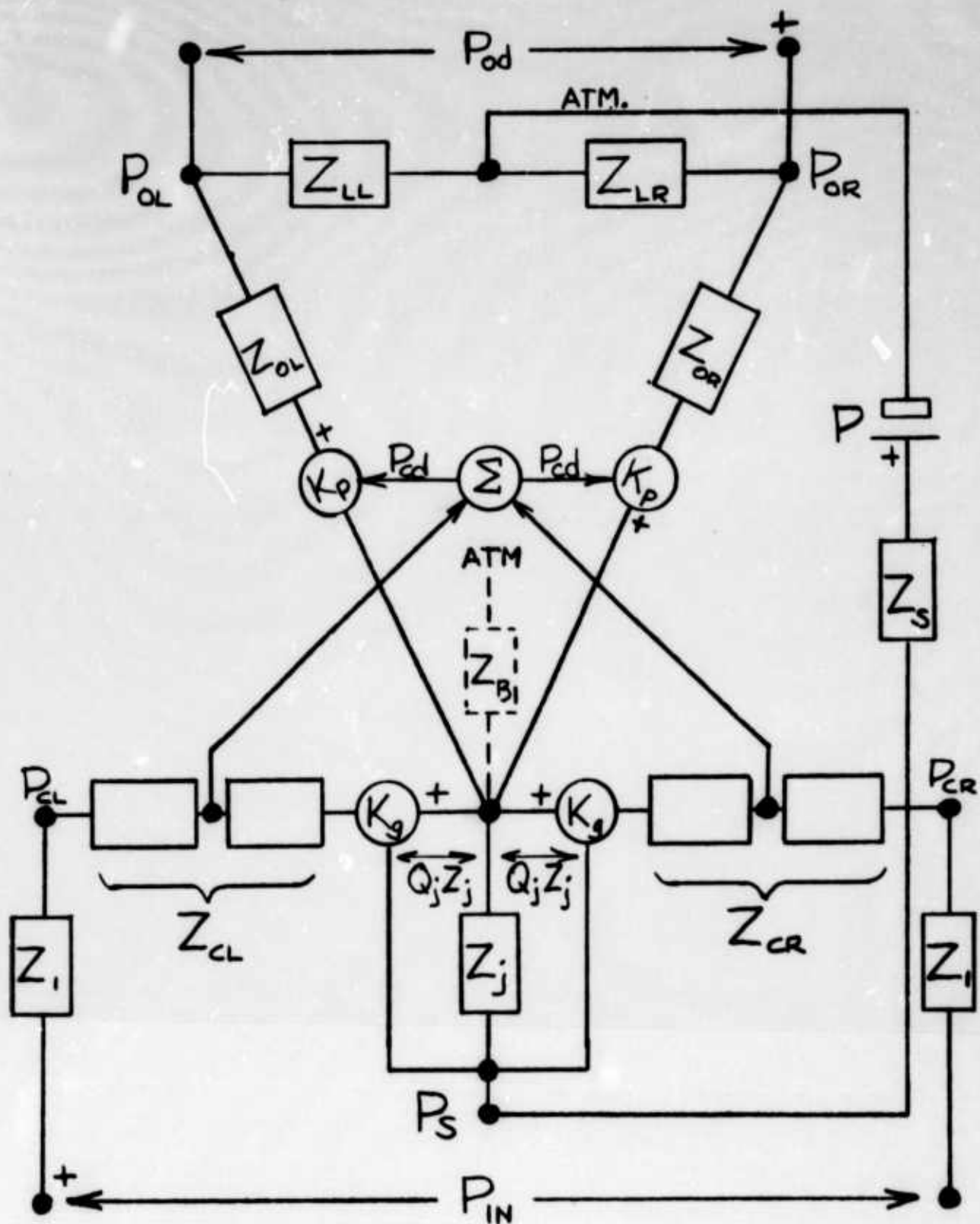


FIG 7- EQUIVALENT ELECTRICAL CIRCUIT

we have

$$2K_p P_{cd} = \Delta Q_0 (2Z_0 + 2Z_L) \quad (6)$$

This represents an equivalent electrical circuit with a generator of output  $2K_p P_{cd}$ , an internal impedance of  $2Z_0$  and a load of  $2Z_L$ .

Similarly in the control circuits we have

$$P_{CL} + \Delta P_{CL} = (Q_{CL} + \Delta Q_{CL})Z_{CL} - (Q_j + \Delta Q_j)Z_j K_g \quad (7)$$

and

$$P_{CR} - \Delta P_{CR} = (Q_{CR} - \Delta Q_{CR})Z_{CR} - (Q_j + \Delta Q_j)Z_j K_g \quad (8)$$

Subtracting equation (8) from (7) to eliminate steady conditions and assuming

$$\Delta P_{CL} = \Delta P_{CR} = \Delta P_c \text{ and } \Delta Q_{CL} = \Delta Q_{CR} = \Delta Q_c \text{ and } Z_{CL} = Z_{CR} = Z_c$$

we have

$$2 \Delta P_c = 2 \Delta Q_c Z_c \quad (9)$$

If we define the differential pressure  $P_{cd} = 2 \Delta P_c$  and the differential flow  $Q_{cd} = 2 \Delta Q_c$ , then equation 9 expresses the conditions in an electrical circuit with a generator of  $P_{cd}$  and an impedance  $Z_c$ .

Thus the linearized incremental equivalent circuit can be drawn as illustrated in Figure 8.

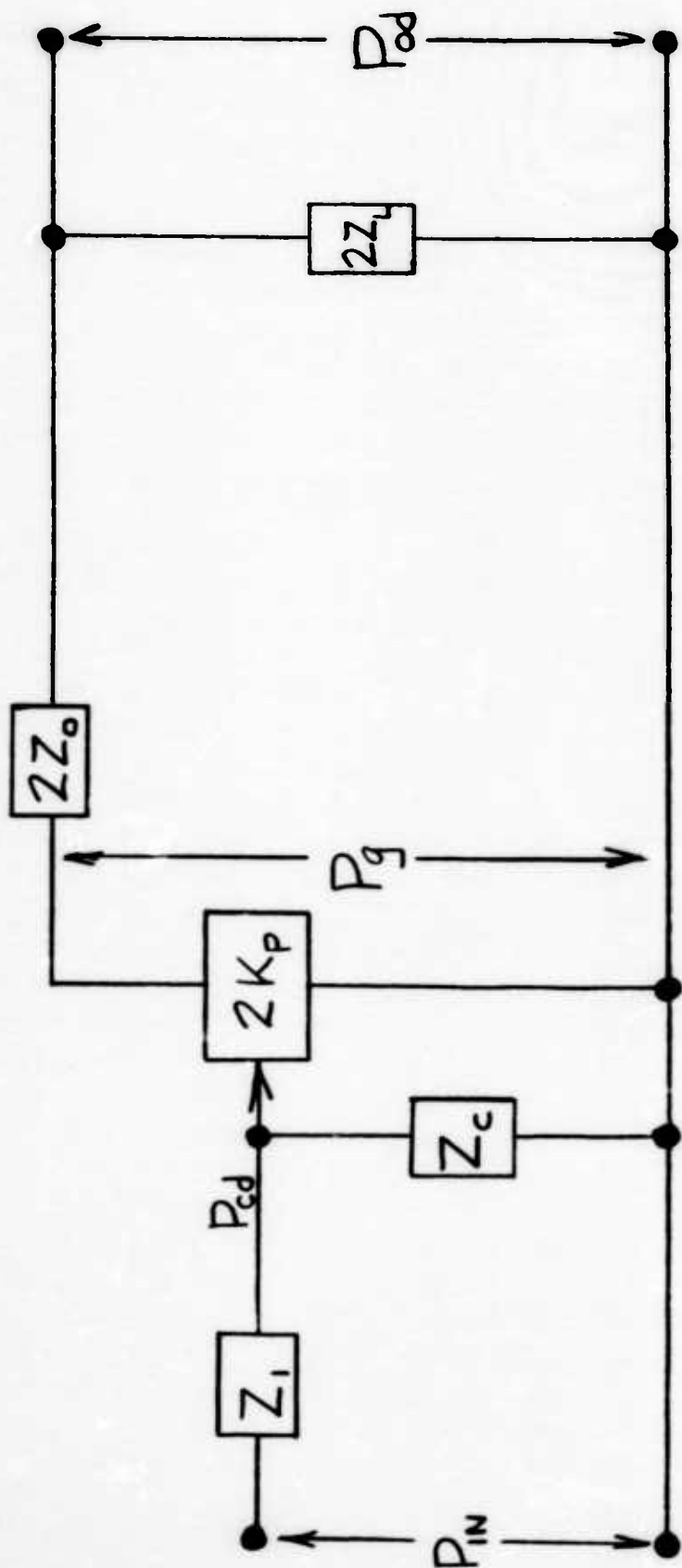
### 3. The Dynamic Equivalent Circuit

Considering the dynamical problem in more detail, we note that all the impedances in Figure 8 can have significant reactive components and the response of the equivalent generator can involve significant lags. Analysis of the amplifier configuration and experimental dynamic performance has led us to hypothesize the dynamical equivalent circuit shown in Figure 9.

In the input circuit,  $Z_1$  is the impedance of the circuits leading to the control ports.  $R_c$  is the static input impedance and  $C_c$  is the equivalent capacitance due to the compression and displacement of the volume of fluid internal to the amplifier. The response of the amplifier, represented by the transfer function

$$\frac{P_g}{P_{cd}} = 2K_p e^{-st_d}$$



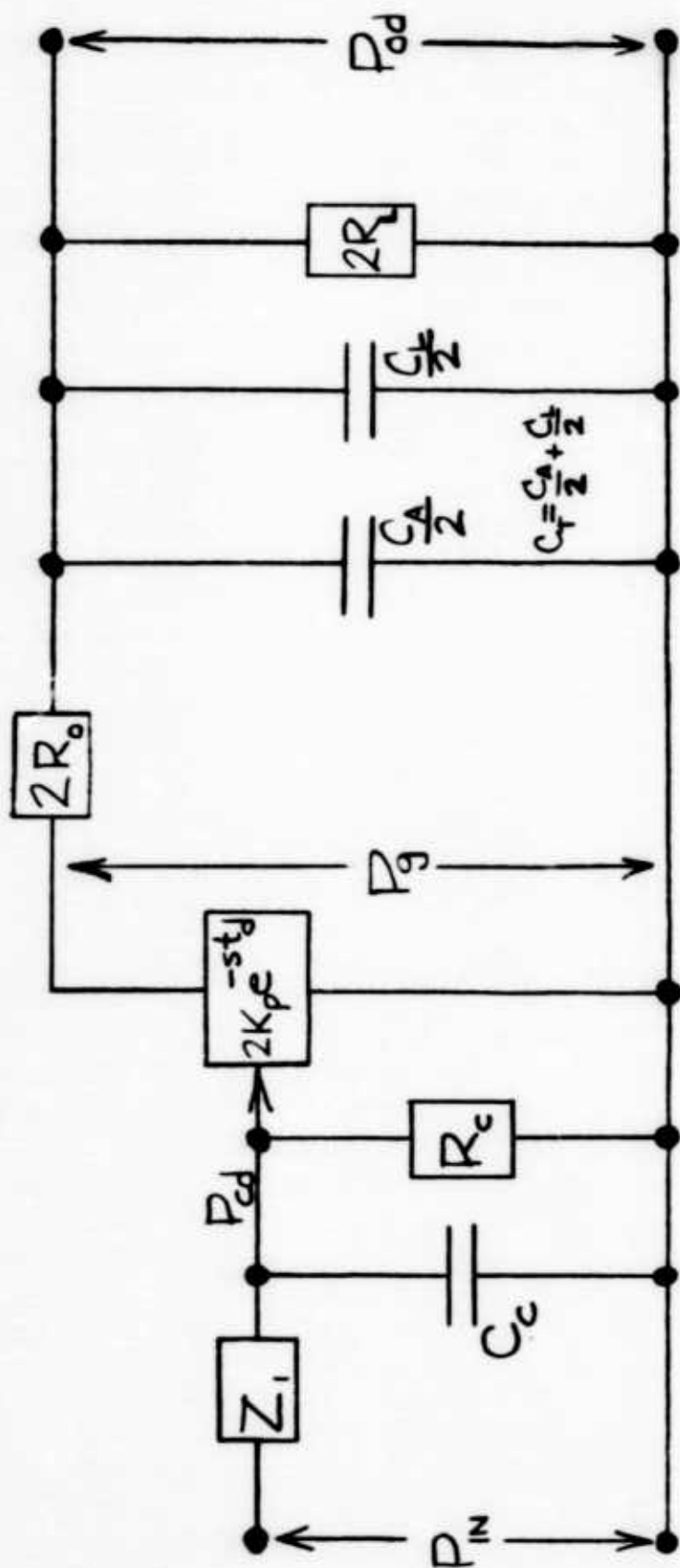


LOW FREQUENCY TRANSFER FUNCTIONS

$$\frac{P_{OD}}{P_{CD}} = \frac{2K_P Z_L}{(Z_O + Z_L)}$$

$$\frac{P_{OD}}{P_{IN}} = \frac{Z_C}{(Z_I + Z_C)} \frac{2K_P Z_L}{(Z_O + Z_L)}$$

FIG 8- LINEARIZED INCREMENTAL EQUIVALENT CIRCUIT



### MID-FREQUENCY TRANSFER FUNCTIONS

$$\frac{P_{od}}{P_{cd}} = \frac{2K_P R_L}{(R_o + R_L)} \frac{e^{-st_d}}{(1 + s C_T \frac{2R_o R_L}{R_o + R_L})}$$

$$\frac{P_{od}}{P_{in}} = \frac{2K_P R_c R_L}{(Z_i + R_c)(R_o + R_L)} \frac{e^{-st_d}}{(1 + s C_c \frac{Z_i R_c}{Z_i + R_c})(1 + s C_T \frac{2R_o R_L}{R_o + R_L})}$$

FIG 9- EQUIVALENT CIRCUIT FOR INTERMEDIATE FREQUENCIES

appears as a delay due to transit time of the particles in the power jet. Other delays due to viscosity or compressibility in the interaction chamber have been neglected. At the output channels of the amplifier we have the equivalent capacitance  $C_A$  of the internal volume fed by the static output impedance  $R_O$ . In the external circuit there are the equivalent capacitance  $C_L$  (due to the volume of the air in the output circuits) and the resistive component of the load  $R_L$ .

In applying these equivalent circuits to analyze the small-signal performance of an amplifier, the operating point is first determined from either the graphical characteristics or the complete equivalent circuit. The values of the parameters  $Z_C$ ,  $K_p$ ,  $Z_O$  and  $Z_L$  at that point are calculated as constants. The quantities are then inserted into the linearized equivalent for circuit analysis by well-known methods. The equivalent circuit approach is particularly valuable in the treatment of external feedback paths, cascaded stages and dynamic circuits.

### III. EXPERIMENTAL

#### A. Experimental Amplifiers

Two amplifiers of radically different design were used in the experimental phase of this work. One was a relatively large unit with a 0.07 x 0.50 inch power nozzle fabricated in the machine shop of The Franklin Institute. The second had a power nozzle 0.02 x 0.05 inches, was fabricated by Corning Glass and supplied to us by the Harry Diamond Laboratories.

#### B. Test Circuits

The experimental circuit for static tests is shown in Figure 10. Fixed restrictors calibrated against laboratory Rotameters were used to measure flow.

The experimental circuit for dynamic tests is shown in Figure 11. Length of lines to pressure transducers and trapped volumes in the input and output circuits were kept to a minimum. The function generator is a pneumatic Wheatstone bridge containing two nozzles impinging on a motor-driven wobble-plate.

### IV. TEST RESULTS

Typical characteristic curves for the experimental amplifiers are shown in Figures 12 and 13. Figure 14 is the frequency response of the HDL 933 amplifier.

In Figures 15 and 16 the performance of the experimental amplifier is correlated with performance calculated by the load line

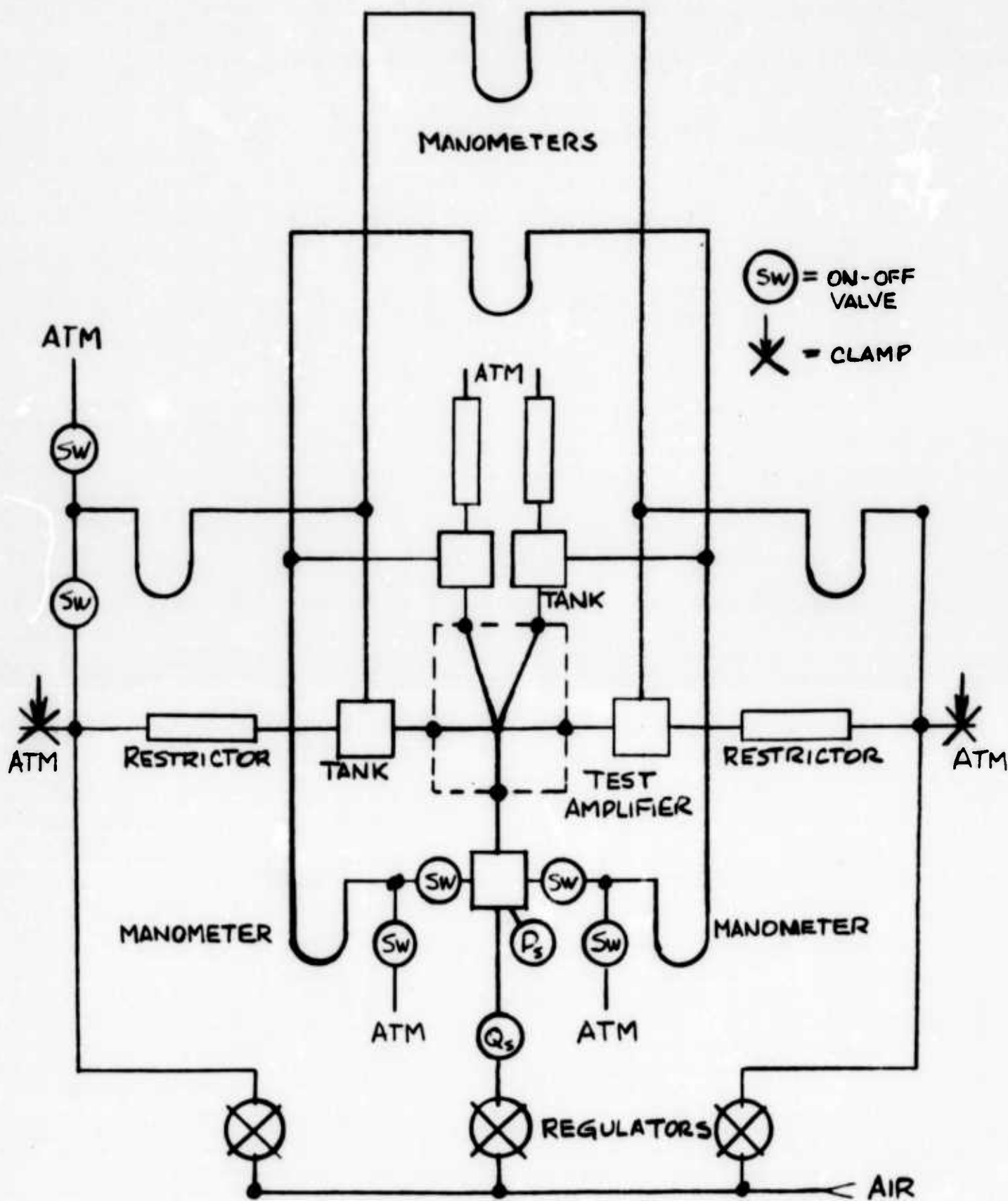


FIG 10- SCHEMATIC OF STATIC TEST CIRCUIT

OSCILLOSCOPE

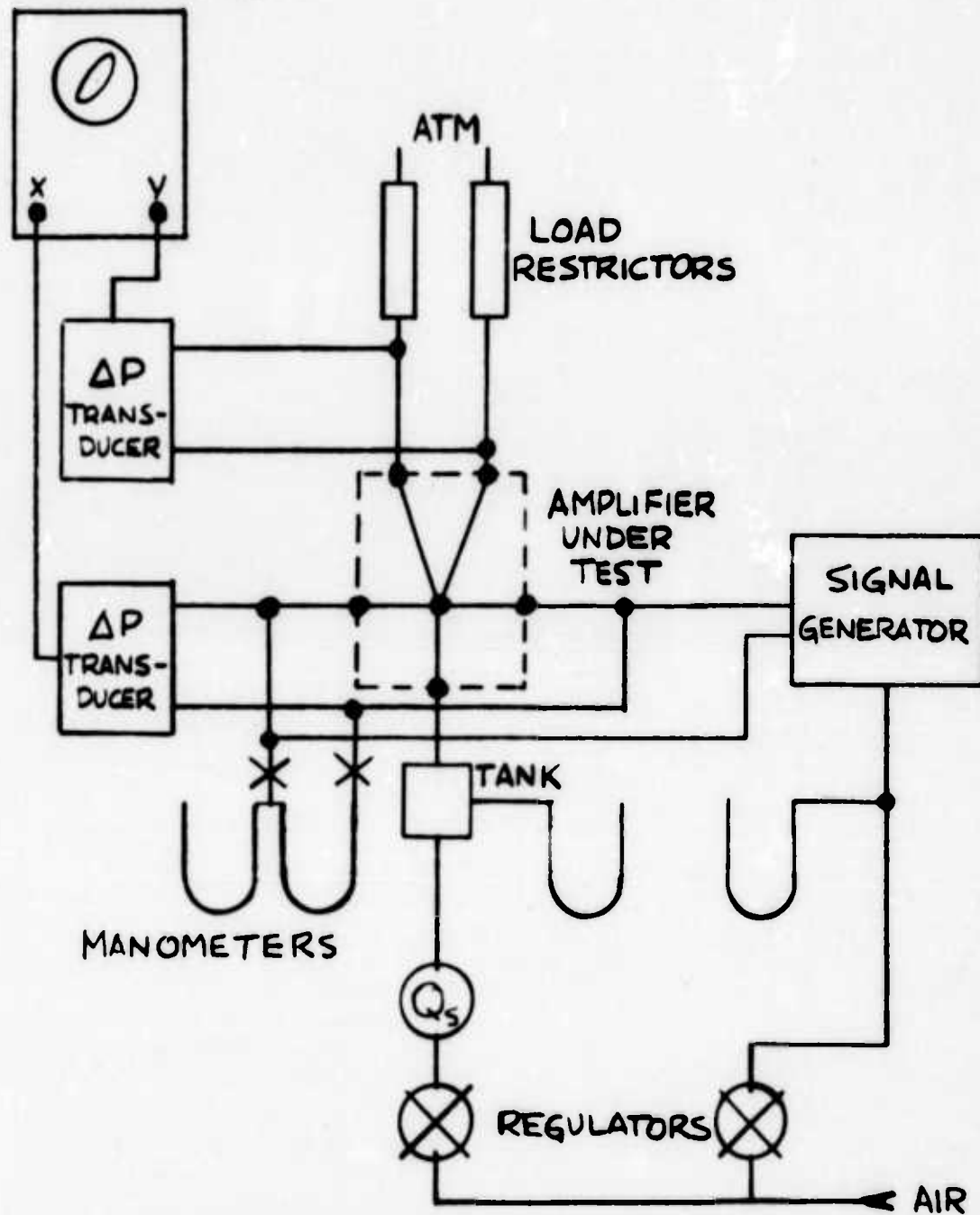


FIG 11- SCHEMATIC OF DYNAMIC TEST CIRCUIT

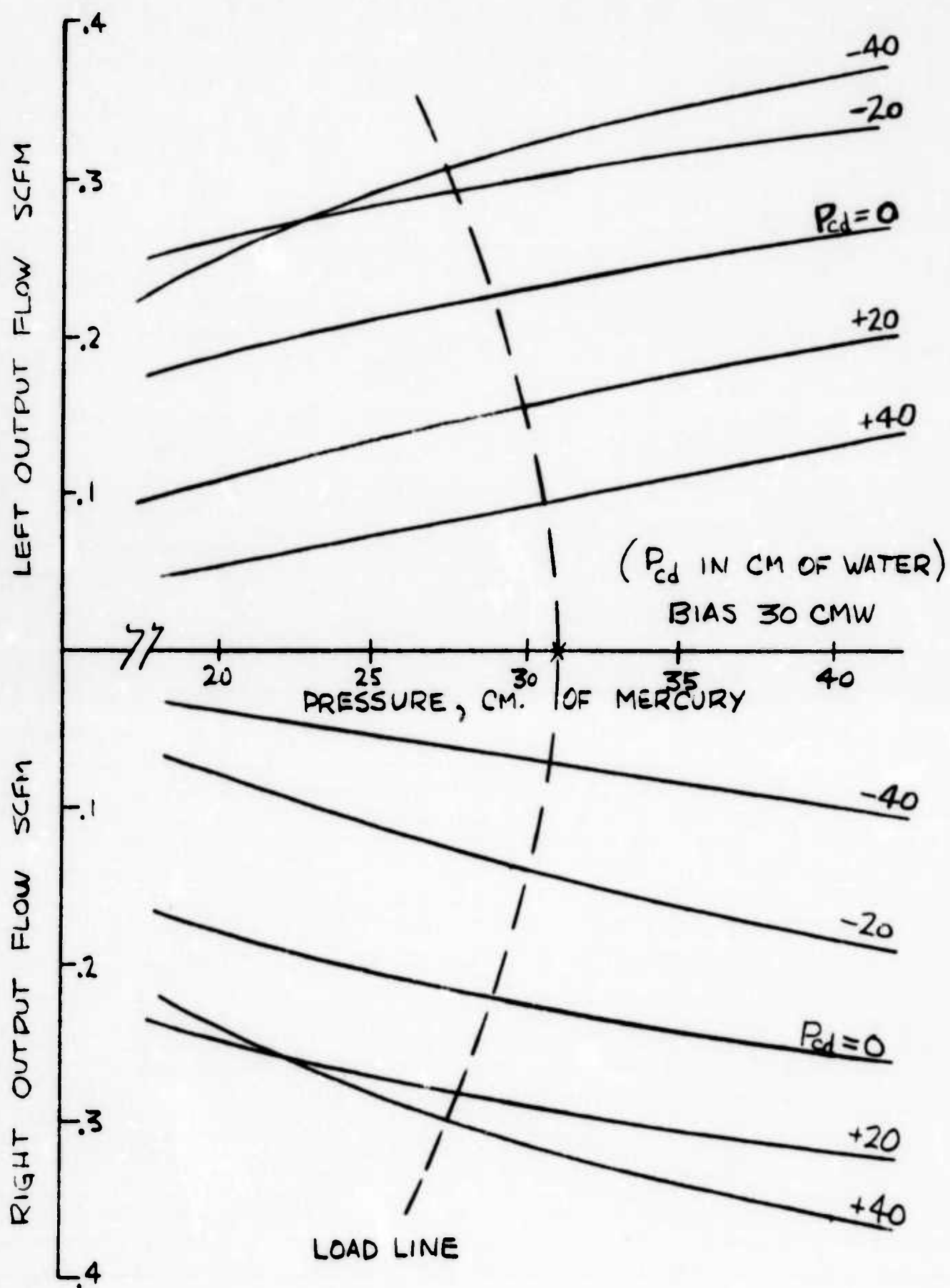


FIG.12 - LOAD CIRCUIT CHARACTERISTICS -HDL 933

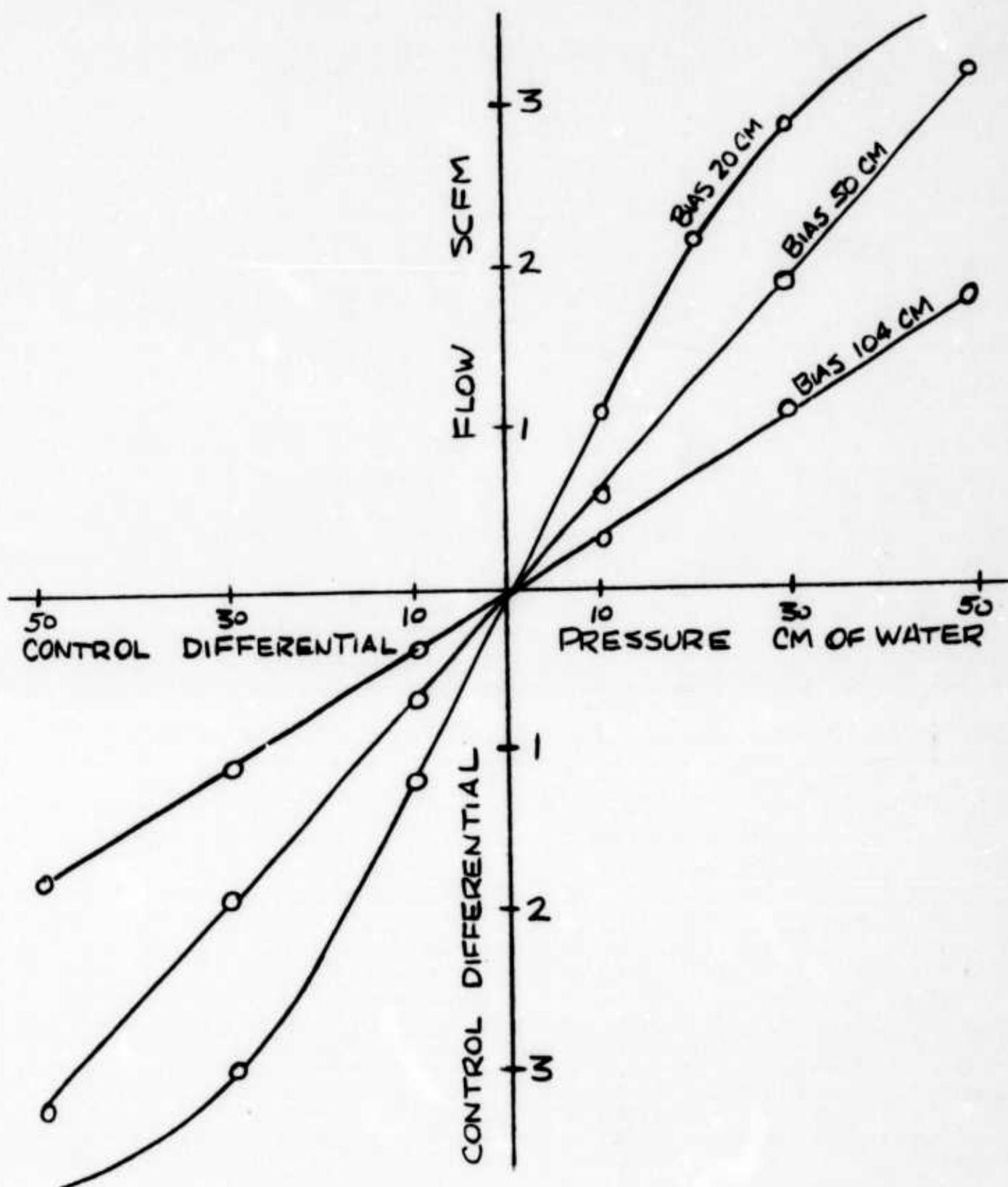


FIG. 13 - DIFFERENTIAL INPUT CHARACTERISTICS-FIL\*1

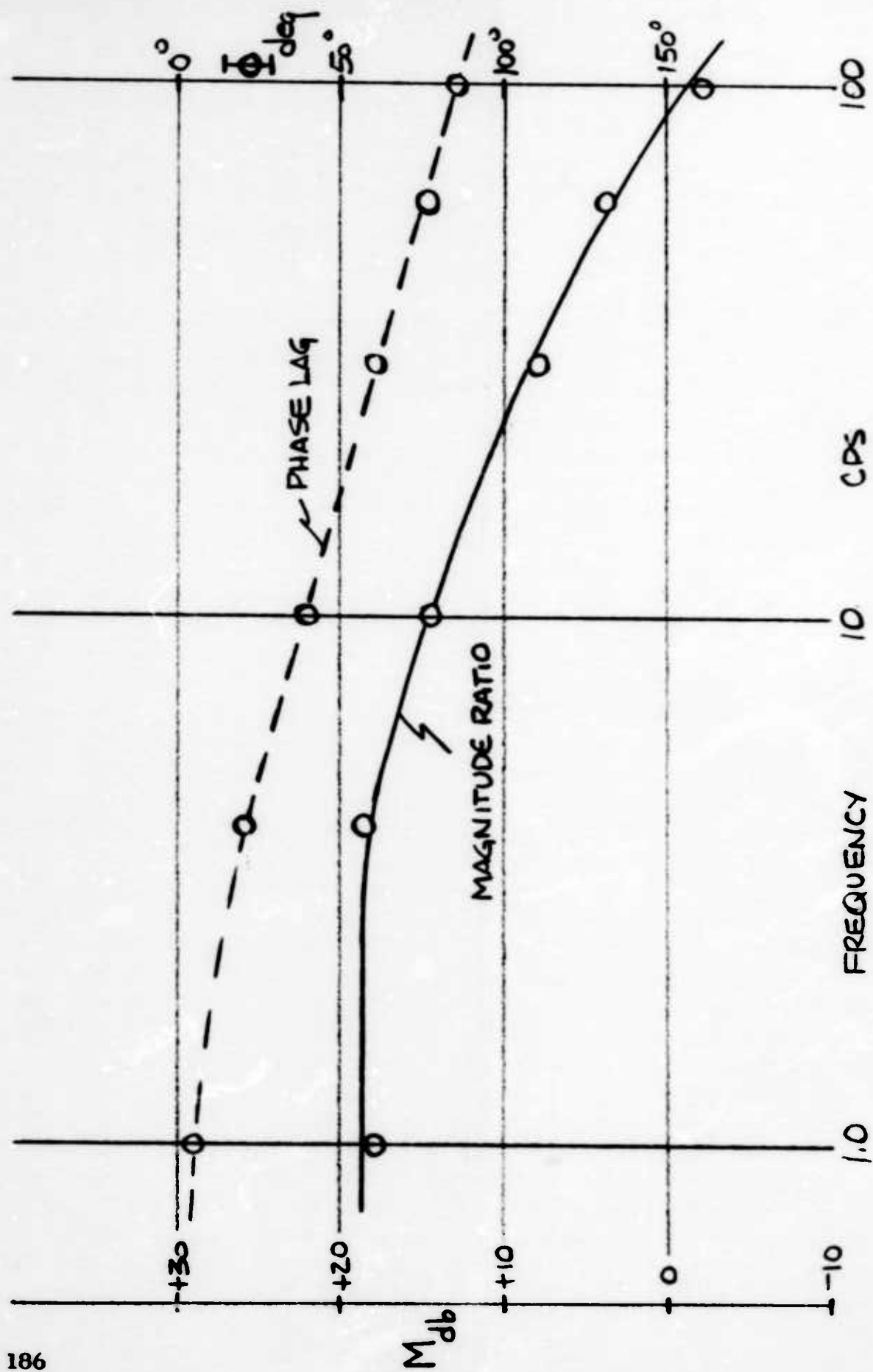


FIG 14--FREQUENCY RESPONSE - HDL 933 AMPLIFIER



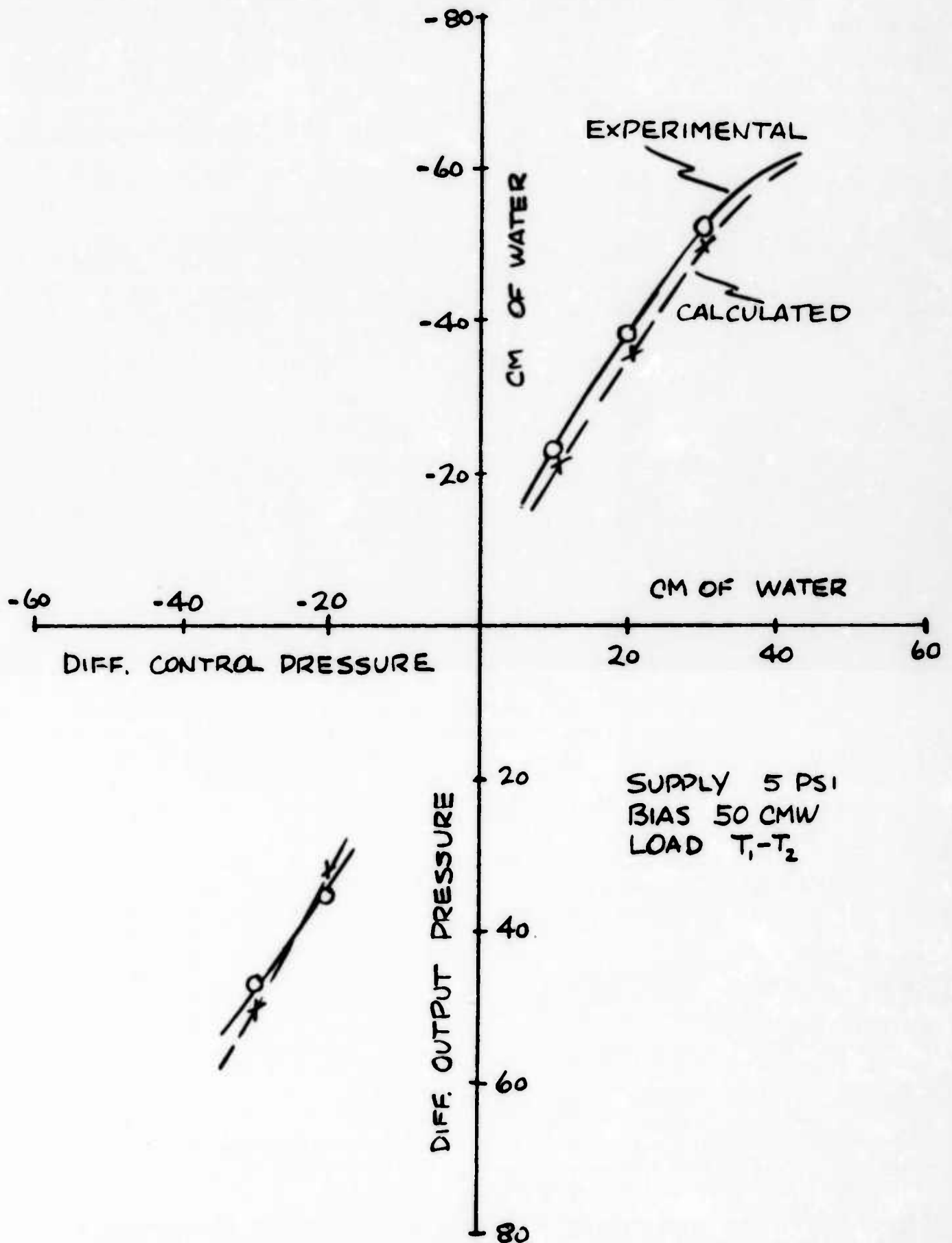


FIG.15- STATIC TRANSFER CURVE - FIL #1

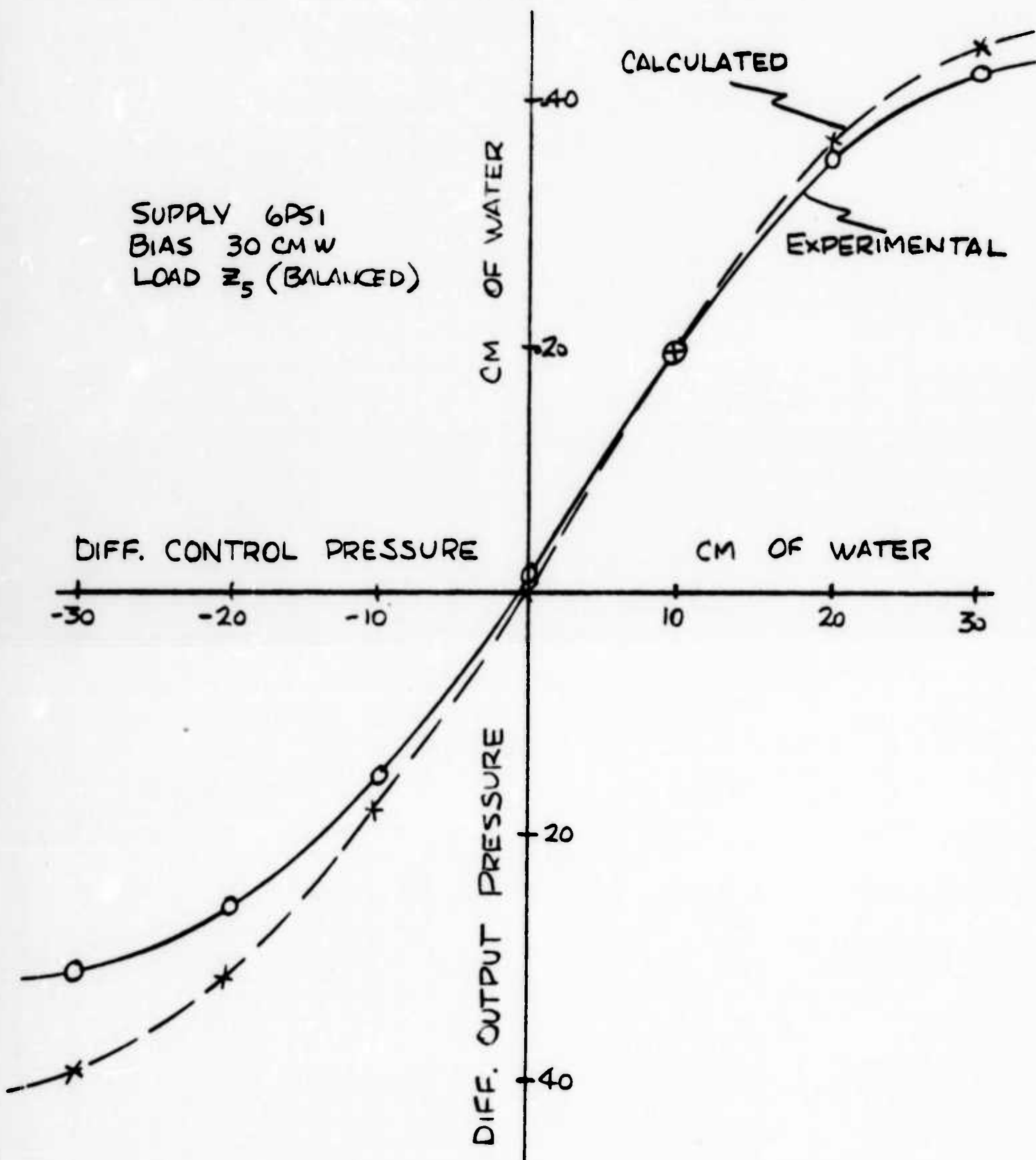


FIG 16 - STATIC TRANSFER CURVE - HDL 933

techniques under static conditions. Using the incremental equivalent circuit under static conditions it has been possible to predict performance for various loads, supply pressures and bias levels with an average accuracy of 5%. Difficulty is encountered when the loads are extremely different from those used in plotting the characteristics.

Figure 17 shows the correlation using the equivalent circuit technique under dynamic conditions. To this date we have been successful in predicting the effect of changes in the load circuit only.

## V. CONCLUSIONS

In conclusion, the analytical and graphical techniques developed in the present research program show promise of being a convenient and valid method for defining a proportional fluid amplifier's characteristics and predicting its in-circuit performance. When they have been refined and verified (especially in the dynamic case) these techniques should be of great value in promoting the application of pure fluid amplifiers in control systems.

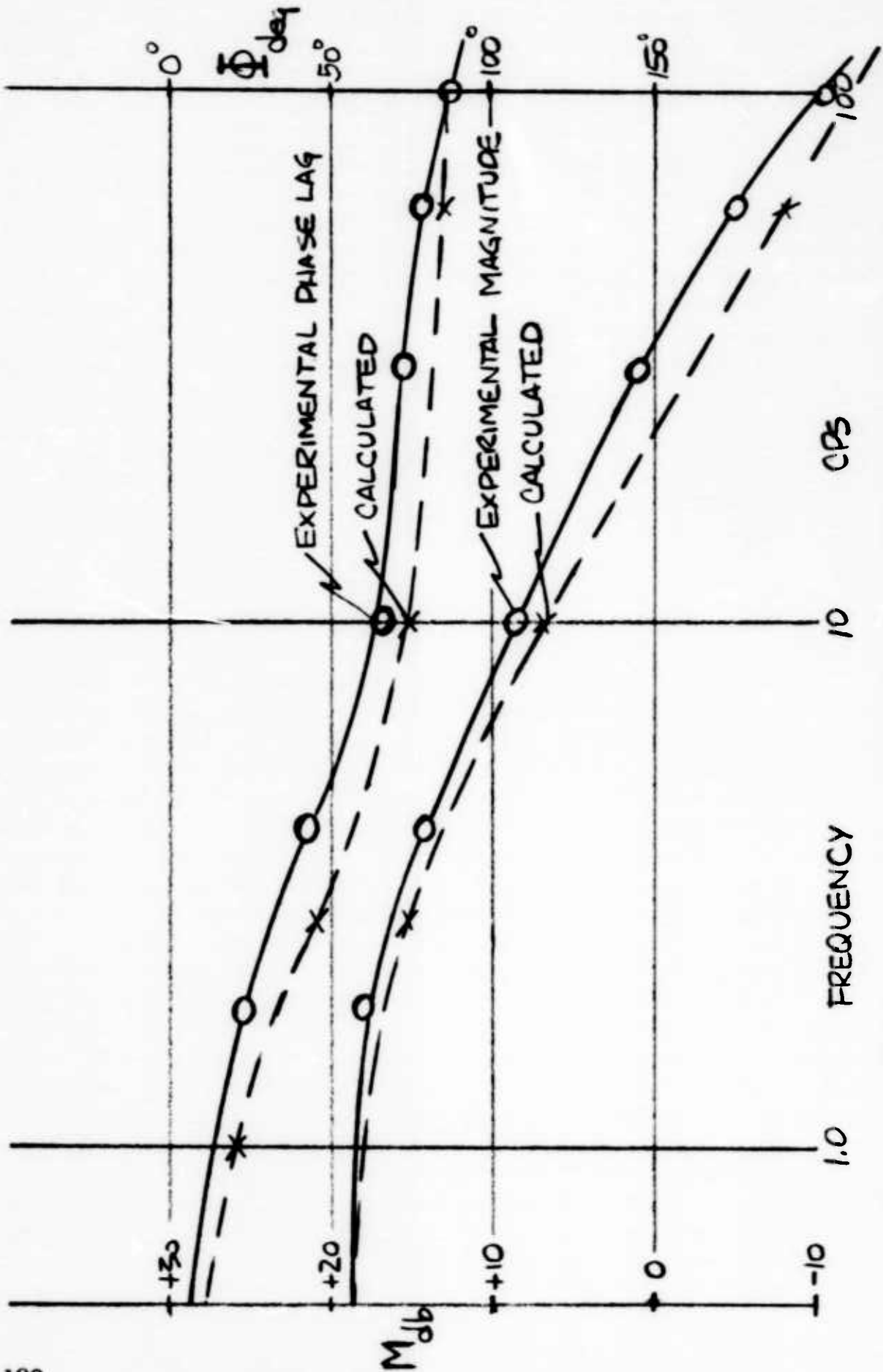


FIG 17-FREQUENCY RESPONSE WITH ADDED VOLUME- HDL 933 AMPLIFIER

# STATIC DESIGN OF PNEUMATIC LOGIC CIRCUITS

by  
H. T. Saghafi  
IBM General Products Division  
Development Laboratory  
Endicott, New York

## ABSTRACT

This paper describes the static design of pneumatic logic circuits using jet amplifiers. The design approach is presented in the graphical form for better visualization of circuit operations. Basically, we are concerned with a generalized logic circuit which is modified to build resistor and diode AND and OR blocks. Initially, two algebraic circuit equations are derived for the output network of this generalized block. Then, the existence of a focus point for the switching points (a useful property of the input network) is demonstrated. Finally, the graphical design approach of several resistor and diode logic circuits is presented.

The result of the analysis is the qualitative determination of an over-all relationship between fan-in, instability distance, switch points, and input impedance of the attachment amplifier. From these relationships a theoretically ideal input characteristic was evolved which would result in circuit design flexibility as well as maximum fan-in for a given instability region.

Logical properties of the mono-output and duo-output fluid jet amplifiers are also discussed in terms of several possible pneumatic logic systems.

## I INTRODUCTION

Operation of the attachment fluid jet amplifier is inherently digital; this characteristic makes it suitable for the implementation of pneumatic logic circuits. The pneumatic jet amplifier is considered as a four-port device whose characteristics are determined experimentally. Then, static analyses of pneumatic circuits using this amplifier are presented in terms of a set of hypothetical characteristics which are similar to the experimental curves. To eliminate confusion in presenting the methods of analysis, manufacturing tolerance effects are not included in the determination of the circuit operating points.

## II PNEUMATIC AMPLIFIERS

Based on the attachment and the amplification phenomena, many different pneumatic amplifiers can be designed. However, from the standpoint of logical design only two types of amplifier elements are needed — a decision element and a memory element. The "decision

element" is used in mechanizing certain logic rules such as the AND and the OR operations. The "memory element" is capable of storing a bit of information which can be used either for sequencing operations or for storing binary characters.

Physically, pneumatic decision and memory elements are similar in characteristics, but differ in some geometrical details. Typical input impedance characteristics are shown in Figure 1.

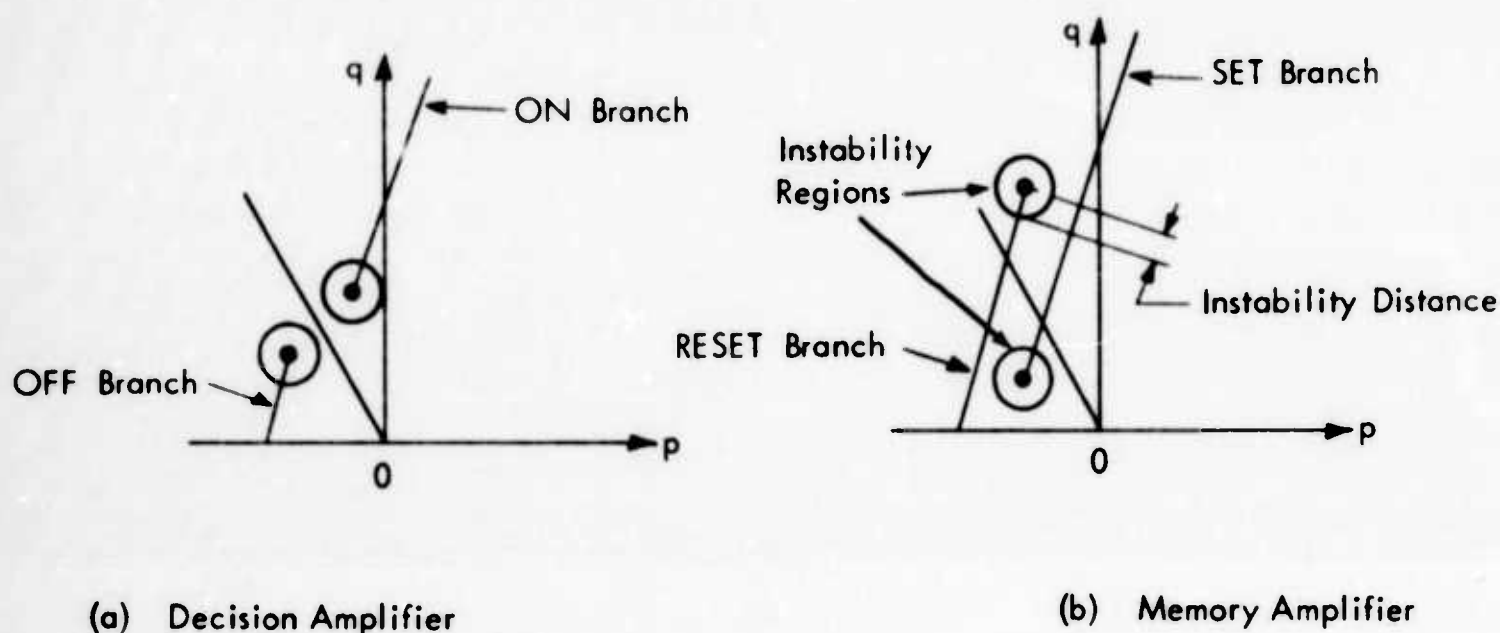


Fig. 1 - Typical Input Impedance of Pneumatic Amplifiers

The decision (or the biased) element changes its logical state when a control signal is applied but returns to its original state when the control pulse is removed. In terms of the impedance characteristics, a straight line through the origin (i.e. a certain driving impedance) would not intersect both branches of the input impedance of the decision amplifier.

The memory element has two controls. It changes its state when one of the controls is pulsed and remains in the new state when the control signal is removed. To return the memory element to its initial state, an input signal is applied at the other control. In terms of the input characteristics, a straight line through the origin would intersect both branches of its input impedance.

To safeguard against erroneous or oscillatory circuit operations, it is best to specify an instability region by a circle around the switch points whose radius (instability distance) can be found experimentally. Then, in any circuit design, the operating points can be either on or outside the boundary of this region. This means that any driving impedance line can, at most, be tangent to the instability circle; otherwise it should pass outside the region. On the other hand, if the operating points are designed too far from the switch points, the switching time of the amplifier will increase.

According to their logical characteristics, three different decision amplifiers and three different memory amplifiers are possible (Figure 2). Notice that it is possible to combine two decision amplifiers and form a memory element (Figure 3).


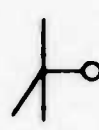





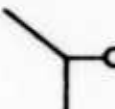
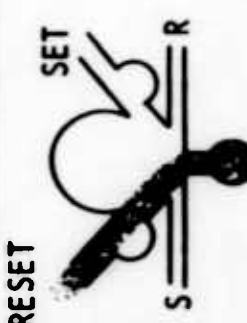
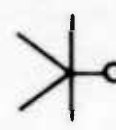
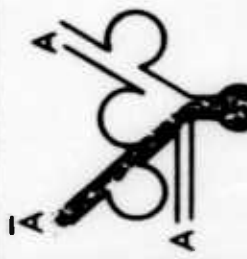

Memory Amplifiers (Latching)			Decision Amplifiers (Biased)		
	Description	Symbol		Description	Symbol
Mono-output Inverter Amplifiers	 SET = 0 RESET = 1				
Mono-output Amplifier	 SET = 1 RESET = 0				
Duo-output Amplifier	 SET RESET				

Fig. 2 - Logical Classification of Pneumatic Amplifiers

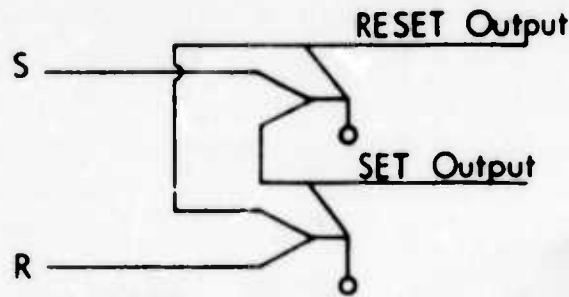


Fig. 3 - Memory Element Built From Two Decision Amplifiers

For the design of pneumatic circuits we must also know the output characteristics of the amplifiers. Typical output characteristic curves are shown in Figure 4. These characteristics behave as a constant pressure source in the region of low flow, where the switching points of the input impedance curves are also normally located. This is a significant relationship, particularly with respect to the design of the directional logic circuits.

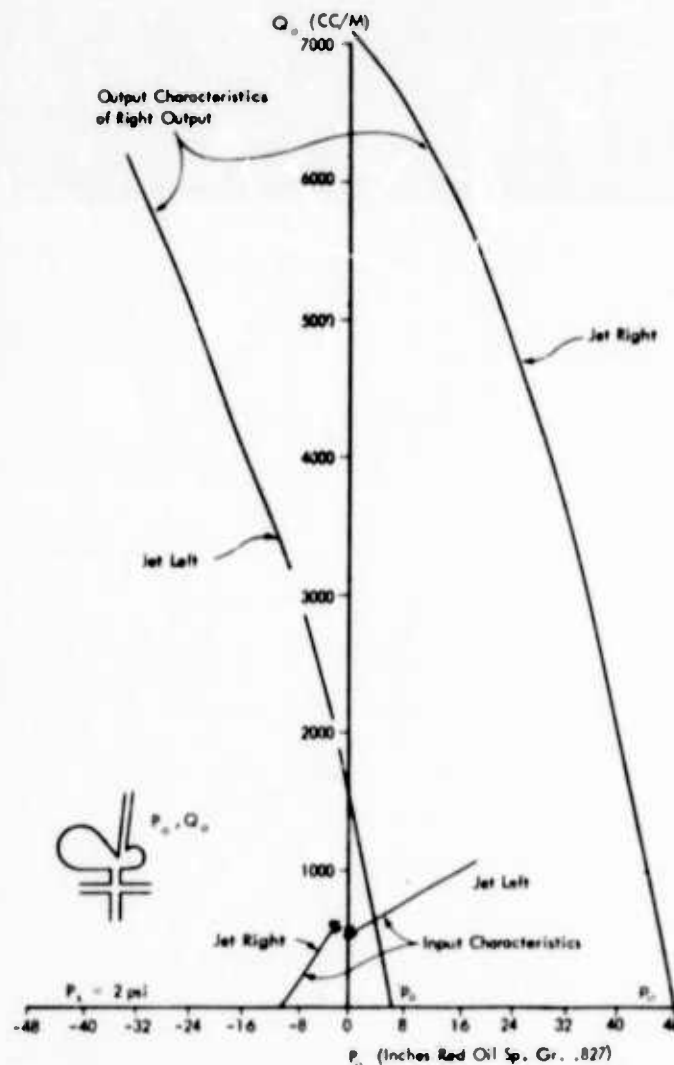


Fig. 4 - Typical Input and Output Impedance of Pneumatic Amplifiers (2 PSI Supply Pressure)



### III PNEUMATIC CIRCUITS

All necessary logical circuits can be designed by interconnecting pneumatic amplifiers with diodes or resistors. The circuit variables of such pneumatic circuits are pressure and flow; these correspond to their electrical analogs, voltage and current.

The simplest and most basic pneumatic circuit is shown in Figure 5.

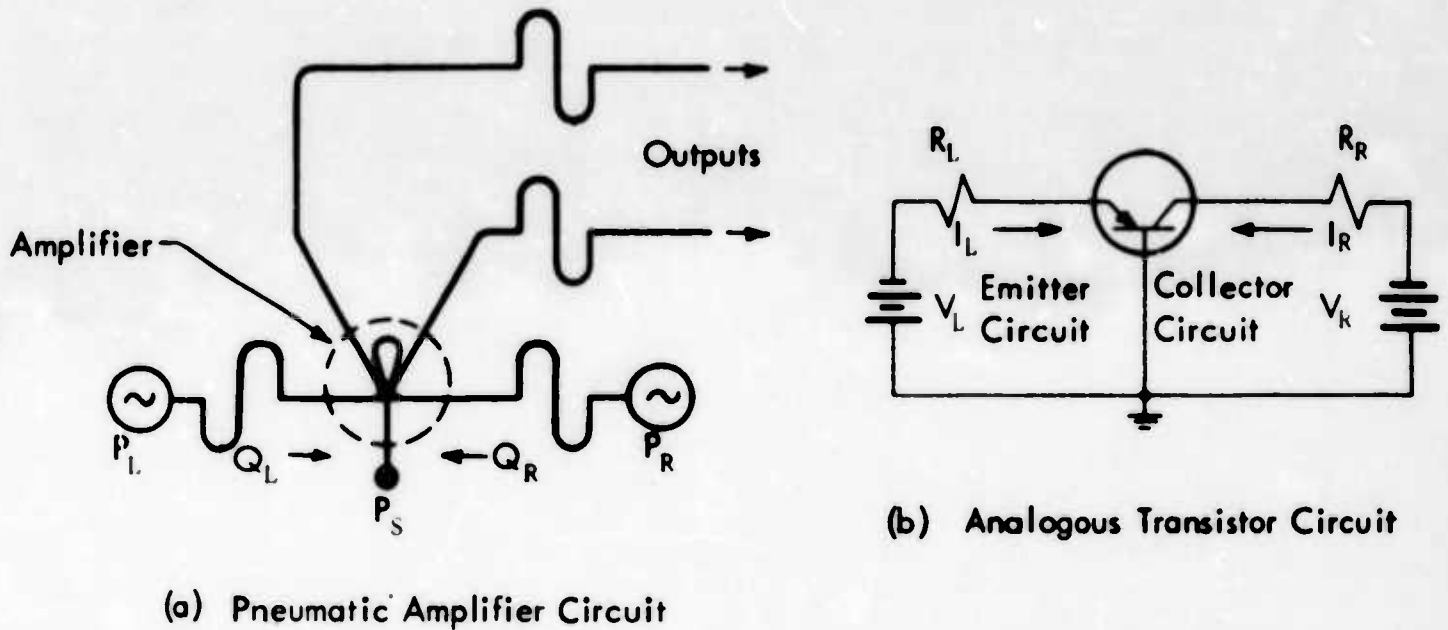


Fig. 5 - The Basic Pneumatic Circuit

Its characteristic curves are shown in Figure 6.

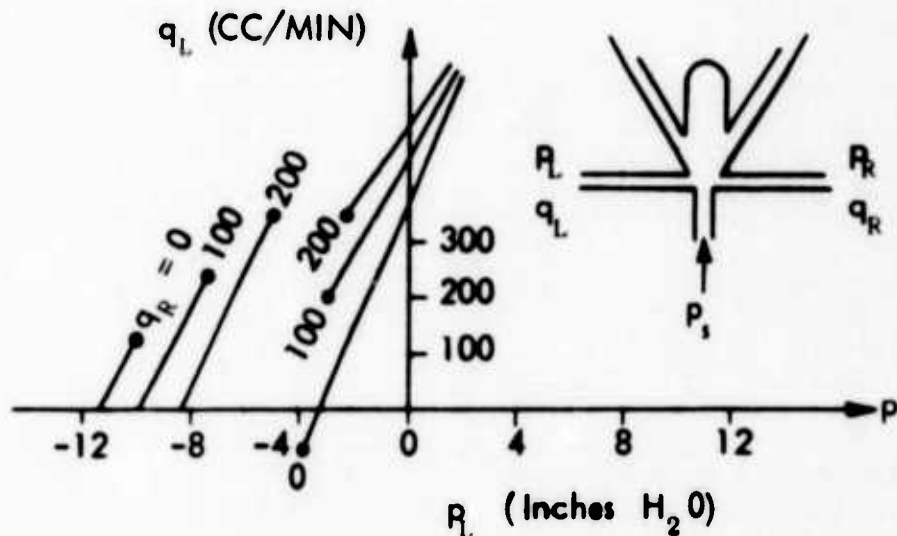


Fig. 6 - Typical Left Input Impedance for Several Right Bias Flows

These curves are obtained by keeping the flow into the right control port at various constant values, and observing the pressure-flow characteristics of the left control port. For any given  $q_R$  the input impedance of the left control port is essentially linear with a discontinuity which represents the switching action of the amplifier. Points on the left branches of these curves correspond to the main amplifier jet being attached to the left wall; points on the right branches correspond to the main jet being attached to the right wall. For the sake of convenience, when the jet is on the right wall, the amplifier is said to be ON, otherwise it is OFF. These curves show that the left and the right control circuits are related in an analog manner, while the outputs respond digitally.

For the purposes of logical implementation, only a limited number of circuit blocks are needed. The most common ones are AND, OR, and INVERTER blocks. Actually, it is unnecessary to have all three blocks; the INVERTER and either the OR or the AND block would be sufficient for the implementation of all logical functions.

In general, a logic block (whether it is an AND or an OR) can be represented by the network shown in Figure 7.

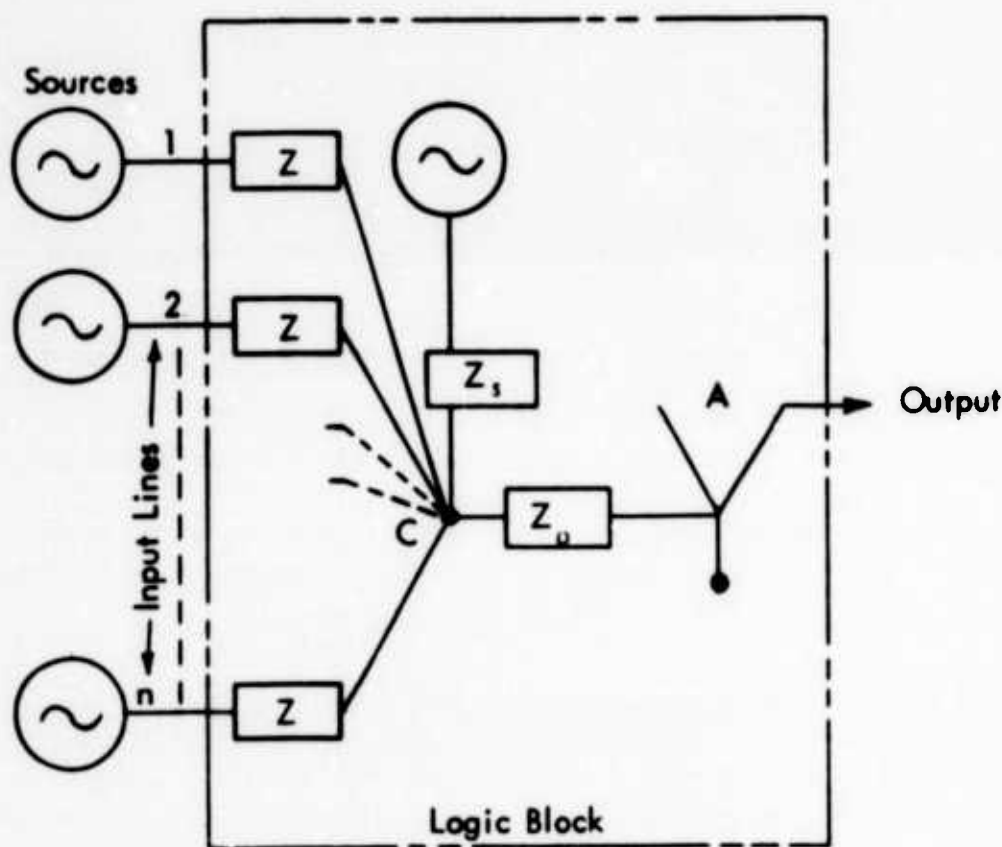


Fig. 7 - Generalized Logic Block

In general, the impedances  $Z_o$  and  $Z$  could involve a number of the elements such as resistors, inductors, diodes, etc.

Depending on the type of circuit elements used in  $Z_o$  and  $Z$ , three different circuit types can be considered: (1) resistor logic, (2) directional logic, (3) diode logic. In resistor logic, pure resistors are used for  $Z_o$  and  $Z$ . The biasing resistor,  $R_s$ , is removed. In directional logic, the direction of the air flow is the significant element in performing logical functions. The passive blocks of directional logic are shown in Figure 21. In diode logic the impedances  $Z$  are replaced by diodes. Depending on whether an OR circuit, or an AND circuit is desired, the biasing resistor  $R_s$  is removed or left in the circuit, respectively. Basic passive diode circuits are shown in Figure 23.

Static design of the three logic circuits is basically very similar. Impedances  $Z_o$  and  $Z$  are pure resistors  $R_o$  and  $R$ . The value of  $R_o$  may vary from zero (directional circuits) to some finite value (resistor and diode circuits). The resistances are either due to the inherent interconnecting resistances (directional logic) or are purposely added in the circuit to obtain logical operations (resistor and diode circuits). For the analysis, the network of Figure 7 can be divided into an output circuit and an input circuit as shown in Figure 8.

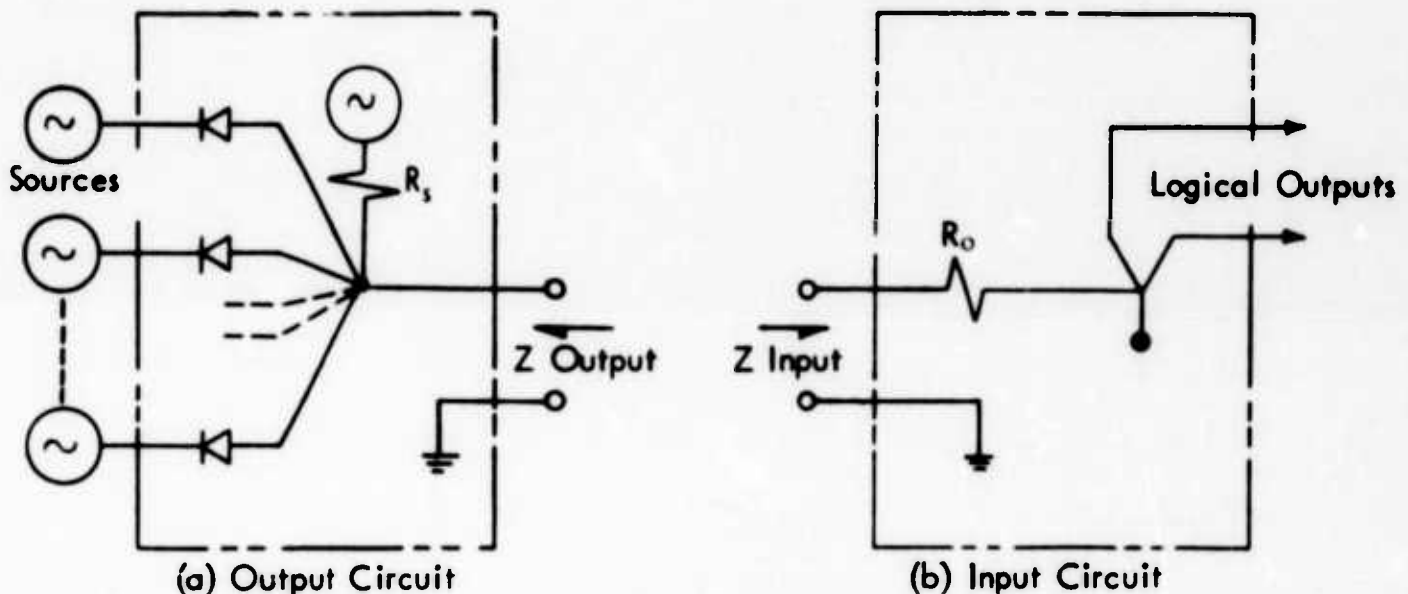


Fig. 8 - Input and Output Circuits of the Generalized Logic Block

Diodes are shown in the diagram, so that the results of the following analysis can be applied to diode logic circuits as well as the resistor circuits. In the corresponding resistor circuit the forward and reverse resistances ( $R_f$  and  $R_b$ ) are set equal to  $R$ , and  $R_s$  is removed. Design of pneumatic logic circuits involves impedance matching between the output portion and the input portion of the above circuits.

### Output Impedance Characteristics

Case 1:  $p_o \leq p \leq p_n$ ;  $p_o$  and  $p_n$  are the blocked-output pressures for a source amplifier —  $p_o$  for the OFF condition and  $p_n$  for the ON condition.

Let us assume that  $x$  of the input lines of the output circuit in Figure 7 are ON. Then, the equivalent circuit would be:

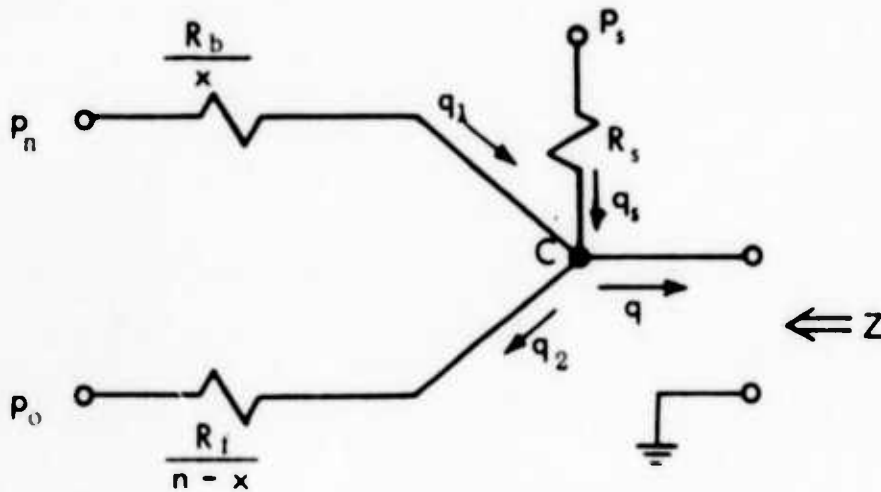


Fig. 8c - Equivalent Output Circuit

where  $R_f$  and  $R_b$  are the forward and backward diode resistances.

The principle of conservation of mass at point C, for the steady state, will give:

$$q = q_s + q_1 - q_2$$

From the above circuit:

$$q = \frac{p_s - p}{R_s} + \frac{(p_n - p)x}{R_b} - \frac{(p - p_o)(n - x)}{R_f}$$

which reduces to:

$$p = \frac{-1}{\frac{1}{R_s} + \frac{n}{R_f} + \left(\frac{1}{R_b} - \frac{1}{R_f}\right)x} q + \frac{\frac{1}{R_s} p_s + \frac{n}{R_f} p_o + \left(\frac{p_n}{R_b} - \frac{p_o}{R_f}\right)x}{\frac{1}{R_s} + \frac{n}{R_f} + \left(\frac{1}{R_b} - \frac{1}{R_f}\right)x} \quad (1)$$

where  $p_o \leq p \leq p_n$  and  $x = 0, 1, 2, 3, \dots, n$ .

Case 2:  $p < p_o$

In this case  $R_f$  is replaced by  $R_b$  in Equation (1), since the flow  $q_2$  reverses its direction:

$$p = - \frac{1}{\frac{1}{R_s} + \frac{n}{R_b}} q + \frac{\frac{1}{R_s} p_s + \frac{np_o + (p_n - p_o)x}{R_b}}{\frac{1}{R_s} + \frac{n}{R_b}} \quad (2)$$

where  $p < p_0$  and  $x = 0, 1, 2, 3, \dots, n$ .

Equations (1) and (2) represent the output characteristics of the generalized logic block of Figure 8. They represent a family of lines with  $x$  and  $n$  as parameters. These equations can be used as they are for the diode logic AND circuit. For the diode logic OR circuit,  $R_s$  is removed ( $R_s = \infty$ ) and,  $R_f$  and  $R_b$  are interchanged. For the resistor logic,  $R_s$  is removed and diodes are replaced by a pure resistance ( $R \equiv R_f = R_b$ ). The details of each of these circuits and the usefulness of Equations (1) and (2) will be discussed in later sections.

### Input Impedance Characteristics

For the static design,  $Z_0$  is a pure resistance. The input impedance characteristics of Figure 8b can best be described by the following property.

The switch points of the input-impedance characteristics always lie along the same straight line with the same point on the pressure-axis, regardless of the value of  $R_0$ .

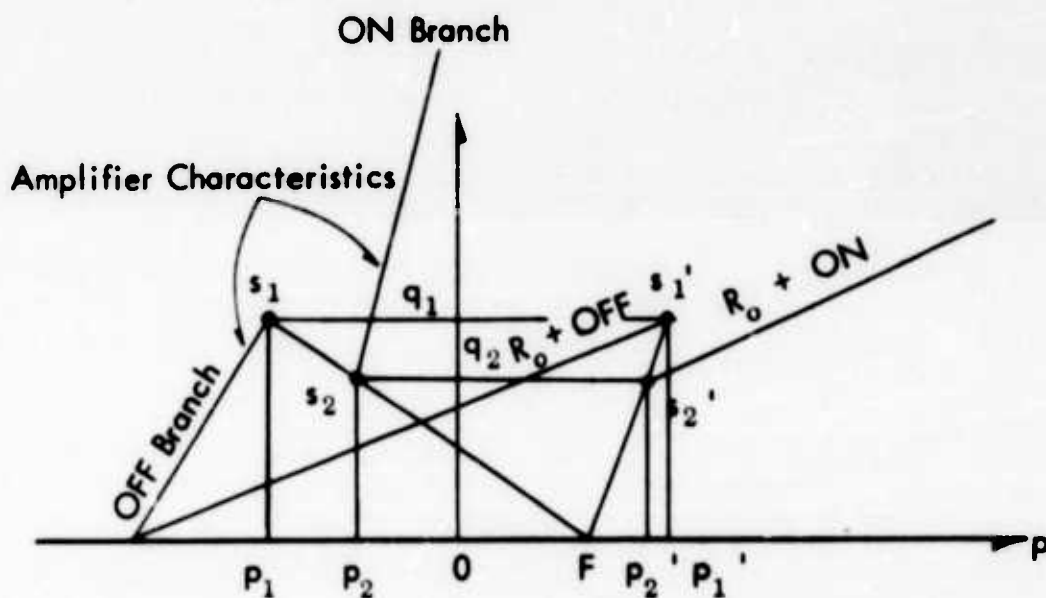


Fig. 9 - Input Impedance Characteristics of the Generalized Logic Block

Proof: In Figure 9,  $R_0$  is graphically added to each branch of the amplifier. The new switch points are labeled  $s_1'$  and  $s_2'$ . From geometrical considerations the line going through switch points  $s_1$  and  $s_2$  intersects the  $p$ -axis at

$$F = p_1 - \frac{p_1 - p_2}{q_1 - q_2} q_1$$

The line going through the switch points  $s'_1$  and  $s'_2$  intersects the  $p$ -axis at

$$F' = p'_1 - \frac{p'_1 - p'_2}{q'_1 - q'_2} q_1$$

Since  $p'_1 = p_1 + q_1 \tan \theta$  and  $p'_2 = p_2 + q_2 \tan \theta$ ,  $\theta$  being the angle that  $R_o$  makes with the vertical line, we have:

$$F' = p + q \tan \theta - \frac{p_1 - q_1 \tan \theta - p_2 - q_2 \tan \theta}{q_1 - q_2} q_1$$

which reduces to

$$F' = p_1 - \frac{p_1 - p_2}{q_1 - q_2} q_1$$

Therefore,  $F$  and  $F'$  are coincident points.

The existence of the focus point,  $F$ , facilitates the design of the basic logic circuits discussed in the next sections.

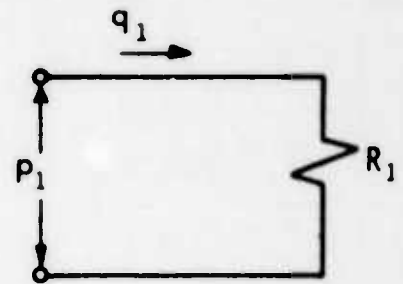
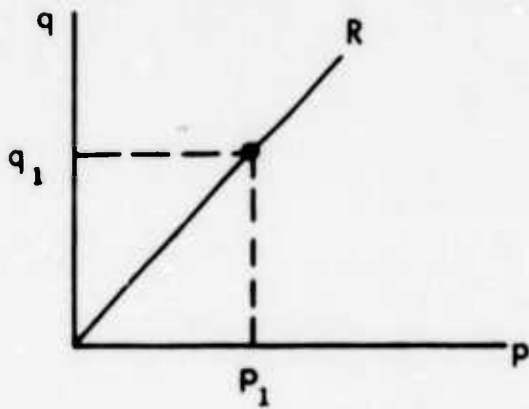
In general, the static design problem involves the determination of the operating points — the intersections of the output characteristics and the input characteristics. These operating points must be designed sufficiently away from the switch points in order to obtain reliable and stable conditions.

### Resistor Logic

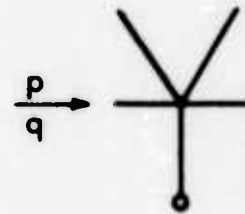
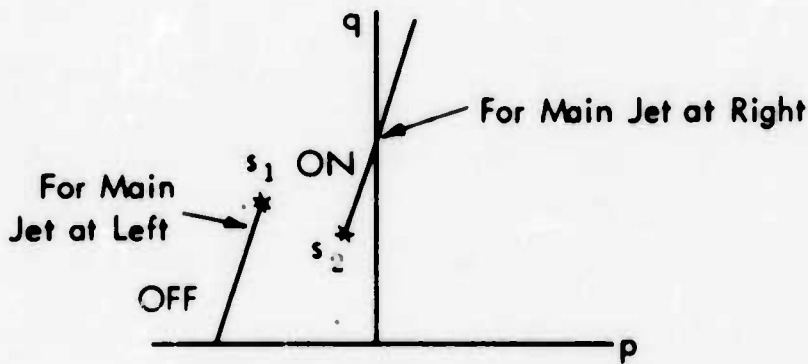
In resistor logic, implementation of the logical functions are accomplished by means of resistors whose design values include two parts. One part is the unavoidable inter-connecting channel resistance; the other part is the resistance intentionally added in order to arrive at the correct design value. Obviously, this situation requires careful considerations since the geometrical variations of the packaging schemes must also be included in the resistor logic design.

As mentioned before, static design of pneumatic logic circuits is carried out by graphical means. The basic rules of graphical approach are presented for linear resistors in Figure 10. These rules also hold true for nonlinear resistors. Figure 10a shows the graphical representation of a linear pneumatic resistor such as a long channel. Figure 10b shows the input impedance of a pneumatic amplifier; it is discontinuous, but linear in each branch. Determination of the resultant resistance of two resistors in series and in parallel is shown in Figures 10c and 10d.

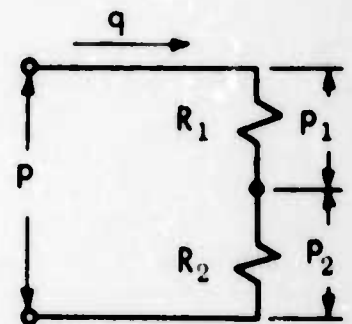
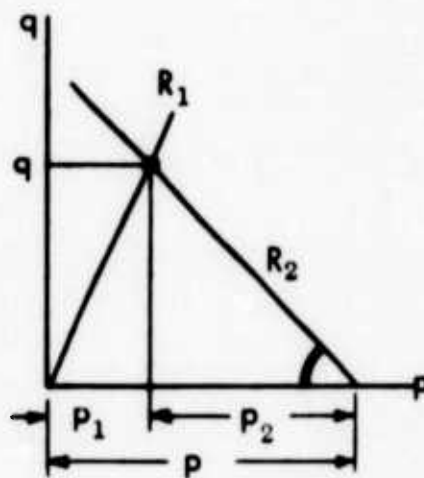
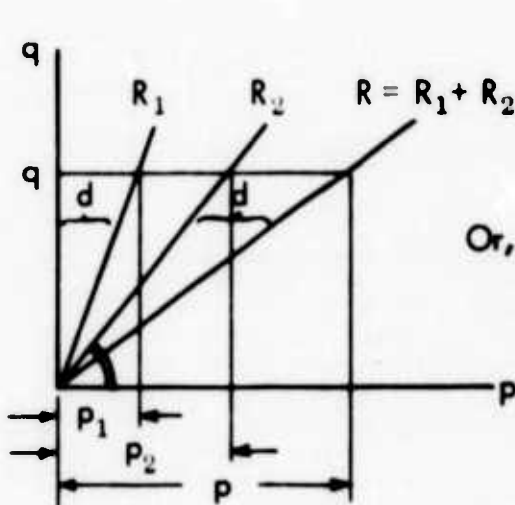
Before the static design of pneumatic logic circuits is discussed, a simple example will be presented to clarify the graphical approach and to state a few definitions.



(a) Impedance Characteristic of a Linear Resistor



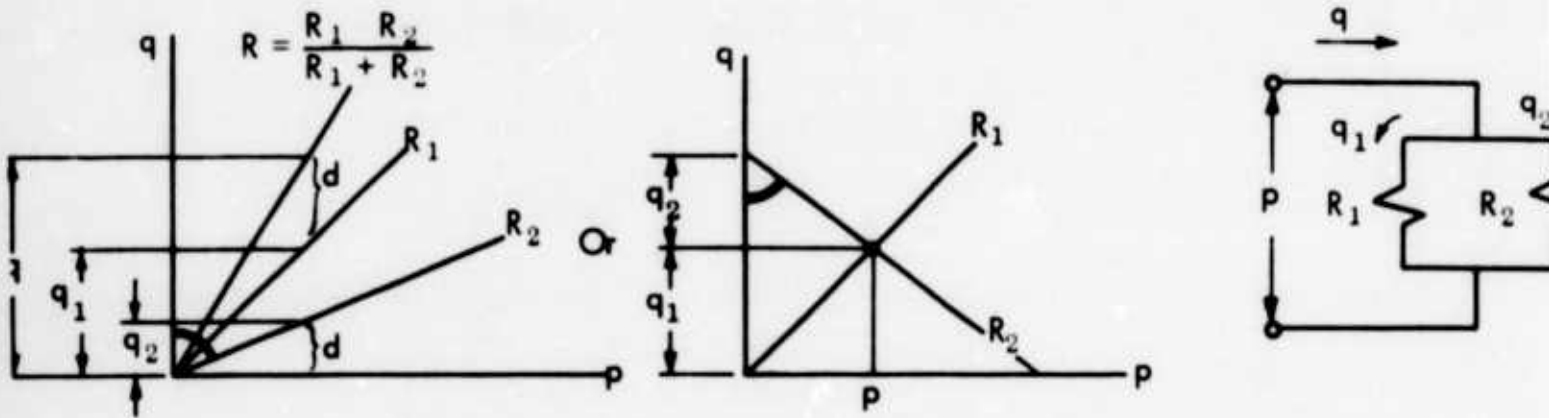
(b) Input Impedance Characteristic of a Pneumatic Amplifier



(c) Graphical Addition of Impedances in Series

Fig.10 - Rules of Graphical Design





(d) Graphical Addition of Impedances in Parallel

Fig. 10 (Cont.)

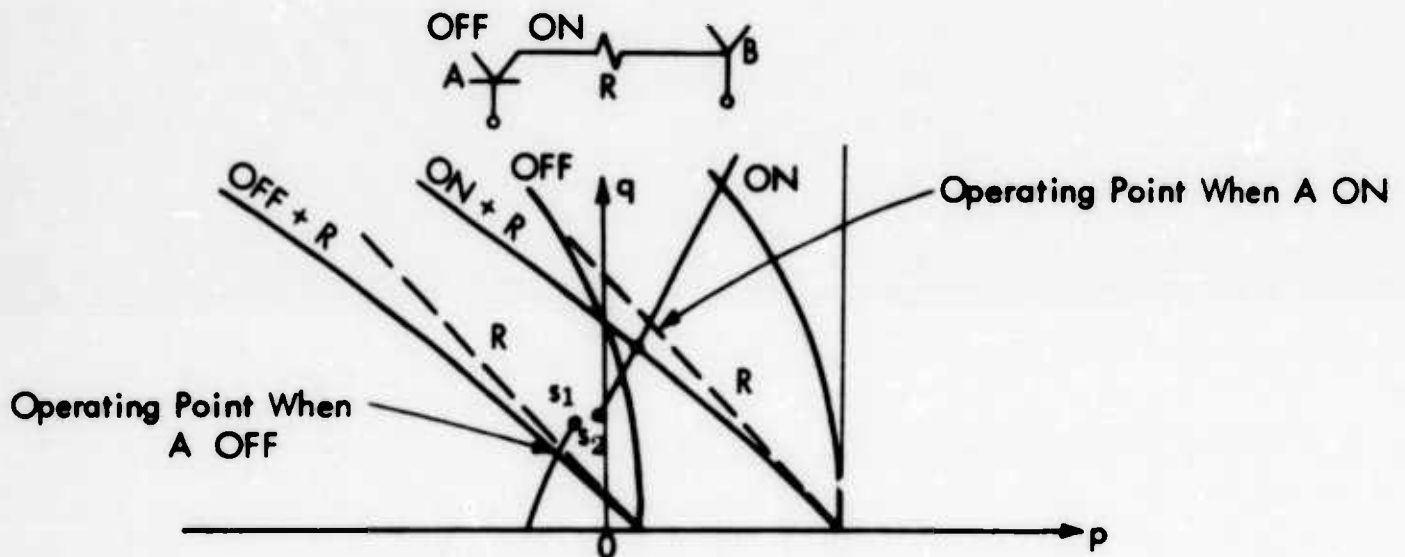


Fig. 11 - Graphical Design of a Simple Pneumatic Circuit

Figure 11 shows the static operation of one pneumatic amplifier connected to another through a resistor. On the graph, the impedance of resistor  $R$  is added to the ON and OFF branches of the output impedance of Amplifier A. These new curves are the output impedance (driving characteristics) that Amplifier B will receive. The intersections of the output impedance curves with the input characteristics of Amplifier B are the "operating points" of the circuit. In this case, the value of  $R$  has been chosen such that Amplifier B is switched ON whenever the A amplifier is turned ON.

Other values of  $R$  will result in different sets of operating points. For instance, for  $R = 0$  both operating points would fall on the ON branch of the input characteristics of Amplifier B. This means that Amplifier B will always be ON regardless of the state of Amplifier A.



Another point of interest in the design of pneumatic circuits is the question of operational stability (and thus the reliability) of the circuits. If the operating points are designed too close to the switching points, any slight variations in manufacturing tolerances or operating pressures might cause malfunctions. For this reason, a minimum distance away from the switching points — the "stability distance" — must always be specified in the design of pneumatic circuits. Generally speaking, the most desirable design would be to have the switch points symmetrically located with respect to the output impedance lines and at the same time meet the requirement of minimum stability distance.

In resistor logic the impedances  $Z_o$  and  $Z$  of Figure 7 are assumed to be pure linear resistances. An important property will be proved for the case where all of the sources (Figure 7) are similar pressure sources such as single amplifiers. The output impedance characteristic of the generalized logic network consists of a family of parallel and equidistant lines (Figure 12).

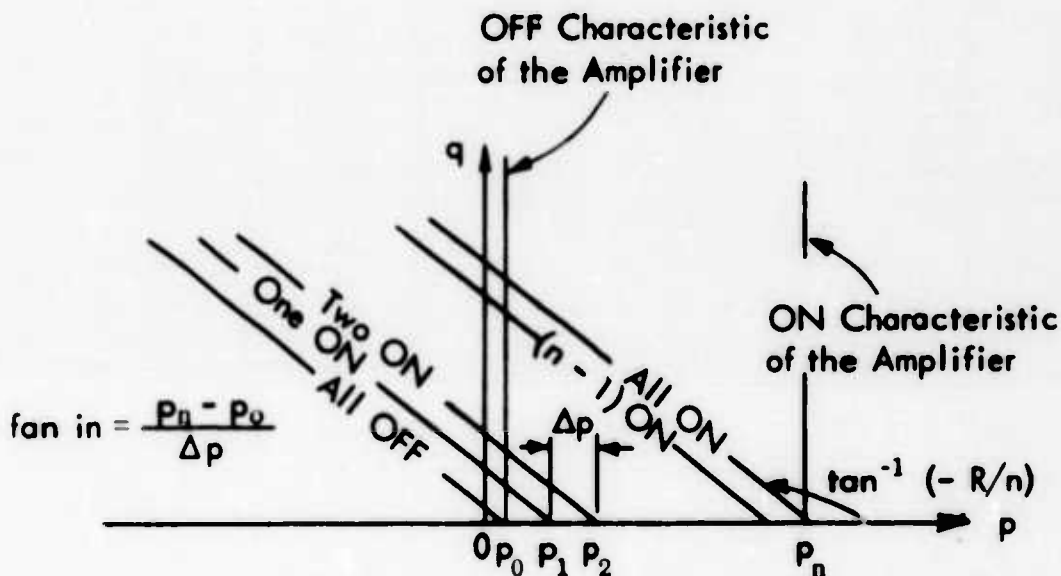


Fig. 12 - Output Impedance Characteristics of the Generalized Logic Block

Proof: In resistor logic the output impedance Equations (1) and (2) both reduce to:

$$p = -\frac{R}{n} q + p_o + \frac{x}{n} (p_n - p_o)$$

Since for a given fan in,  $n$  is constant, the slopes of the member lines remain the same regardless of the value of  $x$ . However, the pressure intercept is a function of  $x$ . Therefore, the output lines are a set of parallel lines with  $n$  and  $x$  as the parameters. " $n$ " determines the number of lines (fan in), and  $x$  locates the particular member lines.

To show that these lines are equally spaced, we will find the general expression for the pressure-axis line-segment between two consecutive lines. For  $q = 0$ :

$$p_{x+1} \Big|_{q=0} = p_o + \frac{x+1}{n} (p_n - p_o)$$

$$p_x \Big|_{q=0} = p_o + \frac{x}{n} (p_n - p_o)$$

Therefore,

$$\left[ p_{x+1} - p_x \right]_{q=0} = \frac{1}{n} (p_n - p_o)$$

which is a constant for a given amplifier.

It should be noted that smaller values of  $n$  result in larger separations between the output impedance lines. As we will see later on, this separation distance affects the reliability of circuit operation.

### The OR Circuit

For the OR circuit, values of  $R_o$  and  $R$  must be selected so that pressurizing any one of the inp lines would result in a logical output. The graphical model of this behavior is shown in Figure 13.

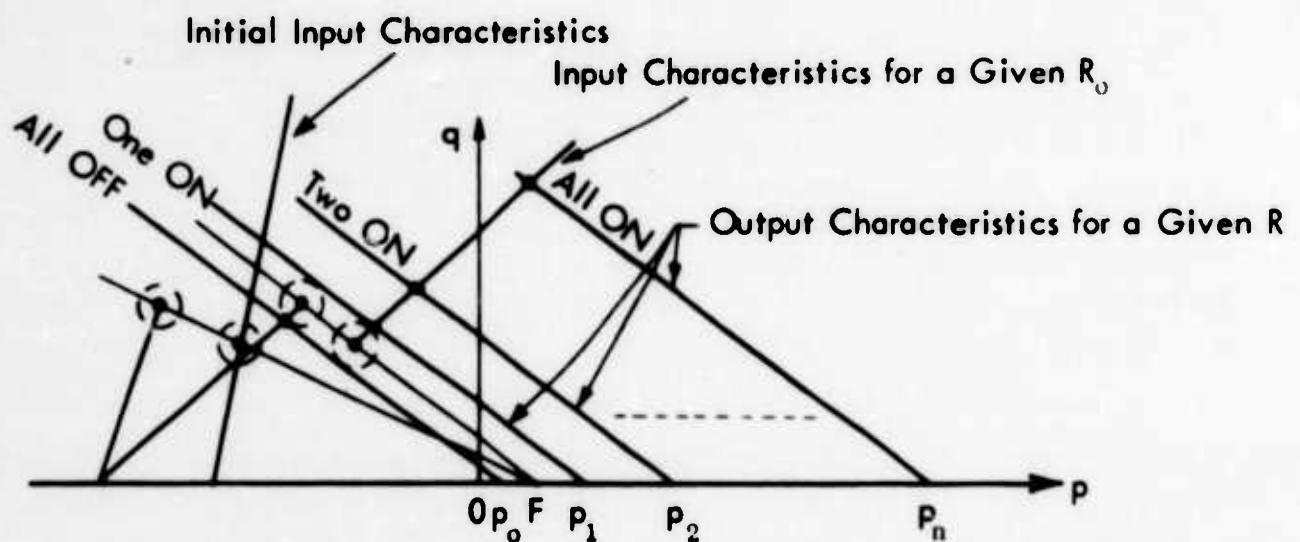


Fig. 13 - The Design of the OR Circuit

When all of the inputs are off, the operating point is on the OFF branch of the input impedance of the amplifier. When any one of the inputs is on, the operating point falls on the ON branch. If more than one input is turned on, the operating point assumes higher and higher positions on the ON branch.

Obviously, Figure 13 has been drawn for a particular set of values of  $R_0$  and  $R$ . Many other pairs of values can be found which would satisfy the logical requirement of the circuit. As the value of  $R_0$  is increased the switch points are moved to the right. This means that the value of  $R$  must be decreased in order to keep the switch points between the first two output impedance lines.

If the highest possible fan-in is to be obtained, the optimum position of the focus point  $F$  would be midpoint of the first two intersections of the output impedance lines and the pressure axis. This can be seen in Figure 13.

For a given  $R_0$ , the value of  $R$  can be determined by drawing a tangent from  $p_0$  to the instability circle for the OFF branch of the input impedance curves. This line is the "ALL OFF" line which corresponds to the case when all input lines are OFF. Now, in order to get the minimum distance between  $p_0$  and  $p_1$  (which results in maximum fan-in) we must choose the ONE ON line as close to the ALL OFF line as possible. On the other hand the ONE ON line cannot be any closer to the OFF-branch switch-point than the tangent line to the opposite side of the instability circle. This tangent line is drawn parallel to the ALL OFF line and is the optimum ONE ON line as far as the OFF branch is concerned. It is easily seen from the figure that this line also satisfies the stability requirements for the ON branch if the focus point falls midway between  $p_0$  and  $p_1$ .

### The AND Circuit

For the AND circuit, values of  $R_0$  and  $R$  must be selected so that all of the driving amplifiers must be turned on before a logical output is obtained. The graphical model of the AND circuit is shown in Figure 14. Here the optimum position of the focus point,  $F$ , is the midpoint of the last two intersections of the output impedance lines with the pressure-axis.

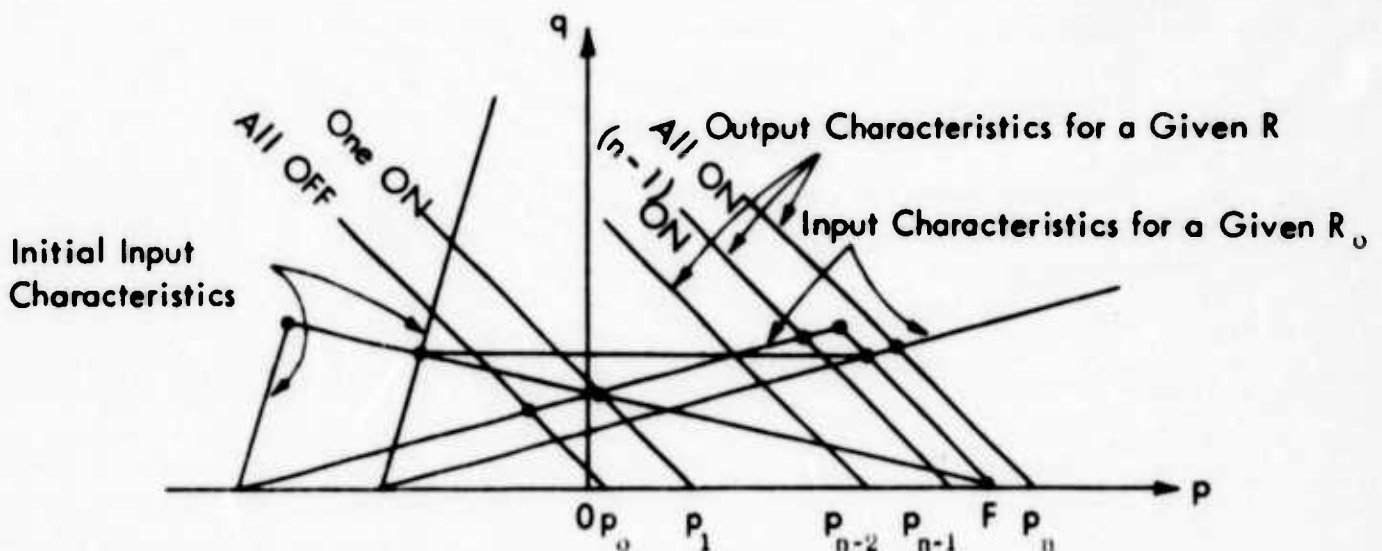


Fig. 14 - The Design of the AND Circuit

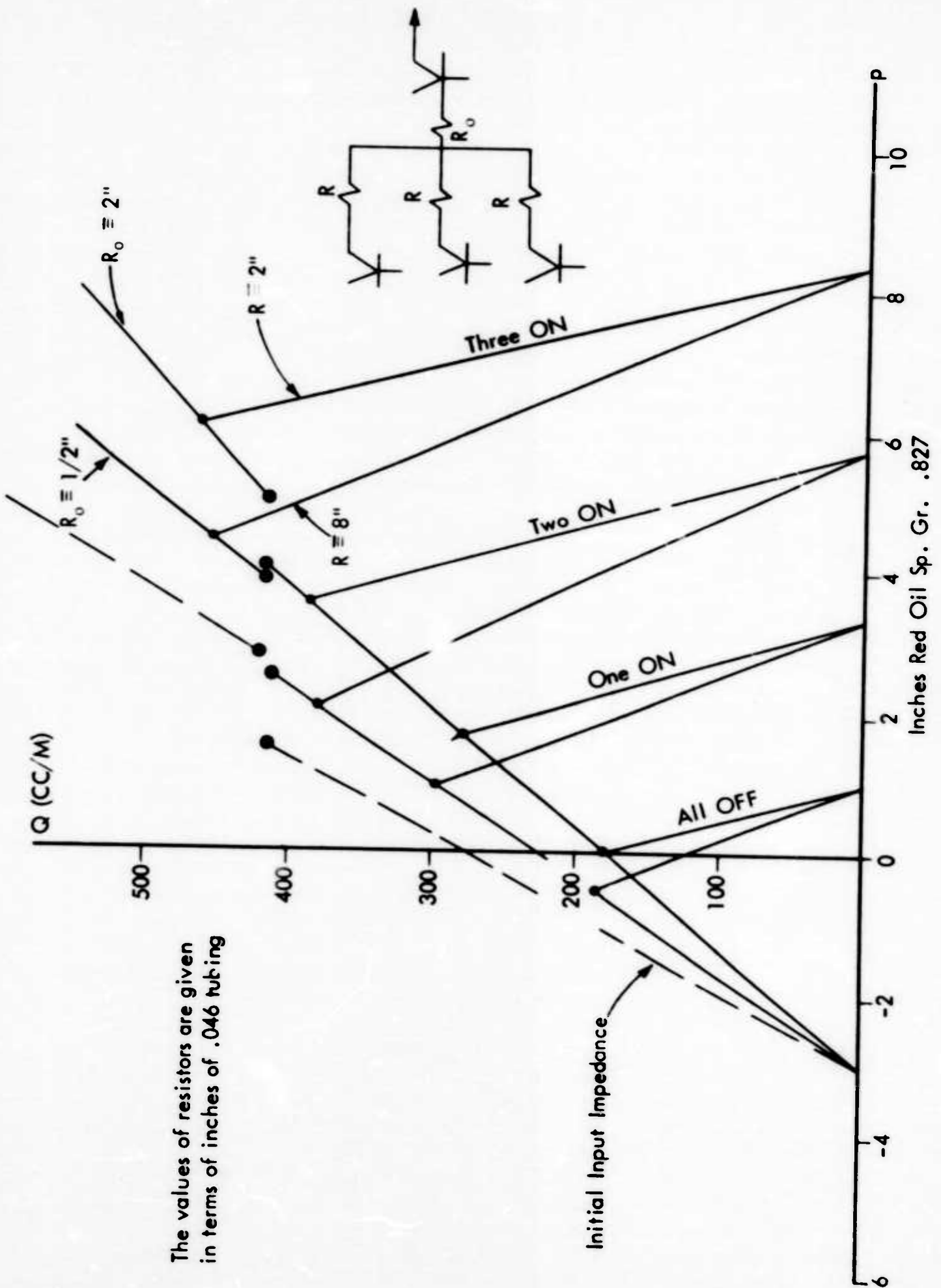


Fig. 15 - Experimental Design of the AND Circuit

Similar to the OR circuit there are many values for  $R_o$  and  $R$  which would satisfy the requirements for the AND circuit. The experimental verifications of the circuit properties and designs are shown in Figure 15. In this figure the input and output properties of the generalized logic block of Figure 7 as well as the design procedure of the AND circuit have been verified.

The AND circuit itself was constructed in a breadboard fashion. Three amplifiers were connected to another amplifier through external resistors made from .046 in. I.D. tubing.

### Resistor Logic Optimum Amplifier Design

From the design of the AND and OR circuits, we saw that two different biased amplifiers are necessary for the resistor logic. For the OR circuit, the focus point  $F$  should be between the first two output lines. This will allow maximum fan-in for a given stability distance. If the focus point is not midway between the first two lines, it is not possible to obtain a high fan-in. Similarly, for the AND circuit the focus point should be between the last two lines for maximum possible fan-in.

At some sacrifice of fan-in capability, we could design a compromise amplifier that would satisfy the requirements of both the OR and the AND circuits. This compromise design (Figure 16) eliminates the necessity of having two different amplifiers.

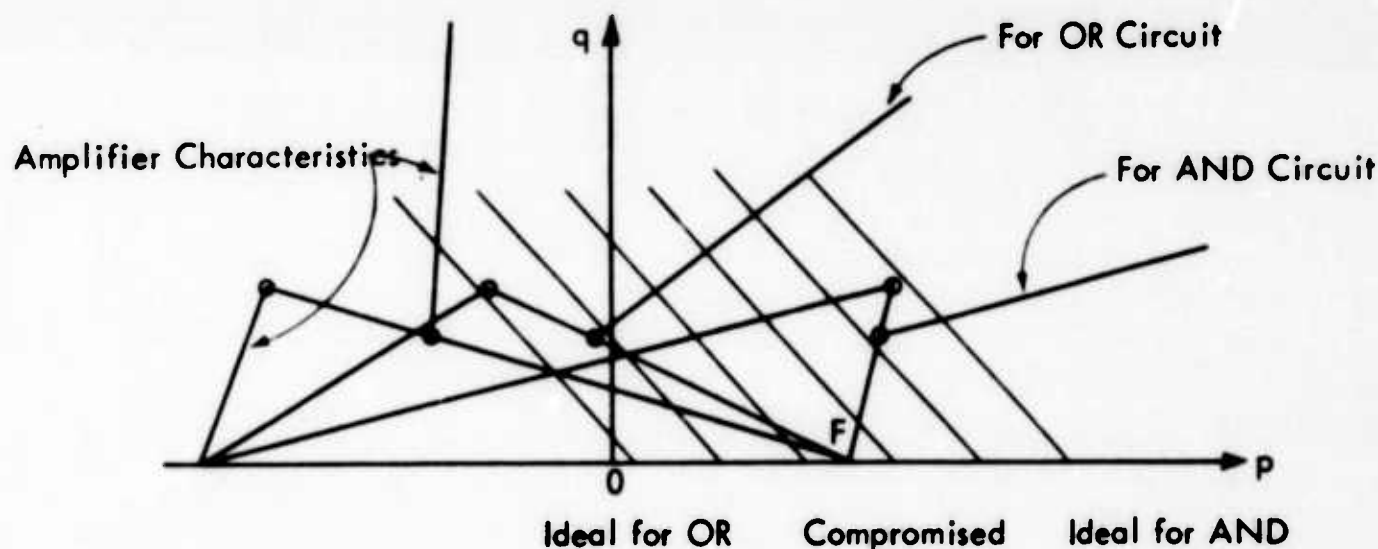


Fig. 16 - Compromise Input Characteristics and the Design of the Basic Logic Blocks

The amplifier must be designed such that its focus point falls on the midpoint between the two ideal locations. (This midpoint is also the midpoint between the points  $p_o$  and  $p_n$ .) This presents an interesting relationship between the input and output impedance characteristics of the compromise amplifier. First, the terminated output pressures  $p_o$  and  $p_n$  must be found. Then, the geometry of the amplifier must be designed such that its switch point would fall on the midpoint of the line segment  $p_o$ - $p_n$ .

In actual practice, design of the compromise amplifier presents several difficulties since the location of the focus point  $F$  on the pressure-axis is very sensitive to the relative positions of the switch points. That is, slight deviations in switching pressure and/or flows of one or both of the switch points could cause large movements in the location of  $F$  on the pressure-axis. Another factor to be considered is the fan-incapability. When a compromise amplifier is used, the fan-in depends on the distance between the switch points as well as the value of  $R$ . If the distance between  $s_1$  and  $s_2$  is increased the absolute value of  $\Delta p = p_1 - p_0$  is also increased (Figure 17).

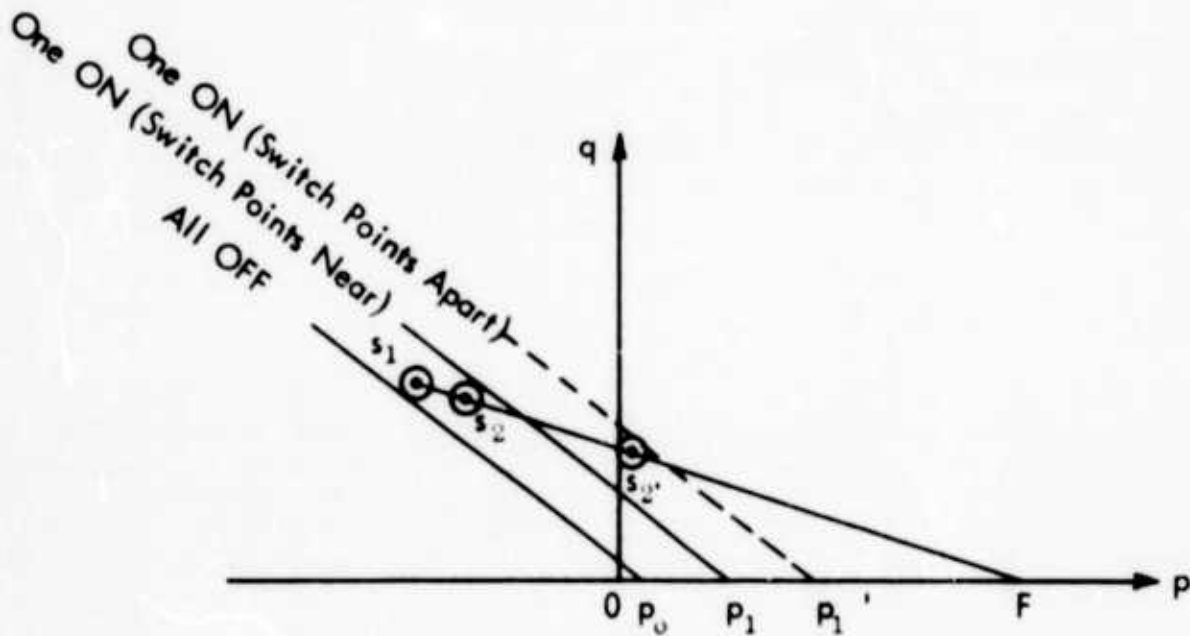


Fig. 17 - Effect of Switch Point Distance on Fan-In

Increasing  $\Delta p$  decreases the fan-in capacity:

$$\text{fan-in} = \frac{p_n - p_0}{p_1 - p_0} = \frac{\text{const.}}{\Delta p}$$

Also, increasing the value of  $R$  decreases the fan-in (Figure 18).

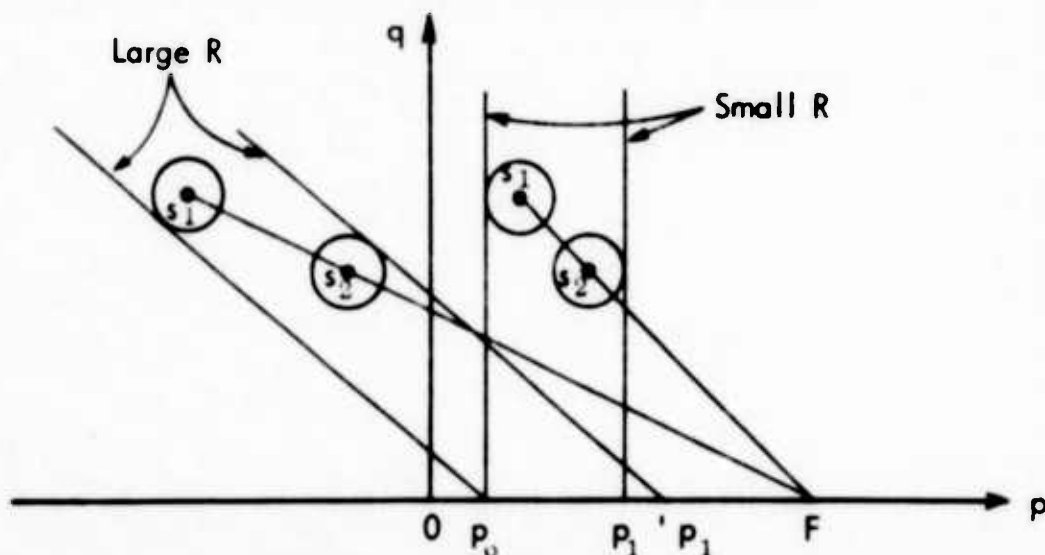


Fig. 18 - Effect of  $R$  on Fan-In



Ideally, if the switch points are coincident, the OR and AND circuits can be implemented without any sacrifice in stability or fan-in. In the ideal case the focus point  $F$  is indeterminate on the pressure axis, and the fan-in would only depend on the manufacturing tolerances and supply variations. However, in the non-ideal cases, where a compromise amplifier is used, the fan-in also depends on the switch-point distance and  $R$ . From the system's point of view, the ON branch of the ideal amplifier should be parallel to the pressure axis. Such an ON branch position would result in low-flow operating points which reduces the demand on air supplies.

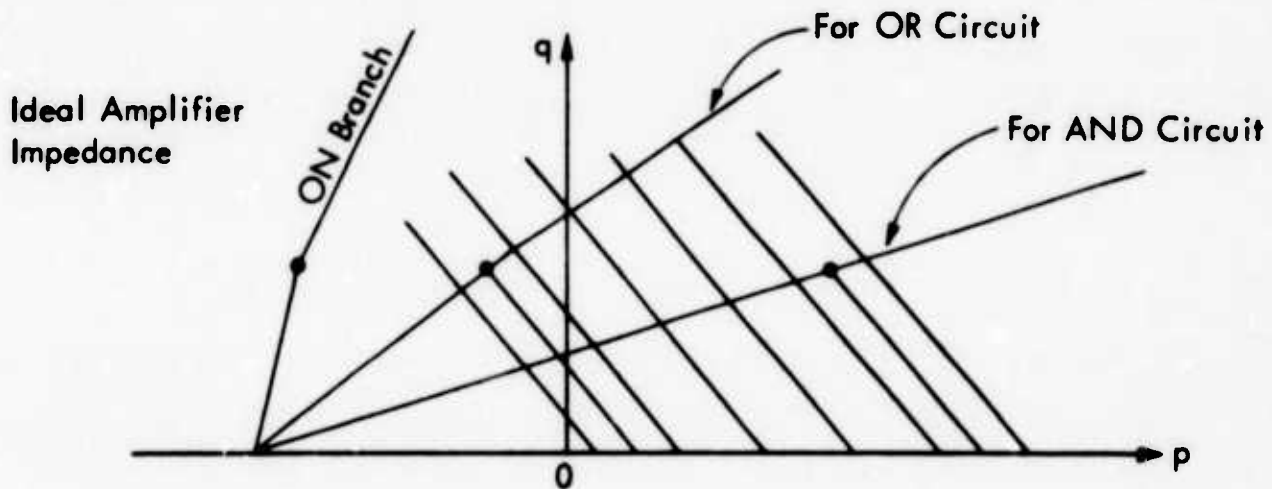


Fig. 19 - Ideal Input Impedance and the Design of the Basic Logic Blocks

### Directional Logic

During the experimental studies, it was observed that deviations of the switch points due to manufacturing tolerances were not totally random. The switching pressures remained constant from model to model, despite large variations in the switching flows (Figure 20).

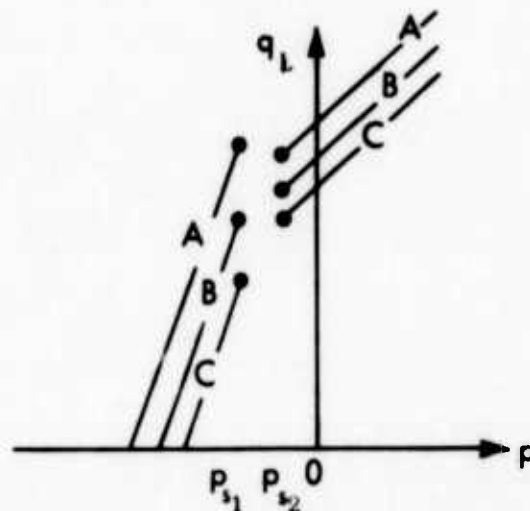


Fig. 20 - Input Impedance of Several Amplifiers Having a Common Design

Based on this observation an amplifier was designed which could be used in conjunction with the directional logic elements shown in Figure 21. The design of this amplifier is such that the switch points of its input impedance occur at very low flows and near the atmospheric constant-pressure line (Figure 22).

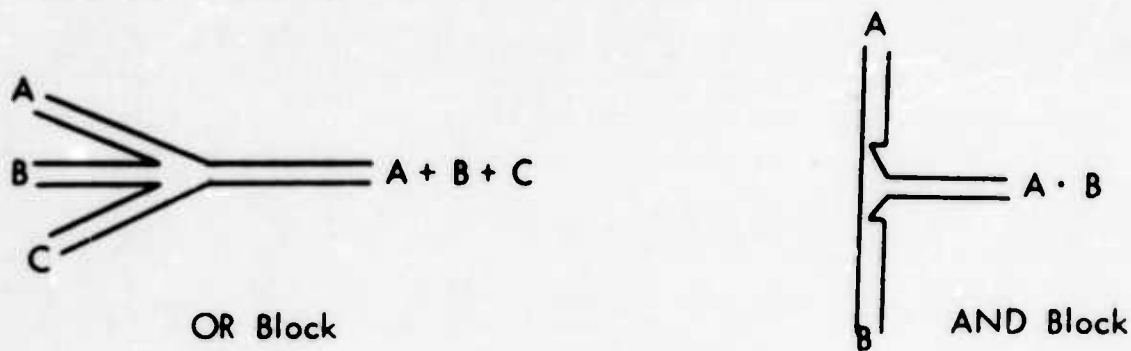


Fig. 21 - Directional Passive Logic Blocks

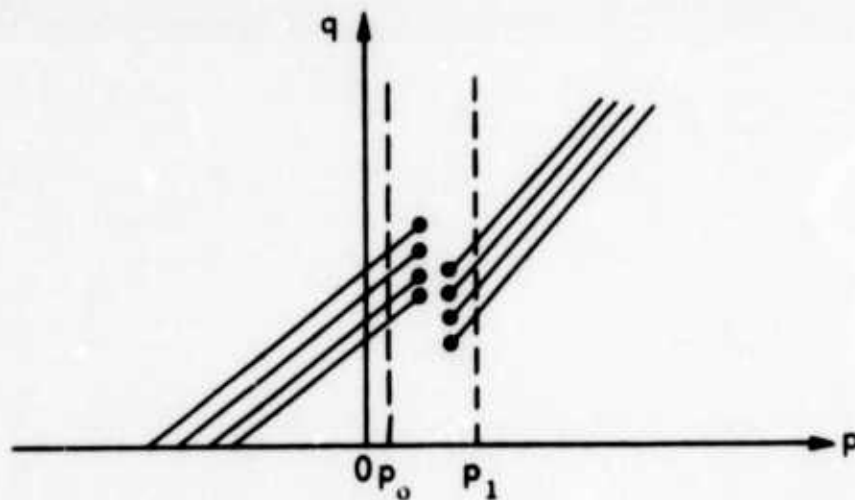


Fig. 22 - Static Characteristics of the Amplifier for Directional OR-NOR Logic

For switching this amplifier all that is needed is a pressure slightly above the atmospheric, since the switch points have been placed in the linear region of the output lines. Thus, with this pressure mode of operation, no particular attention needs to be devoted to the flow deviations of the switch points. An amplifier with characteristics as shown in Figure 22 would be suitable for the design of OR, or NOR logic blocks.

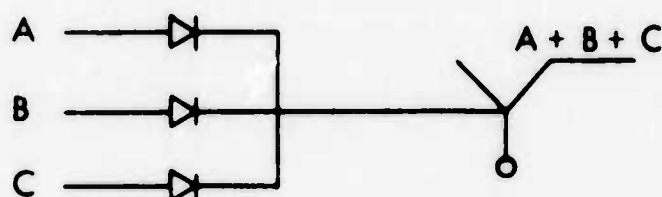


Directional logic circuits have two advantages over resistor logic circuits: (1) the flow variations due to manufacturing tolerances do not become critical, (2) the logic resistors are all eliminated. However, the experimental circuits that have been implemented so far have shown relatively poor fan-out capability.

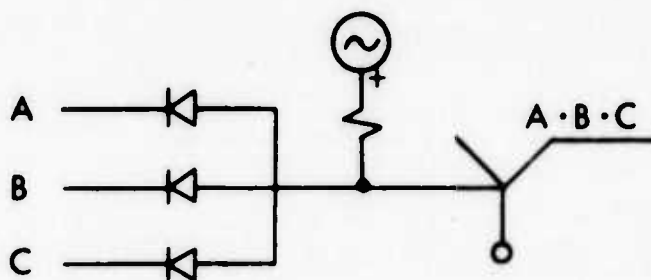
Logical functions of pneumatic circuits using the directional elements can be visualized simply by considering the direction of air flow in the channels. Actually, even with these directional elements, the impedance matching of the circuit design still exists. However, the over-all logical operations are more sensitive to the flow direction than the impedance matching. For this reason, pneumatic circuits that use these elements are called directional circuits.

### Diode Logic

The basic AND and OR blocks for diode logic are shown in Figure 22.



(a) OR Circuit



(b) AND Circuit

Fig. 23 - Diode Logic Blocks

For the OR block any one or more of the input signals is sufficient to switch an amplifier. On the other hand, for the AND block, the flow from the positive bias supply is normally going through the forward direction of the diodes. This condition is satisfied by making the input impedance of the amplifier greater than the forward impedance of a single diode. Thus, even when only one input line is OFF, the impedance of the forward direction of that diode presents little resistance to the impressed bias pressure and keeps the pressure at the control port of the amplifier below its switching value. Only when all the diodes are

pressurized in the reverse direction will the bias pressure be sufficient for switching the amplifier.

### The OR Circuit

The output impedance equation for the diode OR circuit is found by setting  $R_s = \infty$  and interchanging  $R_f$  and  $R_b$  in Equations (1) and (2). Then:

$$p = - \frac{1}{\frac{n}{R_b} + \left( \frac{1}{R_f} - \frac{1}{R_b} \right) x} q + \frac{\frac{x}{R_f} p_n + \frac{n-x}{R_b} p_o}{\frac{n}{R_f} + \left( \frac{1}{R_f} - \frac{1}{R_b} \right) x}$$

for  $p_o \leq p \leq p_n$

and

$$p = - \frac{R_f}{n} q + p_o + \frac{x}{n} (p_n - p_o) ; \text{ for } p < p_o$$

represent the family of output impedance lines for the OR circuit. These lines are not parallel to each other as they are in resistor logic. The general pattern of the lines is shown in Figure 24 for arbitrary values of  $R_f = .01$ ,  $R_b = 1$ ,  $n = 10$ ,  $p_o = 0$  and  $p_n = 10$ .

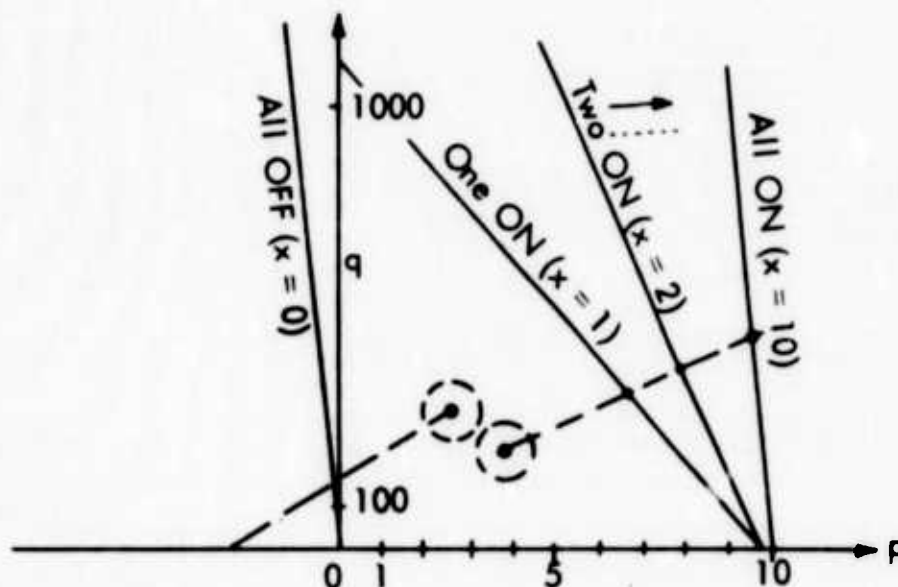


Fig. 24 - Output Impedance Characteristics of the Diode OR Block

The slope of the impedance lines decreases as more and more input lines are pressurized (i.e. as  $x$  increases) and the pressure intercepts are very close to the  $p_n$  value except for the line corresponding to  $x = 0$ , whose pressure intercept is at  $p_o$ . The region between the ALL OFF line and the ONE ON line is relatively large resulting in a wide safety margin between the OFF and the ON operating points.

From the equation given above, we can see that as the fan-in increases, the OFF operating point approaches the instability region, while the ON operating points move further away from their corresponding instability region. Therefore, for a given amplifier characteristic, the maximum fan-in is determined solely by considering the ALL OFF line and the instability regions of the input amplifier — the criteria being that the ALL OFF line can be tangent to one or both circles without intersecting either one.

### The AND Circuit

Equations (1) and (2) can be used for the diode AND circuit. They represent a family of straight lines which are not parallel to each other.

$$p = - \frac{1}{\frac{1}{R_s} + \frac{n}{R_f} + \left(\frac{1}{R_b} - \frac{1}{R_f}\right)x} \quad q = - \frac{\frac{1}{R_s} p_s + \frac{n}{R_f} p_o + \left(\frac{p_n}{R_b} - \frac{p_o}{R_f}\right)x}{\frac{1}{R_s} + \frac{n}{R_f} + \left(\frac{1}{R_b} - \frac{1}{R_f}\right)x} ;$$

$$p_o \leq p < p_n$$

$$p = - \frac{1}{\frac{1}{R_s} + \frac{n}{R_b}} \quad q = - \frac{\frac{1}{R_s} p_s + \frac{np_o + (p_n - p_o)x}{R_b}}{\frac{1}{R_s} + \frac{n}{R_b}} ; \quad p < p_o$$

The general pattern of these lines is shown in Figure 25 for arbitrary values of:  $R_f = .01$ ,  $R_b = .1$ ,  $n = 10$ ,  $p_o = 0$ ,  $p_n = 10$ ,  $p_s = 10$ , and  $R_s = .1$ . The slopes of the impedance lines decrease as more and more of the input lines are pressurized and the pressure intercepts are very close to the  $p_o$  value, except for the line corresponding to  $x = 10$ , whose pressure intercept is at  $p_o$ . The region between the ALL ON line and the NINE ON line is relatively large.

In comparing Figures 24 and 25, an interesting duality can be observed. Any statement made about one figure is also true about the other, provided the dual of words ON (i.e. OFF), ALL (i.e. NONE), SLOPE (i.e. pressure intercept),  $p_o$  (i.e.  $p_n$ ), ON BRANCH (i.e. OFF BRANCH), etc. are used.

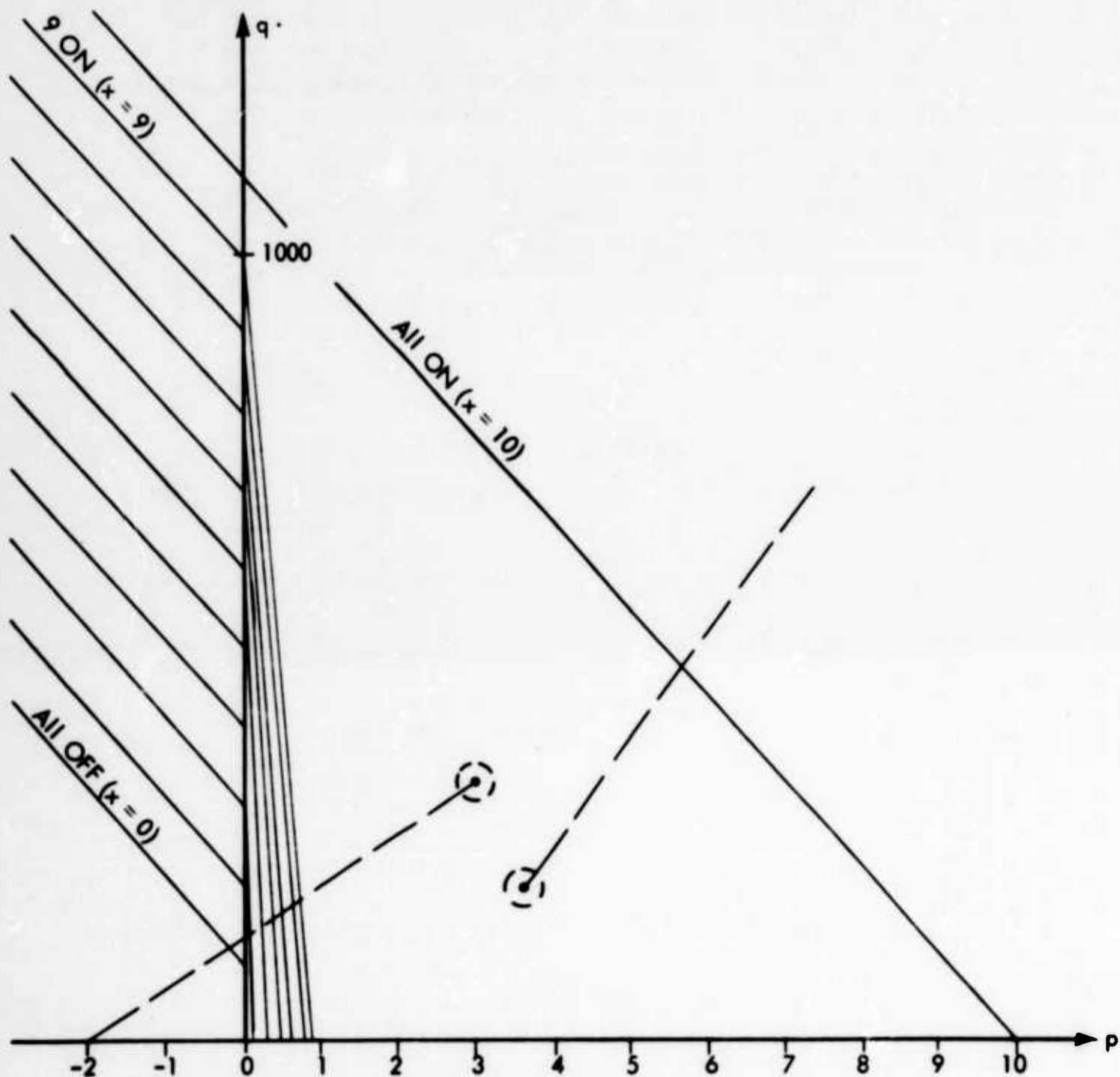


Fig. 25 - Output-Impedance Characteristics of the Diode AND Block

The output characteristics of diode logic are much more desirable than those of resistor logic. In diode logic only one amplifier design suffices for both the AND and the OR circuits. This is accomplished by providing sufficient overlap between the two open regions of the AND and the OR output characteristics. This overlap is determined by the variables and the parameters in Equations (1) and (2). For diode logic the location of the focus point is immaterial as long as the switch points are reasonably close. Due to the wide operational regions in diode logic, a higher fan-in can be obtained than for resistor or directional circuits; also, much better reliability and wider manufacturing tolerances are possible.

#### IV LOGICAL SYSTEMS USING PNEUMATIC JET AMPLIFIERS

There are several different logical systems that can be adopted for pneumatic logic circuits. Two categories of logical systems can be recognized, depending on whether mono-output or duo-output amplifiers are used (Figures      and

The fundamental system is the AND-OR-INVERTER. When using this system, the logical functions of machine capabilities must first be converted into AND, OR, and NOT statements. Then the physical implementation of such a machine is simply a matter of substitution of logical blocks for each functional statement.

The basic AND-OR-I system has been used in many electronic machines. Some minor modifications of this system result in several other interesting and useful logical systems. For example, only the OR- and the INVERTER-blocks would be sufficient for the implementation of any functional requirements. This is due to the fact that the AND block can be constructed from the OR- and INVERTER-blocks. The corresponding Boolean expression for the AND block, in terms of OR and I, would be:

$$A \cdot B = \overline{\overline{A \cdot B}} = \overline{\overline{A} + \overline{B}}$$

Physical implementation of  $\overline{\overline{A} + \overline{B}}$  only requires the INVERTER and the OR-blocks. Such a system using only the OR- and the INVERTER-blocks is called NOR logic.

In a similar manner, in NAND logic, only the AND- and the INVERTER-blocks are used. The OR function is constructed from these two blocks, since:

$$A + B = \overline{\overline{A + B}} = \overline{\overline{A} \cdot \overline{B}}$$

Further variations of these three systems (AND-OR-I, NOR, and NAND) can be recognized; they are listed in Figures 26 and 27. In each case the AND- and OR-block constructions are shown for the single level logic. These constructions are a measure of the adaptability of the corresponding system in implementation of logical functions. However, it should be noticed that the "optimum logical system" is not necessarily a function of the number of the logic elements which are necessary for the construction of AND- and OR-blocks. Other factors such as: over-all cost, circuit type (resistive, directional, or diode), fan-in and fan-out, logic level, operational speeds, timing tolerance accumulation, reliability, packaging schemes, and even particular applications must be considered.

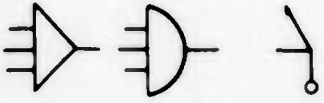
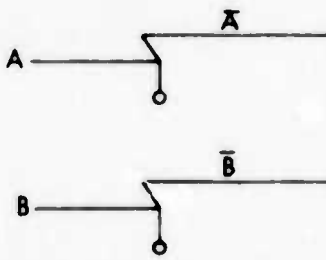
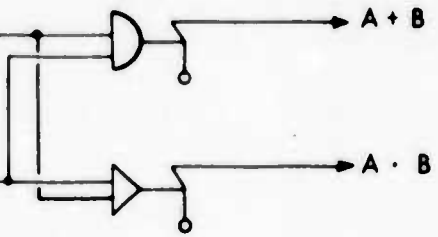

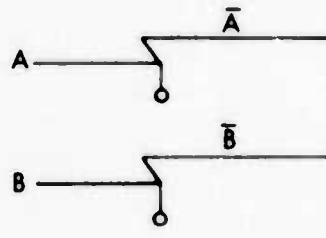
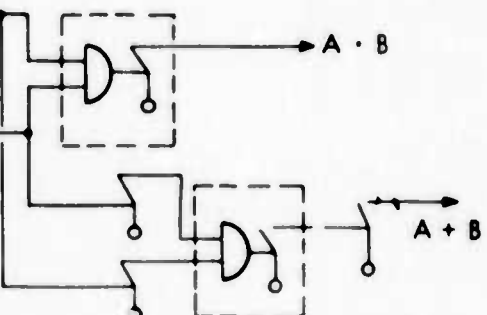
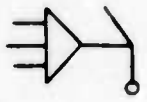
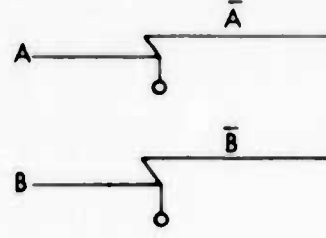
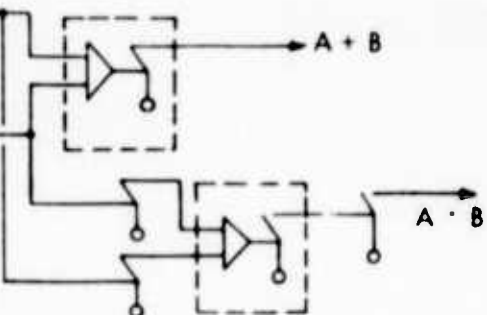

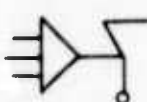
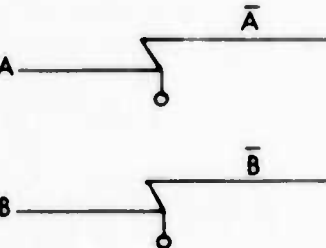
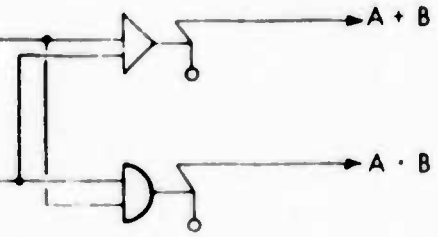
SYSTEM	SIGNAL AMPLIFICATION STAGE	IMPLEMENTATION OF AND & OR USING SINGLE LEVEL LOGIC
<p>AND - OR - I Logic</p> 		
<p>NOR Logic OR - I</p> 		
<p>NAND Logic AND - I</p> 		
<p>NOR - NAND Logic</p> <p> NOR</p> <p> NAND</p>		

Fig. 26 - Logic Systems Using Mono-output Decision Amplifiers

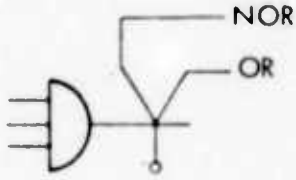
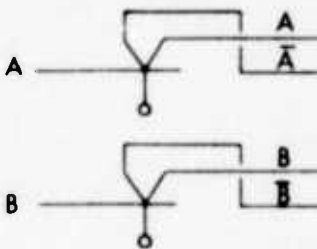
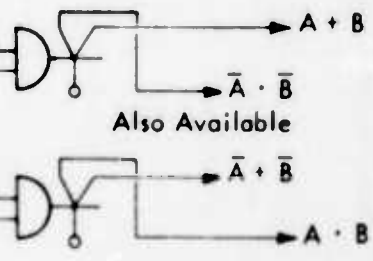
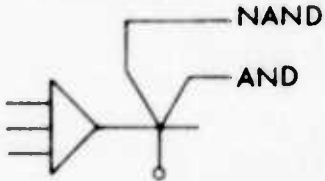
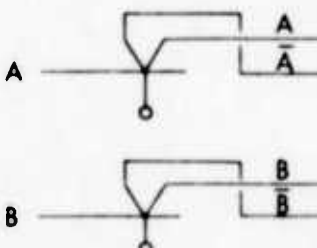
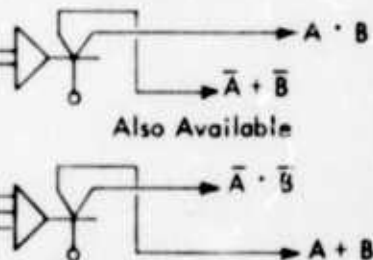
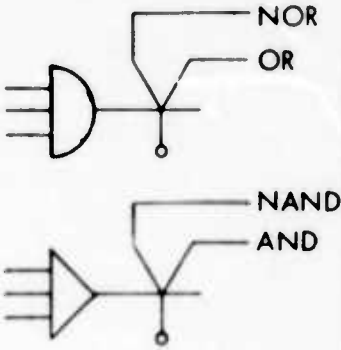
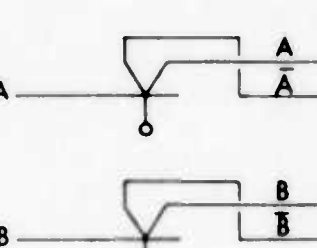
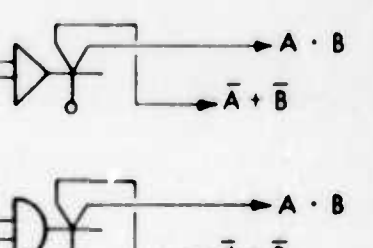
SYSTEM	SIGNAL AMPLIFICATION STAGE	IMPLEMENTATION OF AND & OR USING SINGLE LEVEL LOGIC
<p>OR - NOR</p> 		
<p>AND - NAND</p> 		
<p>OR - NOR - AND - NAND</p>  <p>In this system the AND and the OR functions can be implemented in two different ways.</p>		

Fig. 27 - Logic Systems Using Duo-output Decision Amplifiers



Logic Function	Pneumatic	Electronic
Memory Element (Latch)		
Inversion and Amplification		
OR - NOR		
AND - NAND		

Fig. 28 - Comparisons Between Pneumatic and Electronic Logic Blocks



With regard to certain particular applications, better utilization and economy might be obtained from circuits especially tailored to the given requirements than from standardized circuits. Each segment of logical functions of a given application can be broken down to smaller functional blocks whose circuits can be specially designed. In such a case, the optimization of the logical circuits would only be limited by the designer's skill, since he would be able to use special circuits such as exclusive OR, majority circuits, etc., in order to satisfy specific needs in a more efficient manner.

### Comparisons of Pneumatic and Electronic Logic Blocks

Several interesting comparisons can be made between some of the basic pneumatic logic blocks and the corresponding electronic blocks. These comparisons are listed in Figure 28. From this figure it can be deduced that the implementation of logical functions in pneumatics would require considerably less logic elements than it would with electronic elements. This is true even in case of nonlogical circuits such as driving circuits. For example, Figure 29 shows two equivalent circuits which provide a 1 to 18 driving magnification. In both the electronic and pneumatic circuits a driving capability of three per amplifier is assumed. Notice that all of the pneumatic outputs are in step, while the electronic outputs are not. In the pneumatic circuit the inverted outputs are also available as a bonus. Furthermore, only seven pneumatic amplifiers are required compared to nine transistors. These advantages are realized only if duo-output amplifiers are used. If mono-output amplifiers are used, none of these advantages would be possible. On the other hand the mono-output amplifiers have higher switching speeds as well as better adaptability to miniaturization. Therefore, the choice between the mono-output or duo-output amplifiers, again, must be based on some engineering compromises. Such engineering compromises, in turn, would be based on a quantitative analysis of the costs and the operational speeds that can be expected.

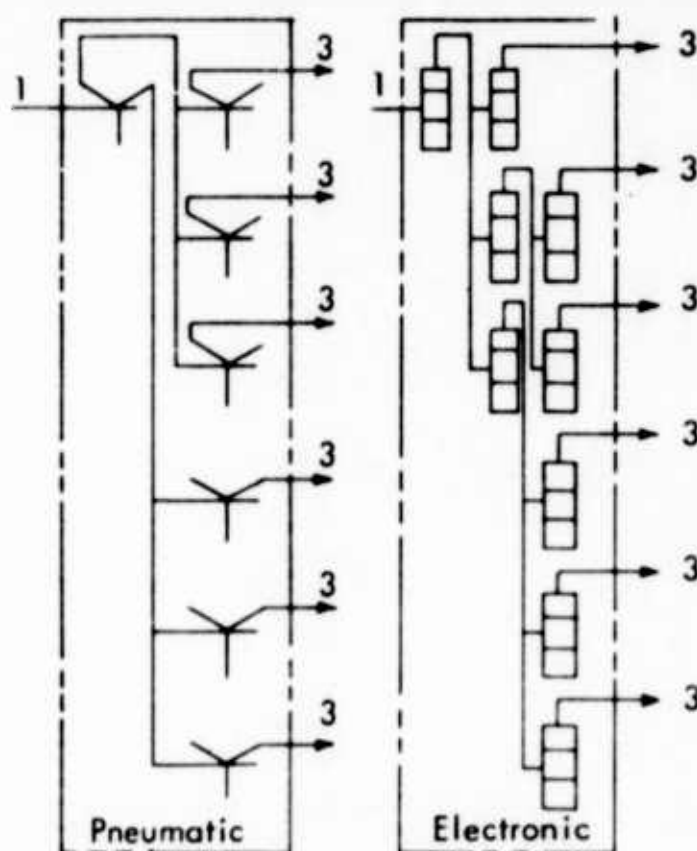


Fig. 29 - Analogous Pneumatic and Electronic Circuits

## V ACKNOWLEDGEMENTS

The author wishes to acknowledge the technical advice and assistance of Dr. R.E. Norwood, IBM Endicott.

## VI REFERENCES

1. Proceedings of the DOFL Fluid Amplification Symposium, Vol. I, October 1962.
2. Norwood, R.E., "A Performance Criterion for Fluid Jet Amplification," ASME Symposium on Fluid Jet Control Devices, November 1962.

The report on

APPLICATION OF PURE FLUID LOGIC TO ON-OFF CONTROL SYSTEMS,  
pages 221 - 241 have been deleted and will appear in Volume 4.

**THEORETICAL ANALYSIS OF  
FLUID AMPLIFIER DESIGN**

by

**R. E. Denker**

**Project Engineer**

**Whittaker Controls and Guidance  
Division of  
Telecomputing Corporation**

**Abstract**

This paper develops a formula which interrelates the major factors involved in a pneumatic bi-stable amplifier that operates above critical pressure ratios. The formula enables accurate scaling of a design and indicates the direction required for optimization. The analysis is based upon techniques that are used in the missile components industry for design of submerged pneumatic flow systems.

## Introduction

The short lead times allocated for design and development of reliable hardware in the missile components industry preclude both rigorous mathematical analyses and cut-and-try methods, and have forced the evolution of dimensional qualitative analysis wherein the component is described theoretically, except for experimentally determined coefficients which become applicable to scaling. This approach is particularly suitable to solution of problems in fluid dynamics wherein the rigorous solutions defy the efforts of genius.

Furthermore, the rigorous solutions that are peculiar to a specific design are generally useless to another. In the more complicated problems, they often obscure qualitative factors and thereby render scaling meaningless.

The following analysis is over-simplified for purposes of extreme clarity. The quantitative values assigned, although conservative and reasonable, are for first approximations only.

## Outline

Inasmuch as this paper develops several independent equations which are hereinafter combined, the following outline is presented:

- (a) Determination of the pressure,  $P_H$ , required to deflect the stream a distance  $y$ , as shown in Figure 1. This phase of the calculations is divided into the following steps:
  - (1) Presentation of equations for sonic compressible flow through a sharp edged orifice.
  - (2) Calculation of the pressure,  $P_L$ , in the bubble on the attached side of the stream.
  - (3) Calculation of the mass of the main stream in an incremental volume (see Figure 2).
  - (4) Calculation of the pressure differential,  $P_D$ , required to deflect the stream.
  - (5) Calculation of the pressure,  $P_H$ , on the detached side of the stream (equals  $P_D$  from step (4) plus  $P_L$  from step (2)).
- (b) Calculation of the secondary injectant flow rate required to cause switching.

## Analysis

### A-I Presentation of Equations for Sonic Compressible Orifice Flow

For reference in subsequent equations, the equations for sonic flow of a compressible gas through an orifice are presented:

$$W = \frac{K C P_1 A}{\sqrt{T}} = \frac{K C P_1 S H}{\sqrt{T}} \quad (1)$$

and/or

$$P_1 = \frac{\dot{W} \sqrt{T}}{K C S H} \quad (2)$$

Where:

$\dot{W}$  = Weight flow rate

$K$  = Constant, depending upon units used

$C$  = Coefficient of discharge of an orifice

$H$  = Height of orifice

$S$  = Width of orifice

$P_1$  = Total pressure upstream of orifice

$T$  = Total temperature upstream of orifice

## **A-II Calculation of Boundary Layer Pressure on Attached Side of The** **Main Stream**

The first step in the analysis is to analyze the pressure condition in the "bubble" between the stream and the wall to which it is attached, as shown in Figure 1. First it must be recognized that a pressure gradient exists in the bubble, with the pressure at the attachment point being equal to the stream static pressure, and with the pressure at a point immediately downstream of the orifice being equal to the stream static pressure, minus the stream velocity pressure.

For this analysis, the pressure gradients in the bubble are neglected, and it is assumed that a certain pressure,  $P_L$ , exists in the bubble between the orifice and the attachment point. The pressure is assumed to be the average of the pressure at the attachment point and of the pressure immediately downstream of the orifice or:

$$P_L = \frac{(P_S) + (P_S - P_V)}{2}$$

or

$$P_L = P_S - 1/2 P_V \quad (3)$$

Since the flow stream is sonic, we know the relationship between  $P_V$  and  $P_S$ .



$$\frac{P_S}{P_1} = \frac{P_S}{P_S + P_V} = \left( \frac{2}{\gamma + 1} \right)^{\frac{\gamma}{\gamma - 1}} = .535$$

$$P_S = .535 P_1$$

or:

$$P_V = .465 P_1 \quad \text{for} \quad \gamma = 1.4 \quad (3)$$

Substituting into equation (3), we have the average pressure that always exists in the bubble in terms of  $P_1$ , or:

$$P_L = .303 P_1 \quad \text{for} \quad \gamma = 1.4 \quad (4)$$

It is noted that this pressure in the bubble will remain constant regardless of the pressure on the opposite side of the stream.

The only effect of increased pressure on the opposite side of the stream would be to decrease the size of the bubble.

Allowing for possible error in equation (4), we can write:

$$P_L = K_1 P_1 \quad (5)$$

where  $K_1$  is an experimentally determined coefficient.

In order to obtain  $P_L$  in terms of main stream weight flow, we can substitute equation (2) into equation (5), yielding:

$$P_L = \frac{K_1 \dot{W} \sqrt{T}}{K C S H} \quad (6)$$

### A-III Calculation of Mass Density of an Incremental Volume of The Main Stream

The mass of an incremental cross section of a stream, discharging from a sharp edged orifice can be defined as: (see Figure 2)

$$dM = \rho \frac{dV_o}{g}$$

or:

$$dM = \frac{\dot{W}}{VA} \frac{dV_o}{g}$$

Where:

$dM$  = Mass of an incremental cross section of the main stream, lb sec<sup>2</sup> per ft.

$\dot{W}$  = Weight flow rate of the main stream  
 $= \frac{K C P_1 S H}{\sqrt{T}}$

$dV_o$  = Volume of the incremental cross section  
 $= \frac{S H_L dx}{\quad}$  (see Figure 2)

$V$  = Velocity of the main stream  
 $=$  Velocity of sound  
 $= \sqrt{\gamma g R T}$

$A$  = Cross section of the stream  
 $= S H_L$

$g$  = Accerlation of gravity

$\rho$  = Density, lb. per ft<sup>3</sup>

Substituting, we have:

$$dM = \frac{W}{\sqrt{\gamma g R T}} \cdot \frac{(d x)}{g} \quad (7)$$

Where:

$dx$  = Incremental length of main stream (see Figure 2)

## A-VI Calculation of Pressure Differential Required to Deflect The Main Stream

The parameters of the main stream trajectory are shown in Figures 1 and 2.

Treating the incremental mass as a projectile, the time required for the incremental mass to travel over the distance  $x$  is:

$$t = \frac{x}{V} = \frac{x}{\sqrt{\gamma g R T}} \quad (8)$$

The time required for the center of the incremental mass to fall the distance  $y$  is:

$$t^2 = \frac{2 y dM}{dF}$$

or

$$t = \sqrt{\frac{2 y dM}{dF}}$$

Where:

$$\begin{aligned} dF &= \text{Net force acting upon the incremental mass} \\ &= P_D S dx \end{aligned}$$

Substituting to eliminate  $dF$ , we have:

$$t = \sqrt{\frac{2 y dM}{P_D S dx}} \quad (9)$$

Combining equations (8) and (9) to eliminate  $t$ , we have :

$$\frac{x}{\sqrt{\gamma g R T}} = \sqrt{\frac{2 y dM}{P_D S dx}}$$

or:

$$P_d = \left( \frac{2 y}{x^2 S dx} \right) (\gamma g R T) (dM)$$

Substituting the value of  $dM$  from equation (7) we have:

$$P_d = \left( \frac{2y}{x^2 S dx} \right) (\gamma g R T) \frac{\dot{W}}{\sqrt{\gamma g R T}} \frac{dx}{g}$$

or

$$P_d = \dot{W} \left( \frac{2y}{x^2 S} \right) \sqrt{\frac{\gamma R T}{g}} \quad (10)$$

#### A-V Calculation of the Pressure on the Detached Side of the Stream

The pressure,  $P_H$ , on the detached side of the main stream is assumed to be the sum of the average pressure in the bubble,  $P_L$ , and the pressure required to deflect the stream,  $P_D$ , or, from equations (6) and (10)

$$\begin{aligned} P_H &= P_L + P_D \\ &= \dot{W} \left( \frac{2y}{x^2 S} \right) \sqrt{\frac{\gamma R T}{g}} + \frac{K_1 \dot{W} \sqrt{T}}{K C S H} \end{aligned} \quad (11)$$

## **B     Determination of Control Flow Rate Required to Cause Switching**

Figure 3 depicts the main stream in an incipient switching condition.

The stream has been detached from the one wall by the application of control flow,  $W_C$ . It is noted that the following conditions occur during the switching operation.

- (1) If the pressure induced on the attached side of the stream by the control flow is to detach the stream, this pressure must at some time exceed the pressure on the detached side.
- (2) Mixing of the main stream and the control gas accelerates the control gas downstream. The ultimate velocity of the boundary layer formed by the control gas is a complex function, being related to the duct aspect ratio and to the main stream Reynolds number, but primarily to the velocity of the main stream. This function should be determined experimentally for each design, however, with the high Reynolds numbers that attend the sonic flow of the main stream it is tentatively assumed that the velocity of the boundary layer gas is one-half the main stream velocity.
- (3) With the stream in the incipient position shown in Figure 3, the cross sectional area of the boundary layer can be defined as a function of the duct cross section, and is assumed to be  $1/2 H_L S$ , or  $y S$ .

(4) Knowing the pressure in a flow stream, the stream velocity, and the stream cross section, the weight flow rate can be determined. Assuming that the pressure described above in item (1) exists simultaneously with the velocity and area described in items (2) and (3), the control flow rate can be determined. The above quantitative assumptions, although considered to be reasonable and conservative, may vary substantially with the amplifier design. Qualitatively, however, the above approach is basically sound and should lend itself to scaling once a coefficient is determined experimentally. The following equations reflect the above discussion.

$$\begin{aligned}\dot{W}_C &= \left( \rho \right) \left( \frac{V_s}{2} \right) (A) \\ &= \left( \frac{P_H}{RT} \right) \left( \frac{\sqrt{\gamma g RT}}{2} \right) (\gamma S)\end{aligned}$$

Substituting the value of  $P_H$  from equation (11)

$$\dot{W} = \left( \frac{1}{RT} \right) \left[ \dot{W} \left( \frac{2\gamma}{x^2 S} \right) \sqrt{\frac{\gamma RT}{g}} + \frac{K_1 \dot{W} \sqrt{T}}{K C S H} \right] \left( \frac{\sqrt{\gamma g RT}}{2} \right) (\gamma S)$$

or:

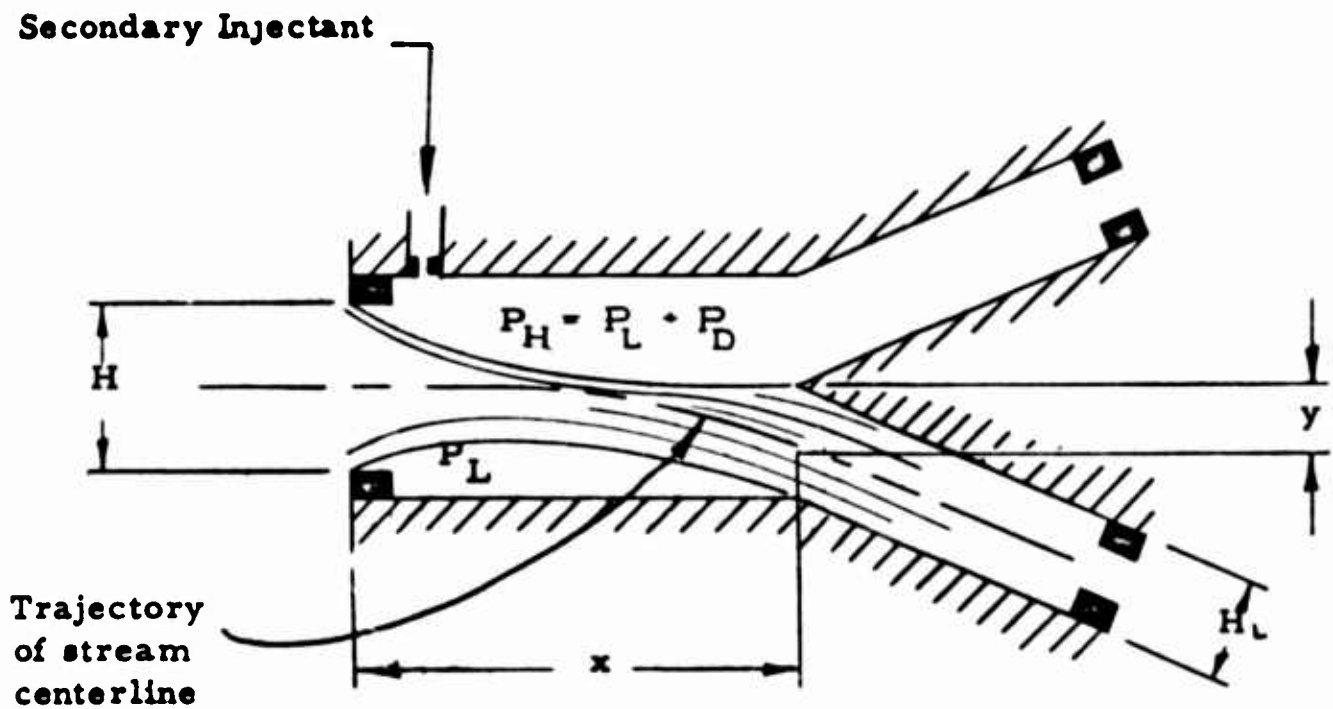
$$\dot{W} = \left( \frac{\dot{W} \gamma y^2}{x^2} \right) + \left( \frac{\dot{W} K_1 Y}{2 K C H} \right) \cdot \sqrt{\frac{\gamma g}{R}} \quad (12)$$

The flow gain may easily be derived from equation (12). The size of the control orifice can be determined, given  $P_1$  and upon having determined  $P_H$  and  $\dot{W}_C$ .



Typical of other simplifications, the effect of entrainment of the control flow by the main stream prior to switching has been omitted from this analysis. Its effect, if any, will be reflected by the above coefficients. For first approximation calculations its omission introduces negligible error since the entrainment will be at its maximum prior to switching; being small at the instant that switching occurs.

## FLUID AMPLIFIER IN "SWITCHED" CONDITION



Where:  $x$  Distance from Orifice (Inlet to Branch, Inches)  
 $y$  Stream Deflection Over Distance  $x$ , Inches

Figure 1

## INCREMENTAL REPRESENTATION OF FLOW STREAM

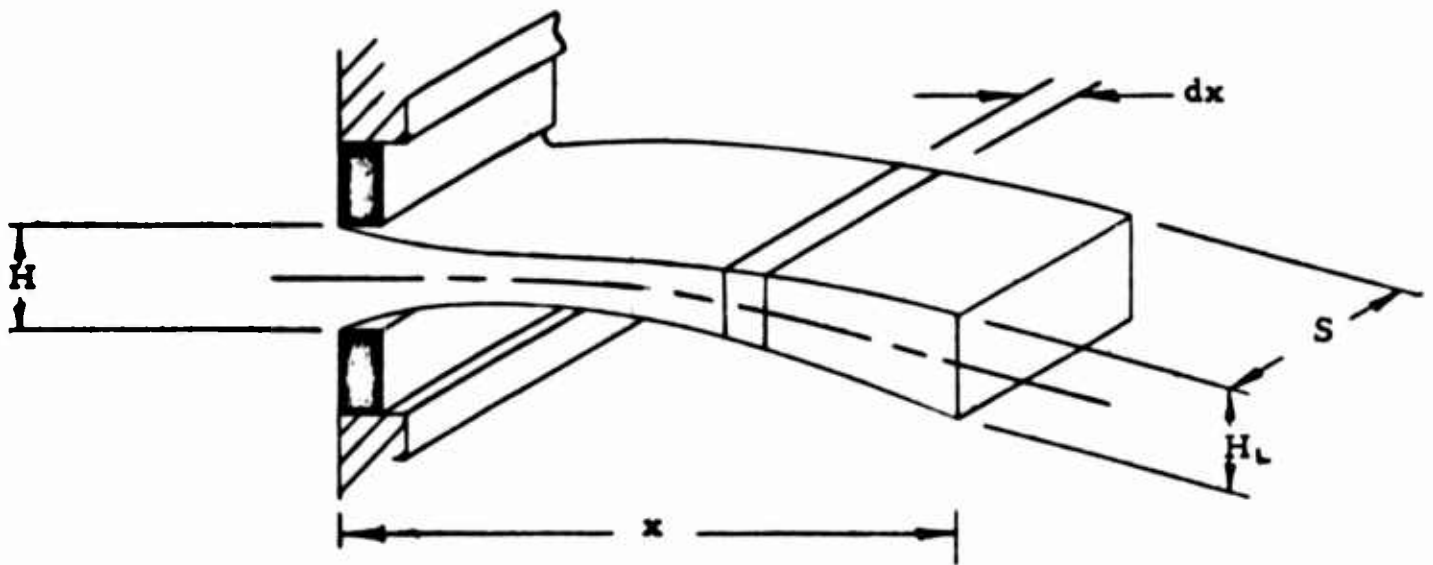
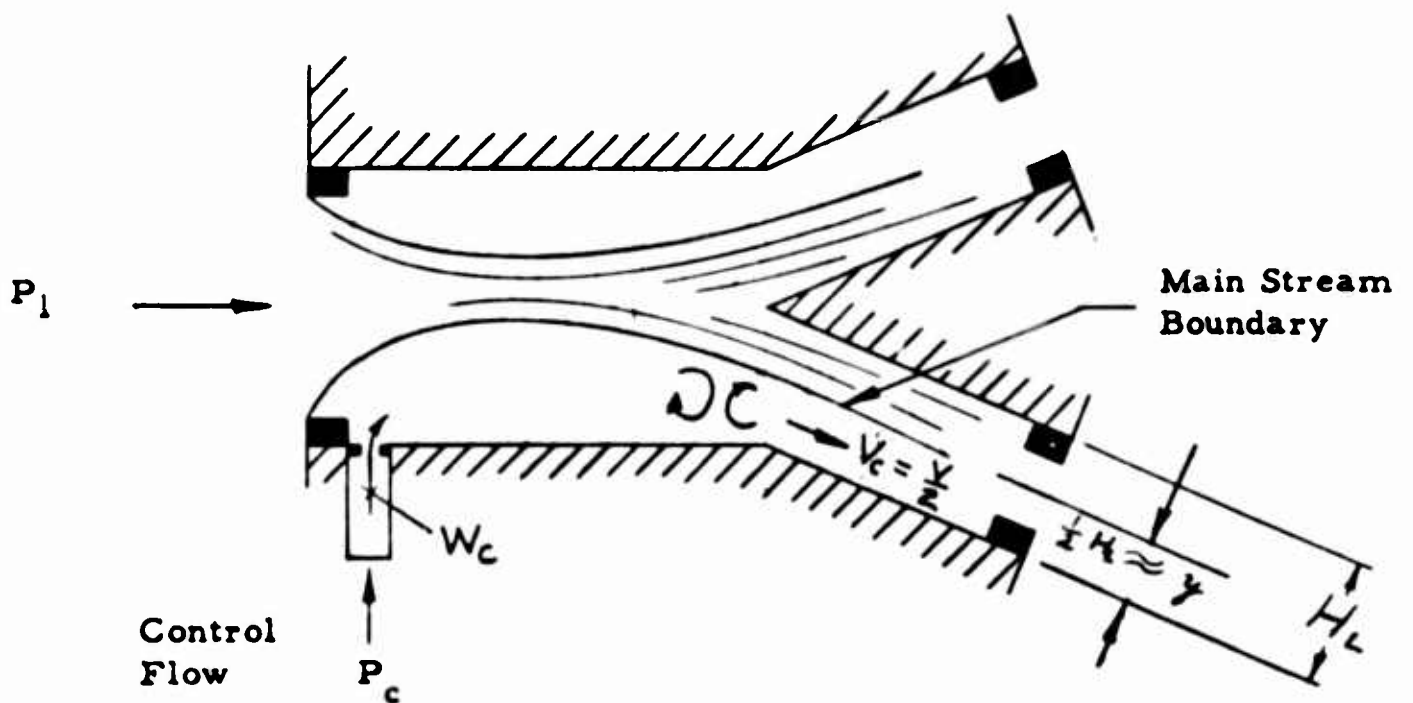


Figure 2

# **FLUID AMPLIFIER IN HYPOTHETICAL NULL CONDITION**



**Figure 3**

## **References**

1. Warren, R. W. "Wall Effect and Binary Devices",  
'Proceedings of the Fluid Amplification Symposium'  
Volume 1, October 1962.
2. Schlichting, H. "Boundary Layer Theory",  
McGraw-Hill Book Company, 1960.

# THE TURBULENCE AMPLIFIER IN CONTROL SYSTEMS

by

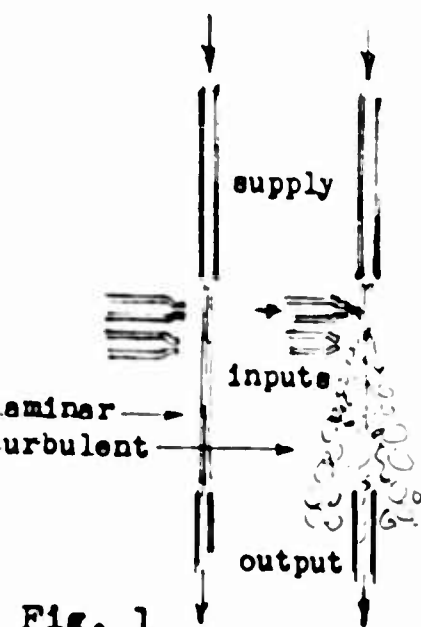
Raymond N. Auger

of

Fluid Logic Control Systems  
New York 27, N.Y.

**Introduction** - The turbulence amplifier was first described as a component for fluid logic systems at the 1962 Symposium on Fluid Amplification. At that time hundreds of these devices had been built for use in experiments and model systems. Control circuits using various input techniques, logic functions and output transducers had been thoroughly tested to verify the practicality of the turbulence amplifier as a control and switching element. Since then progress has been made in both improving the design of TAs and fabrication techniques for manufacturing them and also in applying them to an increasing number of situations. Extensive experience has now been gained in their use in industrial environments. It has been established that complex systems using hundreds of TAs can reliably operate day after day on conventional shop air, summer and winter, in the presence of severe noise, vibration and moisture in the air supply and that TA systems can be integrated with complex machine systems by industrial personnel who are not specialists in the fluid logic field.

Standard housing cabinets, input devices, output elements, filter-regulators and manifolding methods have now been established, so that large TA systems can be offered on a fast-delivery basis to solve many different types of industrial control problems. TA systems have been integrated in the center of electrical systems in some instances, and in others used to completely eliminate electrical devices. This paper will briefly outline the characteristics of the turbulence amplifier and then cover some of its applications.



**How the TA Works** - The turbulence amplifier is a high-gain, very low pressure, low cost, no-moving-parts pneumatic amplifier which can be used as the primary switching and sensing device in many control systems which might use or presently use electromagnetic relays, photocells, limit switches or transistor logic modules. The major advantages of the TA are: 1) high reliability; 2) simplicity in circuit design; and 3) low cost. The turbulence amplifier uses the disturbance amplification properties of long laminar streams. Such streams are formed by 0.030" i.d. tube in standard TAs and directed at a "collector" of the same diameter. If there is no air flow from any of the input tubes, Fig. 1, the projected laminar

Fig. 1

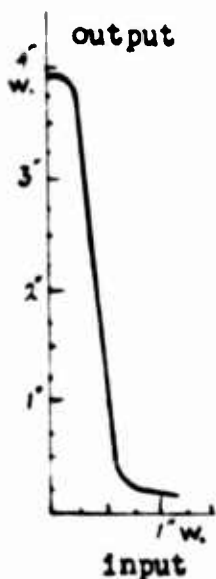


Fig. 2

stream loses relatively little of its energy during its free travel to the collector. When an air stream from any of the input tubes strikes the laminar stream, however, it becomes turbulent and relatively little of its air enters the collector. Fig. 1 illustrates the manner in which turbulence affects the variation in output pressure, and Fig. 2 indicates the input-output pressure curve. A year ago 2" of water was an acceptable stable maximum TA output. Now we can regularly obtain 5" and expect that in the future 6" will be obtainable. High-Pressure TAs are being made at present with better than 6" w. maximum outputs. In the future we expect to have 10" w. High-Pressure units. Although one-third of a psi is hardly a high pressure by conventional pneumatic standards, nonetheless it can provide a 2 pound force from a 3" diameter diaphragm, for example, which proves to be more than sufficient for operating small valves, snap-action switches, mechanical latches, etc. The i.d. of the collector tube is 0.030" and that of the input tubes 0.010", resulting in a volume gain in excess of 10, and a pressure gain also in excess of 10, so that our power gain is well over 100.

Standard TAs presently available from the H & H Machine Company of Norristown, Pennsylvania, are: two inputs, single output; four inputs, three outputs; two inputs, high-pressure single output; and a single low-impedance input, to be discussed later, with a single output. These amplifiers are being made on a production basis at the present time, in addition to various other components required for the assembly of fluid logic systems. The characteristics of these components represent choices in size, air consumption, fabrication convenience and other factors, so as to yield as universal a group of logic elements as possible. Were a demand to arise for smaller or faster TAs, these could be built, but in general it appears that a component volumetric reduction to  $\frac{1}{4}$  the present size would approach certain physical limits imposed by the phenomenon being utilized.



Fig. 3

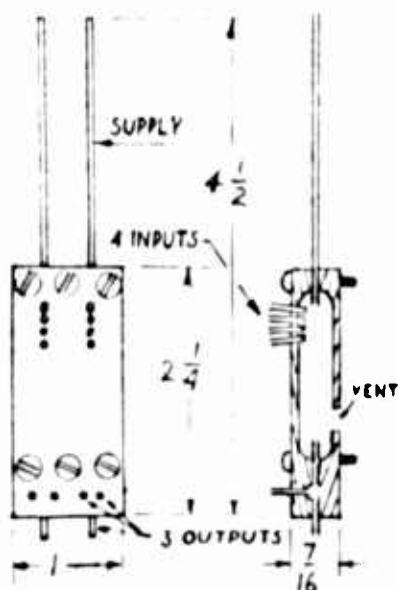


Fig. 4

Standard TAs are being built in pairs at present, except for the low-impedance input unit, the ASD. Figs. 3 and 4 illustrate a pair of four-input, three-output amplifiers.

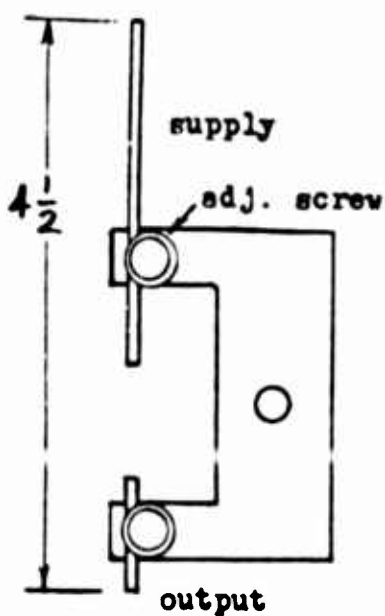


Fig. 5

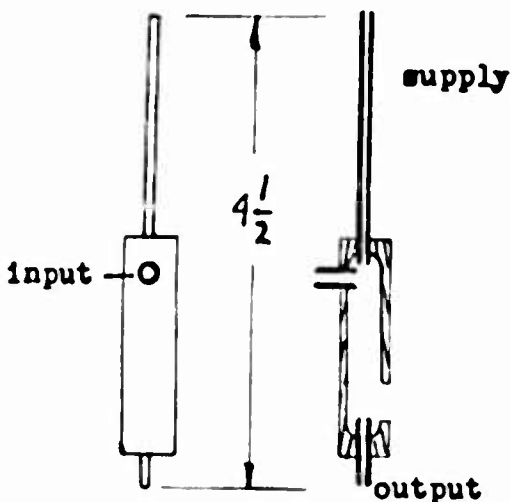


Fig. 6



Fig. 7

Inputs - Many different techniques and devices can produce pneumatic signals which can be used as inputs to TA systems. The interruptible jet (IJ), shown in Fig. 5, is the most versatile input device. It is a very precise way of detecting the location of a mechanical object without making contact with it. The IJ projects a laminar stream over a distance which may be less than  $\frac{1}{4}$ " or as long as  $1\frac{1}{2}$ ", depending on the need of the application. The physical interruption of this stream causes the collector's pressure to drop to zero. When used as an input to TAs, the IJ will be repeatable in its detection of the interrupting device to within 0.001". Unlike conventional electrical switches, the IJ has no overtravel limits and imposes so little force on the sensed object that it can be used to detect the position of electrical meter needles. IJs can transmit interruptions of less than 2 ms, or non-interruptions of less than 7 ms.

In using TA systems with complex machine systems, the IJ is used whenever possible as a substitute for a limit switch. It has these major advantages over electromechanical limit switches: 1) no wear or friction with the sensed object; 2) no overtravel limits; 3) extremely fast response; and 4) extraordinarily high precision when required.

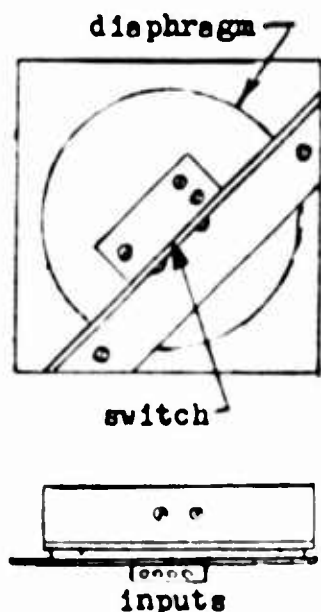
The Air Stream Detector (ASD), shown in Fig. 6, is the TAs counterpart of a photocell. The ASD is very similar in construction to a standard TA except for its single large diameter input. The large input tube allows the ASD to respond to pressures almost too low to measure. The ASD can sense air streams blown from jets or small blowers over distances ranging from a few inches to over 10'. The interruption of such streams by objects moving through them allows the ASDs internal stream to become laminar.

Inputs to TAs can be obtained by blocking orifices, such as in Fig. 7, which are venting small amounts of air to the atmosphere. This



arrangement creates a backpressure behind the blocked orifice. This technique can be used for precision gaging systems to sense variations in orifice-closure of less than 0.0001". Because of the low pressure required at the orifice, it can be used to sense the thickness of wet paint or soft coatings of various types.

Outputs - The pressure obtained from TAs can be converted into physical motion through the use of suitable diaphragms. Various sizes of mylar diaphragms are available to operate electrical switches of various types, high-pressure pneumatic or hydraulic valves, pressure-sensitive electrical transducers, sensitive instrument clutches, ratchets, dogs, etc. Standard TAs provide enough pressure to actuate snap-action switches with a small diaphragm, although High-Pressure TAs are recommended for operating devices requiring more than one pound of force. A 150 psi air or hydraulic valve is available with a 5" diameter diaphragm for applications requiring high-pressure fluid control. A 3" diameter diaphragm provides ample force for operating most snap-action switches. Speed of response is determined by the number of TAs used to provide air volume, 20 ms being the practical minimum. Visual indication of TA pressures is conveniently obtained using manometers.



Although a number of pressure switches on the market at the present time have sufficient sensitivity to be used with TAs, many have large internal volumes with capacities which result in delays of one or two seconds before actuation if a single TA is used to drive them. For that reason we have developed a simple minimum-volume diaphragm actuator. Any type of snap-action switch can be used with it. High-precision small-differential switches will respond within 1/10 second when such diaphragms are powered only by one TA. Larger switches or high-pressure valves requiring actuation forces in excess of 1 pound and travels on the order of 1/16" will require four or more amplifiers to respond with equal speed. Fig. 8 illustrates a typical diaphragm-switch structure.

Fig. 8

Using TAs in Logic Circuits - The NOR function is the most basic and universal logic concept. A NOR device produces no output when any of its inputs is active. The TA is a "natural" NOR device because if any of its inputs has a signal the projected stream becomes turbulent and the TAs output is effectively zero. Of course, if only one input of a NOR is used by a circuit, the NOR is operating simply as a NOR, or simple inverter.

One TAs output can be connected to the inputs of over 10 others, and conversely, 10 TA outputs can be connected to the inputs of one TA. Signal transmission in complex circuits takes place at about 3 ms/ft of tubing. Switching time for the TA, from laminar to turbulent, is effectively zero in addition to transmission time, but

switching time from turbulent to laminar is from 2 to 10 ms, depending on the size of the previous input signal and the demand of the device being operated. When the output of a TA is connected to its own input, for example, with a total circuit path of about  $\frac{1}{4}$ " including transmission distance in the TA itself, oscillation at about 330 cps occurs, indicating formation of some output signal within 2 milliseconds. One TA can operate another over 100' away through  $\frac{3}{32}$ " i.d. plastic tubing. Greater distance can be obtained by using more than one TA to provide the signal or by using larger tubing.

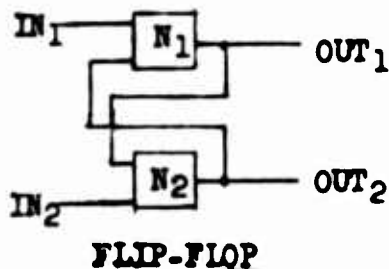


Fig. 9

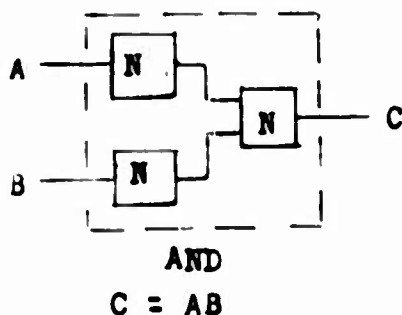


Fig. 10

Memory, AND, OR - Obtaining memory capability in logic circuits is accomplished through a flip-flop (FF) circuit. Its electromechanical counterpart is a latching relay. Two TAs are used to make a FF by the circuit shown in Fig. 9. When  $N_1$  has an output,  $N_2$  is kept turbulent. A brief pulse (3 to 10 ms. or longer) into  $IN_1$  will cause  $N_1$  to become turbulent, thereby allowing  $N_2$  to become laminar which keeps  $N_1$  turbulent. A pulse into  $IN_2$  will reverse the state of the FF.

The AND function is the same as the NOR function with inverted inputs. All of the inputs into an AND must be present for the AND to yield an output. The AND's circuit is shown in Fig. 10.

The OR function is obtained by inverting the output of a NOR. An OR produces an output when any input is present.

Standard counting, industrial logic and arithmetic circuits are found in the booklet "FLUID LOGIC FUNDAMENTALS AND THE TURBULENCE AMPLIFIER".

Power Supplies - TAs are very low power devices. The electrical energy required to provide the pneumatic power for one TA is less than 150 milliwatts if an efficient motor and low-pressure pump are used. Conventional "shop air" pneumatic power can be used if care is taken to remove water vapor through suitable traps. Large TA systems have been used with air very heavily laden with moisture, but in general the life of a TA system is limited only by the quality of the air used with it. When TA systems using over a few hundred amplifiers are installed, it may be desirable to use a low-pressure pump to provide air specifically for the TAs. The air from such a pump will have little oil or water vapor and will use little electricity for its compression. Standard filter-regulators are available which can provide more than sufficient regulation for TA systems despite wide variations in supply pressures. Each TA consumes approximately 0.05 cfm at  $\frac{1}{3}$  psi.

Manifolding TAs to the supply source presents no special problem except that care must be taken to prevent high velocity air in any manifolding system from generating high-frequency acoustical noise. Pulsating air sources present no problems as long as the pulses are below 100 or 200 cycles per second and the minimum pressure between pulses is no less than 60% of maximum pressure at the peak of the pulses.



Fig. 11

Fig. 11 indicates how compactly a complete TA system can be built. The 22" long model boat shown contains a battery-operated pump, a sound-sensitive laminar stream device, and a pressure switch in addition to the model's drive motor and steering mechanism. This toy boat can be reversed and steered to the left or right by the sound of a whistle being blown from up to 150 feet away. The sound-sensitivity of long laminar streams of the dimensions used in this model is limited to the 5 to 10 kc range; consequently the model is not responsive to normal vocal sounds or even the noise produced by its own pump.

Applications - The circuit in Fig. 12 illustrates the use of the TA as a pneumatic amplifier. An ASD, described earlier, detects an air stream projected by a blower or jet. The output of the ASD is fed to six TAs which in turn operate a diaphragm-operated valve. A box or other object which breaks the projected stream will cause the valve to respond within 1/10 second and with a positional repeatability of the interrupting object of better than 1/8". Delayed response can be obtained by using fewer TAs to drive the diaphragm.

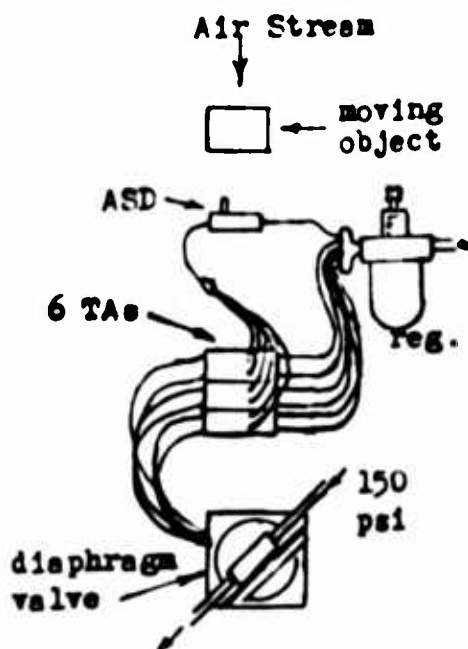


Fig. 12

Were two ASDs used, each being fed to the six TAs, it would be possible to have the system respond only to objects long enough to block the inputs of both ASDs. The components of the system shown (regulator, TAs, ASD, diaphragm-operated valve, manifolds, etc.) can be purchased for about \$50.00. Assembled in a suitable housing, their cost is \$75.

Fig. 13 illustrates a set-up at the H & H Machine Co. for testing the speed of response of Fig. 12's circuit. A synchronous clock motor rotates a plastic disk at a speed which causes ears on the disk to interrupt a projected stream of air  $1\frac{1}{2}$  times a second. The air is projected over a distance of

about 4 inches from a 1/16" tube with a supply pressure of less than 4 psi. This projected turbulent stream is intercepted by a 1/8" i.d. tube, and then carried about one foot to the input of an Air Stream Detector. The output of the Detector then drives six High-Pressure TAs, which activate a diaphragm-operated spool valve with 50 psi at its inlet. The output of the valve then operates a small 1" bore cylinder through a 1" stroke.

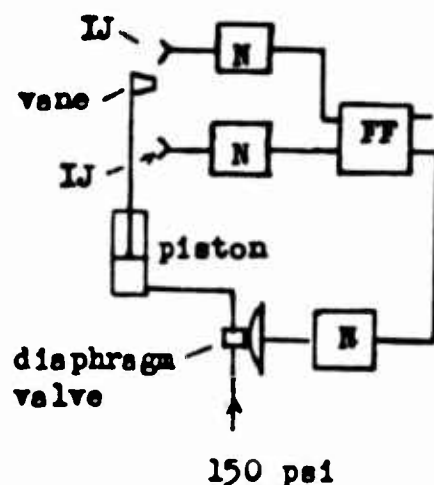
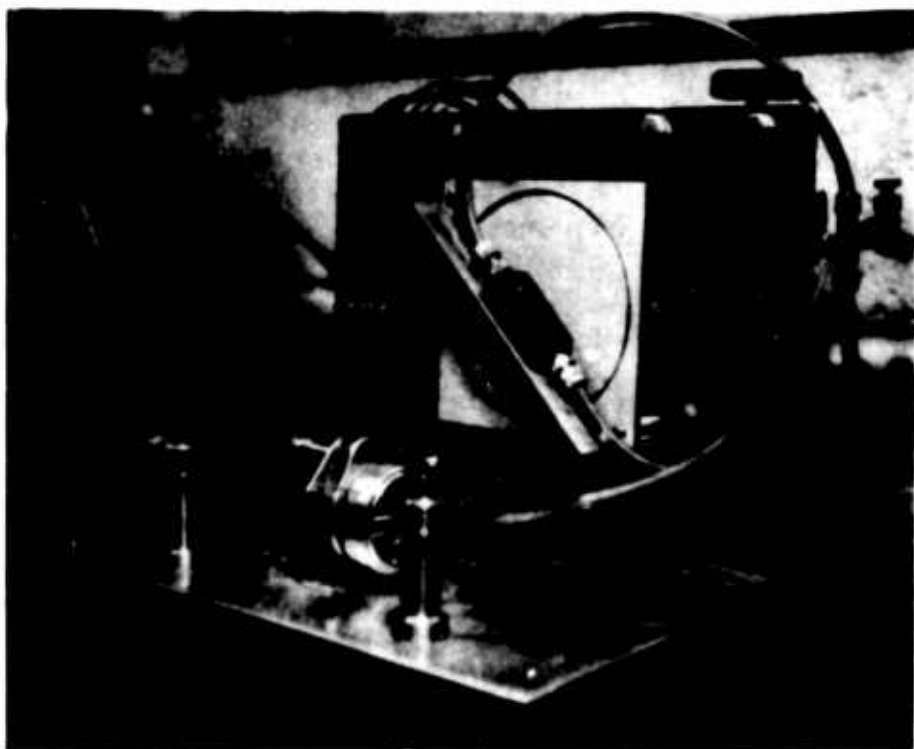


Fig. 14 (above)

Fig. 13 (left)

Hydraulic or pneumatic positioning systems used in automation equipment often have the requirement of having easily adjusted stops and occasionally mid-range stops. This can be done by cam-operated valves. Greater positioning accuracy, however, and freedom from cam wear can be obtained by using IJs to detect light weight vanes and then amplifying the IJ's output with TAs to operate high-pressure valves. The circuit in Fig. 14 shows how a spring-returned pneumatic piston can be made to automatically cycle between two IJs driving a FF. Other IJs and a simple TA circuit can be used to create a slow-down prior to the final stops.

Because IJs place virtually no load on the object they sense, they can be used to follow the profile of cardboard or light metal cams. By amplifying the output of an IJ with TAs to operate a diaphragm valve, a pneumatic or hydraulic piston can be positioned so as to keep the IJ on the edge of the cam. IJ positioning to within 0.001" is possible with such an arrangement.

Fig. 15 illustrates the first complex turbulence amplifier demonstration control system, built in early 1962. It is a model conveyor control which senses the movement of objects down a conveyor by their interruption of projected streams across the belt. Signals from the air stream detectors are fed to ANDs along with

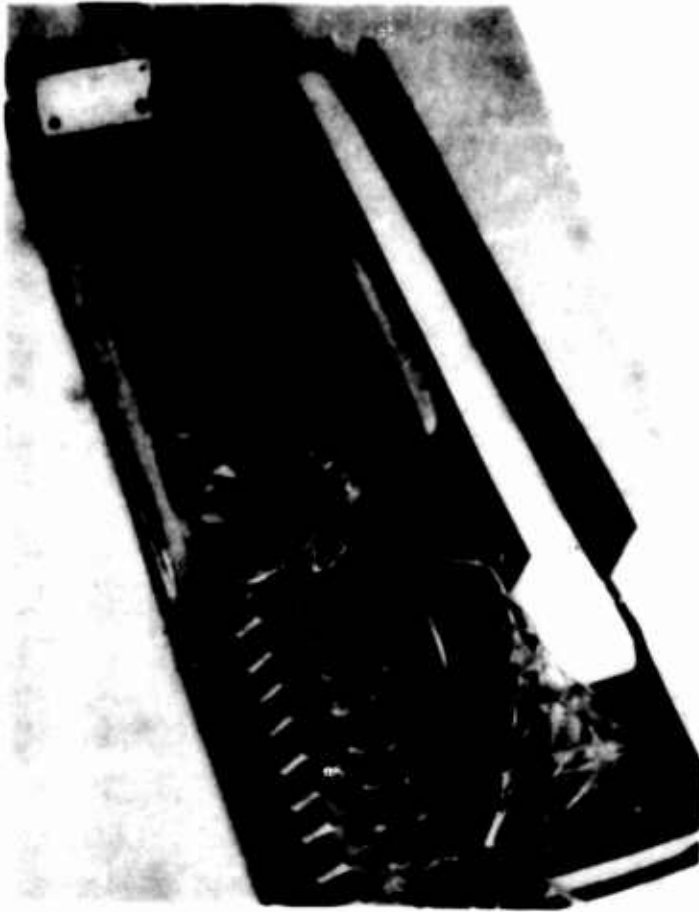


Fig. 15

signals from flip-flops operated by orifice closure type "push buttons." Coincidence of a signal from a flip-flop and an Air Stream Detector causes a pressure switch to operate, stopping the belt.

Fig. 16 illustrates a set-up also at H & H to demonstrate the effectiveness of laminar streams themselves to detect objects. Three small blocks having holes through their centers are rotated on a turntable at 30 rpm through a group of laminar streams. Depending upon the orientation of the blocks, the streams provide different signals into a simple logic circuit which distinguishes the orientation of the blocks and holds this information in a flip-flop until the part is located elsewhere on the table. This circuit simulates the requirement for distinguishing the orientation of a part on a conveyor belt or when delivered from a vibratory feeder and then, at some later point on the conveyor system, doing something, such as stamping, marking or rejecting the part.

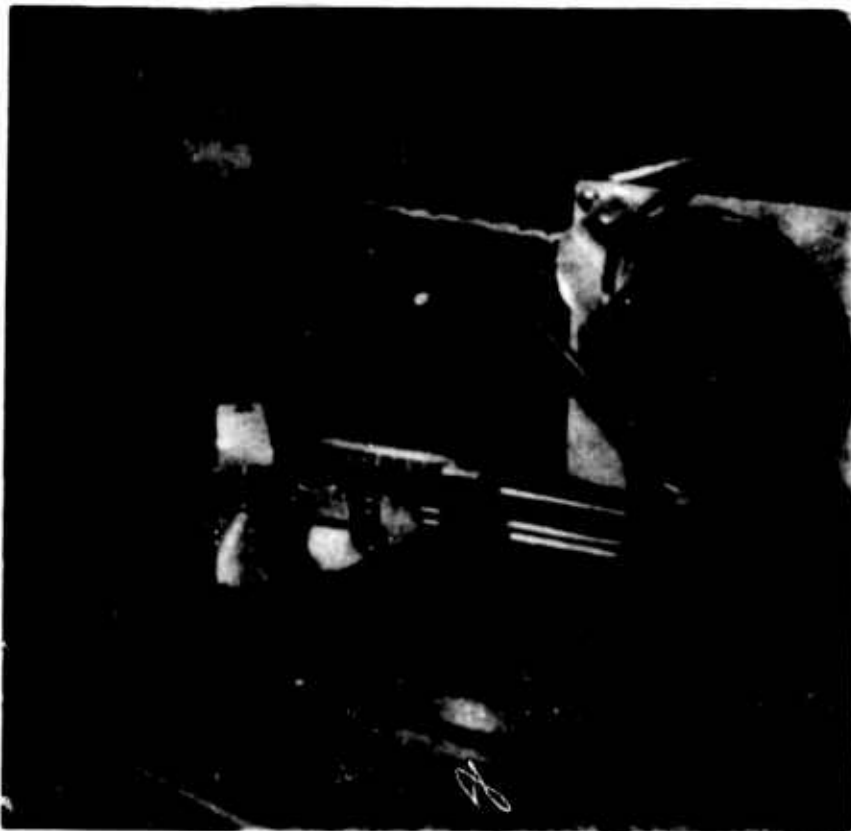


Fig. 16

Fig. 17 is a photograph of the most complicated and most thoroughly tested TA system built to date. It contains over 120 amplifiers connected to form a 6 stage binary counter. Manometers on the front of the panel indicate the condition of the counters. The inputs to this machine are derived from blocked orifices at the shaft of an automatic assembly machine. During the counting cycle various numbers are recognized, flip-flops set and pressure switches actuated. The counter automatically



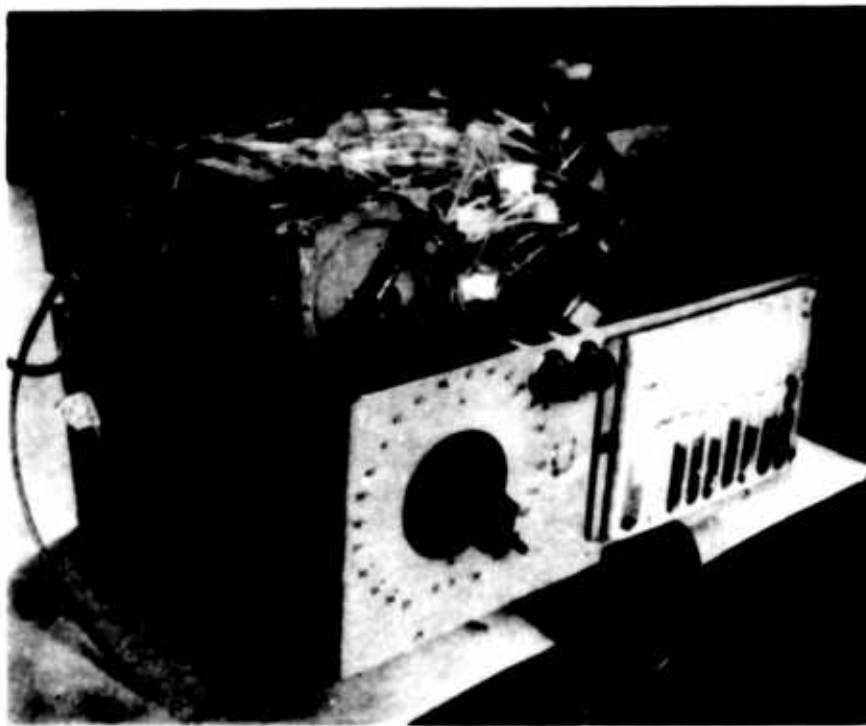


Fig. 17

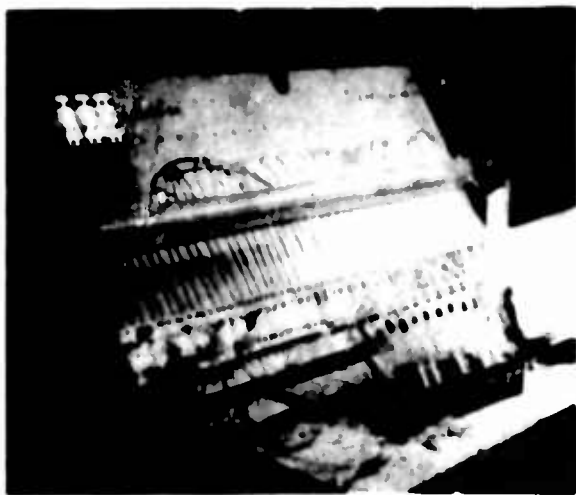


Fig. 18

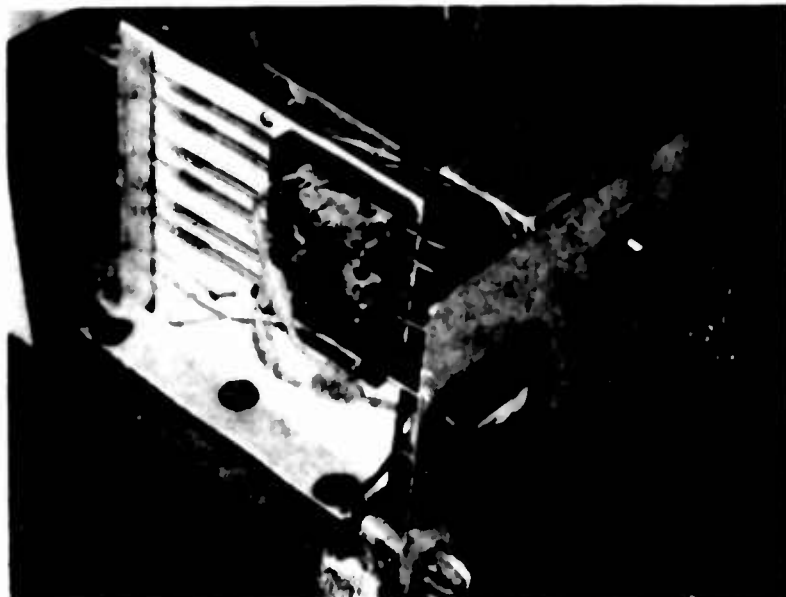


Fig. 19

recycles on reaching a number determined by the dial on the front of the machine. This dial mechanism proved unreliable after some use and was replaced with a patchboard set-up so that the operator of the machine actually alters connections on its panel with plastic tubing in order to obtain responses for different numbers. The arrangement of turbulence amplifiers in this device provided some difficulty during final assembly as a result of tubing congestion, and so a second counter of this general type was built with all of the amplifiers on a single panel. The machine illustrated in Fig. 18 is in early stages of assembly, and not all of its 100 amplifiers are in position,

but the connections of the first group of amplifiers at lower left illustrate the tubing density which resulted in the final machine. This housing technique appears to be the most suitable for industrial installations. A group of TAs completely connected can be mounted in a housing only  $2\frac{1}{2}$ " thick, complete with pressure switches or high pressure valve outputs. 100 amplifiers and two pressure switches plus a supply pressure gage fit in a cabinet 15" by 31".

Fig. 19 illustrates the ease with which TAs can be integrated into electrical assemblies. The device illustrated is a current balancing bridge circuit with a meter indication of bridge unbalance. A change in current of less than  $1/10$  Ampere in a load of up to 15 Amperes moves the pointer of the milliammeter enough to interrupt a short laminar stream. The air volume and pressure of this stream is

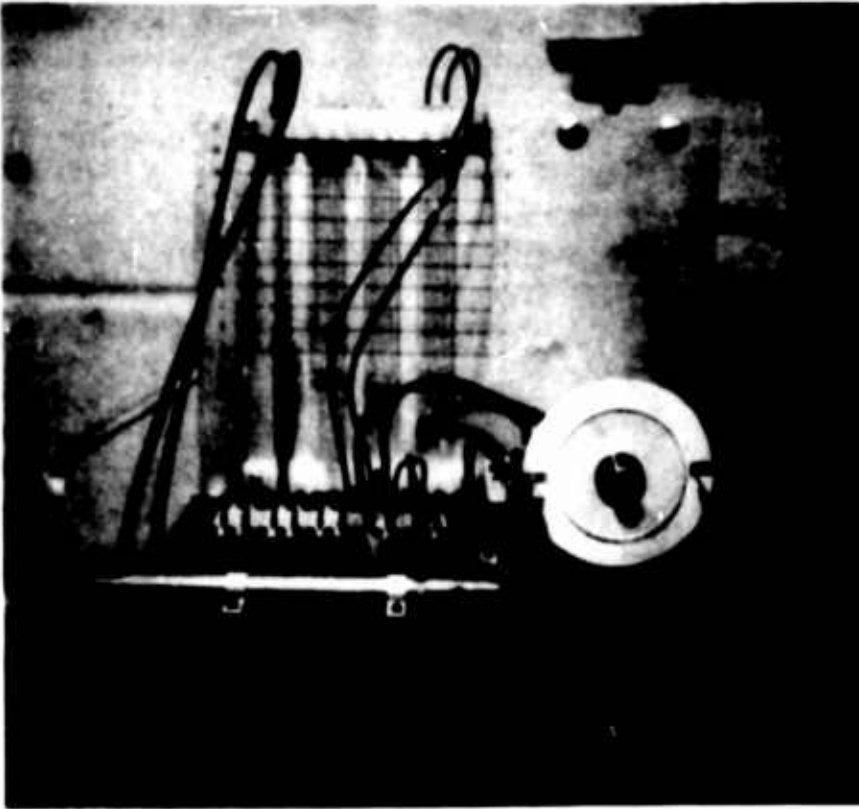


Fig. 20

amplified by a group of TAs and then used to operate a pressure switch. Speed of response to small changes is less than  $1/5$  second. This device is used to control the feed motor of a buffing machine, so as to account for buffing wheel wear.

Designing a TA System - Fig. 20 illustrates a device designed specifically to enable control system designers and those interested in fluid logic to conveniently study turbulence amplifier operation. It employs 10 TAs, six indicator manometers and a supply pressure manometer, a synchronous motor to facilitate the generation of precise pulses, two Interruptable Jets, an Air Stream Detector, a 37-page instruction book and a filter-regulator. This device has

proven very useful for the study of logic system design as well as demonstrating TA system capabilities. It is a standard produce of the H & H Machine Company.

The experience gained in working with TA systems during the last two years indicates that they presently offer a highly reliable non-electric solution to many control problems conventionally solved through the use of electromagnetic relays. TA control systems are economical in terms of power consumption, original device cost, weight, design-time, size, and installation. Of course they present no fire, explosion or shock hazard. Input techniques offer precision and life capability far beyond the ranges of electrical contact devices. Components are now available for delivery on short notice, and we expect to have dealer stocks of them in various cities before too long. Completely assembled TA systems of any size can be built to order generally within 60 days. Small systems, such as the circuit shown in Fig. 12, for the direct amplification of the output of an ASD or IJ to operate a pressure switch or high-pressure valve, can be supplied in much less time and will also be stocked items shortly. With quantity utilization, the price of TA components will inevitably be reduced. Future minimum prices are doubtlessly quite distant from present prices, which are, nonetheless, generally competitive with electrical counterparts.

We are prepared to provide every assistance to organizations wishing to use the TA for the control of new or old equipment or as a crucial or minor part of new products. We have great faith in the future of TAs and would like to invite all those in the fluid logic field to join us in profiting in their use.

## References

1. Auger, Raymond: Fluid Logic Fundamentals and the Turbulence Amplifier. H & H Machine Co., Norristown, Pennsylvania.
2. Auger, Raymond: A New "Solid State" Pneumatic Amplifier for Logic Systems. Automatic Control, December, 1962, p. 28.



# MULTIPLE-BALL PNEUMATIC AMPLIFIERS

by

John J. Eige  
Research Engineer  
Control Systems Laboratory  
Stanford Research Institute  
Menlo Park, California

## SUMMARY

A new class of fluid amplifier has been devised in which a balance of forces on balls of two sizes valves air-pressure signals. The few simple parts allow high input flow resistance, low output resistance, low power dissipation, visual indication of state, and compatibility with a variety of outputs including bellows, nozzles, and electrical contacts.

Two balls form a logical inhibitor, and three balls comprise a two-input NOR, either element being sufficient to combine in networks for all binary logic functions. A wide range of size and pressure level is possible. Units have been made as small as 0.04 in.<sup>3</sup> per NOR with interconnections. Power consumption of 10 milliwatts and switching times of 1.7 milliseconds have been measured. Ball diameters of from 1/16 to 3/8 in. are representative. Supply pressures have ranged from 0.1 to 100 psig.

The two-ball element can also be combined with flow restrictors to act as an operational amplifier for analog summing and integrating. All-solid parts of a variety of materials can tolerate high temperature and hard radiation.

## INTRODUCTION

Tiny valves, containing only sliding balls of two sizes, can control and amplify air-pressure signals. The advantages and limitations of this pneumatic component have been studied in digital and analog systems, both analytically and experimentally. The multiple-ball amplifiers, designed to fit the requirements outlined below, are capable of even more general application.

## DESIGN PHILOSOPHY

The valves were intended to control directly a useful mechanical load such as a spring-returned piston, a bellows, or a nozzle with appreciable back pressure. Therefore, operating as a binary logic element, the device should put out a steady pressure in one state, and should exhaust the trapped compressed air to the atmosphere in the other state. These states will arbitrarily be called ON, or one, and OFF, or zero, respectively.

In order to supply power to nozzles and other leaky chambers, the pressure in these chambers must be sustained by continual flow. This calls for low resistance to flow out of each amplifier. In addition, if each amplifier input has high leakage resistance, then one element will be able to fan out to drive many others in a logic network.

The interconnections between these logic elements are to be simple to design. Therefore, each input should have gain, to boost weak signals back to full strength, and the inputs should be well isolated from each other, to avoid setting up stray signal paths. The connecting lines should be simply fluid conductors, requiring no special shapes or resistances. These requirements can be met if the input chambers are closed by solid parts, moved by fluid pressure.

Elastomers and mechanical springs or flexing parts were avoided because of their tendencies to deteriorate with temperature, stress, and time, and because they would probably complicate assembly of the amplifiers. The inclusion of compliant parts would also imply that the air supply pressure must be closely regulated to a narrow range in order to accommodate the predetermined spring forces, but units that can operate over a wide range of supply pressure are more useful.

If the elements are to be low cost, they must consist of simple parts, easily made or readily available. Solid balls sliding in through-drilled holes in stacked flat plates are a suitable example of inexpensive precision.

#### THE BASIC ELEMENT

The switching motion must be caused by an unbalanced force, which could be due to differing pressures on opposing equal areas. This approach was rejected in our case because it seemed to call for either complicating the interconnecting passage with flow resistors, or else for supplying two exactly spaced pressure levels. The other way of causing the valve to move, equal pressures on opposed differing areas, occurs when two balls of different diameters are arranged as shown in Fig. 1.

The balls slide freely in round holes through plates fastened together. End plates cover the holes, limiting travel. Pressure signals enter and leave the bores as shown. The exhaust port between the balls dumps the air when the output is turned OFF, and it also prevents the leakage around the balls from building up pressure between them and separating them.

#### INHIBITOR

When only Input A is pressurized, both balls are pushed to the right, and the output is ON. But, if Input B is supplied with the same (or even somewhat lower) pressure, the balance of forces will accelerate the balls to the left, whether or not Input A is ON. The smaller ball slides across the output port, letting it exhaust, and seals off Input A. Thus, this two-ball element is ON only if: A is ON, and B is not ON. The AND and NOT functions of this logical "inhibitor" are especially useful in decoding systems.

#### TWO-INPUT NOR

The addition of another ball converts the inhibitor into the two-input NOR device shown in cross section in Fig. 2. The left-hand port is now permanently connected to the supply pressure, and the input-signal ports both terminate in closed chambers formed by the larger balls and their bore. Thus, the inputs are isolated from each other and from the output. By action similar

to that of the two-ball unit, the output of the NOR is ON only when neither Input A nor Input B is ON. Another large ball could be added to the NOR for each additional input desired.

An ideal leakless unit, in which the projected area of the larger balls was twice that of the smaller ball (diameter ratio of  $\sqrt{2}$ ) would have a switching threshold just halfway between the level of the supply and exhaust pressures. Input signals at full supply pressure would result in equal switching force in each direction. Stock ball sizes do not allow for the theoretical diameter ratio of 1.414, but the ratios 1.333 and 1.500 are readily available. The smaller ball-area ratios tend to give smaller over-all size and mass with resulting faster speeds, but the larger ratios can give more sensitivity (gain) and ability to drive more other units (fanout). The ball-area ratio is not critical, and can be varied to fit particular requirements.

Another design detail that is open to choice is the location and relative size of the (left-hand) port from the supply-pressure manifold. If this port is small and on the centerline of the bore, the small ball will close it off as it moves to the left, damping incipient bounce, lowering the standby leakage, and giving a snap action when the valve next opens. On the other hand, if the port is large and off center, there will be less hysteresis around the switching threshold, and the lower output resistance will allow more fanout.

After trying several ball materials, we have tentatively decided upon steel in small elements because of its precision and toughness, and nylon in larger devices (where less precision is needed) for its low density and long wear. Both are readily available at low cost.

Figure 3 is a photograph of a typical block of eight separate three-ball NOR elements in one supply manifold. Brass tubes pressed into the input and output ports form a patchboard on which signal connections are made by slipping vinyl sleeving over the tubes. (These simple connections have been used successfully at pressures up to 20 psig.) The balls in this unit are of 3/32-in. and 1/8-in. diameter steel, the center plates are aluminum, and the end plates acrylic. These materials were chosen for easy fabrication of an experimental model, but held up well for over 50 million on-off cycles. The ball diametral clearance is readily held to within a fraction of a mil by through-drilling and reaming each hole, then pressing through an oversized tungsten-carbide ball.

The exact size and shape of the signal paths are not important, nor do the stacked plates need to be exactly aligned, so construction is rapid.

Units this size have been operated from pressure supplies of from 0.1 to 100 psig. A pressure level between 1 and 4 psig was found experimentally to give a good balance between the high speed and good acceleration-tolerance of high pressures and the reduced bounce and low power drain attainable at low pressures. Calculations predict that the units could tolerate up to 9 g's per psi of supply pressure without erroneous switching.

These NOR's have a fanout of about 5, and their operating power requirement at 1 psig in logic systems is about 10 milliwatts. Standby power drain is about 90% of that, indicating that most of the air power is dissipated by leakage, rather than by pressurizing and exhausting the input chambers.

Other laboratory models have been made in various configurations and sizes. The smallest and fastest NOR elements of this type (see Fig. 4) have steel balls of 1/16-in. diameter. They occupy a volume of 0.04 in.<sup>3</sup> per element, including interconnections in the form of grooved plates (like printed circuits) that cover the input-output holes. The period of oscillation of three elements in a free-running ring indicated that their individual switching time at 8 psig was 1.7 millisecc.

## SPEED OF RESPONSE

The switching speed of these elements is, to a first approximation, the sum of three terms: the time delay for a pressure wave to be transmitted from one device to the next, the lag in pressurizing an air chamber through a port, and finally the time required to accelerate the moving parts to a new position after full pressure is present.

Scaling the element down to smaller size reduces all of these terms proportionally.

An increase in supply pressure has little effect on the transmission delay; it actually increases the lag time because of increased compressibility effects, but decreases the acceleration time as the square root of pressure level.

The acceleration time is also proportional to the square root of the mass density of the ball material, so that a change from steel to nylon balls can better this term by almost a factor of 3. The fact that the response of most of these amplifiers is mainly limited by the acceleration time does have one advantage: the response of all elements in a dynamic logic system will remain the same regardless of minor differences in fanout, line lengths, and restrictions.

A more complicated analysis is required when the element is speeded up (by reducing size, increasing pressure, and lightening the balls) to the point where all three response terms are of the same order of magnitude. This has not been done in detail, but a switching speed of about 1 ms appears to be a practical limit.

## BINARY CIRCUITS

Either the inhibitor or the two-input NOR is logically sufficient as the sole building block in all binary functions and computations.

In the block diagrams of some typical circuits, the inhibitor is represented by a rectangle containing the letters AN. This is a mnemonic to indicate that the signal entering the A (for AND) side is connected with an AND to the Boolean negation of the signal entering the N (for NOT) side. Physically, the N side is that of the larger ball.

The NOR symbol is a triangle, with signals going into a side and the output at the opposite vertex. The supply pressure and exhaust connections

to each NOR are omitted in the diagrams. Where additional supply pressure connections are needed, they are denoted by a one.

Figure 5 shows that an inhibitor, supplied with constant pressure and fed back so that its output tends to negate itself, becomes an oscillator.

In Fig. 6, two NOR's in a loop form a basic memory element, the two-input "flip-flop."

The next diagram, Fig. 7, refers to the rudimentary punched-tape reader and decoder seen in the photograph, Fig. 8. Two holes in the tape are read and decoded, and appropriate action is taken (simulated by pressurizing one of several gages), all pneumatically.

Two binary numbers are added in the circuit of Figs. 9 and 10. The numbers are entered as parallel combinations on push-button valves, and their sum is displayed in parallel binary code on pressure gages (as on-off indicators).

The last example network, Figs. 11 and 12, continually cycles three outputs as shown in the timing diagram of Fig. 11. The outputs in this case create air jets from nozzles for an experiment dealing with tactile perception, i.e., information sensing through the skin. The flow resistances R and the tanks C form lag circuits that slow the cycle down to the desired rate.

#### PNEUMATIC OPERATIONAL AMPLIFIER CIRCUITS

The two-ball pneumatic element previously described as an inhibitor for digital circuits can also be used as an operational amplifier, the basic unit of analog computing circuits.

Figure 13 shows one form of such an amplifier provided with flow resistances to give the inverted sum of two input pressure signals.

The balls are freely sliding but well fitted to the holes. The smaller ball throttles the output port, acting as a pressure divider between the supply and exhaust pressures. If the cross-sectional area of one ball is twice that of the other, then the balls will be in static equilibrium only when  $P_x - P_a = \frac{1}{2}(P_s - P_a)$ . But, since  $P_s$  is a fixed reference pressure, then  $P_x$  will also be a fixed known pressure level (except for transient disturbances.) This  $P_x$  corresponds to the "virtual ground" at the summing junction of an electronic summing amplifier. The input signals are represented by the pressure differentials  $(P_1 - P_x)$  and  $(P_2 - P_x)$ , and can therefore be positive or negative (with respect to "computer ground,"  $P_x$ ).

The R's shown in the preceding diagram are linear flow resistances, e.g., capillaries or porous plugs. (Resistance here has the units of pressure drop divided by volume flow rate.) The needle valve, b, can be adjusted so as to balance out the effect of leakage past the large ball, thus eliminating zero offset of the output.

A summation of flow rates into the  $P_x$  chamber will show that the output is the negative weighted sum of the inputs, as follows:

$$(P_o - P_x) = - \frac{R_f}{R_1} (P_1 - P_x) - \frac{R_f}{R_2} (P_2 - P_x).$$

Note that  $P_1$  and  $P_2$  are assumed to be pressure sources, of low internal resistance. They must be able to put out or to accept some flow at constant pressure. It can be seen that these operational amplifiers can drive and be driven by other units like themselves in circuits.

The usual electronic way to integrate a function with respect to time using an operational amplifier is to feed back around the amplifier through a coupling capacitor. The pneumatic analogy to this coupling capacitor is two chambers separated by a spring-loaded partition or compliant membrane. For applications where these springy elements are not desirable, there is another scheme for integrating that is based upon the fact that a rigid tank containing air is analogous to a capacitor with one end tied to ground.

Electronically, a current source feeding such a capacitor would generate a voltage at the capacitor proportional to the integral of the current. The current could be controlled by monitoring the drop across a resistor. The pneumatic analog is shown in Fig. 14. Arrows show information flow, not necessarily air-flow direction. The restrictors marked  $R_1$  are all of equal (linear) resistance;  $C$  is the "pneumatic capacitance" of the air tank. Analysis of the circuit shows that we have the desired function:

$$(P_o - P_x) = \frac{1}{R_2 C} \int (P_1 - P_x) dt.$$

The two-ball element can also be used as a high-gain amplifier for control as well as computing. Figure 15 shows a fluid servomechanism for positioning a variable load in continuous response to a low-power pressure signal. There are no springs or diaphragms to creep or deteriorate at high temperatures. The load displacement,  $x$ , will be proportional to  $(P_1 - P_x)$ . Valve  $b$  can be used to set the zero position.

The capillary gap around the enlarged portion of the piston rod provides a feedback flow rate proportional to position. The resulting flow summation at the amplifier input causes the balls to shift and valve fluid to or from the head end of the cylinder until an equilibrium position is reached, in correspondence to the input signal.

A pressurized air bearing forms a different position control system in which the insertion of a fluid amplifier and an air gage can improve stiffness and stability.

Hybrid circuits with the same kind of element throughout are internally compatible since these elements are designed to drive each other readily. A sample portion of a circuit is shown in Fig. 16 to illustrate: analog sensing of displacement, an analog buffering and inverting amplifier, analog summing, and binary switching after threshold detection. The balance valve

in the summer could be used to vary the threshold. The weight associated with each input to the summer is adjustable, as shown previously. The output could obviously continue on to other binary (or analog) devices.

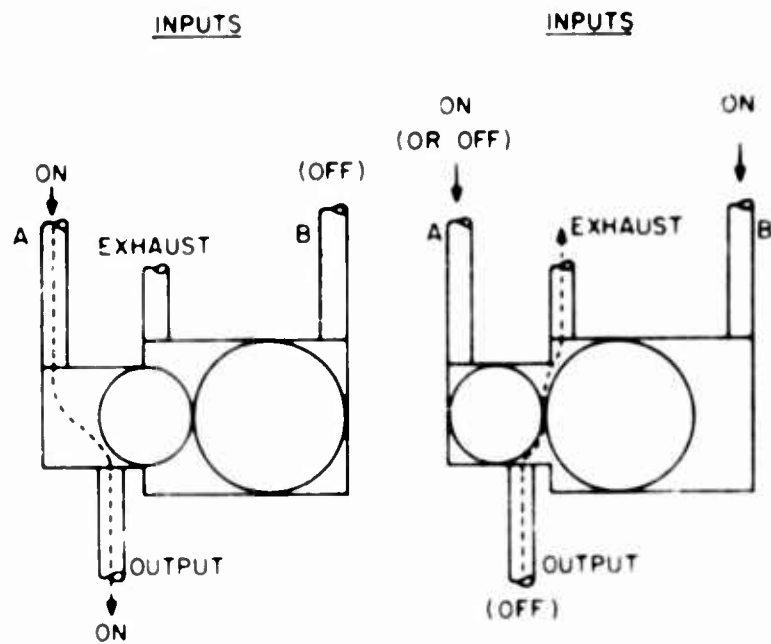


Fig. 1  
The Basic Two-Ball Element (Inhibitor)

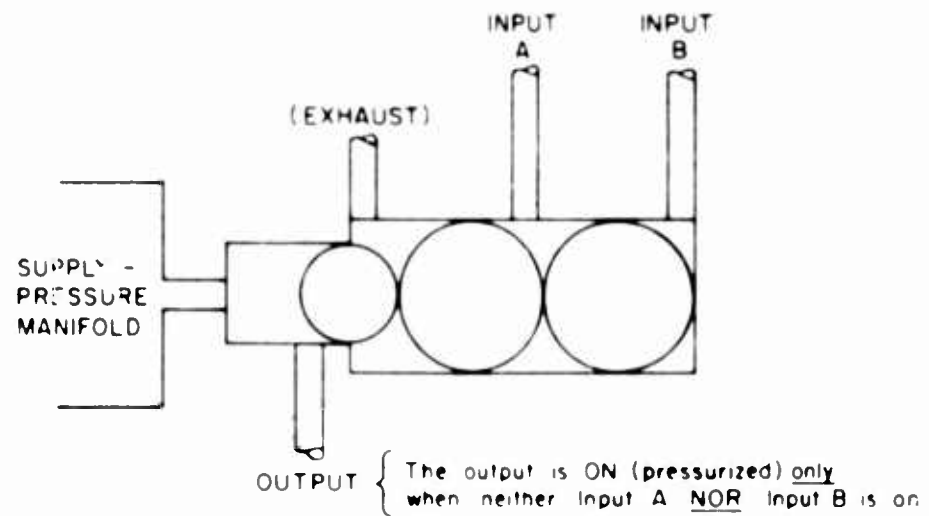
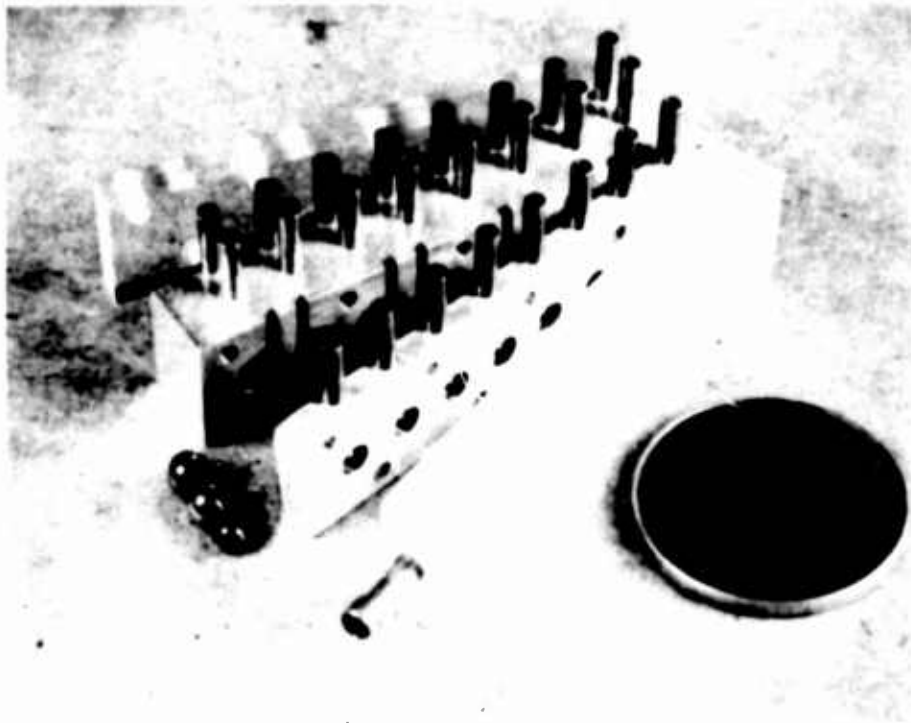
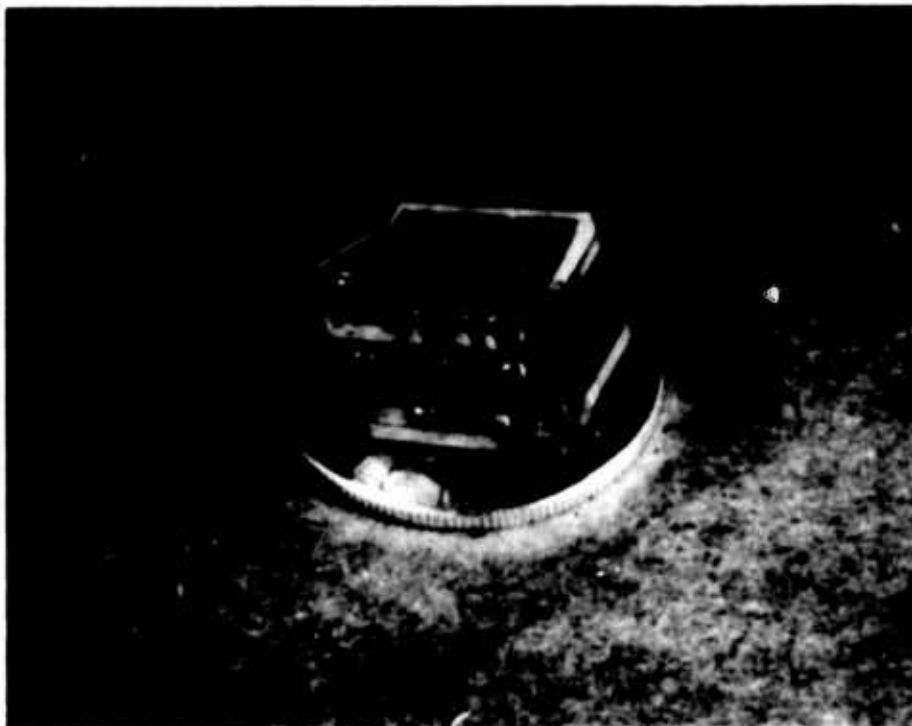


Fig. 2  
The Three-Ball NOR

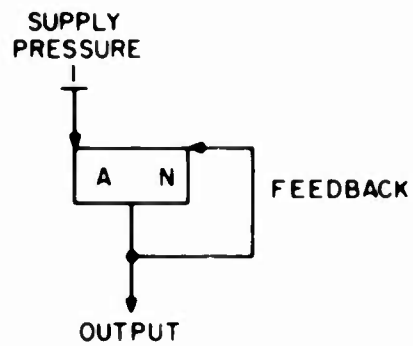




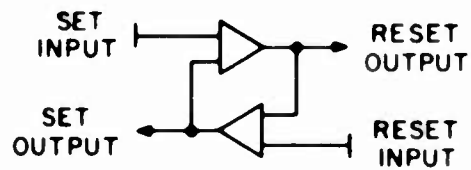
**Fig. 3**  
**Exploded View of a Block of Eight NOR Elements**



**Fig. 4**  
**A Package of Four NOR's with Signal Manifolds**



**Fig. 5**  
**An Inhibitor Connected as an Oscillator**



**Fig. 6**  
**Two NOR's Form a Flip-Flop**

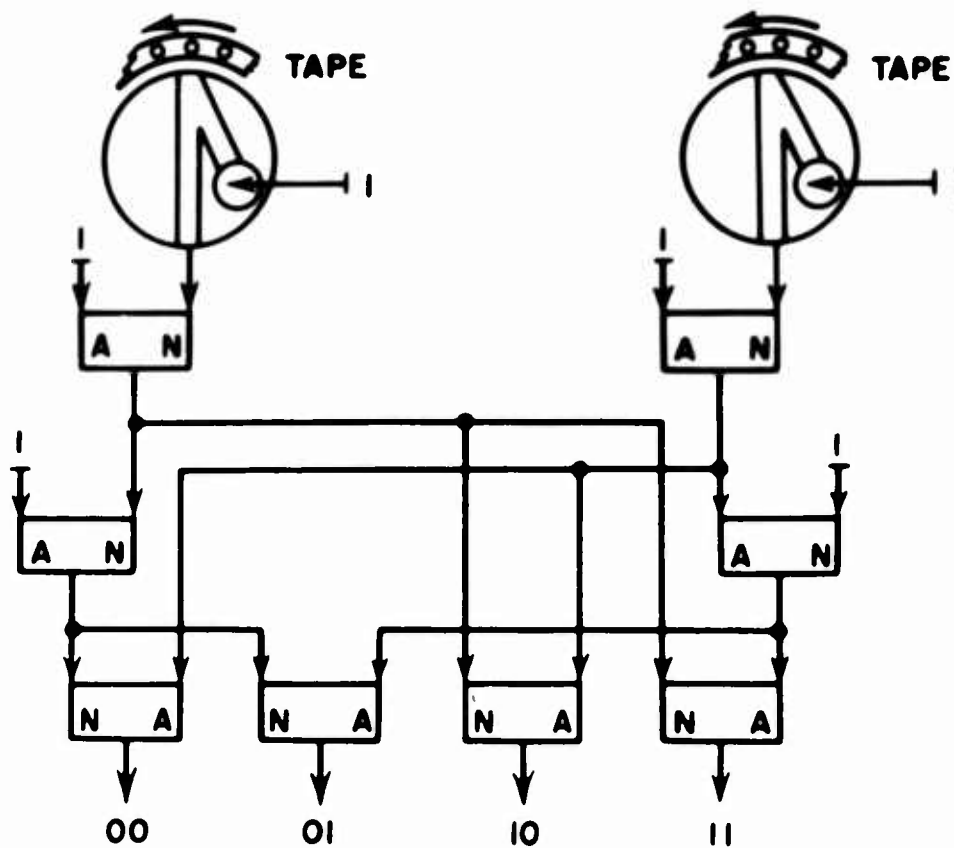


Fig. 7  
A Punched-Tape Reader and Decoder, Schematic

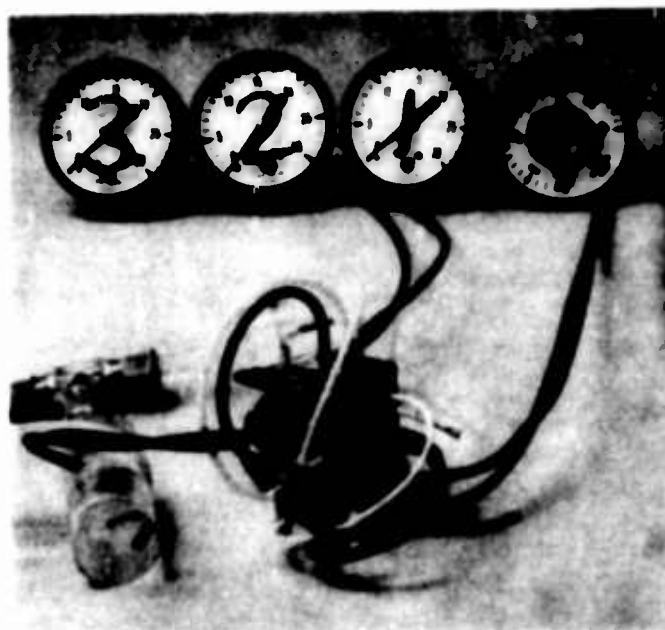
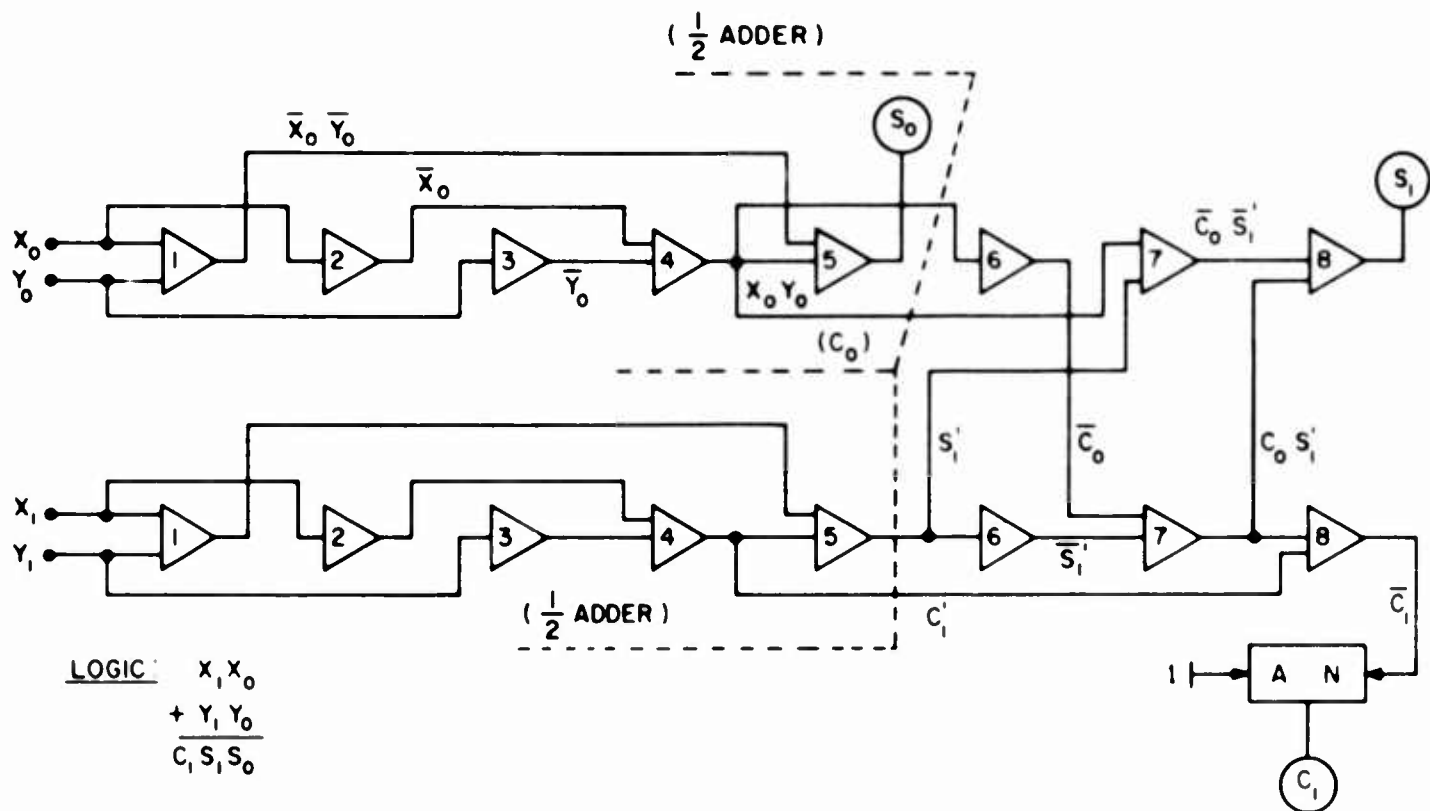
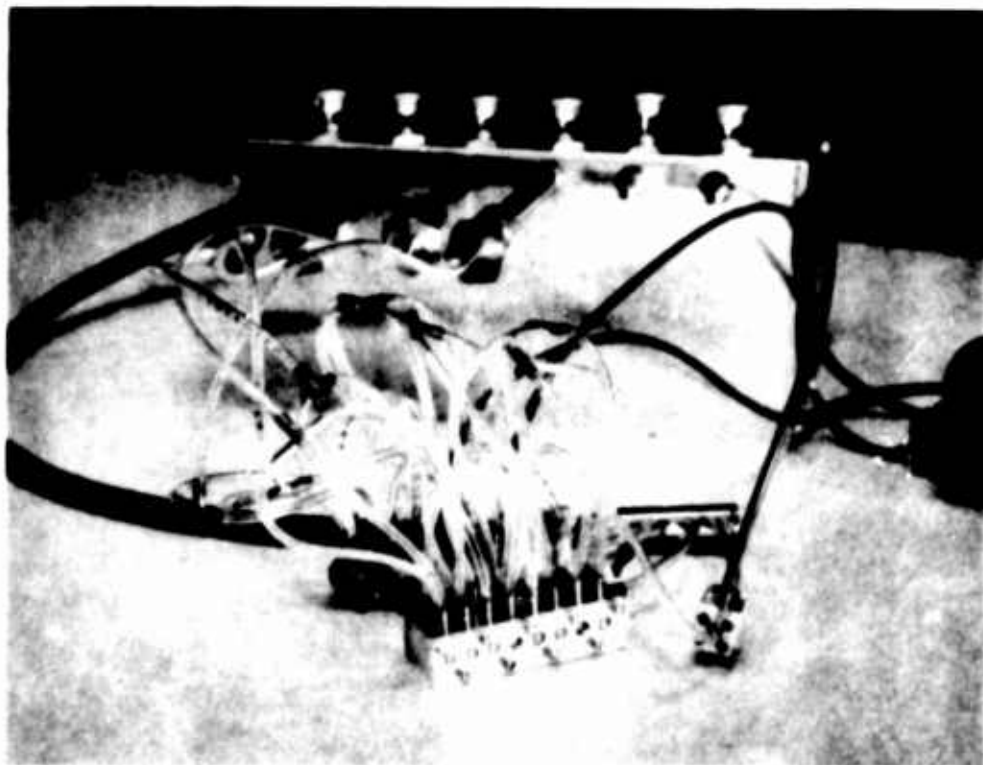


Fig. 8  
A Punched-Tape Reader and Decoder, Photograph



**Fig. 9**  
**A Parallel Binary Adder, Schematic**



**Fig. 10**  
**A Parallel Binary Adder, Photograph**

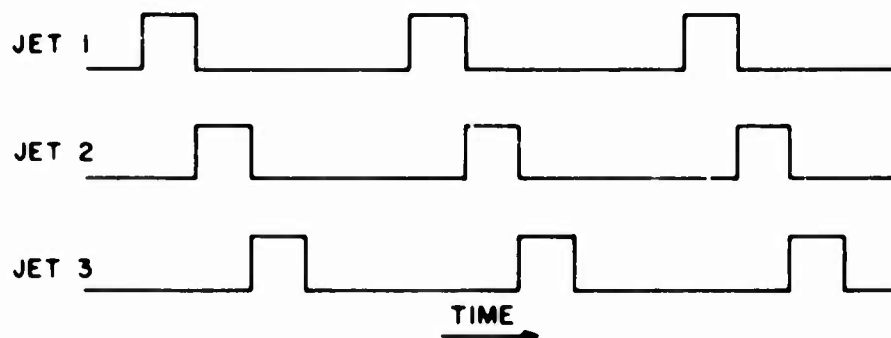
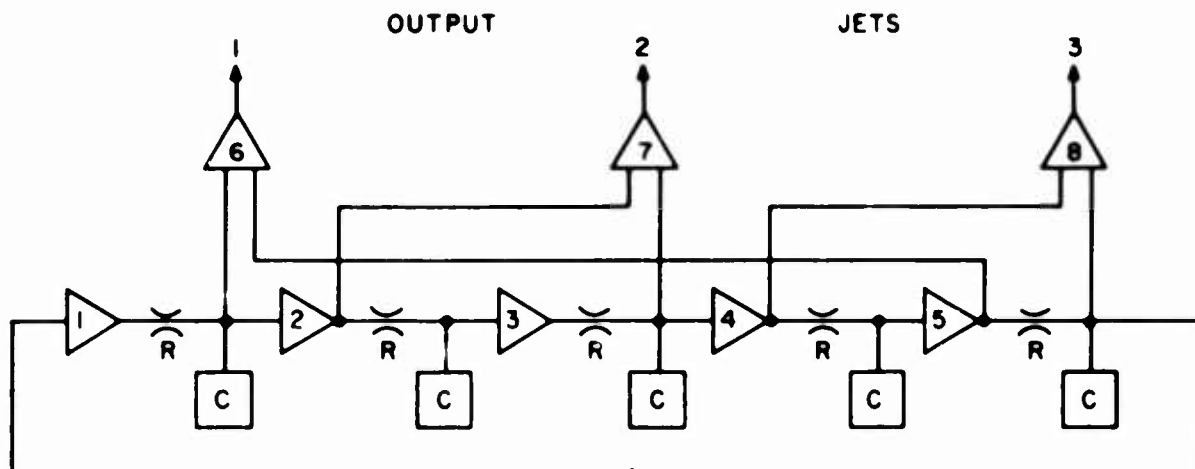


Fig. 11  
A Sequencer, Circuit and Timing Diagram

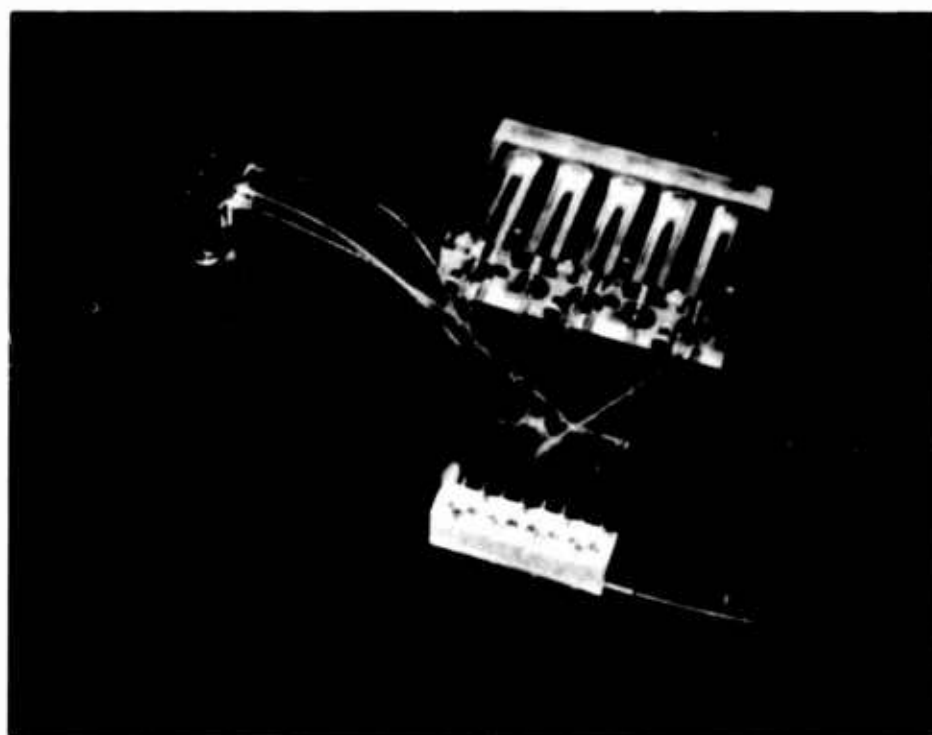


Fig. 12  
A Sequencer, Photograph

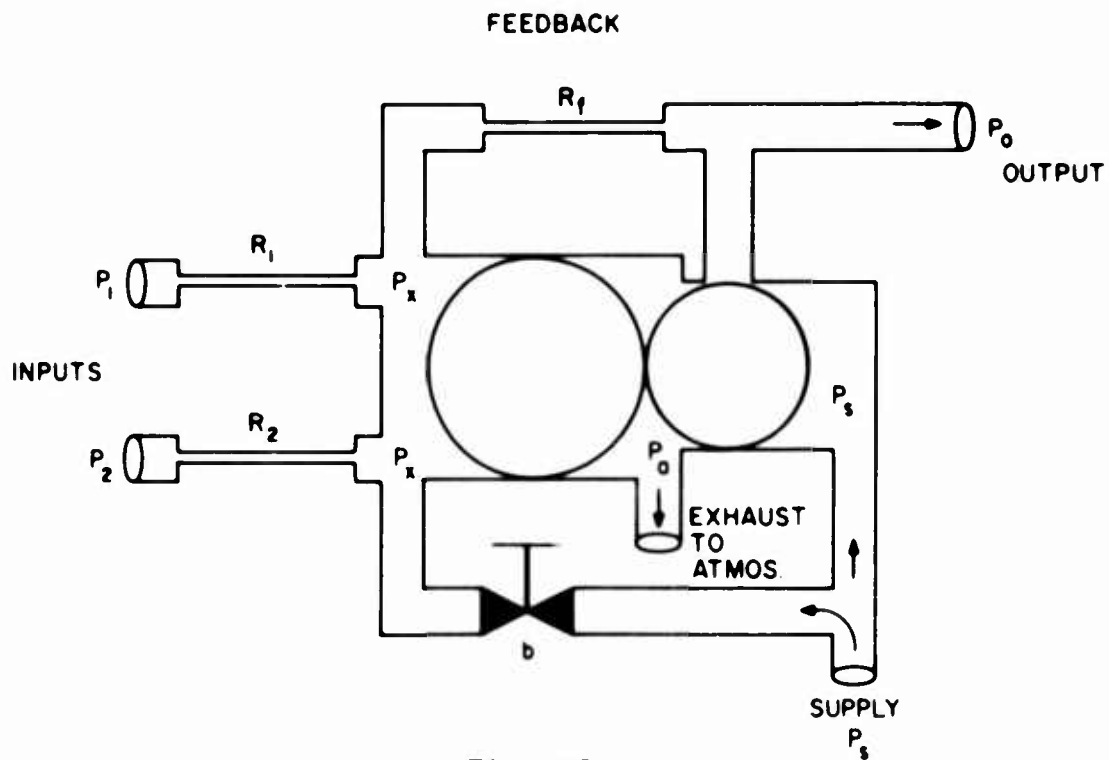


Fig. 13  
Analog Summation

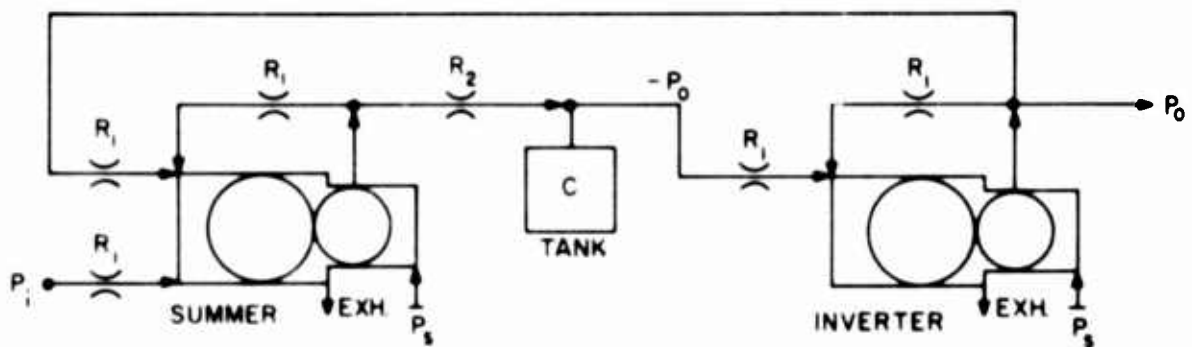


Fig. 14  
Analog Integration

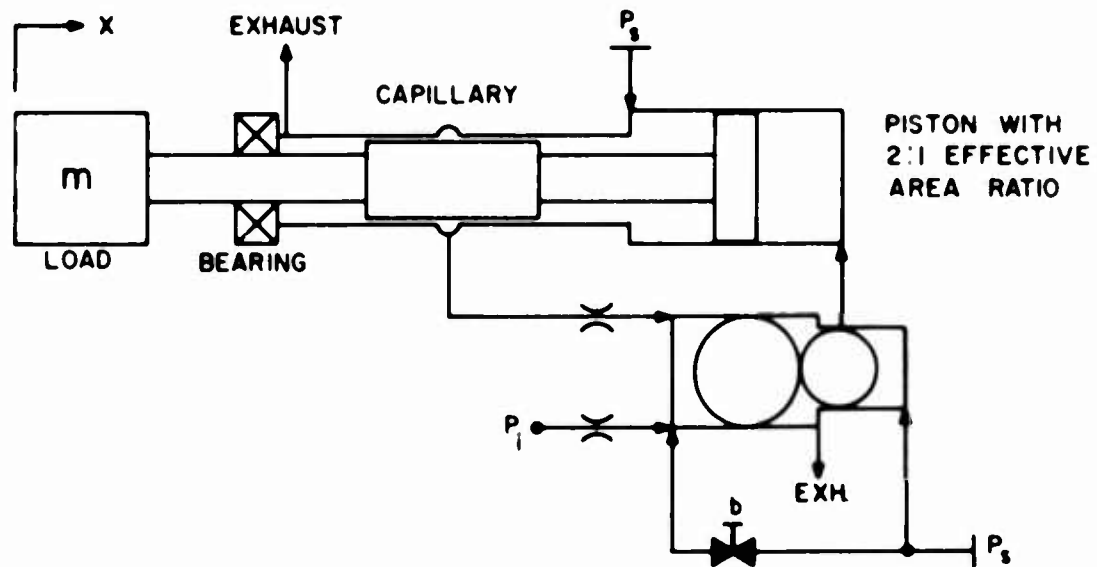


Fig. 15  
Position Control

#### NOZZLE-AND-FLAPPER SENSOR

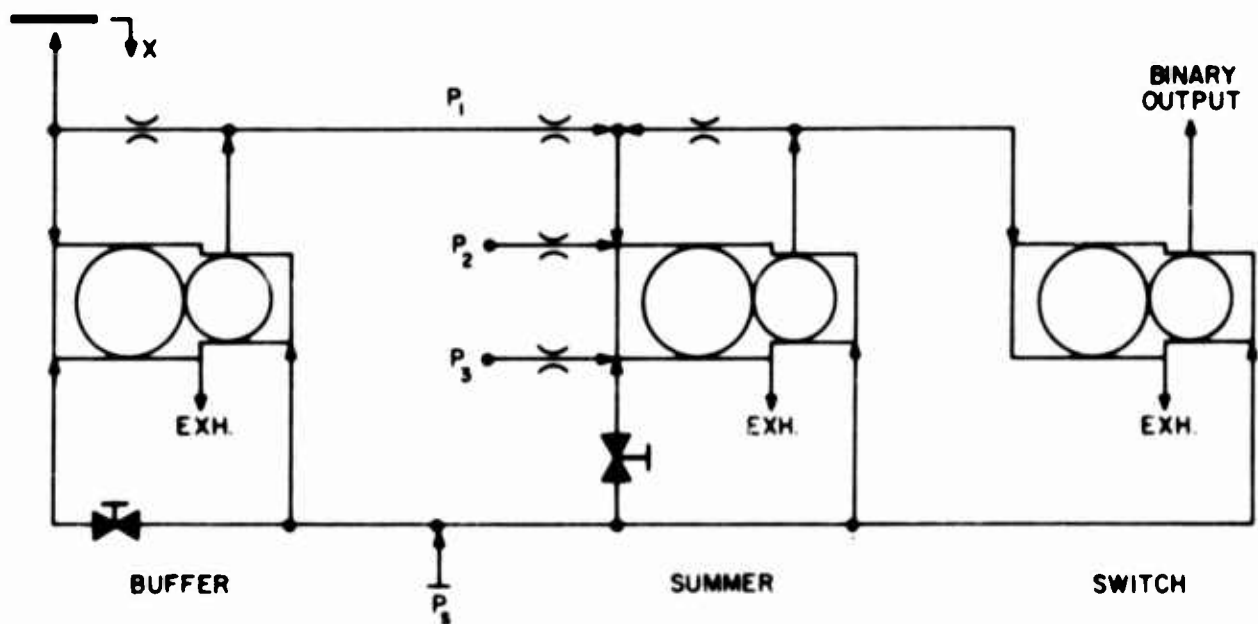


Fig. 16  
Analog-Digital Combination

The Staging of Pressure Proportional Amplifiers to Provide Stable,  
Medium Gain, Dual Control, Single Output Pure Fluid Systems

By

W. L. Cochran

And

R. W. Van Tilburg

of

CORNING GLASS WORKS



## ABSTRACT

Fabrication and testing techniques used in the development of multistage pressure proportional amplifier pure fluid systems are discussed and practical solutions to some of the problems inherent in the development of interconnected fluid subsystems are given where available. Performance of individual elements are discussed as they relate to staged system performance. Staged system noise and individual element noise is described and the attempts to locate and eliminate the sources of the noise are discussed. In each case only those solutions which have been demonstrated as possible and practical are offered.

A solution to the problem of providing a common power inlet to a multistaged system is presented and the effect of using such a common source is discussed.

The description and output characteristics of a modified passive difference amplifier are given. The passive difference amplifier was originally designed by HDL personnel and when used in conjunction with a staged system provides a single pneumatic signal approximating the difference in pneumatic signals appearing at the outputs of the staged system. With the use of this device it is possible to have output signals which are compatible with the control signal requirements of the staged system.

# I INTRODUCTION

## A) General

This paper covers work performed under contract to the Harry Diamond Laboratories by Corning Glass Works and represents in some cases a combination of effort from the two facilities.

## B) Goals

It has been the goal of Corning Glass Works to determine the operational characteristics of certain fluid amplifiers as fabricated in Fotoform Glass in semi-production quantities. More recently the goal has been to interconnect these designs in glass to provide working useful pure fluid systems.

## C) The Pressure Proportional Amplifier-The Primary Active Element

The pressure proportional amplifier operational characteristics are of fundamental interest when considered as a link in a larger system. For this reason, considerable discussion will be centered around the basic device even though this paper deals primarily with a system containing several devices. No attempt is made herein to present the theory of operation of the pressure proportional amplifier since adequate presentation has been made by others and is available. <sup>(1)</sup> The step from theory to practice is often large and theory must be translated into practice before a useful piece of hardware results. It is hoped then that the data, conclusions, and techniques discussed herein which were borne out of practice will be of value to the reader since many of these can apply to other phases of fluid amplifier development as well as they apply to the development of the primary active element, the pressure proportional amplifier.

## D) Staging

In order to achieve reasonable gains, individual low gain elements must be staged together. Unfortunately, many experiences associated with staging have not been pleasant. Devices can be staged together, though, and can be made to work with a considerable degree of success. Although the present state of the art is not as advanced as we would like, the outlook is far from discouraging. It appears that systems need to be designed as systems rather than automatically accepting that which comes out of a series of X numbered similar devices as being the best system performance available. While this

concept is perhaps more difficult and has not been fully developed, it may be the shortest path toward achieving in practice the inherent reliability of which pure fluid systems are capable.

#### E) Passive Elements

Passive elements are described as those parts of the system which due to their geometry act on the fluid in a predictable fashion. These elements are not supplied with a source of power and in many cases their theory of operation is straightforward. Such elements can usually be fabricated without undue difficulty. They are mentioned here since they are, in practice, a part of every fluid system.

#### F) The Medium Gain Block

Pressure proportional systems containing five stages of amplification have been fabricated as single systems. The individual stages of amplification are connected together in the same plane and in the same piece of glass. Power is supplied by a fixed manifold system which delivers the flow for each stage of amplification.

## II THE PRIMARY ACTIVE ELEMENT

A considerable number of fluid amplifier elements have been fabricated in Fotoform glass and tested to determine the capability of the manufacturing process for the production of such devices. During the early work at Corning, efforts were directed towards the determination of the operational characteristics of a relatively large number of similar devices at fixed operating conditions. Most of this work utilized the basic DOFL design which is shown in silhouette in Figure I. This image was photographically put into Fotoform glass and when developed was removed by etching which resulted in recesses in the glass corresponding to the silhouette which was used as a negative. The entire image which extended through the glass was not etched away since etching was continued only until the channels reached the required depth. A cover, made by the same technique and also shown in silhouette in Figure I, was then positioned onto the device and the cover and device were sealed together. Efforts to correlate dimensional variations with the performance of the devices made this way were only partly successful. The dimensional variations were small and did not seem to be as important as the factors of assembly and of getting air into and out of the devices. Auxiliary equipment such as fittings made more difference in device performance on occasion than did an obvious defect caused by handling before sealing. While working with these devices led to fairly

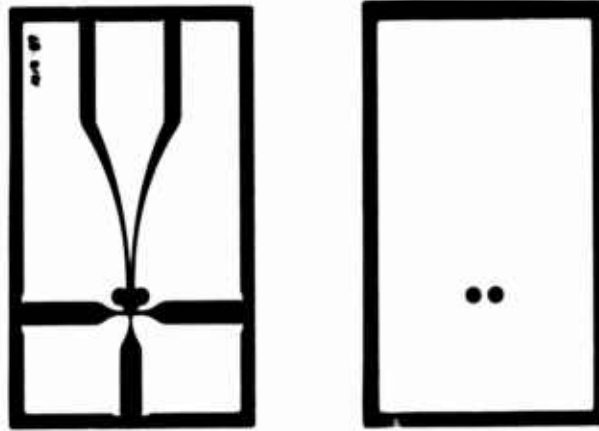


FIG I  
SILHOUETTES OF PRESSURE PROPORTIONAL  
AMPLIFIER AND COVER  
SHOWN AT HALF SIZE

EFFECT OF POWER  
NOZZLE PRESSURE  
ON STREAM VELOCITY  
AT FIXED POSITIONS  
~ 0.125 INCHES  
DOWN STREAM  
POWER NOZZLE WIDTH  
0.020 INCH  
POWER NOZZLE  
DEPTH 0.050 INCH

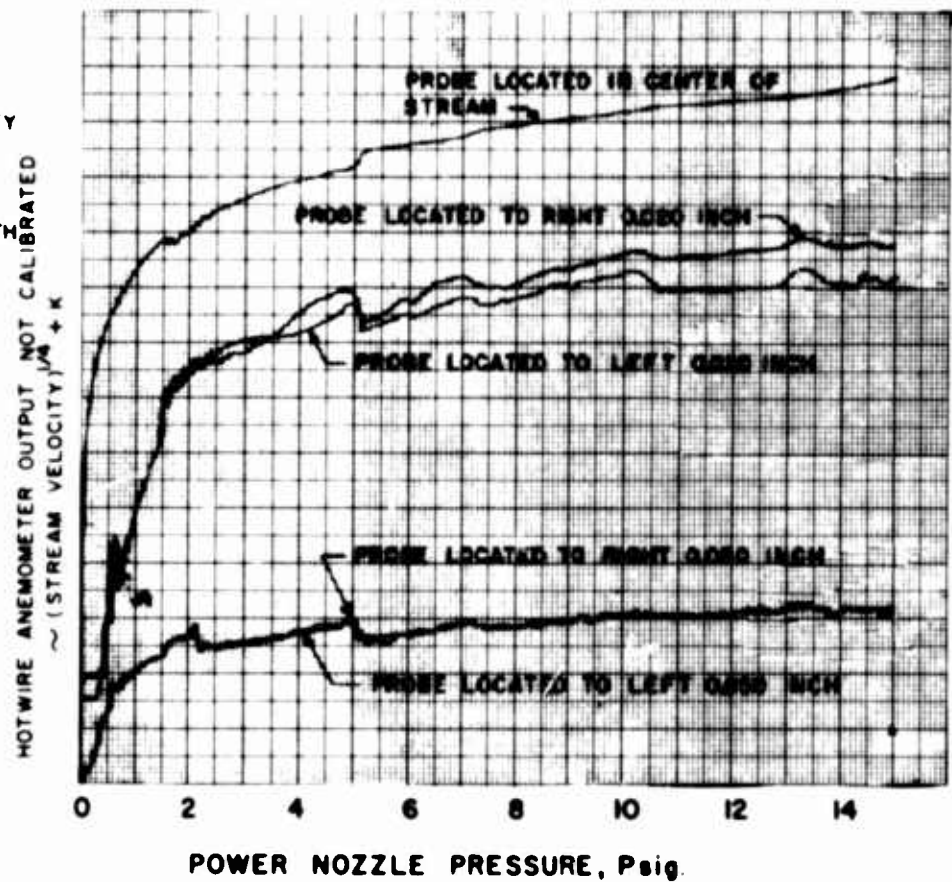


FIG. II

complete knowledge within a narrow range of operating conditions, it led to limited knowledge over the broad range. Recent efforts having to do with interconnecting the devices have required investigation over a much broader range of operating conditions and these later investigations have helped to pin down the characteristics thought to be desirable in the basic element. It would be folly, however, to discuss these characteristics as a unit without first surveying the role played by each geometrical part of the basic device. It is difficult to isolate the function of each section of the device and oftentimes some basic error is developed when attempting to do so. For the sake of clarity, however, the basic device will be discussed by looking at the power nozzle, the control nozzles, the relief geometry, and the receiver separately before considering them as an integrated element.

#### A) The Power Nozzle

The purpose of the power nozzle is to provide a jet stream which can be deflected and whose velocity profile at some distance downstream is uniform and symmetrical about the center line of the nozzle. The profile shape should not be altered by minor changes in operating conditions.

A wide variety of nozzle designs can meet the above criteria if they are operated at very low pressures. As velocities are increased and turbulence increases, nozzles probably need to be more carefully designed and made in order to be within the above limits. A particular fluid amplifier design was found to give some baffling and hard to interpret performance data when connected with four other similar devices in a system to provide 5 stages of amplification. A stepwise testing and component elimination procedure led to the power nozzles as being the primary source of trouble. Further testing with the hot wire anemometer system resulted in the graphs presented as Figures II through IV which give some indications of the phenomenon involved. The curves in Figure II were generated by holding the hot wire in a fixed position downstream and changing the power jet pressure. The probe in this case was held at 0.125 inches downstream which would normally be in between the power jet and the receivers although the receivers and the top and bottom plate were previously removed from the devices and the jet issued freely out into the room for the test. The changes in velocity, as seen in Figure II, were dependent on the power jet pressure and each curve in Figure II could be retraced again and again. It should be noted that the velocity traces determined along the edge of the stream do cross but are generally in phase; so

SAME NOZZLE AS IN  
FIGURE II VELOCITY  
PROFILES DETERMINED  
AT  $\sim 0.100$  INCH DOWN  
STREAM WITH HOTWIRE  
ANEMOMETER  
PROBE TRAVERSED

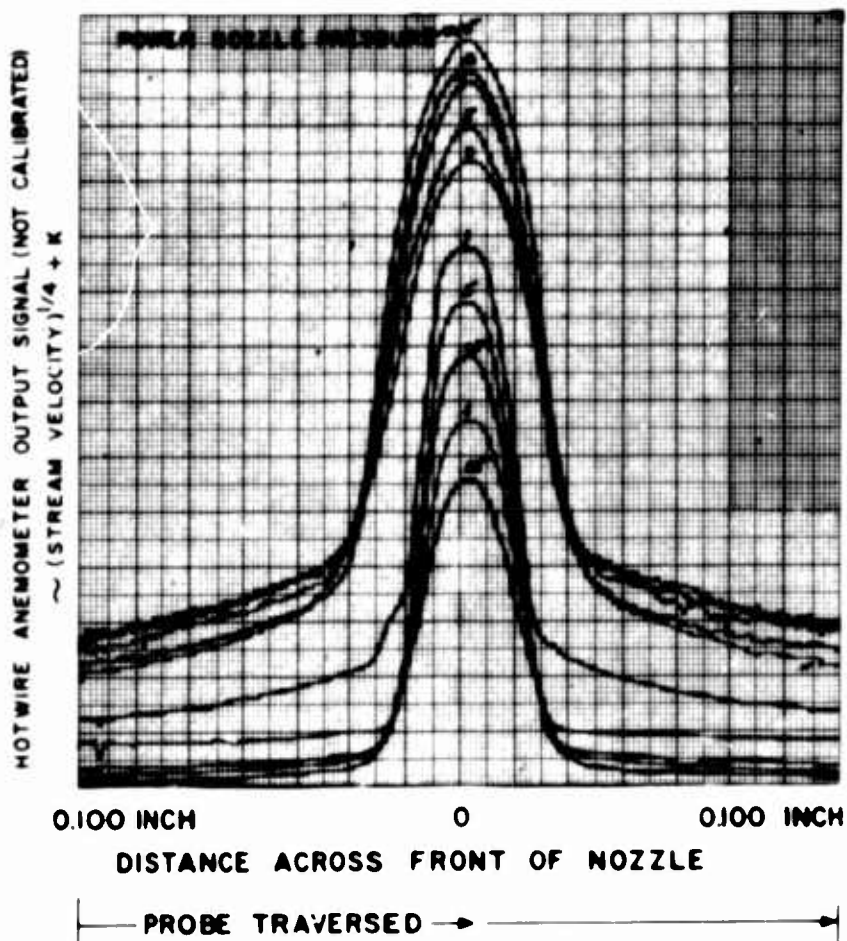


FIG. III

SAME NOZZLE AS IN  
FIGURE II VELOCITY  
PROFILES DETERMINED  
AT  $\sim 0.180$  INCH  
DOWN STREAM WITH HOT  
WIRE ANEMOMETER  
PROBE TRAVERSED

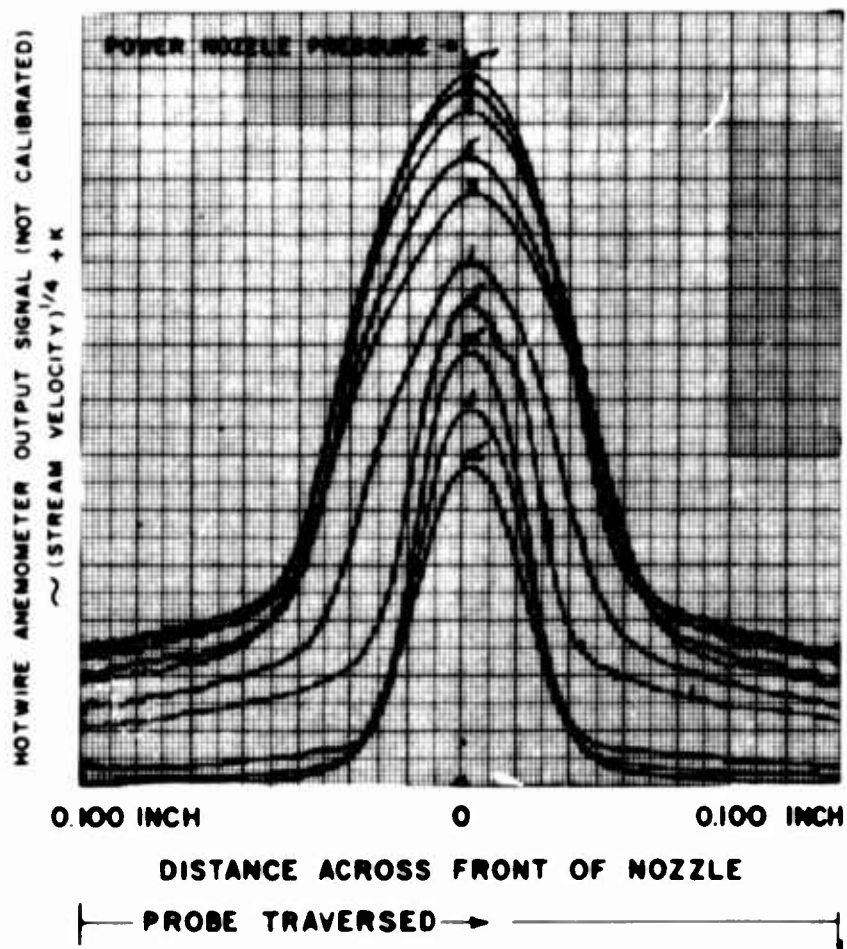


FIG. IV

most of the excursions are probably not due to stream deflection but rather to some action taking place on both sides of the stream simultaneously. Further, the lower edge velocity accompanied by increased center line velocity suggests some pinching effect. The rather wild excursions along the right and left side of the stream through the pressure range of about 1 psig may reflect the transition from laminar to turbulent flow in the jet after it leaves the nozzle. Other data obtained with the probe nearer the nozzle show these excursions to be much less erratic nearer the nozzle and suggest this possible answer. The data shown in Figure II represent a fairly typical nozzle of this particular design. All other nozzles of the same design have shown this same tendency when tested. Similar tests were performed on nozzles of this design which had been fabricated 1/2 size and the effect was more pronounced.

Figure III and IV are velocity profile curves generated by traversing the hot wire probe across the stream while recording distance on the X axis and the hot wire signal on the Y axis. The X-Y recorder was used to directly plot the data as it was being generated. In both Figures III and IV as was the case for Figure II any curve could be retraced again and again. The slightly more erratic nature of the curves presented in Figure IV as opposed to those in Figure III suggests more strongly that the phenomenon looks worse further downstream due to some form of stream disintegration. All the data indicate, however, that the velocity profile is probably being formed asymmetrically somewhere in the nozzle. Since the degree of asymmetry seems dependent on power jet pressure it appears to be a result of some kind of separation taking place in the nozzle itself. If this is true, it would follow that the separation point could shift or there could be a change in separation bubble size with changes in operating pressure(velocity) that could result in the kind of variations which have been observed. Usually, a distorted profile results in the same symptoms in the operating device as does unwanted stream deflection.

Similar tests have been conducted using many different nozzle designs and, in each case, the profiles at very low stream velocities (less than 100 ft/sec) appear to be symmetrical. At the higher velocities however, most of the profiles have been distorted. The most promising nozzle tested to date has still shown some erratic behavior through a small range of velocities, but with this exception, has shown uniform operation over a wide range of operating



EFFECT OF POWER  
NOZZLE PRESSURE  
ON STREAM VELOCITY  
AT FIXED POSITIONS  
0.080 INCHES  
DOWNSTREAM  
POWER NOZZLE  
WIDTH 0.020 INCH  
POWER NOZZLE  
DEPTH 0.050 INCH  
LONG NOZZLE

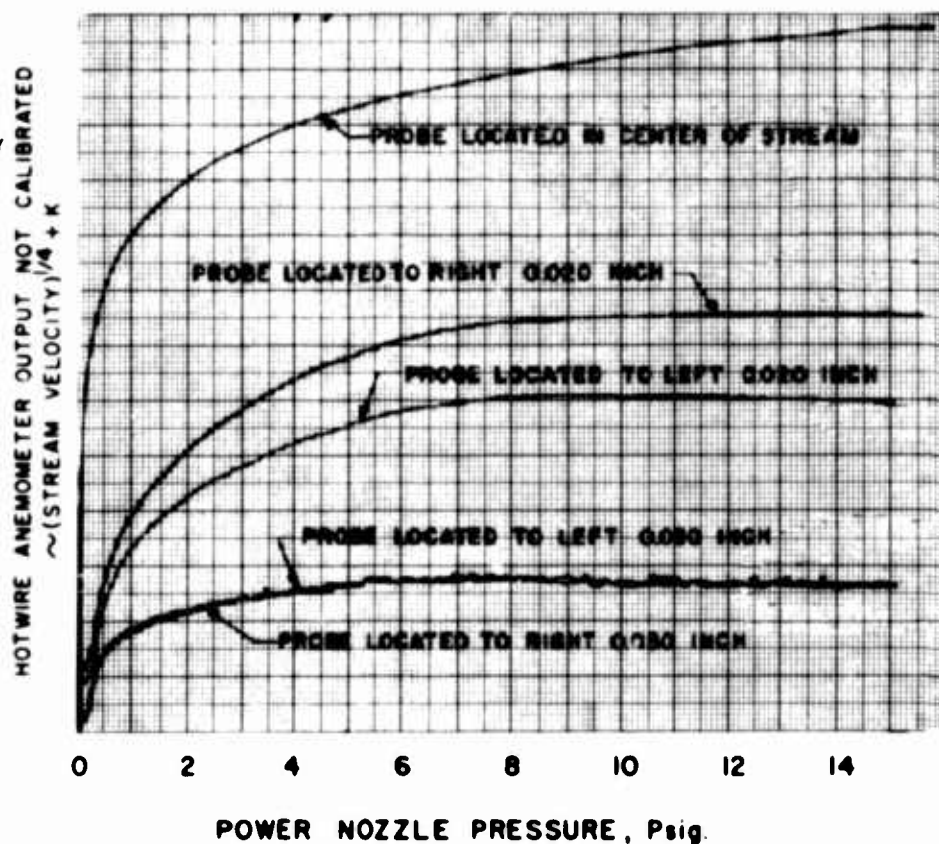


FIG. V

SAME LONG NOZZLE  
AS IN FIGURE V  
VELOCITY PROFILES  
DETERMINED AT  $\sim 0.080$   
INCH DOWN STREAM  
WITH HOT WIRE  
ANEMOMETER  
PROBE TRAVERSED

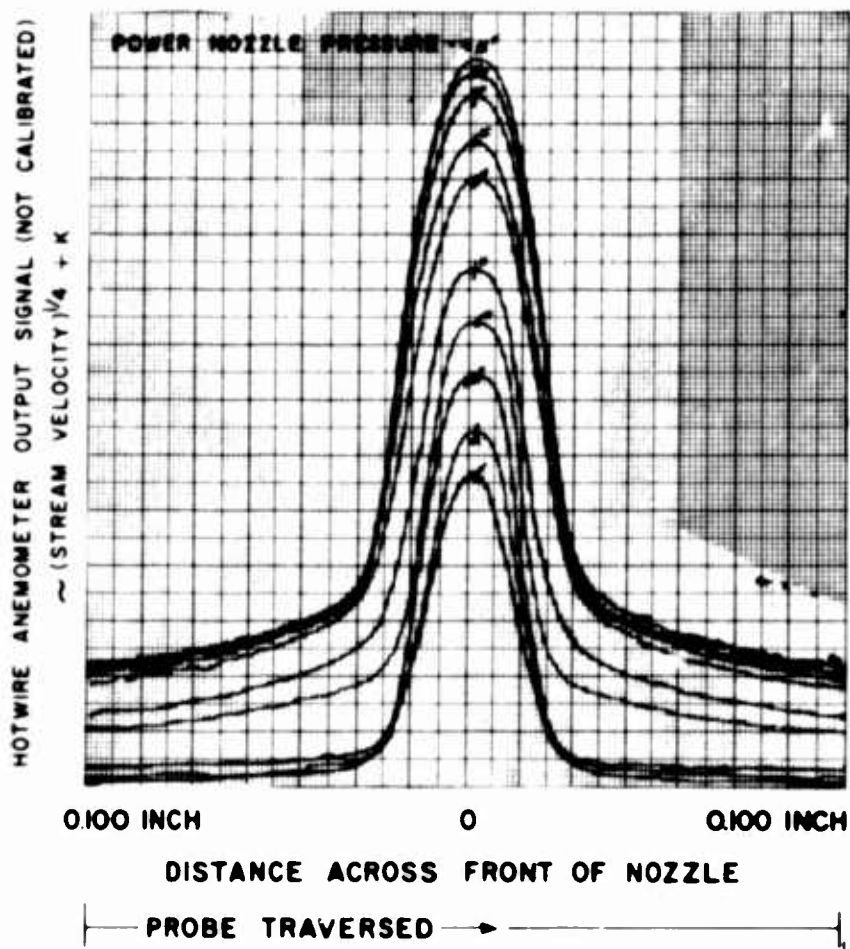


FIG. VI



SAME LONG NOZZLE  
AS IN FIGURE V  
VELOCITY PROFILE  
DETERMINED AT  $\sim 0.180$   
INCH DOWN STREAM  
WITH HOT WIRE  
ANEMOMETER  
PROBE TRAVERSED

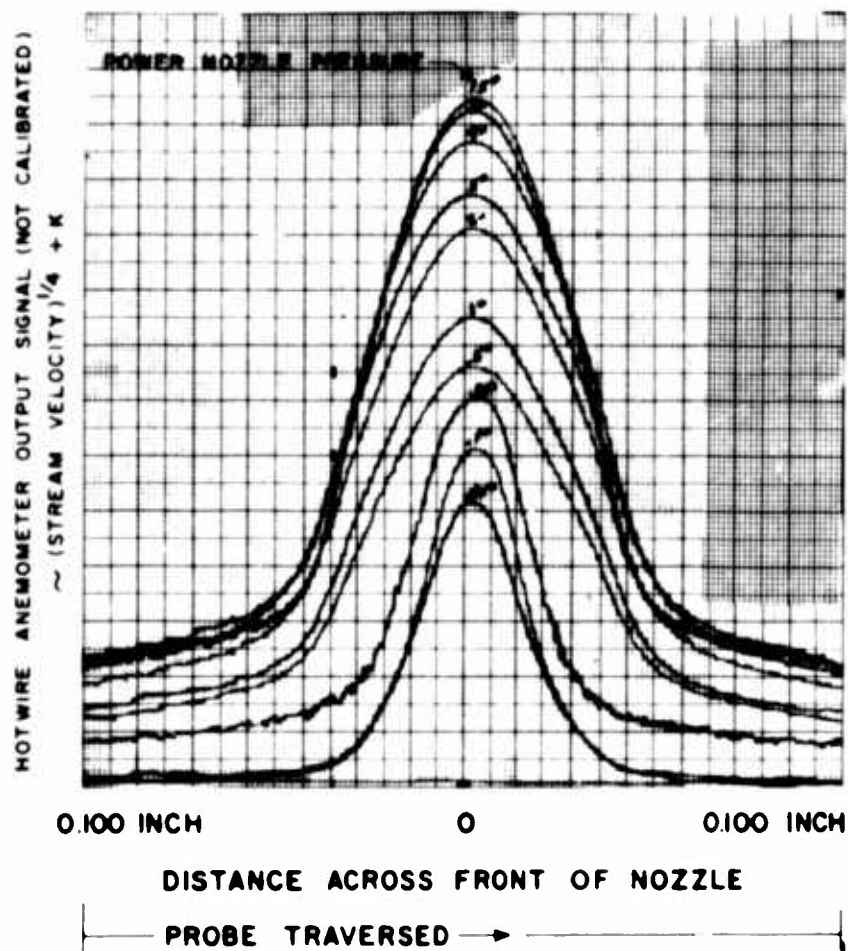


FIG. VII

conditions. Curves for this nozzle are presented as Figures V, VI and VII. This nozzle design differs from the other designs tested in that the straight section is considerably longer and a stream deflector has been placed just upstream of the nozzle. The improved performance is thought to be due to the extra length rather than the stream deflector, since as length is reduced, erratic behavior begins. The extra length apparently provides a sufficient zone for the disturbances to be ironed out before emerging from the nozzle and the longer nozzle appears satisfactory for fluid amplifier use if the region of erratic behavior is avoided. Although specific test data have not been correlated to show the effect of channel to nozzle area ratio and the effect of stream turning angle on jet profile, it appears that the better nozzles have large area ratios and the stream is forced to turn gradually rather than abruptly. A limited amount of literature is available which deals with nozzle design in this size range and for this particular application. There exists a distinct need for such data since a fluid amplifier is not a good fluid amplifier unless it is built around a nozzle with uniform and predictable operating characteristics. Meanwhile, the designer must take every precaution against inadvertently setting down geometries which can be inherently troublesome. Straightening vanes to insure uniform flow going into the necked down portion of the nozzle, large area ratios, and gentle stream turning may all be significant factors which help make a nozzle a good nozzle. The longer nozzle appears to be a temporary stop-gap solution to the basic problem.

#### B) The Control Nozzles

The purpose of the control nozzle(s) is to direct the control stream(s) toward the power stream so that the energies of the two (three) streams can interact and cause power stream deflection. Although no reason has been observed in practice which indicates the need for uniform symmetrical profiles coming from the control streams, there is the distinct need for both controls of a single device to have the same pressure-flow relationship. Considerable attention has been given to the control pressure vs control flow relationship. Since this is discussed in detail elsewhere (2), the remarks here will be limited to a few general observations. Because of the geometry relationship existing between the control nozzle edge and the moving wall of fluid, the power jet, the pressure-flow relationship must be considered with respect to the total fluid path. In practice, it has been found that when the control edges are positioned near the power stream the control flow at a given control pressure can be changed by either changing the power jet pressure or by

changing the pressure in the other control. The control edges should be positioned so that the flow delivered at a given pressure will be the same every time and to do this, the flow must be dependent on fixed geometry alone. In practice this is very difficult to achieve since the pressure at the inside edge of the control nozzle must, under these conditions, remain unchanged. Most times the pressure at this point has been found to be dependent on operating conditions. The most promising change in control nozzle geometry to lessen this effect has been to move the control edge further away from the power stream. No significant reduction in gain occurred by this move although the pressure at which flow begins is still somewhat dependent on power jet pressure. When the gain block is used in any situation, where the summing junction is inside the first stage, it seems to be of utmost importance to have stream deflection take place only when a positive gage pressure difference is applied to the controls. To do this, the pressure just inside the control must, of necessity, be atmospheric, and any deviation from atmospheric will constitute a fixed system error which has to be taken into account.

It is sometimes desirable to insure a particular relationship between pressure and flow in the control channel. The normal relation is usually some form of a power relationship such as  $Q = \sqrt{P}$  and if this normal relationship is altered, the relationship of input signal to output signal for the device will likewise be changed. Unfortunately, the normal dependence of flow on pressure results in a calculated resistance for the control channel  $\frac{(P_c)}{(Q_c)}$  which can change by several hundred percent over a normal operating range. Geometry of the control channel can be changed to make the resistance constant or very nearly so, but any device or geometry change which increases resistance in the control channel results in a loss of gain in the device.

### C) Relief Geometry

Initial design efforts having to do with relief geometry were aimed toward providing equal pressures on either side of the power jet stream while allowing adequate area for venting that portion of power and control streams which does not go out through the receivers. In practice, this has been difficult to achieve particularly when the power jet is operated at higher pressures. It seems that as power jet pressures are increased the interaction area pressure rises, and as it does so less output pressure difference is available for a given amount of stream deflection.

At very low power jet operating pressures, however, the relief areas can be changed considerably without adverse effects. Under certain operating conditions, it has been possible to completely block the reliefs and maintain high gain. Under these conditions, the receivers are capable of discharging all the flow that enters the interaction area. The relief areas apparently needed on any particular design have thus been found to be functions of operating conditions including power nozzle pressure, control nozzle pressure and the capability of the receivers to handle the flow. The last factor is partly dependent on stream width which is also a function of power nozzle pressure. Some attempts have been made to utilize the relief/interaction area geometry to provide negative feedback for stream stabilization. This technique has been found to be quite useful but it has been found that the amount of feedback obtained depends on so many factors that design must proceed on a cut and try basis. In fact, the situation is so delicate that it is fairly easy to make a device which has so much feedback in the interaction area that the power jet stream is completely stable. Under these conditions, of course, gain disappears. Many of the problems with the basic device have been found to be due to some apparently minor assembly or manufacturing error connected with relief geometry. These malfunctions have been difficult to diagnose and sometimes more difficult to eliminate. In the basic design, ports on either side of the stream are open to the atmosphere. The top ports are in the coverplate and the bottom ports are drilled in the device floor. Precise location of the bottom holes was difficult but reasonable accuracy seemed to result in single devices having consistent gains one to the other. Coverplate registration was accomplished along the edge of the coverplate and piece and slight misregistrations did not appear to affect gain. When 5 devices were made together in a single piece the situation was altered. In five stage systems, the location of the top and bottom ports seemed to change the system balance and it became possible to observe the relief hole registration and predict with considerable accuracy the ultimate off-balance direction. Other factors may well have influenced the tendency of the streams to center themselves between the reliefs since a coverplate misregistration also resulted in misregistration of the coverplate hole to the power nozzle channel. More care in positioning was of some benefit but did not completely solve the problem. The basic principle of operation of the device depends on the impinging of one stream on another and this seems to set up many varied and random vortices and disturbances which are difficult to control. In addition, an examination of the velocity profiles presented earlier shows rather large velocity components normal to the power stream. If these large velocity components are altered asymmetrically,

unwanted stream deflection can occur. A practical solution to this general problem of relief geometry is to remove the top and bottom plate from the area just downstream of the control nozzles to the leading edge of the receivers. A device made this way is somewhat more difficult to manufacture and it seems that there may be some adverse effects. The adverse effects seem to be more than offset by the fact that the devices are less sensitive to load, are quieter, and stream deflection seems more predictable. Although thorough testing has not been accomplished, it appears that the later stages are much less dependent on operating pressures than those with standard shaped reliefs.

#### D) Receiver & Diffusor Geometry

The purpose of the receiver-diffusor is to capture segments of the power stream and guide these increments of energy to the point of use. No efforts have been directed toward receiver design except to make some minor modifications to splitter width to compensate for the 2-1/2° wall taper present in the manufacturing process. Difficulties have not been known to be directly due to receiver and diffusor design but it is possible that many inefficiencies exist. It seems that receiver diffusor design must be a compromise between losses due to friction if the velocities are kept high or losses due to expansion if interstage velocities are allowed to drop. In practice, pressure taps have been located between the stages near the next stage control nozzle to determine pressure gain for a device while under actual operating conditions. The presence of these taps has not proven to be detrimental and seem to be absolutely necessary particularly when working with new designs.

#### E) The Single Device

The various parts of the basic device have been discussed singly and the operation of each part seems rather straightforward. Upon analysis however, the basic element is found to be quite complex in its operation. The complexity seems to be only partly due to the phenomena involved, i. e. stream interaction, about which limited information is available. A larger and perhaps more difficult area of concern which adds to the complexity is the interdependence of the various parts of the basic device. These effects are real but are sometimes so subtle in nature that they easily become indistinguishable in the reams of data being collected by those working with fluid amplifiers.

It has been found that to change the geometrical relationship

between two parts of a device can and does often affect the operation of the other parts. For example, if the control edge width is changed, the pressure being exerted on the side of the stream is probably changed, the momentum relationship between the power stream and control streams is changed and the loading on the previous stage is altered. Fortunately, many of these effects are opposite in nature so that if a single parameter is tested, such as pressure gain, little total effect is noted. The effects are real however and could possibly make the difference between a device operating satisfactorily in a staged system or being a source of trouble. One course of action has been to attempt to decrease this interdependence as much as possible even if at the expense of a slight compromise in performance. Too much cannot be written or said of the need for having a perfectly symmetrical device with respect to geometry and performance. It usually matters little in a single device whether both sides operate identically for there is usually plenty of room allowed for error. When this small error is considered in light of total system performance, however, it can make the difference between having a useable or useless system. Accurate dimensions on a piece of paper do not automatically insure device symmetry for these dimensions must be faithfully transformed into flow channels before they can be used to perform some useful function. Any device asymmetry constitutes a system error if the device asymmetry causes the gain to be different on one side of the device than on the other side. In addition to the error caused by gain asymmetry, errors are generated when the pressure proportional amplifier delivers an output signal without the presence of a control signal. These errors are brought about since the linear portion of the gain curve is fixed and an initial signal on the output automatically limits the linear range in one direction or the other. With a shortened linear range available on one side it is much easier to over drive that side of a device to the position on the curve which is not linear and this results in an error signal. So, even if the gain is the same on both sides of the device initially, device symmetry plays an important role in total system performance and every reasonable effort should be expended to make sure that the performance on one side of a device acts like a mirror image of the other side.

### III STAGING

- A) Since the purpose of staging is to ultimately control a very large amount of energy with a very small amount of energy, it follows that with limited gain available in individual stages, the stages must be coupled together. This coupling should allow large power stream deflections in each stage. The deflections need



to be larger than any inherent stream deflection brought about by minor disturbances. To reach this condition, the energy level of each stage must be higher than the previous stage. There are at least two ways that this can be accomplished.

- a) A small device could drive a larger device and so on until the desired gain was reached, or
- b) Similar sized devices could be operated at ever increasing energy levels to accomplish the same purpose.

Both methods have certain advantages to offer and have certain inherent limitations. For instance, if the device size is graded a rather large range of sizes are required to reach reasonable gain levels. (The size factor of the basic DOFL design is approximately  $2.0w$  for the power jet width of each additional stage.  $w$  being the width of the first stage power jet). If power consumption is to be considered and this should limit the size of the largest device, then the smallest device would need be very much smaller in a 5 stage system. As devices are made smaller, inherent process variations of any process which are small within themselves become large percentage variations. In addition, there are many questions concerning the effect of size scaling which have yet to be answered. These factors have made the more prudent approach that of keeping device size constant and varying the energy level of each stage by changing the power jet pressure. This approach has been troublesome but recent developments have pointed very clearly to the reasons for most of the difficulties (see Section II-A). The earliest attempts to stage devices together were somewhat discouraging. Two devices, each having a gain of about 5 resulted in a combined gain of about 15. This was repeated with different devices many times over and the gains of two devices connected together rarely equalled the product of the gains as determined separately. In each case, however, the two devices were operated at the same power jet pressure of 5 psig. When the power jet pressure of the first of the two stages was lowered, the system gain increased and equalled the product of the gain of the two measured separately. It seems that by operating both devices at the same pressure, the second device was being operated with too much control bias and the first device with incorrect load. Various techniques can be utilized to determine whether a particular design will operate properly when loaded with the control nozzles of another. No details will be shown here except to say that only one flow is possible through each output leg with any given design, load, and power jet pressure. The same

is true of pressure in the output legs. This pressure and flow should be reasonably near that required on the controls of the next stage at the operating point. If devices are tested singly, loading should be the same as will be present when driving another device. It should be remembered that the control input pressure-flow relationship is dependent on conditions inside the device as well as on basic geometry. By keeping this fact in mind it was possible, by careful tuning, to get most any system of devices to operate with some degree of satisfaction. Each group of devices staged together seemed to require a special set of power jet pressures in order to meet any kind of optimum performance and because it was desired to operate the bank of devices with fixed manifold systems, the yields were very low. The degree of complexity was made worse by the jet profile distortion effect discussed earlier. This effect made system balance highly dependent on the manifold header pressure and a slight change in that pressure could drive the system output pressure to the maximum limits. It also seemed that a slight change in one of the stage pressures could make the difference between large fluctuations in the output of the system or having relatively quite operation. It was possible to use the staged systems as gain blocks and their use allowed the assembly of a pure fluid scale changer whose multiplication constant could be selected at any whole number between 1 and 10. Many new facts continuously develop as more experience with staging is gained. A continuous monitor of the pressures throughout the staged systems have made it possible to gain much useful data and experience even from systems whose total performance has been much less than ideal. Working with staged systems is considerably more complex than working with individual devices but oftentimes it is the only way to develop devices truly capable of being staged together.

Although the present state of the art has not developed to the point where an individual can sit down and design a pure fluid system which will operate exactly as desired when built, it appears that future pure fluid systems will be designed as complete systems where each device included will be operated under its most optimum conditions.

## B) System Noise

Noise is generally defined as any unwanted signal in the system not introduced through the controls of the first stage which will cause stream deflection or do work at the point of use. Pressure proportional amplifiers of the basic design are found to contain somewhat more noise in the outputs than is desired. When staged



together, some of these unwanted signals are multiplied as if they were good signals and this results in systems having a relatively high noise level. Efforts to measure noise with the hot wire anemometer have been only partly successful since the hot wire signal contains many different velocity components, some of which are capable of causing stream deflection while others are not. It has not been possible to distinguish between the two types of signals. The use of the hot wire has shown that normally the control input signals to the first stage are very nearly turbulence free. It can be concluded then that the unwanted signals come from some point in the system downstream of the summing junction of the first stage.

The unwanted signals can be divided into two rather broad categories, namely

- a) Those caused by stream deflection, and
- b) Those caused by some form of turbulence.

Those disturbances caused by stream deflection are generally characterized by being out of phase while those caused by turbulence are of a random nature. No attempt has been made to further describe the kind of noise present. It has been found that many factors influence the noise level of a system and a system can usually be tuned by adjustment of power jet pressures to the point where noise is low enough to be able to use the system while still maintaining a reasonable gain level. It seems that noise is lower when all stages are operating around the balance point and noise increases as any stage is operated toward off balance. This seems contrary to that which would be expected and may indicate a feedback phenomena which is increased and is of a cyclic nature when the stream is slightly off center. The noise level of a system can be changed by changing the relief geometry but the results are not always in the anticipated direction. Noise of the turbulent type is probably due in part to turbulence in the power stream itself in addition to that generated in the receiver-diffuser.

#### IV THE GAIN BLOCK

Staged systems containing 5 stages of amplification have been successfully built and operated. Gains greater than 2000 are readily obtainable and higher gains are possible even though there is some degree of difficulty experienced when attempting to accurately determine the higher gains. The gain blocks have power fed through a manifold which provides a fixed flow for each stage of the system. Both controls of the first stage are used since the interaction area of the first stage serves

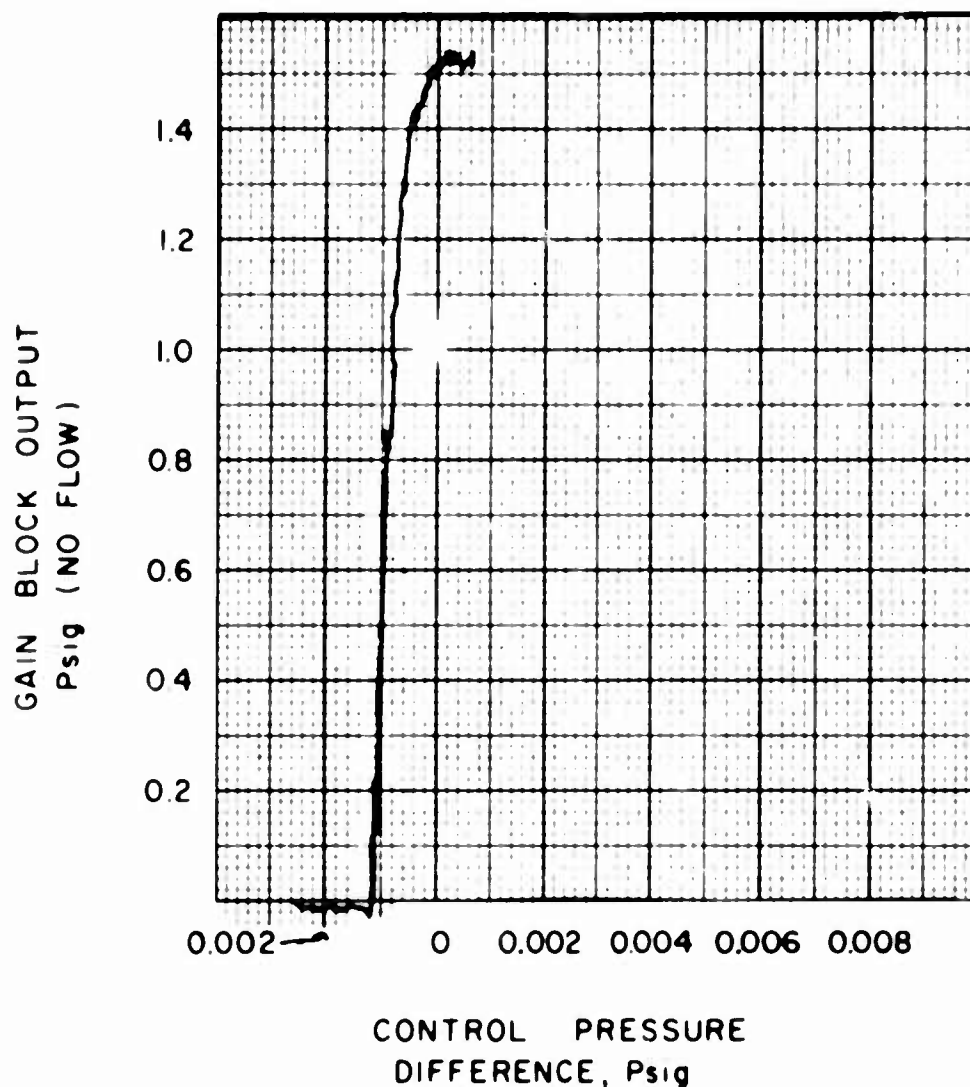


FIG. VIII

GAIN BLOCK OUTPUT PRESSURE VS CONTROL PRESSURE  
 GAIN BLOCK INCLUDES 5 STAGES OF AMPLIFICATION,  
 FIXED MANIFOLD TO PROVIDE POWER JET PRESSURES  
 AND PASSIVE DIFFERENCE AMPLIFIER AT THE OUTPUTS  
 OF THE STAGED SYSTEM.

$P_0$  BAL = 2.5 INCHES WATER PRESSURE

$G_p = 3366$

as a summing junction. This feature is particularly useful when the gain block is used with feedback to perform some logic function. A single output signal is made possible through the use of the passive difference amplifier which is described in paragraph V-C.

No attempt has been made to install trimming valves or extra nozzles in the gain blocks for centering purposes since their presence tends to complicate the system. Each of the gain blocks have slightly different operating characteristics and some of the reasons for the differences are understood while other of the reasons are yet to be determined. In this respect, the gain blocks should be considered as first generation devices which can stand considerable improvement. Figure VIII is the gain curve for one such gain block.

## V PASSIVE ELEMENTS

### A) General

The passive elements act on the fluid stream due to their geometry. In this category would be resistances, capacitances, passive difference amplifiers and in a broader sense hoses and hose fittings. Of primary interest here is the resistor and the passive difference amplifier.

### B) The Pneumatic Resistor

One of the basic pneumatic circuit building blocks is the resistor. Of necessity, the resistor is different in design from either a nozzle or an orifice since it should offer the same resistance to flow even if the operating conditions should change. The relationship of pressure to flow, therefore, must be linear over the operating range. In practice, small channels sufficiently long to insure fully developed laminar flow are used and result in linear resistance over a wide range of operation. With suitable cross sectional area, and length, and the ability to connect in series or parallel, any desired resistance value can be obtained which is linear within 5% up to pressures of 5 psig. These resistors can be used in conjunction with the gain block to make a variety of useful circuits and are mentioned here only because they are a necessary part of most any circuit which uses feedback.

### C) The Passive Difference Amplifier

Due to the large differences in pressures between the first

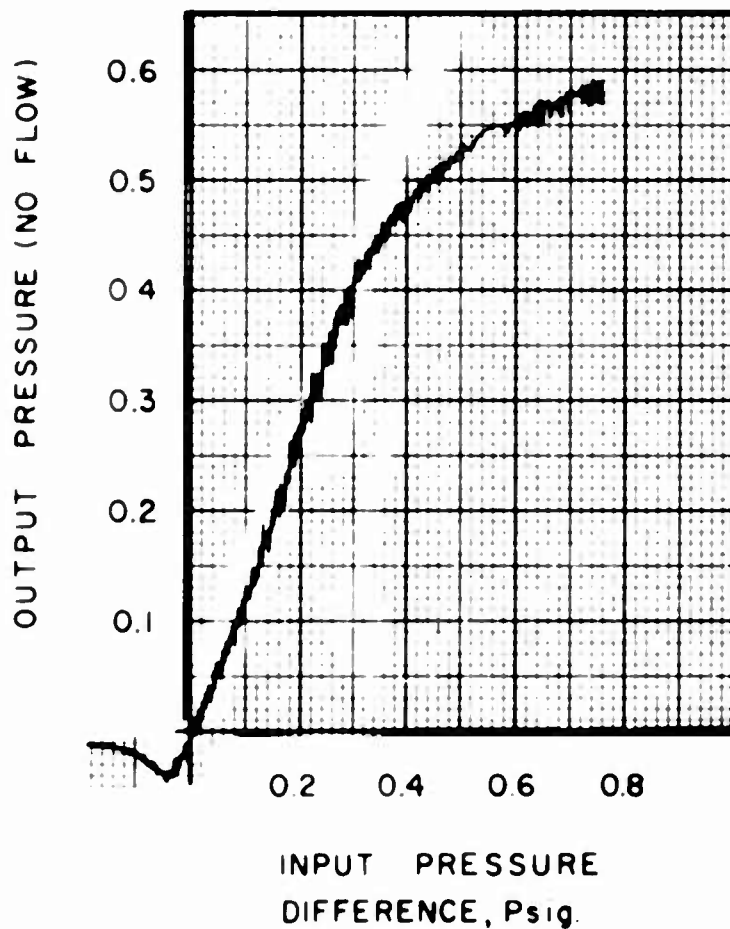
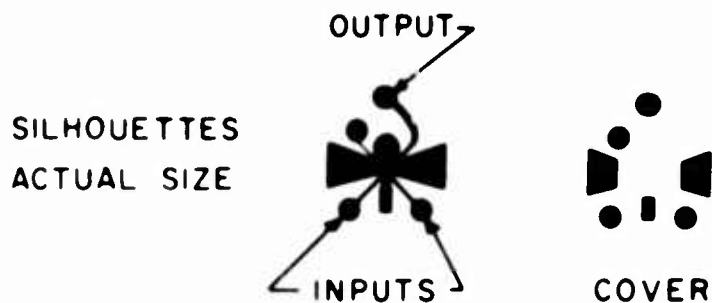


FIG. IX

PASSIVE DIFFERENCE AMPLIFIER CHARACTERISTIC  
GAIN CURVE.

INPUTS DRIVEN BY OUTPUTS OF PRESSURE PROPORTIONAL  
AMPLIFIER. AT ZERO INPUT DIFFERENCE, BOTH INPUT  
SIGNALS AT 1 Psig.

$G_p \sim 1.25$

stage and last stage of the normal pressure proportional amplifier multi-stage system, output signals are not compatible with input control signals. Where the control signal should operate from zero pressure upward, the final stage output signal is usually developed around some elevated point (usually about 20% of the final stage power jet pressure). In addition, the useable output signal is actually the difference in signal which is obtained when one of the output pressures is subtracted from the other output pressure. This is normally an electrical signal computed by a difference transducer and heretofore pure pneumatic signals to express this difference have not been available. The passive difference amplifier performs the subtraction and through its use a pure pneumatic signal is generated which approximates the difference in pressure between the two output legs of the last stage device. The basic design of this device was made by Harry Diamond Laboratories personnel and some design improvements have been made by us to adopt the design to the systems in use. Figure IX shows the operational characteristics of a typical passive difference amplifier. The passive difference amplifier operates by impinging the two output flow streams together at 90°. A receiver is situated such that no pressure is developed in the receiver when the streams have equal energy and full pressure is developed when the positive stream is maximum.

#### D) The Fixed Resistor Manifold

The manifold provides the necessary flow to operate the power jet of each stage of a staged system. The use of the manifold reduces the number of pressure regulators needed since with it only one point of regulation is required. In practice, the final stage power jet of a system operates from the pressure regulated section of the manifold and flow limiting sections (resistors) are operated in series to drop the header pressure to the required operating level for each stage. Since the pressures decrease in the system from the last to first stage, it is possible to utilize resistors of nearly the same size down the line. The resistor size is calculated on the basis of pressure and flow needed for each stage of operation. With this technique each resistor must supply flow for all the later points of the manifold while providing the proper pressure for only one point. More stable staged system operation is possible with the manifold since the resistors tend to even out the small cyclic pressure variations normally present in most pressure regulators.

## CONCLUSIONS

Although progress has not been as rapid as would be desired, past efforts have resulted in staged systems whose performance is adequate for the initial attempts to perform logic functions. This, in itself, represents considerable progress for the short time involved. There will no doubt be many improvements in staged systems in the next few months which will open many new areas of application. The new areas of application will, in turn, demand staged systems to be designed to perform specific tasks. It is anticipated that problems will continue to be present as they have been in the past. The solution to these problems will, of course, determine the ultimate success of fluid amplifiers.

## ACKNOWLEDGMENT

The authors wish to thank Robert Bellman and others on the staff at Corning Glass Works who have been most helpful in data collection and constructive criticism which have made this paper possible.

## REFERENCES

- (1) Dexter, E. M., An Analog Pure Fluid Amplifier. Fluid Jet Control Devices, ASME Meeting November, 1962.

Reilly, R. J., et al., Notes on a Proportional Fluid Amplifier. Fluid Jet Control Devices, ASME Meeting November, 1962.

Peperone, S. J., Katz, Silas, Goto, John M., Gain Analysis of the Proportional Fluid Amplifier. Fluid Amplification Symposium - DOFL 1962.

- (2) Powell, Alan, Characteristics and Control of Free Laminar Jets. Fluid Amplification Symposium, DOFL 1962.

Van Tilburg, R. W., Cochran, W. L., Application of Optical Fabrication Techniques to the Development of Fluid Amplifiers. Contract Report to The Harry Diamond Laboratories Covering Tenth Through Eighteenth Months Work ending October 31, 1963.

.

# Development Of A Proportional Fluid Amplifier For Multi

## Stage Operation

by

R. W. Van Tilburg

and

W. L. Cochran

of

CORNING GLASS WORKS

### ABSTRACT:

A presentation is made of the data and general information obtained during the development of a basic proportional device for use in fabrication of a multistage, high gain proportional amplifier.

Starting with a sound basic design of a pressure gain device submitted by Harry Diamond Laboratories personnel in conjunction with a fabrication program, a comprehensive study was undertaken directed toward maximizing the pressure gain while maintaining operating conditions which would permit direct in-line coupling of several identical devices.

All design and operational parameters which were felt to have a direct effect on pressure gain were investigated, with primary emphasis on aspect ratio, control edge width, size, and the relationship between power jet pressure and control jet pressure.

The program was basically empirical in nature, utilizing the optical fabrication techniques developed to permit fabrication of pure fluid components and systems in Fotoform glass and Fotoceram glass ceramics. Data were obtained from thermally fused units using air as the fluid in the pressure range of 0 to 20 psig. Sizes tested were in the power nozzle width range of .005" to .050".

As previously indicated, the original design from Harry Diamond Laboratory was sound, and only marginal improvements in pressure gain were realized. Results indicate that the pressure gain is relatively sensitive to aspect ratio and control jet to power jet ratio, and relatively insensitive to control edge width and size. However, the smaller the device the more sensitive it becomes to fabricating and operating variables.

## INTRODUCTION

Under the sponsorship of The Harry Diamond Laboratories, and with considerable technical assistance from the personnel of that organization, a program has been in effect for approximately two years, directed toward the development of a stable, pressure gain proportional fluid amplifier which could be connected in multiples to form a high gain multi-stage amplifier, adaptable to control and computational circuits. Within the scope of this program it has been necessary to develop fabrication techniques and processes to a degree which would permit the assembly of large numbers of identical devices, the performance of which was closely enough reproducible to permit the adequate evaluation of marginal changes resulting from incremental adjustments to the physical dimensions of the basic design. Further, the original design, as supplied by HDL, had been developed and optimized in a size much greater than was to be used, and it was felt to be advisable to process a sufficient number of minor design changes to establish what adjustments, if any, were necessitated by the size reduction.

In any development program, a great deal of data are generated which are of value not only to the achievement of the goals under consideration, but which may also prove to be useful in programs utilizing similar components, or directed toward end products of the same general nature. This particular program was, of course, no exception, and many things were learned, in some cases after prolonged periods of frustration, which might well prove to be of general interest. It has not as yet been established which, if any, of the relationships discussed herein are directly related to the techniques used in the fabrication of Fotoform glass and Fotoceram glass ceramic fluid amplifiers, and it might be somewhat dangerous to assume that similar conditions would exist in identical devices fabricated in a substantially different manner, but it is felt that the majority of the information is related to the design, and should be included. It has proven extremely difficult to adequately present the results of over 1000 tests performed on several hundred devices, within the scope of this paper, and in most cases composite curves and average values are used, but every effort has been made to simplify the data without affecting their validity.

The basic dimensional changes discussed are size, aspect ratio, and control edge width, as they are related to pressure gain when operated under a fixed set of conditions; and the basic operating conditions examined are the power jet pressure level, and the control bias pressure level as it is related to the power jet pressure.



## DISCUSSION OF BASIC DESIGN

The original basic design, as provided by Harry Diamond Laboratory personnel, is shown in silhouette in Figure 1, along with some of the more important dimensions as referenced to the power nozzle width. All of the preliminary fabrication and testing was directed toward establishing performance criteria for this design when reduced to a power nozzle width of 0.020" and etched to a depth of 0.060" and data were limited to pressures and pressure gains, although some flow information is available.



DIMENSIONS AS REFERENCED TO  
POWER JET WIDTH.

CONTROL EDGE WIDTH: 3.0

CONTROL NOZZLE WIDTH: 1.5

RECEIVER DISTANCE DOWNSTREAM: 10.0

RECEIVER WIDTH: 1.5

FIG. 1 SILHOUETTE OF ORIGINAL PRESSURE PROPORTIONAL  
AMPLIFIER WITH PERTINENT DIMENSIONS.

Approximately twenty supposedly identical devices were processed using epoxy cement as the sealant, and, upon establishing nozzle characteristics and pressure gain values, it was determined that the pressure gain of the design was extremely sensitive to one or more of the variables of the fabrication and assembly processes. Although the flow-pressure curves of the three nozzles were generally as consistent as would be expected from the dimensional values obtained prior to sealing, pressure gain values averaged about 3.0, which is less than half of the theoretical value, and ranged from 1.0 to 5.3, which is a range approximately one order of magnitude greater than expected.

The coverplates were removed from the devices in order to permit internal inspection, and upon reassembly and testing it was found that not only had the gain level not improved, but also that the reproducibility of gain from seal to seal, using the same unit, was so poor that the unsatisfactory performance could definitely be attributed to an assembly variable, as opposed to a weakness in the basic amplifier fabrication techniques.

It was apparent that the data being accumulated were representative of the device being tested, and not of the design, and that a major improvement in assembly procedures was essential to adequate analysis of the design. Any marginal improvements in performance which might be effected by stepwise adjustment of dimensions would be overshadowed by the variations inherent in assembly. As previously indicated, a comprehensive program of nozzle analysis showed good reproducibility from unit to unit, and the only performance variable which appeared to correlate with gain was the pressure recovery of the units when tested under equal conditions. Further testing showed a variation in power jet profile which was found to be affected by the positioning of the fittings epoxied to the glass coverplate perpendicular to the plane of the device, and it was reasoned that the air expanding from the relatively small fittings into the power jet chamber through a  $90^\circ$  angle to the nozzle was in such a state of turbulence as to preclude the formation of a consistently reproducible jet. The unit was modified to provide input and output flows parallel to the plane of the device as shown in Figure 2,

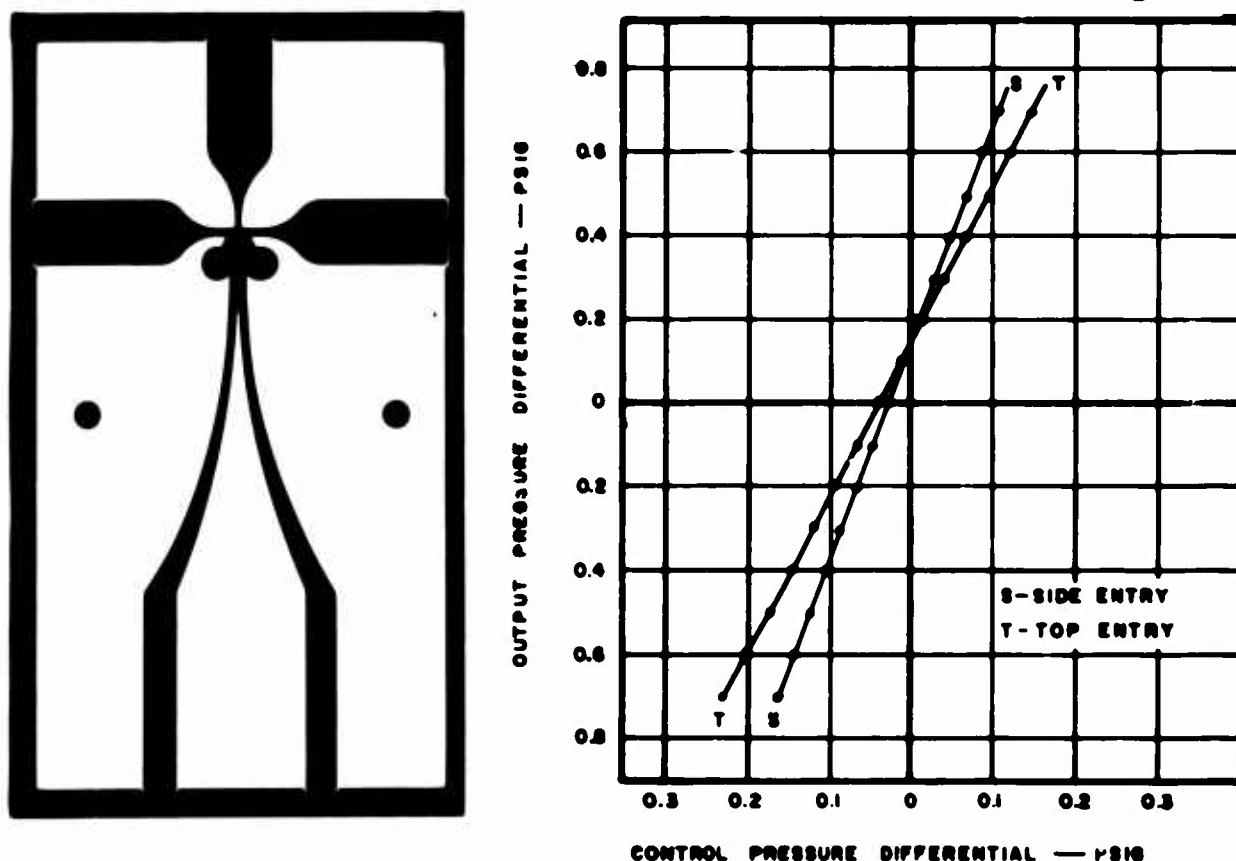


FIG. 2 SILHOUETTE OF SIDE ENTRY MODIFICATION WITH COMPARATIVE CURVES.

and the improved performance indicated has been definitely established by the results of testing the several hundred devices which have been fabricated in this manner.

Further improvements in assembly have been realized through development of a thermal diffusion seal which eliminates the tendency of the sealant, either epoxy cement or gasket material, to press into the nozzles and channels. The combination of parallel inputs and thermal sealing has resulted in performance reproducibility from unit to unit of approximately  $\pm 5\%$ , and although this value still leaves something to be desired, it was felt to be adequate to permit accurate analysis of the results of marginal design changes. It is interesting to note that, even with performance variations reduced to the degree indicated, it has so far proven to be impossible to correlate these variations with any measurable dimensional or surface roughness values. This would tend to indicate that the variability originates in the relatively inaccessible area of the nozzle, if it is a function of fabrication; or in the stability of the power stream as it is channeled into the nozzle; if it is a function of design or assembly. Whatever the case may be, experience gained during the fabrication of hundreds of devices, both proportional and bistable, indicates that the design of the power nozzle, and the condition of the stream entering the nozzle can be critical, and if not properly handled, can result in performance data which are peculiar to the device as assembled, and are not representative of the design being evaluated.

## DESIGN MODIFICATIONS

Toward the end of gaining a better understanding of the operation of the device, a design parameter study was undertaken directed toward optimizing the location of the various functional parts, relative to the power nozzle. The design had been optimized previously at HDL, but in a much larger size, and it was felt to be desirable to repeat some of the tests with units reduced to a power nozzle width .020".

Changes were made in both directions to the dimensions shown in Figure 1, for the receiver width, receiver distance downstream, control nozzle width, and control edge width; and the results showed that photographic reduction of the device did not alter the optimum position of the component parts. Although the pressure gain theoretically should increase somewhat as the receiver width is decreased, it was found that the gain was maximum at the standard width. Maximum gain was achieved with the standard downstream location of the receivers, and, as expected, the pressure gain increased directly with increases in control nozzle width. In all of these cases the changes were relatively large, and this is not to imply that marginal improvements in gain could not result from marginal changes in these dimensions, but it does show that a large decrease in overall size does not appreciably alter the dimensional relationship established for the larger sizes.

The data obtained for different control edge widths, sometimes referred to as interaction aperture widths, indicated the possibility of achieving minor gain improvements by moving the control nozzles closer together. Since the control input impedance, which is an extremely important performance variable in staged systems utilizing feedback, is directly related to the control edge width, it was decided to vary this dimension in smaller increments so that both data and testable devices would be available. A series of units were fabricated with control edge widths ranging from .020" to .080", and, the power nozzle width of the standard device being .020", the range tested when referenced to setback was zero to .030", and when referenced to the ratio of control edge width to the power nozzle width, was 1.0w to 4.0w. The program included edge widths of 1.0w, 1.25w, 1.50w, 1.75w, 2.0w, 2.5w, 3.0w, 3.5w, and 4.0w, and eight devices were fabricated and tested at each of these values except 3.0w which is the standard unit. Gain values were determined with the power jet pressure set at 5 psig, the left control pressure set at 15 inches of water, the right control varied, and the output loading area equal to the receiver aperture area.

The basic data obtained from this test are shown in Figure 3, from

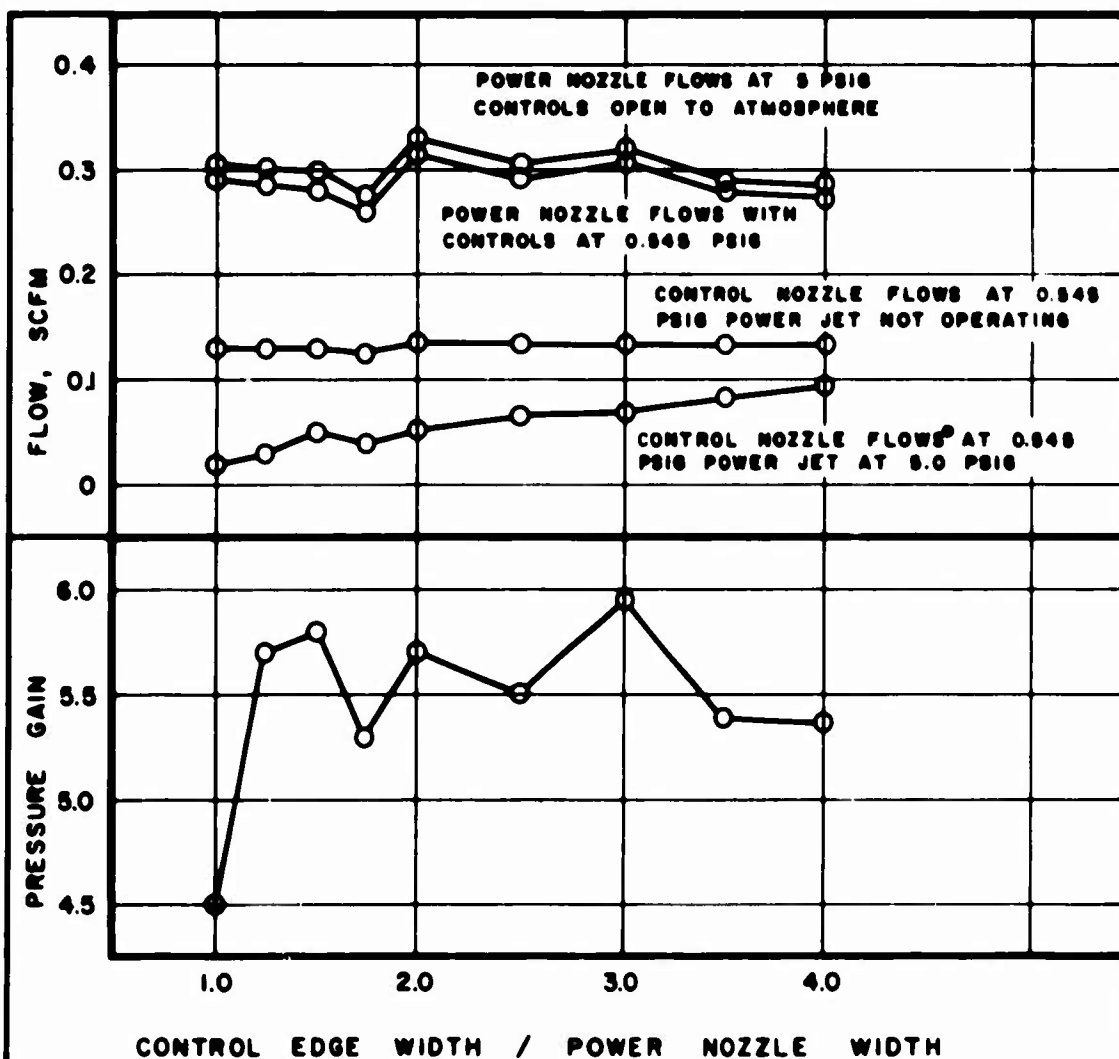


FIG. 3 EFFECT OF CONTROL EDGE WIDTH ON PRESSURE GAIN AND NOZZLE FLOWS.

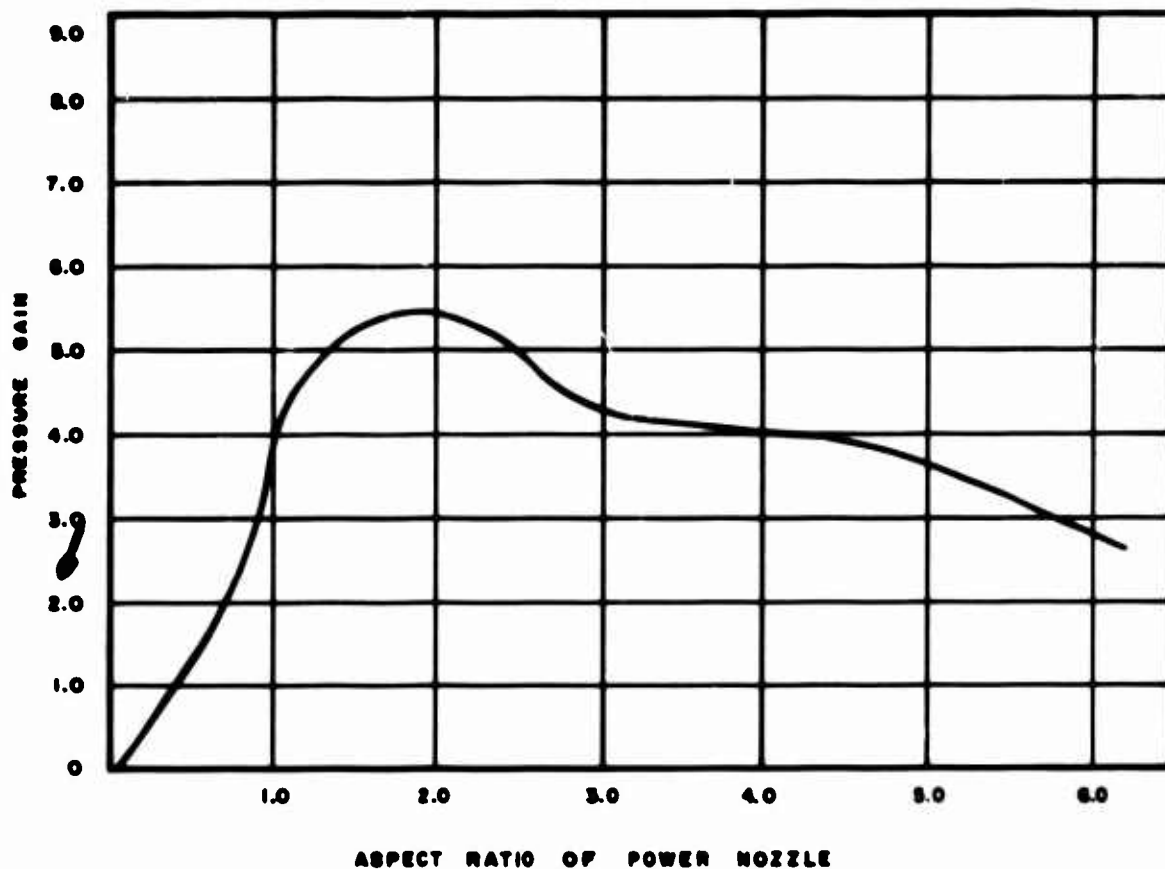


FIG. 5 RELATIONSHIP BETWEEN PRESSURE GAIN AND ASPECT RATIO FOR STANDARD UNIT WITH BLUNTED DIVIDER

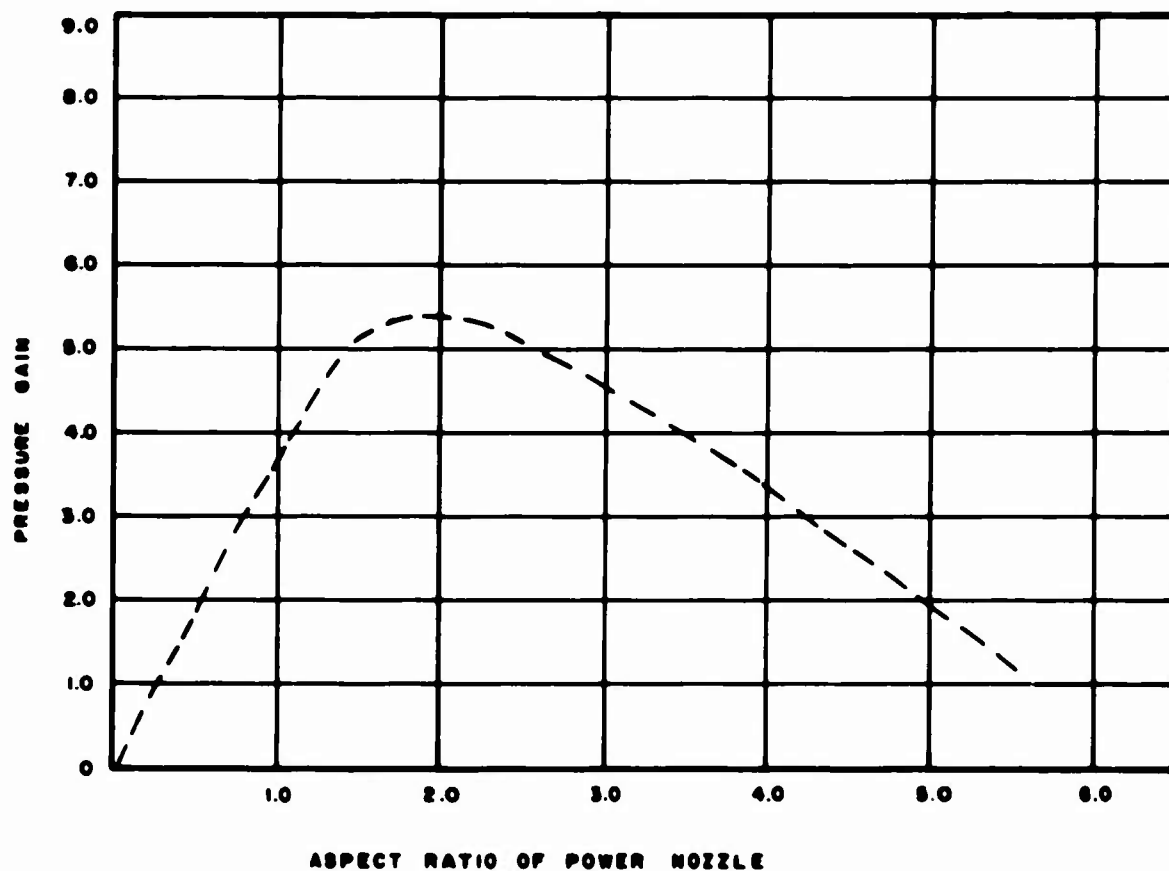


FIG. 4 RELATIONSHIP BETWEEN PRESSURE GAIN AND ASPECT RATIO FOR STANDARD UNIT WITH SHARP DIVIDER

which it can be seen that the gain seems to trend slightly upward to 1.25w and then fall off substantially at 1.0w. The high value at 3.0w might be explained by the fact that this is the standard dimension and these devices were not fabricated at the same time as the others, although the difference of about 0.6 is somewhat higher than would be expected. The reason for the low value at 1.75w has not been established, but careful examination of the artwork and devices at 50X magnification did not reveal any basic geometrical inconsistencies and it is felt that a definite change in the relationship of the power jet to the control edges occurs at this point. The upper curves in Figure 3 represent nozzle flows at the conditions shown, and as can be seen, the characteristics of the power nozzle and the control nozzles are definitely interdependent, and their effect upon each other increases as the control edge width decreases. This interdependence is to be expected, but it must be minimized in multi-stage systems operating from a common power supply, or an externally induced pressure change at any nozzle in the system could result in a pressure change in all of the nozzles of that system. Other factors must be considered, of course, but since an increase in the control edge width results in a substantial decrease in nozzle interdependence and only a slight decrease in pressure gain, all other things being equal, any device intended for operation at these pressures should be designed with a control edge width of at least 4.0w.

In addition to the previously mentioned changes, an aspect ratio study was undertaken, partly to verify the theory and partly to determine the effect of minor depth variations on pressure gain. Identical devices were etched to depths ranging from .020" to .100", thereby covering aspect ratios from 1 to 5, and pressure gain values were determined for the condition of 5.0 psig power jet, 15 inches of water control bias, and output load area equal to the receiver aperture area. As can be seen in Figure 4 the gain values increased steadily up to an aspect ratio of approximately 2.5, as predicted by theory, but then, contrary to theory, decreased almost as rapidly. It had been noted during fabrication that the relatively sharp stream divider began to etch back noticeably at aspect ratios higher than three, and it was felt that this fact presented a logical explanation for the deterioration in performance. In an effort to establish this relationship the artwork was modified by doubling the radius on the end of the stream divider, and the test was repeated. Data from the second run are shown in Figure 5, and although substantial improvement is evident at the higher aspect ratios, a definite decrease in gain does occur. The reason for this loss of gain has not been established, but it is apparent that with the basic design as shown, the highest gain values are obtained at an aspect ratio of 2.0. It is interesting to note that increasing the width of the stream divider did not adversely affect gain at the maximum value, and devices fabricated since that time have incorporated the stronger splitter.

## DIMENSIONAL SCALING

One of the advantages claimed for pure fluid systems is the degree of miniaturization which can be achieved, and one of the basic advantages offered by Fotoform glass to the field of pure fluid systems is the ease of changing size over a fairly broad range, down to power jets as narrow as .003" or less. Since many of the potential applications for these devices involve low power levels, and since it is almost always desirable to minimize power consumption, it was decided to run some preliminary tests on units reduced to one-half and one-quarter the size of the standard .020" power nozzle amplifier. The size reductions were made photographically with no modifications to the basic artwork, and the normal conditions of 5 psig power jet pressure, 10% control bias, and output loading equal in area to the receiver aperture area, were used in testing. In general, the average gain values obtained were the same over the entire size range, but the standard deviation from the mean value increased drastically as the size decreased. For example, the gain values for the .020" power nozzle devices normally fall between 5.7 and 6.3, whereas the gain for the 0.25 times size device ranged from 3.6 to 7.6 with values evenly spaced in between. The gain values for the 0.5 times size device approximated those for the standard device in both magnitude and standard deviation, although there was a noticeable increase in the range of values obtained.

There are many possible reasons why good unit to unit performance reproducibility might become increasingly difficult to maintain as the over-all size of the devices are reduced. It is to be expected that miniaturization would demand tighter tolerances on those processing variables which are not directly related to size. Among these are the depth, which is a function of time, the wall taper, which is a function of the process, and the positioning of the relief holes, which is a function of assembly, and which becomes increasingly more difficult as the over-all size of the unit is decreased. One variable that is related to size which might have contributed to the poor reproducibility in the smallest device is the width of the stream divider, the end radius of which was reduced to the degree that considerable erosion was noted prior to sealing.

All of these variables can be improved upon, and it is not intended to imply that production of .005" power nozzle devices is impossible, or even difficult, but it is felt to be wise to work with power nozzles at least .010" in width until such time as all of the other problems inherent to the particular system under development have been solved.

## EFFECT OF POWER JET PRESSURE LEVEL

The power gain of these units is such that direct interconnection of full size devices operating from a common power supply is neither practical nor economical, and in staging work some means must be found to control the output power level of each stage so that a reason-

able relationship between the power and control jets will exist in the succeeding stage. There are several possible approaches to this problem, including bleeding the excess power, and increasing the size, depth, or power jet pressure from the input stage through to the output stage. Bleeding power would not only be uneconomical, but would also require very closely matched bleed resistances in the opposite interconnecting channels of each stage. Increasing the size of the stages from input through output would require operation of either very small devices, which is undesirable from a reproducibility standpoint, or very large devices which would soon become excessive in both size and power consumption. Increasing the depth, without a corresponding increase in the overall size, would result in a wide range of aspect ratios, and this has been shown to be undesirable from the standpoint of achieving maximum gain. Increasing the power jet pressures in steps from the input stage through to the output stage appeared to be the logical choice.

All test data which were available for these pressure gain devices were taken during operation under the single set of fixed conditions previously mentioned. This was done because it was felt to be unwise to adjust either the design or the test conditions until such time as satisfactory performance reproducibility could be achieved for a single design run under fixed conditions. The decision to develop the first generation of multi-stage units with the device size fixed and the power jet pressure graded, brought out the need to retest the devices on hand to determine what effect, if any, could be expected from operation at pressures other than the standard 5 psig.

A reasonably comprehensive test program was undertaken in which gain curves were generated at power jet pressures of 0.5, 1.0, 2.5, 5.0, 10.0, and 20.0 psig on units from the control edge width study, and the aspect ratio study. Data were also obtained in the zero to 10 psig range on units from the dimensional scaling study. It would, of course, be impractical to attempt to present all of these data within the scope of this paper, and composite curves have been prepared which are felt to be representative of the relationship which exists between the power jet pressure and each of the dimensions studied.

Figure 6 is a plot of the pressure gain vs the power jet pressure as obtained from the control edge width study. All tests were run with the output loading area equal to the receiver aperture area, however, the control bias pressure which is normally held at 10% of the power jet pressure, was adjusted over a limited range to give a more realistic picture of problems which might be expected in operation, and the data shown are averages of the gain at these different bias levels. A more detailed discussion of the effects of adjusting the bias level is included in the following section. As shown, one curve presents the averages for all of the different control widths for each of the pressures tested, and the other curve is that of the original design which has a control edge width of 3.0 times the power nozzle



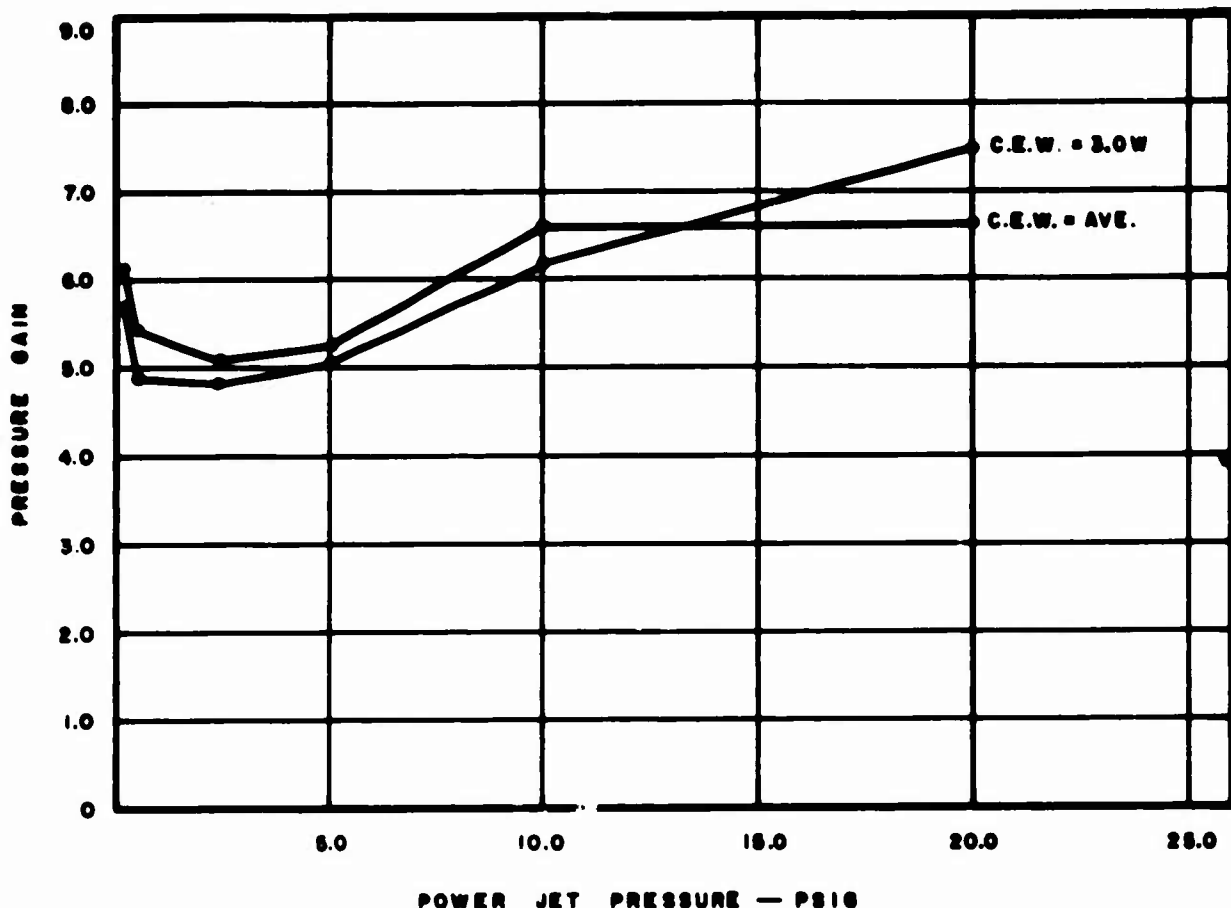


FIG. 6 RELATIONSHIP BETWEEN PRESSURE GAIN AND POWER JET PRESSURE FOR DIFFERENT CONTROL EDGE WIDTH

width. The latter curve is included to show that the shape of the curves for individual values of control edge width is in reasonably good agreement with that of the average. The lone exception to this occurs at a control edge width of 1.0 times the power nozzle width, in which case the gain at 0.5 psig power jet is in line with the average, but the value for 1.0 psig is somewhat low, and as the pressure increases, the gain does not. All of the remaining control edge widths between 1.25w and 4.0w follow the shape of the average curve, and the total range of values at 5 and 10 psig power jet pressure is relatively small. At 20 psig power jet the range of values increase somewhat, and at 2.5 psig and below, the data, although they follow the general trend, become quite erratic.

Figure 7 presents the relationships between pressure gain, power jet pressure, and aspect ratio. Again, the values are averages of those obtained at several different control bias levels, and the output loading was held constant at an area equal to that of the receiver aperture area of the standard device, which has an aspect ratio of 2.5. This latter condition results in the shallow devices operating under relatively light load conditions and the deeper devices operating under relatively heavy load conditions. The test was carried out in this manner in an

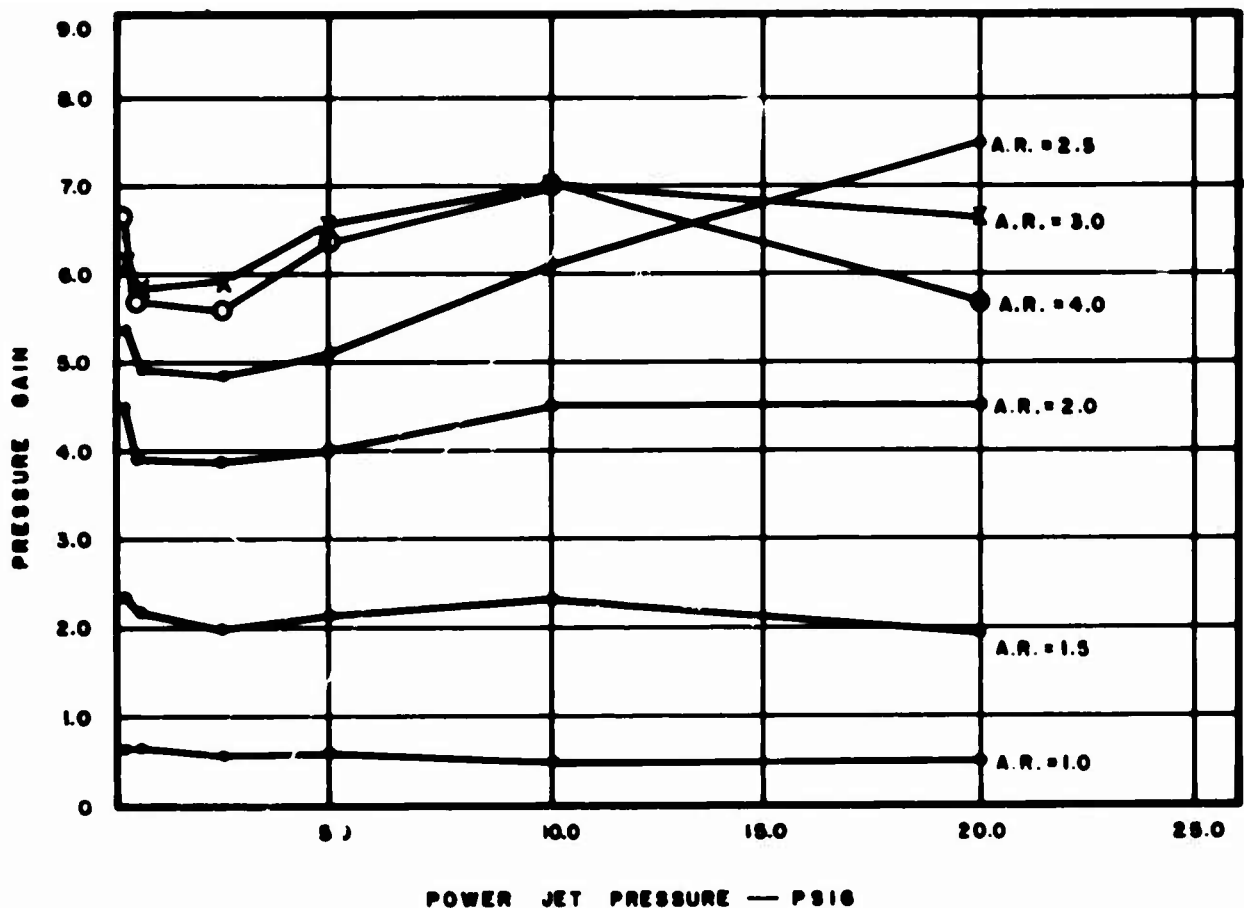


FIG. 7 RELATIONSHIP BETWEEN PRESSURE GAIN AND POWER JET PRESSURE FOR DIFFERENT ASPECT RATIOS

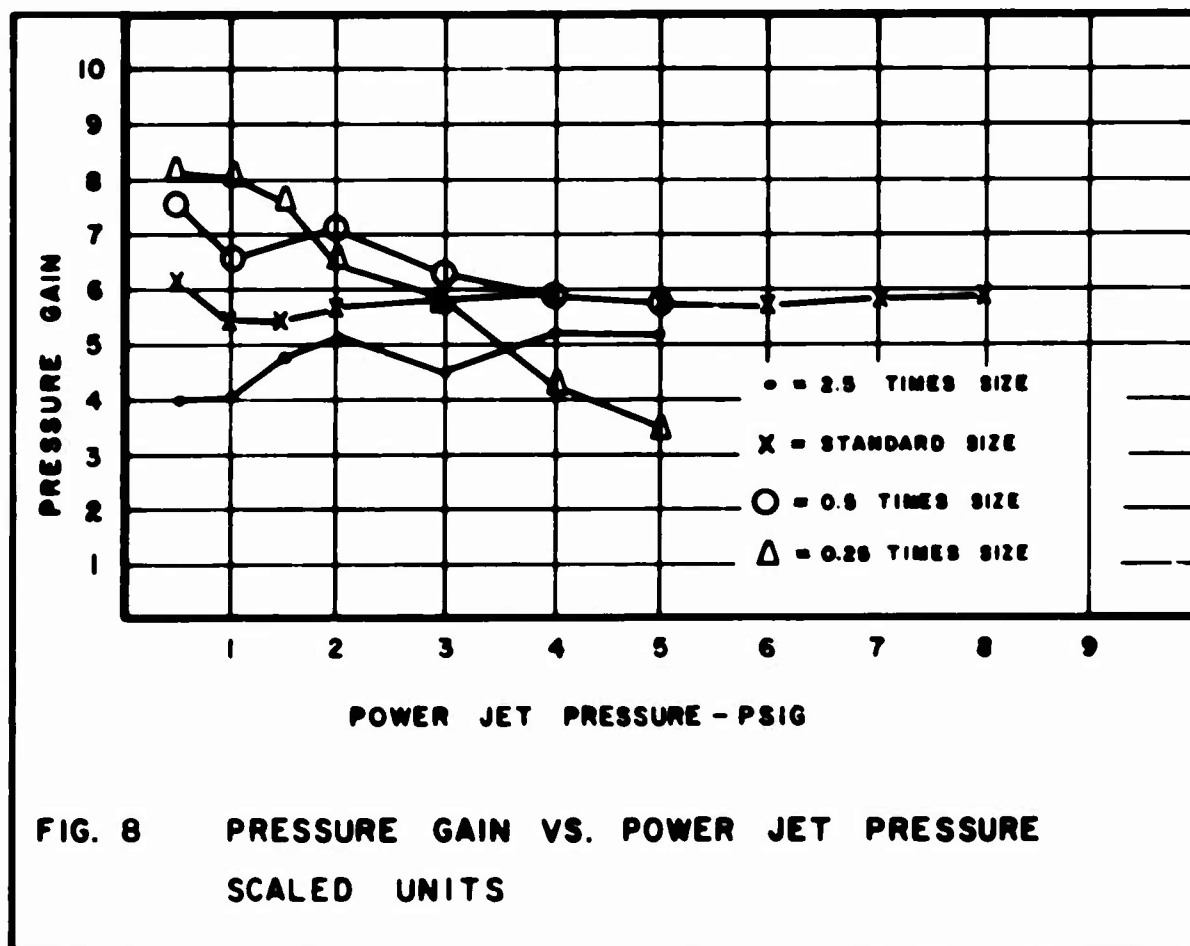
effort to gain some insight into the effect of variable loading on performance, because all of the stages in a multi-stage device are loaded by the control nozzles of the succeeding stage, and as previously stated, the characteristics of the control nozzles of these devices in operation are a function not only of the nozzle dimensions, but also of the power jet pressure level. Since the operating power jet pressures have not as yet been established, it is not possible to predict the loading conditions which will exist in multi-stage operation, and an understanding of the effects of variable loading is desirable.

As would be expected, Figure 7 shows the gain at an aspect ratio of 1.0 to be very low. As the depth is increased the gain increases up to an aspect ratio of 3.0, at which point it levels off. The primary reason for 3.0 representing maximum gain, whereas 2.5 was the peak value in the aspect ratio study, is the difference in output loading. In this case, the 3.0 sample is loaded with an area equal to the receiver aperture area of the 2.5 sample, and, as such, recovers more pressure and would be expected to show a higher pressure gain. In each instance with the exception of the lowest curve, the relationship between gain and power jet pressure follows the same general pattern as in the control edge width study, in that the gain

decreases from 0.5 psig to 2.5 psig, increases to 10 psig, and then tends to level off. Only the curve for an aspect ratio of 2.5, which is the same device represented by the curve for a control edge width of 3.0w in Figure 6, continues to increase at 20 psig. Although it is not shown in the curves presented, it is worth noting that the outputs of the 3.0 and 4.0 aspect ratio devices operating at 20 psig are quite noisy, and this turbulence might explain the deterioration in gain at those points.

Figure 8 is a plot of the relationship between power jet pressure and pressure gain for the size range from .005" power nozzle width to .050" power nozzle width. All of these units were etched to an aspect ratio of 2.5, and the tests were run with a control bias pressure of 10% of the power jet pressure, and output loading equal in area to the area of the receiver apertures of the device being tested. At these low pressures there is an increase in gain as the size decreases, but, as previously stated, the standard deviation from the average value also increases significantly as size decreases. Data recently obtained show the gain for the 0.5 times size device to increase slightly at a power jet pressure of 10 psig, and then drop off to 4.7 at a power jet pressure of 20 psig.

Within the scope of these tests it would seem that operation at any



power jet pressure from .05 psig to 20 psig would be safe, and that gain and stability would not be overly sensitive to variations in power nozzle width, depth, or control edge width. However, some noise is evident in many of the 20 psig curves.

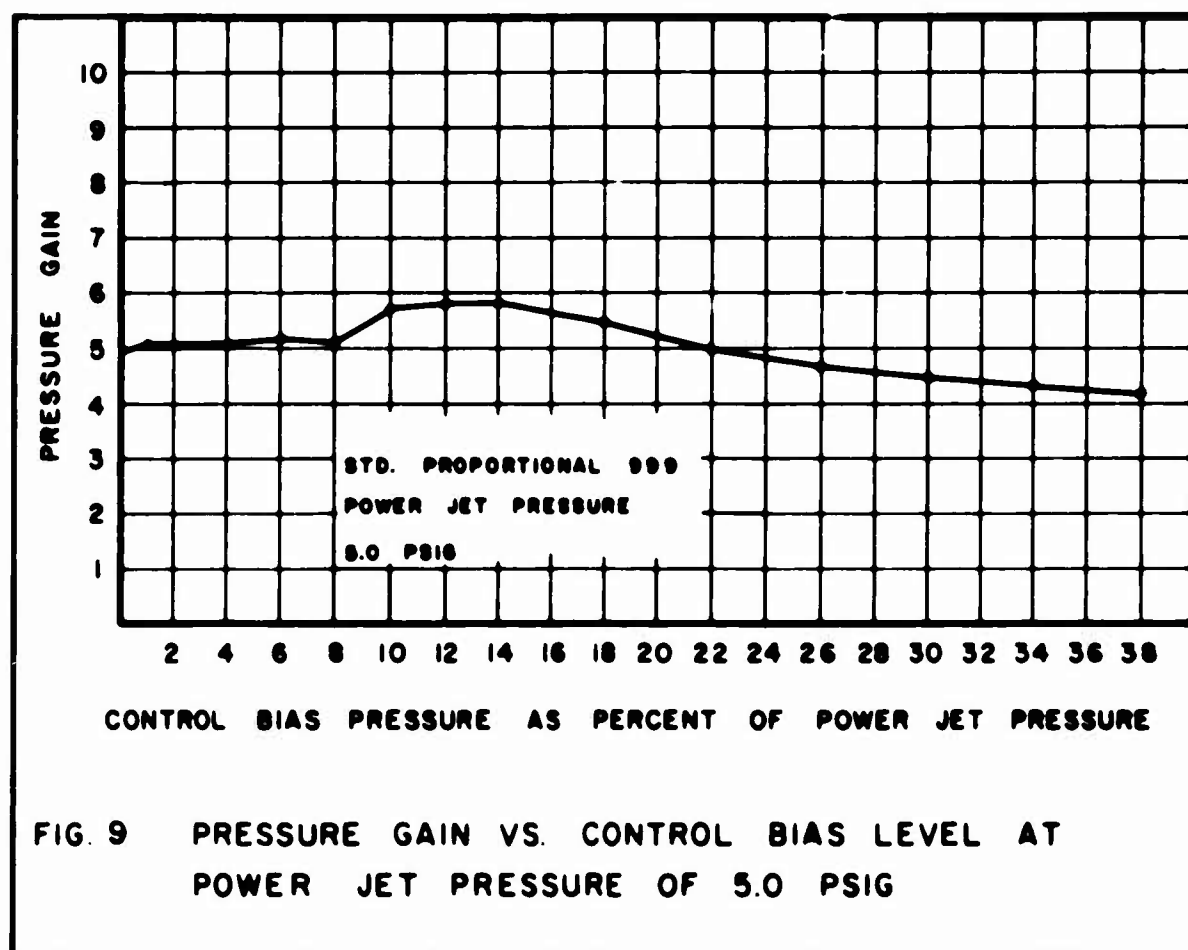
### EFFECT OF CONTROL BIAS LEVEL

In any directly interconnected multiple of these devices operating each at a different power jet pressure level it is impossible to maintain a control bias level at any predetermined point, and although data obtained at a fixed bias value such as 10% are invaluable in developing reproducible fabrication techniques, and in establishing optimum dimensions for specific conditions; before any serious staging work can be undertaken it is essential that the effect of a variable bias level on gain and stability be understood.

In this case, as in that of the previous section, a large amount of data have been accumulated, and it would be impractical to try to include all of the pertinent curves within the scope of this paper. However, there are some specific relationships worth noting, and while discussing these, every effort will be made to cover the general picture as thoroughly as possible.

The data included in this section are taken from the same sets of curves discussed in the previous section, and all test conditions for the control edge width study, the aspect ratio study, the size study, and the standard device, are as described therein.

Initial testing of the "standard" device under "standard" conditions indicated that the pressure gain was not altered appreciably by moderate changes in power jet pressure or control bias level. Figure 9 represents fixed standard conditions with the exception of control bias level which is varied over a substantial range, and, as can be seen, the gain is surprisingly steady. In addition, the device was stable and the gain linear throughout this entire range. A duplicate set of curves were run at 12 psig power jet pressure, and the curve was almost identical to that for 5 psig power jet with the single exception that all gain values were higher, the maximum gain being 7.3 instead of 5.8. In this case also, all of the gain curves were linear and no instability was noted. A further increase in power jet pressure to 20 psig resulted in a curve almost identical to that for 12 psig at 2% and 30% bias level, but substantially higher in the 12% to 16% range where the gain increased to 9.0. The higher gain is, of course, desirable, but the rate of change was disturbing in that small changes in bias level resulted in relatively large changes in gain. Once again, all curves were linear and no instability was detected.



No tests were run at pressures above 20 psig, but it was decided to develop these relationships at the very low pressures which would exist in the input stages of a multi-stage device. With the power jet pressure set at 0.1 psig, gain curves were run from 10% control bias pressure up to 30% and the resultant curve was almost exactly identical to that section of the 12 psig curve. Because of the extremely low pressures involved below 10% ( $< .01$  psig), no curves were run and it has not been established that the gain would follow the normal trend and decrease at lower bias levels. This test was repeated at 0.5 psig power jet pressure, and although the resultant gain vs bias level curve was similar in shape to the others, the peak value occurred at 22% bias level instead of 12%, and in the relatively narrow range of bias levels from 24% to 30% the gain dropped from 7.0 to 4.3.

The final set of values were obtained at a power jet pressure of 1.0 psig, and, as shown in Figure 10, by the curve representing the standard proportional unit, the relationship was generally similar to that for the 0.5 psig curve. Maximum gain was once again approximately 7 and it occurred at 22% bias level, above which it dropped to 4.3 at 25%. At these pressures a 3% change amounts to something

less than an inch of water pressure change, and this is certainly an undesirable condition, in that a relatively small change in the power jet pressure of a stage preceding one operating in this manner could result in a 40% decrease in the gain of the entire staged system.

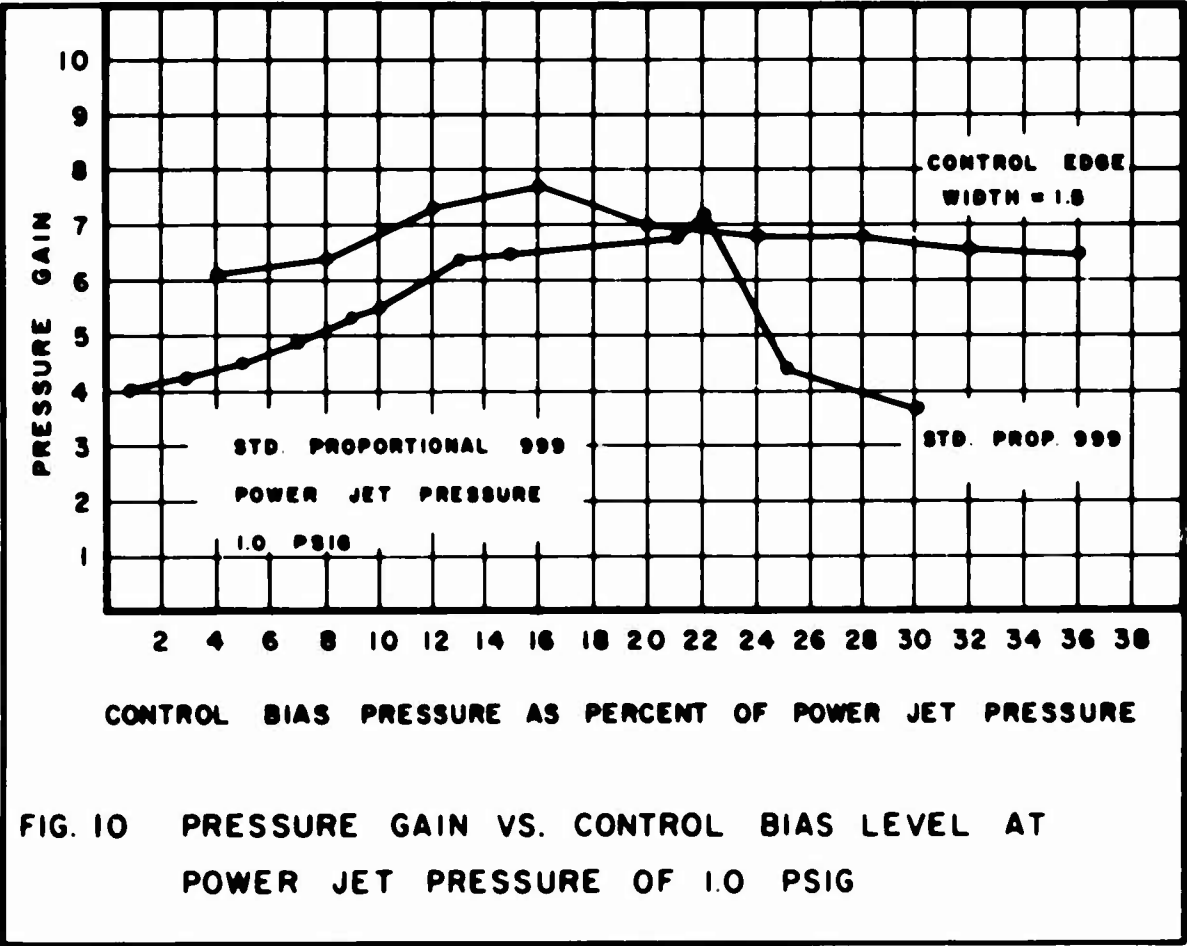


FIG. 10 PRESSURE GAIN VS. CONTROL BIAS LEVEL AT POWER JET PRESSURE OF 1.0 PSIG

In an effort to eliminate, or at least minimize this gain sensitivity to minor bias level changes it was reasoned that, since the characteristics of both the power and control jets could be altered by changing their physical relationship (control edge width), similar data should be generated using the devices from the control edge width study. The curve representing a control edge width of 1.5w in Figure 10 is very encouraging in that this change in control edge width from 3.0w to 1.5w not only virtually eliminated the extreme sensitivity of gain to bias level, but did so without decreasing the gain at any point. In fact, the gain is substantially higher at every point except the peak of the curve. Similar data were obtained for all available control edge widths at a power jet pressure of 0.5 psig, and it was discovered that the devices with a control edge width of 2.0w were just as effective in eliminating the large gain fluctuations at that pressure as were the 1.5w control edge width devices at 1.0 psig. There was a minor decrease in gain at the maximum value, from 7.0 to 6.8 but this is insignificant when compared to the fact that the high end of the curve

was brought up from 4.3 to 6.5 at the 30% bias level. Similar results were achieved at 20 psig power jet pressure using the 2.0w control edge width devices in that the total gain difference across the entire 30% range was reduced from 3.4 to 1.6, and the reduction of the maximum gain value from 9.0 to 8.5 was again insignificant. Checking further it was discovered that the range of gain across the 30% bias range could be improved at every pressure run, including 5 psig. In this case the gain ranged from 4.5 at 30% bias level to 5.8 at 14% bias level when checked with 3.0w control edge width devices, and when 2.0w control edge width devices were substituted, the minimum was 5.3 at 1% and the maximum was 5.8 at 20%. Speaking specifically in terms of gain stability as a function of control bias level it would certainly be advisable to fabricate these devices with a control edge width of 2.0 times the power nozzle width.

Control bias pressure level data were generated for the aspect ratio devices also, but no valuable conclusions could be reached. The range of gain values for each power jet pressure increased in almost direct proportion to the average gain value, but it appears that the aspect ratio of 2.5 which is currently considered to be "standard", is as good as, or perhaps better than, any of the others tested.

A set of curves were run comparing the "standard devices" with 1/2 size devices of the same control edge width and aspect ratio, and in most cases the smaller units were more sensitive to changes in bias level. However, at 2.5 psig power jet pressure they were comparable, and at 1.0 psig the small unit was somewhat superior, and very stable up to a bias level of 20%.

The smaller device proved to be unsatisfactory at 20 psig power jet pressure in that it was completely unstable at the lower and higher bias levels, and most certainly should not be operated at that pressure until it has been more thoroughly investigated. At the lower pressures there is no reason to believe that minor changes in control edge width would not result in a perfectly satisfactory device.

## ZERO BALANCE

Although this entire program was originally intended to be a study of the effects of the pressure relationships between the power jet and the control jets, as these relationships influence the pressure gain, further analysis of the curves has resulted in the collection of a substantial amount of data relative to zero balance, which may prove to be of more value than the gain data. Zero balance, which is herein defined as the pressure difference across the outputs of a device when the controls are in perfect balance, is obviously an extremely vital factor when direct in-line coupling of a multi-stage system is

attempted. If any one stage is far enough out of balance, it will drive the succeeding stage out of the linear gain range into a condition of negative gain, in which case the multi-stage system will not function.

Figure 11 was prepared from data taken from the curves used in the previous sections, and as such, the operating conditions are the same, and need not be outlined again. As previously stated, the zero balance plotted on the Y axis is the pressure difference in psig which exists across the output channels of a device when the controls are in perfect balance, and it can be seen that, in addition to being a function of the power jet pressure, as would be expected, it is also to some degree a function of the control edge width. Considerable work has been done outside of the scope of this program, which has shown zero balance to be primarily dependent on power nozzle design, and it is not intended to imply that, without regard to design or fabrication techniques employed, the devices can be balanced by adjusting the control edge width. However, it does appear that the degree of unbalance can be minimized by choosing the proper control nozzle setback, and, since it is unlikely that perfect symmetry will be achieved in practice, it would seem reasonable to design toward minimizing this variable, assuming that the change in control edge width does not adversely effect any of the other performance variables. Further data which have been taken since this graph was prepared indicate that the increase in offset above a control edge width of  $2.5w$  may be somewhat exaggerated, but there does appear to be an increase in the unbalance at widths below  $2.0w$  and above  $2.5w$ .

As shown, all of the unbalance occurred in one direction except for the higher pressures at a control edge width of  $4.0w$ . Thus, in a directly coupled, in-line system wherein the right output of each device is coupled directly to the right control of each succeeding device there is a tendency for the unbalance to compensate down through the system, and assuming that none of the stages are excessively out of balance, the entire circuit will function in the narrow range of high gain without the need for carefully adjusting power jet pressures, or compensating with intra-stage negative feedback.

An analysis of the curves used in the aspect ratio study showed the amount of unbalance to increase with both increases in power jet pressure and increases in aspect ratio, whereas the control bias level proved to be relatively unimportant. In effect, all other things being equal, the unbalance is not affected by aspect ratio as such, and the increase noted was a function of the level of pressure recovered in the outputs. Under the condition of fixed output load resistances used in this test, the pressure recovered increased directly with power nozzle area, at constant power jet pressure,



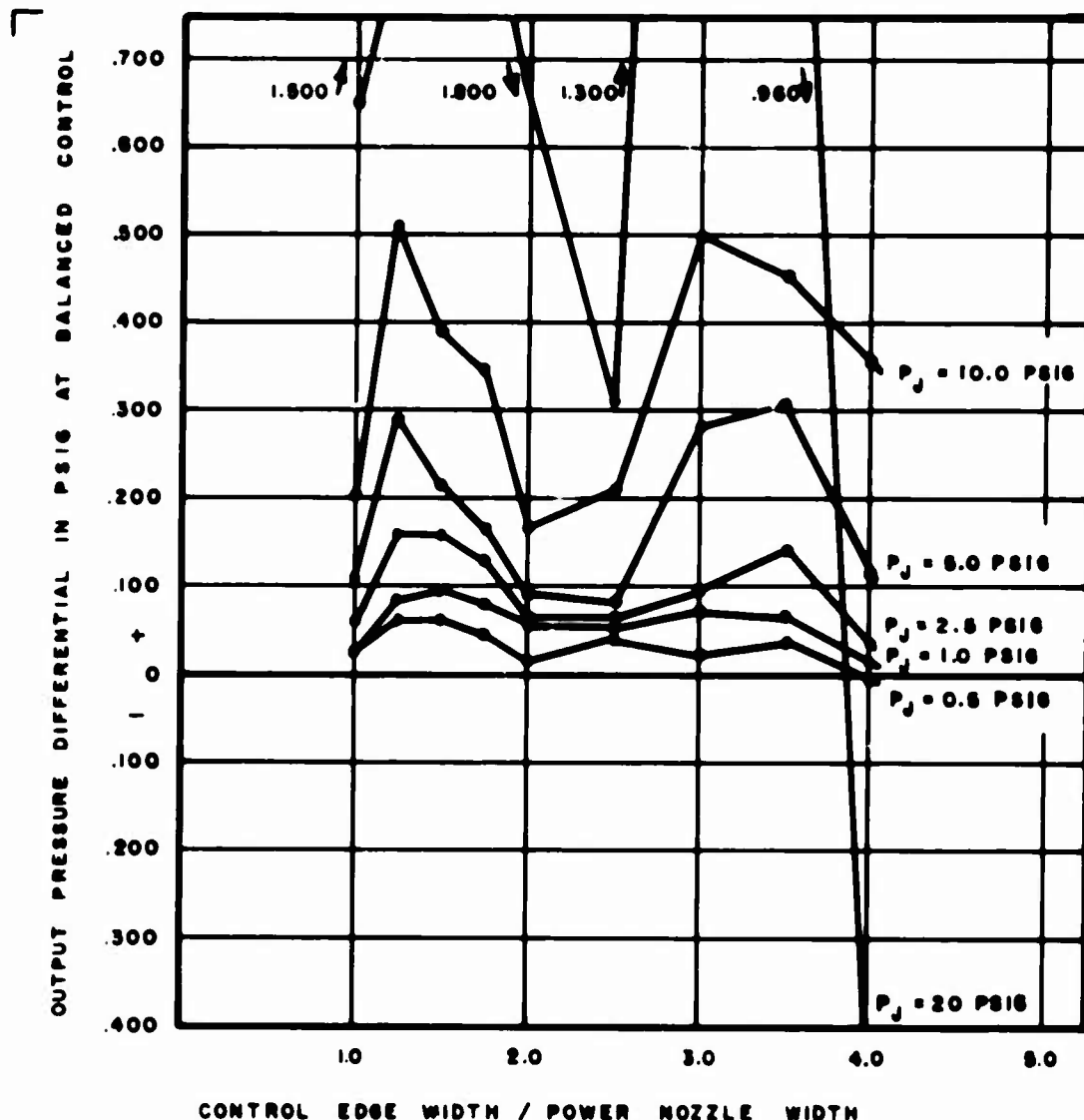


FIG. 11 RELATIONSHIP BETWEEN ZERO BALANCE AND CONTROL EDGE WIDTH FOR DIFFERENT POWER JET PRESSURES

and with power jet pressure, at constant power nozzle area, and the unbalance was approximately 25% of the pressure recovered in every case except that of an aspect ratio of 3.0, where 20% would be a more accurate figure. These data indicate that there is nothing to gain in the area of zero balance which would justify operating at an aspect ratio which would result in a sacrifice of pressure gain.

The gain curves generated for the one-half size devices showed them to be substantially better balanced in every case, than were the standard size devices. These smaller devices were loaded with resistances equal in area to the receiver apertures, and the pressure recovered was effectively as high as that for the large devices, so this is not a case of the offset being a percentage of the recovery pressure as it was in the aspect ratio study, but rather,

there seems to be a definite improvement in zero balance in this smaller size. Unfortunately, these devices are unpredictable, and this, combined with the fact that they do not function properly at the higher power jet pressures is sufficient to limit their use until such time as techniques are developed which will result in consistent reproducibility.

Throughout this particular test only the relatively slow response X-Y recorders were used, and no analysis of noise was attempted. However, the devices with a control edge width of 1.0w, and an aspect ratio of 1.0, and the 1/2 times size units tended to be non-linear at high power jet pressures, the 3.5w and 4.0w control edge width units were somewhat unstable at lower power jet pressures, and these two designs, plus the aspect ratio units of 3.0 and above, were noisy at high power jet pressures.

## CONCLUSIONS

In summary, the results of this program can probably best be expressed in outline form, and the following conclusions appear to be true in so far as Fotoform and Fotoceram glass ceramic fluid amplifiers of the particular design discussed, are concerned.

### I. Assembly

The performance of these devices is extremely sensitive to certain assembly variations, particularly the technique used to introduce the power stream.

### II Fixed Test Conditions vs Variations in Dimensions

- A) Control edge width changes do not have an appreciable effect on pressure gain if held between 1.25w and 4.0w, but to minimize the interdependence of the jets, should be held at the higher value.
- B) Aspect ratio has a distinct effect on gain, with the maximum value occurring at approximately 2.0.
- C) Size should be maintained at a .010" minimum power nozzle width because of poor unit to unit reproducibility in the very small devices.

### III Variations in Power Jet Pressure vs Variations in Dimensions

- A) Control edge width exerts little influence on gain with power jet pressures up to 20 psig, but should be held between 2.0w and 3.0w to minimize variations.

- B) Aspect ratio as related to pressure gain is relatively insensitive to power jet pressure changes in this range.
- C) Size should be maintained at a .020" minimum power nozzle width because the smaller devices do not function properly at 20 psig power jet pressure.

#### IV Variations in Control Bias Pressure Level vs Power Jet Pressure vs Dimensions

---

- A) Control edge width exerts an influence in gain constancy as the bias level is changed, for any given power jet pressure, and should be held at 2.0w.
- B) Aspect ratio changes do not have an appreciable effect on the relationship between bias pressure and power jet pressure.
- C) Size data for the particular control edge width tested at .010" power jet width were comparable to those for the .020" power nozzle except that, at 20 psig power jet pressure the device did not function properly.

#### V Zero Balance

Zero balance is primarily a function of power nozzle design, but it does appear to be influenced somewhat by control edge width, which should be held between 2.0w and 2.5w.

**HARRY DIAMOND LABORATORIES  
WASHINGTON 25, D. C.**

**EXPERIMENTS IN ANALOG COMPUTATION  
WITH FLUIDS**

by

**SILAS KATZ  
JOHN M. GOTO  
ROBERT J. DOCKERY**

## ABSTRACT

A study is made of the use of passive and active fluid components without mechanical moving parts to perform analog computations. The active fluid component is the proportional fluid amplifier with feedback. Multiplication by a constant greater than unity and integration are demonstrated. The errors in computation are considered with a view toward designing better components.

## 1 INTRODUCTION

The theory and practice of analog computation are well developed. When passive and active components are placed in computational circuits, a wide variety of mathematical operations and automatic control functions can be performed.

Active fluid devices with no moving mechanical parts are now being studied. The presently available devices have low-frequency (below 1000 cps) characteristics that are analogous to some of the well developed electrical and mechanical circuit components. Theoretically, then, it is possible to perform analog computations using these devices in conjunction with existing passive fluid components.

The purposes of this report are as follows:

- (1) To demonstrate that fluid computation with these components is possible.
- (2) To show that for low-frequency or slowly changing input signals the computation follows the basic laws of lumped parameter circuit theory.
- (3) To determine what efforts are necessary in the future design and fabrication of fluid components to obtain more accurate and versatile analog computation.
- (4) Review the functioning of analogous components.

## 2 BASIC PASSIVE COMPONENTS

### 2.1 Resistance

Linear fluid resistive components can be obtained with capillary tubing. The fluid resistance is defined as the ratio of pressure drop,  $\Delta p$ , across the component to the volumetric flow rate  $Q$  through the component. When the flow is laminar, the resistor is linear and the magnitude can be calculated from the Hagen-Poiseuille law as

$$R = \frac{\Delta p}{Q} = \frac{128 \mu l}{\pi N D^4} \quad (1)$$

where

- $R$  = fluid resistance, lbf-sec/in<sup>5</sup>
- $\mu$  = viscosity of the fluid, lbf-sec/in<sup>2</sup>
- $l$  = length of capillary tube, in.
- $N$  = number of capillary tubes
- $D$  = internal diameter of a capillary tube, in.

Since a small error in the measurement of the internal diameter of the capillary tubes results in a large error in calculated resistance, the values of resistance are measured directly. This is accomplished with a flowmeter, accurate to 2 percent of rate, and a manometer. Typical data for a resistor are shown in figure 1 in which the pressure drop across the resistor is plotted against volume flow rate. The best line through the data is calculated by the method of least squares. The slope of this line is the resistance. This value of resistance is believed to be accurate to within 2 percent of the true value over the range of pressures used.

### 2.2 Capacitance

One type of capacitive component can be obtained with a chamber or tank. The fluid capacitance of this component is defined as the ratio of the volumetric flow difference to the rate of change of tank pressure. When the pressure changes are relatively slow, isothermal conditions exist and the magnitude of the fluid capacitance can be calculated using the conservation of mass equation. This results in

$$C = \frac{Q_i - Q_o}{s p_T} = \frac{V}{p_T} \quad (2)$$

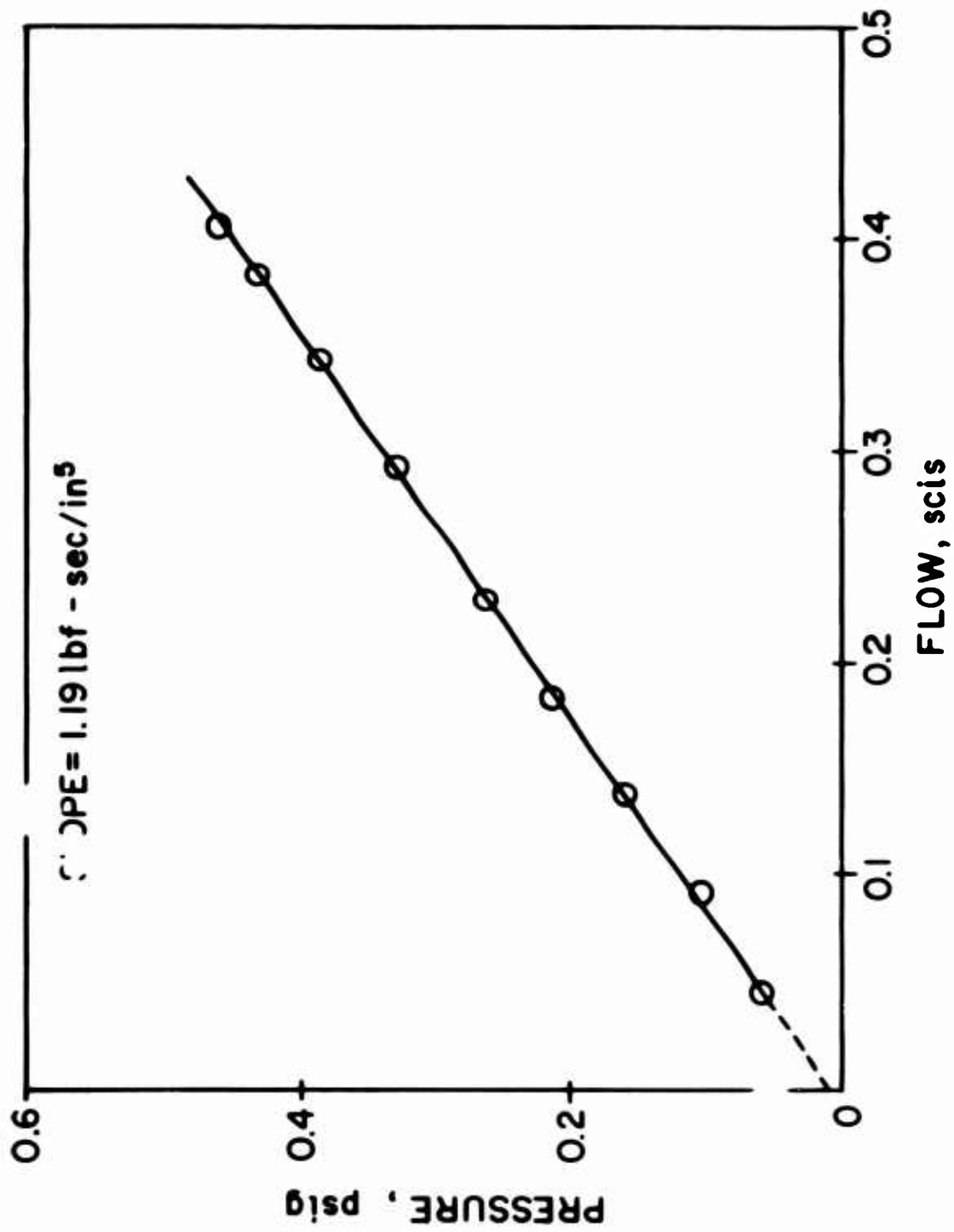


Figure 1 Typical Capillary Tubing Resistance Data

where

$C$  = capacitance,  $\text{in}^5/\text{lbf}$   
 $V$  = volume of tank or chamber,  $\text{in}^3$   
 $P_T$  = pressure in the tank,  $\text{psia}$   
 $Q_i$  = volumetric flow rate into tank,  $\text{in}^3/\text{sec}$   
 $Q_o$  = volumetric flow rate out of tank,  $\text{in}^3/\text{sec}$   
 $s$  = differential operator,  $d/dt$

Since the absolute value of pressure in the tank is always very close to atmospheric pressure, the capacitance was calculated from equation (2) using atmospheric pressure. This calculated value was checked experimentally by connecting a known fluid resistance to the tank and applying a step input to the combination. The experimental and calculated values agreed within 5 percent.

At the present time there is no known point-to-point fluid capacitance that does not utilize moving parts. This fact considerably reduces the number of circuits available for pure fluid computational purposes. This lack of a point-to-point capacitor led to the use of the "bootstrap" integrator discussed in detail in section 4.

### 2.3 Inductance

Fluid inductance is defined as the ratio of pressure drop to the time rate of change of volumetric flow rate. If  $L$  is the inductance, then

$$L = \frac{\Delta p}{sQ} \quad (3)$$

where, once again,  $s = d/dt$ .

In terms of a length of tubing  $l$  with inside cross-sectional area  $A$ , the inductance may be derived from Newton's second law. The sum of the forces is  $A\Delta p$  and the mass times acceleration is  $\rho A l dV/dt$  so that

$$A\Delta p = \rho A l \frac{dV}{dt}$$

or, since  $V = Q/A$ ,

$$\Delta p = \frac{\rho l}{A} \frac{dQ}{dt}$$



The area of the tubing is  $A = \pi D^2/4$  so that after rearranging, the inductance is

$$L = \frac{\Delta p}{\frac{dQ}{dt}} = \frac{4\eta l}{\pi D^2} \quad \frac{\text{lbf sec}^2}{\text{in}^5} \quad (4)$$

No inductive components were used in these experiments because of the low frequency limitations imposed by the active components. At these low frequencies the inductive reactance of most practical size components is very small.

### 3 ACTIVE COMPONENTS

#### 3.1 The Proportional Fluid Amplifier

The active fluid component used for computation is the proportional fluid amplifier (ref 1). A typical amplifier is shown in figure 2.

This amplifier operates predominantly on the exchange of momentum flux between the power jet and the control jets. When the control pressures are equal, the power jet divides equally between the two output collectors (fig. 3a). As one control pressure is changed, the power jet is redirected and one output pressure increases while the other decreases. At a constant power jet pressure, the functional dependence of the difference in pressures at the output on the control pressures may be written as

$$p_{ol} - p_{or} = f(p_{cr}, p_{cl}) \quad (5)$$

where  $p_{ol}$  = total pressure at left output  
 $p_{or}$  = total pressure at right output  
 $p_{cl}$  = total pressure at left control  
 $p_{cr}$  = total pressure at right control

The variational components obtained from equation (5) are

$$\Delta(p_{ol} - p_{or}) = \left. \frac{\partial(p_{ol} - p_{or})}{\partial p_{cr}} \right]_{p_{cl} = \text{const.}} \Delta p_{cr} + \left. \frac{\partial(p_{ol} - p_{or})}{\partial p_{cl}} \right]_{p_{cr} = \text{const.}} \Delta p_{cl} \quad (6)$$

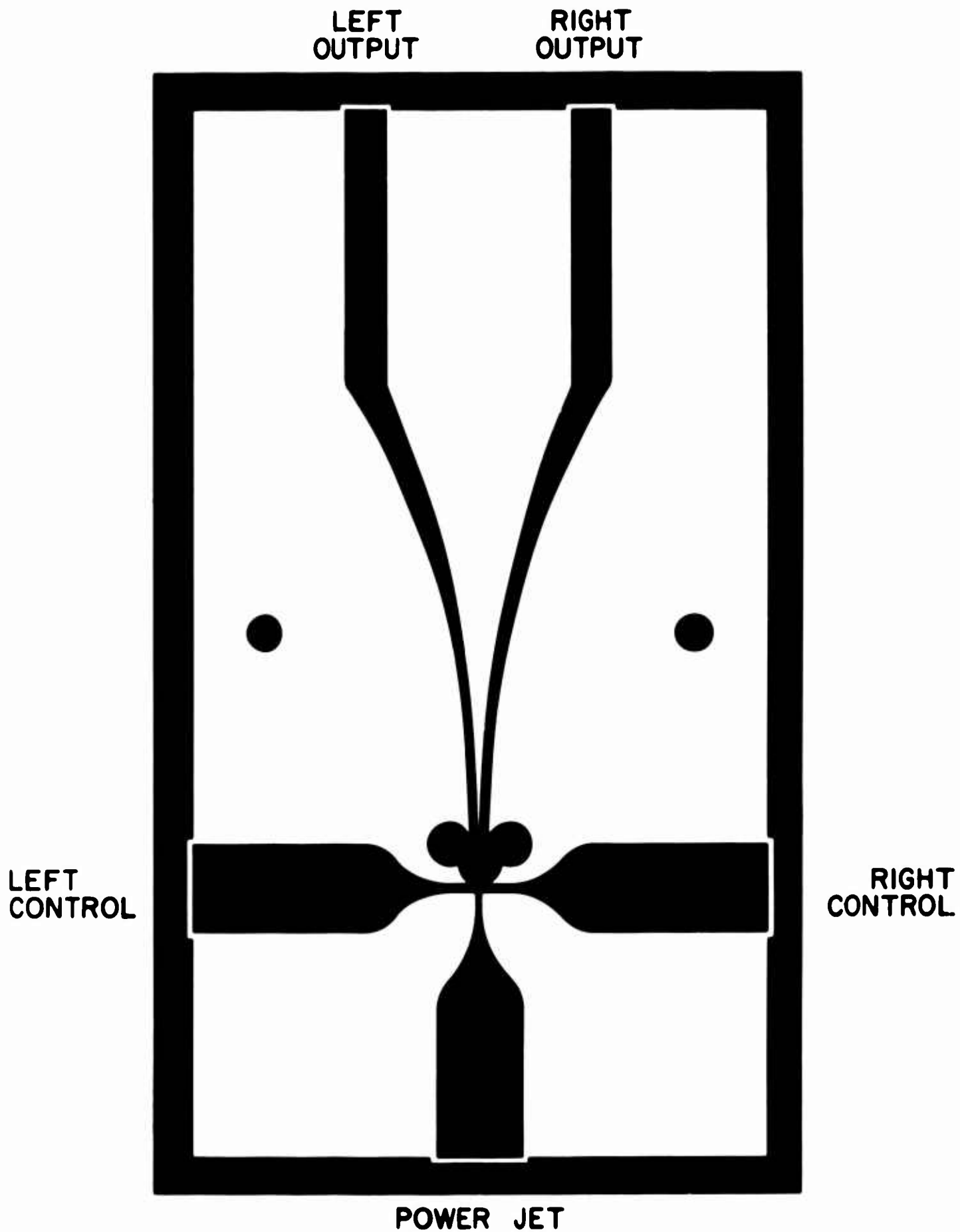
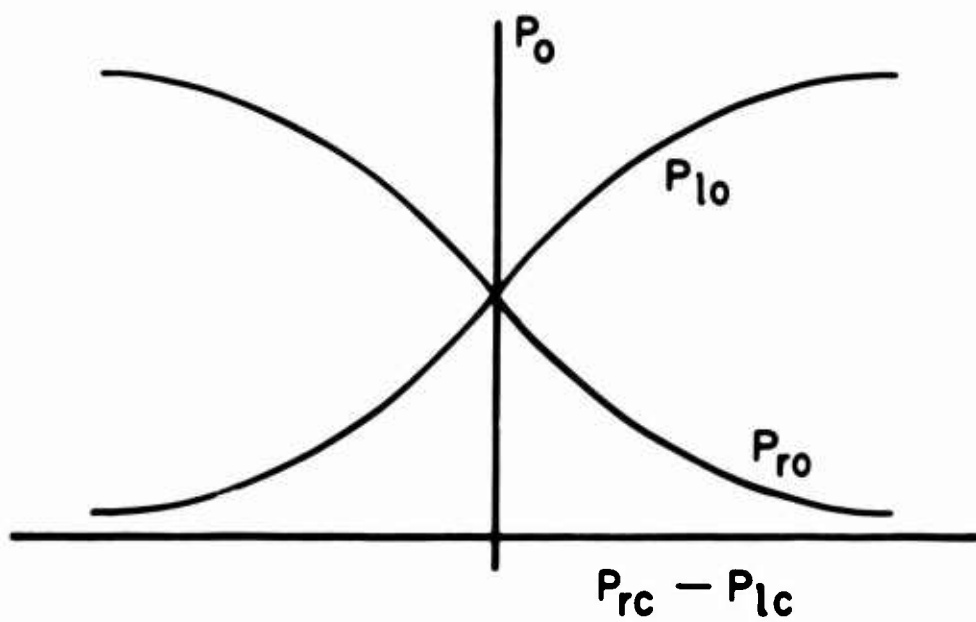
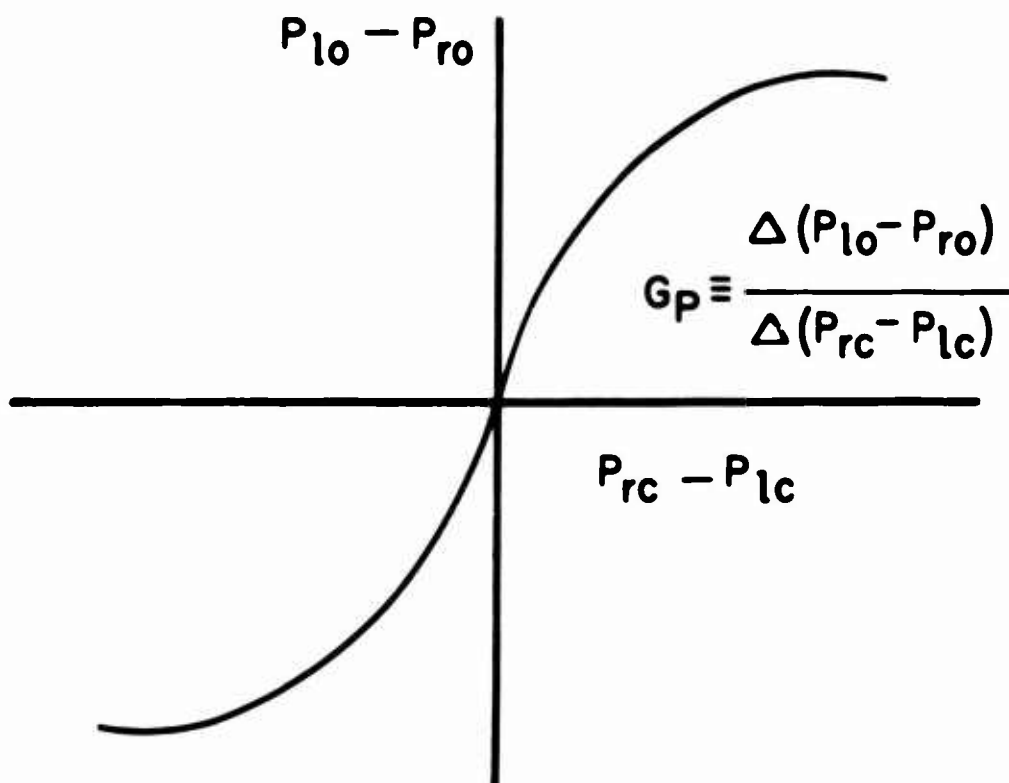


Figure 2 Typical Proportional Fluid Amplifier



(a)



(b)

**Figure 3** Typical Output-Control Characteristics of a Proportional Fluid Amplifier

If the amplifier is symmetrical, the left control pressure and the right control pressure are equally effective in deflecting the power jet. In this case

$$\left. \frac{\partial (p_{ol} - p_{or})}{\partial p_{cr}} \right]_{p_{cl} = \text{const}} = - \left. \frac{\partial (p_{ol} - p_{or})}{\partial p_{cl}} \right]_{p_{cr} = \text{const}} \quad (7)$$

The negative sign appears on the right side of the equation because an increase in the left control pressure raises the right output pressure and lowers the left output pressure. Equations (6) and (7) can be combined to give an expression for the pressure gain of the proportional fluid amplifier

$$G_p \equiv \frac{\Delta (p_{ol} - p_{or})}{\Delta (p_{cr} - p_{cl})} = \frac{\partial (p_{ol} - p_{or})}{\partial p_c} \quad (8)$$

where  $G_p$  = pressure gain

$p_c$  = pressure at one control when the other control pressure is fixed

The pressure gain is indicated in Figure 3b.

Ordinarily proportional fluid amplifiers are designed to be symmetrical; however, at present, fabricating techniques are not sufficiently advanced to insure symmetry in high-gain amplifiers. When amplifiers are not symmetrical, the equality given by equation (7) does not hold. The controls are not equally effective in deflecting the power jet. Then, a right-side pressure gain  $G_{pr}$  and a left-side pressure gain  $G_{pl}$  may be defined as

$$\left. \begin{aligned} G_{pr} &\equiv \left. \frac{\partial (p_{ol} - p_{or})}{\partial p_{cr}} \right]_{p_{cl} = \text{const}} \\ G_{pl} &\equiv \left. \frac{\partial (p_{ol} - p_{or})}{\partial p_{cl}} \right]_{p_{cr} = \text{const}} \end{aligned} \right\} \quad (9)$$

Substitution of equation (9) into equation (6) gives

$$\Delta(p_{ol} - p_{or}) = G_{pr} \Delta p_{cr} - G_{pl} \Delta p_{cl} \quad (10)$$

Other characteristics of proportional fluid amplifiers are that the forward gain can be either positive or negative and that the output and input impedances are both low. In addition, the output signal of the amplifier is a difference signal. Although this output difference may be zero, the pressure at either output is above ambient. Since the output operates about a higher reference level than the input, feedback from the outputs to the controls will carry flow even when the outputs are balanced.

### 3.2 Proportional Amplifier with Feedback

The unsymmetrical properties of the fluid amplifier adversely affect its use in computational circuits. This can be seen by examination of the lumped parameter system equations for a fluid amplifier with positive and negative feedback.

The circuit is shown in figure 4. From the continuity equation the two loop equations are

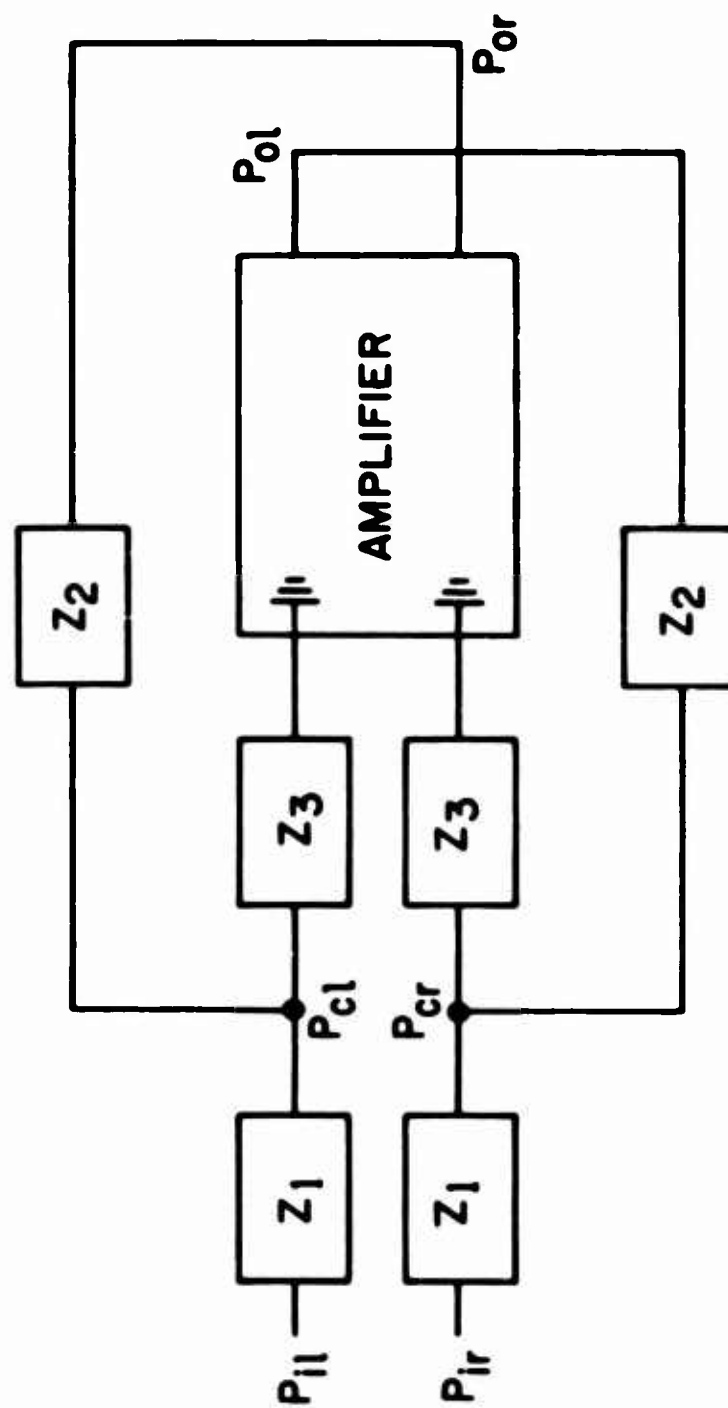
$$\frac{p_{lr} - p_{cr}}{Z_1} + \frac{p_{ol} - p_{cr}}{Z_2} = \frac{p_{cr}}{Z_3} \quad (11a)$$

and

$$\frac{p_{il} - p_{cl}}{Z_1} + \frac{p_{or} - p_{cl}}{Z_2} = \frac{p_{cl}}{Z_3} \quad (11b)$$

or by rearranging

$$\frac{p_{lr}}{Z_1} + \frac{p_{ol}}{Z_2} = p_{cr} \sum_{i=1}^3 \frac{1}{Z_i} \quad (12a)$$



**Figure 4** Proportional Fluid Amplifier With Feedback

$$\frac{p_{il}}{Z_1} + \frac{p_{or}}{Z_2} = p_{cl} \sum_{i=1}^3 \frac{1}{Z_i} \quad (12b)$$

Subtracting (12b) from (12a) gives

$$\frac{p_{ir} - p_{il}}{Z_1} + \frac{p_{ol} - p_{or}}{Z_2} = (p_{cr} - p_{cl}) \sum_{i=1}^3 \frac{1}{Z_i} \quad (13)$$

Replacing  $p_{cr}$  with the gain expression, equation (10), for the unsymmetrical amplifier and considering only the linear operating range yields

$$\frac{p_{ir} - p_{il}}{Z_1} + \frac{p_{ol} - p_{or}}{Z_2} = \left( \frac{p_{ol} - p_{or}}{G_{pr}} + \frac{G_{pl}}{G_{pr}} p_{cl} - p_{cl} \right) \sum_{i=1}^3 \frac{1}{Z_i} \quad (14)$$

Rearranging gives

$$\frac{p_{ir} - p_{il}}{Z_1} + (p_{ol} - p_{or}) \left[ \frac{1}{Z_2} - \frac{1}{G_{pr}} \sum_{i=1}^3 \frac{1}{Z_i} \right] = p_{cl} \left[ \frac{G_{pl}}{G_{pr}} - 1 \right] \sum_{i=1}^3 \frac{1}{Z_i} \quad (15)$$

When there are no input signals,  $(p_{ir} - p_{il}) = 0$  and

$$(p_{ol} - p_{or}) = \frac{p_{cl} \left[ \frac{G_{pl}}{G_{pr}} - 1 \right] \sum_{i=1}^3 \frac{1}{Z_i}}{\frac{1}{Z_2} - \frac{1}{G_{pr}} \sum_{i=1}^3 \frac{1}{Z_i}} \quad (16)$$

It is essential for the stability of some feedback circuits that there be no output pressure difference when there is no input pressure difference. According to equation (16) this requirement is met if either the control pressure  $p_{cl}$  is zero or the gain ratio  $G_{pl}/G_{pr}$  is equal to one.

The control pressure,  $p_{cl}$ , cannot equal zero when the outputs and inputs operate at different reference levels. Therefore, the amplifier must be symmetrical. This is especially critical when the denominator of equation (16) is very small.

### 3.3 Proportional Amplifier and Passive Difference Junction

The component shown in figure 5a is called a passive difference junction. Its purpose is to convert the output pressure difference signal of the proportional amplifier into a pressure signal with atmospheric pressure as a reference.

In operation, the left- and right-side output pressures of the proportional amplifier become the inputs to the passive difference junction. The inputs are directed perpendicular to each other within the passive difference chamber. A single output is positioned downstream of the intersection of the jets to collect the fluid. This output signal  $p_o$  is related to the individual outputs of the proportional amplifier by

$$\begin{aligned} p_{ol} - p_{or} &= K p_o, \quad p_{ol} > p_{or} \\ 0 &= K p_o, \quad p_{ol} \leq p_{or} \end{aligned} \tag{17}$$

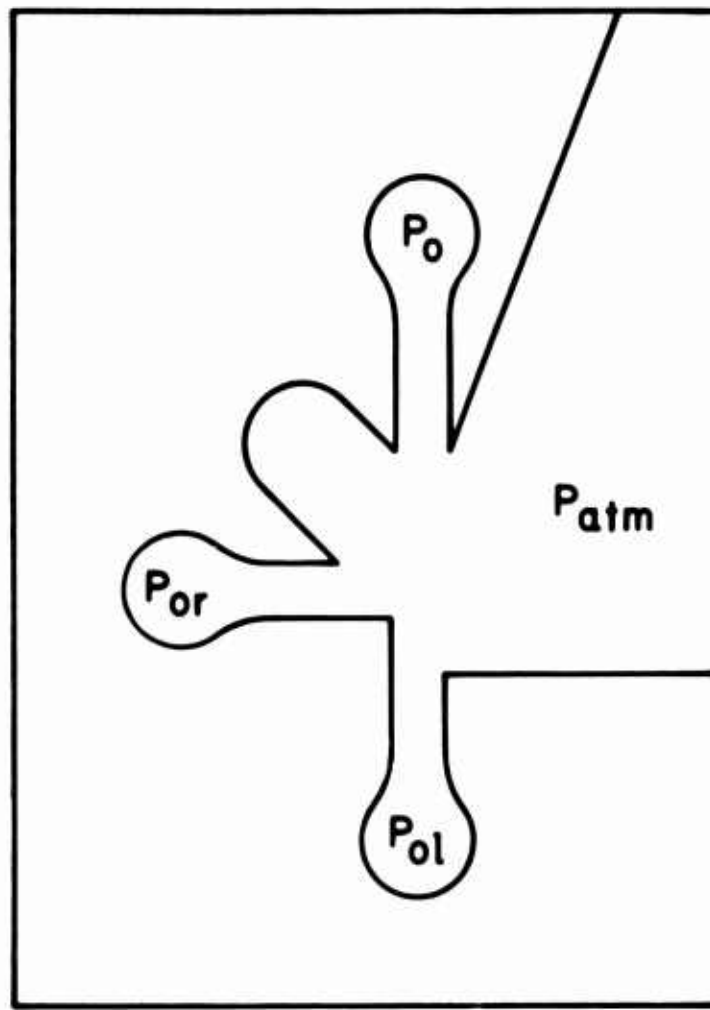
where  $p_o$  = total output pressure of the passive difference junction

$K$  = proportionality constant

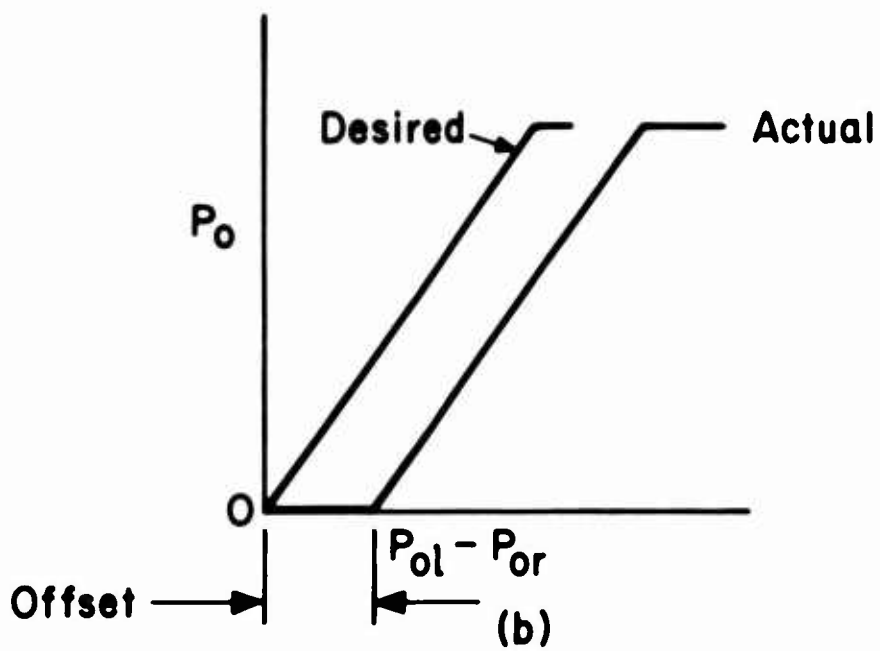
Figure 5(b) shows the desired performance and the actual performance of a passive difference junction. The offset is usually small but must be accounted for in the computation

Feedback circuits constructed using the proportional amplifier-passive difference junction combination, have no flow in the feedback loop when no input signal is applied to the proportional amplifiers. This differs from the case of the amplifier without the passive difference junction. Another advantage of the passive difference junction is that it eliminates half the passive components on which the computation depends.





(a)  
Geometry



(b)  
Characteristic

Figure 5 The Passive Difference Junction

The expression for the output of the difference junction may be written in terms of the proportional amplifier control pressures by combining equations (10) and (17).

$$K \Delta p_o = G_{pr} \Delta p_{cr} - G_{pl} \Delta p_{cl} \quad (18)$$

Finally, in the range of linear operation, the difference symbol  $\Delta$  may be dropped and equation (18) becomes

$$K p_o = G_{pr} p_{cr} - G_{pl} p_{cl} \quad (19)$$

#### 3.4 Proportional Amplifier and Passive Difference Junction with Feedback

On the circuit diagram shown in figure 6, all the impedances are considered lumped. This has been found to be a good approximation at low frequencies. In addition, the passive elements are assumed to be linear.

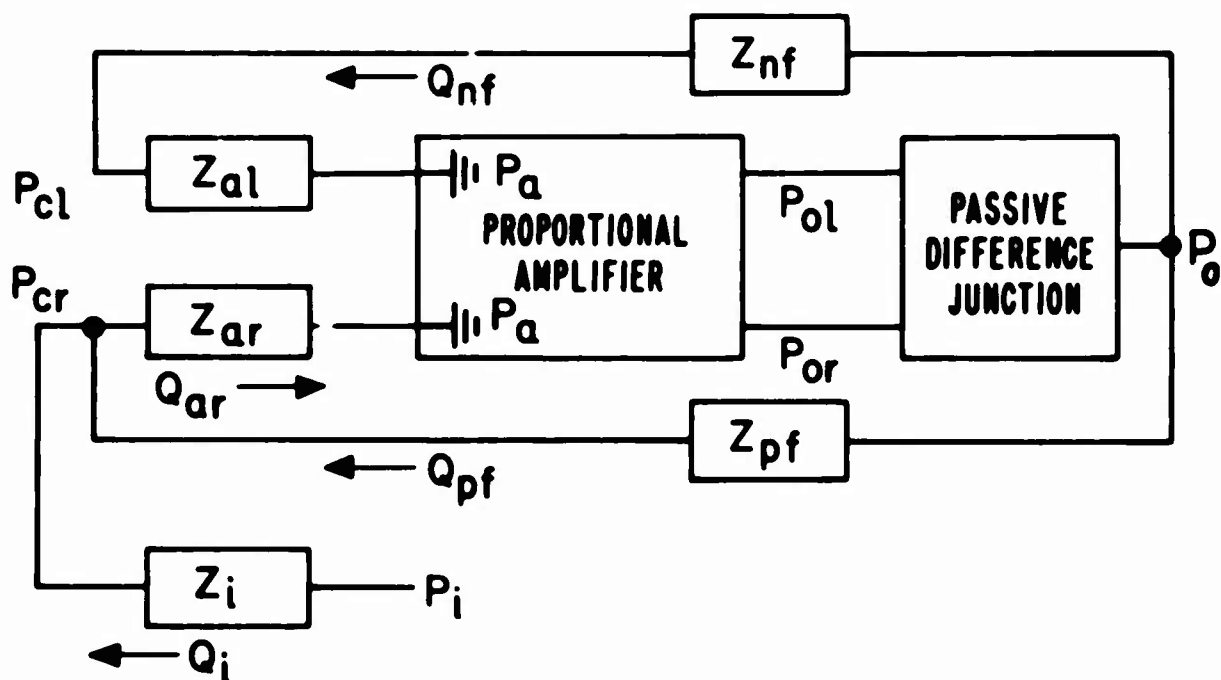
In figure 6, a proportional amplifier with input impedances,  $Z_{al}$  and  $Z_{ar}$ , is connected to a passive difference junction. The output of the difference junction is connected back to the inputs of the proportional amplifier through a positive feedback impedance,  $Z_{pf}$ , and a negative feedback impedance,  $Z_{nf}$ . The signal is applied to one input of the proportional amplifier through the forward loop input impedance,  $Z_i$ . This circuit can be analyzed using the continuity equation for incompressible flow. Thus

$$Q_{pf} + Q_i = Q_{ar} \quad (20)$$

where  $Q_{pf}$  = positive feedback volume flow

$Q_i$  = input volume flow

$Q_{ar}$  = amplifier right input volume flow



$Z_i$  = Forward loop input impedance

$Z_{al}$  = Left input impedance

$Z_{ar}$  = Right input impedance

$Z_{nf}$  = Negative feedback loop impedance

$Z_{pf}$  = Positive feedback loop impedance

$P_i$  = Input pressure signal

$P_a$  = Ambient pressure

$Q_i$  = Input volume flow

$Q_{ar}$  = Amplifier volume flow

$Q_{nf}$  = Negative feedback volume flow

$Q_{pf}$  = Positive feedback volume flow

**Figure 6** Proportional Amplifier and Passive Difference Junction  
With Feedback

The impedances are assumed linear, so equation (20) can be written in terms of pressure as

$$\frac{p_i - p_{cr}}{Z_i} + \frac{p_o - p_{cr}}{Z_{pf}} = \frac{p_{cr}}{Z_{ar}} \quad (21)$$

In the negative feedback loop, the feedback impedance and the amplifier left-input impedance are in series. The flow in the negative feedback path is given by

$$Q_{nf} = \frac{p_o - p_{cl}}{Z_{nf}} = \frac{p_{cl}}{Z_{al}} \quad (22)$$

If the left control pressure,  $p_{cl}$ , is eliminated between equations (19) and (22) the result is

$$p_{cr} = p_o \left[ \frac{G_{pl}}{G_{pr}} \left( \frac{Z_{al}}{Z_{al} + Z_{nf}} \right) + \frac{K}{G_{pr}} \right] \quad (23)$$

Substitution of (23) into (21) gives

$$\frac{p_o}{p_i} = \frac{1}{Z_i \left[ \left( \frac{K}{G_{pr}} + \frac{G_{pl}}{G_{pr}} \frac{Z_{al}}{Z_{al} + Z_{nf}} \right) \left( \frac{1}{Z_i} + \frac{1}{Z_{pf}} + \frac{1}{Z_{ar}} \right) - \frac{1}{Z_{pf}} \right]} \quad (24)$$

It is seen that the passive difference junction used in conjunction with an unsymmetrical amplifier gives zero output

for a zero input. With reference to equation (16), this is in contrast to the nonzero output of an unsymmetrical amplifier with feedback.

### 3.5 Description of Amplifiers

Two fluid amplifiers were used in the experiments, a two-stage and a five-stage cascade of proportional amplifiers designed for pressure gain (rather than for flow gain). All stages are identical in design (fig. 7 and 8).

Both the two- and the five-stage amplifiers have an aspect ratio of 2.5 (ratio of depth to power nozzle width).

For the two-stage amplifier the power nozzle widths are 0.020 in. and the control nozzle widths are .030 in.; for the five-stage device the power nozzles are 0.010 in. and the control nozzles are 0.015 in. The five-stage amplifier power nozzles are supplied from a common manifold. Supply pressure is applied to the last stage and is dropped successively through resistances before being fed to each of the other four stages.

The passive difference junctions used with the two- and five-stage amplifiers are shown in figures 5 and 9, respectively. The pressure gain curves for the amplifiers are shown in figures 10, 11, and 12.

The relation between output pressures and input pressures for the five-stage amplifier is shown in figures 11 and 12. The pressure gains of the left and right side are seen to vary. Thus the ratio of the pressure gains is not constant. The average right-side pressure gain is about 430 and the average left-side pressure gain is about 300. The gains of this five-stage unit are relatively low because of the resistances in series with control input nozzles of the first stage (fig. 8). This construction results in a linear amplifier input resistance of  $R_{al} = R_{ar} = 1.55 \text{ lbf-sec/in.}^5$

## 4 COMPUTATIONS

### 4.1 Scaling (Multiplication by a Constant)

The arrangement of the fluid components to perform scaling or multiplication by a constant is shown in figure 13a. This circuit contains fluid resistors, a proportional fluid amplifier, and a passive difference junction. The electrical analog is diagrammed in figure 13b, which is equivalent to the feedback circuit of figure 6 with infinite positive feedback impedance ( $Z_{pf} = \infty$ ). The ratio

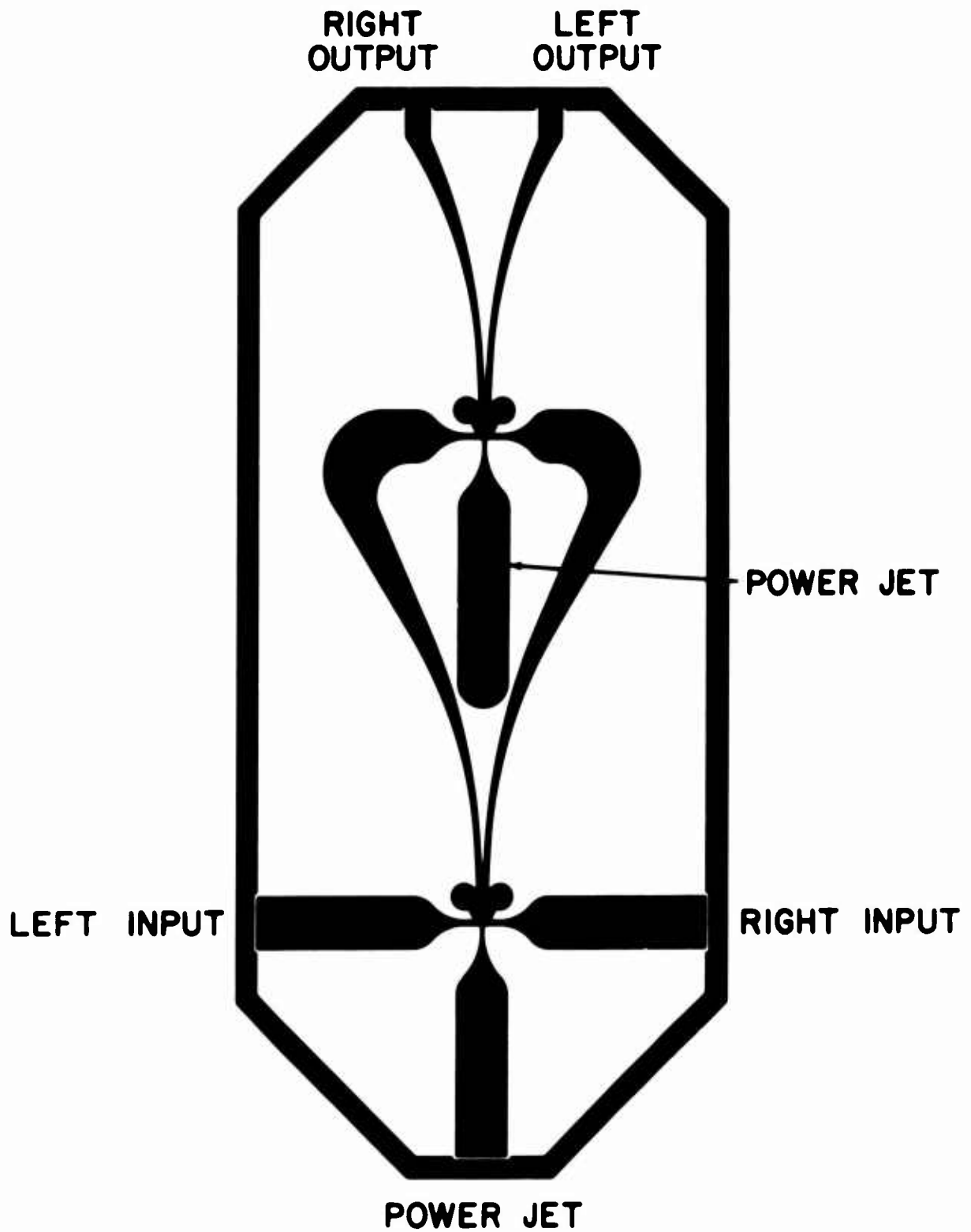
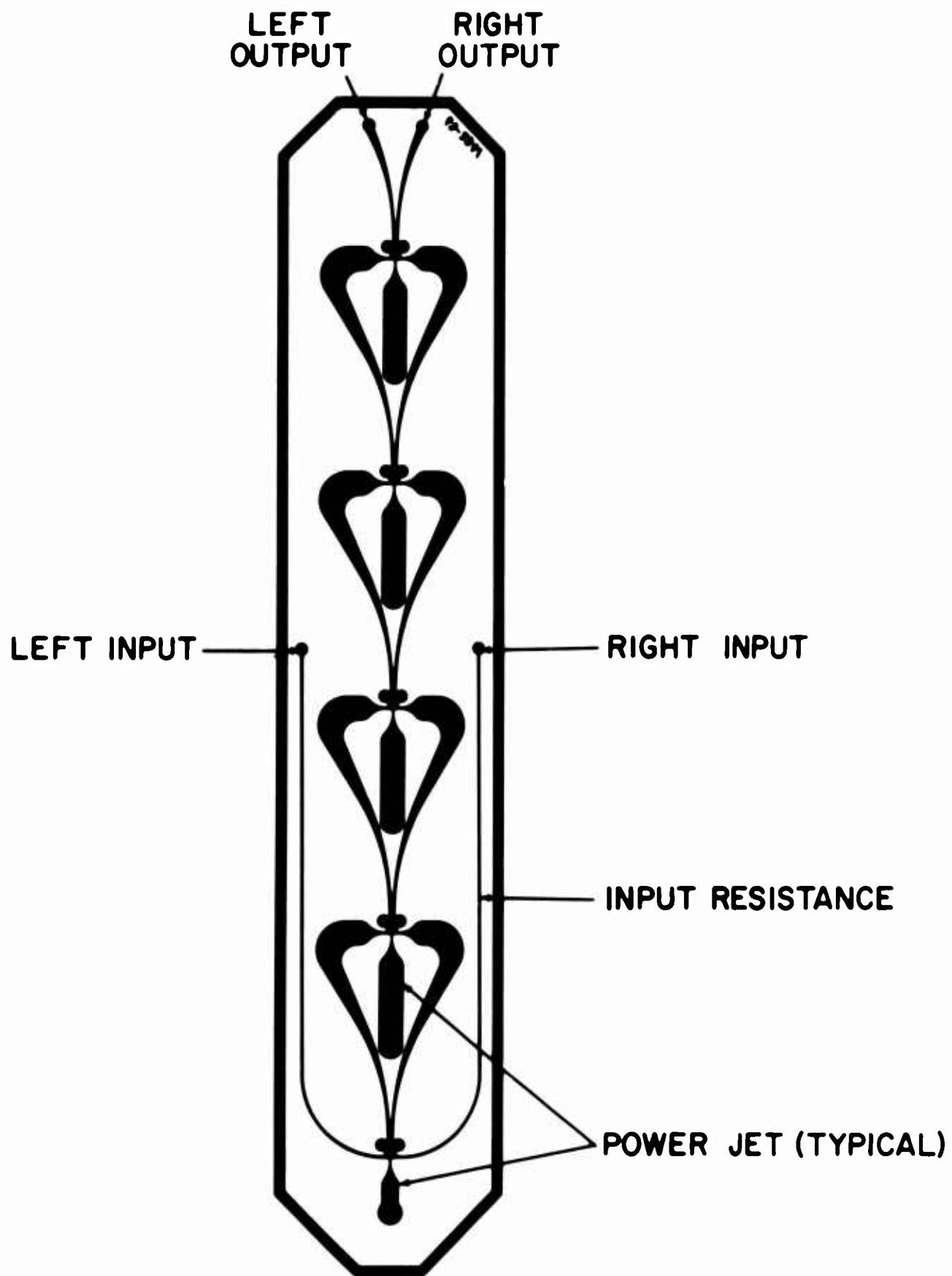
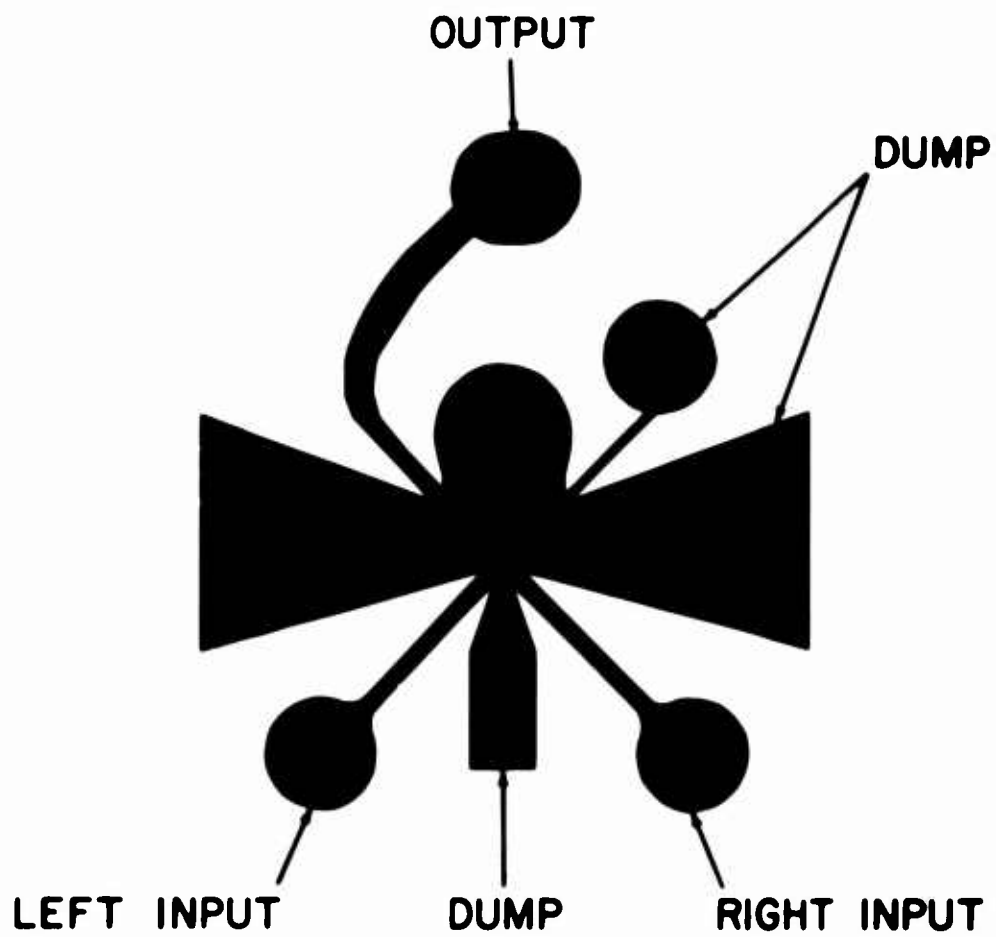


Figure 7 Two Stage Proportional Fluid Amplifier



**Figure 8**     **Five Stage Proportional Fluid Amplifier**



**Figure 9**    **Passive Difference Junction**



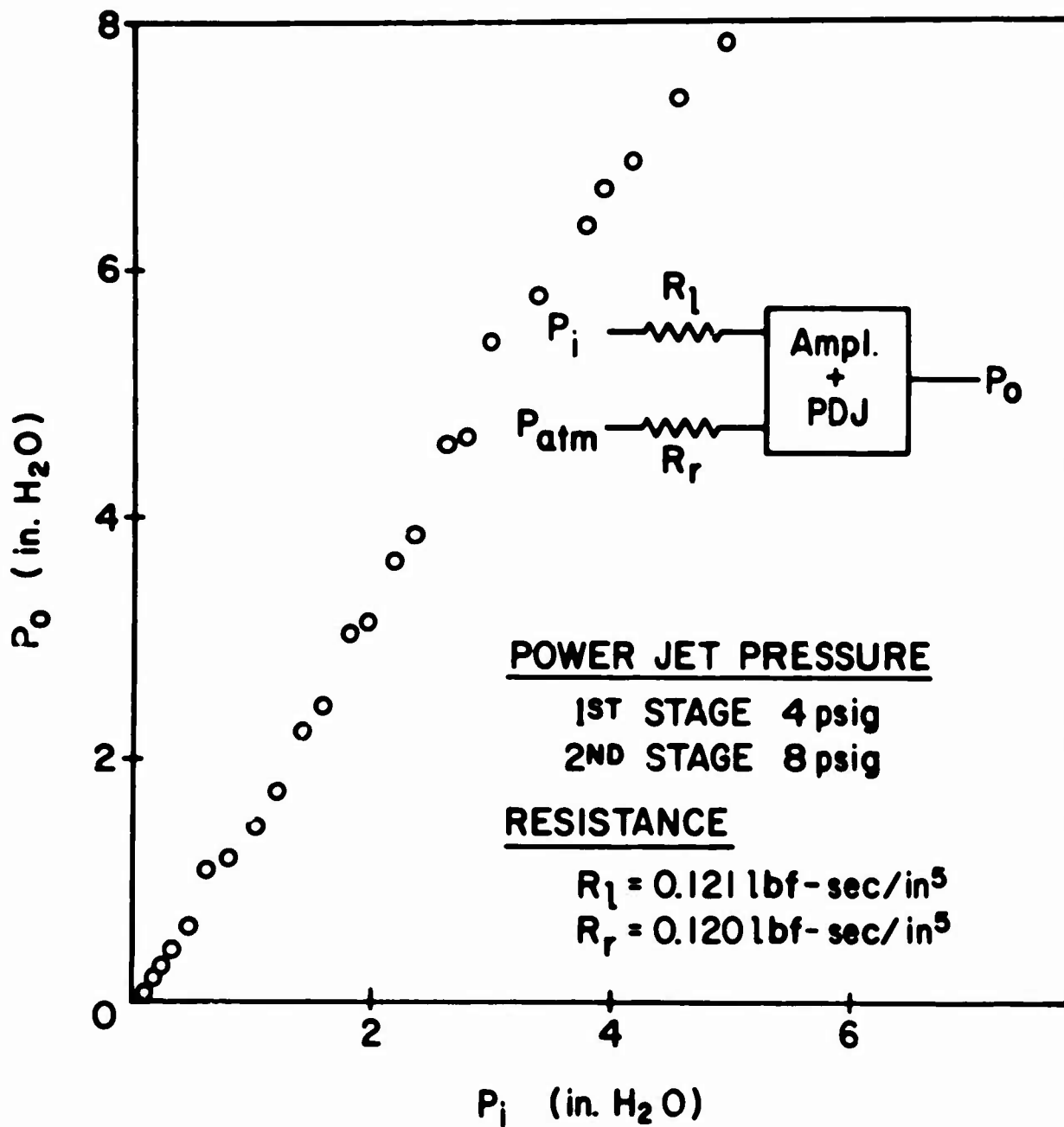


Figure 10 Pressure Gain of the Two Stage Proportional Amplifier With Passive Difference Junction (PDJ)

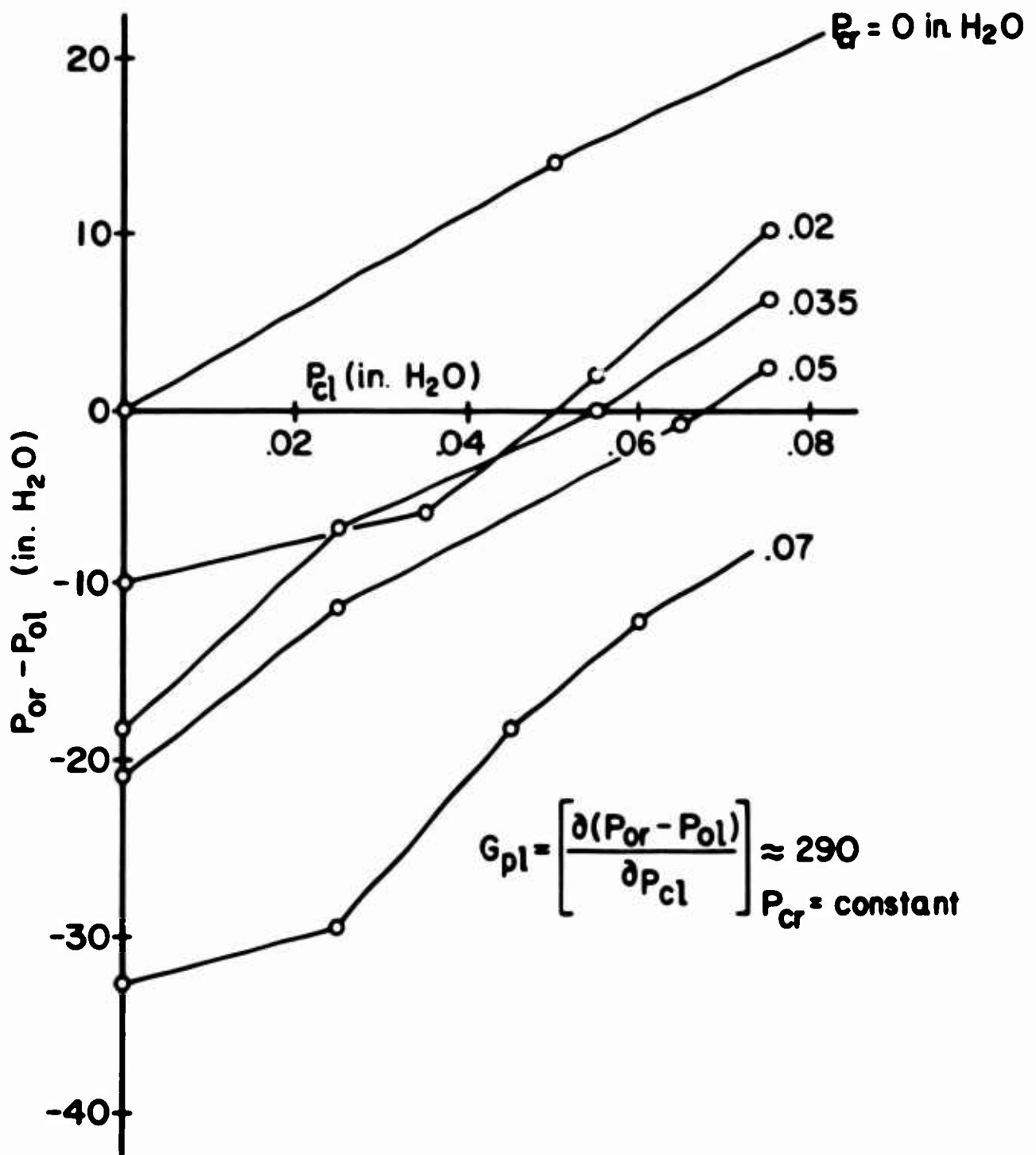
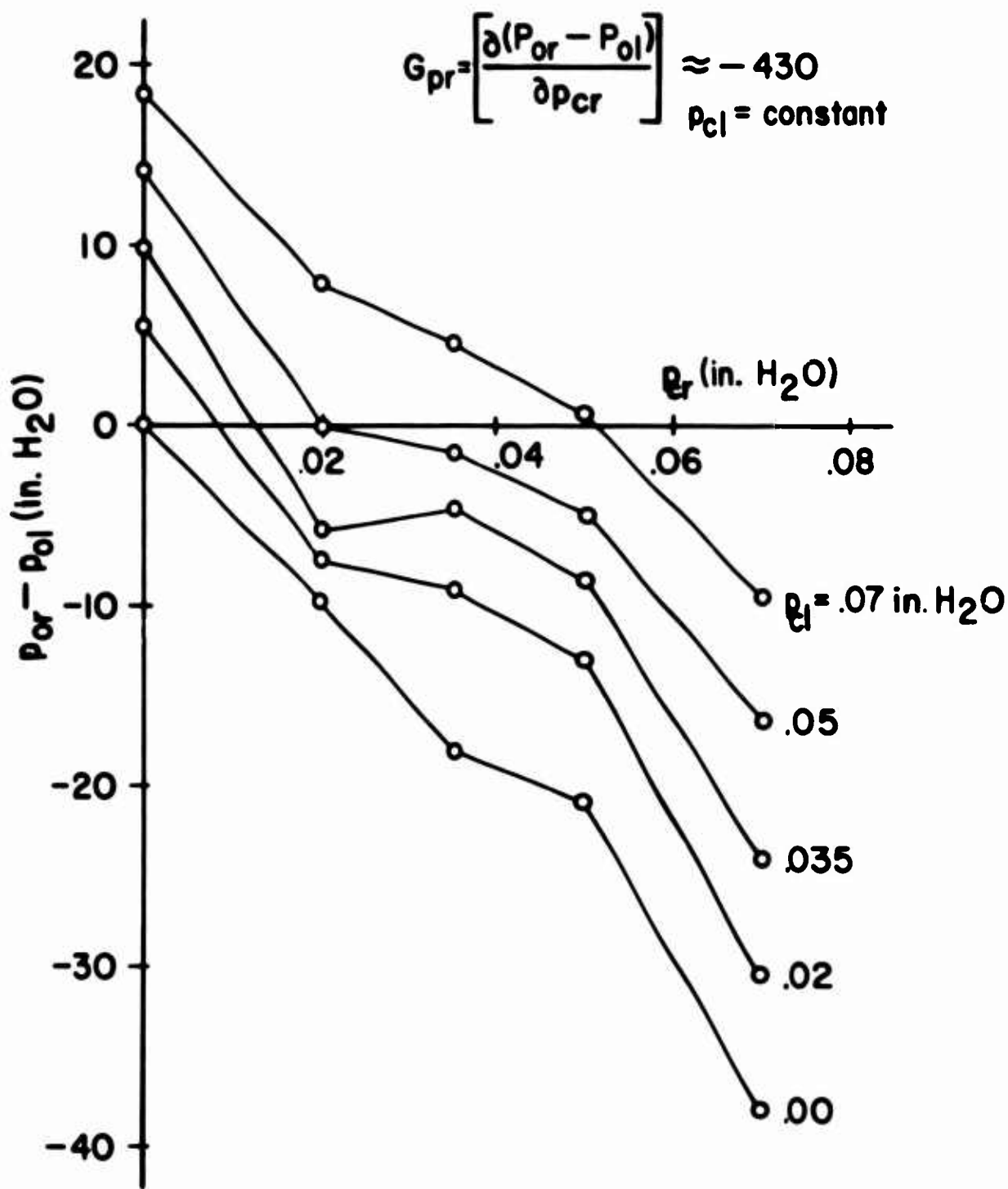
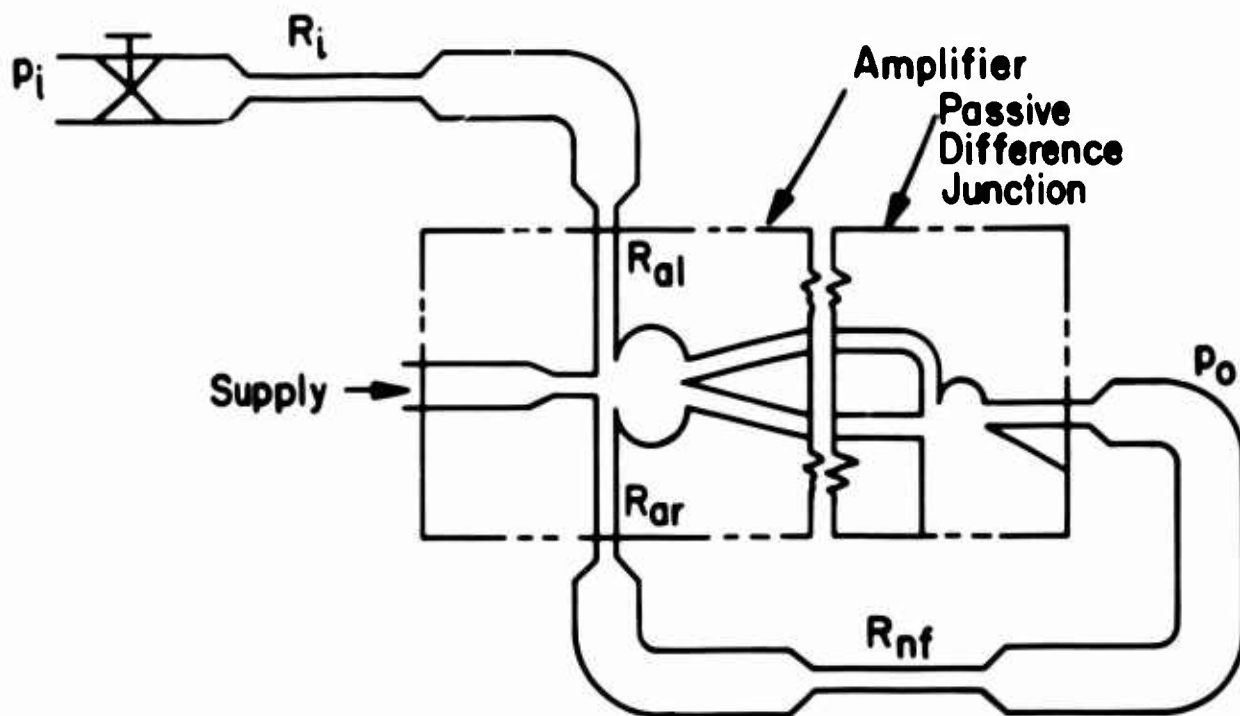


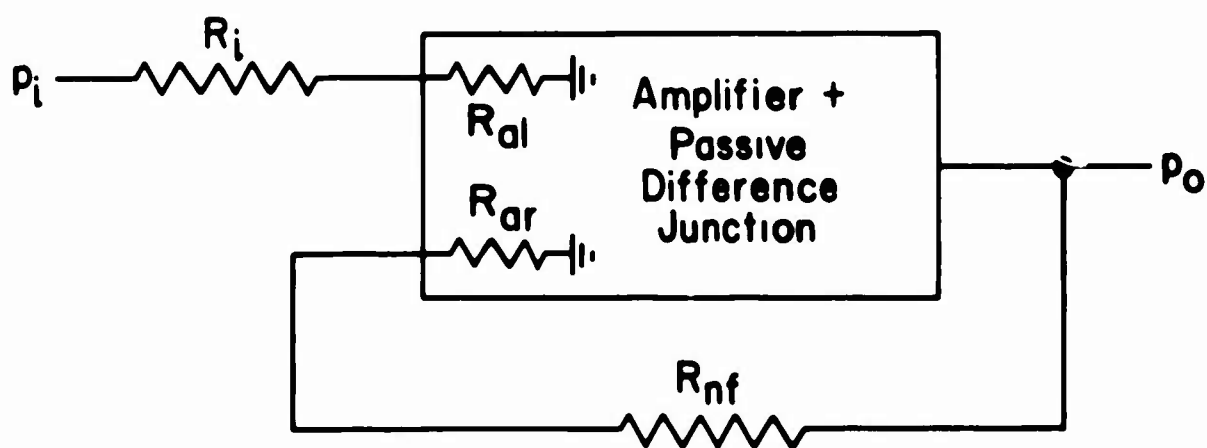
Figure 1.1 Pressure Gain of the Five Stage Proportional Fluid Amplifier - Left Side



**Figure 12**      **Pressure Gain of the Five Stage Proportional Fluid Amplifier - Right Side**



(a)  
Fluid Circuit



(b)  
Electrical Analog

Figure 13 Scaling Circuit

of output pressure,  $p_o$ , to input pressure,  $p_i$ , is obtained from equation (24) by substituting resistances for the unknown impedances. This yields

$$\frac{p_o}{p_i} = \frac{R_{nf} + R_{al}}{R_i + R_{ar}} \left[ \frac{1}{\left(\frac{K}{G_{pr}}\right) \frac{R_{al} + R_{nf}}{R_{ar}} + \left(\frac{G_{pr}}{G_{pr}}\right) \frac{R_{al}}{R_{ar}}} \right] \quad (25)$$

The cascaded five-stage proportional amplifier was used for the scaling operation. The power jet pressures used were 0.06, 0.12, 0.40, 1.28, and 5.26 psig.

Since the experimentally determined pressure gain ratio  $G_{pl}/G_{pr}$  varied widely, it was decided to compare the experimental scaling operation with the theory by assuming a symmetrical amplifier. Equation (25) then reduces to

$$\frac{p_o}{p_i} = \frac{R_{nf} + 1.55}{R_i + 1.55} \quad (26)$$

where  $R_{al} = R_{ar} = 1.55 \text{ lbf-sec/in}^5$ ,  $K = 1$ ,  $\frac{K}{G_p} \frac{R_{al} + R_{nf}}{R_{ar}} \ll 0$

With  $R_i = 0.60 \text{ lbf-sec/in}^5$ , the negative feedback resistor,  $R_{nf}$ , is varied from 1.94 to 23.12 lbf-sec/in<sup>5</sup>. This is equivalent to multiplications from 1.6 to 10.6. The results of this experiment are shown in figures 14 and 15 along with the theory predicted by equation 26.

#### 4.2 Integration

The choice of a circuit to perform integration is limited by the types of passive components available. One possibility is the "bootstrap" integrator circuit shown in figure 16a. (ref. 3) This circuit contains fluid resistors, a fluid capacitor, a proportional fluid amplifier and a passive difference junction. The electrical analog of this circuit is shown in figure 16b. In this integrator regenerative or positive feedback is used to boost the pressure in the tank by an amount equal to the difference between true integration and RC integration. The impedances in figure 6 are replaced by resistors except for one amplifier input impedance (either right

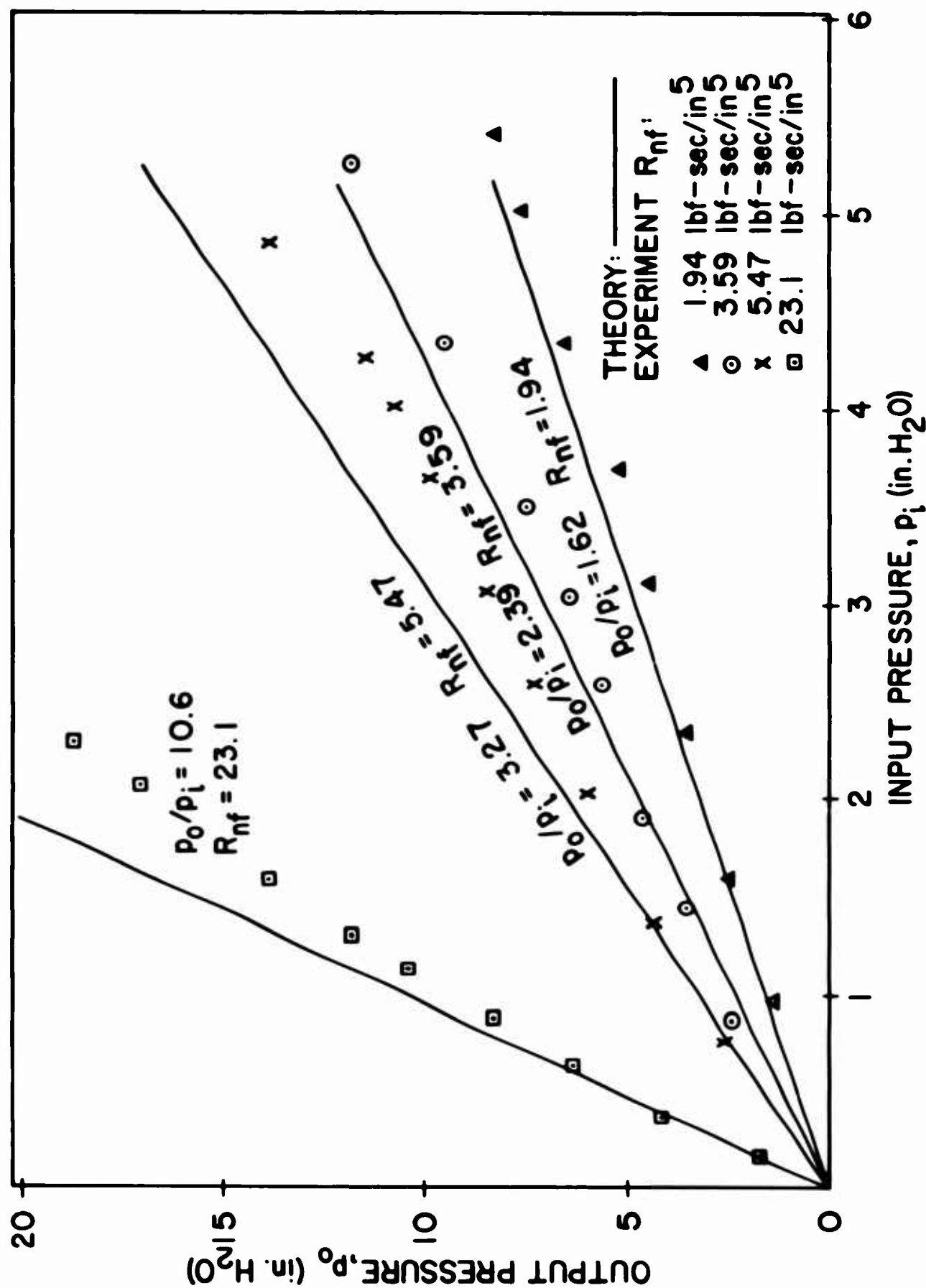


Figure 14 Comparison of Experimental and Theoretical Scaling  
Signal to Right Control With  $R_a=1.55$  and  $R_i=0.60$  lb-sec/in<sup>5</sup>

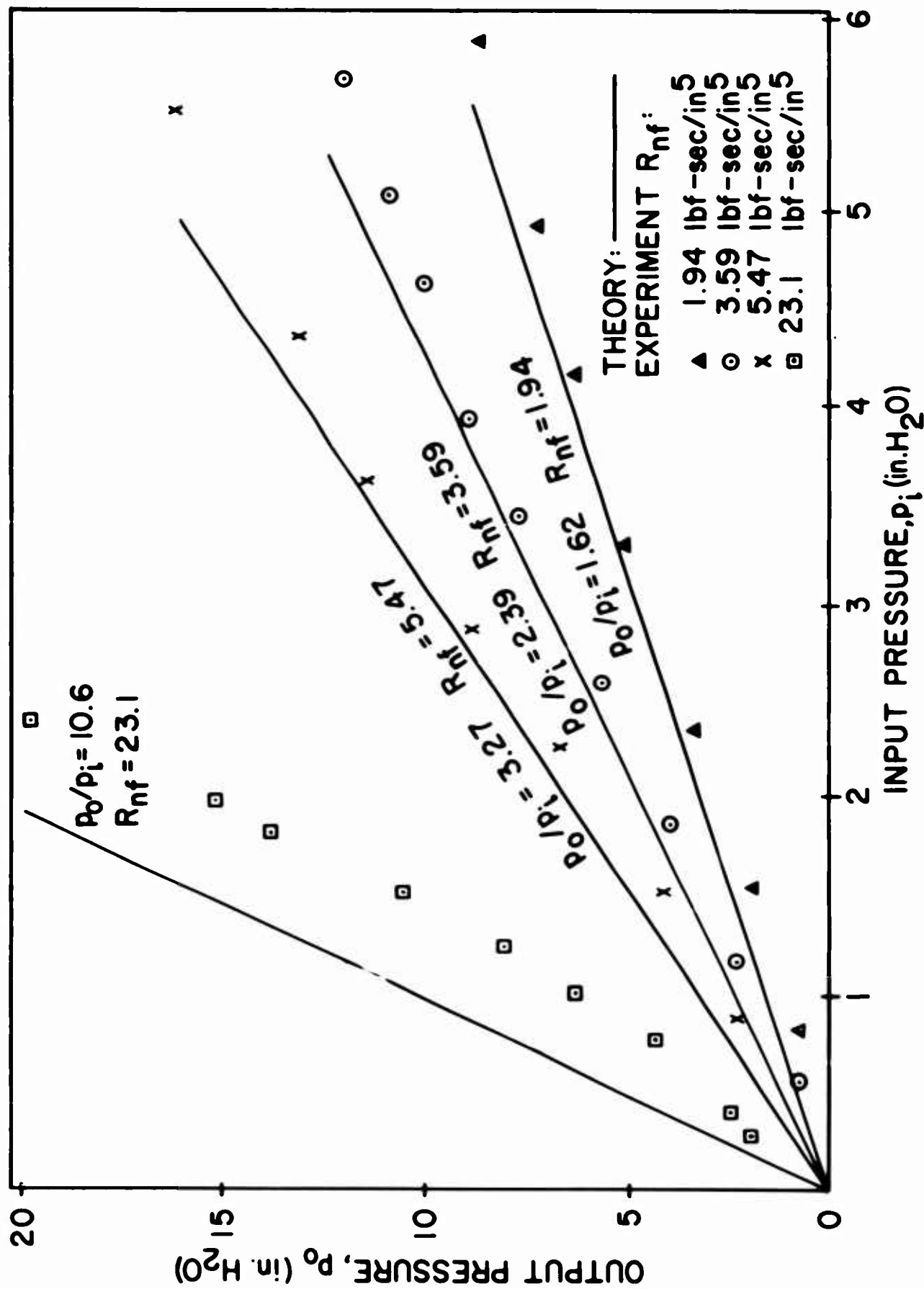
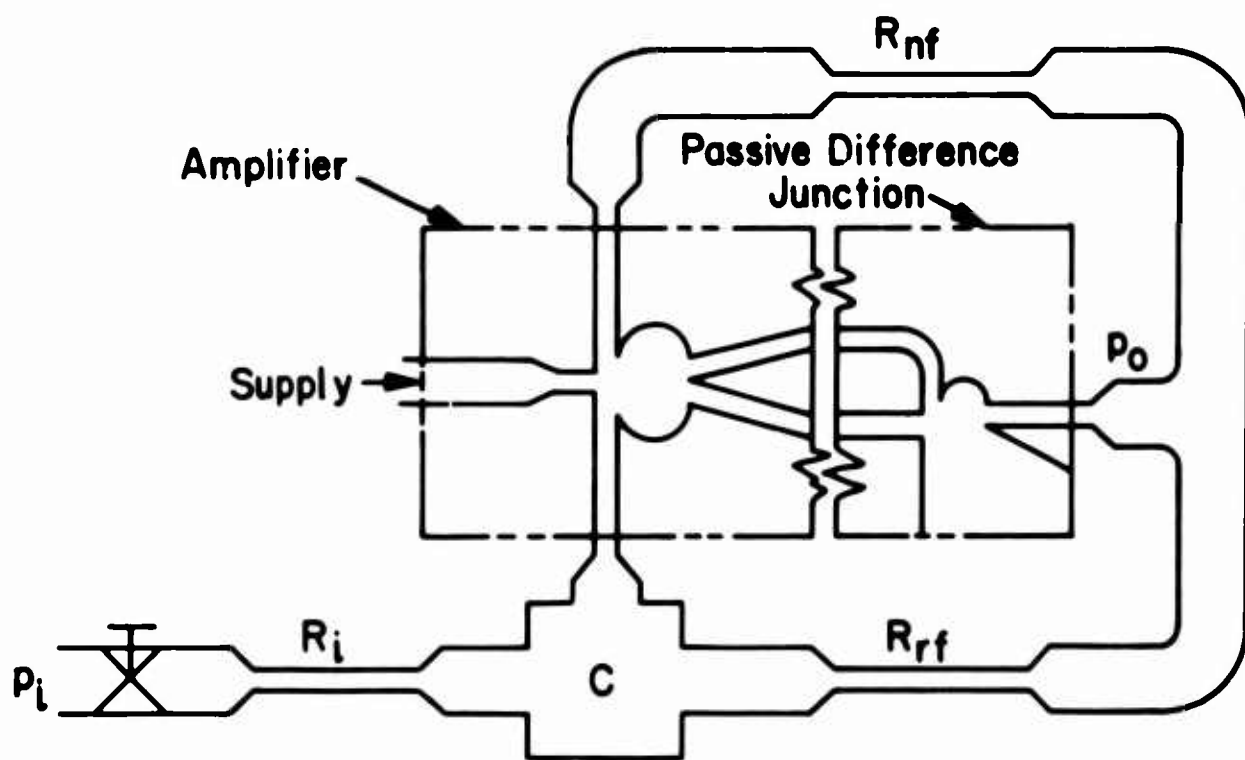
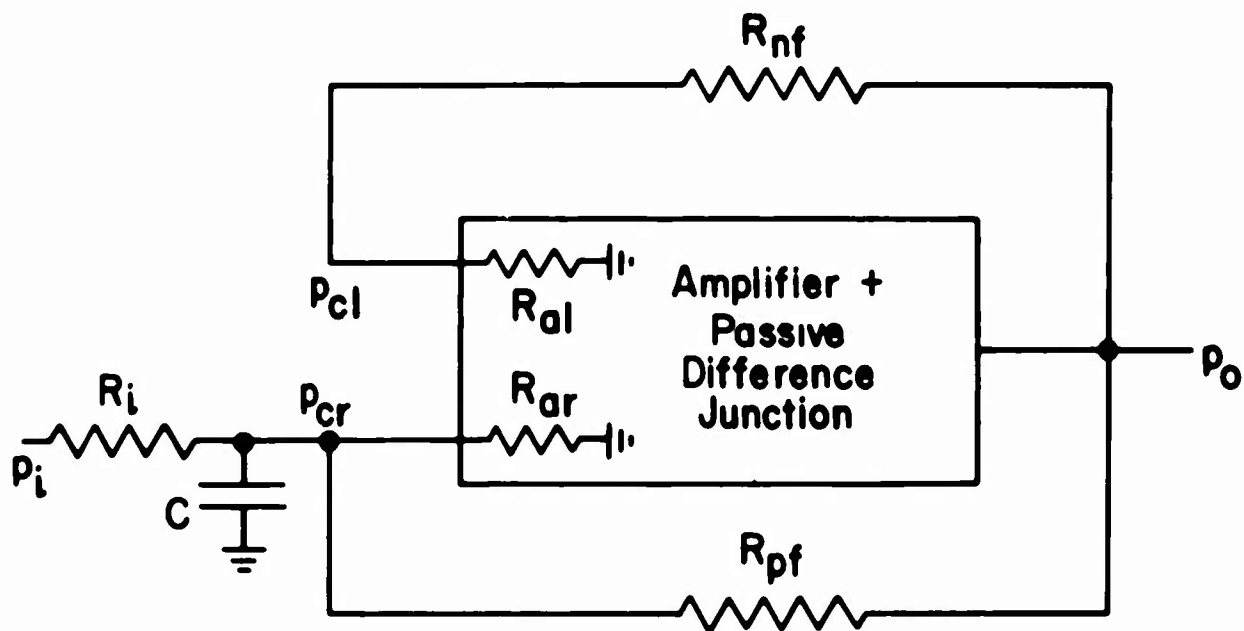


Figure 15 Comparison of Experimental and Theoretical Scaling

Signal to Left Control With  $R_a=1.55$  and  $R_l=0.60$  lbf-sec/in<sup>5</sup>



(a)  
Fluid Circuit



(b)  
Electrical Analog

Figure 16

Integrating Circuit



or left). This input impedance is replaced by the parallel combination of a resistor and a capacitor to ground. This is expressed mathematically as

$$Z_{ar} = \frac{R_{ar}}{R_{ar}Cs + 1} \quad (27)$$

Substituting equation (27) into equation (24) and changing the other impedances into resistances yields

$$\frac{p_o}{F_i} = \frac{1}{R_i Cs \left[ \frac{K}{G_{pr}} + \frac{R_{al}}{R_{al} + R_{nf}} \frac{G_{pl}}{G_{pr}} \right] + \left[ \left( \frac{K}{G_{pr}} + \frac{G_{pl}}{G_{pr}} \frac{R_{al}}{R_{al} + R_{nf}} \right) \left( 1 + \frac{R_i}{R_{pf}} + \frac{R_l}{R_{ar}} \right) - \frac{R_l}{R_{pf}} \right]} \quad (28)$$

When the input pressure,  $p_i$ , is a step function, the solution of equation (28) is

$$\frac{p_o}{p_i} = \frac{1}{B} \left[ 1 - e^{-\frac{Bt}{\tau}} \right] = \frac{t}{\tau} - \frac{B}{2} \left( \frac{t}{\tau} \right)^2 + \frac{B^2}{6} \left( \frac{t}{\tau} \right)^3 - \dots \quad (29)$$

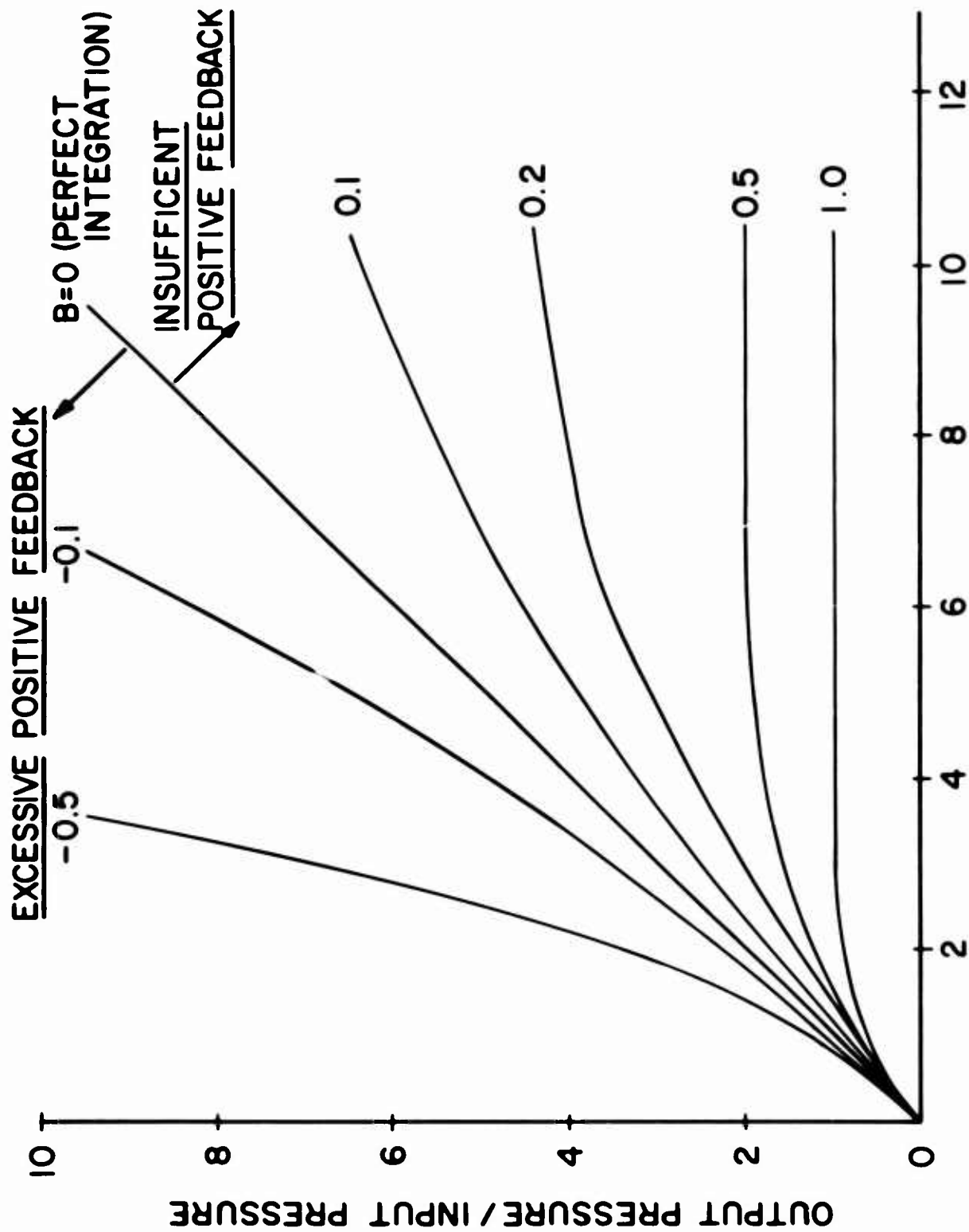
where

$$B = \left[ \left( \frac{K}{G_{pr}} + \frac{R_{al}}{R_{al} + R_{nf}} \frac{G_{pl}}{G_{pr}} \right) \left( 1 + \frac{R_i}{R_{pf}} + \frac{R_l}{R_{ar}} \right) - \frac{R_l}{R_{pf}} \right]$$

and

$$\tau = R_i C \left[ \frac{K}{G_{pr}} + \frac{R_{al}}{R_{al} + R_{nf}} \frac{G_{pl}}{G_{pr}} \right]$$

When  $B = 0$ , true integration results. The theoretical effect of  $B \neq 0$  on the integration of a step is shown in figure 17. Positive values of  $B$  indicate that there is not enough positive feedback. Negative values of  $B$  indicate an excess of positive feedback. The resistances can always be adjusted so that  $B$  is zero as long as an active component with positive forward loop pressure gain greater than unity is available. Without this



**DIMENSIONLESS TIME RATIO  $t/\tau$**

**Figure 17** Effect of Positive Feedback on the Accuracy of Integration of a Step Input

active component a physically unrealizable negative resistive component would be required. Figure 18 demonstrates this same point experimentally. Here, a step input is supplied to the circuit with and without positive feedback. The result is as predicted theoretically by equation (29).

Two integrators were constructed. One used the two-stage amplifier with passive difference junction ( $G_p = 1.75$ ). In this case there was a small offset (fig. 5b). The other used the five-stage amplifier with passive difference junction ( $G_p = 350$ ). The circuit with the two-stage amplifier used only positive feedback ( $R_{nf} = \infty$ ). This arrangement has the advantage of eliminating the symmetry problem. However, the quality of the integration depends on the pressure gain remaining constant. Under this condition, with the resistors adjusted to make  $B$  equal to zero, equation (28) becomes

$$\frac{p_o}{p_i} = \frac{G_p}{KR_iCs} \quad (30)$$

In these tests, the capacitance had a volume of approximately 200 in.<sup>3</sup>. The equivalent capacitance was 13.52 in.<sup>5</sup>/lbf. The forward loop resistance  $R_1$  was chosen as 1.936 lbf-sec/in.<sup>5</sup>, and  $K = 1$ . Substituting these values into equation (30) results in

$$p_o = \frac{1.75}{(13.52)(1.936)} \int p_i dt = 0.0667 \int p_i dt \quad (31)$$

When  $p_i$  is a step pressure, equation (31) may be plotted as the output pressure against time for various input levels. This is shown in figure 19 along with the experimental data. The theory has been adjusted to include the initial offset. The response to a pulse of finite width is shown in figure 20. The output does not continue to rise during the second pulse because the amplifier has reached saturation.

The integrator formed with the higher gain five-stage amplifier used both positive and negative feedback. In this arrangement the magnitude of the gain can vary without causing appreciable effects on the integration. Theoretically the integration depends solely on passive components. However, the disadvantage here is that the symmetry of the amplifier becomes a major factor. Equation (28) with the assumption of a high gain symmetrical amplifier becomes

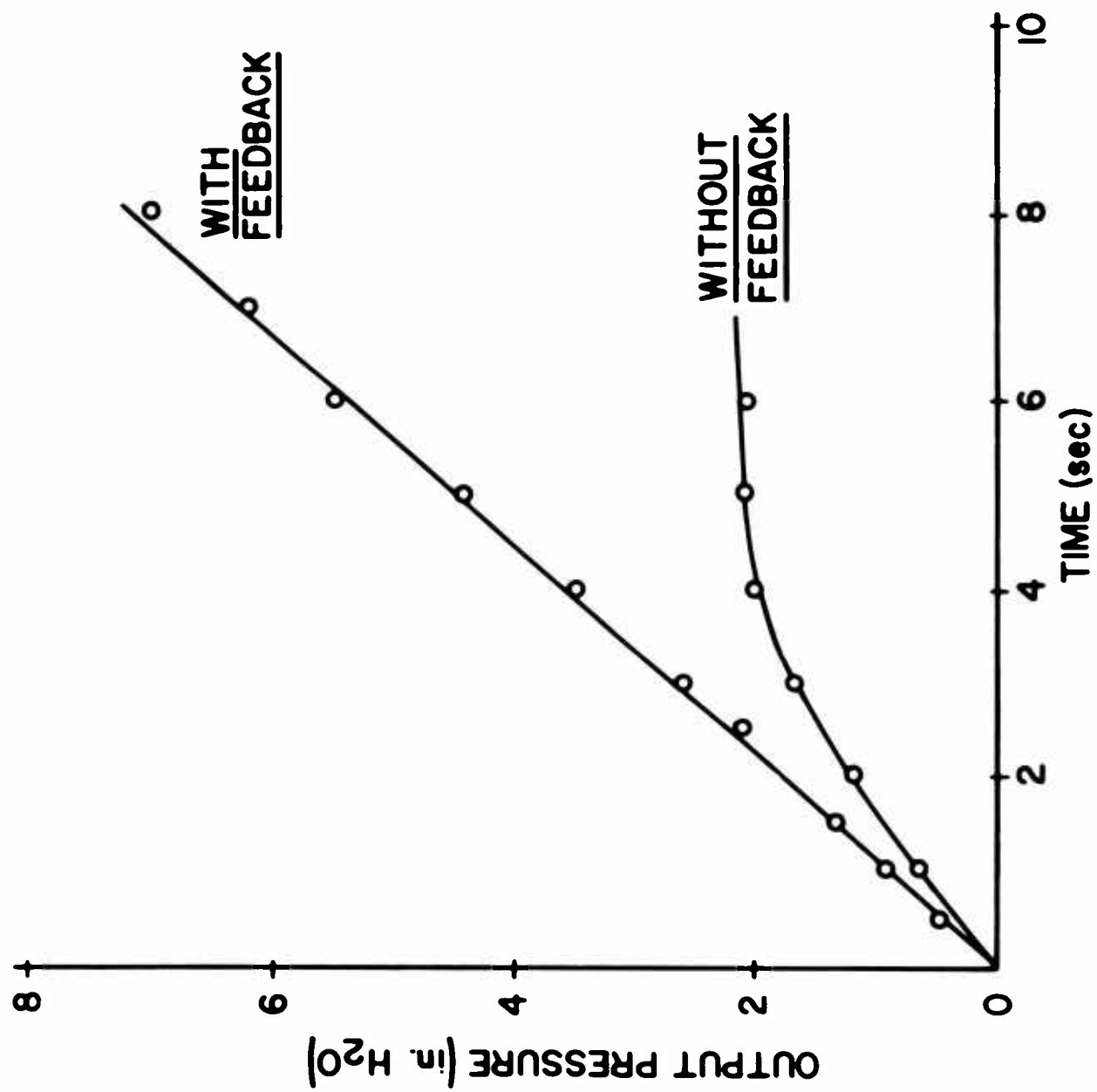


Figure 18 Experimental Comparison of Integration Circuit

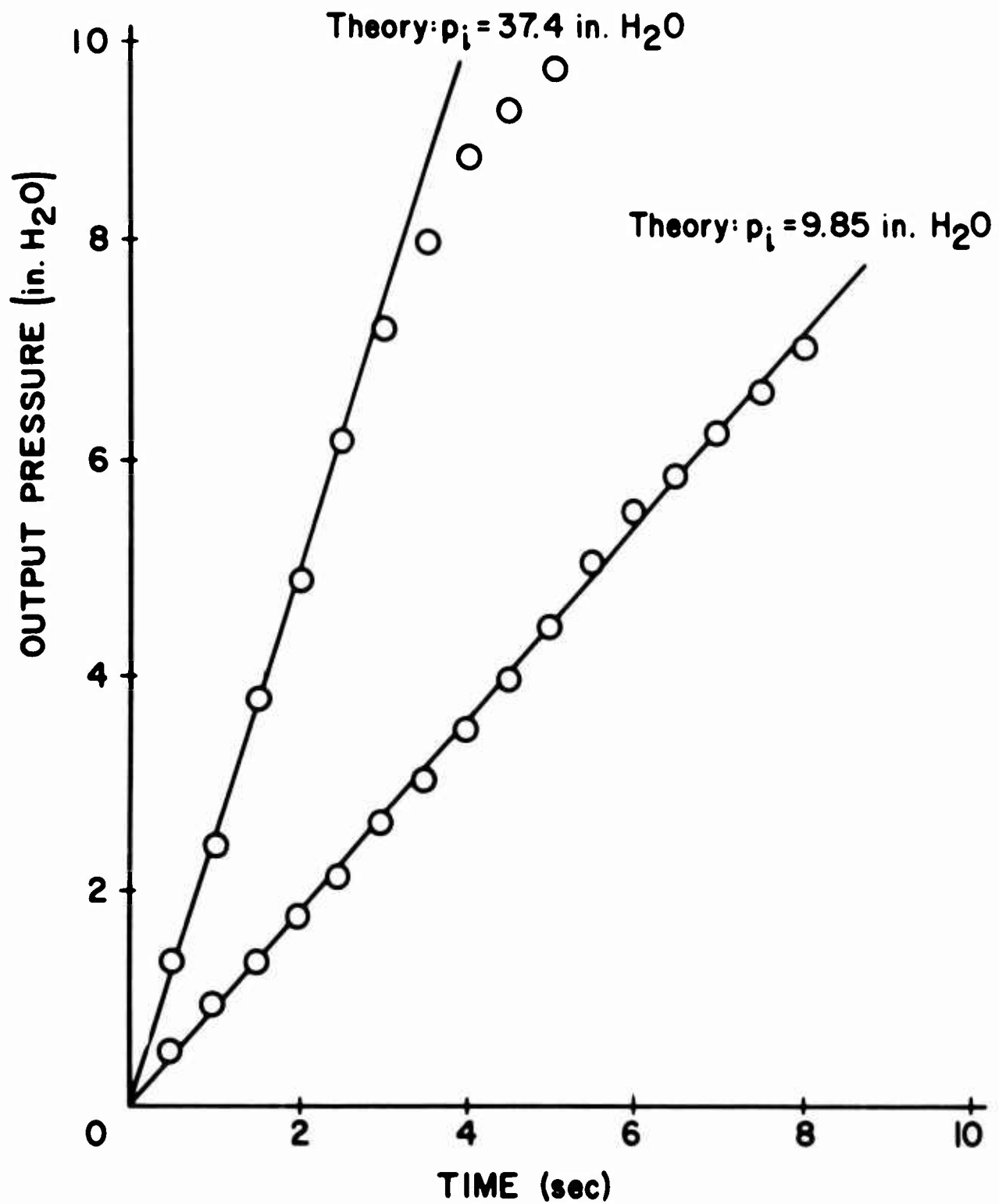


Figure 19 Comparison of Experimental and Theoretical Integration of a Step Input - Two Stage Amplifier

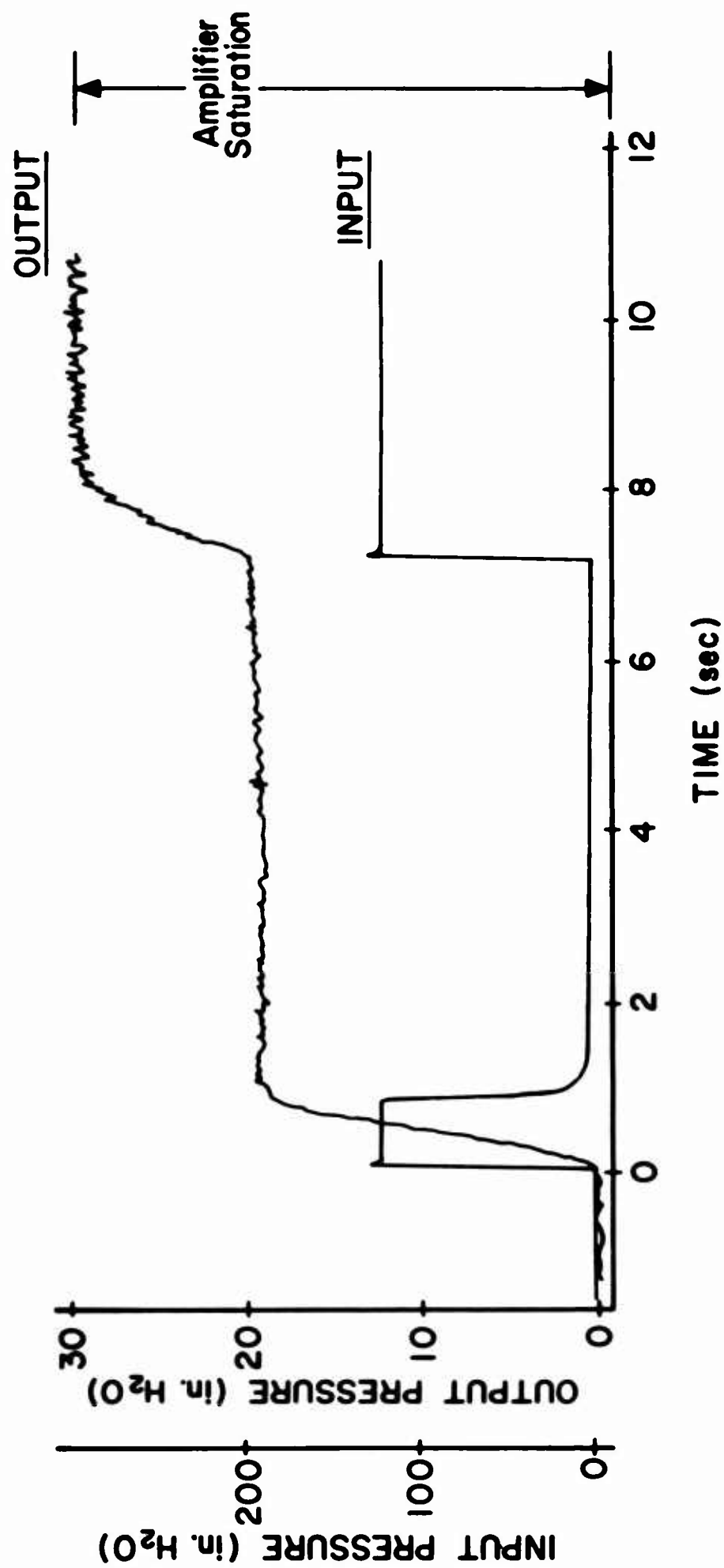


Figure 20 Integrator Response to a Step Input - Two Stage Amplifier

$$\frac{p_o}{p_i} = \frac{1}{R_i C_s} \frac{R_{al} + R_{nf}}{R_{al}} \quad (32)$$

when the resistances are adjusted to make  $\beta$  equal to zero.

In this integrator,  $R_i$  was chosen equal to 2.45 lbf-sec/in.<sup>5</sup>  $R_{nf}$  was taken as 1.94 lbf-sec/in.<sup>5</sup>. Substituting these values into equation (32) yields

$$p_o = \left[ \frac{1.55 + 1.94}{1.55} \right] \left[ \frac{1}{(2.45)(13.52)} \right] \int p_i dt = 0.068 \int p_i dt \quad (33)$$

This equation is plotted in figure 21 for various step pressure levels of the input pressure. The experimental values are also shown.

## 5 DISCUSSION

The experimental results of the scaling operation are compared with the theoretical predictions in figures 14 and 15. Figure 14 presents the data when the input pressure signal is applied to the right side with feedback to the left side; in the data of figure 15 the input and feedback sides were reversed. These results, which agree in a general way, clearly indicate that the overriding influence on accurate computation is the lack of symmetry rather than the relatively low pressure gain of the amplifier. It is believed that more symmetrical amplifiers and matched pairs of accurate resistive components will perform accurate scaling operations without the passive difference junction. Scaling does not present any stability problems in the low operating frequency range.

Integration, on the other hand, presents much more difficult problems. The limitation on useful passive fluid components has led to the adoption of circuitry with positive feedback. The stability has been maintained artificially through the use of the passive difference junction. Figures 19 and 21 compare theory and experiment for two modes of integration. In one mode, the integra-

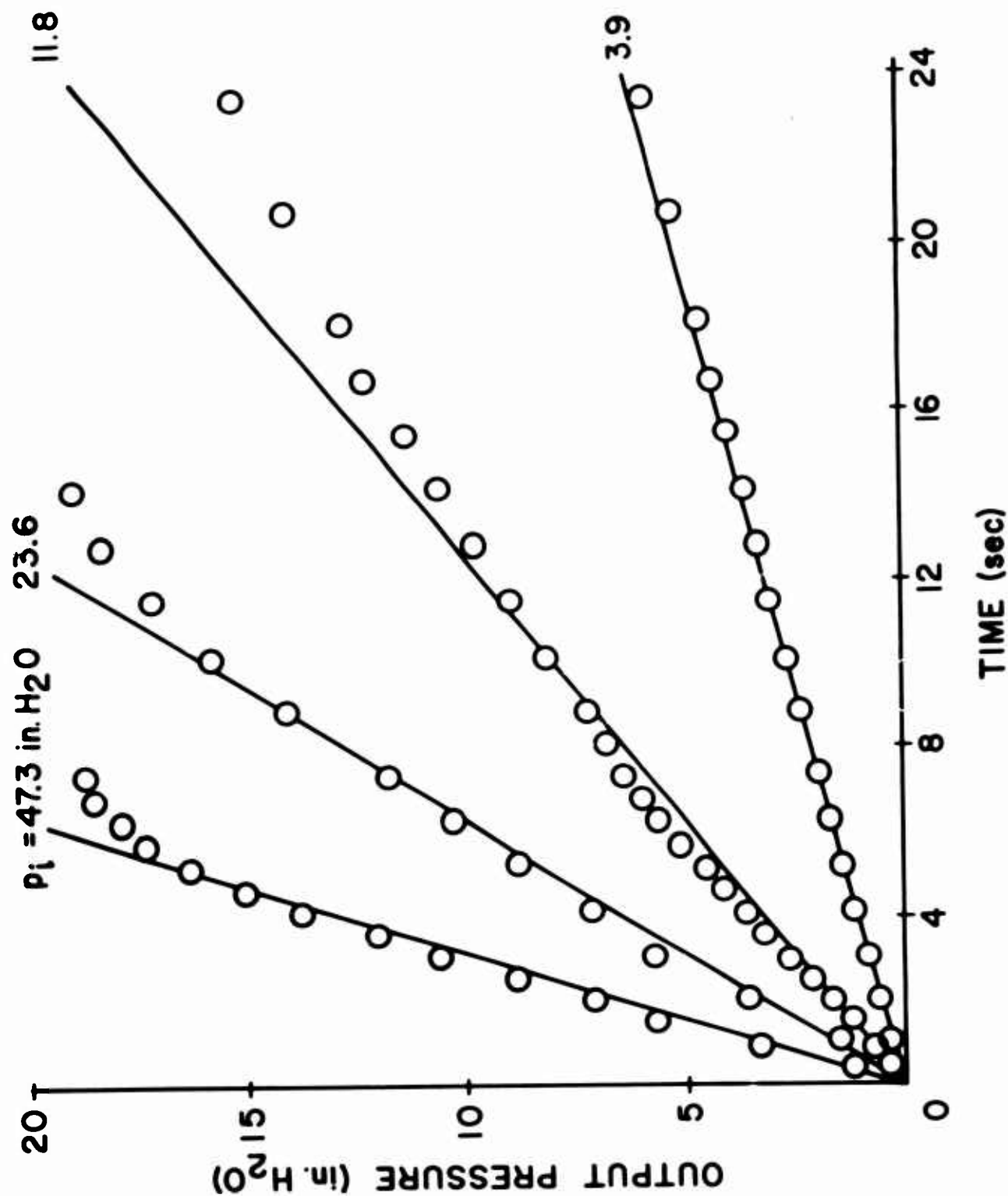


Figure 21 Comparison of Experimental and Analytical Integration of Various Step Input Pressures - Five Stage Amplifier



tion is dependent to a large degree on the symmetry of the amplifier, but not significantly on the magnitude of the gain. It is desirable in analog computation to make the computation independent of the amplifier gain so that this mode is preferable. In both modes the agreement between theory and experiment is good. However, the use of the passive difference junction results in a great sacrifice in versatility. Thus only positive integration is possible as the amplifier proceeds monotonically toward saturation. This component prevents negative integration. To perform both positive and negative integration, the amplifier must be operated entirely as a differential amplifier. This requires perfect symmetry or the integrator will be unstable at low frequencies. It is believed that in this case the accuracy of integration will have to be exchanged for increased stability.

It

It is recognized that a very important consideration, the dynamic performance of the components, has not been mentioned. At the present time the transfer functions for the proportional amplifier have not been measured. Work along this line is planned. However, in the present tests, passive components were chosen such that the time constants were several orders of magnitude higher than the expected amplifier time constant. In addition transport times through the components were short so that the lumped parameter circuit theory was closely approximated.

The dynamic range of these computer circuits is between 50 and 100. This is the ratio of the largest possible signal to the smallest signal discernible above noise.

## 6 CONCLUSIONS

The operations of scaling and integration have been performed with no mechanical moving part fluid components. The agreement between theory and experiment is only fair. The discrepancies are attributed mainly to the lack of symmetry in the proportional amplifiers rather than to relatively low pressure gain values.

Due to the nonexistence of a no-moving-part fluid blocking capacitor, a positive feedback circuit (the bootstrap integrator) was used for integration. This circuit has poor stability in the low frequency range where the proportional amplifier operates. Stability was established artificially with a new component, the passive difference junction, but computational versatility was sacrificed.

## REFERENCES

1. Warren, R. W., and Peperone, S. J., "Fluid Amplification 1. Basic Principles," TR-1039, Diamond Ordnance Fuze Laboratories, August, 1962.
2. Peperone, S. J., Katz, S., and Goto, J. M., "Fluid Amplification 4. Gain Analysis of the Proportional Fluid Amplifier," TR-1073, Diamond Ordnance Fuze Laboratories, October, 1962.
3. Korn and Korn, "Electronic Analog Computer," McGraw-Hill, 1956.

## A FLUID ENCODING SYSTEM

The development of an encoding system using pure fluid devices is described. The system consists of three portions: a device to quantize an angular rotation into incremental digital fluid signals, a logic section to shape the fluid pulses, a section to sense direction of rotation and a bidirectional counter. The input to the counter is the angular position in quanta from the point at which the counter is reset. The counter sums algebraically the number of feedback pulses received. A slotted disk, rotating between two sets of opposed nozzles, is employed as the quantizer. The slots, equally spaced circumferentially, allow fluid flow from supply nozzle to receiver nozzle while the spaces between slots inhibit such flow. The outputs of the receiver nozzles are fed to pulse forming circuitry and logical gating which senses direction of rotation. The fluid pulses from this section are gated to the appropriate input of a bidirectional counter. The counter is comprised of T or trigger memory elements in addition to the necessary logical gating elements.

The speed of operation and sensitivity relationships will be discussed. Experimental verification of the design will be presented which demonstrates the advantages and disadvantages of this type of digital position transducer.

# **FEASIBILITY STUDY OF A FLUID AMPLIFIER** **STEAM TURBINE SPEED CONTROL**

By W. A. Boothe, Project Engineer  
Advanced Technology Laboratories  
General Electric Company  
Schenectady, N. Y.

(For presentation at the Second Fluid Amplification Symposium,  
Harry Diamond Laboratories, May 1964)

## **ABSTRACT**

This paper describes a study of the feasibility of applying fluid amplifiers to the control of a steam turbine. Work was performed under Contract Nonr 4001(00) sponsored by the Office of Naval Research. The study included an extensive computer analysis to determine the relative merits of all-analog, all-digital, or hybrid analog/digital operation. Circuit requirements to meet the more rigid Specification MIL-G-21410 were determined. Using fluid amplifier elements, it appears feasible to get performance equivalent to that now obtained by electrohydraulic speed controls.

A description is given of a working demonstrator using tuned reed speed references. The demonstrator consists of a small air turbine with a pneumatic drag-brake load. In this circuit there are no moving parts other than the turbine and the tuned reeds. Problems of extrapolating the design to full scale machines will be discussed.

## **INTRODUCTION**

Specifications for ship-board steam turbine-generator governors stress both performance and reliability. In present applications, these governors are either hydromechanical or electrohydraulic devices. This paper describes a study of the feasibility of using fluid amplifiers with a minimum of moving parts to implement such a control.

The advantages of these devices are their potential for extremely high reliability over long time periods, and the fact that they can withstand extreme environments of temperature, nuclear radiation, shock and vibration. In addition, they are capable of operating with virtually any working fluid, regardless of its lubricating qualities. By proper choice of materials, corrosion of the elements is not a problem. While fluid amplifiers cannot be used arbitrarily as substitutes for electronic or hydromechanical controls, there are many applications they can satisfy with unique advantage. It will be seen that the speed control of a ship's service turbine is one application where fluid controls have such an advantage. Not only are they capable of the

performance necessary, but they would be more reliable and can use the available water or steam as a working fluid and eliminate the need for a separate fluid supply system. This is consistent with the Navy's long range interest in encapsulated equipment using a single fluid.

The study described in this paper consisted of an analytical investigation of various possible systems together with a hardware study of critical components. For brevity, only the most promising systems will be described, and discussion of components will be confined to those of the Reed Governor system that was finally selected.

### INITIAL SYSTEMS ANALYSIS

The basic guideline for the systems analysis was Specification MIL-G-21410 (Ships). This specification calls for the capability for isochronous operation and rapid recovery from large load transients. Ship-board turbine generator sets often operate singly, and do not tie in to an equivalent "infinite bus" as do large land-based central station power plant turbines. As a result, the speed control requirements of the above specs are stringent. Currently, electrohydraulic systems are generally used to meet the control requirements of the above specification and hydromechanical systems are used to meet earlier, less stringent specs.

Requirements of particular interest stated in MIL-G-21410 include:

- a.  $\pm 0.2\%$  steady state speed accuracy.
- b. Maximum transient speed deviation of  $2\%$  when a load drop or load increase of  $100\%$  of rated load is applied to the turbine. In addition, speed must recover to within  $\pm 0.5\%$  in less than 1.5 seconds of the load change.

Analytical studies were performed on a wide variety of systems that fall into the three general categories of:

- a. All-digital,
- b. Hybrid analog and digital,
- c. All-analog.

The studies made extensive use of both the analog and digital computer facilities available at the Advanced Technology Laboratories. The results presented in this paper represent a distillation of the many studies, and dwell primarily on the most attractive system studied in each of the above three categories.

## All-Digital System

The straightforward approach to an all-digital control would require counting the number of revolutions over a fixed time period, comparing this to a desired number of revolutions in that time period, storing this information in a register and passing it on to produce corrective action in the control. The error signal will not change until a new sample is taken, at which time the error signal in the register is changed and new corrective action is taken. To obtain high accuracy of control, a large number of counts must be made in each sample. To obtain rapid response, the samples must be taken at extremely short intervals. As the sampling rate increases, the performance of the control becomes more and more like that of an analog control. Computer studies show that, to obtain both the necessary accuracy of steady-state speed, as well as the ability to stay within specifications on transients, a count rate of 400 cycles per second per percent of speed error is necessary. This would require an information rate capability of several KC in an all-digital control of this type, and, if it must maintain control from start-up through full speed, this implies a pulse rate as high as 40 KC. This obviously is beyond the present state of the art of practical fluid controls.

By careful system design it is possible to greatly reduce the pulse rate requirement of an all-digital system. The most appealing system of this type that has been studied to date is shown in Figure 1. This system consists of a proportional plus reset type of system, where the reset action is provided by a reversible counter, and the proportional action is provided by three speed samplers. The speed samplers are arranged in such a way that they produce a relatively low proportional gain for small speed errors and higher gains for higher errors. Due to the extreme non-linear nature of such a system, it was studied on the GE-225 digital computer at the Advanced Technology Laboratories. Typical results of this study are shown in Figure 2. The curves are presented in terms of percent turbine speed deviation vs. time due to a 100% step application of load. Figure 2 shows results for a system where a basic pulse rate of 32 pulses per second per percent speed error is used. In this system, each pulse results in a 2-1/2% change (quanta) of steam flow. Many other pulse rates and quanta sizes were considered.

One basic conclusion of the digital study was that the transient response remains approximately the same, as long as the product of the pulse rate times the quanta size is held constant. However, increasing the quanta size will result in a larger limit cycle. Without resorting to additional circuitry for suppression of the limit cycle, it appears to be quite difficult to eliminate it completely. If the possible limit cycle is held to an extremely small value, the true limit cycle may not show up in actual operation, due to the effects of deflection of

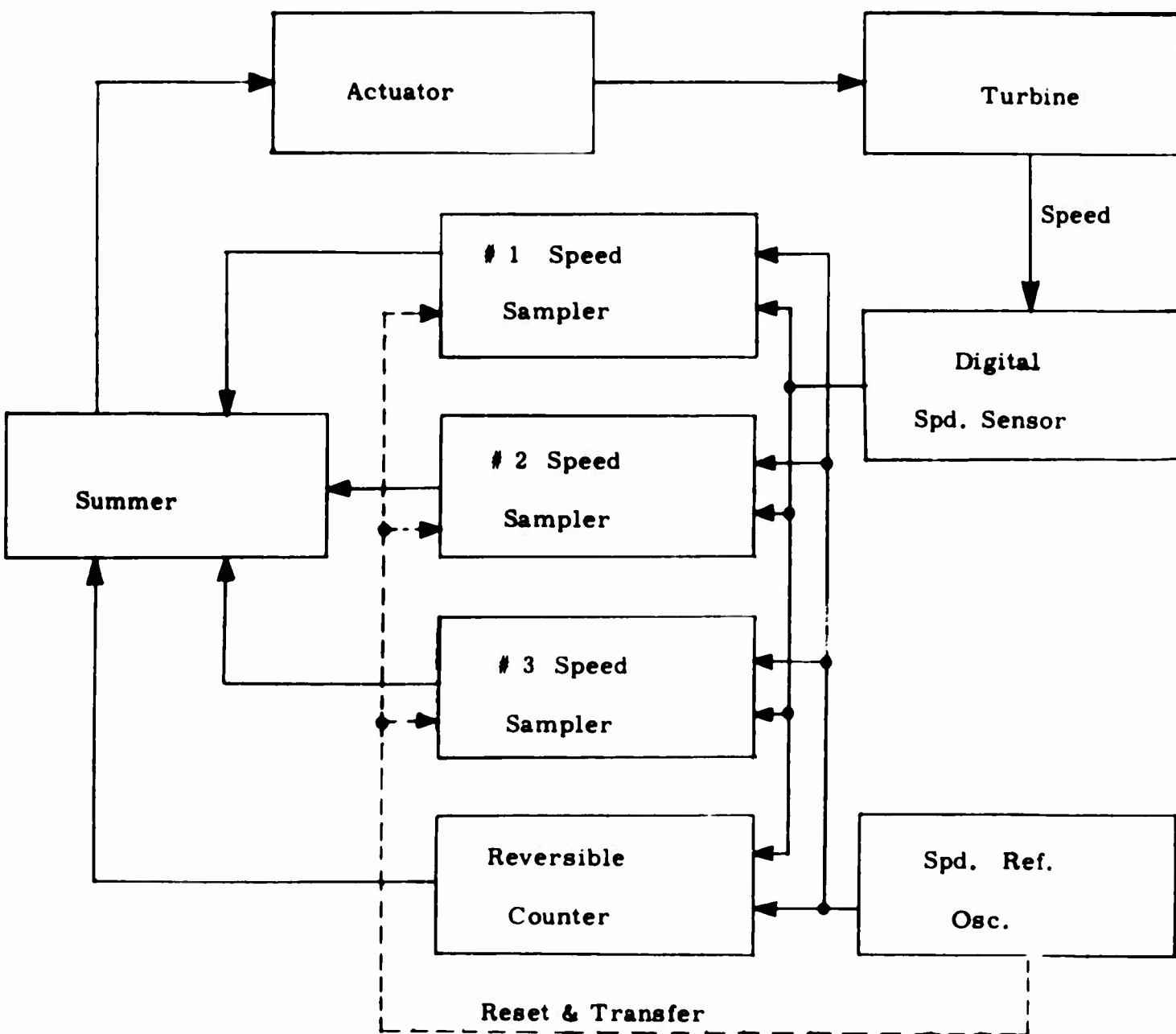


Figure 1 Block Diagram -  
Modified All - Digital Control  
(Proportional plus reset)

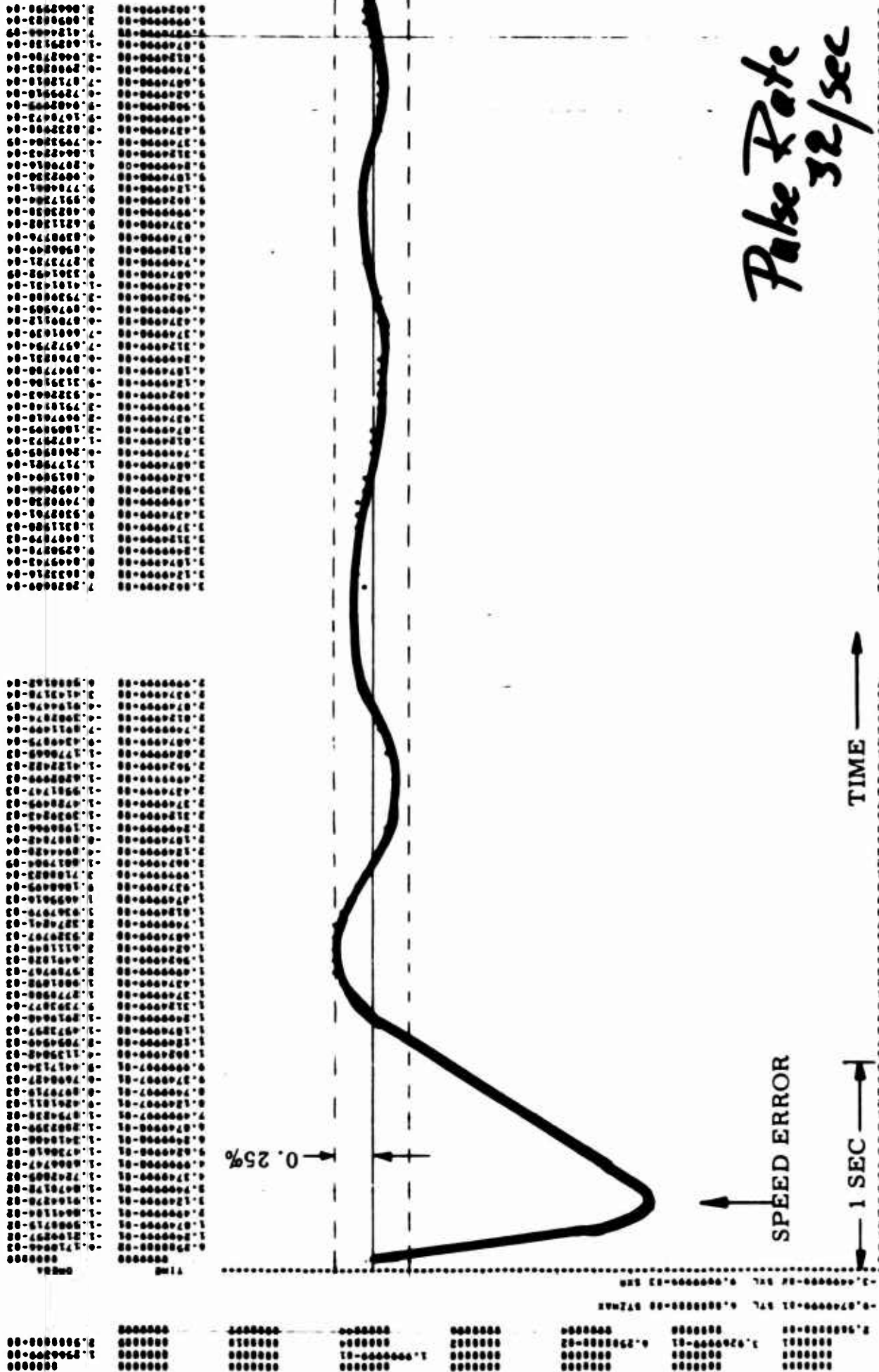


Figure 2

Response to Step Load Change  
(Modified All-Digital Control)

32 pps/% speed error, 2 1/2% quanta



parts, friction and other factors. Such reduction of limit cycle size implies a finer control requiring more elements.

The conclusion of the studies of all-digital systems was negative, due to several reasons. First, such a system will require a large number of active fluid elements to perform the necessary functions if performance specs are to be met. Secondly, undesirable limit cycle oscillations will exist unless still more system elements are used. The limit cycle oscillation in itself would be most undesirable due to the resulting low quality of the electrical output signal, and also because of the continuous motion of the steam valve parts that would result.

### Hybrid Digital/Analog System

A hybrid digital/analog system would make use of the best features of both the analog and digital types of fluid transistor elements. Normally, an analog control would feature fast response but not extreme accuracy, particularly if integration is to be performed. On the other hand, easily realizable digital systems would be limited by a speed of response, but would be capable of high accuracy, particularly when performing the integration function, such as in a reversible counter. Therefore, a system of the type shown in block diagram form in Figure 3 was investigated. This system makes use of the well-known proportional plus reset approach, where an analog speed sensor obtains a proportional signal necessary for good transient performance, and a digital speed sensor in conjunction with a reversible counter is used for the slower reset action which is necessary for steady-state accuracy. A typical analog computer trace is shown in Figure 4, where several reset rates are studied, having 2-1/2% proportional speed regulation (temporary droop) and a steam valve actuator that moves in 6% steps. The trace shows that the reset rate of four pulses per second per percent error will provide adequate transient and steady-state speed accuracy. For this condition, a pulse rate of only 40 pulses per second would result for speed errors as large as 10%. This is much larger than any expected error that will be encountered, and is well within the existing frequency capability of fluid amplifier devices. It can also be seen that equivalent transient control can be obtained using a system of smaller quanta size steps, provided the pulse rate is increased. Thus, if the quanta size is reduced to 1%, equivalent transient response can be obtained if the pulse rate is increased to 24 pulses per second per percent speed error. The hybrid system will also have a steady-state limit cycle, as shown in Figure 4. The size of this limit cycle will be quite small as long as small quanta sizes are used, and this may result in no noticeable movement of the steam control valve or bobble in the actual turbine speed in a practical system.

It is possible to eliminate the limit cycle in theory as well

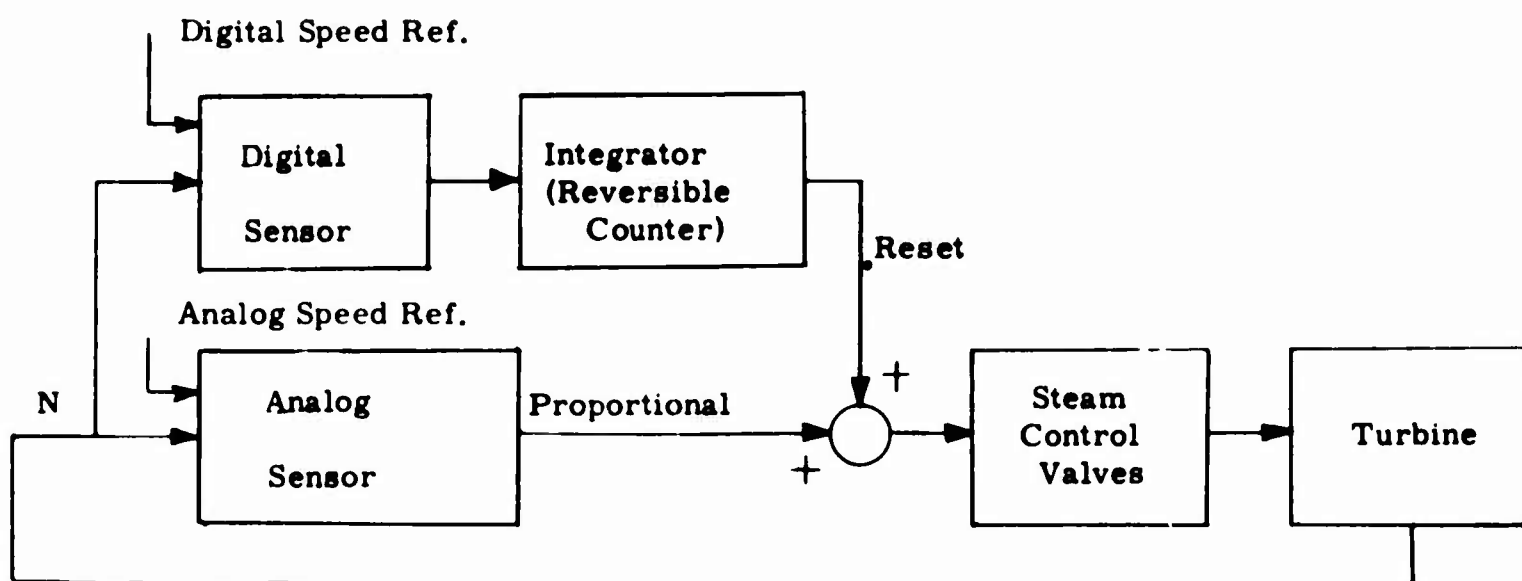


Figure 3 Block Diagram Hybrid Analog - Digital Control

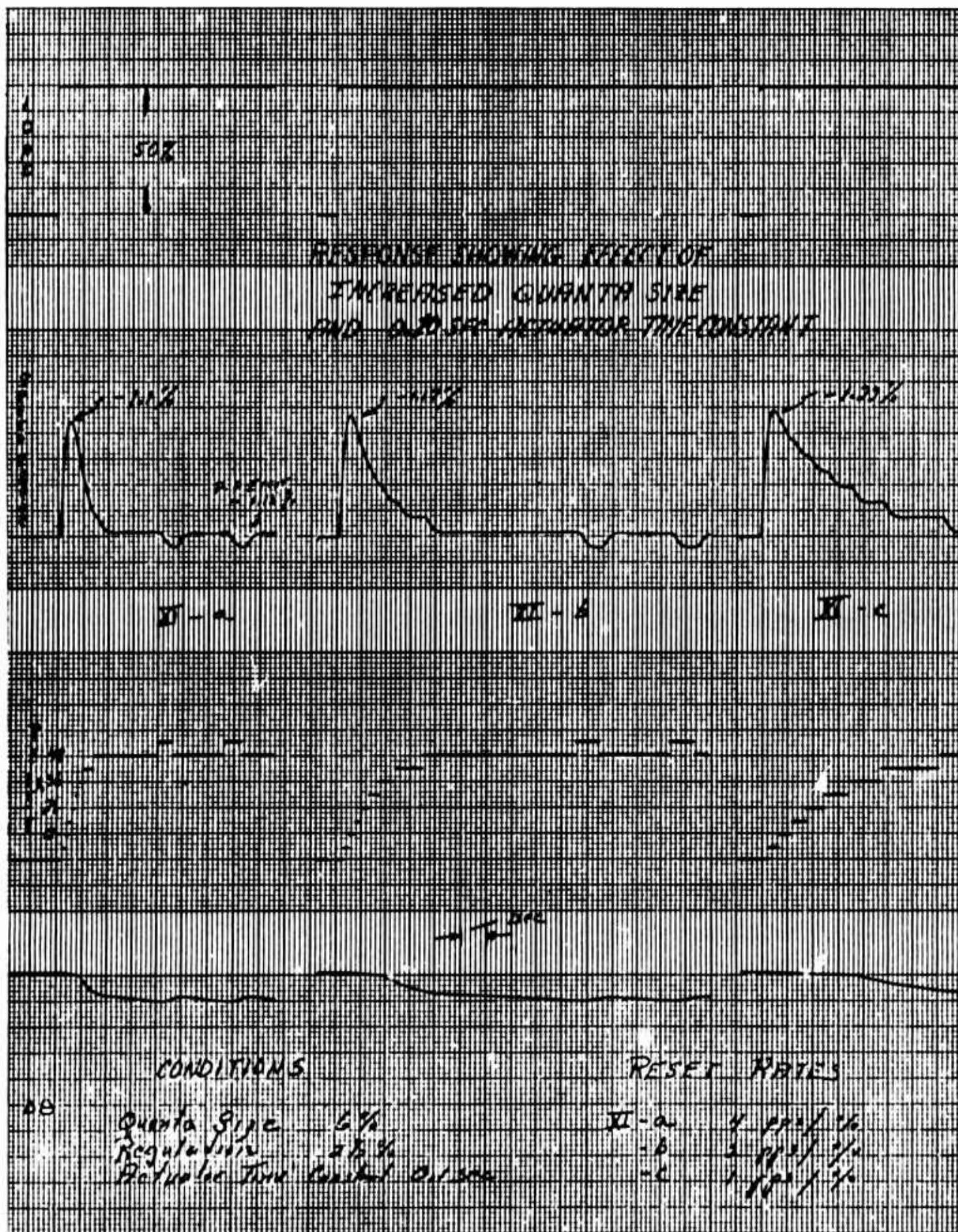


Figure 4 Response to 50% Step Load Change - Hybrid Analog/Digital Control

as practice by a relatively simple addition to the circuitry in the hybrid system, at some expense in speed accuracy. If the quanta sizes are small enough, the resulting decrease in steady-state accuracy will not be objectionable. It should also be pointed out here that the quantum changes in steam flow can be obtained by a stepping type actuator, as described above, or could be obtained equally well (and probably more practically) from a proportional actuator where the signals to this actuator are changed in quantum steps by the output of the reversible counter. It is felt that the hybrid system can be implemented by devices that exist in the present or near future state of the art. However, a study of the hardware requirements of this system showed that it will require many more active fluid amplifier elements than an all-analog system.

### All-Analog System

Analysis of an all-analog system is straightforward and shows that the required control action can be obtained using either a proportional-plus-reset system or an integrating system with lead-lag stabilization. The problem in an all-analog system is to get a speed sensor of sufficient accuracy. After a survey of various approaches, it was concluded that a Reed or Tuning Fork Governor system was the best approach to the all-analog system. The remainder of this paper will be devoted to this approach, including both the hardware design and system analysis aspects.

### REED (OR TUNING FORK) TYPE ANALOG SPEED SENSOR

The Reed Governor principle for hydraulic and pneumatic speed control was invented and developed at General Electric Company several years ago. This approach offers advantages in reliability and accuracy that cannot be found in other speed sensing means. To directly sense the shaft speed, the Reed Governor uses a sinusoidal chopper consisting of a wobble plate mounted on the turbine shaft, which provides a sinusoidal variation in restriction of the outlet of two nozzles (spaced  $180^\circ$  apart), as shown in Figure 5. The result is a sinusoidal output pressure signal from each nozzle, the signal  $B_1$  from nozzle 1 being  $180^\circ$  out of phase with  $B_2$  from nozzle 2. The two pressure signals are transmitted to driving nozzles which apply a sinusoidal driving force to a tuned resonant reed, as shown in Figure 6. Attached to the end of the reed is a small spatula which intercepts the flow of fluid from a sensing nozzle. Below the spatula is a sensing receiver directly in line with the nozzle. When the reed is at rest, the spatula intercepts all of the fluid from the sensing nozzle, and none impinges on the sensing receiver. When the driving signal from the sinusoidal chopper reaches a frequency approaching the resonant frequency of the reed, the reed will start to vibrate, resulting in intermittent opening of the path from the sensing nozzle to the sensing receiver. As the reed goes through resonance, the output

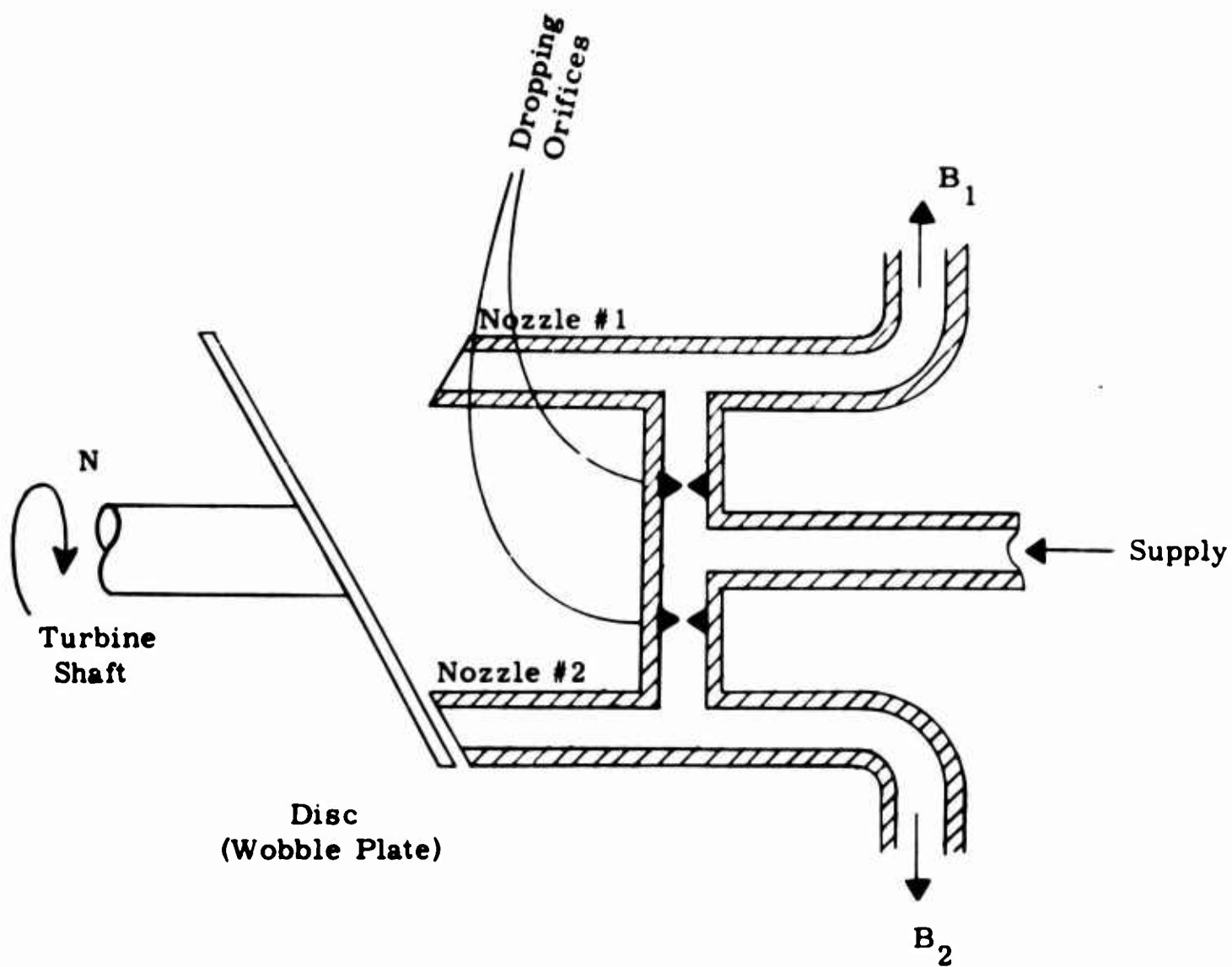


Figure 5 Sinusoidal Chopper

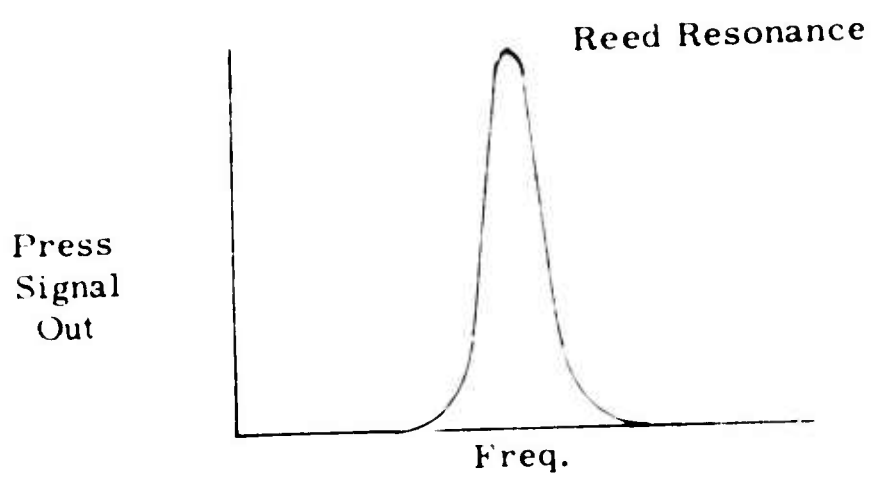
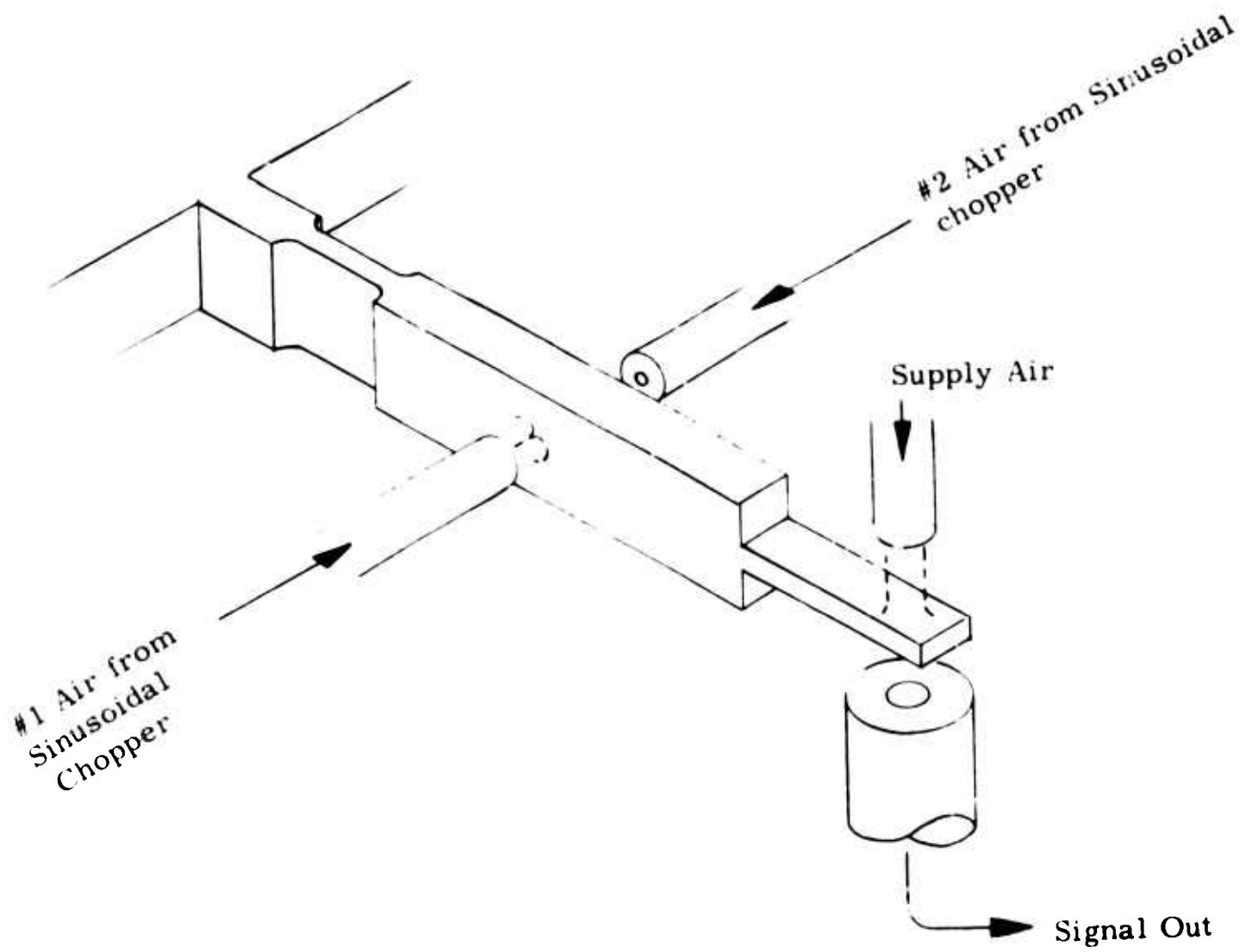


Figure 6 Vibrating Reed Speed Sensor.



pressure signal from the sensing receiver will go through a maximum, as shown in the diagram on Figure 6. Beyond resonance, the signal will die out again as the reed amplitude decreases. The same principle can be applied to a tuning fork, as well as a tuned reed, the reed being used here for simplicity of illustration. A tuning fork will have certain advantages in that it is less sensitive to vibration and to means of anchoring it to its base.

When two tuned reeds that are tuned at somewhat different frequencies are combined, a speed error sensor can be formed as shown in Figure 7. The output from the sensing receivers are fed to an analog valve which produces a subtracting function. When the two signals are subtracted from each other, a characteristic output differential pressure is generated as a function of signal frequency, as shown in Figure 7. The reed frequencies are tuned so that the desired set frequency is midway between the two. As a result, at the desired operating point, the differential output pressure from the analog valve will be zero. When speed is below the desired value, the differential output pressure will be positive, and when above the desired value, the differential output pressure will be negative. A Reed Governor of this type has been built and operated as part of the ONR Fluid Controls Program. Actual test results of the output characteristic are shown in Figure 8, where the working fluid is air, and the supply pressure to the analog valve is 4 psi.

The vibrating reed speed sensor is a very straightforward method of sensing shaft speed and would be assumed to be as fast in response as the basic reed resonance itself. The steady-state characteristic curve for a single reed is shown in the top curve of Figure 9. The amplitude of the reed motion is expressed in decibels and is plotted versus the logarithm of the steady-state input frequency. The dynamic response of the Reed Governor, however, depends on the modulation frequency in the signal, not on the prime frequency. A reed that has a steady-state resonance of 200 cycles per second may have a "sensor" resonance of less than 20 cycles per second, as shown in the bottom curve of Figure 9. It is the dynamic performance of the reed that must be considered in a stability analysis of a system utilizing the vibrating reed speed error sensor. References 1 and 2 describe mathematical techniques of predicting "sensor" resonance and give design curves verified by tests.

Tests performed on the Reed Governor used air as the working fluid. This was done for economy and convenience. However, the earlier G. E. sponsored work of References 1 and 2 successfully demonstrated hydraulic oil as a working fluid.

To evaluate the Reed Governor, it was used to control a small

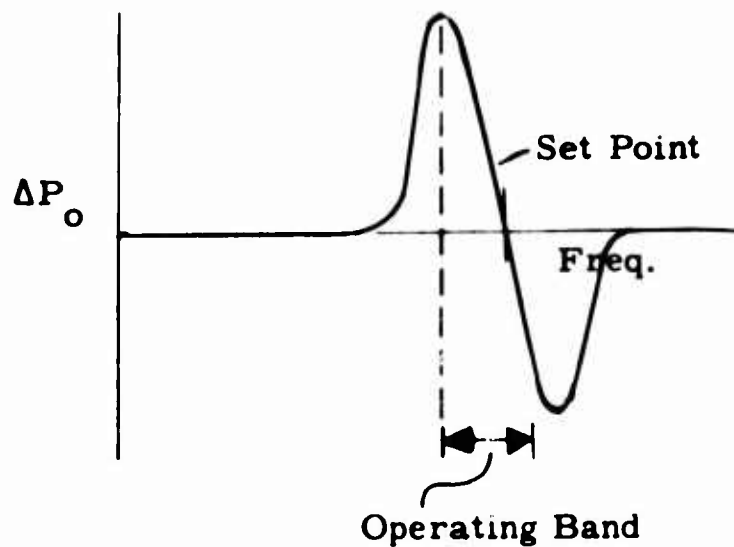
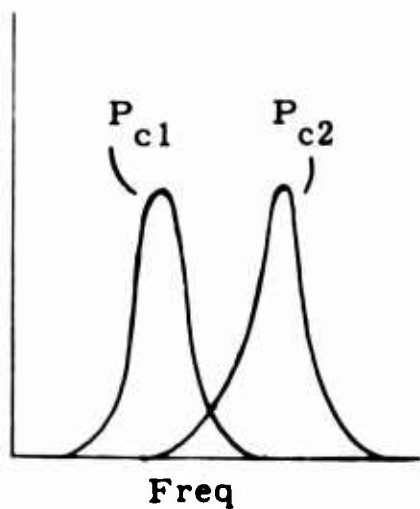
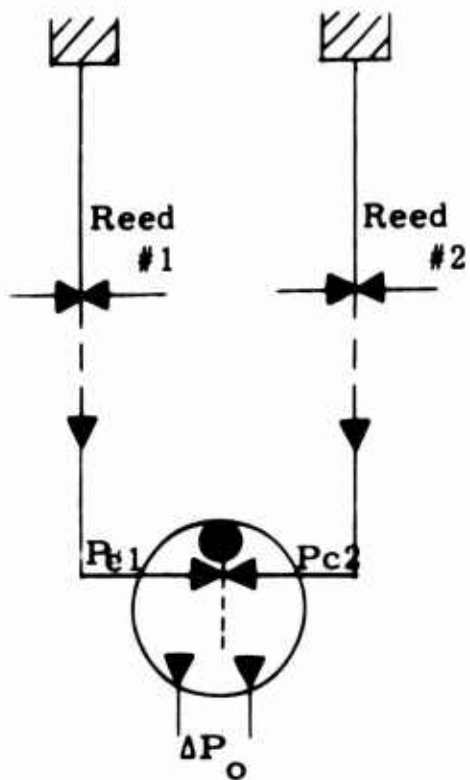
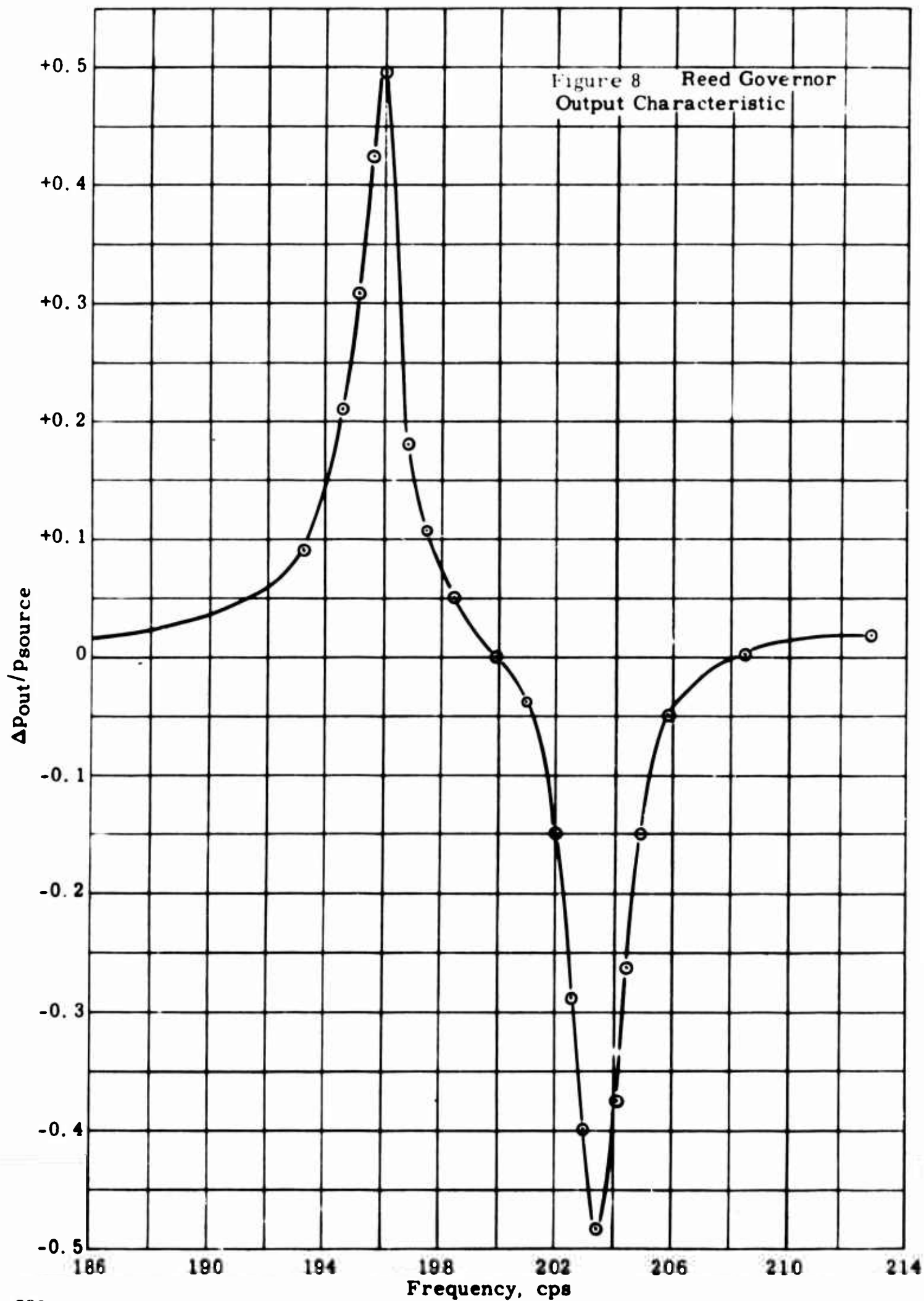


Figure 7

**Vibrating Reed Speed Error Sensor  
(Reed Governor)**





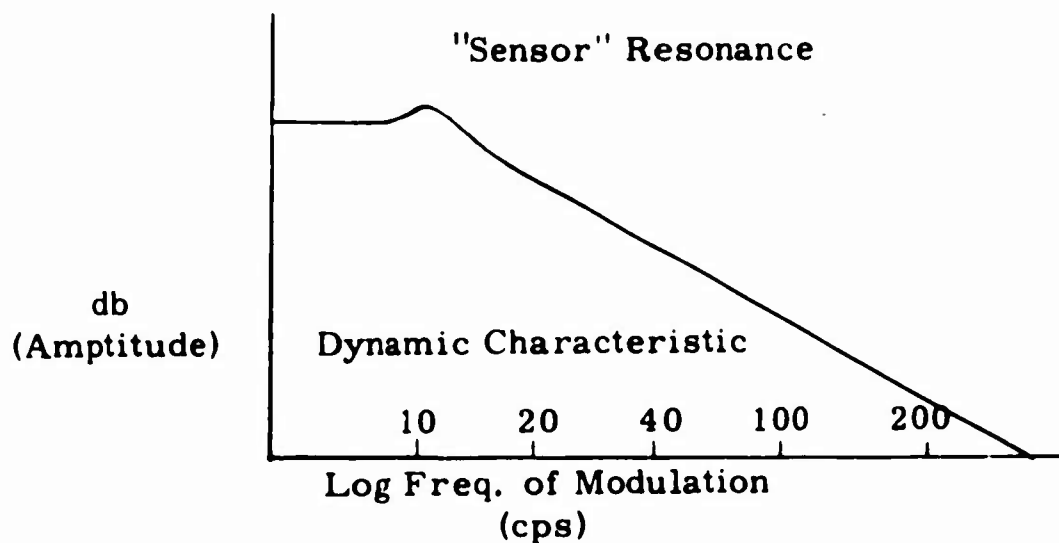
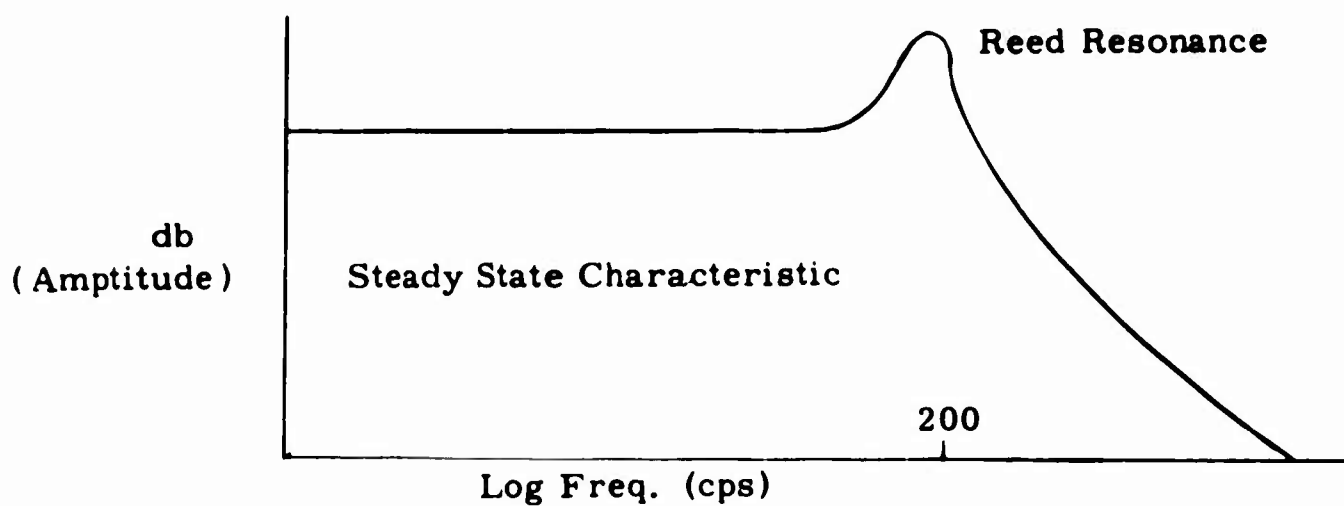


Figure 9 Reed Resonance and Sensor Resonance of Reed Governor

air turbine, as shown in Figure 10. The output of the Reed Governor was amplified and used to modulate the air flow to the turbine. A complete schematic diagram of this circuit is given in Figure 11. The turbine itself was loaded by a gear wheel against which a jet of air could be impinged to obtain a wide range of load. Figure 12 shows the steady-state speed holding capability of the governor. It should be emphasized that the test rig in its present form is a proportional speed control without re-set. As a result, some regulation will be present which will not appear in a final design. Figure 12 shows a total variation from 201 cps down to 198.5 cps over the load range tested. Demonstrations were also conducted where the Reed Governor maintained speed of the turbine during both positive and negative load transients.

### REED GOVERNOR SYSTEM ANALYSIS

The initial system analysis showed that an all-analog system will have a block diagram of the form of Figure 13. The Reed Governor will serve as the speed error sensor. The output from the speed error sensor must be passed thru a correction network to assure adequate stability of the loop, together with isochronous operation. The output of the correction network controls steam flow by means of a steam valve, which in turn controls the turbine speed. The system analysis described below was performed using parameters characteristic of the Reed Governor. The Reed Governor exhibits a flat frequency response up to a frequency  $\omega_L$  where it exhibits a second order break, or resonance, with damping. (The frequency referred to in this case is the frequency of oscillation of shaft speed, not the output frequency of the alternator.) References 1 and 2 give a detailed analytical derivation of this characteristic, as well as design curve test results verifying the analysis. The derivations of References 1 and 2 apply equally well to any resonant type of sensor, be it a tuning fork, Helmholtz Resonator, or electronic circuit. The ratio of the "sensor resonance" frequency,  $\omega_L$ , to the tuned frequency is a function of design. Values of 5 to 20% are typical.

Figure 14 shows a simplified Bode attenuation plot of the analog system. Here the characteristics are exaggerated, and straight line approximations are used with the exception of the sensor resonance. The system characteristic includes a lead break at frequency  $\omega_1$ , a lag break at frequency  $\omega_2$ , and the sensor resonance at frequency  $\omega_L$ .

Analog computer studies were performed on a system having the general characteristics of Figure 14. The analog computer study showed that the system represented by Figure 14 would produce satisfactory responses of the type shown in Figure 15. Here the peak frequency change due to a 100% load drop is 1.9%, and frequency settles out to within 0.1%, 1-1/2 seconds after the transient.

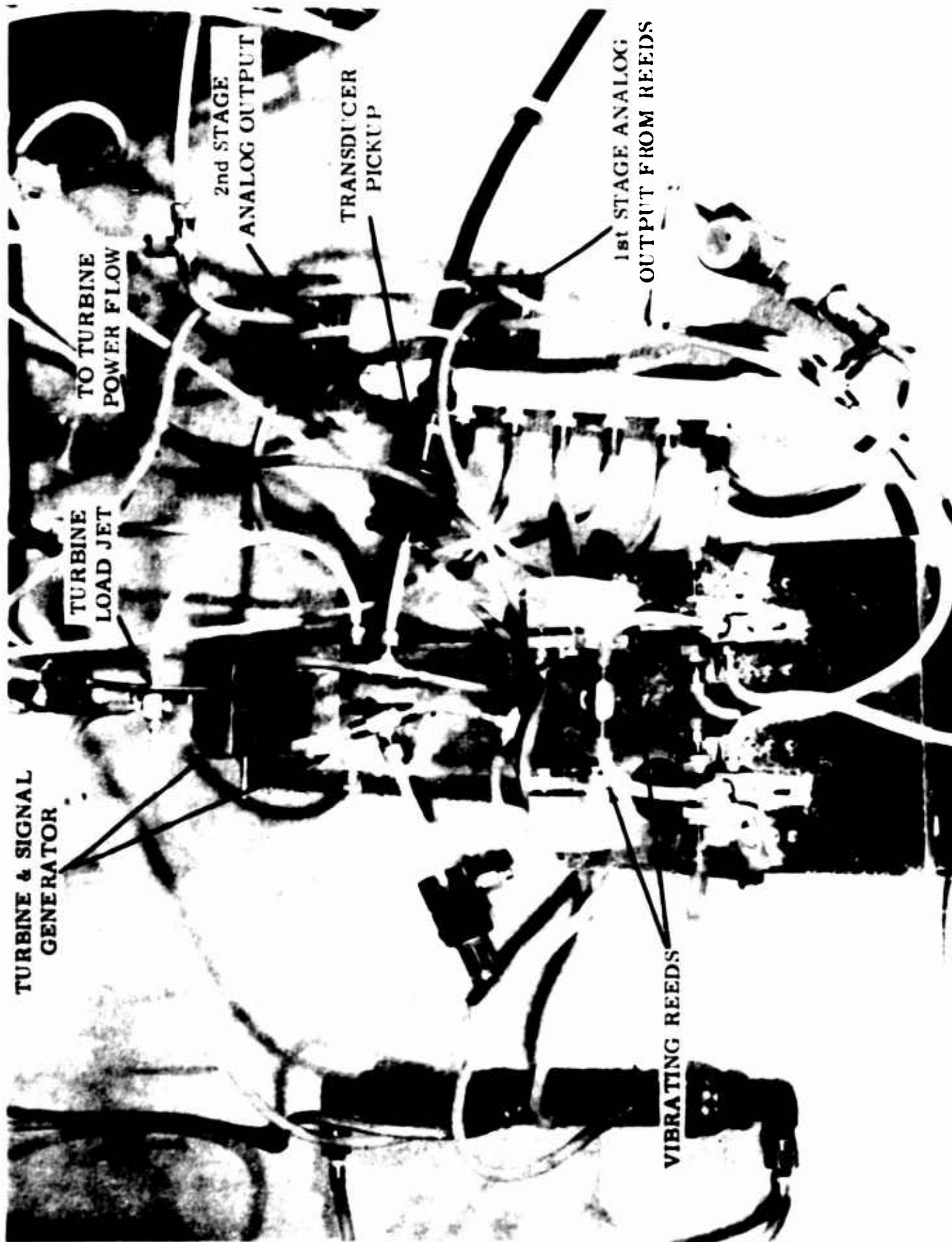


Figure 10 Reed Governor Test Rig  
- Loop Closed Through Air Turbine

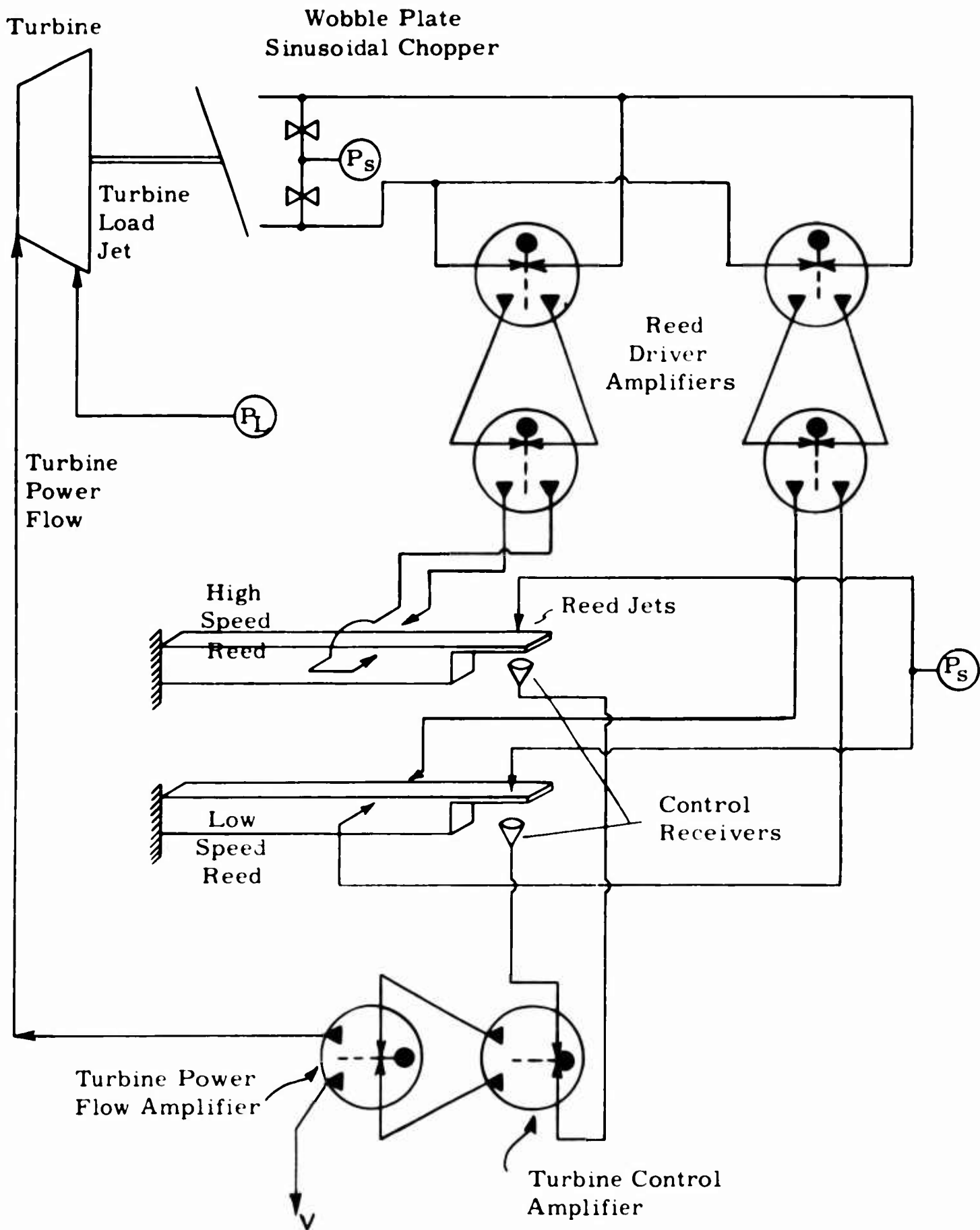


Figure 11 Schematic Diagram - Reed Governor Test Rig.

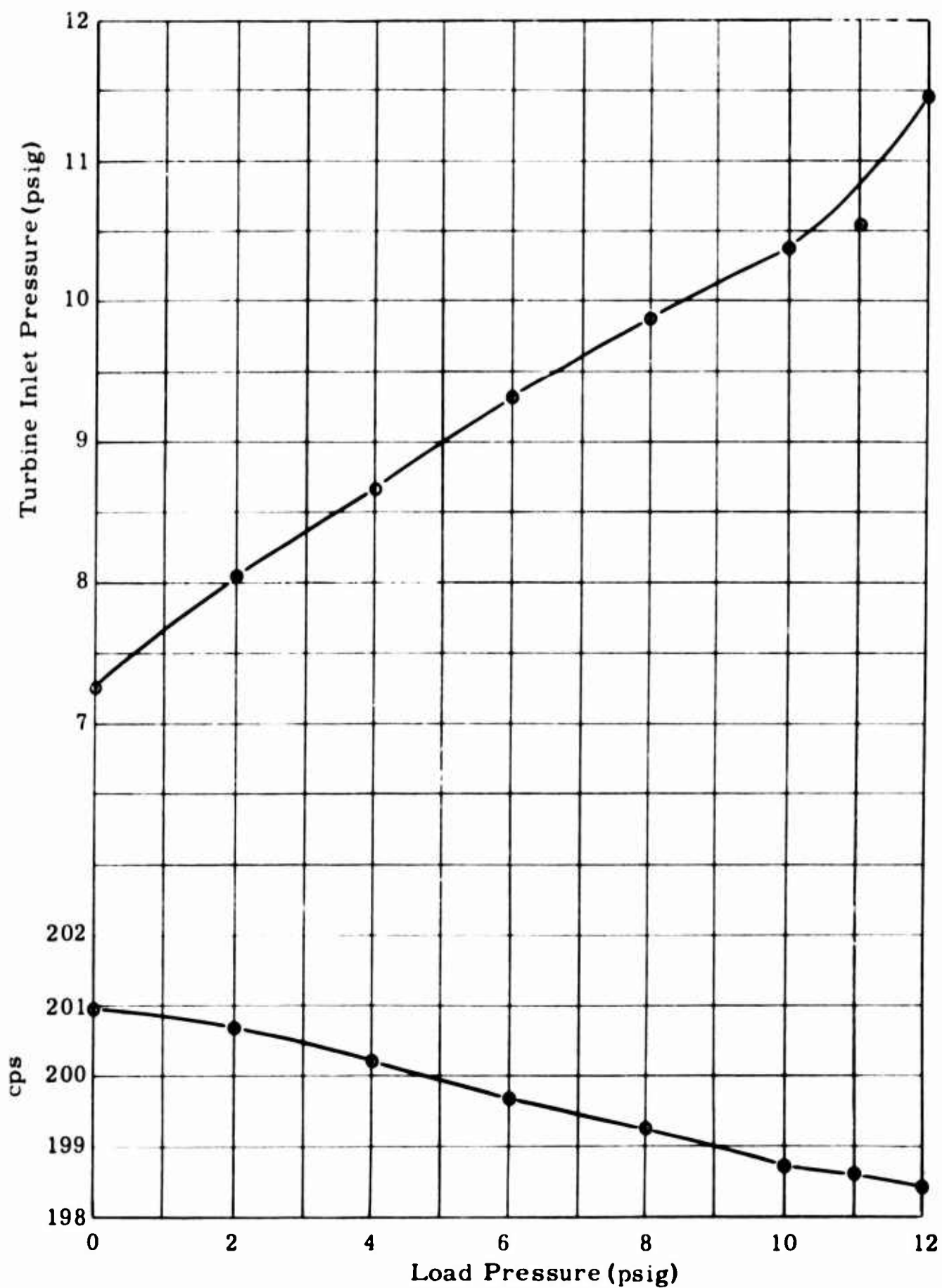


Figure 12 Regulating Characteristics of Air Turbine Reed Governor.

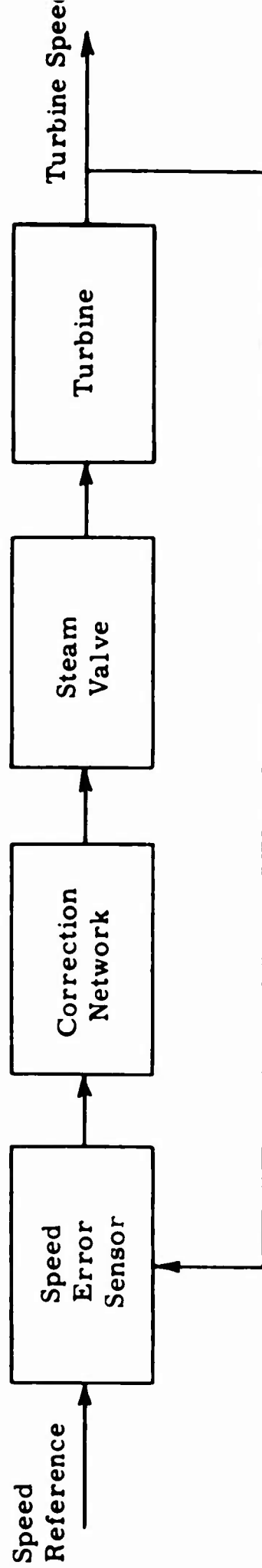


Figure 13 Block Diagram - All-Analog Control.

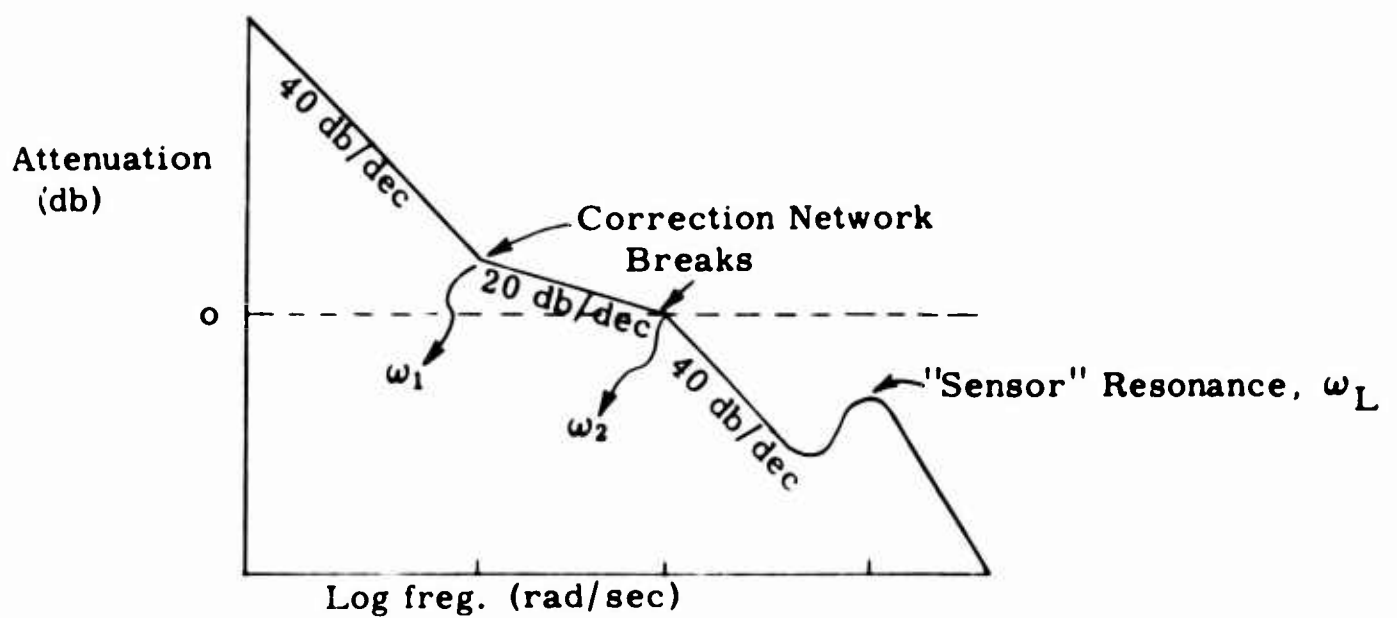


Figure 14 Simplified Bode Attenuation Diagram  
All - Analog Control.



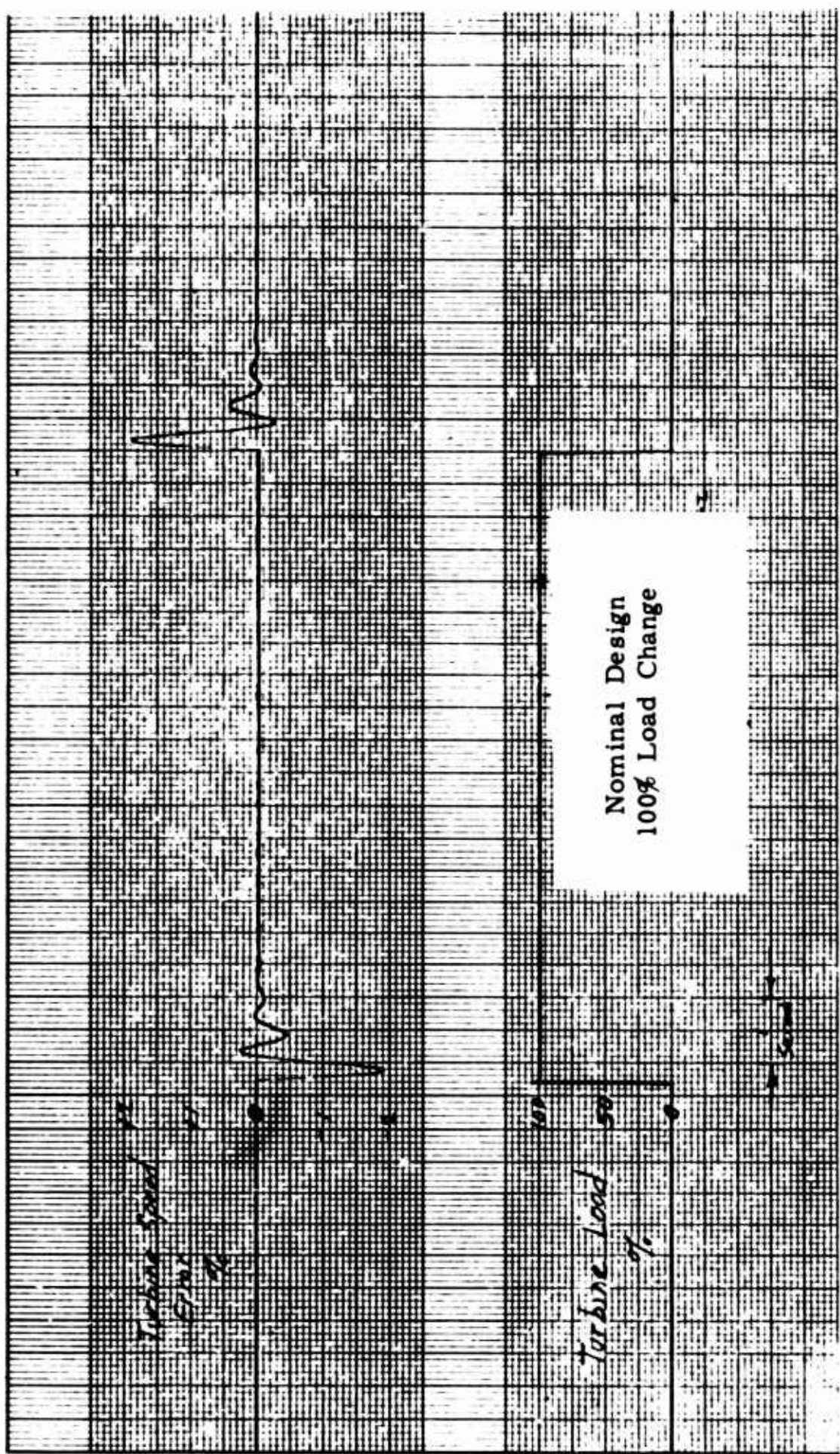


Figure 15 Response to 100% Step Load Change - All-Analog Control

Performance was simulated for conditions bracketing the optimum operating range to determine the criticality of such a design. Figures 16 and 17 show typical variations of parameters which were investigated. Figure 16 shows that a low sensor resonance frequency,  $\omega_L$ , reduces stability. Figure 17 verifies the desirability of a high value of  $\omega_2$ .

The computer traces are intended to bring out critical points in the system design. It should also be noted that the analog computer studies reported here were made with a five second turbine time constant. This is the smallest time constant expected to be encountered in any of the ship's service steam turbine generators, and more typical values for the units running on boiler steam supply would be 10 to 12 seconds. The higher time constant machines will tend to be more stable. Hence, the computer studies performed above are based on conservative assumptions.

### REED GOVERNOR SYSTEM DESIGN

The basic Reed Governor system using lead-lag stabilization is shown in simplified schematic form in Figure 18. The system described here would use water as the working fluid throughout<sup>(3)</sup>. It is possible, however, to use steam or compressed air as the working fluid, although certain stability problems will arise. If the actuator working fluid must be steam or air, added stability compensation of the actuator is needed. One compromise approach is to use air or steam up through the lead-lag stage. At this point, it would be necessary to add several buffer stages of analog amplification which use water as the working fluid and would use the air or steam output of the lead-lag as their control. The operation of a water-operated analog amplifier, using air as the control medium, has been demonstrated at Advanced Technology Laboratories.

The basic loop will control the turbine speed while inside the range of the simple two-reed governor. However, it is necessary to provide override signals for situations where the turbine speed falls outside the operating range of the governor. These override signals can also be generated by fluid logic elements.

It was determined that the entire Reed Governor lead-lag system including the auxiliary logic, can be accomplished using a total of 16 fluid amplifier elements. Of this total, 9 would be active elements where a separate fluid supply must be provided, and 7 are passive elements which do not require a separate fluid supply.

A proportional-plus-reset approach requires four more active elements than the lead-lag system. As a result, the lead-lag system is slightly more attractive from the standpoint of system simplicity. However, the proportional-plus-reset system offers greater flexibility in that the lead and lag frequencies can be adjusted separately.

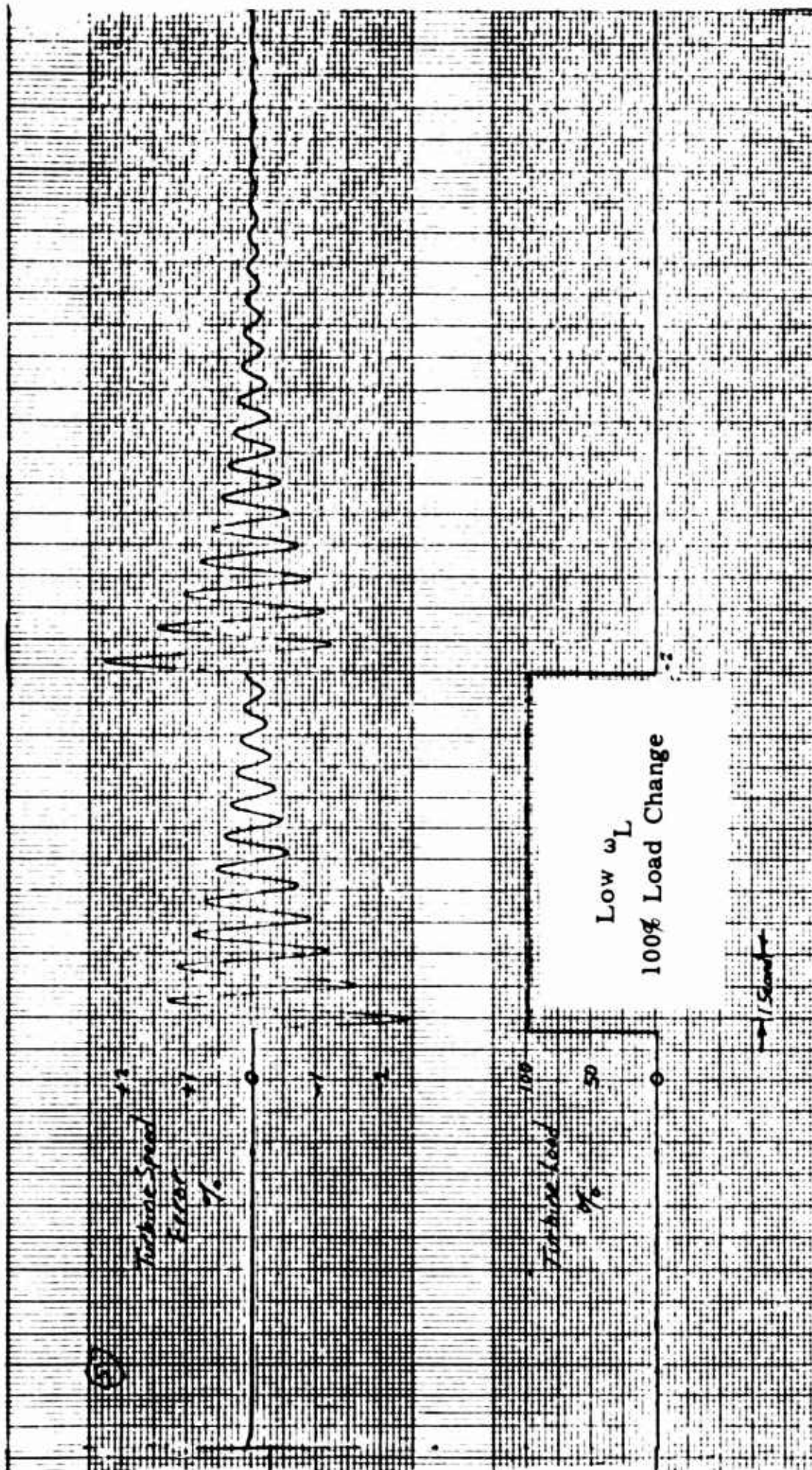


Figure 16 Response to 100% Step Load Change - All-Analog Control with Low Sensor Resonance Frequency



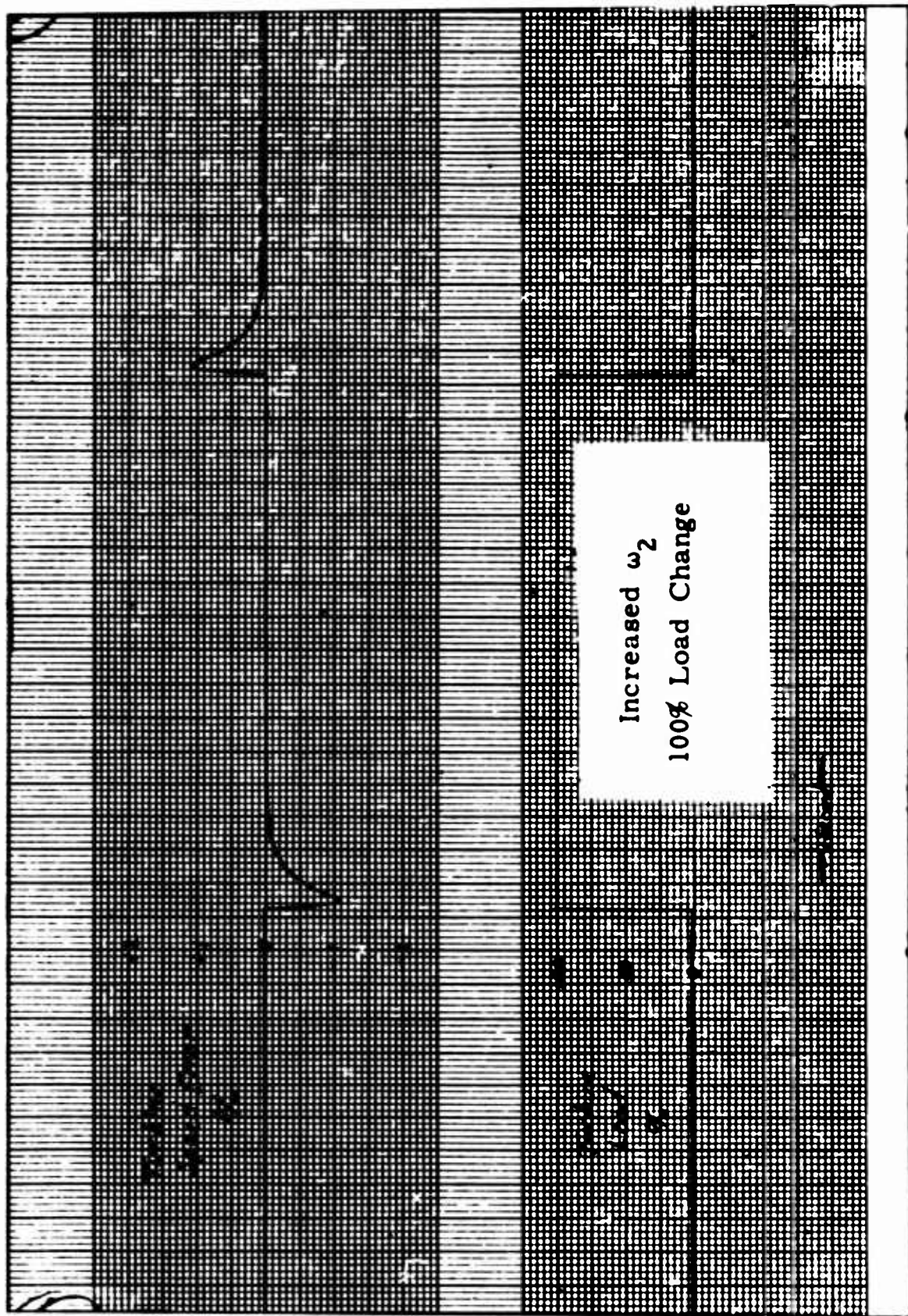


Figure 17 Response to 100% Step Load Change -  
All-Analog Control with High  $\omega_2$  Frequency

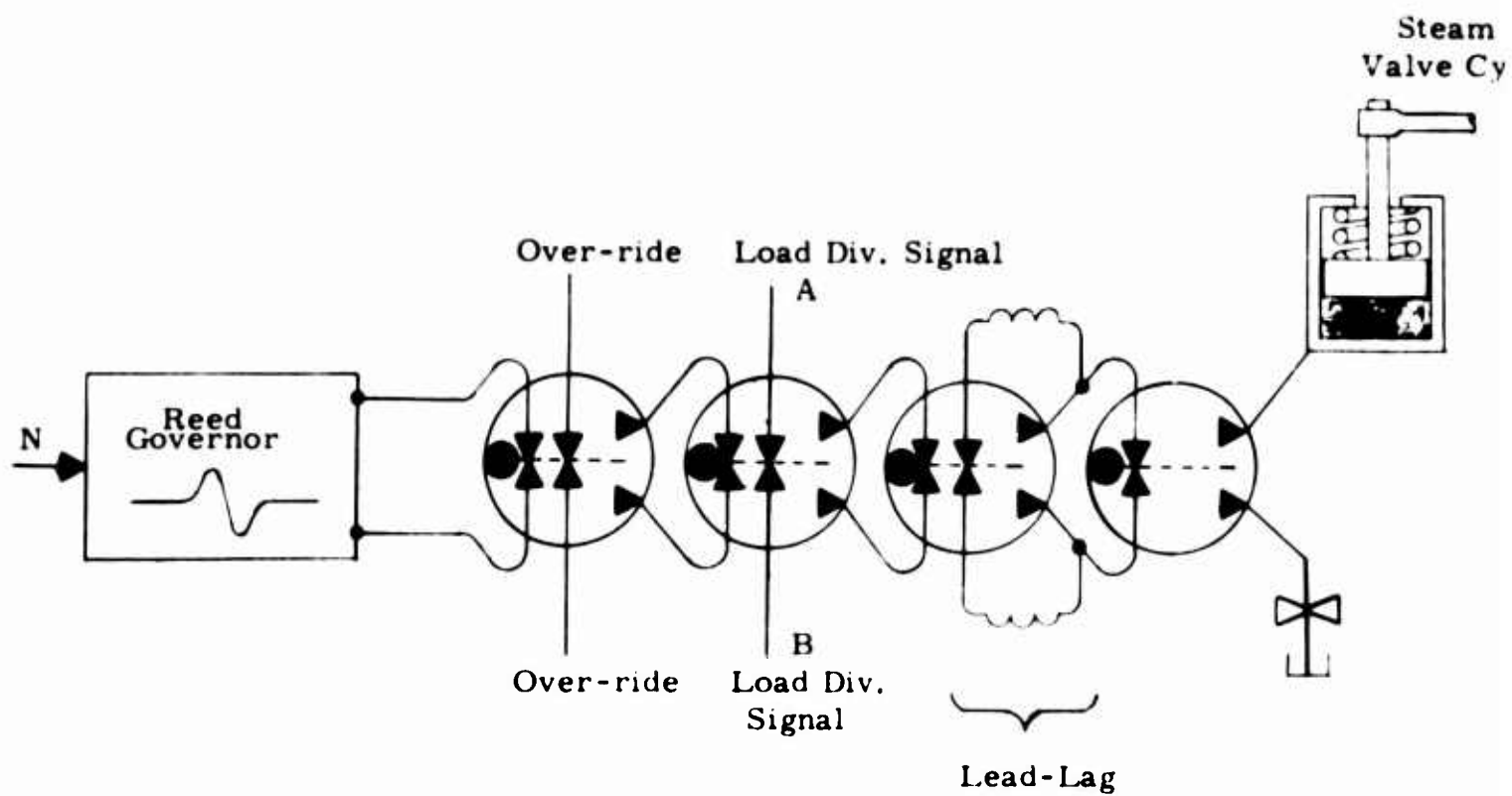


Figure 18 Lead-Lag Reed Governor System Schematic

## REFERENCES

1. General Electric Co., TIS Report R56A0348  
"Hydraulic Discriminator Speed Control" by T. S. Honda and  
C. C. Christianson, October 23, 1956.
2. ASME Paper 57IRD-14  
"Dynamic Response Study of a Mechanical-Hydraulic Frequency  
Discriminator Governor" by C. C. Christianson, April 8, 1957.
3. "A Water Control System for Steam Turbines" by V. N. Veller,  
G. A. Kirakosyants, and D. M. Levin (Moscow). Paper  
presented at Fifth Session of All-Union Seminar on Pneumatic-  
Hydraulic Automation held in Leningrad, USSR, June 11-13,  
1962. This is abstracted on page 1617 of the English Trans-  
lation of Vol. 23, No. 12, Dec. 1962 issue of Automation and  
Remote Control.

# Applications of Pure Fluid Techniques to a Speed Control

by

J. R. Colston  
E. M. Dexter

Pure fluid controls are attractive as speed controls because they reduce mechanical complexity which reduces cost and improves reliability. These controls can use the fluids which already are available in the system. This paper is concerned with an application for the Office of Naval Research where the objective is a 500 KW power plant using the steam for the control and for bearings; thus eliminating the need for electromechanical devices and a second fluid completely.

The result of the survey of possible approaches to speed control using pure fluid circuits concluded with the system shown in Figure 3 which is a frequency modulation technique. The frequency difference between signals generated by the turbine shaft and the frequency reference, which is a tuning fork, is used to drive two parallel fluid resonant circuits which are part of the discriminator circuit. The error frequency is designed to be 40 cycles per second at the desired turbine speed. This 40 cycle per second pressure pulse train drives the parallel resonances which are tuned for 30 cycles per second and 60 cycles per second respectively. A change of the turbine speed either increases or decreases the error frequency, changing the amplitude in the resonant circuits, to distinguish in which direction the change has occurred. For example, if the turbine speed increases so that the output frequency from the speed detector is 810 cycles per second the error frequency is reduced to 30 cycles per second. This results in an increase in output from the 30 cycle resonant circuit and a decrease in output from the 60 cycle resonant circuit. This change of amplitude results in a correction signal to decrease the size of the valve opening which supplies fluid to the turbine.

Because of the dynamics of this system, a double integration, a stabilizing network is required. This is a lead-lag network.

The fourth major block in Figure 3 is the pressure-to-flow amplifier. This device produces an output flow which is proportional to the pressure error signal. The objective of this component is to provide a valve actuator velocity which is proportional to the pressure error signal.

The breadboard model of this system, which was tested with air, is shown in Figure 2. The size of the controls and actuator are compatible with the 500 KW plant application. The alternator turbine has been scaled down holding constant torque inertia damping ratios so that the dynamic performance is the same as the planned application.

The following sections of the paper include a survey of system approaches to this problem, a description of each component of the feasibility model, and the results of tests which showed that the specification of 1/2% speed control for a 10% load change could readily be met.



## SYSTEM SURVEY

The five types of basic speed control systems are shown in Fig. 1. Any of these types can be executed with pure fluid means. The pertinent features of these controls are the type of reference signal, the error-sensing technique and the actuator type.

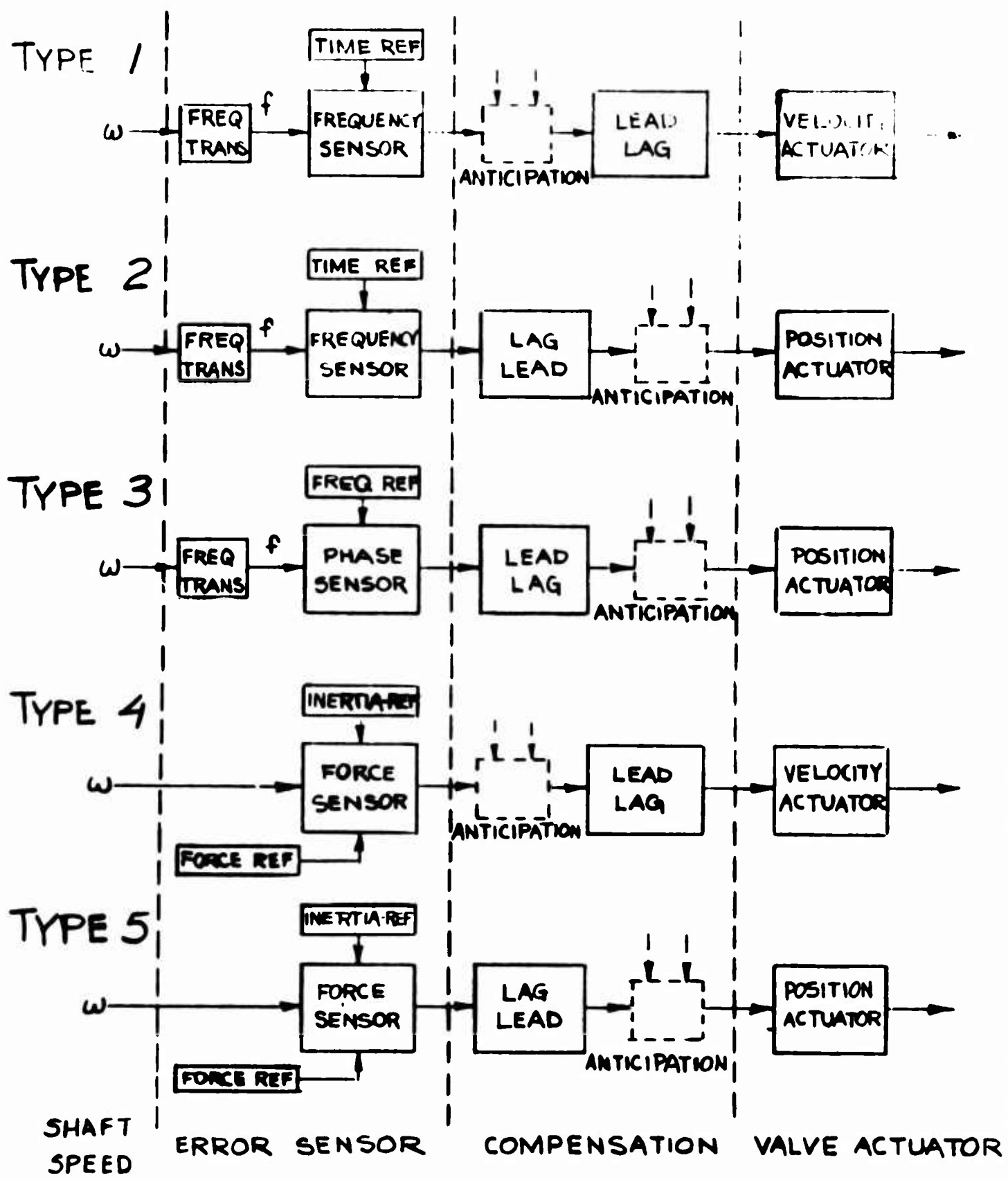
The three basic types of reference signal are time reference, frequency reference, and inertia reference. The error detectors sense frequency error, phase error or force error. In the phase sensor the reference signal phase angle is compared with the phase of the shaft signal. The frequency sensor on the other hand primarily recognizes differences in intervals of cycle time between the shaft signals and speed reference signals. The use of the phase sensor infers that the objective of the control system is to hold the shaft speed and frequency reference locked in synchronism at all times. This is a relatively difficult control function to perform. The frequency control maintains equal time intervals.

The force error systems are the well known flyball system in which a force from the flyweights is compared to a set spring or weight force. This system can also employ a comparison between the pressure generated by an impeller and a pressure reference signal.

The two types of actuators shown are the velocity actuator and position actuator. In the position actuator the output position is proportional to input signal. This in general requires a position feedback network or, as normally done, a feedback linkage system. The velocity actuator has an output velocity which is about proportional to input signal. This is a damped piston which has a velocity as a function of differential pressure.

The compensation networks that must be used with each system are also shown in Fig. 1. For example, in type 1, the open-loop system has potentially two integration functions. The actuator is itself an integrator as its output position is proportional to the time integral of input signal. In addition the speed of the turbine shaft is an integral of valve position change. These two open-loop components produce a potentially unstable system which may be compensated by a lead-lag in order to increase the phase margin at crossover. There may also be external compensation or "Anticipation" signals. These in general require additional sensors, so were not included in the system choice.

Fig. 1



BASIC SPEED CONTROL SYSTEMS

## Speed Reference Signal Generator

A survey of reference signal generators that are compatible with the system requirement of  $1/2\%$  accuracy indicates that the tuning fork is most desirable. A mechanical force generator such as a flyweight system is ruled out because of the mechanical complexity. The use of a condensate pump to produce a pressure as a function of speed is unsatisfactory because of the variation in fluid density over the range of temperatures. Fluid elements such as a fluid oscillator, time delay or time constant are also affected by the temperature change. At the temperatures of the operating system a 50 degree Fahrenheit change of temperature will produce a 1.84% time reference change based upon variations in sonic velocity with temperature. A tuning fork without special compensation for temperature has a potential frequency change of .05% over the 50 degree Fahrenheit change anticipated. Since this is one tenth the allowable system error it is a usable reference frequency.

Time reference generated from both sonic delay lines or from inductance-capacitance circuits are affected by the changes of sound velocity with temperature. Sound velocity is proportional to the square root of absolute temperature. A change of 50 degrees Fahrenheit at 900 degrees Fahrenheit produces a percentage change of absolute temperature of 3.68%. The sound velocity variation is 1.84%. Calculations to substantiate these conclusions are given in Appendix A.

The resonant frequency of the tuning fork is the square root of spring constant divided by mass. Assuming a constant modulus of elasticity, the change in spring constant is inversely proportional to the cube of length. As length increases with temperature the natural frequency will vary inversely with the  $3/2$  power of temperature. There are materials available which are called constant modulus alloys which utilize both the change in size and variation of modulus with temperature to produce tuning forks which actually maintain constant resonant frequency over a wide temperature range. The calculation of change in frequency from the change in length with temperature is given in Appendix A.

## Error Detector

A most significant concept is the technique for establishing a near absolute reference at the desired speed level. For example, in analog systems the speed signal is normally proportional to the speed. At zero speed the output is zero and at maximum speed a maximum signal is obtained. As a result, there is a very small percentage change in speed signal over the speed range desired. By establishing a speed reference at or near the desired speed the magnitude of the output signal sensitivity for a speed error is increased.

As a result, the recalibration of the signal with temperature is minimized. A change in temperature only affects the speed error signal which is a small percentage of the absolute speed. It is assumed that the tuning fork frequency can be compensated for temperature changes by the selection of appropriate materials.

## Actuator

The velocity actuator is a desirable component because it reduces the complexity of the mechanical system. Secondly, its design is compatible with the system design objectives; an actuator that does not require very close tolerances and can be designed with reliable metal piston ring seals. Some consideration was given to the use of a pure fluid steam valve. The necessity for the high efficiency in this system precludes its use.

## Conclusion

As a result of this survey the development of the control system was directed toward the use of a velocity actuated steam valve and a tuning fork time reference in a frequency sensitive control. This is type 1 in Fig. 1.

## FEASIBILITY MODEL

Figure 2 is a photograph of the feasibility model, and Fig. 3 is a schematic. It consists of a scaled turbine generator, piston-operated valve and constant speed control system. The control system is composed of the speed error detector, which measures the difference between the shaft speed and the frequency of a tuning fork, the control circuit plate and associated passive networks. The control system has only one moving part, the tuning fork time reference. Air was selected as the working fluid for this model to simplify construction on the basis of tests which confirmed that there were no significant differences in the operation of fluid amplifiers using air or steam as long as the steam was dry. Sample results of these tests are presented in Appendix B.

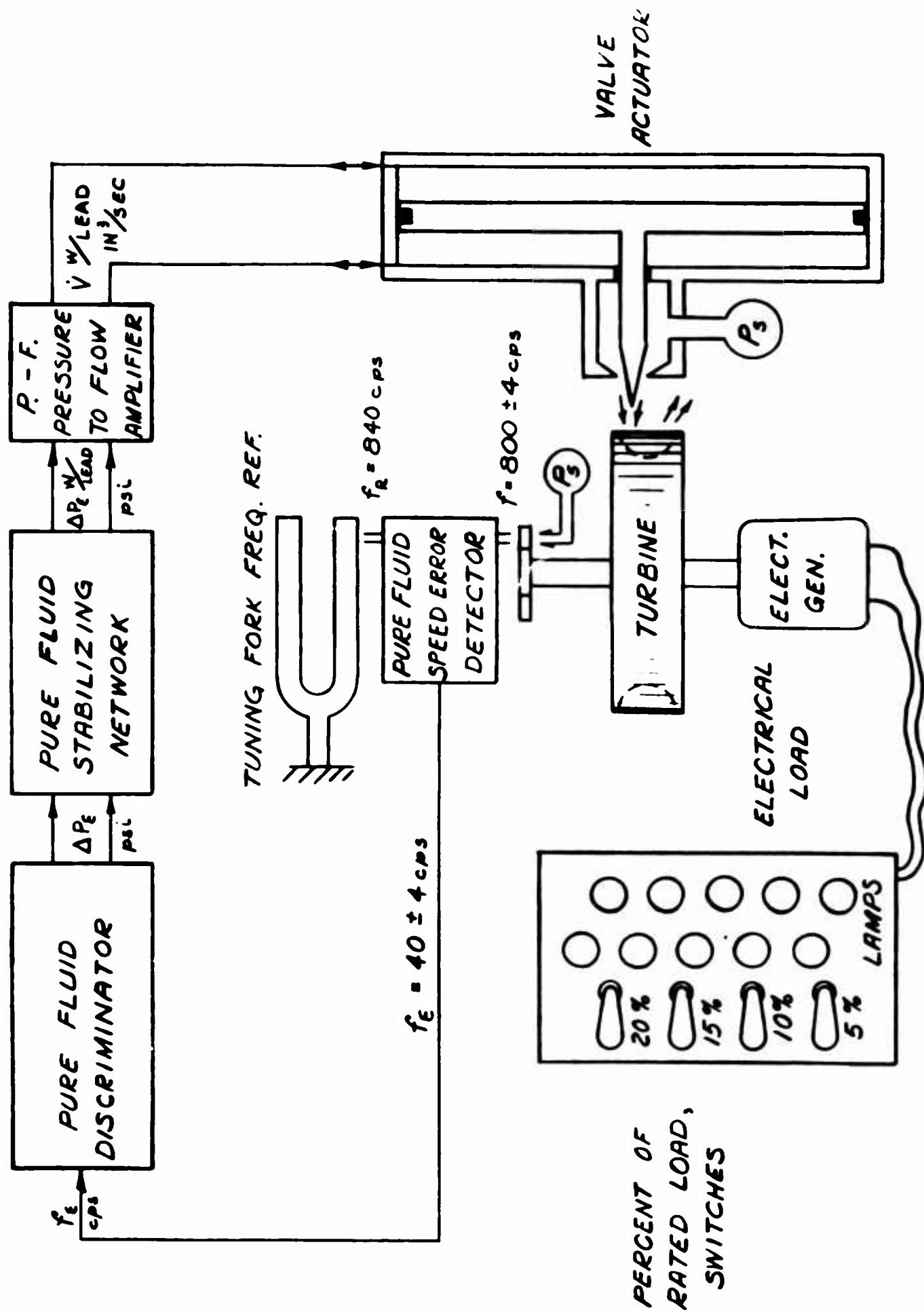
The speed error detector measures the frequency difference between pulses from the rotating shaft and from the tuning fork. The output beat frequency drives two parallel resonant circuits which are adjusted for resonance above and below the desired forty cycle per second beat frequency. When the shaft speed is at the desired 12,000 rpm, the beat frequency is 40 cycles per second and the outputs from the two parallel resonant circuits are equal. When the speed exceeds the desired value, the output from one resonant circuit increases and the other decreases producing a corrective control signal. Appropriate lead-lag networks are included in the control to provide stability.

It should be pointed out that the turbine generator shaft assembly has been scaled to provide a time constant equivalent to that of the full-scale model. In addition, the size of the breadboard components including the actuator is compatible with the full-scale model. (In such a full-scale model the tanks and interconnections would be incorporated in a common manifold rather than being composed of many individual tubes). As a result, the control system has the same dynamic performance as would be required by a full-scale assembly. A detailed description of the speed error detector and control circuitry is given below.

Fig. 2



Oblique view of Pneumatic Pure Fluid Speed Control showing the bench test of the control driving a scaled air driven turbine generator.



FINE SPEED CONTROL SYSTEM, SCHEMATIC

## Speed Error Detector

As shown in Fig. 3, the signal from the turbine shaft is a jet interrupted at four cycles per revolution which produces a nominal frequency of 800 cycles per second. This jet is directed toward receiver 1 of Fig. 4 which produces a control signal in the amplifier at 2. The supply pressure,  $P_+$ , for the first amplifier in Fig. 4 produces a pressure in volume 3 which exhausts in a jet from 4 to the tuning fork. The function of this jet is to both excite and, by the mechanical construction of this jet nozzle, to damp the motion of the tuning fork. Its oscillation in turn produces a fluctuation in the pressure at 3, at nominally 840 cycles per second, the resonant frequency of the tuning fork. The signals at 2 and 3 are subtracted in the first amplifier, amplified and rectified at 5 producing the signal shown at the bottom of Fig. 4. The output is filtered for high frequencies, to some extent, by the volumes and resistances of the lines and pure fluid elements. The resulting frequency is a sensitive measure of the speed.

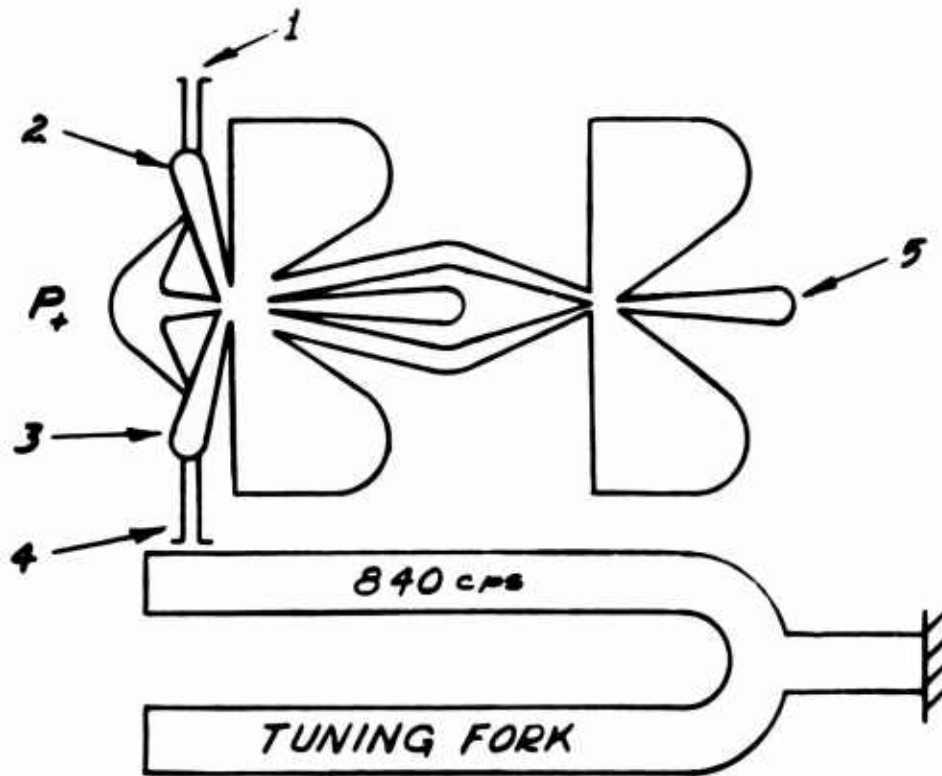
## Discriminator, Parallel Resonant Circuits

The output signal 5 is used to drive the parallel resonant circuits as shown in Fig. 5. The input signal 5 drives amplifiers 6 and 7. The output circuits of the two amplifiers are tuned respectively for 60 and 30 cycles per second, as shown, by a combination of an inductive line and volumes. The volumes are connected at 8 and 9 external to the circuit plate. Due to the adjustments of the resonant circuits the amplitudes at 40 cycles per second at locations 8 and 9 are identical. However, if the frequency drops below 40 cycles per second the amplitude of the signal at 8 is greater than that at 9. The signals at 8 and 9 are subsequently amplified and rectified producing a DC output at 10 and 11 which reflects the frequency error from 40 cycles per second. For example, in the diagram of Fig. 5 the output amplitude curves as a function of frequency are shown for the 60 and 30 cycle per second resonant networks. The output amplitudes for the condition described above are shown. Note that for frequencies less than 40 cycles per second the output amplitude from the 30 cycle per second network is always greater than from the 60 cycle per second network and above 40 cycles per second the reverse is true.

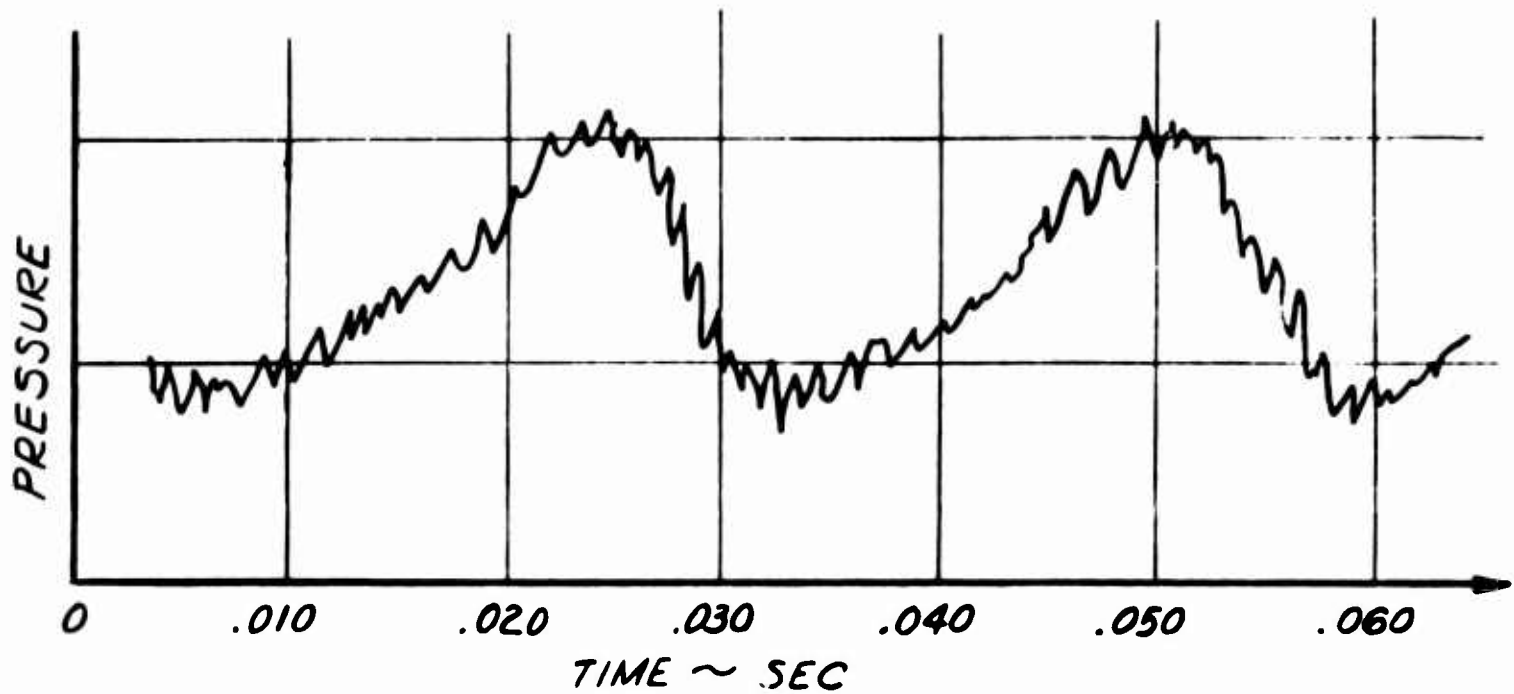
These signals are subsequently subtracted resulting in the output curve shown dotted in Fig. 5.



FIG. 4

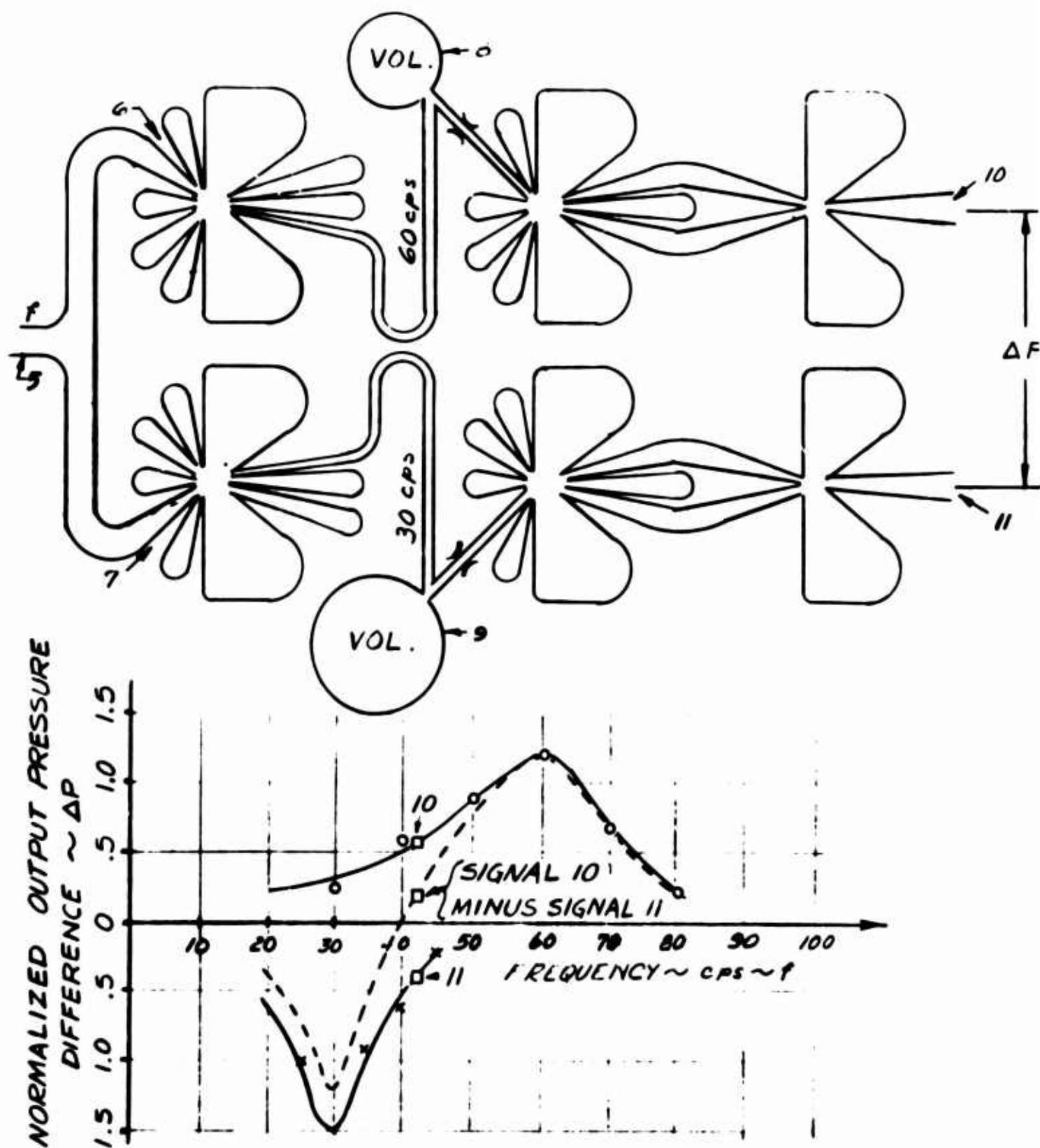


PRESSURE WAVE SHAPE AT 5



SPEED ERROR DETECTOR

FIG. 5



DISCRIMINATOR, PARALLEL RESONANT CIRCUITS

## Lead-Lag Stabilizing Network

The lead-lag stabilizing network is shown in Fig. 6. Signals 10 and 11, which are subtracting, produce the input  $\Delta P_1$ . The output from this circuit is  $\Delta P_3$  and has a gain and phase effect as shown in the curve of Fig. 6. A stability analysis and calculations for the development of the lead-lag network are given later.

The network shown is a negative feedback circuit. The output  $\Delta P_2$  is fed back to the input of the first amplifier through the resistances 12 and 13 and capacitive tanks 14 and 15 which are external to the circuit. The time constant of this resistive capacitive network is adjusted so that at frequencies less than one radian per second the output  $\Delta P_2$  serves to oppose the input signal  $\Delta P_1$ . At higher frequencies the feedback circuit is not effective and the output gain, the ratio of  $\Delta P_2$  to  $\Delta P_1$ , is the forward gain of the three amplifiers. The result is a reduced gain at frequencies less than one radian per second and full gain at frequencies above eleven radians per second. This output  $\Delta P_2$  is subsequently amplified which produces the signal  $\Delta P_3$ .

## Pressure-Flow Amplifier

The pressure-flow amplifier is shown in Fig. 7. This amplifier is designed to produce an output flow which is proportional to the control signal  $\Delta P_3$ . As a result, since the mechanical load on the actuator is small, compared to maximum pressure force, the velocity of the actuator is proportional to  $\Delta P_3$ . This function is accomplished by producing an output of the amplifier,  $\Delta P_4$ , which is the square of  $\Delta P_3$ . The receivers of the amplifier are separated more than the normal amount so that the received pressure is a nonlinear portion of the jet velocity profile. This produces the desired square effect.

FIG. 6

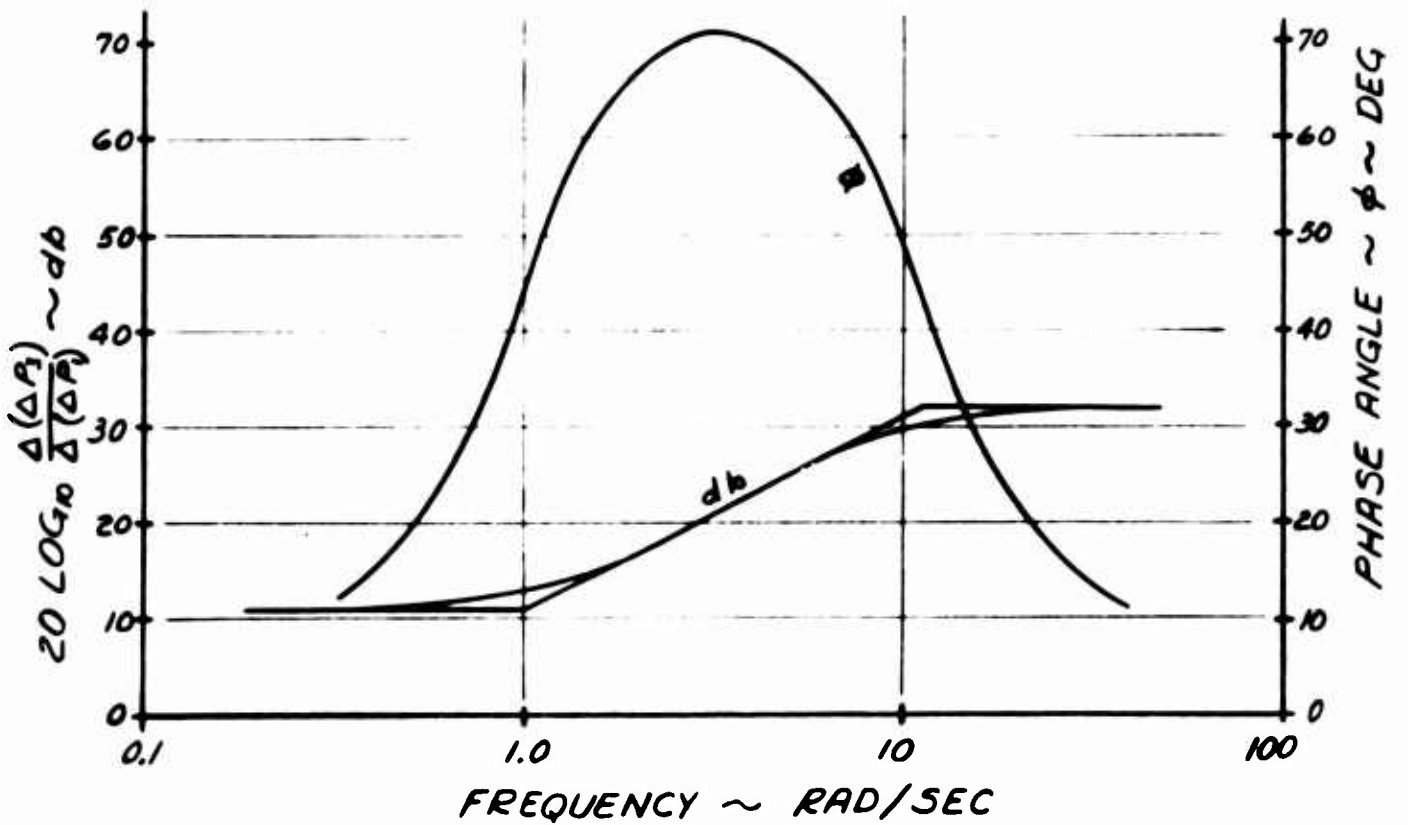
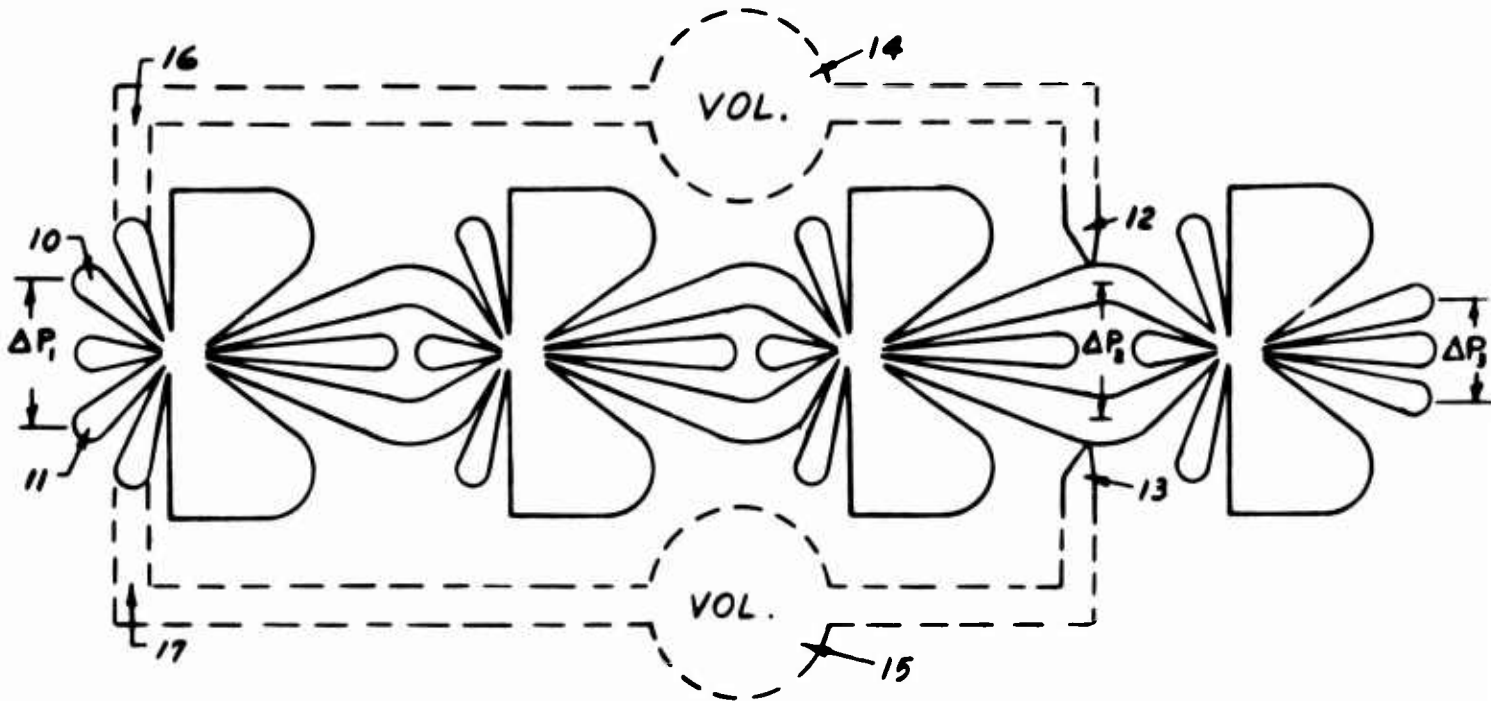
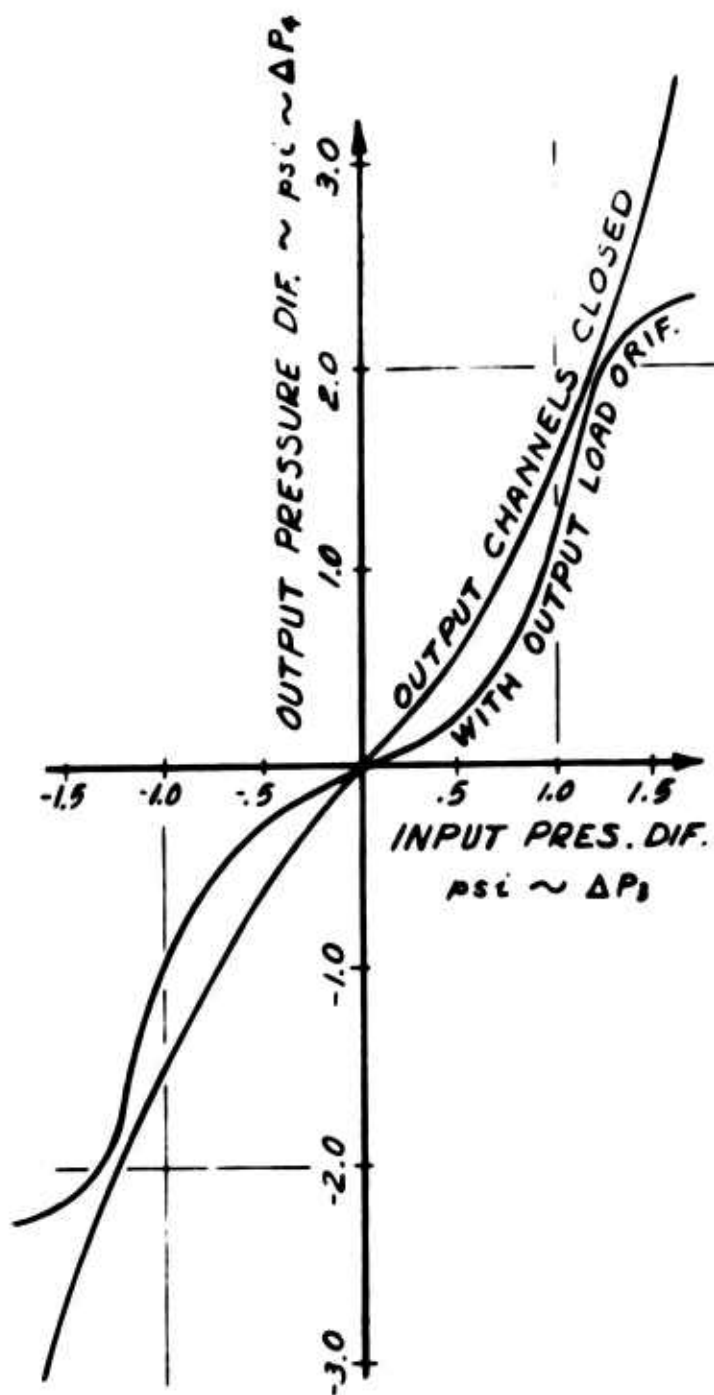
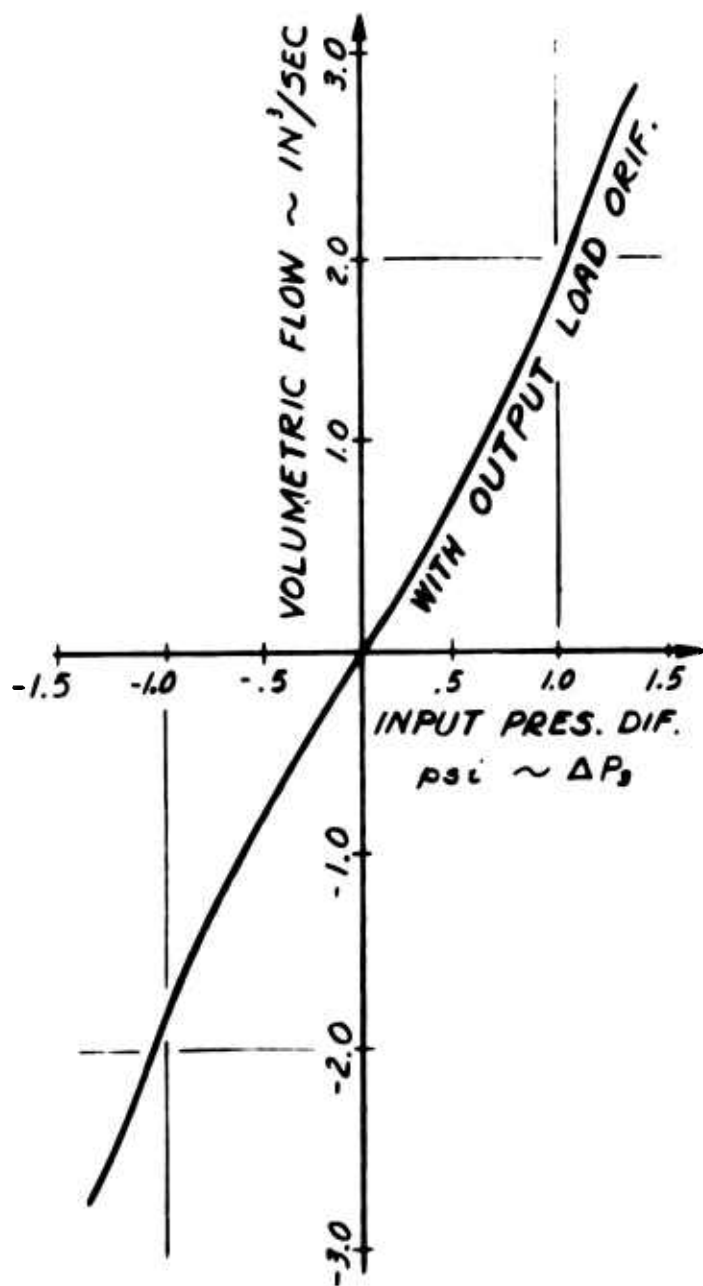
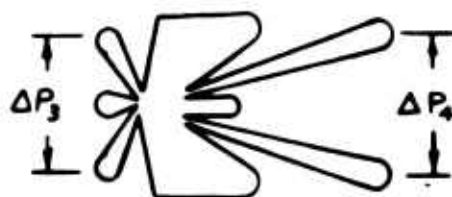


FIG. 7



## Stability Analysis

The open loop performance of the system is given in Fig. 8. It includes the performance of each component and the resulting open loop frequency response of the system.

The crossover slope or phase margin is set by the lead-lag network. The calculations for this network are given in Appendix C.

It should be noted here that the turbine generator shaft torque, inertia, and speed ratios in the model unit are scaled in such a manner as to provide the same time constant as in the intended application. The equation below shows that units which have the same ratio of speed error change to power change have the same values of the ratio: rated speed squared, inertia to power. As a result, the model unit has the same relationship of per cent speed error to per cent power change as in the intended application.

$$T_c = \text{Constant} = \frac{N_e \%}{P_e \%} \frac{N_r^2 I}{P}$$

$N_e$  = Speed Error

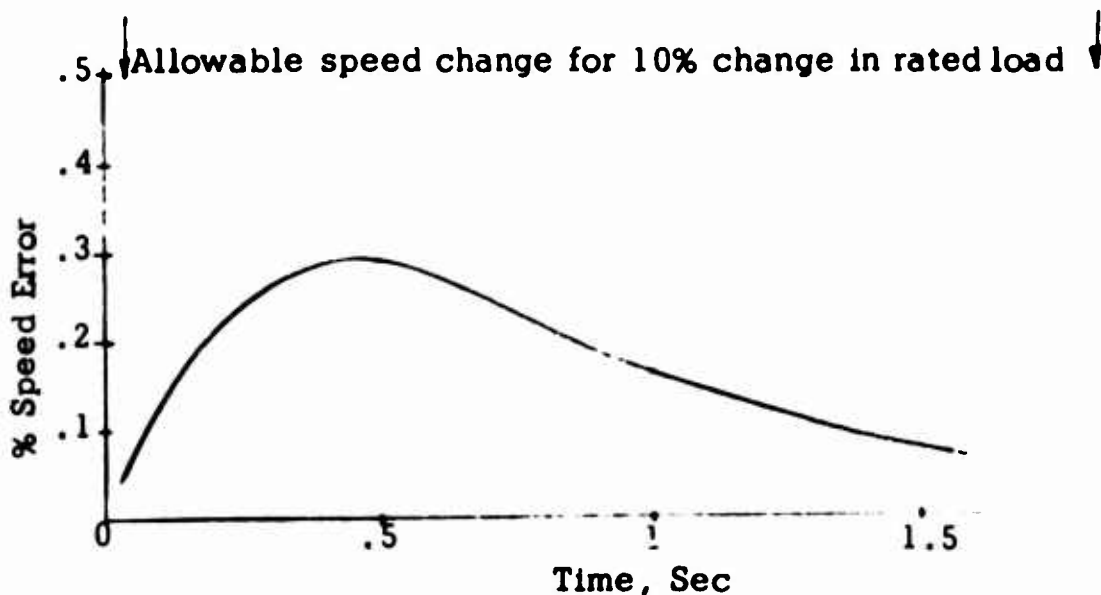
$P_e$  = Power Change

$N_r$  = Rated Speed

$I$  = Inertia

$P$  = Power, Rated

The expected transient response from the open loop characteristic is given below for a 10% load change.



$$\frac{\Delta \dot{\theta}_i}{\Delta \theta_i} = \frac{\Delta \dot{\theta}_o}{\Delta T} \times \frac{\Delta T}{\Delta X} \times \frac{\Delta X}{\Delta \dot{V}} \times \frac{\Delta \dot{V}}{\Delta P_2} \times \frac{\Delta P_2}{\Delta P_1} \times \frac{\Delta P_1}{\Delta f} \times \frac{\Delta f}{\Delta \theta_i}$$

$\dot{\theta}$  SPEED

T TORQUE

X VALVE DISPLACEMENT

$\dot{V}$  FLOW TO ACTUATOR

$P_2$  PRESSURE, FIG. 6

$P_1$  PRESSURE, FIG. 6

$\Delta f$  FREQUENCY CHANGE

$$\frac{\Delta \dot{\theta}}{\Delta T} = \frac{1430}{s} \frac{\text{RAD/SEC}}{\text{in-lb}}$$

$$\frac{\Delta T}{\Delta X} = 0.392 \frac{\text{in-lb}}{\text{in}}$$

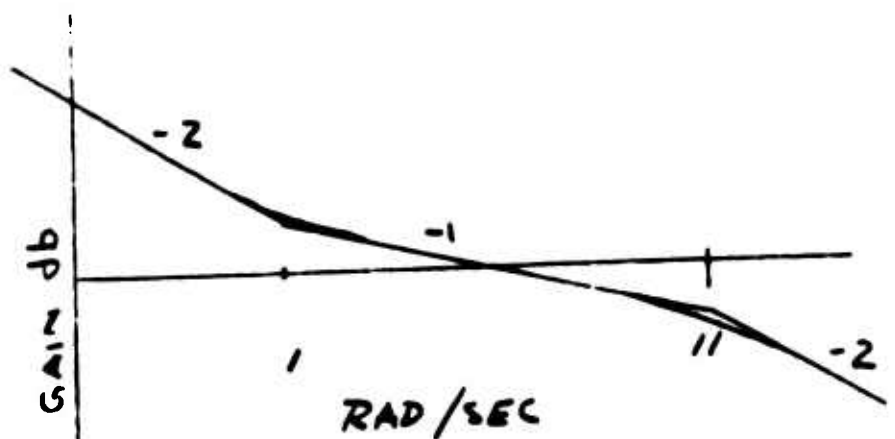
$$\frac{\Delta X}{\Delta \dot{V}} = \frac{.02}{s} \frac{\text{in}}{\text{in}^3/\text{SEC}}$$

$$\frac{\Delta \dot{V}}{\Delta P_2} = 1.82 \frac{\text{in}^3/\text{SEC}}{\text{PSI}}$$

$$\frac{\Delta P_2}{\Delta P_1} = \frac{3.64 \left( \frac{s}{40} + 1 \right)}{\left( \frac{s}{11} + 1 \right)} \frac{\text{PSI}}{\text{PSI}}$$

$$\frac{\Delta P_1}{\Delta f} = 0.057 \frac{\text{PSI}}{\text{C/SEC}}$$

$$\frac{\Delta f}{\Delta \theta_i} = \frac{2}{\pi} \frac{\text{C/SEC}}{\text{RAD/SEC}}$$



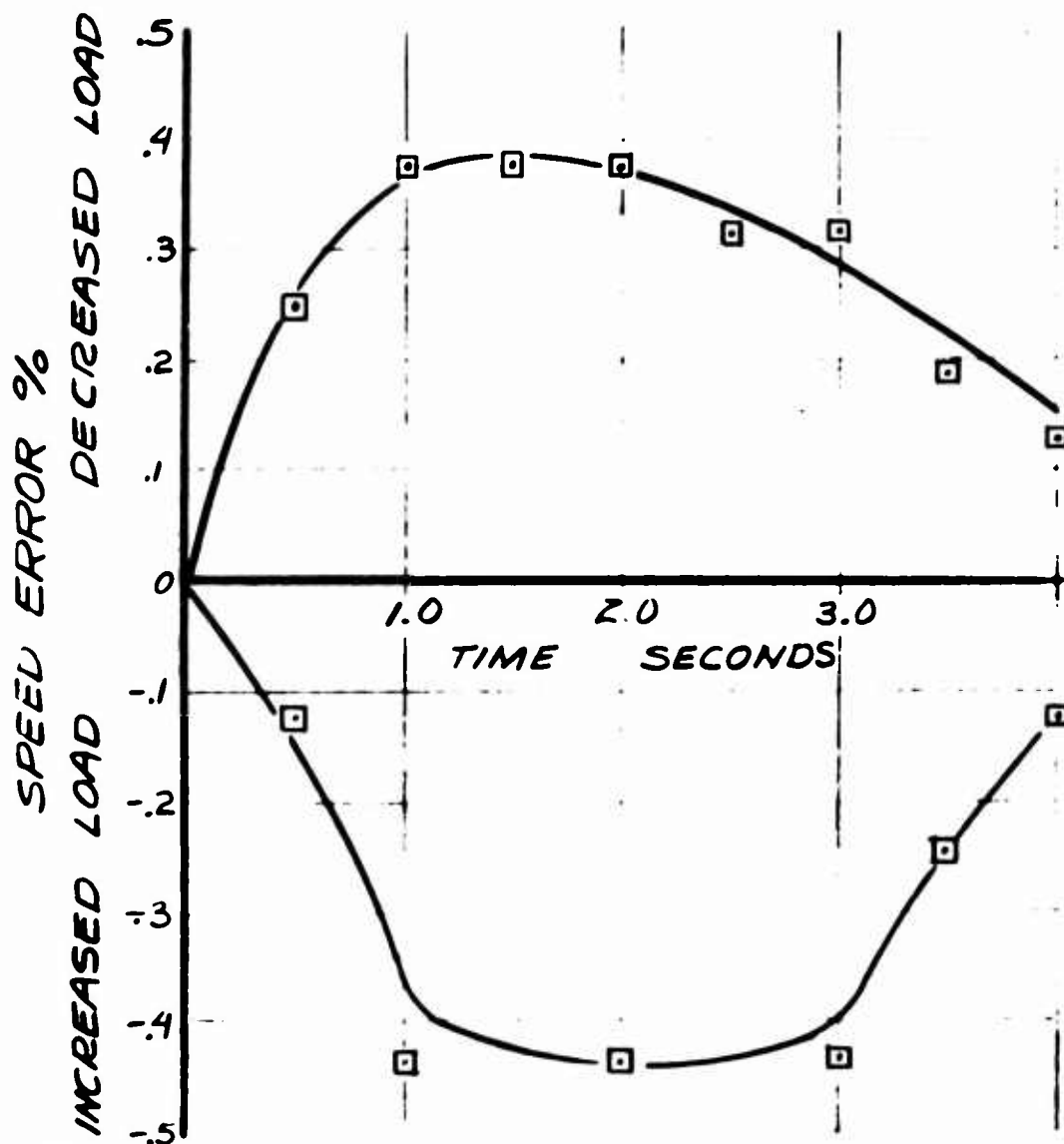
OPEN LOOP RESPONSE

## Test Results

The transient performance of the speed control was measured for speed error with a step load change. The results for a step change, both increasing and decreasing load, are given below.

The speed error was measured at the output of the discriminator circuit. This frequency, nominally 40 cps, changes proportionally with speed error. The pulses were recorded using a strain gage pressure transducer and a Massa recorder. The instantaneous speed error was measured by the period change of the output trace.

The test results below are for a  $\pm 20\%$  load change from a power level of 45%. In neither case did the speed error exceed 0.5%. The time to return to 0.1% speed error is about 4.5 seconds. For a  $\pm 10\%$  load change the speed error does not exceed 0.3% and the time to return to .1% error is about 2 seconds. This agrees reasonably well with the expected performance. Limited tests have shown that the response time is reduced when system gain is set at a larger value.





## APPENDIX A

### Effects of Steam Temperature Variation

ALLOWABLE STEAM TEMPERATURE VARIATION  
 $900^{\circ}\text{F} \pm 50^{\circ}\text{F}$

SONIC VELOCITY VARIATION

$$(\text{SONIC VEL}) \propto \sqrt{T_{\text{ABS}}}$$

$$\% T_{\text{ABS}} = (100) \frac{\pm 50^{\circ}\text{F}}{460 + 900^{\circ}\text{F}} = \pm 3.68 \%$$

$$\% (\text{SONIC VEL}) \sqrt{100 \pm 3.68} - 100 = \pm 1.84 \%$$

TIME REF. VARIATION FOR SONIC DELAY LINE

$$(\text{TIME REF}) \propto \frac{\text{LINE LENGTH}}{\text{SONIC VEL}}$$

$$\% (\text{TIME REF}) = \frac{100}{100 \pm 1.84} (100) - 100 = \mp 1.84 \%$$

TIME REF. VARIATION FOR VOLUME AND INDUCTANCE LINE

$$(\text{TIME REF}) \propto \frac{1}{(\text{SONIC VEL})} \sqrt{\frac{(\text{VOLUME})(\text{LINE LENGTH})}{(\text{LINE AREA})(\text{CROSS SECTION})}}$$

$$\% (\text{TIME REF}) = \frac{100}{100 \pm 1.84} (100) - 100 = \mp 1.84 \%$$

TIME REF VARIATION FOR TUNING FORK

1. ASSUME MOD. OF ELAS. DOES NOT VARY APPRECIABLY
2. ASSUME COEF. OF EXPANSION SAME AS STEEL AT ROOM TEMPERATURE
3. ASSUME EXPANSION ONLY IN LENGTH

$$\% (\text{LENGTH}) = 100 [1 + 6.5 \times 10^{-6} (\pm 50)] - 100 = \pm .032 \%$$

$$(K_{\text{SPRING}}) \propto \frac{1}{(\text{LENGTH})^3}$$

$$\% (K_{\text{SPRING}}) = 100 \frac{1}{(1.00032)^3} - 100 = \mp .096 \%$$

$$(\text{TIME REF}) \propto \frac{1}{\sqrt{K_{\text{SPRING}}}}$$

$$\% (\text{TIME REF}) = 100 \frac{1}{\sqrt{1.00096}} - 100 = \pm .05 \%$$

## APPENDIX B

### Comparison of Analog Valve Performance on Steam and Air

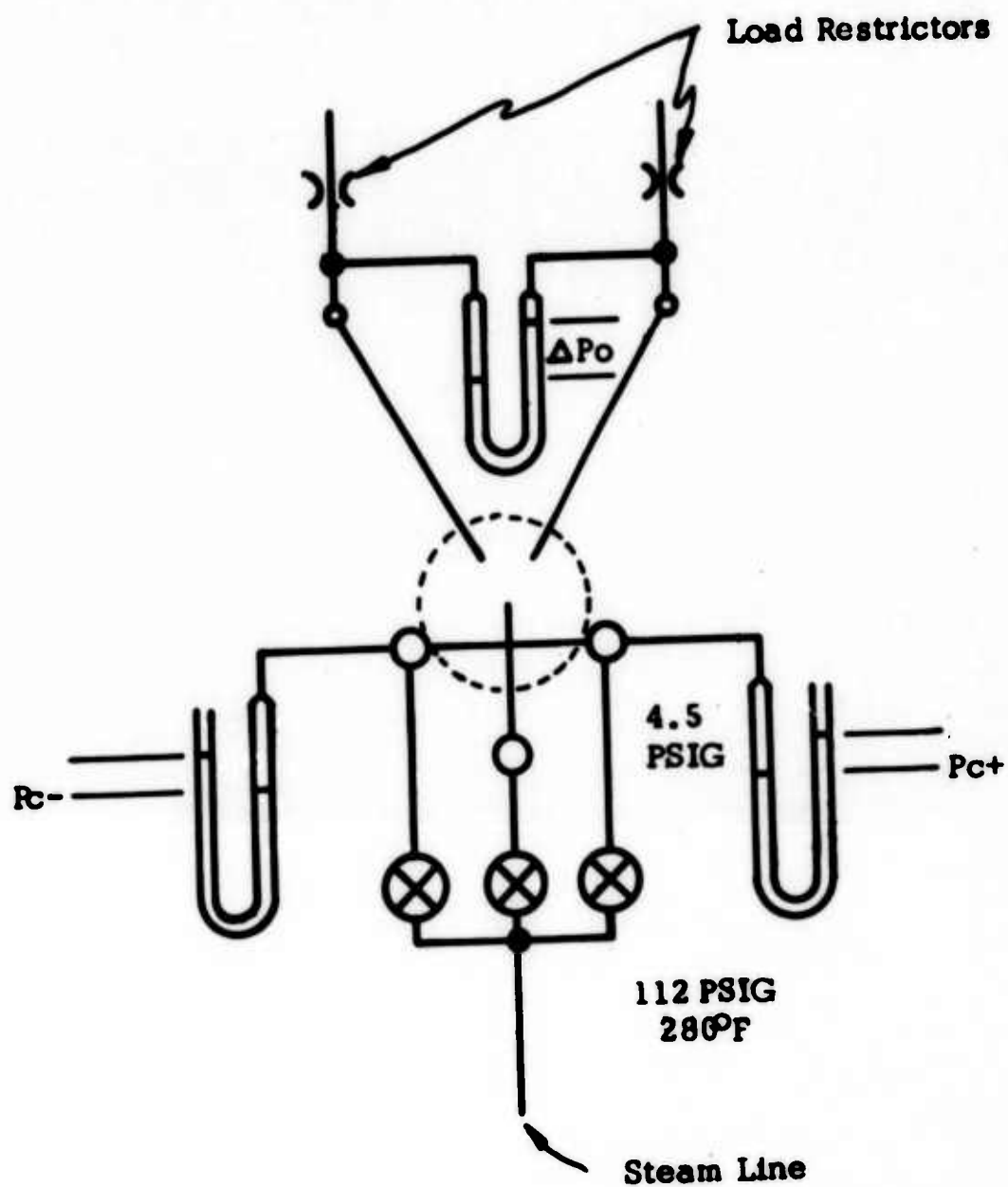
Steam and air tests were made on an analog amplifier with a supply pressure of 4.5 psig. A series of gain tests were made with steam over a range of control pressure levels which indicated that a control level of 0.54 psi produced the best gain. The gain obtained was 2.0. Room temperature air tests at this same control level produced a gain of 2.2. These tests indicate that there is no significant differences between operation with steam and air. The tests did show that moisture in the steam produces marked disturbances as water tends to come through the power nozzle in slugs. Operation on steam will require that the steam be to some degree superheated and that the unit be kept above the saturation temperature.

### Tests

The unit was supplied from a saturated steam line at 112 psig and dropped to 4.5 psig at 280°F. This indicates a superheat condition, but water droplet accumulation did occur in the unit. Some attempt was made to reduce this effect by lagging. This was only partially effective. The output orifices occasionally passed solid water through the load orifice with resulting momentary increase in outlet pressures.

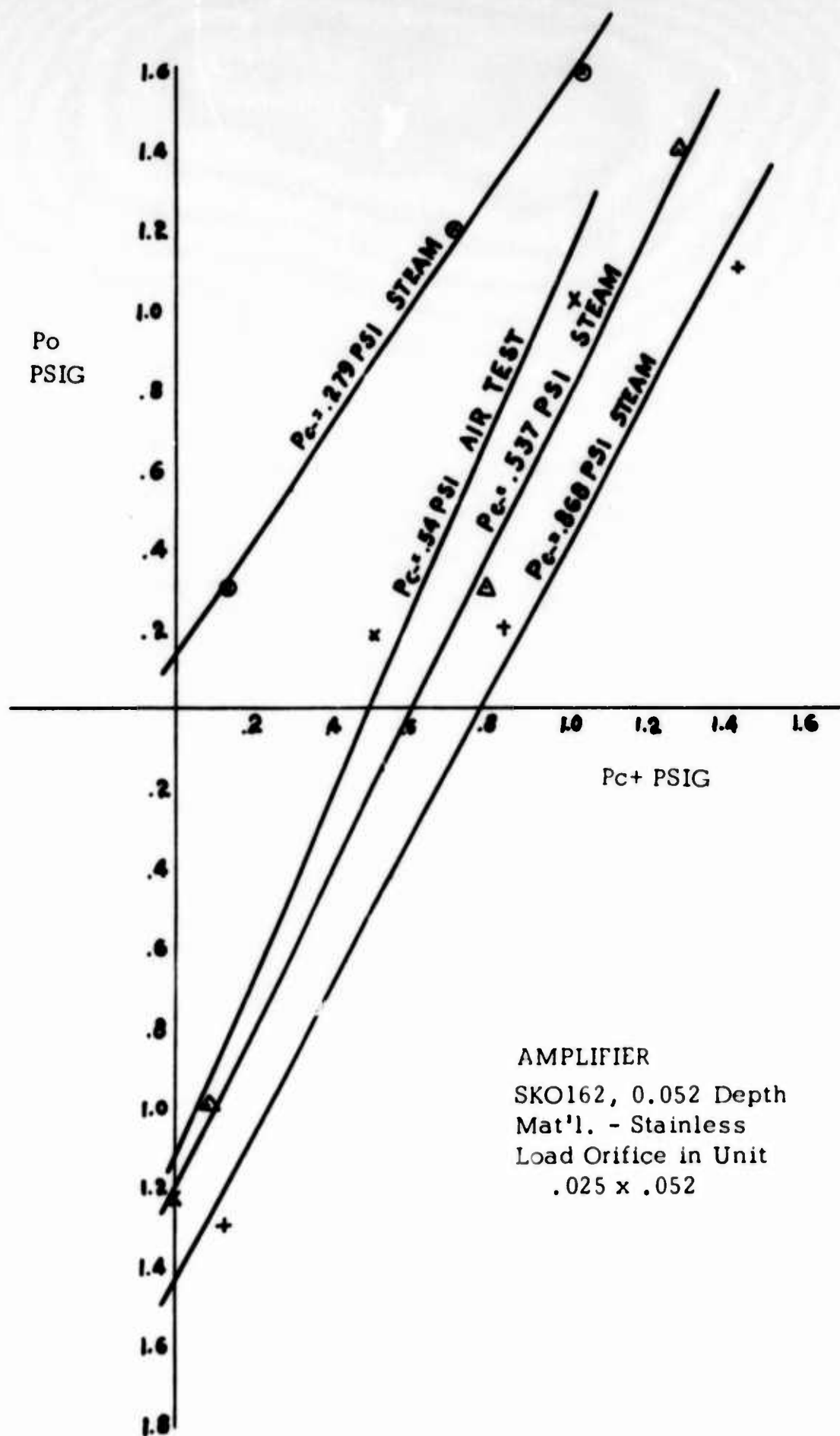
The test schematic is shown in Fig. 1. The supply pressure was maintained at 4.5 psig. The left control was held at 0.279, 0.537, and 0.868 psi for each test respectively on steam. The air test was made with the left control at 0.54 psig. For each test the right control pressure was varied from 0.0 to about 1 psig.

Fig. 1



Analog Valve Steam Test

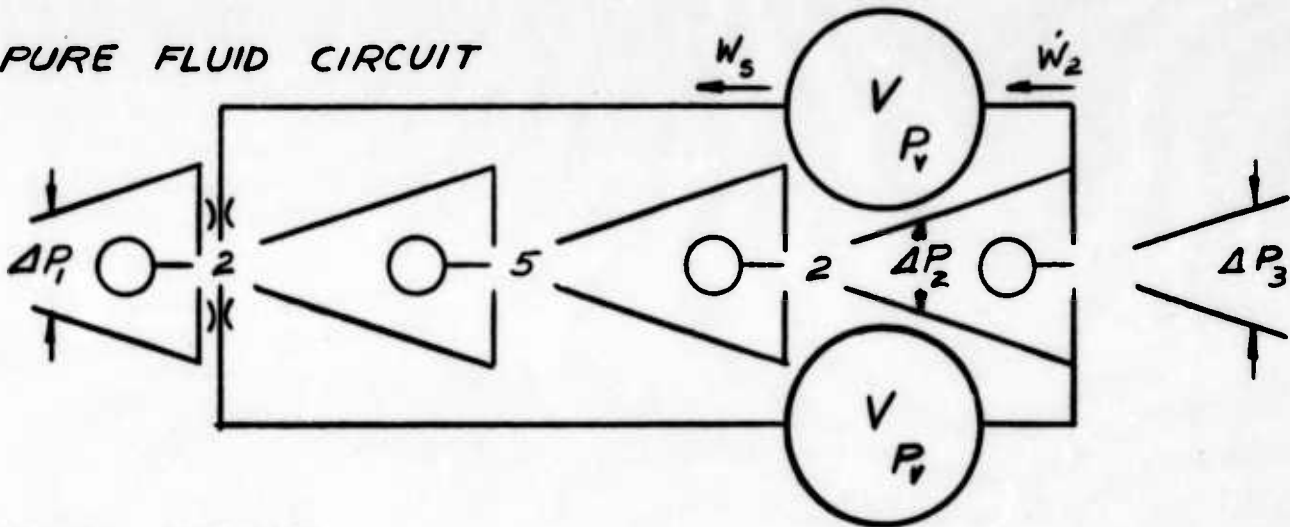
Fig. 2



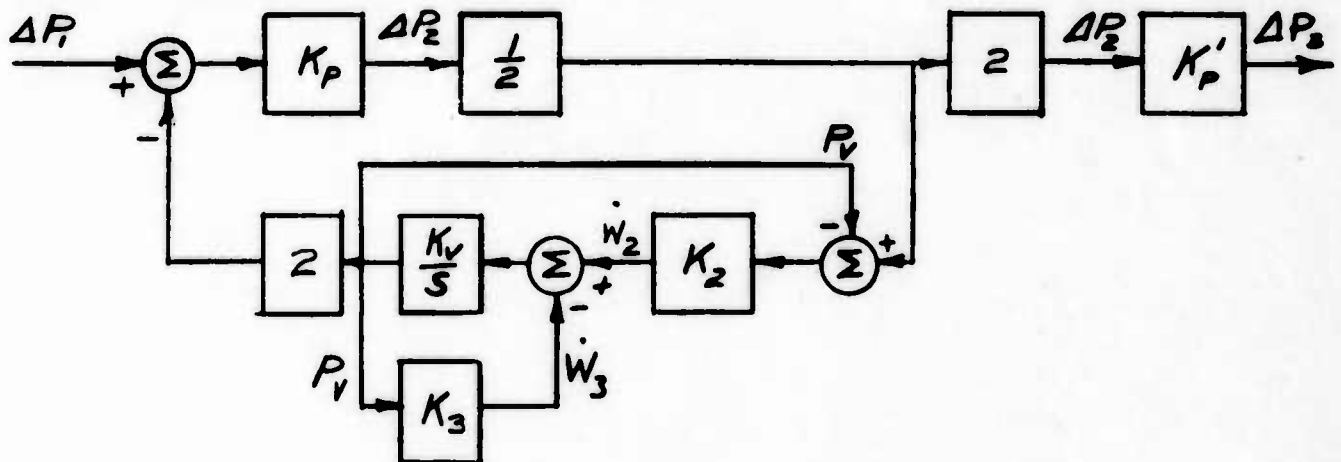
# APPENDIX C

## LEAD-LAG CIRCUIT CALCULATIONS

PURE FLUID CIRCUIT



BLOCK DIAGRAM



TRANSFER FUNCTION

$$\frac{\Delta P_3}{\Delta P_1} = \frac{\frac{K_p K_{p'}}{1 + \frac{K_p K_3}{K_2 + K_3}} (\tau s + 1)}{\left( \frac{\tau}{1 + \frac{K_p K_3}{K_2 + K_3}} s + 1 \right)}$$

WHERE

$$\tau = \frac{1}{K_v (K_2 + K_3)}$$

THE REQUIRED LEAD TIME CONSTANT IS 1.0 SEC

$$\tau = \frac{1}{K_v(K_2+K_3)} = 1.0 \text{ SEC.}$$

THE VOLUME CONSTANT FOR ISENTROPIC EXPANSION

$$K_v = \frac{\Delta P}{\Delta W} = 1.4 \quad \frac{RT}{V} = 1.4 \frac{(640)530}{V} = \frac{475,000}{V} \frac{\text{PSI}}{\#}$$

$$R = 640 \frac{\text{IN}}{\text{OR}}, \quad T = 530^\circ\text{R} = 70^\circ\text{F}$$

THE ORIFICE CONSTANTS,  $K_2$  &  $K_3$  ARE THE SAME

$$K_2 = K_3 = \alpha \sqrt{\frac{\rho_o}{2(P_a - P_d)}} = .0008 \sqrt{\frac{.0000443(386)}{2(.3)}}$$

$$K_2 = K_3 = \frac{\Delta \dot{W}}{\Delta P} = .000135 \frac{\#/\text{s}}{\text{PSI}}$$

THE REQUIRED VOLUME IN EACH FEED BACK IS

$$V = \tau (K_v V) (K_2 + K_3) = 1.0 (475,000) (.00027)$$

$$V = 128 \text{ IN}^3$$

THE HIGH FREQUENCY GAIN IS

$$\left. \frac{\Delta(\Delta P_3)}{\Delta(\Delta P_1)} \right|_{\text{HIGH FREQ}} = K_p K_p' = (2 \times 5 \times 2) 2 = 40$$

THE LOW FREQUENCY GAIN IS

$$\left. \frac{\Delta(\Delta P_3)}{\Delta(\Delta P_1)} \right|_{\text{LOW FREQ}} = \frac{K_p K_p'}{1 + \frac{K_p K_2}{K_2 + K_3}} = \frac{40}{1 + 20(\frac{1}{2})} = 3.64$$

$$\frac{K_2}{K_2 + K_3} = \frac{1}{2}$$

THE LEAD TIME CONSTANT IS

$$\tau = 1.0 \text{ SEC}$$

THE LAG TIME CONSTANT IS

$$1 + \frac{\tau}{\frac{K_P K_2}{K_2 + K_3}} = \frac{1.0}{1 + 20\left(\frac{1}{2}\right)} = \frac{1}{11} = .091 \text{ SEC}$$

THE EVALUATED TRANSFER FUNCTION IS

$$\boxed{\frac{\Delta(\Delta P_3)}{\Delta(\Delta P_1)} = \frac{3.64 (1.0s + 1)}{(.095s + 1)}}$$

# **A Pure Fluid Hydrofoil Control System**

**by**

**Romald E. Bowles  
Edwin U. Sowers III**

## **Introduction**

**There is at present a rapidly growing interest in Hydrofoil Boats .**

**There has existed a gap in the modes of transportation over bodies of water .  
Transportation by the conventional type of ship is relatively inexpensive but  
slow . If time is of sufficient importance , flying , though much more expensive ,  
becomes justifiable . The hydrofoil appears to fit into the space between these  
two means .**

**The hydrofoil craft "flies" on foils , in many cases similar to airfoils .  
At cruising speeds the hull is lifted out of the water , with only the foils and  
supporting struts contributing drag forces . The speed barrier encountered in  
conventional craft due to hull friction forces and energy losses in large  
gravity waves is thus overcome .**

**The greater speeds and improved maneuverability of hydrofoil craft  
offer great possibilities militarily , such as in high speed attack and landing  
craft . There are already many hydrofoil boats in commercial use , primarily  
in passenger ferry service on inland waterways . In the majority of cases  
these commercial craft are supported by surface piercing foils which , over**



a range , are inherently stable and require a minimum of external control. Looking from the front of the craft , the foils appear as a large V with only the lower portion submerged at cruise speed. As the craft starts to settle into the water more foil surface is submerged and lift is increased; if the ship starts to rise out of the water lift decreases. Thus , the foils tend to follow the water surface in a manner roughly similar to water skis. Although stable under relatively smooth conditions , under more adverse conditions the ride becomes unacceptably rough and can become unstable.

The largest percentage of current development is directed towards submerged foil systems where the supporting foils are wholly submerged and truly "fly" in the manner of airfoils. By means of a control system somewhat similar to that of an airplane the lift forces exerted by the supporting foils may be regulated to more nearly sustain level flight through rough seas. Vertical acceleration forces can be minimized and sea conditions not navigable by surface piercing foil systems can be accommodated.

Bowles Engineering Corporation is engaged in a program directed towards the development of pure fluid type hydrofoil control systems. The work is being carried out under contract with the U. S. Navy Bureau of Ships , with Mr. M. D. Martin , Code 632 , responsible for the technical aspects of the program.

A scaled, submerged foil, fluid control system model has been designed and successfully tested. This report will consider the development and testing of this model. The design approach will be described. It will be shown that the performance predicted by linearized flow theory was substantiated by dynamic testing of the model system.

### Hydrofoil Craft Control System

The hydrofoil craft control system is required to control craft vertical position. In controlling vertical position two requirements exist which are not under all conditions compatible. It is desired that vertical acceleration forces be minimized, approaching the condition of the craft moving along in a fixed plane independent of wave motion. This condition cannot be satisfied under all conditions however, such as when waves become of sufficient height as to slap against the hull bottom or cause the supporting foils to broach. Thus vertical position must be controlled taking into account both height above water surface and vertical acceleration.

In addition to height, pitch and roll, as well as pitch and roll rates must be controlled. The system must facilitate take off and landing and permit coordinated banked turns.

Since the hydrofoil craft is supported completely by foils, the problem reduces to control of the instantaneous lift force exerted by the various foils so as to meet the above requirements.

### Control System Considered by BEC

In this phase of the program we were concerned primarily with a system for controlling the lift forces of a single foil. Having accomplished this goal a number of foils can then be coordinated into an overall craft control system.

The first approach, with which this paper deals, was to position the hydrofoil about a pivot axis to control foil lift forces. In subsequent work other means of lift control, such as jet flaps, are being investigated.

Specifically the function of the fluid control system is to maintain a constant lift force in the presence of waves. It is desired that the instantaneous relationship of foil angle to flow angle be controlled so as to minimize deviations from a constant lift value.

A schematic of the first control system is shown in Figure 1, a closed loop system including:

- (1) a means of measuring deviations of lift, as indicated by the product of dynamic pressure and relative angle of attack, from the desired value,

- (2) a means of amplifying this error signal,
- (3) a means of actuating the foil,
- (4) a means of providing position feedback.

Advantages of a closed loop servo system are the elimination of unduly rigid linearity requirements and highly accurate calibration, along with improved reliability.

The foil was mounted such that it could pivot about an axis nearly  $1/4$  chord from the leading edge. A foil type lift sensor, developed by Bowles Engineering Corporation, was incorporated into the leading edge of this foil. The signal output obtained from this sensor being proportional to the product of the angle of attack,  $\alpha$ , and dynamic pressure,  $\frac{1}{2} \rho V^2$ , is proportional to foil lift within the necessary range of parameters. Any error in lift was amplified and fed into a piston type actuator. By means of an actuating strut connected to the foil a corrective rotation of the foil was achieved. As the sensor was mounted in the foil the resulting lift correction was directly fed back to the system by the sensor.

Figure 8 shows the hydrofoil test model with the foil supported by two vertical struts. Figure 10 shows the hydrofoil model mounted in a water tunnel during testing. Waves were generated by an oscillating foil upstream from the hydrofoil. Lift forces generated by the foil due to the generated waves were measured with the control system operating and with

the foil locked. It was found that variations in lift force were greatly reduced with the control system in operation.

All of the involved control functions were accomplished by means of pure fluid elements, using air as the operating medium.

### Lift Sensor

In looking at the various parts of the system the lift sensor will be considered first. The foil type lift sensor makes use of the variation in pressure distribution on the surface of a foil with angle of attack<sup>1</sup>. Figure 2 shows the basic lift sensor.

If the pressure at two properly located points on the surface of a foil, on opposite sides of the centerline, are monitored, and the difference between these pressures sensed, this difference is proportional to angle of attack and lift under steady state conditions. Holes intersecting the foil surface connect to chambers within the foil. Steady state water channel tests showed  $\Delta P$  to be linear with respect to angle of attack to nearly  $\pm 6^\circ$ .

As mentioned earlier, the control system was to be completely pneumatic. Thus, an interface was required between the water external to the foil and the first pneumatic logic element.

The sensor system devised to meet this requirement is shown in Figure 3. A flow to pressure converter was added to the sensor foil. From a constant pressure supply,  $P+$ , air was passed through pressure dropping orifices to chambers within the sensor, exiting from a series of holes in the sensor leading edge.

The hole exit pressure being a function of angle of attack, flow then through the sensor holes was likewise dependent upon angle of attack. For an angle of attack other than zero the flow through the series of holes in the upper and lower surfaces differed, thus producing differing pressure drops across the two orifices. The pressure difference taken across the downstream sides of the two dropping orifices was proportional to angle of attack.

Figure 4 shows a plot of non-dimensional pressure difference as a function of angle of attack in degrees. Linearity was fairly good over a range of  $12^\circ$ . The curve not passing through the origin was due to a bias in angle measurement. Figure 4 also shows gain to be nearly independent of supply pressure.

This sensor system then, at least under steady state conditions, satisfied two most important requirements. It provided a pressure signal proportional to angle of attack or hydrofoil lift, and a hydraulic/pneumatic interface.

Dynamic tests were made on the sensor system to obtain the dynamic characteristics necessary for design of the control system. The sensor foil was oscillated about a number of different pivot locations while submerged in a constant velocity flow of water. From the dynamic test data frequency response was determined. Bode plots were made showing amplitude attenuation and phase shift with respect to angle of attack as a function of frequency. From these Bode plots the transfer function for the sensor system was derived.

### Foil Actuating Characteristics

A theoretical determination was carried out by Hydronautics, Inc.<sup>2</sup> to determine the required foil actuating forces. The moment required to sinusoidally oscillate the foil was determined in terms of amplitude and phase as a function of frequency. Requirements were determined for a number of pivot axis locations.

Based on this information the pivot axis was located at nearly  $1/4$  chord downstream from the leading edge. Locating the pivot axis further than  $1/4$  chord from the leading edge would introduce foil instability, externally applied moments being in phase with rotation. Locating the pivot point further forward would require a higher actuating moment at higher oscillation frequencies.

## System Design

Design of the control system was carried out using standard techniques. The system was analyzed by means of Bode plots obtained from transfer functions of the various parts of the system. Transfer functions for the pneumatic system components were derived using linearized pressure flow theory. Sonic time delays within the system were included in the system analysis.

Figure 5 shows a block diagram of the complete system. For the initial tests the system was set to maintain a zero lift condition, any deviation from zero being considered an error. A reference other than zero can be called for by the addition of a bias to the system.

The error signal output of the sensor system, a function of the product of dynamic pressure and foil relative angle of attack, was amplified in a computer circuit and fed into a power amplifier. Output of the power amplifier directed into a piston actuator produced a corrective rotation of the foil, readjusting the lift amplitude and causing a new signal to be fed directly back to the sensor, due to mounting of the sensor in the foil itself.

Figure 6 shows the system in more detail. Actual silhouettes of the elements used are shown, though not in actual relative size in all cases. All of the elements used except for the power amplifier were standard Bowles



Engineering Corporation analog elements. The elements shown in black silhouette were fabricated by our Optiform process.

The output from the sensor system, not shown, was fed into a buffer amplifier, whose function was to maintain known sensor performance independent of adjustments to the remainder of the system. The buffer amplifier was followed by a 5 stage analog amplifier with pressure gain greater than the anticipated requirement. Between the buffer and 5 stage amplifier, bleeds were incorporated to permit gain and bias adjustment during testing. A Colston Ladder type low pass filter was included in the 5 stage amplifier circuit between the third and fourth stages for high frequency noise attenuation. Between the output of the 5 stage amplifier and the power amplifier a pressure to flow amplifier was used to obtain proper impedance matching. Output of the power amplifier was fed to a piston type actuator as shown.

Of considerable concern in designing the system was the minimizing of signal lag through the system. An open loop mathematical analysis of the system showed that when applying a sinusoidally varying error signal the lag in corrective rotation of the foil would become a problem at fairly low frequencies. The foil actuating piston, where flow is converted into an actuating force, inherently contributed a  $90^{\circ}$  lag. Flow variations passing through large volumes with relatively small entrance and exit orifices introduce phase lag, the amount of lag being frequency dependent. Sonic delay

through the system can and must be interpreted as a phase lag. To facilitate the laboratory tests and modification, it was required that, for the test model, the logic elements be mounted remotely from the sensor and actuator. As a result fairly long interconnecting lines were dictated thus introducing considerable phase lag in the laboratory model due to line capacitance and sonic delay.

To partially overcome this phase lag an RC lead-lag feedback loop was added to the 5 stage amplifier circuit. It is shown in Figure 6 where a signal is taken out at the input to the fourth stage and fed back to the first stage input. With the phase lead produced by the feedback loop, stable operation was anticipated to sufficiently high frequencies. In an actual installation the control circuit is to be mounted in close proximity to the sensor-actuator subsystems, thus minimizing interconnection line lag.

The above analysis was carried out by means of Bode plots, having calculated the transfer functions for the various parts of the system.

It was indicated earlier that the desired function of the control system was to cause the foil to respond to changes of the speed and the angle of the flow passing over the foil. Figure 7 shows the anticipated closed loop frequency response of the system. The upper curve gives the ratio of foil angle peak to peak amplitude to flow angle peak to peak amplitude under

conditions of constant dynamic pressure, the ratio given in decibels. Good amplitude correspondence to 7 or 8 cps is predicted. The lower curve shows the phase lag of foil angle with respect to flow angle with constant dynamic pressure, indicating a lag increasing rapidly with frequency.

An estimate was made of the ability of such a system to control lift variation. It was found that a significant reduction of variations of foil lift forces, or attenuation of vertical acceleration forces, should be obtained for frequencies less than 10 cps.

### System Testing

In testing the model system it was desired that the performance of the system be evaluated under conditions simulating those encountered by typical hydrofoil craft. Hydrodynamic similarity is prescribed by angle of incident flow and reduced frequency of encounter,  $k$ , where  $k$  is a function of foil chord, velocity of water passing over the foil, and in this case frequency of the sinusoidally varying flow angle incident on the foil. A range of test conditions were determined based on this criteria, the available variables being water velocity, flow angle peak to peak amplitude and frequency.

Figure 8 shows the hydrofoil model. The three section pivoted foil was supported by two vertical foil shaped struts. The foil was of the NACA 633-018 configuration with a 4" chord and total span of 12". Both the foil sections and the struts were epoxy castings. Sensor holes were

located in the center foil section and were connected through tubes in the left hand strut to the converter shown attached to the upper mounting plate. The actuating cylinder was attached to the mounting plate and connected to the foil by means of an aluminum actuating strut.

Figure 9 shows the panel mounted computer circuit with needle valves and gauges for regulating and monitoring supply pressures to the individual amplifier stages.

Dynamic system tests were carried out in the Hydronautics, Inc. water tunnel. The hydrofoil model was mounted to a support beam in the water tunnel. Wave motion was generated by a large oscillating foil mounted in the channel upstream from the location of the hydrofoil model. Both amplitude and frequency of the sinusoidally oscillating generator foil were controllable, thus making available a large range of approximately sinusoidal flow angle disturbances.

Figure 10 shows the hydrofoil model and disturbance generator mounted in the water tunnel with water flow from left to right.

Tests were run over a range of predetermined conditions. Actual lift forces generated were sensed by means of reluctance type force transducers and recorded in strip chart form by a C.E.C. light galvanometer recorder. For the same set of conditions variations in lift force were recorded with:

- (1) The control system in operation.
- (2) The foil locked in a position parallel to the mean flow velocity.

As a means of evaluating performance, the variation of lift force with the system operating was compared with the variation of lift force with the foil locked, the foil being subjected to the same flow disturbance in each case.

Figure 11 shows the results of one test series. The ratio of controlled to uncontrolled lift variation is given as a function of frequency and reduced frequency. Lift variation was reduced to 35% of that variation produced by a fixed foil.

Along with the experimentally determined values a theoretical lift ratio curve is given. This curve was obtained by means of existing unsteady airfoil theory<sup>3,4</sup>, making use of the angle relationships prescribed by the closed loop system response.

Correspondence between the experimentally determined values and the theoretical curve is good. Data was obtained over a range of reduced frequencies from .05 to .5, a range covering many sea conditions encountered by full scale craft. The results obtained from these tests are thus most encouraging.

## Conclusion

Three of the principle results accomplished by the design and testing of this scaled model system are as follows:

1. This system is responsive to the environment of changing velocity and angle of attack common to wave motion.
2. It has been demonstrated that a hydrofoil lift control system of this type will be effective in controlling vertical acceleration forces on a hydrofoil craft under actual sea conditions.
3. The mathematical model derived to represent the system was sound, hence the procedure may be used with confidence in the design of future systems.

The next step, towards which we are presently directed, is the design of a complete control system for a full-scale hydrofoil craft.

### References

1. McCullough, George B., & Gault, Donald E., "Examples of Three Representative Airfoil Sections - Stall at Low Speed", NACA TN2502, 1951.
2. Martin, M., "Unsteady Moments on a Model Hydrofoil to Be Used in an Experimental Investigation of Fluid Controls", Hydronautics, Inc., Technical Report 351-1, June 1963.
3. Scanlan, R. H., & Rosenbaum, R., "Introduction to The Study of Aircraft Vibration and Flutter", The MacMillan Company, New York, 1951.
4. Lawrence, H. R., & Gerber, E. H., "The Aerodynamic Forces on Low Aspect Ratio Wings Oscillating in An Incompressible Flow", Cornell Aeronautical Laboratory, Inc., March 1952.

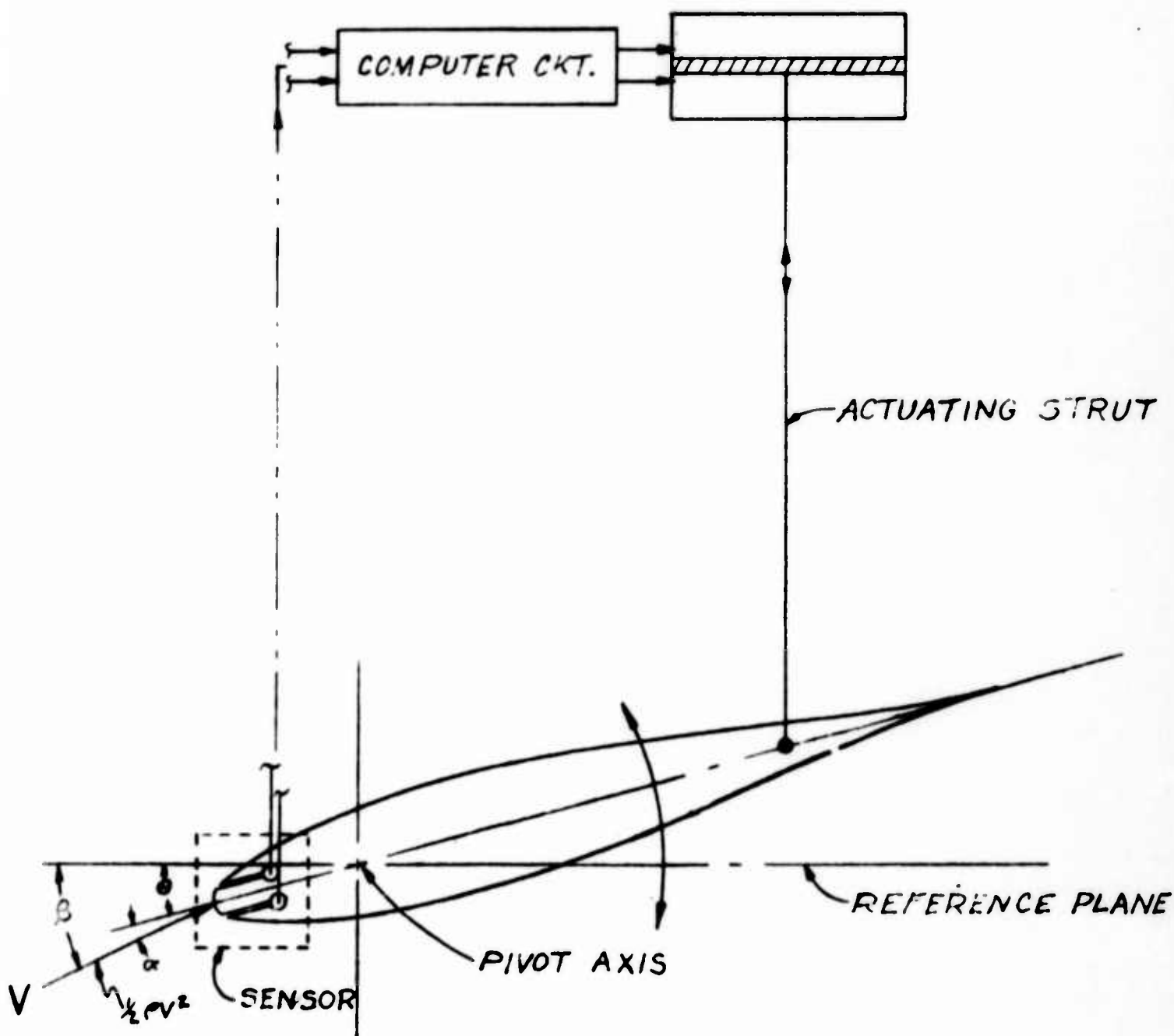


FIG. 1  
HYDROFOIL CONTROL SYSTEM



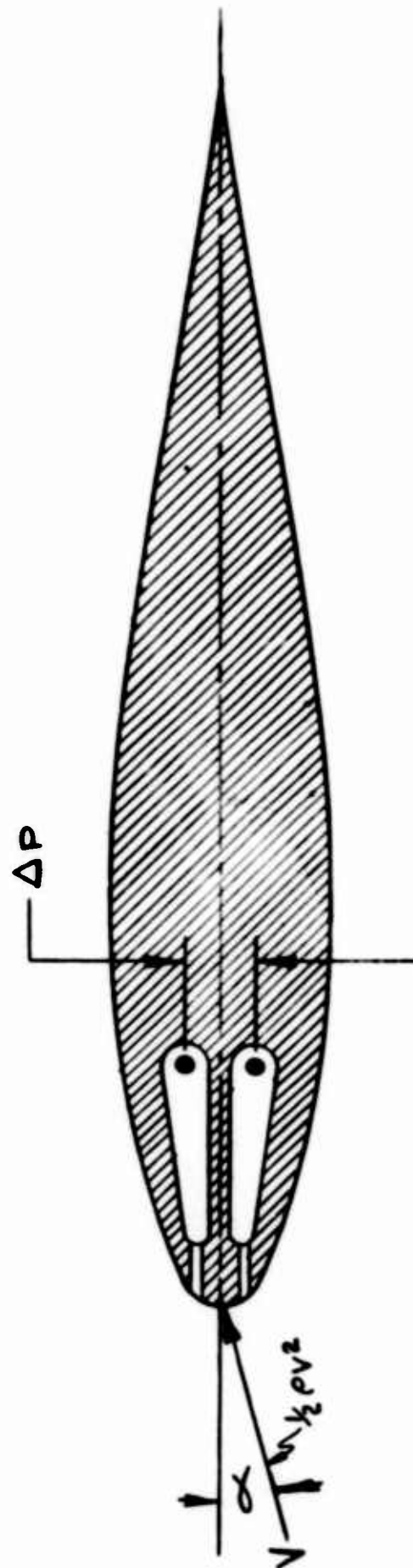


FIG. 2  
FOIL LIFT SENSOR

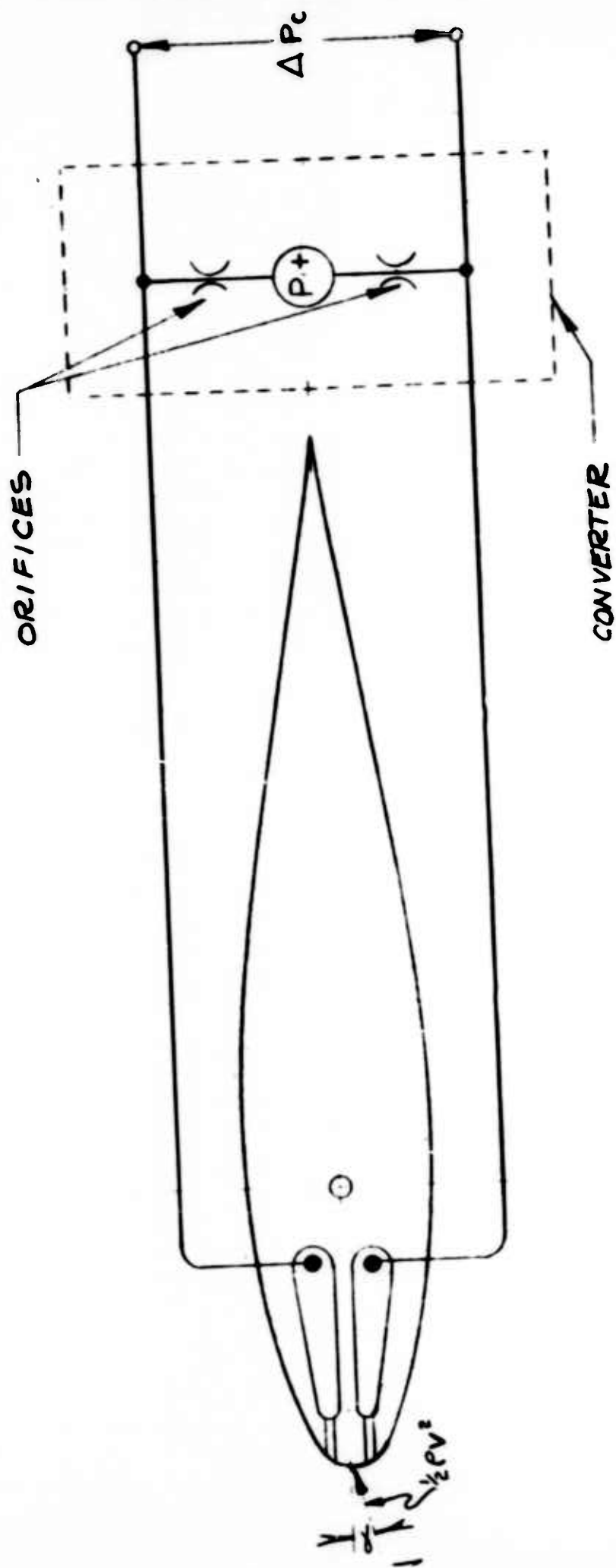


FIG. 3  
LIFT SENSOR SYSTEM

$\Delta P/q$

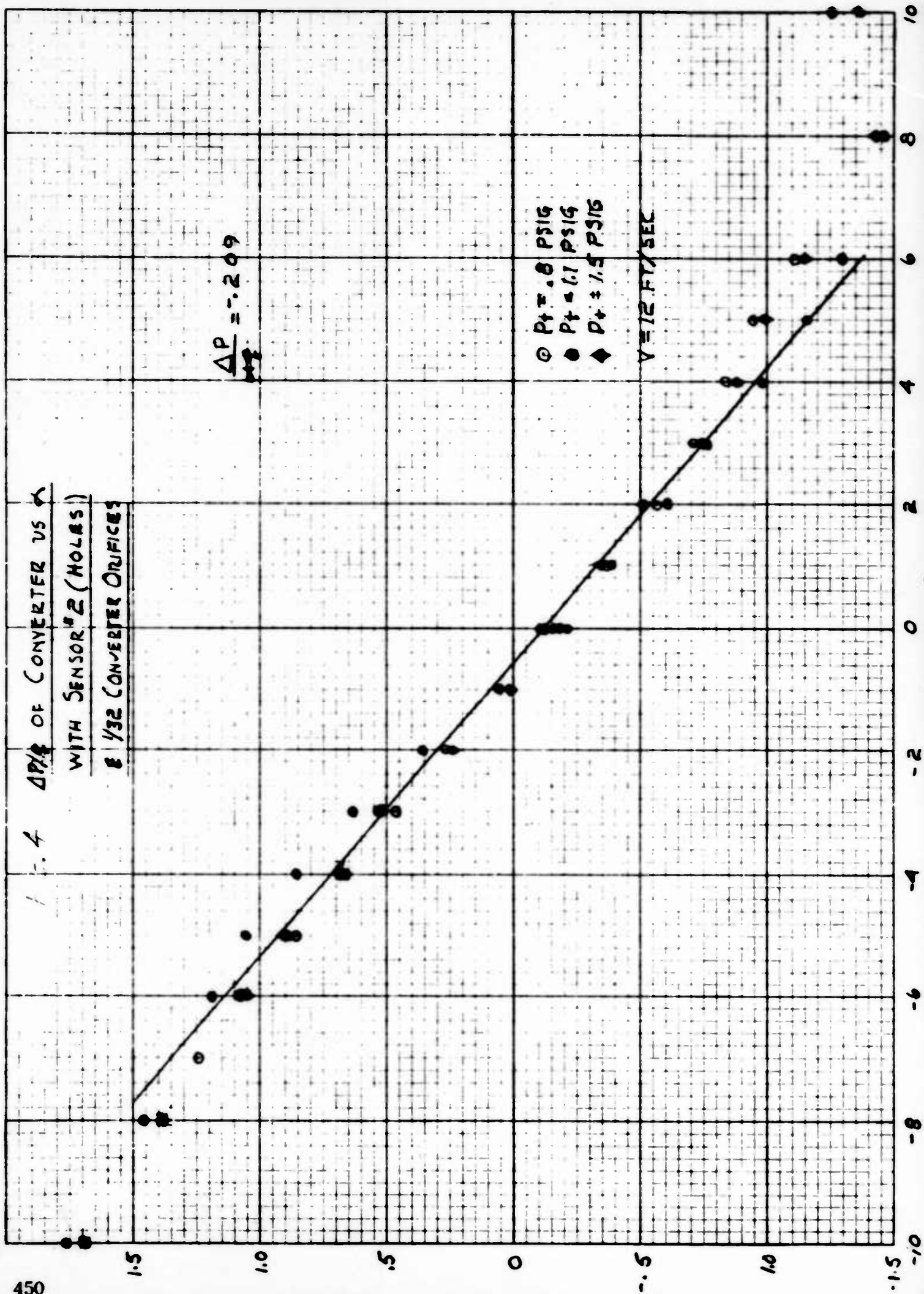
450

1-4  $\Delta P/q$  OF CONVERTER VS  $\Delta$   
WITH SENSOR #2 (HOLDS)  
8  $1/32$  CONVERTER ORIFICES

$$\frac{\Delta P}{q} = -0.209$$

- $P_t = 0.8$  PSIG
- $P_t = 1.1$  PSIG
- ◆  $P_t = 1.5$  PSIG

$$V = 12 \text{ FT/SEC}$$



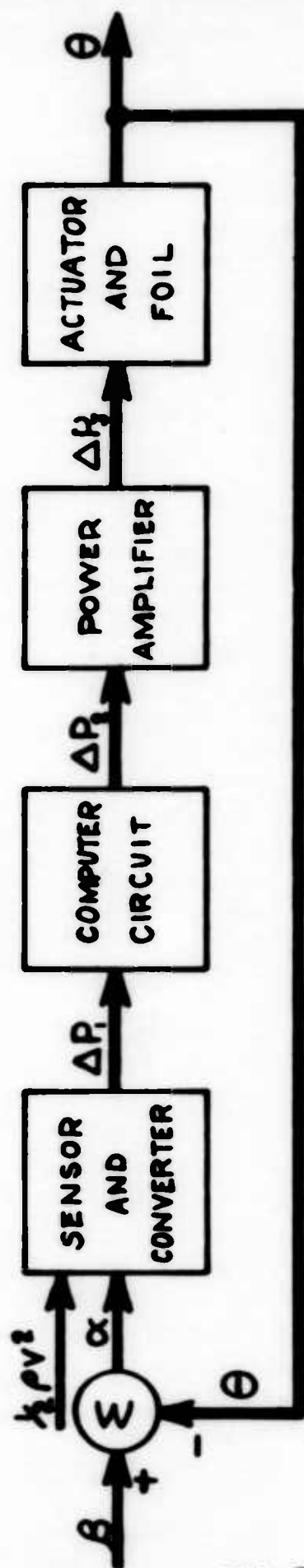


FIG. 5

# LIFT CONTROL SYSTEM BLOCK DIAGRAM

## WHERE

$\alpha$  is angle of attack

$\beta$  is water flow angle with respect to horizontal foil

$\theta$  is angle of foil with respect to horizontal

$\Delta P_1$  is pressure difference out of sensor and converter

$\Delta P_2$  is pressure difference out of computer circuit

$\Delta P_3$  is pressure difference out of power amplifier under no flow condition

$\rho$  is water density

$v$  is water speed

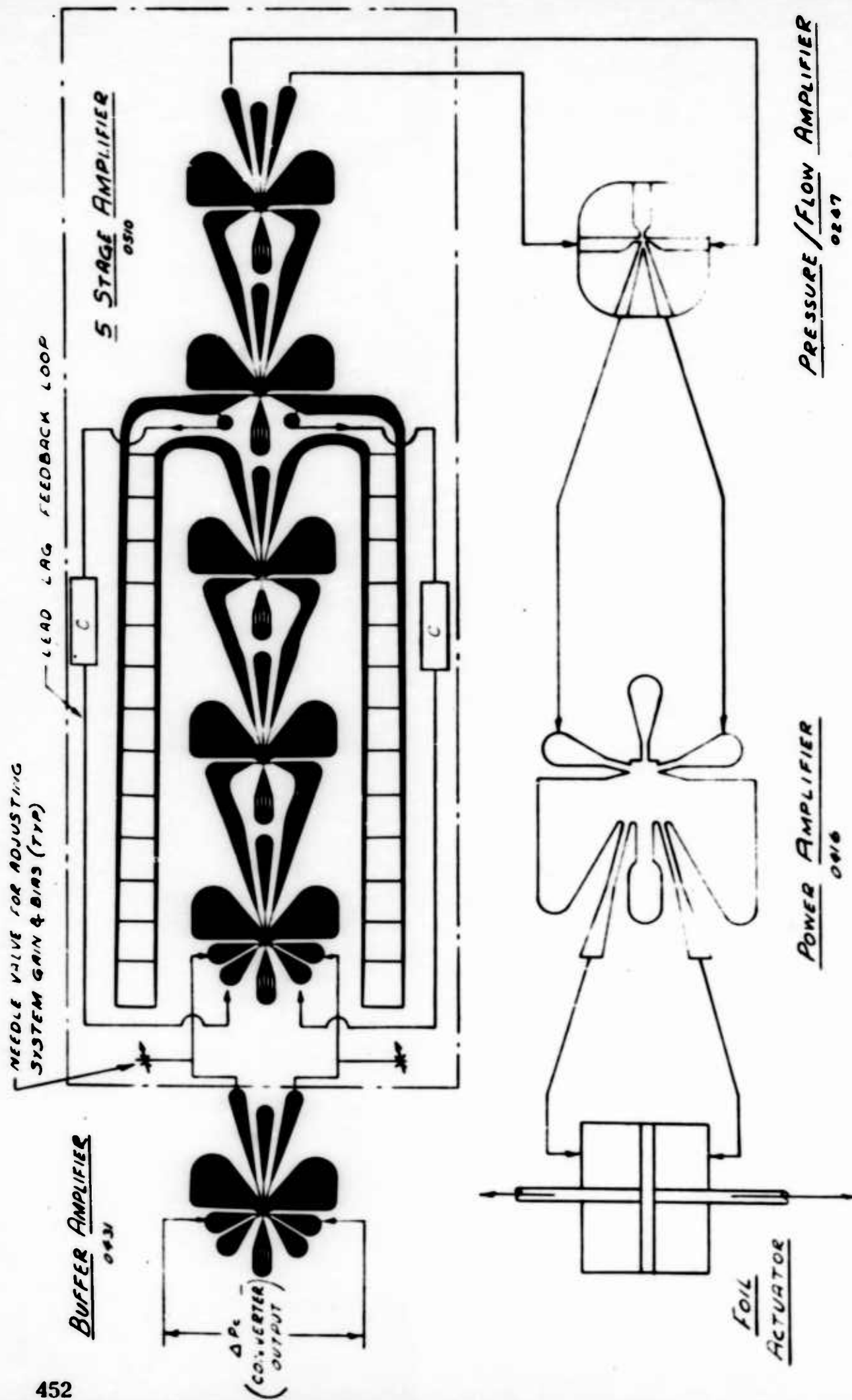


FIG. 6

**FLUID CONTROL LOGIC**

FOR PIVOTED SERVO CONTROLLED HYDROFOIL

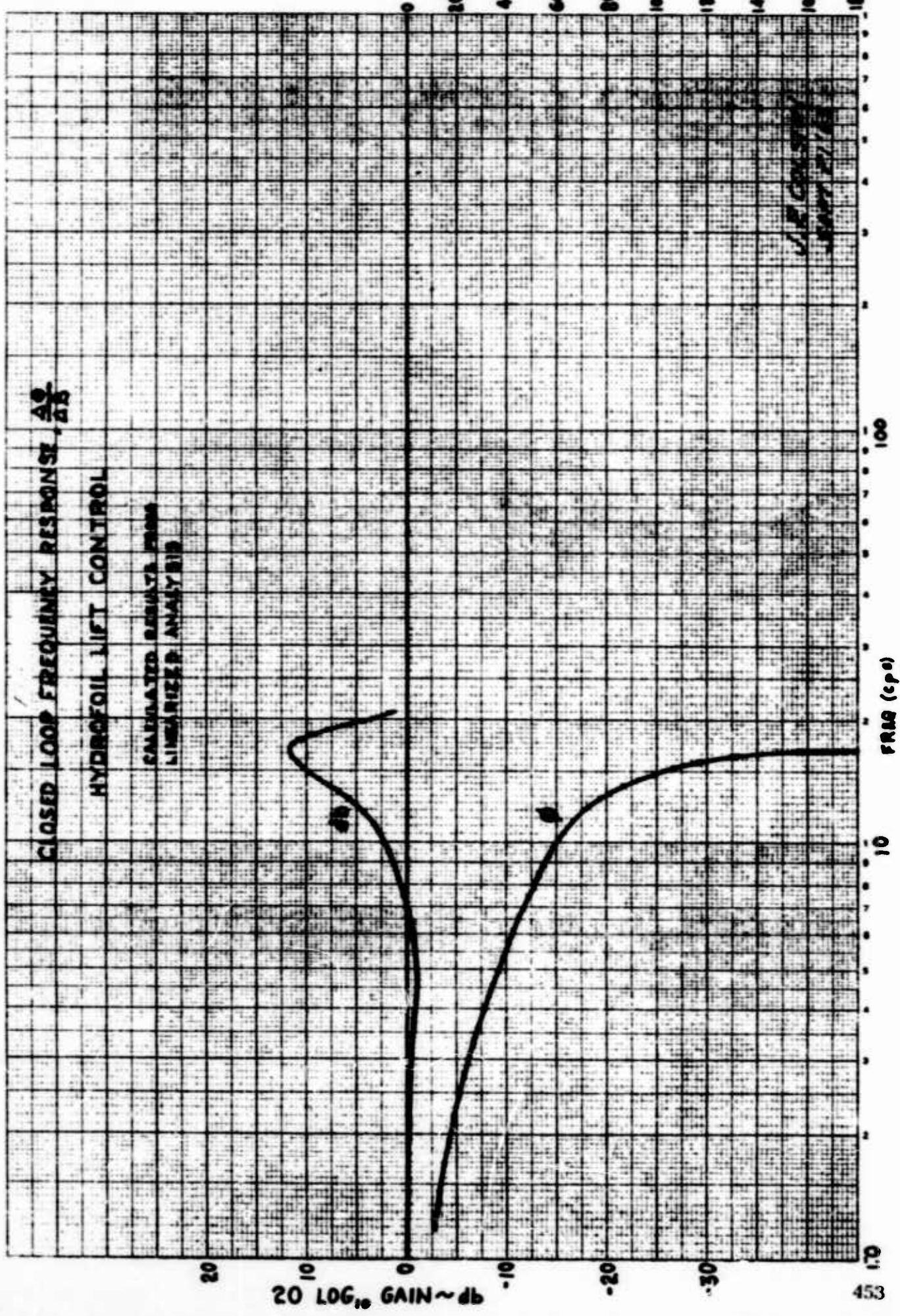


CLOSED LOOP FREQUENCY RESPONSE,  $\frac{A\omega}{B\omega}$

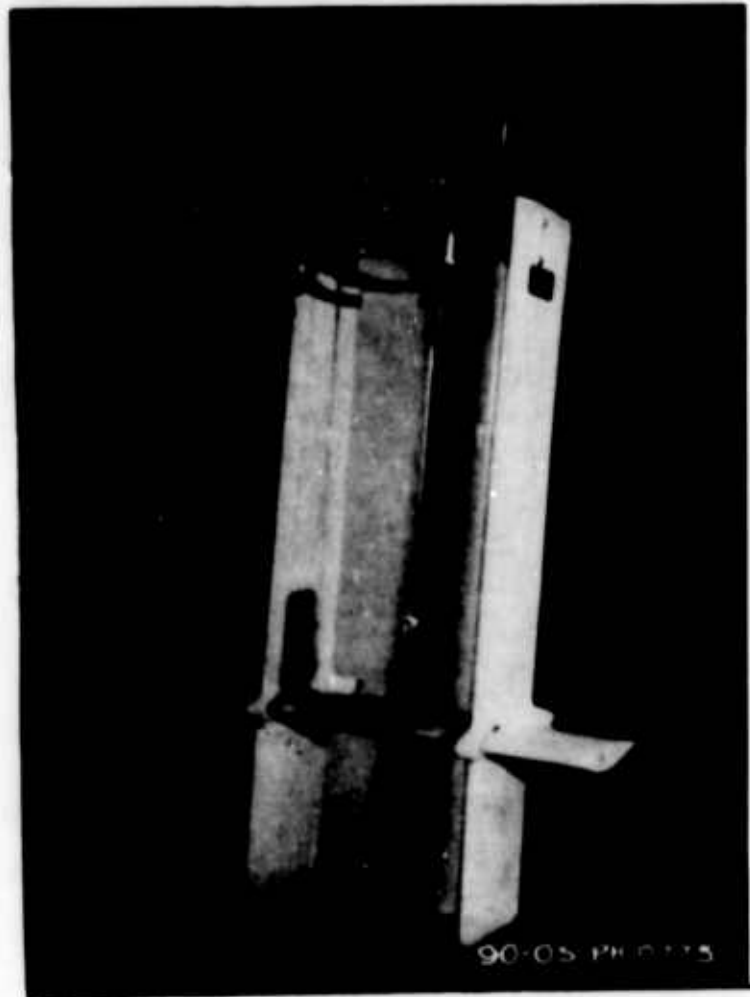
HYDROFOIL LIFT CONTROL

CALCULATED RESULTS FROM  
LINEARIZED ANALYSIS

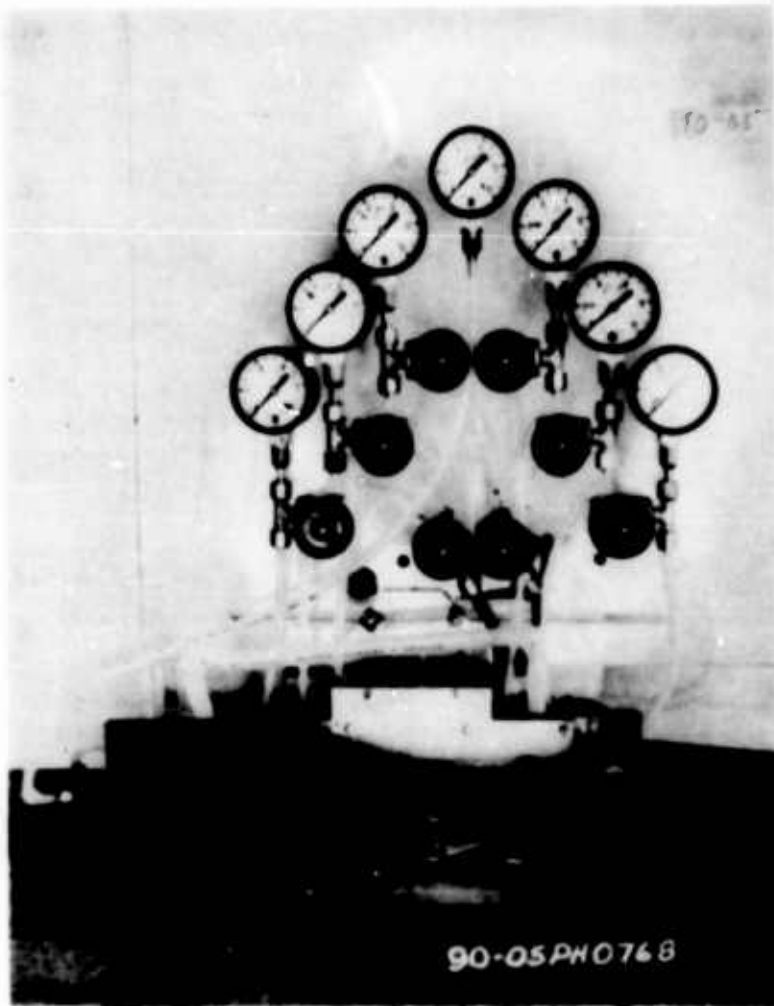
PHASE ANGLE  $\sim \phi \sim \text{DEG.}$



*FIG. 8*



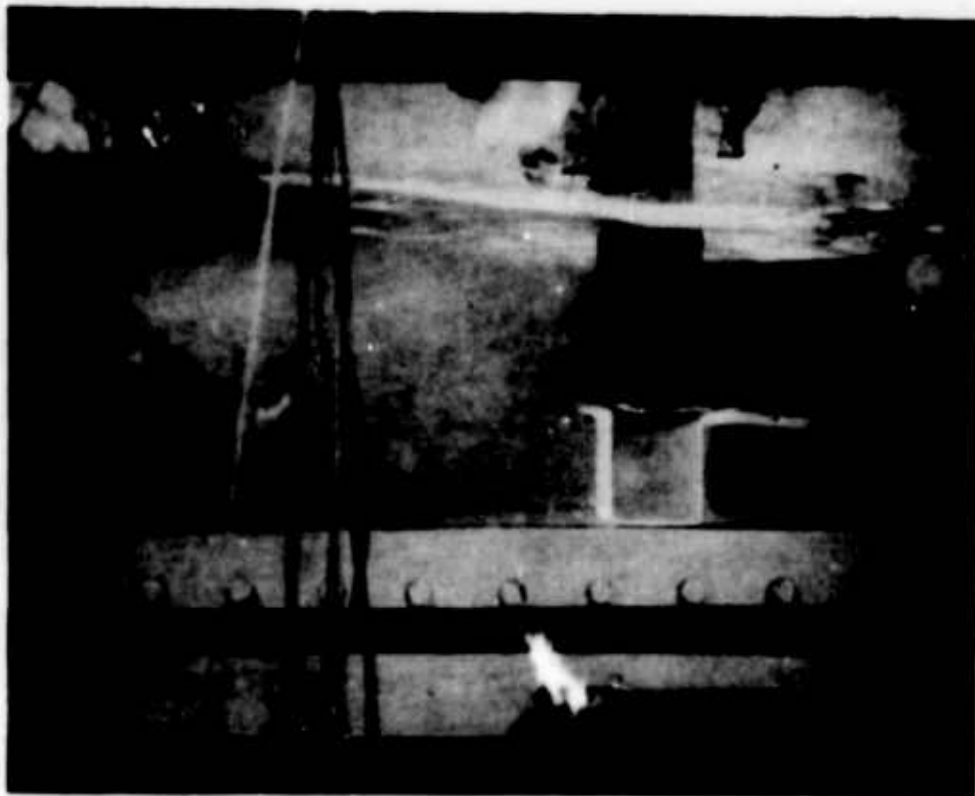
HYDROFOIL RIG



COMPUTER CIRCUIT PANEL



*FIG.10*



FOIL RIG & DISTURBANCE GENERATOR  
MOUNTED IN WATER TUNNEL

FIG. 11

RATIO CONTROLLED TO UNCONTROLLED  
ΔT/T VARIATION VS FREQUENCY

$V = 14.1 \text{ FT/SEC}$

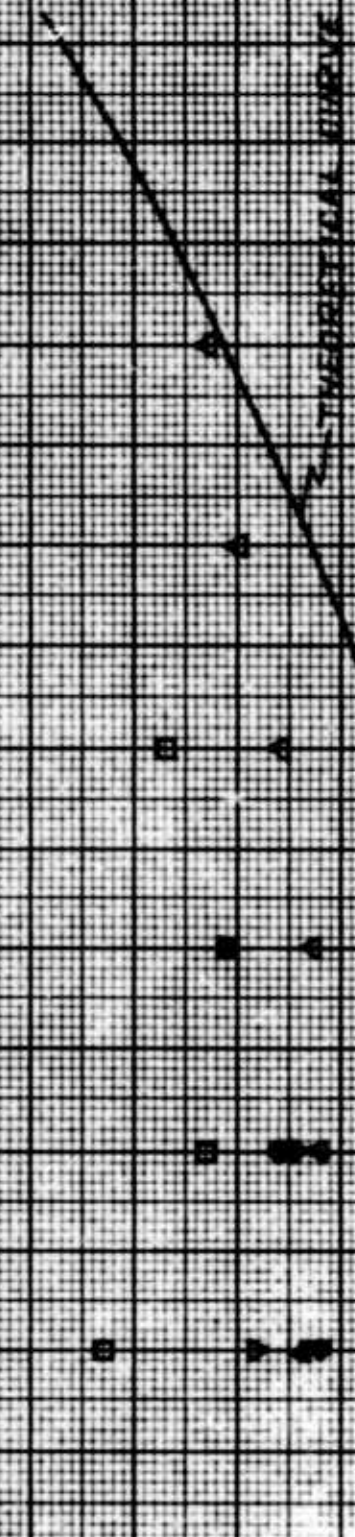
$\Delta V/g = 0.0 \text{ P-P}$

$V/g = 1.4 \text{ P-P}$

$\Delta V/g = 0.0 \text{ P-P}$

$\Delta V/g = 0.0 \text{ P-P}$

$\frac{\Delta T}{T}$



THEORETICAL CURVE

FREQ (CP/S)  
 $K = 0.05$

**A STATUS REPORT ON THE EXPERIMENTAL  
DEVELOPMENT OF A HOT GAS VALVE**

by

**J. C. DUNAWAY & V. H. AYRE**

of

**CONTROL SYSTEMS BRANCH  
ARMY INERTIAL GUIDANCE AND CONTROL LABORATORY  
DIRECTORATE OF RESEARCH AND DEVELOPMENT  
ARMY MISSILE COMMAND  
REDSTONE ARSENAL, ALABAMA**

**ABSTRACT**

This report describes an effort toward development of a hot gas jet reaction valve utilizing boundary layer technique to control a high pressure, high temperature gas stream. The result of this program to date has been the successful design of a hot gas valve in a reaction control system utilizing fluid-controlled bi-stable amplifier principles, requiring no moving parts in the gas stream and no source of secondary pressure.

Valves have been fabricated and successfully tested with gases at pressures to 1300 psi and temperatures to 2350° F. with flow rates to 1#/sec cold air.

This status report on the program presents a summary of results of experimental design work completed and a review of packaging and environmental problems with an existing missile system.

## INTRODUCTION:

As missiles have become more advanced, the design engineer has been required to deliver a less expensive, more reliable system. Size and weight restrictions have simultaneously become more severe, particularly in the case of small missiles whose performance is extremely dependent on these parameters. To meet these size and weight requirements, the use of solid propellant grains as an energy source for the control system output force has become more attractive. As gas temperature is increased, the weight of propellant for a given duty cycle can be reduced. However, problems are encountered with conventional valving techniques when a high temperature, contaminated gas is used. The exposure of moving parts to the hot gas stream often results in erosion, warping or sticking of these parts. Fluid amplifier techniques appeared to be an attractive method of controlling hot gases without moving parts in the gas stream.

## PROGRAM OBJECTIVE:

The objective of this program was to apply fluid amplifier techniques to a hot gas reaction control system for a particular missile. Since the application was specified, the valve had to be designed to the requirements of the existing reaction control system. The valve package was to contain 3 valves for 3 axis control (See Figure 1). This pitch and yaw valve output force requirements were 18 pounds and the roll valve requirement was 12 pounds. The valve package was to be capable of operating with gas temperatures up to 2400° and a supply pressure of from 550 to 1250 psi. The input to the valves was a pulse duration modulated signal with a 25 cps carrier frequency.

## EXPERIMENTAL DEVELOPMENT:

Bistable amplifier techniques based on early work at Harry Diamond Laboratories were used to design the first prototype valves. By modifying the receiver section, satisfactory operation was obtained up to a supply pressure of about 200 psi.

Experimental and analytical work showed that with a supply pressure of 1000 psi and a sonic nozzle, stream integrity could not be retained due to the large pressure difference between the stream and ambient conditions into which the nozzle was exhausting. Supersonic nozzles with varying expansion ratios were tested and stream profiles plotted to determine the type of nozzle required to retain stream integrity at the high pressures. After determining the correct nozzle configuration, adjustable type receiver sections were designed to fit the nozzles. The receiver sections were built with provisions to vary the setback, wall length, control port size, and wall angles. Tests were conducted to determine the optimum receiver section configuration. During these tests, it was discovered that switching could be obtained by using atmospheric air as a control fluid. This type of switching eliminated the need to carry a control fluid supply aboard the missile, since switching could be obtained by opening and closing the control ports. Table 1 shows the results of the cold gas tests with variable nozzle and receiver parameters. The results showed that as the nozzle exit pressure was decreased, the range over which the unit would switch occurred at higher supply pressures.

Attempts were made to diffuse and recover pressure to be expanded through jet reaction nozzles to provide control forces. Two difficulties were encountered: (1) Supersonic diffusers were very inefficient so that enough useful pressure could not be recovered to produce the required reaction forces. (2) The valve could not be made to switch into a back pressure of more than a few psi.



Since enough pressure could not be recovered to meet the force requirement, it appeared that a possible method of producing the control forces was to duct the high velocity gases through  $90^\circ$  bends to obtain the proper force vector. A velocity of Mach 2 was required to produce the required control force. Figure 2 shows a typical valve configuration.

A variety of different shaped nozzles were designed and tested. The first nozzles tested were rectangular shaped with exit plane aspect ratios of from 1:1 to 4:1. The 1:1 aspect ratio nozzles were short in length but required a longer receiver section to operate correctly. The 4:1 aspect ratio nozzles were longer than the 1:1 aspect ratio nozzles but could be switched into a shorter receiver section. The overall length of the valve with different aspect nozzles were about the same. Valves with rectangular nozzles had good switching characteristics but were inefficient. Primary thrust efficiencies were as low as 70% of ideal isentropic thrust.

Round nozzles were tried in an effort to get more efficient nozzles. These nozzles were short in length, and could be switched into receiver sections of approximately the same length as the 1:1 aspect ratio rectangular nozzles. In addition to being more efficient, these nozzles were easier to fabricate.

Since the valve used atmospheric air for the control fluid, some method had to be devised to open and close the control ports to the atmosphere. The actuator devised was an electro-mechanical flapper actuator (See Figure 3). The pressure forces on the actuator were balanced by pistons. This reduced the electrical power requirement.

The Missile Command (MICOM) Valve has two problem areas when it is packaged for the intended missile application:

1. Packaging: The exit ducts are large and cannot tolerate more than a single  $90^\circ$  turn from the exit of the nozzle until the gas exits the

missile. Missile command link components and motor blast tubes interfere with the Missile Command (MICOM) Valve package. Modifications to these components are being studied and it is believed that modifications can be made which will allow installation of the MICOM Valve package in the missile. Figure 4 shows one packaging approach. For reference, the missile diameter is 6".

2. Low Base Pressure: The pressure in the aft portion of the missile, where the MICOM Valve is located, can vary from atmospheric (14.7 psia) to approximately 10 psia. Since ambient air pressure is used as the control fluid, the control flow and valve performance is reduced. Valves will have to be designed for acceptable performance over this range.

In order to gain an insight into the MICOM Valve operating characteristics at a reduced ambient pressure, two series of altitude test were run. One valve with the following dimensions is considered here (See Figure 5):

#### Nozzle

Throat Area = .00518 in<sup>2</sup>

Area Ratio = 17.35

Divergent Angle = 20°

Convergent Angle = 60°

#### Receiver Section

Control Port Area = .084 in<sup>2</sup>

Setback = .150"

Divergent Angle = 15°

Splitter Location = 1.525" from nozzle exit

#### Exit Ducts

Exit Area = .25 in<sup>2</sup>

Bend = 90°

## TEST PROCEDURE:

The test setup is shown in Figure 6. The entire valve assembly was installed in a 16' diameter X 56' long vacuum chamber. The electro-mechanical actuator was switched at  $\frac{1}{2}$  cps. The vacuum chamber was brought to the desired pressure. The pressure ( $P_u$ ) on the valve was brought to the maximum, then brought down in steps of about 100 psi.

The following variables were recorded:

$P_u$	Upstream Pressure
$P_R, P_L$	Right & Left Control Port Pressures
$F$	Side Force
$P_c$	Pressure Inside the Vacuum Chamber
$S_w$	Voltage Applied to the Electro-Mechanical Actuator

## RESULTS:

As seen in Figure 7 with a  $P_c$  of 14.7 psia, the valve had an operating pressure range (i.e. greater than 60% relative efficiency) of 750 to 1750 psi.

This gives a

$$\frac{\text{Pressure Nozzle Exit}}{\text{Pressure Vacuum Chamber}} = \frac{P_e}{P_c} \text{ of from .456 to .169}$$

Following the above reasoning:

at a  $P_c$  of 7.7 psia,  $\frac{P_e}{P_c}$  is from .474 to .173

at a  $P_c$  of 6.7 psia,  $\frac{P_e}{P_c}$  is from .485 to .173

at a  $P_c$  of 3.7 psia,  $\frac{P_e}{P_c}$  is from .414 to .143

at a  $P_c$  of 2.7 psia,  $\frac{P_e}{P_c}$  is from .493 to .307



The similarity of the  $P_e/P_c$  range at the various altitudes gives an indication that once the operating range of a unit at one altitude is known, the operating range at any other altitude can be predicted.

#### TESTS TO DATE:

The MICOM Valve Development Program to date has resulted in about 65 hot gas tests. These tests were conducted utilizing a single axis thrust stand (Figure 8) whereby the normal thrust developed by the valve and its associated ductwork can be measured directly on a tension compression load cell. The instrumentation included pressure transducers and thermocouples located such that the valve inlet pressure and temperature could be recorded.

These tests have demonstrated that the valve can satisfy the original requirements as to control forces, frequency response, efficiency and range of operating pressure and temperature.

The valves utilized in these tests were fabricated using standard model shop fabrication techniques to produce the power jet nozzle from stainless steel, the receiver section from aluminum, and the ductwork from copper or stainless steel tubing (both have proven satisfactory). However, it appears that stainless steel tubing has the advantage because thinner walls can be utilized and thus total weight can be reduced. The use of these rather low temperature materials is permissible due to the reduction in the gas temperature by the previous expansion of the gas stream through the power jet nozzle. Thinner walls are permissible because the pressure of the gas has been reduced to near atmospheric. It is also interesting to note that the use of thin walls and low density metals has resulted already in a weight reduction of about 25% over the conventional valve. This has been accomplished while using the rather inefficient (from the standpoint of weight reduction) methods of fabrication available in the model shop.

## CONCLUSIONS:

The following conclusions were made from the hot gas tests run on various valve configurations. These tests are summarized in Table II.

### 1. Nozzle Configurations:

Nozzles with nominal area ratios of from 8.6 to 13.3 were tested. Normally a higher supply pressure could be switched by increasing the area ratio.

### 2. Receiver Section Configuration:

Tests showed that two receiver section variables effected the valve switching characteristics: (1) A longer receiver section increased the high pressure limit at which a valve would switch. (2) Increasing control port areas resulted in a wider switching range.

### 3. Exit Manifold:

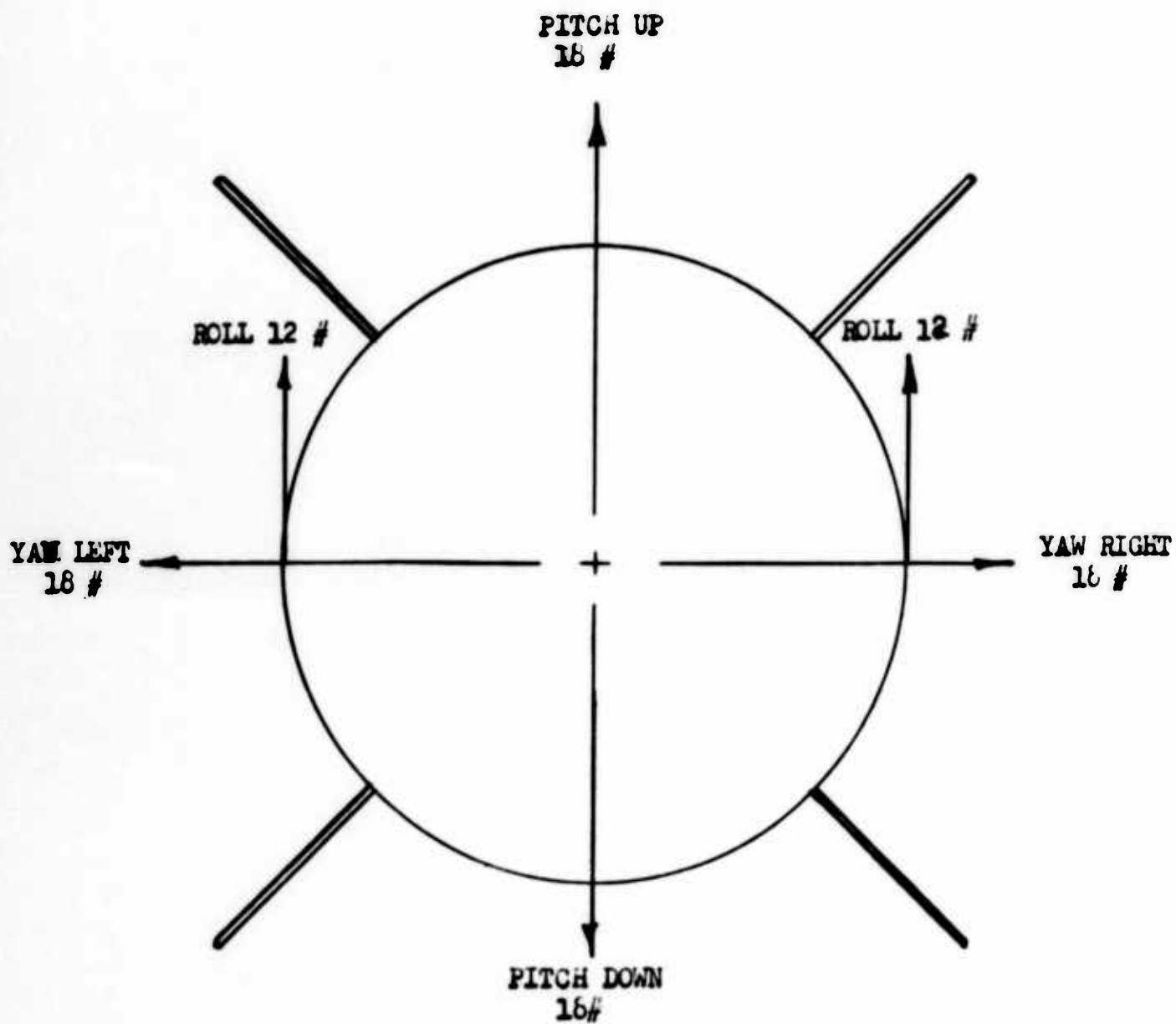
Exit manifold areas were normally equal to the areas of the exit of the receiver section. Increasing the exit manifold areas resulted in switching at a higher supply pressure but decreased the valve efficiency at lower supply pressures.

## FUTURE DEVELOPMENT:

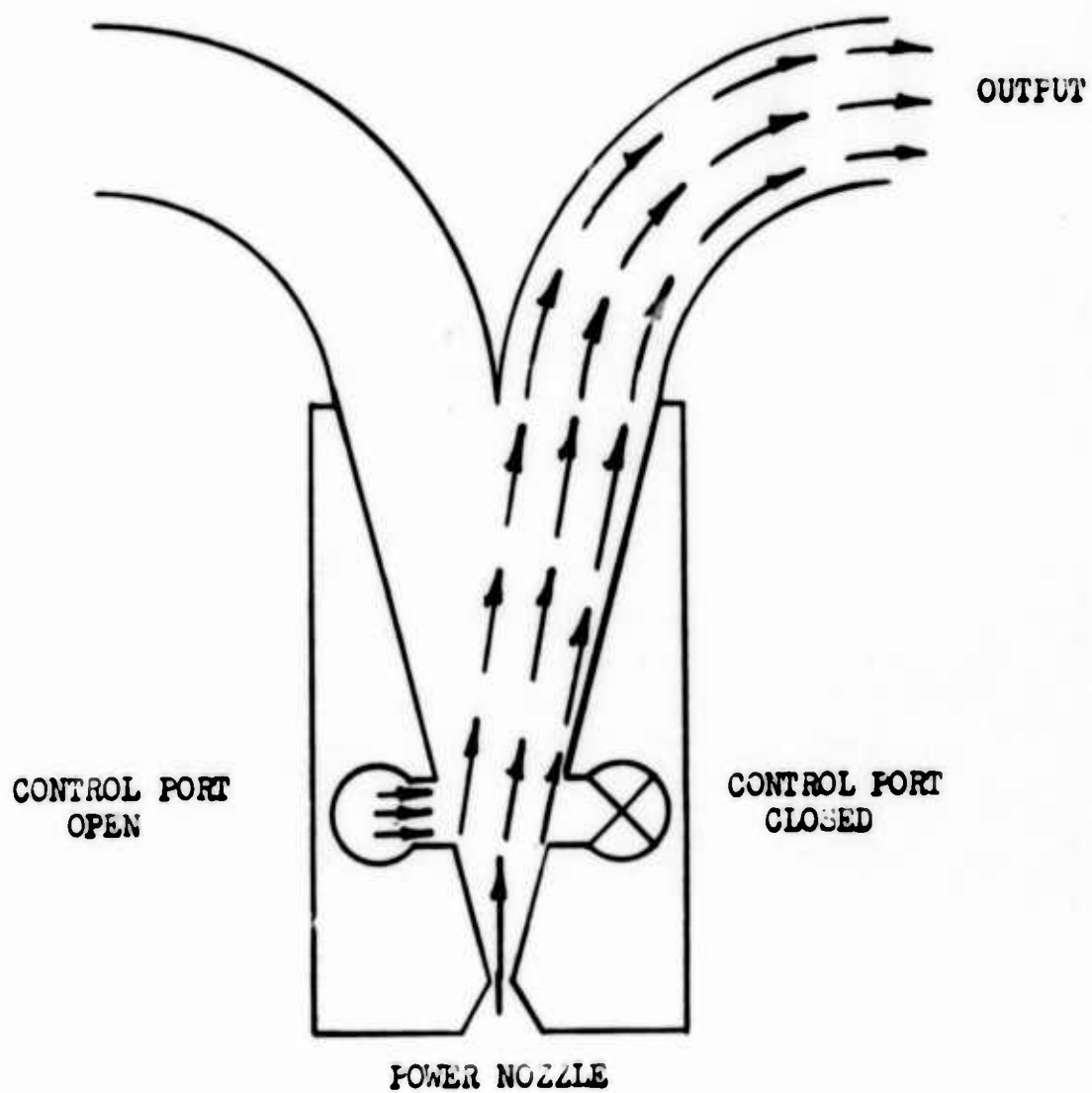
Future development will be directed toward making the MICOM Valve compatible with the missile. Reducing the exit duct size and improving valve operation at reduced base pressures would make the two compatible.

Two approaches are being taken: (1) A staged valve approach is being aimed at reducing the exit duct size and eliminating the base pressure problem. (2) Altitude chamber test indicate that it might be possible to modify the present one-stage valve to operate over required base pressure range. Both approaches are related because the first stage of the two staged

valve will also have to operate at the reduced base pressure. Test indicate that the larger the power nozzle area ratio, the lower the ambient pressure necessary to control the valve. Physical size will probably determine which final approach will be used. The one-stage valve will probably be larger but easier to produce than the two-stage unit.

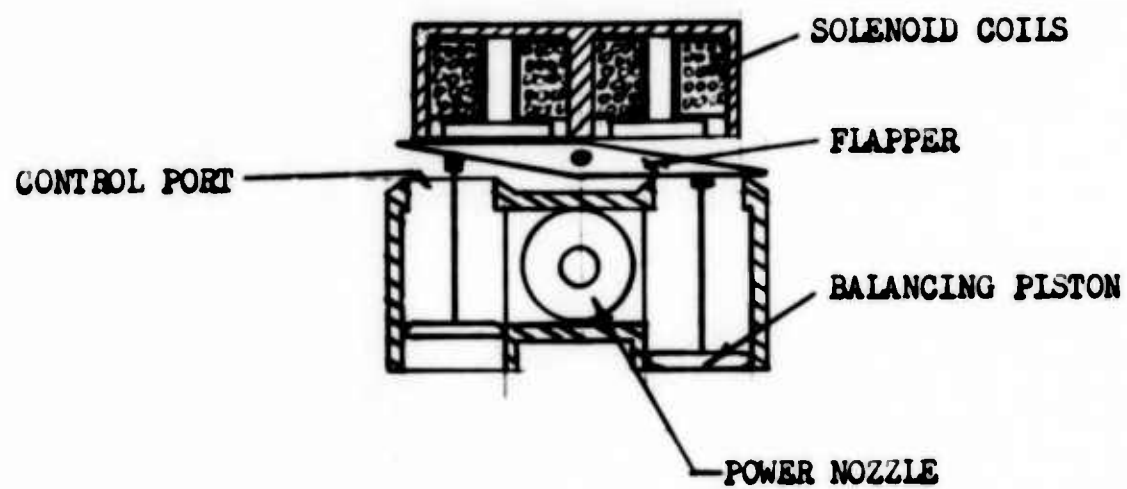


CONTROL FORCES FIG. 1



TYPICAL VALVE CONFIGURATION

FIGURE 2



MICOM VALVE ACTUATOR

FIGURE 3

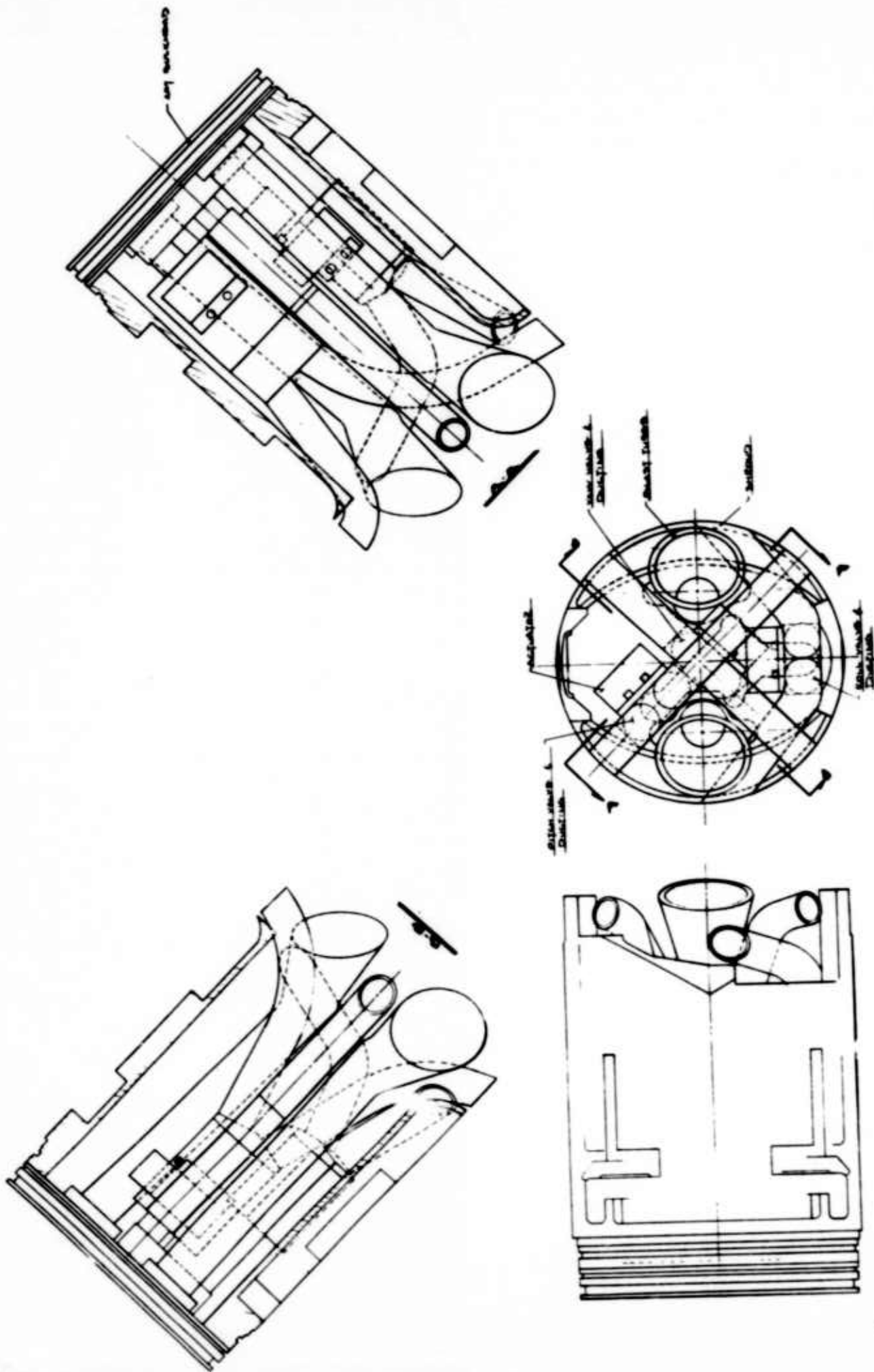
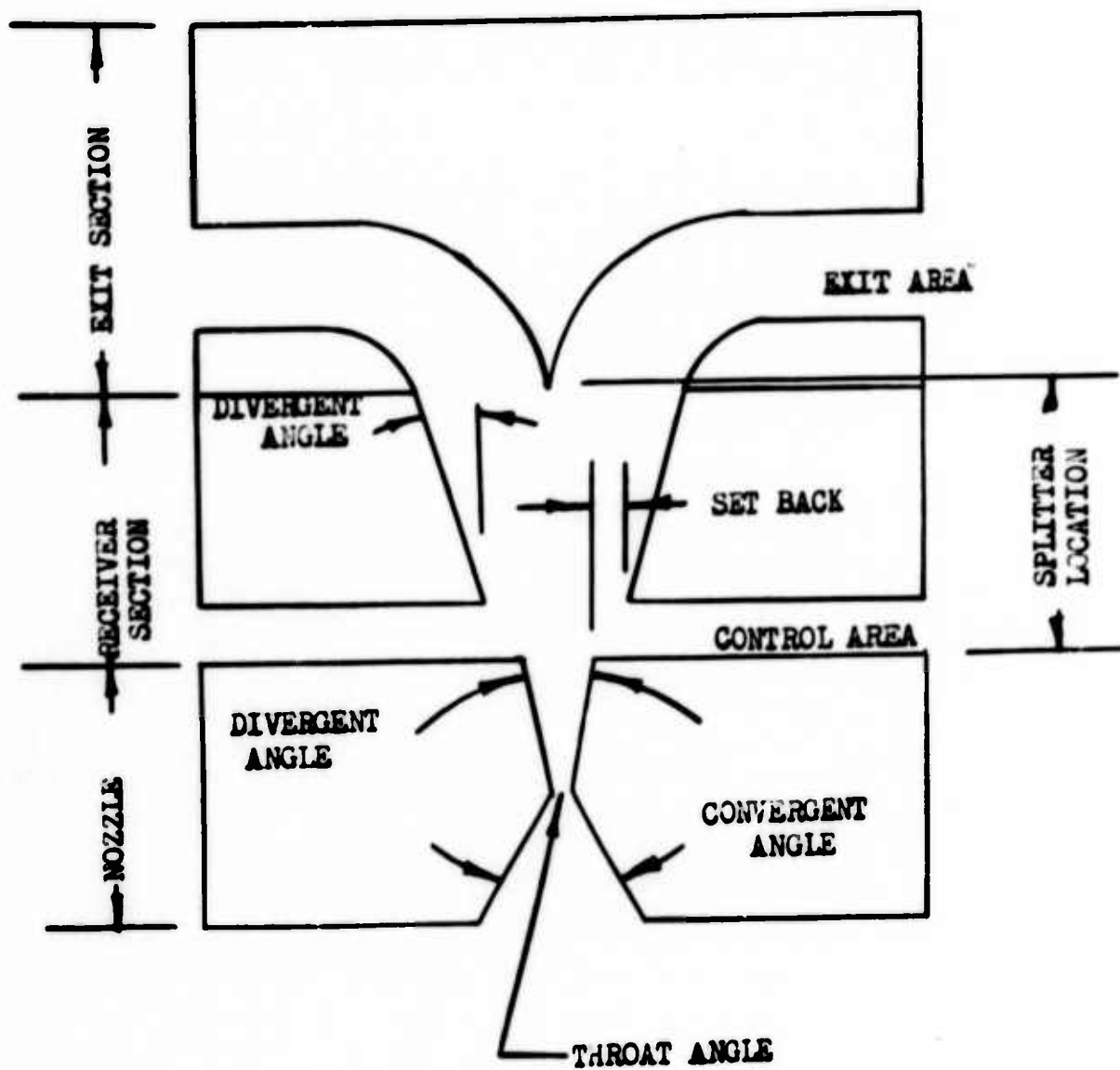


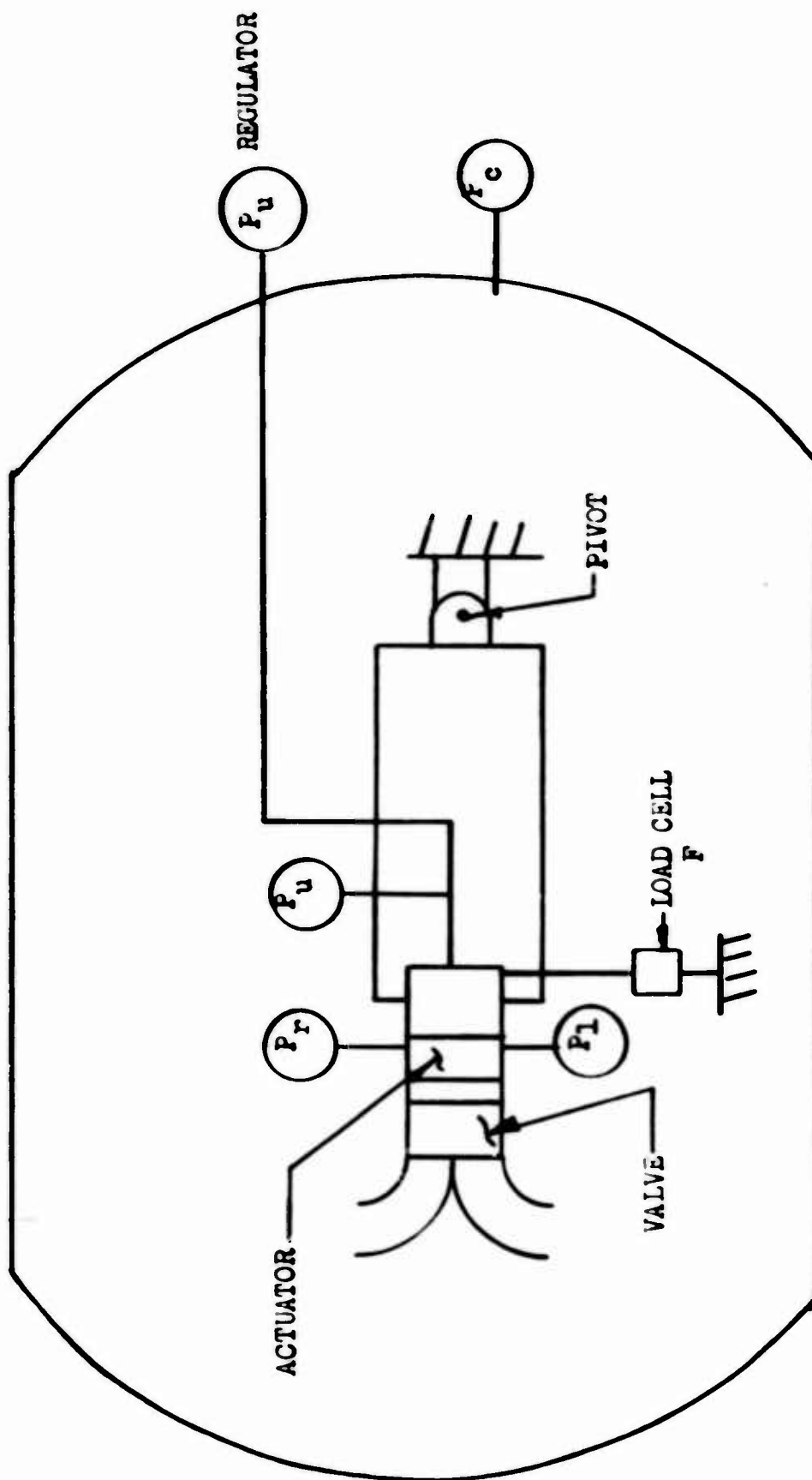
FIGURE 4



ADJUSTABLE VALVE CONFIGURATION

FIGURE 5





VACUUM CHAMBER TEST SETUP

FIGURE 6

ALTITUDE TEST Series 2, Run 1 Test 310.763.500.001-310.763.500.016  
Altitude Chamber Pressure ( $P_c$ )

14.7 psia —○—  
7.7 psia —□—  
3.7 psia —◇—

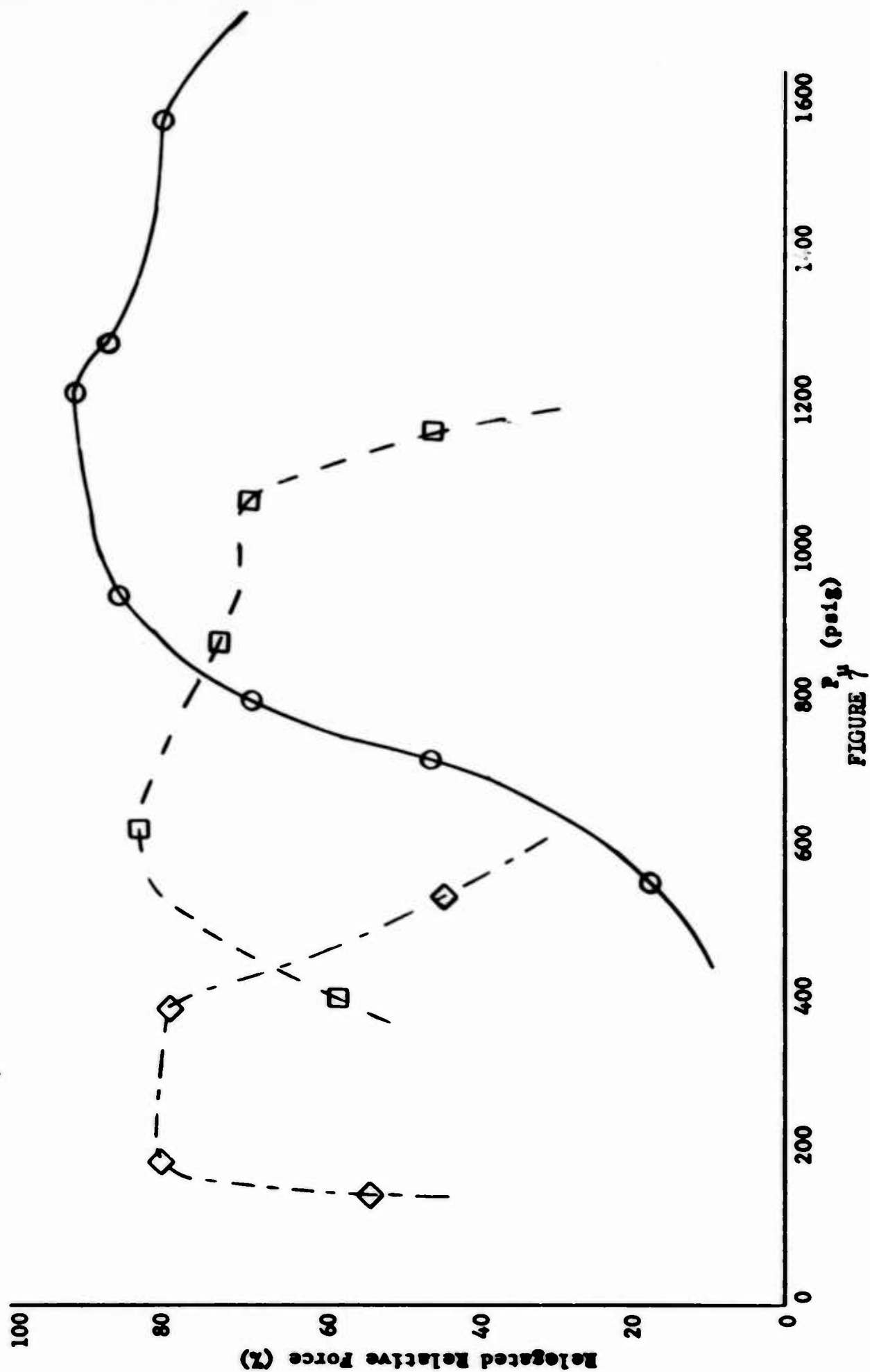
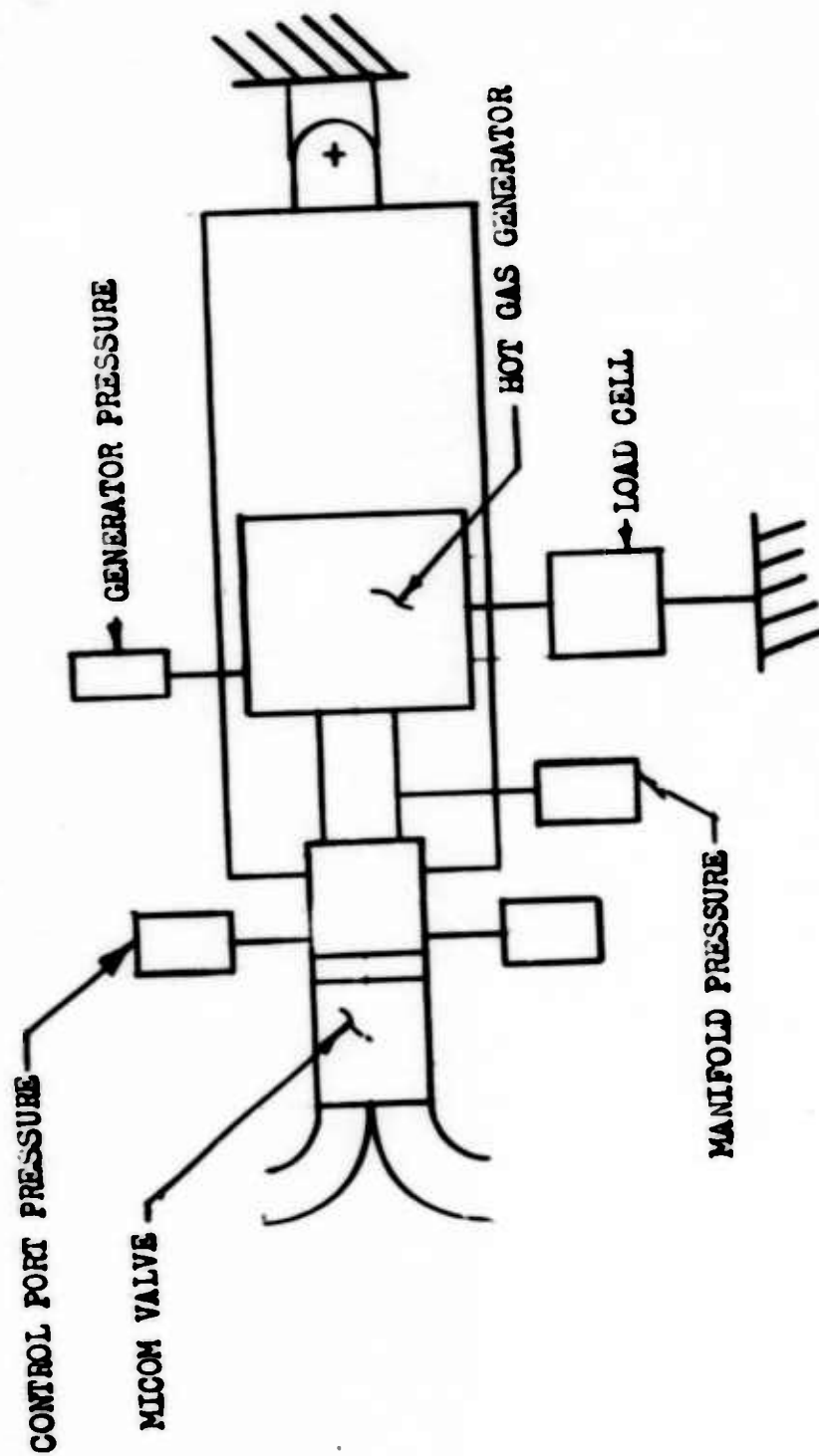


FIGURE 7



HOT GAS TEST STAND

FIGURE 8

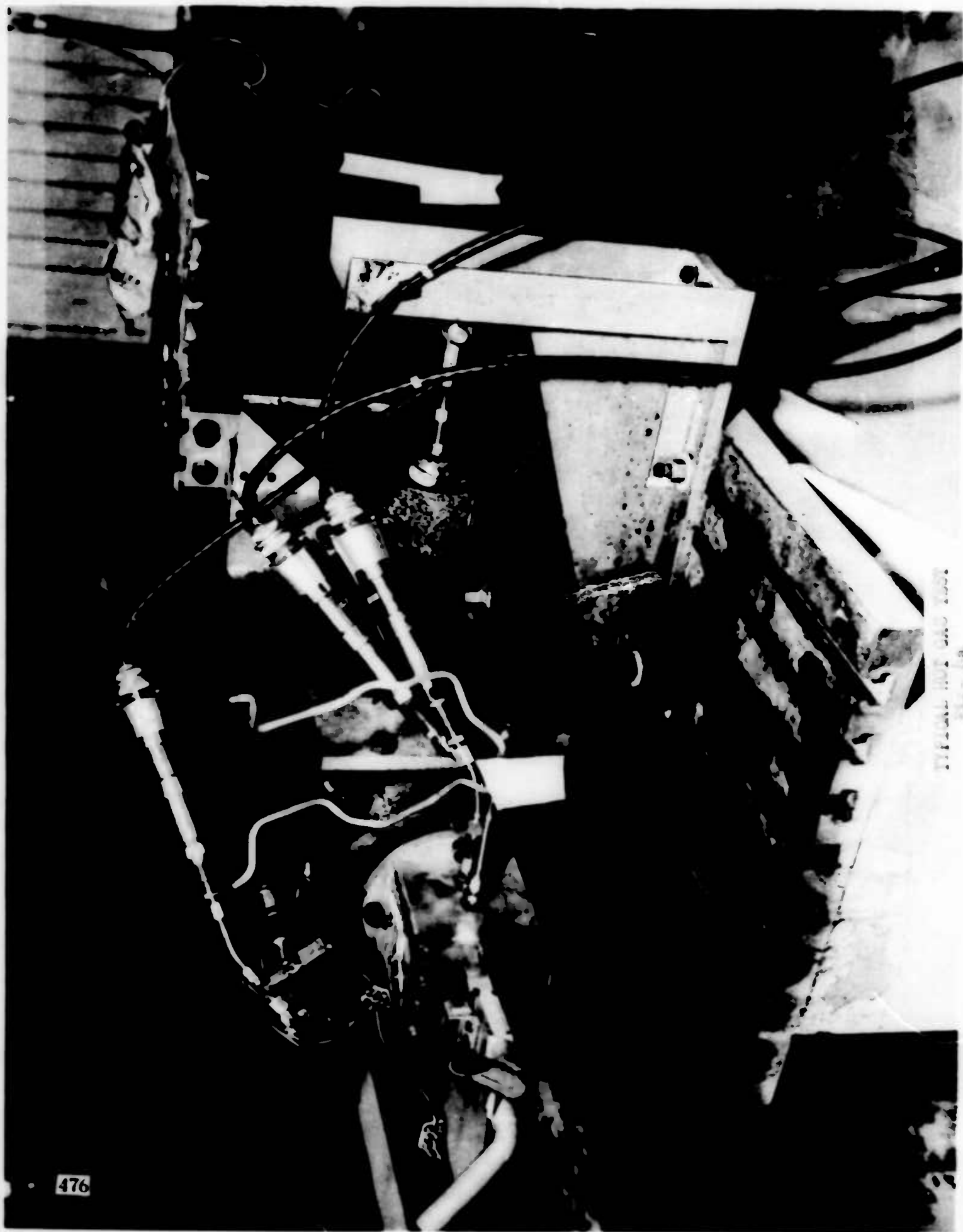


Table I. - EXPERIMENTAL COLD GAS VALVES

Import- metal valve No.	Test No.	Supply pres- sure, psi	Exhaust pres- sure, psi	Nozzle div angle, deg	Nozzle throat aspect R	Nozzle exit aspect R	Nozzle exit (in <sup>2</sup> ) area	Control port-area exit area	Setback, in.	Offset, in.	Receiver wall angle, deg	Receiver wall length, in.	Dist to splitter, in.	Remarks
8-1	1	125-375	22-65	15	.7	.7	.01	1.3	.2		15	3	.275	Sharp splitter switching range 125-375 psi
	2	125-375	22-65	15	.7	.7	.01	1.3	.2		15	3	None	No splitter switching range 125-375 psi
	3	125-375	22-65	15	.7	.7	.01	1.3	.25		15	3	None	No splitter switching range 125-375 psi
	4	125-600	22-104	15	.7	.7	.01	1.9	.25		15	3	None	No splitter switching range 125-600 psi
	5	125-375	22-65	15	.7	.7	.01	1.7	.25		15	3	None	No splitter switching range 125-375 psi
	6	125-600	22-104	15	.7	.7	.01	2.9	.32		25	3	None	No splitter switching range 125-600 psi
	7	No switch	22-104	15	.7	.7	.01	2.9	.32		25	3	1.45	Sharp splitter, no switching
1	1	0-1000	0-328	None	8:1	8:1	.0049							No satisfactory results were obtained
2	1	0-1000	0-27	15	8:1	2:1	.0135	2	.064	0	15	.75	None	Switching, stream width unsatisfactory
3	1	0-1000	0-27	7 1/2	8:1	2:1	.0135	2	.064	0	15	1.5	1.3	Good to 800 psi
4	1	0-1000	0-14.7	7 1/2	8:1	2:1	.0428	1.5	1 1/4	0	22.5	1.5	None	Switching unsatisfactory
	2	0-1000	0-14.7	7 1/2	8:1	2:1	.0428	1.5	1 1/4	0	22.5	1.5	None	Switching 500-750 psi
	3	0-1000	0-14.7	7 1/2	8:1	2:1	.0428	1.0	1 1/4	0	22.5	1.5	None	Switching 900-1000 psi
	4	0-1000	0-14.7	7 1/2	8:1	2:1	.0428	1.5	2 1/4	0	22.5	1.5	None	Switching 500-1000 psi
	5	0-1000	0-14.7	7 1/2	8:1	2:1	.0428	1.5	2 1/4	0	15	1.5	None	Switching unsatisfactory
	6	0-1000	0-14.7	7 1/2	8:1	2:1	.0428	1.5	1 1/4	0	15	1.5	None	Switching unsatisfactory
	7	0-1000	0-14.7	7 1/2	8:1	2:1	.0428	1.5	1 1/4	0	15	1.5	None	Switching 500-1000 psi
	8	0-1000	0-14.7	7 1/2	8:1	2:1	.0428	1	1 1/4	0	7 1/2	1.5	None	Switching good except 900-1000 psi
	9	0-1000	0-14.7	7 1/2	8:1	2:1	.0428	1	1 1/4	0	7 1/2	1.5	None	Switching good except 900-1000 psi
	10	0-1000	0-14.7	7 1/2	8:1	2:1	.0428	1.5	1 1/4	0	7 1/2	1.5	None	Switching good except 900-1000 psi
	11	0-1000	0-14.7	7 1/2	8:1	2:1	.0428	1.5	2 1/4	0	7 1/2	1.5	None	Switching good
	12	0-1000	0-14.7	7 1/2	8:1	2:1	.0428	1.5	2 1/4	0	7 1/2	1.5	None	Switching good
	13	0-1000	0-14.7	7 1/2	8:1	2:1	.0428	1.5	2 1/4	0	7 1/2	1.5	None	Unsatisfactory
5	1	0-1100	0-10	7 1/2	8:1	1.74:1	.0555	1.25	.1	.07	15	1.5	1.30	.06 concave splitter switching 850-1100 psi
	2	0-1100	0-10	7 1/2	8:1	1.74:1	.0555	1.25	.1	.07	15	1.5	1.33	.07 concave splitter switching 750 psi
	3	0-1100	0-10	7 1/2	8:1	1.74:1	.0555	1.25	.1	.07	15	1.5	1.37	.12 concave splitter no switching
	4	0-1100	0-10	7 1/2	8:1	1.74:1	.0555	1.25	.1	.07	15	1.5	1.20	.09 concave splitter switching 750-1100 psi
	5	0-1100	0-10	7 1/2	8:1	1.74:1	.0555	1.25	.1	.07	15	1.5	1.00	.07 concave splitter switching 750-1000
	6	0-1100	0-10	7 1/2	8:1	1.74:1	.0555	1.25	.1	.07	15	1.5	1.30	.06 concave splitter switching 700-800 psi
	7	0-1100	0-10	7 1/2	8:1	1.74:1	.0555	1.25	.1	.07	15	1.5	1.33	.07 concave splitter switching 850-1050
	8	0-1100	0-10	7 1/2	8:1	1.74:1	.0555	1.25	.1	.07	15	1.5	1.37	.12 concave splitter switching 1025-1100
	9	0-1100	0-10	7 1/2	8:1	1.74:1	.0555	1.25	.1	.07	15	1.5	1.20	.09 concave splitter no switching
	10	0-1100	0-10	7 1/2	8:1	1.74:1	.0555	1.25	.1	.07	15	1.5	1.00	.07 concave splitter switching 850-900

Experimental nozzle No. 5, tests 6 through 10 were conducted with .51 ID manifold and were used as a model for further work.  
 .07 in width of nozzle at exit section.

Table II.

Valve No.	Test No.	Throat area, in. <sup>2</sup>	Nozzle expansion ratio	Exit aspect ratio	Vertical offset, in.	Control port dia., in.	Control port width, in.	Set-back, in.	Wall half angle, deg.	Distance nozzle to splitter, in.	Exit duct size, in.	Switching	Gas pressure range, psi	Range on air, psi	No. of pipes	Force, lb.
1	1	.0104	10.23	1.74:1	.141	.212	.08	.11	15°	1.3	N/A	None	875/920		None	N/A
	2										.625ID	None	910/1075		2	
	3											Good	1010			
	4											Poor	822/887			
	5	.0105				.30	.15	.06/.07			.53ID	Poor	860/965	900/1050		
	6										.625ID	Good	865/925			
	7	.0102						.065				Exc	825/895			
2	1	.0191	9.5	1.74:1	.070	.30	.15	.10	16°	1.3	.73ID	None	875/920		2	N/A
	2											None	910/1075			
	3											None	1010/-			
	4											None	-687/822			
3	1	.0191	9.5	1.74:1	.070	.30	.15	.10	16°	1.3	N/A	Pair	875/920		None	N/A
	2										.9ID	Poor	910/1075		2	
	3											None	1010			
	4											Exc	687/822		4	
	5	.0159				.348		.063/.071			.55ID	Exc	860/965			
	6	.0176						.063/.073				Pair	865/925			
	7	.0204										Good	825/895			
4	5	.0157	12.4	1.73:1	.076	.348	.15	.10/.11	23°	1.3	.74ID	None	860/965		2	N/A
	6	.0154	13	1.07:1	.076	.35	.137	.11/.116	15°	1.3	.73ID	None	865/925	900/1000	2	N/A
5	7							.063/.067			.5ID	Good	825/895	750/1150	4	
	9										.45ID	Exc	860/975	900/1400	None	9-14.5°
	10											N/A	825/890	N/A		10-15.8°
	11	.0104	13.28	2.48:1	None	3	.11	.10	15	.8	.4X.75	Good	900/1040		2	3.9-5.2°
Ble 1	12											Exc	885/975			2.9-9.5°
	15	.012	13	2.84:1	None	.35	.13	.07	15	N/A	None	N/A	860/940		None	6.5-1.4°
7	13	.0176	13	1.42:1	.04	.35	.15	.07	15°	1.45	None	N/A	875/885		None	20.7-20.4°
	14										.75ID	Pair	865/885		2	12.6-16.9°
	17											Exc	860/980			15-16.5°
	21							.10		2.05	.75X.65	Exc	890	200/800		17-18°
	24											Exc	790/965			17-18.3°
	28										.55ID	Exc	880/920	500/1000	4	
	29															
Moly 1	16	.0119	13.3	3.9:1	.042	.437	.185	.075	15°	1.375	None	N/A	860/940		None	11.5-13.3°
	20							.09			.87X.53	Exc	525/890	250/1300	2	6.2-28°
	25							.09				Exc	640/1040	500/1300		8.5-10.9°
	26															
10A	18	.0176	13.3	Ed	None	.39	.2	.07	15	2.05	.8X.55	Exc	870/940		2	15.1-16.5°
	19							.09			.95X.55	Exc	900/960			14.6-16.4°
	22										.65ID	Exc	870/970	500/1300	4	17-19.3°
	23										.55ID	Q	710/975			1.4-16.6°
	27											Exc	810/925	500/900		1.5-14.7°
	29											Exc	900	200/800	2	16-18°
	32										.68ID	Exc	850/900			16.5°
	33										.55X.8	Exc	900/1000			14-17°
	36											Poor	1050/1400			10-15°
	38											Exc	750/1050			18°
	41															16.5-18°
	42															

Table II. (Continued)

Valve No.	Test No.	Throat area, in. <sup>2</sup>	Nozzle expansion ratio	Exit aspect ratio	Vertical offset, in.	Control port dia., in.	Control port width, in.	Setback, in.	Wall half angle, deg.	Distance nozzle to splitter, in.	Exit duct size, in.	Switching	Gas pressure range, psi	Range on air, psi	No. of pipes	Force, lb.
11	30	.0117	7.9	Rd	None	.39	.35	.096	15	1.9	.63E.34 .51ID	Exc	~900		2	10.5-11.5*
	31											Exc	~950			9-11*
	34											Exc	~900			11-12.5*
87	26	.0108	11.85	Rd	None	.3	.17	.09	15	1.65	.63ID	Exc	670/1005	600/1100	2	10.4-11.9*
	40	.0107	11.85	Rd	None	.35		.124	15		.68ID	Poor	900		2	9-10*
Noly 3	39	.0175	11.75	Rd	None	.437	.350	.08	15	2.1	.68ID	Poor	600/975		2	14*
87a	44	.0108	11.85	Rd	None	.35	.4	.109	15	1.75	.68ID	Exc	500/975	500/975	2	11*
	50											Pair				6*
	52											Good				5*
	61						.45					Exc		650/1100		9.5*
BM131-15	43	.0161	8.06	Rd	None	.5	N/A	.55	0	2.1	.68ID	Good		to 800	2	5.5*
	45	.0150				.47	.80	.24	15			None		600/900		6*
	46											Some		to 800		5-12*
	48					.5				2.25		Good		500/1050		12*
	49	.0154										Poor				14*
	51											Poor				15*
	53											Poor		to 1000		13.5*
	54											None		to 1000		12.8*
	56											Pair				15*
	57											Poor		700/950		14*
	58										.74ID	Poor		700/1050		13*
	59										.68ID	Pair				11*
	60															14.2*
BM131-7	62	.016	13.3	Rd	.030	.39	.48	.06	15	2.1	.74ID	Good		700/1075	2	14.5*
	63				None	.45					.68ID	Poor		600/885		13.2*
	64										.74ID	Exc		775/1000		13.5*
	65										.74ID	Exc				11.2*

\* Side Force - Receiver Section on Valve  
 \*\* Total Thrust - No Receiver Section on Valve

# DEVELOPMENT OF TWO PURE FLUID TIMERS

BY

G. V. Lemmon - Sandia Corporation

E. R. Phillips - UNIVAC, Div. of Sperry Rand Corp.

## INTRODUCTION

Sandia Corporation has many applications for timers to perform various functions. In the past, these components have been designed using what are now proven mechanical and electrical principles, and reliable and satisfactory timing components have been built on each of these and on a combination of both. With the introduction of pure fluid systems, it was felt that the advantages of reliability, cost, accuracy, package size and insensitivity to environment should be investigated. Accordingly, a survey of components was made and two specifications for timers were selected as a basis for the investigation. It was hoped that the development of these timers would provide a practical test of the applicability of pure fluid systems to the whole family of components of interest to Sandia.

The specifications adopted for this development called for two timers of varying complexity. The first of these was estimated to be producible from present capabilities in the field of pure fluids, and the second was estimated to be of such complexity and size as to be more challenging. These detailed specifications are as follows:

## SPECIFICATIONS

### TIMER NO. 1

Type:	Sequential Timer
Construction:	Except for valves, regulators and electrical controls, to be made from nonmoving, solid parts and operated with fluids.
Times Required:	7.0 $\pm$ 1.0 seconds 11.0 $\pm$ 1.25 seconds 16.0 $\pm$ 2.5 seconds - 0 seconds



21.0 + 2.5 seconds  
- 0 seconds

25.0 + 3.0 seconds  
- 0 seconds

30.0 + 4.0 seconds  
- 0 seconds

The 30-second contact must always provide a  $5^{+1}_{-0}$ -second interval after closure of the 25-second contact. Each time channel must have an output

**Output:**

The output will be in the form of a closure of normally open contacts for each of the channels specified.

**Operation:**

The timer shall be capable of being remotely started through the closure of an external switch.

**TIMER NO. 2**

**Times Required:**

**A) Variable**

TA: 10-59 seconds in 1-second increments.

TB: 10-59 seconds in 1-second increments.

TA & TB must be interlocked so that TB cannot be set to a shorter time interval than the TA setting, and this setting must be capable of accomplishment under field operation conditions.

**Tolerance:  $\pm .5$  second + 1% of T setting**

**B) Fixed**

**.20  $\pm$  .10 second**

**.82  $\pm$  .17 second**

**1.00  $\pm$  .25 second**

1.37  $\pm$  .37 second  
- .17 second

All other requirements for Timer No. 2 are the same as for Timer No. 1.

The power required for each of these timers must be completely contained as a part of the timer. It should be noted that miniaturization in weight and volume will make these timers more attractive as components.

The operating environment under which these timers must be capable of operating include the following conditions:

- A) Temperature: -65°F to + 160°F.
- B) Ambient Pressure: 2.12 to 70 inches of mercury
- C) Shock: Up to 100 g with 1.0-millisecond rise time in each direction along each of three mutually perpendicular axes.
- D) Humidity: Relative humidity up to 100%.
- E) Vibration: 10-73 cps, .036-inch double amplitude  
73-500 cps, 10 g  
500-2000 cps, 5 g

Each of these to be on three mutually perpendicular axes with a total frequency time up and down of 60 minutes.

#### CONTRACT AWARD AND STATUS:

After consultation with several competent agencies in the field and after receipt of formal bids from several companies the development purchase order for these two timers was granted to the UNIVAC Division of Sperry Rand Corporation. It was mutually decided that the development work would be done in three phases:

- 1) Prototype Phase - in which components would be built and proven in large scale models at room temperature.
- 2) Environmental Compensation Phase - in which the sensitivity to the specified environments would be studied and suitable methods of compensation developed.

- 3) Miniaturization Phase - in which production techniques would be adapted or developed to meet the weight and size specifications.

At the time of the submittal of this paper the prototype phase has been completed and work has started on both the temperature compensation and miniaturization phases. A prototype of Timer #1 was brought into Sandia Corporation and successfully demonstrated several times. Then this timer was modified and expanded to produce a prototype of Timer #2 which has been received at Sandia Corporation. The remainder of this paper is devoted to the details of the prototype of Timer #2. The logic of prototype Timer #1 is very similar except that no variable selection of times is provided and all decoding is done in a straight binary fashion.

### CLOCK

The time base for this pure fluid timer consists of a fluid oscillator utilizing RC feedback. The oscillator provides the basic "clock" pulse to the system. The pulses are introduced to the frequency divider network to reduce the clock rate to the basic frequency required by the counter. This reduced frequency is applied to the counter stages where the desired time intervals are selected by the decoding logic. Each time interval selected by the logic circuit sets a fluid flip-flop which in turn operates a pressure sensitive switch. The time from the starting of the oscillator to the closing of the switch represents a complete cycle of one time interval. The timer described contains six time channels and each channel operation results in a switch closure.

The active element in the clock consists of a monostable toggle action fluid device with two possible outputs and one signal input port. One output (inverter output) exists only in the absence of an input signal and the other output (amplifier output) exists only in the presence of an input signal. This amplifier output is the active output of the clock. A feedback signal from the inverter output is applied to the signal input of the device (see Figure 1). The wave form of the feedback signal is altered by the presence of a resistance-capacitance network in the feedback line. The resistance is simply an orifice and the capacitance is a small chamber. By varying the resistance a 50% change in the oscillator frequency is possible.

The oscillator frequency was chosen to be 32 cps to reduce the size of the capacitor which would be necessary. The value of the capacitance is, of course, determined by the time constant (RC) necessary and the maximum fluid resistance that can be utilized. The upper limit of resistance is dependent on the input impedance of the amplifier-inverter element comprising the active element in the clock. Thus, where maximum packaging density is required, RC circuits are feasible where the active element exhibits relatively high input impedance.

It is possible to employ sonic feedback to cause the active device to oscillate. Sonic feedback is accomplished by merely feeding back part

of the output through a simple pipe to the input of the active device. The value of the delay is proportional to the length of the pipe and the square root of the absolute temperature of the fluid. This simple method of obtaining the feedback to provide oscillation has the disadvantage of being difficult to afford temperature compensation with the present state of the art. The RC network affords several variables which can be adjusted to obtain a stable oscillator frequency with a varying gas temperature. Also, for the order of magnitude of the delays required, a sonic delay line is likely to require more space than the RC circuit.

### COUNTER CIRCUIT

The basic function of a binary counter is to reduce the input pulse rate by one half. Figures 2 and 3 show how the binary numbers may be obtained by cascading binary counters.

This characteristic of halving the input frequency makes possible the use of the binary counter as a frequency divider. When it is necessary to operate the clock at a higher frequency than that required by the counting stages, binary counters can function to reduce the frequency to that required. Binary Counter No. 1 of Figure 2 performs this role in the timer circuit. The only output from this stage is the "carry" pulse to drive the following stage at half the frequency.

Several counter designs were investigated to determine their particular advantages. After careful examination it seemed advisable to exclude designs which required time delays to avoid timing problems. Associated with time delays are usually excessive volume requirements and the need for temperature stabilization. Therefore, a counter design was developed which required no delays at the expense of somewhat more elements. As a result, within the entire timer circuit, the effects of temperature changes need be considered only for the oscillator circuit. Because of the elimination of the timing problem, this counter has no low frequency limit, requires no pulse shapers, and each counter stage within the timer circuit is identical.

Figure 3 shows the logic diagram of a single counter stage. NOR gates 1 and 2 in Figure 3 are interconnected to form a flip-flop, as are NOR gates 3 and 4. Figure 4 simplifies the logic diagram and refers to the interconnected NOR gates as flip-flops. A NOR gate is defined as an inverter driven by an OR gate, in this case a 4-input OR gate.

Referring to Figure 4 if FF #1 has simultaneous positive signals to both inputs no output is obtained from either output line. During the time the input signal is applied no change occurs to FF #2. However, either NOR gate 5 or 6, whose outputs are normally low, will produce a high output. Which of these gates turns on depends on the state of FF #2. A high signal at output 4 of FF #2 as shown in Figure 4 will produce a high signal from Gate 5. After the removal of the input pulse to FF #1, the condition of gates 5 and 6 will determine what state FF #1 will assume. It can be shown

that the state of FF #1 will change after the removal of each input pulse. This change in FF #1 then changes the state of FF #2 and turns "OFF" gates 5 and 6 since normally FF's 1 and 2 are in opposite states. The normal binary outputs are obtained from FF #2.

In order to provide a decade count using binary counters it is necessary to deviate from the standard binary counter circuit. As shown in Figure 6, by simultaneously checking the state of each of the four counters (producing binary 1, 2, 4, and 8) a count from 0 to 15 is possible. At the count of 15 all counter stages are in the "ON" state. With the application of the 16th pulse, all stages revert to the zero or "OFF" state. To convert the four binary stages to 10 count circuit, it is necessary to have all counter stages in the "ON" state with the 9th pulse. This can be accomplished by turning on the 2 and 4 counters sometime after the count of 8. Prior to the application of the 9th pulse counters 2, 4, and 8 must be "ON". With the application of the 9th pulse, counter 1 turns "ON". At this time all four stages are in the "ON" condition. With the application of the 10th pulse, all counter stages revert to the "OFF" condition. Thus, the counter is "cleared" at the count of 10 and cycle begins counting again from 1 through 10.

The 2 and 4 counters can be turned "ON" by feeding back the signal from the 8 counter. For timing purposes the application of the turn on signal is delayed by gating until the count of 8-1/2 is reached (see Figure 6).

#### DECODING SECTION

Since binary counters whether set to count to 10 or 16 produce only the binary numbers 1, 2, 4, and 8, combining of these outputs is required to obtain a discrete decimal output. Since two output channels of the timer can be manually set from 10 to 59 seconds, the decoder must be capable of selecting any preset decimal number from 10 to 59. It is also necessary to produce on other channels the elapsed times 0.2, 0.82, 1.00, and 1.37 seconds.

Decoding is essentially an "AND" logic function. For example, for a binary counter producing 1, 2, 4, and 8, to obtain a decimal 5 count the binary 1 must occur simultaneously with the binary 4. While it is true that a 1 and a 4 combination might occur at higher counts (e. g., 7), this does no harm in this particular application, since the 5 count must be held in a flip-flop until the end of operation anyway.

The "AND" function is accomplished by applying all "signals" to be ANDed to the same NOR gate. To use the NOR gate to perform the "AND" function requires signals which have previously been inverted (zero pressure and flow indicate the presence of the binary numbers). The fact that the standard NOR gate employed in the timer has a "fan-in" and "fan-out" of four provides for economical decoding. Figure 7 shows the decoding for the variable time Channel A, capable of picking any elapsed time from 10 to 59 seconds.



## OUTPUT MEMORY

The result of the decoding function is introduced to a fluid flip-flop whose function is to take the output of the decoder which is in pulse form and to produce a steady signal indicating the completion of the time channel function and to supply steady fluid power to the proper pressure switch.

## SELECTOR SWITCH

In order to manually select the proper elapsed time for the two variable time channels, a multiposition selector switch was designed. The switch has a dual dial, one for selecting the units and the other for tens. The switch package incorporates a "dial" read-out which indicates the time selected in decimal notation.

Each switch element is a sliding metal plate with through holes. The location of the holes on the slider plate determines which binary counters are to be connected to the decoding "NOR" gates. With reference to Figure 7 the slider when selecting the decimal unit 3 will connect to the decoder, the binary counter outputs 1 and 2. Since the negative or zero signal contains the binary information, when simultaneously zero signals are obtained from both counters, the "AND" function is performed. Since the slider plate is blocking the binary 4 and 8 these values will already be zero to the decoding "NOR" gates. The tens are selected by the second slider plate in the switch assembly. Figure 8 shows the logic diagram for the timer showing the complete decoding section including the manual selector switches, output memories, flip-flops and pressure switches.

## CONCLUSION

The prototype of Timer #2 contains 100 identical NOR gates plus one monostable toggle device in the clock (Timer #1 contained 84 NOR gates plus the clock). Both timers worked immediately upon assembly (except for one minor logic error in the first one) and required no timing or adjustments of any kind. This demonstrates that with a truly reliable element having adequate fan-in and fan-out characteristics very complex logic networks can be designed and built with ease using pure fluid devices. The elements used in the timers were produced by a casting technique and were 100% tested before assembly.

It is expected that all final specifications for both of these timers will be met during this development contract and that the designs produced therefrom will be a significant contribution to the field of pure fluid systems in timing.

## OSCILLATOR CONFIGURATION

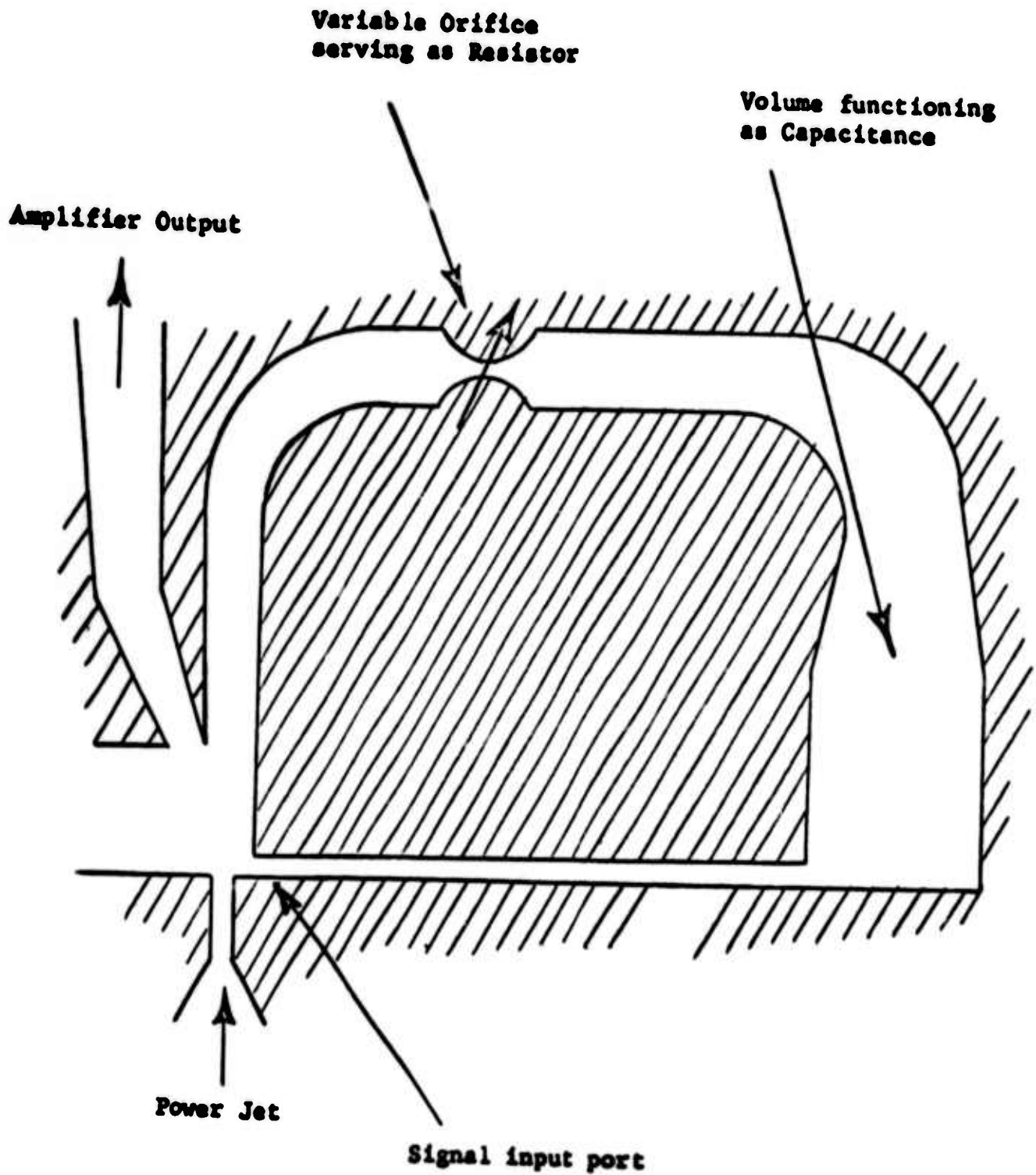


FIGURE 1

COUNTING STAGES  
TIMER No. 2

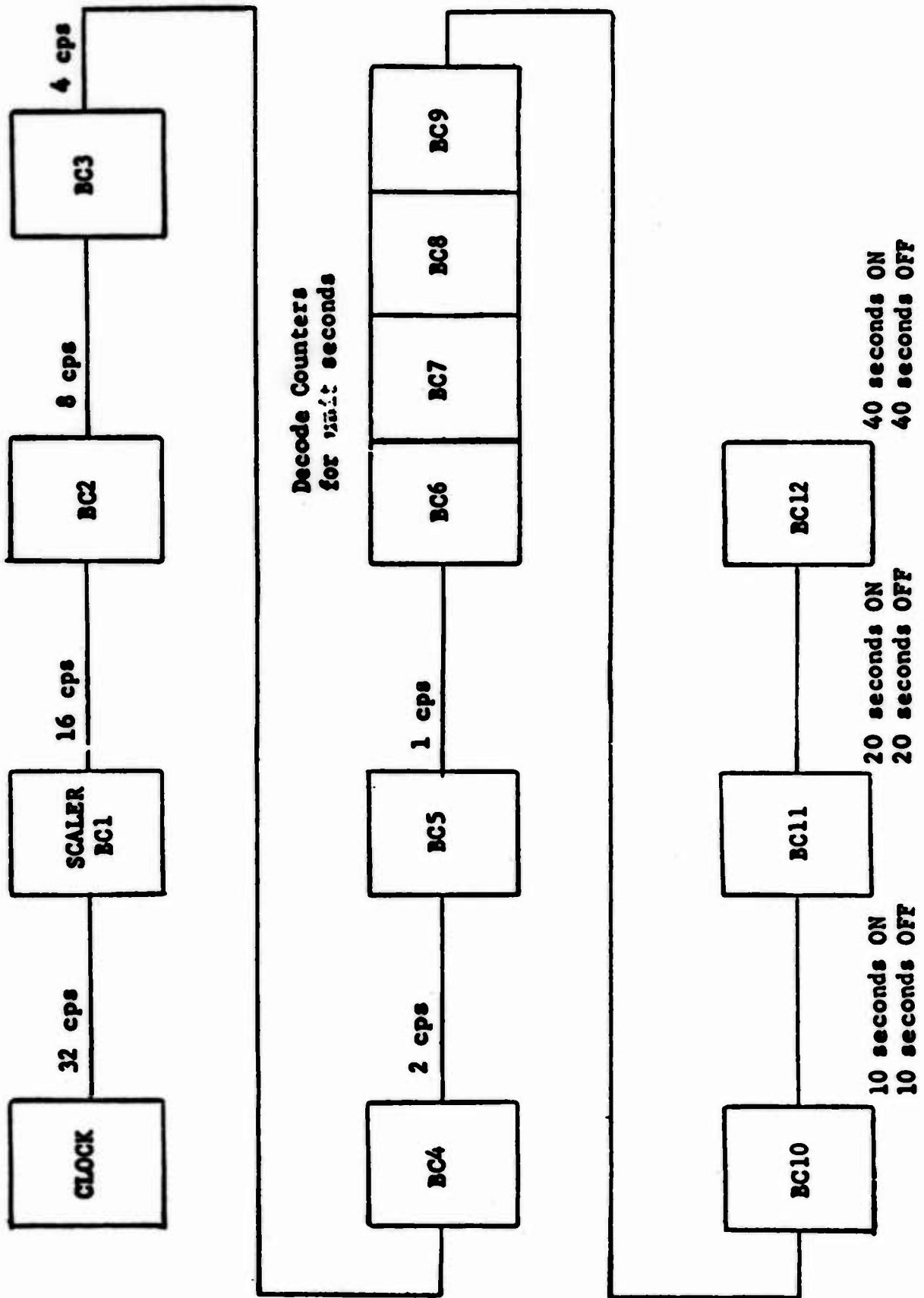


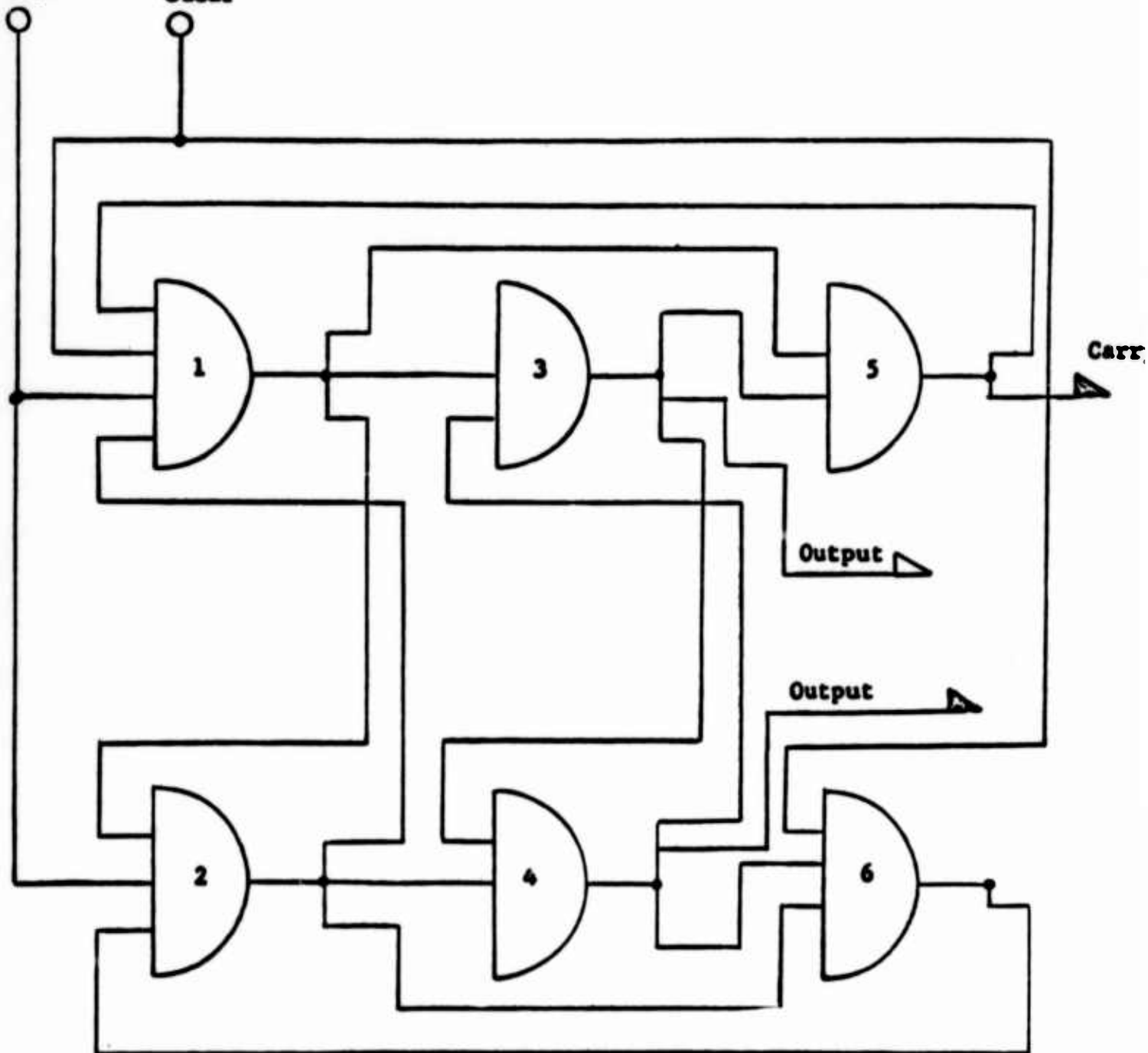
FIGURE 2



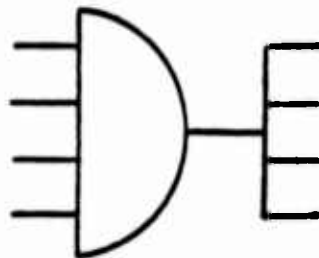
# NOR GATE. BINARY COUNTER CIRCUIT

Signal  
Input

Clear



4 Inputs  
Available

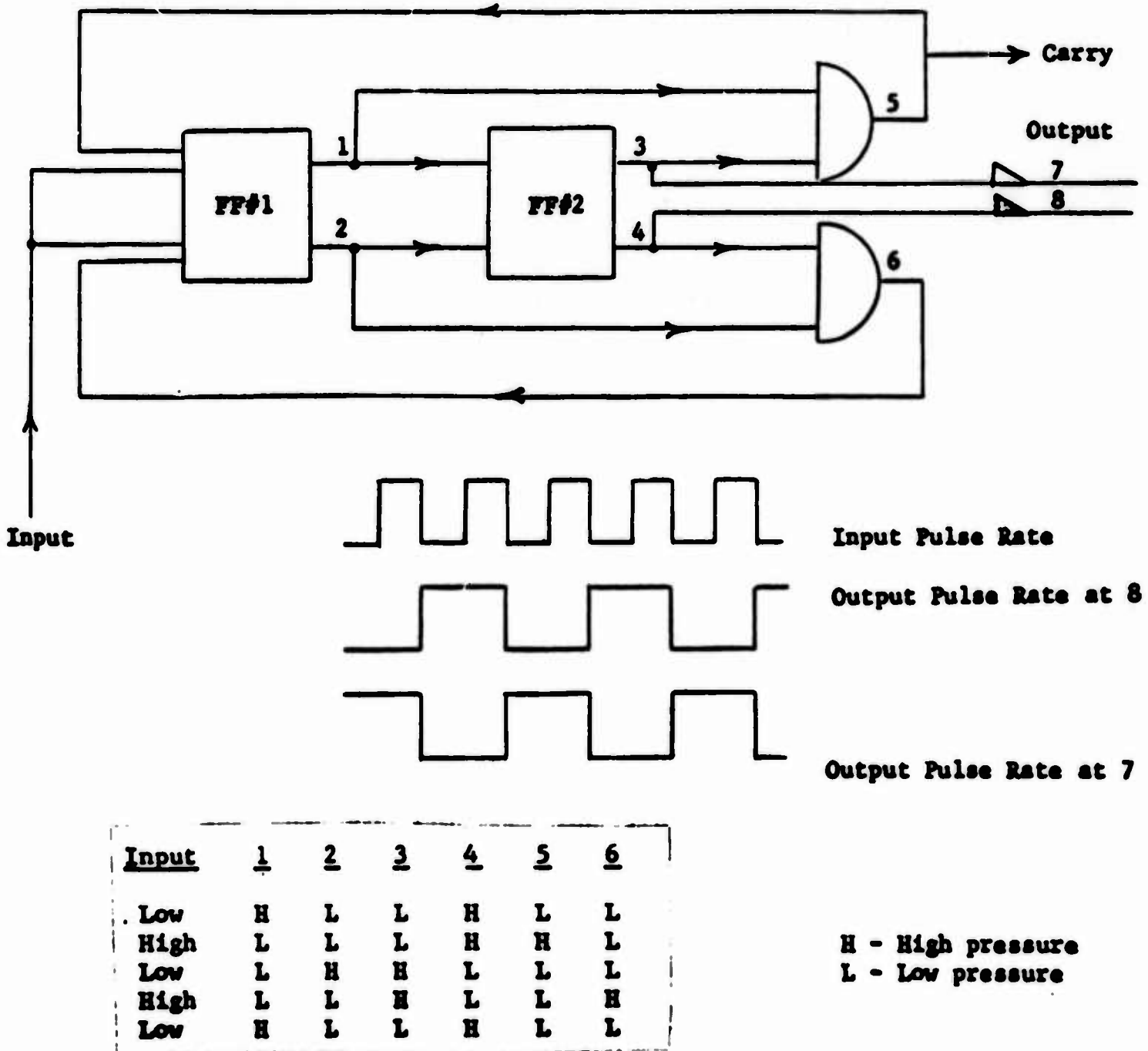


4 Outputs  
Available

NOR Gate Logic Symbol

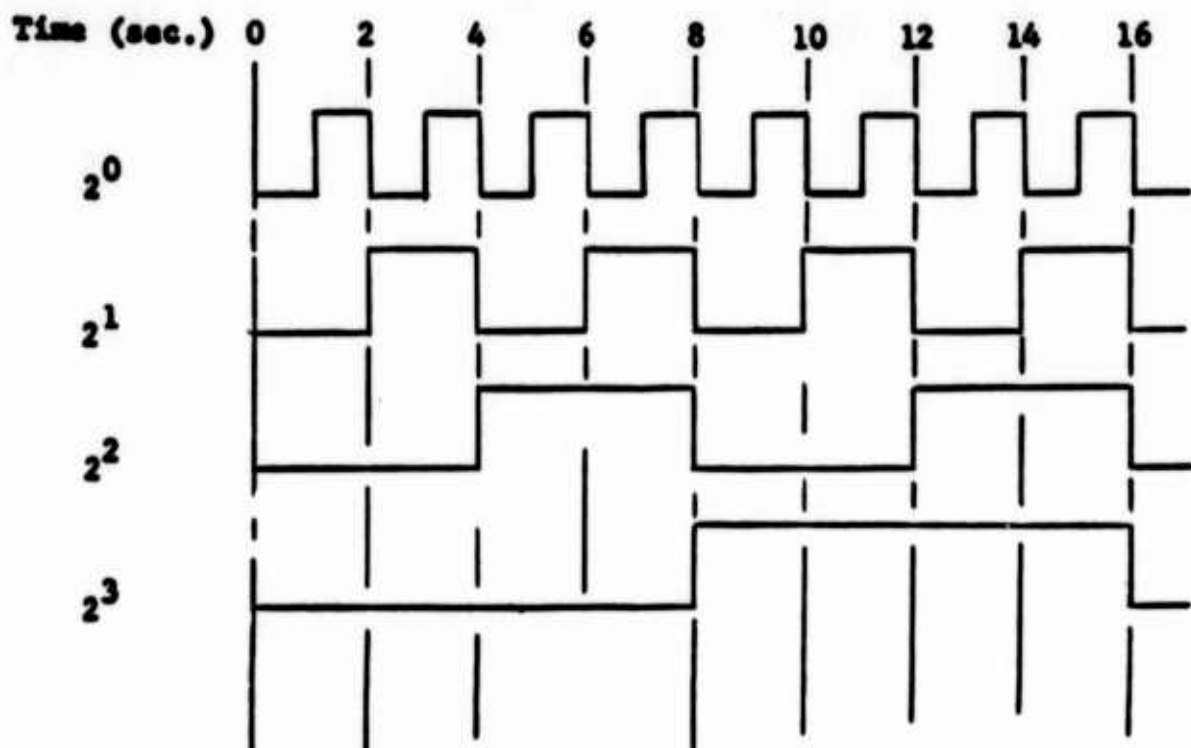
FIGURE 3

# SIMPLIFIED COUNTER CIRCUIT

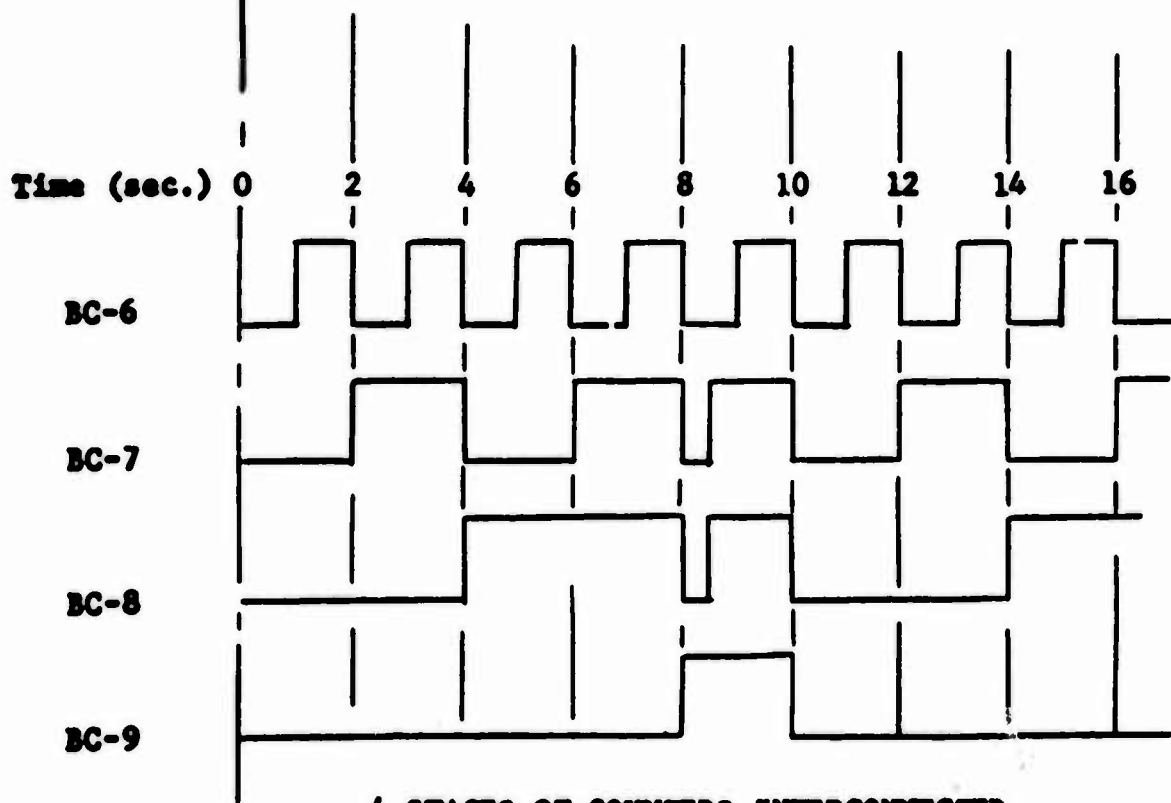


**FIGURE 4**

# COUNTER STATE vs TIME



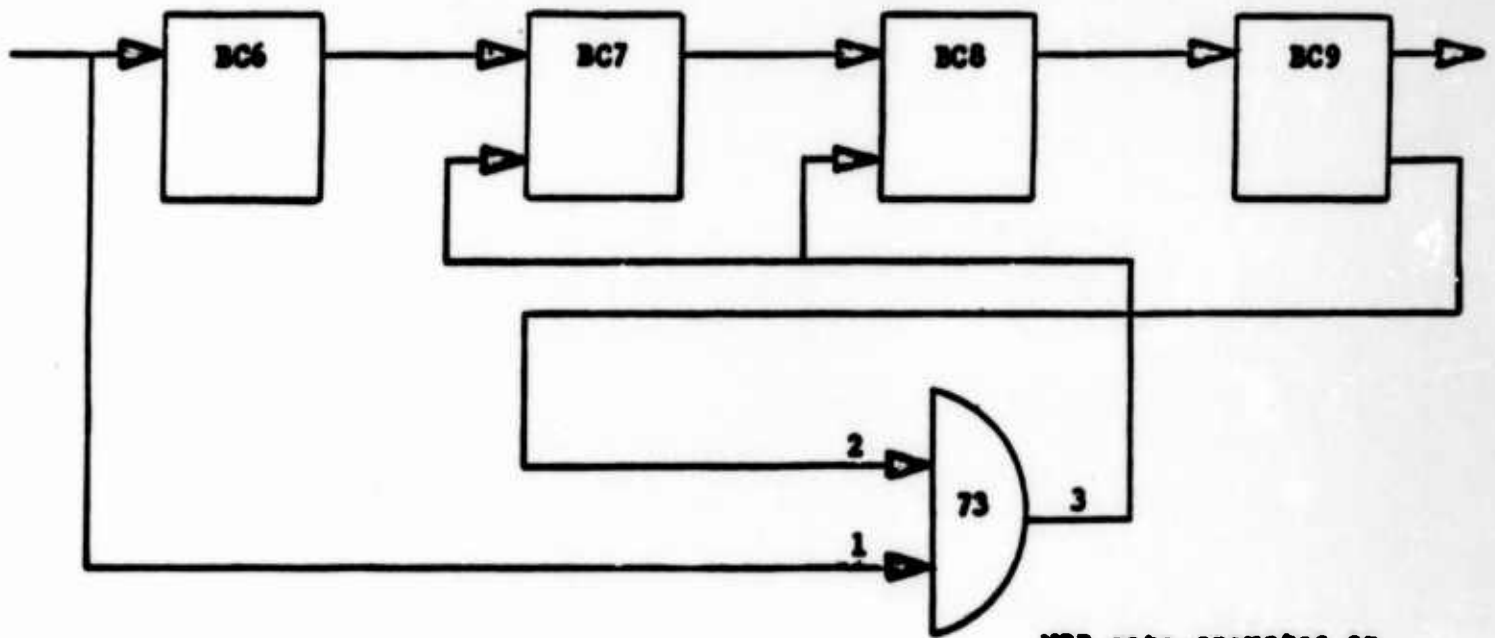
**NORMAL 4 STAGE BINARY COUNTER OUTPUTS**



**4 STAGES OF COUNTERS INTERCONNECTED  
TO COUNT DECADES**

**FIGURE 5**

# DECODE COUNTER INTERCONNECTIONS



NOR gate operates at  
8.5 seconds to turn on  
BC7 and BC8

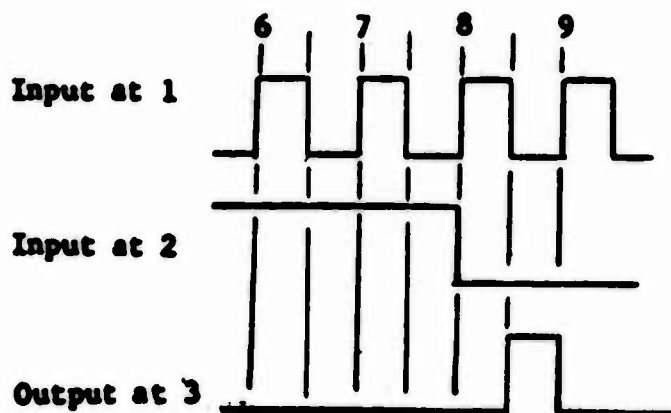


FIGURE 6

# DECODING FOR VARIABLE TIME CHANNEL

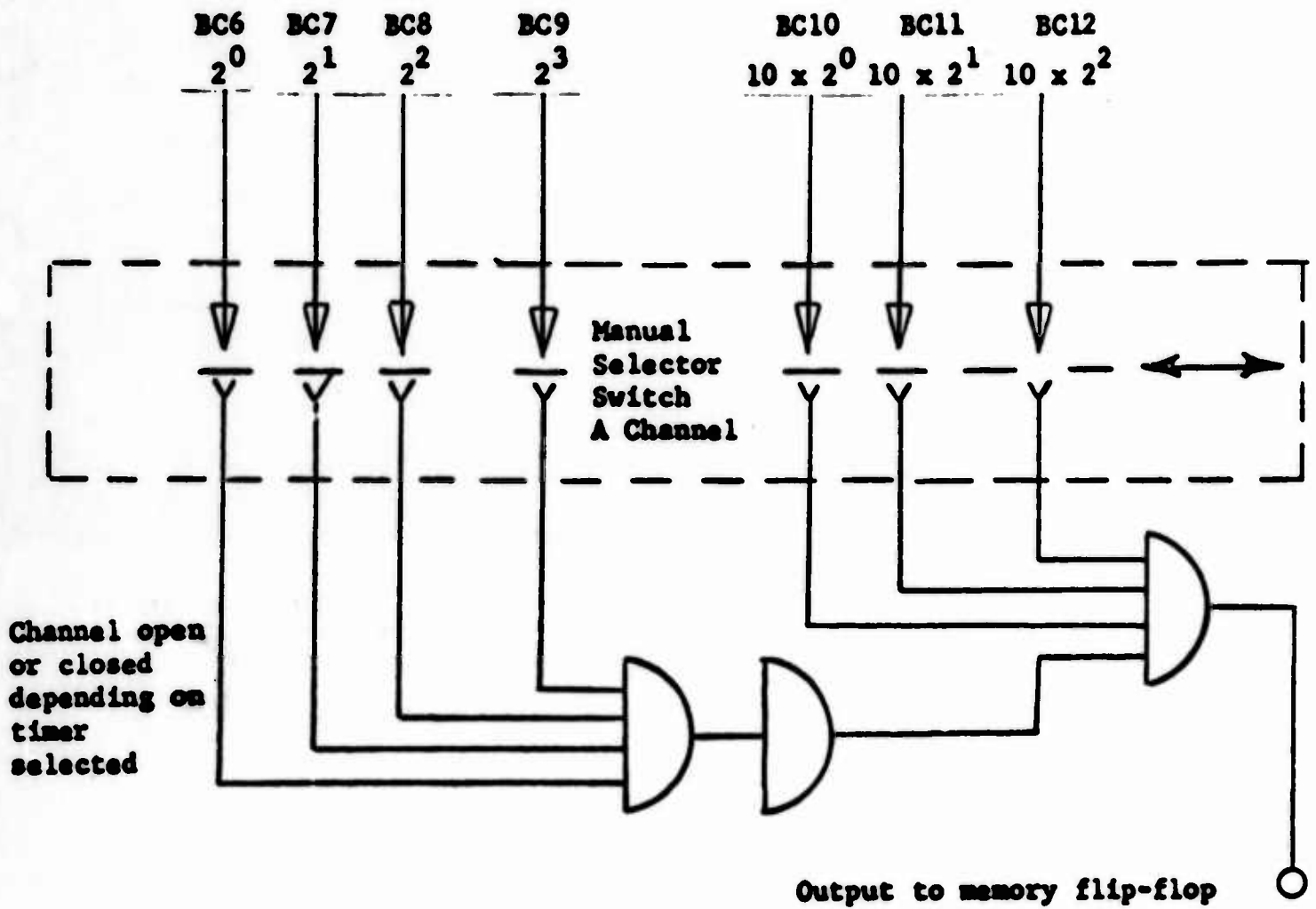


FIGURE 7

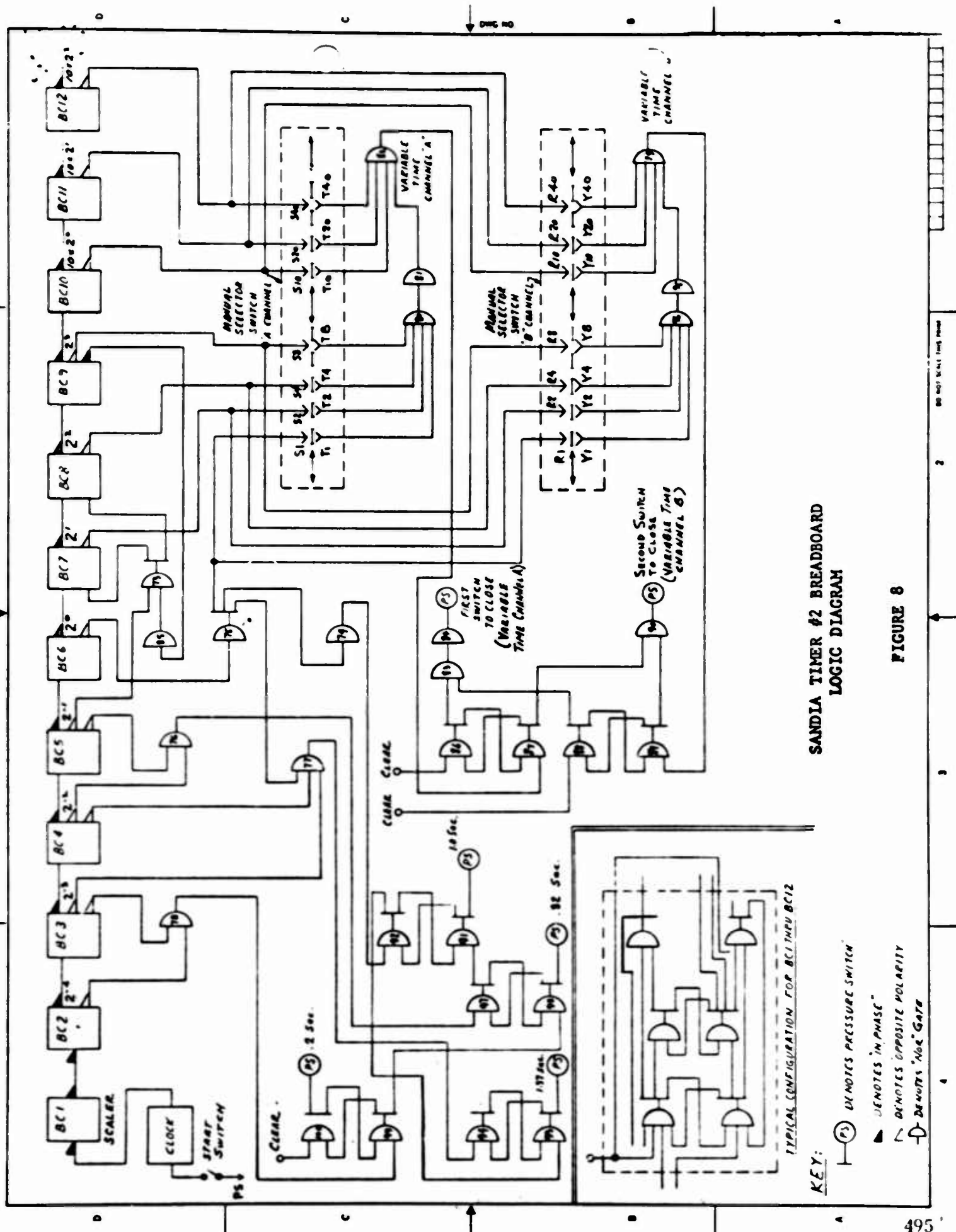


FIG. 9  
PROTOTYPE TIMER #2



## DISTRIBUTION

Office of the Secretary of Defense  
Research and Engineering  
The Pentagon, Washington 25, D. C.  
Attn: Tech Library (Rm 3C128)

Director  
Advanced Research Projects Agency  
Washington 25, D. C.  
Attn: Fred A. Koether

C. A. Lejonhud  
D.C.N.O. (Development)  
Op-07TS  
The Pentagon (Rm5E621)  
Washington 25, D. C.

Director, Army Research Office  
Office, Chief of R & D  
Washington 25, D. C.  
Attn: Library

Department of the Army  
Office of the Chief of R & D  
Washington 25, D. C.  
Attn: Chief, Combat Material Div.

Director, Special Weapons  
Office of the Chief of R & D  
Department of the Army  
Washington 25, D. C.

Department of the Army  
Office, Chief of R & D  
Physical Science Div  
Washington 25, D. C.  
Attn: Dr. R. B. Watson

Commanding General  
Army Materiel Command  
Washington 25, D. C.  
Attn: R & D Directorate, AMCRD-RS-CM  
AMCRD-DE-MI  
AMCRD-DE-N  
AMCRD-RS, Major W. Kerttula

Commanding General  
Army Munitions Command  
Dover, New Jersey  
Attn: Technical Library

Commanding Officer  
U.S. Army Munitions Command  
Frankford Arsenal  
Philadelphia 37, Pennsylvania  
Attn: Library, 0270

Commanding Officer  
Aberdeen Proving Ground, Md.  
Attn: J. A. Tolen

Commanding Officer  
U.S. Army Limited War Lab.  
Aberdeen Proving Ground, Md.  
Attn: Lt. Col J. T. Brown

Commanding Officer  
Picatinny Arsenal  
Dover, New Jersey  
Attn: Tech Library (3 cps)  
SMUPA-VA6

Commanding Officer  
U.S. Army Biological Lab  
Fort Detrick  
Frederick, Maryland

Commanding General  
U.S. Army Engineer Research & Dev Lab.  
Fort Belvoir, Virginia  
Attn: Tech Library  
Attn: Office of Patents, R. Lucke  
Army Security Agency  
Arlington Hall Station  
Arlington 12, Virginia  
Attn: OACS DEV (OBJ-Div)

Commanding Officer  
Army Research Office - Durham  
Box CM - Duke Station  
Durham, N. C.



**DISTRIBUTION (Continued)**

Commanding Officer  
Artillery Combat Dev Agency  
Fort Sill, Okla.

Redstone Scientific Info Center  
U.S. Army Missile Command  
Redstone Arsenal, Alabama  
Attn: Chief, Document Section  
(10 copies)

Commanding General  
U. S. Army Missile Command  
Redstone Arsenal, Alabama  
Attn: Charles Schriener  
Bldg 7446

Commanding General  
U.S. Army Weapons Command  
Technical Information Branch  
Rock Island, Ill.

Commanding Officer  
U.S. Army Weapons Command  
Springfield Armory  
Springfield, Mass.  
Attn. TIU

Commanding Officer  
U.S. Army Materials Research Agency  
Watertown Arsenal  
Watertown 72, Mass.  
Attn: Tech Info Center

Commanding General  
White Sands Missile Range  
White Sands, New Mexico  
Attn: Tech Library

Army Mathematics Research Center  
University of Wisconsin  
Madison 6, Wisconsin  
Attn: Librarian

Commanding Officer  
Watervliet Arsenal  
Watervliet, New York  
Attn: Tech Library B-C

Department of the Navy  
Bureau of Naval Weapons  
Washington 25, D. C.  
Attn: S. J. Gorman, RRRE-31

Director  
U.S. Naval Research Laboratory  
Washington 25, D. C.  
Attn: Code 2027

Office of Naval Research  
Washington 25, D. C.  
Attn: Code 492, Dr. Morscher

Department of the Navy  
Chief, Bureau of Ships  
Washington 25, D. C.  
Attn: Code 210L, 442, 632

Commander  
U.S. Naval Ordnance Laboratory  
Corona, Calif.  
Attn: Tech Library

Commander  
Naval Ordnance Laboratory  
White Oak, Silver Spring, Maryland  
Attn: B. Gilbert

Commander  
U.S. Naval Ordnance Test Station  
China Lake, Calif.  
Attn: Tech Library

Commandant  
U.S. Marine Corps  
Washington 25, D. C.  
Attn: Code AO4F

DDC Headquarters  
Cameron Station, Bldg 5  
5010 Duke Street  
Alexandria, Virginia  
Attn: TISIA (20 copies)

Mr Pervy Griffin  
CIA Headquarters  
Langley, Virginia  
143-7671

**DISTRIBUTION (Continued)**

Aeronautical Systems Division  
Wright-Patterson AFB, Ohio  
Attn: ASRMOD (Mr. M. Shorr)  
Attn: ASRMC-ZO (Mr. Wible)

Aeronautical Systems Division  
Avionics Laboratory  
Wright Patterson AFB, Ohio  
Attn: ASRNG-1

Aeronautical Systems Division  
Propulsion Laboratory  
Wright Patterson AFB, Ohio  
Attn: ASRMP-1 (Mr. Bentz)

Air Force Special Weapons Center  
Kirtland Air Force Base  
Albuquerque, New Mexico  
Attn: Tech Library - SW01

Commander  
Air Proving Ground Center  
Eglin AFB, Florida  
Attn: Library APGC(PGAPI)

Commander  
Edwards Air Force Base, Calif.  
Attn: M. Jones AFTTC (FTOOT)

Sandia Corporation  
Sandia Base  
Albuquerque, New Mexico  
Attn: Tech Library

U.S. Atomic Energy Commission  
Space Nuclear Propulsion Office  
Washington 25, D. C.  
Attn: F. C. Schwenk

U.S. Atomic Energy Commission  
Washington 25, D. C.  
Attn: Library

Oak Ridge National Lab  
P.O. Box Y  
Oak Ridge, Tennessee  
Attn: Technical Library Y-12

Los Alamos Scientific Laboratory  
P.O. Box 1663  
Los Alamos, New Mexico  
Attn: Reports Librarian

Marshall Space Flight Center  
Huntsville, Alabama  
Attn: Roy Currie (R-ASTR-TN)  
Attn: Dr. Walter P. Krause

Scientific & Technical Info Facility  
P.O. Box 5700  
Bethesda, Maryland  
Attn: NASA Representative  
(S-AK/DL)-A366

National Aeronautics & Space Agency  
Lewis Research Center  
Cleveland 35, Ohio  
Attn: K. Hiller

Library of Congress  
Science & Technology Div.  
Washington 25, D. C.

National Bureau of Standards  
Washington 25, D. C.  
Attn: Chief, Sec. 14.01

National Bureau of Standards  
Boulder, Colorado  
Attn: Tech Library

Patent Office  
Washington 25, D. C.  
Attn: Scientific Library  
Acquisitions, Rm 1886-C  
Attn: Group 220, R. Stahl  
Attn: Group 360, W. O'Dea  
Attn: Group 370, R. Nilson  
Attn: Group 430, M. Hoffman  
Attn: Miss Steddom

Armour Research Foundation of  
Illinois Inst. of Tech.  
Chicago 16, Illinois  
Attn: George I. Jacobi  
10 W. 35th Street

**DISTRIBUTION (Continued)**

Franklin Institute of the State of  
Pennsylvania  
Philadelphia 5, Pennsylvania  
Attn: C. W. Hargens, Tech Dir  
Attn: Charles A. Belsterling

Johns Hopkins University  
Applied Physics Lab  
8621 Georgia Avenue  
Silver Spring, Maryland  
Attn: Tech Library (2 copies)

University of Maryland  
College Park, Maryland  
Attn: W. Sherwood, College of  
Aero Engineering  
Attn: Dr. Donald S. Gross,  
Director, Wind Tunnel  
Attn: Dr. S. Pai

University of Southern California  
University Park  
Los Angeles 7, California  
Attn: Library

University of California  
Engineering Library  
405 Hilgard Avenue  
Los Angeles 24, California  
Attn: Mr. J. Tallman

Cornell Aeronautical Laboratories  
P.O. Box 235  
Buffalo, New York  
Attn: Librarian

New York University  
Engineering Library  
University Heights  
Bronx 53, New York

Arizona State University  
Measurement Engr. Lab. Library  
Engineering Center  
Tempe, Arizona

University of Minnesota  
St. Anthony Falls Hydraulic Lab  
Mississippi River at 3rd Ave S. E.  
Minneapolis, Minnesota 55414

Purdue University  
Mechanical Engineering Library  
Mechanical Engineering Building  
West Lafayette, Indiana

Wichita State University  
Documents Department  
Wichita 8, Kansas  
Attn: Library

Johnson Service Company  
507 East Michigan Street  
Milwaukee 1, Wisconsin  
Attn: Thomas J. Lechner

Purdue University  
West Lafayette, Indiana  
Attn: Librarian

Carnegie Institute of Technology  
Pittsburgh, Pennsylvania  
Attn: Technical Library  
Attn: Dr. E. M. Williams

University of California  
Engineering Library  
Berkeley 4, California

Cornell University  
Ithaca, New York  
Attn: Dr. Ed Resler, Jr.

Engineering Societies Library  
345 East 47th Street  
New York 17, New York

Illinois Institute of Technology  
Research Institute  
10 West 35th Street  
Chicago, Illinois  
Attn: Mr. Roy Kamo

Worcester Polytechnic Institute  
Worcester, Massachusetts 01609  
Attn: Library

DISTRIBUTION (Continued)

Mass. Inst. of Technology  
Dept of Mech. Engineering  
Cambridge, Mass.

Attn: J. L. Shearer - B  
Rm 3-453

Manhattan College  
Riverdale 71, New York

Attn: Technical Library

Fairleigh Dickenson University  
Teaneck, New Jersey

Attn: Engineering Library

University of Michigan  
Institute of Science & Technology  
Ann Arbor, Michigan

Attn: Tech Documents Serv (Box 618)

Ohio State University  
M.E. Department Library  
206 W. 18th Ave  
Columbus 10, Ohio

University of New Mexico  
Albuquerque, New Mexico

Attn: Dr. A. H. Koschmann

Case Institute of Technology  
Pittsburgh, Pennsylvania

Attn: E. M. Williams

Catholic University  
Department of Mech Engineering  
Washington, D. C.

Attn: Prof. P. K. Chang

University of Nebraska  
Lincoln 8, Nebraska

Attn: Prof. T. Sarpkaya

Oklahoma State University  
Stillwater, Oklahoma

Attn: Dr. Glen Zumwalt

New York State University  
School of Engineering  
6 Chemistry Road

Buffalo 14, N. Y.

Attn: Tech Library

Rutgers University  
University Library  
New Brunswick, N. J.

Attn: Dr. D. F. Cameron

University of Arizona  
Physics Department  
Tucson, Arizona

Attn: Prof. Ulrich H. Bents

Linda Hall Library  
5109 Cherry Street  
Kansas City 10, Mo.

Attn: Joseph C. Shipman

Ohio State University  
1858 Neil Avenue  
Columbus 10, Ohio

Attn: Documents Division

Pennsylvania State University  
201 Hammond Bldg  
University Park, Pennsylvania 16802

Attn: Engineering Librarian

Attn: David P. Margolis

University of Notre Dame  
Notre Dame, Indiana

Attn: Prof F. N. M. Brown

Dept of Aeronautical Eng.

Minneapolis-Honeywell Regulator Co.  
Military Products Group Research Dept.  
2600 Ridgway Rd. Mail Station 340  
Minneapolis, Minnesota

NASA  
Langley Research Center  
Langley Station  
Hampton, Virginia

Attn: Tech Library

INTERNAL

Horton, B. M./McEvoy, R. W., Lt. Col.  
Apstein, M./Gerwin, H. L./Guarino, P. A./Kalmus, H. P.  
Hardin, C. D., Lab 100  
Sommer, H., Lab 200  
Hatcher, R. D., Lab 300  
Hoff, R. S., Lab 400  
Nilsen, H. Lab 500  
Flyer, I. N., Lab 600  
Campagna, J. H./Apolenis C.J., Div 700  
DeMasi, R., Div 800  
Landis, P. E., Lab 900  
Seaton, J. W., 260  
Kirshner, J., 310 (350 copies)  
Garver, R. V., 250  
Harris, F. T., 320  
Tech Reports Unit, 800 (2 copies)  
Tech Info Office, 010 (10 copies)  
HDL Library (5 copies)  
Rotkin, I./Godfrey, T. B./Bryant, W. T.  
Distad, M. F./McCoskey, R. E./Moorhead, J. G.  
Bonnell, R. 040